



Swansea University
Prifysgol Abertawe



Circles within spirals, wheels within wheels; Body rotation facilitates critical insights into animal behavioural ecology

Richard Michael Gunner

ORCID iD: <https://orcid.org/0000-0002-2054-9944>

Supervised by:

Prof. Rory P. Wilson¹, Prof. Emily L.C. Shepard¹, Dr Luca Börger¹

¹Swansea Laboratory for Animal Movement (SLAM), Department of Biosciences, College of Science, Swansea University, Swansea, SA2 8PP, Wales, UK

*Submitted to Swansea University in fulfilment of the requirements for
the Degree of Doctor of Philosophy*

Swansea University

2021

1

Abstract

How animals behave is fundamental to enhancing their lifetime fitness, so defining how animals move in space and time relates to many ecological questions, including resource selection, activity budgets and animal movement networks. Historically, animal behaviour and movement has been defined by direct observation, however recent advancements in biotelemetry have revolutionised how we now assess behaviour, particularly allowing animals to be monitored when they cannot be seen. Studies now pair ‘convictional’ radio telemetries with motion sensors to facilitate more detailed investigations of animal space-use. Motion sensitive tags (containing e.g., accelerometers and magnetometers) provide precise data on body movements which characterise behaviour, and this has been exemplified in extensive studies using accelerometry data, which has been linked to space-use defined by GPS. Conversely, consideration of body rotation (particularly change in yaw) is virtually absent within the biologging literature, even though various scales of yaw rotation can reveal important patterns in behaviour and movement, with animal heading being a fundamental component characterising space-use. This thesis explores animal body angles, particularly about the yaw axis, for elucidating animal movement ecology. I used five model species (a reptile, a mammal and three birds) to demonstrate the value of assessing body rotation for investigating fine-scale movement-specific behaviours. As part of this, I advanced the ‘dead-reckoning’ method, where fine-scale animal movement between temporally poorly resolved GPS fixes can be deduced using heading vectors and speed. I addressed many issues with this protocol, highlighting errors and potential solutions but was able to show how this approach leads to insights into many difficult-to-study animal behaviours. These ranged from elucidating how and where lions cross supposedly impermeable man-made barriers to examining how penguins react to tidal currents and then navigate their way to their nests far from the sea in colonies enclosed within thick vegetation.

Declaration and statements

This work has not previously been accepted in substance for any degree and is not being concurrently submitted in candidature for any degree.

Signed  (candidate)

Date10/07/21.....

STATEMENT 1

This thesis is the result of my own investigations, except where otherwise stated. Where correction services have been used, the extent and nature of the correction is clearly marked in a footnote(s).

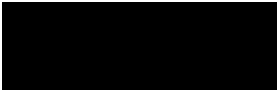
Other sources are acknowledged by footnotes giving explicit references. A bibliography is appended.

Signed  (candidate)

Date10/07/21.....

STATEMENT 2

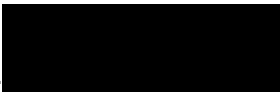
I hereby give consent for my thesis, if accepted, to be available for photocopying and for inter-library loan, and for the title and summary to be made available to outside organisations.

Signed  (candidate)

Date 10/07/21.....

NB: *Candidates on whose behalf a bar on access has been approved by the University (see Note 7), should use the following version of Statement 2:*

I hereby give consent for my thesis, if accepted, to be available for photocopying and for inter-library loans **after expiry of a bar on access approved by the Swansea University.**

Signed  (candidate)

Date10/07/21.....

Contents

Abstract	i
Declaration and statements	ii
Contents	iii
Acknowledgments	ix
Ethics statement and approvals	xii
Contributing authors and funding	xvi
List of Tables and Figures	xix
Chapter 1 Introduction	1
Why is it important to study animal behaviour?	2
How can we measure movement-specific behaviours?.....	5
The relevance of magnetic and inertial measurements for elucidating behaviour	9
Choice of sensor with respect to the animal in question and questions being asked	12
The Daily Diary (DD) & the GiPSy	14
The purpose of this thesis	16
The layout of my data chapters	18
References	26
Chapter 2 A new direction for differentiating animal activity based on measuring angular velocity about the yaw axis	43
Abstract	44
Background	45
Materials and methods	47
Subjects, study area and tagging	47
Derivation of VeDBA.....	48
Derivation of angular velocity.....	48
Data analysis	50
Results	53
Discussion	61
Angular velocity as a metric for animal movement	61
Relationship between AVeY and VeDBA	63
Advantages of AVeY over acceleration estimates.....	64
Conclusion	66

References.....	67
Chapter 3 Activity of loggerhead turtles during the U-shaped dive: insights using angular velocity metrics	72
Abstract	73
Background.....	74
Materials and methods	77
Subjects, study area and tagging	77
Derivation of angular velocity.....	78
Depiction of type 1a dives and activity	79
Statistical analyses	81
Results	82
Discussion	87
AAV and its ability to infer activity in turtles	87
Comparison between acceleration- and angular velocity-derived metrics.....	87
Potential for AAV metrics to elucidate turtle behaviour	88
Behaviour during dives.....	89
Depth use.....	89
Activity extent of type 1a dives.....	89
Conclusion	92
References.....	93
Chapter 4 Decision rules for determining terrestrial movement and the consequences for filtering high-resolution GPS tracks – A case study using the African Lion (<i>Panthera leo</i>).....	99
Abstract	100
Background.....	101
Materials and methods	105
The Movement Verified Filtering (MVF) method	106
Data analyses	109
Results	110
Discussion	114
Evaluation of the MVF protocol	114
Utility of the MVF protocol according to species-specific and environmental circumstance.....	116
Conclusion	119
References.....	121
Chapter 5 Dead-reckoning animal movements in R: a reappraisal using <i>Gundog.Tracks</i>.....	127

Abstract	128
Background	129
Implementation of <i>Gundog.Tracks</i>	134
User functionality.....	135
Reverse dead-reckoning.....	135
Integrating current vectors.....	135
DBA~speed derivation.....	136
Pre-determining speed.....	137
VPC procedure	139
Default inputs for calculations and outputs	142
The case-studies.....	149
VPC dead-reckoning procedure in R	158
Preparing the three axes of rotation for derivation of heading	158
Tilt-compensated heading derivation	159
Preparing speed estimates	168
By-passing DBA as a speed proxy.....	170
Converting speed to a distance coefficient	171
Derivation of co-ordinates.....	172
Reverse dead-reckoning.....	173
Integrating current vectors.....	174
VPC procedure	174
Conclusion	181
References.....	182
Glossary.....	193
Chapter 6 How often should dead-reckoned animal movement paths be corrected for drift?	199
Abstract	200
Background.....	201
Materials and methods	204
Study species	204
VP-corrected dead-reckoning procedure	205
VP correction rate and metrics of analysis.....	206
Results.....	209
Discussion	217

Speed inaccuracies and VP corrected dead-reckoning	217
Heading inaccuracies and VP-corrected dead-reckoning accuracy	221
VP inaccuracies and VP-corrected dead-reckoning accuracy	223
Deciding drift correction rates	224
The utility of dead-reckoning.....	225
Key considerations governing the relationship between VP correction rate and dead-reckoning accuracy.....	227
Conclusion	229
References	230
Chapter 7 Magellanic Penguins navigate effectively on land in multiple landscapes	240
Abstract	241
Introduction	242
Materials and methods	246
Study site	246
Animal-attached tags and capture protocol	247
Colony mapping	248
Track analysis	248
Statistical Analysis	252
Results	254
Discussion	265
Conclusion	269
References.....	270
Chapter 8 Magellanic penguins react to current streams for efficient navigation	275
Abstract	276
Background.....	277
Materials and methods	279
Study site, tags used and attachment method	279
Numerical ocean current model	279
Speed estimates.....	280
Dead-reckoning procedure.....	281
The travelling vectors and their derivation	282
Ease of transport (EOT)	283
Graphical and statistical analysis	285
Results	286

Discussion	290
Orientation strategy	290
Potential errors	294
Conclusion	295
References	296
Chapter 9 Synopsis	299
Why did my thesis take the direction it did?	300
Piecing together the puzzle: the dive and foraging strategy	301
The future	309
References	315
Appendices	321
Chapter 2: Supplementary Information	322
Chapter 3: Supplementary Information	324
Limitation of using Euler angles	326
References	327
Chapter 4: Supplementary Information	328
Text S1 – The study design	328
Study area	328
Collar design and set up	328
Capture protocol	330
Text S2 – The Relationship between VeDBA and GPS speed	332
Text S3 – Descriptive statistics comparing the MVF results	338
Text S4 - mathematical procedures for various DD- and GPS-derived metrics used to compare MVF results	341
Derivation of pitch, roll and heading	341
GPS heading	342
Tortuosity	343
Distance and speed estimates	343
References	345
Chapter 5: Supplementary Information	346
Text S1 – Device set up and capture protocol	346
Text S2 – The importance of having the correct coordinate system and axis alignment	348
Text S3– Magnetometer calibration, rotation correction and deriving yaw (heading)	352

Text S4 – Step counts as a distance estimate	356
Text S5 – Time Data in R (POSIXct).....	360
Text S6 – VPC dead-reckoning – Gundog.Tracks.....	363
References	366
Chapter 6: Supplementary Information	367
Text S1. Dead-reckoning formulae.....	369
Chapter 7: Supplementary Information	371
Text S1 – Identifying walking and pausing periods in DDMT software using the LoCoD method.	371
Text S2 – Descriptors of movement.....	375
Text S3 – Model parameters.....	377
Text S4 – The case-studies.....	380
References	388
Chapter 8: Supplementary Information	389
Text S1 – Additional results	389
Text S2 – Methods expanded	392
Accounting for Pressure drift.....	392
Correcting the dead-reckoned tracks for drift.....	392
Conversions between estimates of U and V components (m/s) and heading (°) and speed (m/s)	393
Calculating the Theoretical ‘best’ heading	393
References	394
Papers that I have co-authored during this thesis.....	395

Acknowledgments

Having finished putting this thesis together, this acknowledgments section was the final task prior to submission. Funny enough, I was a tad nervous about writing this section, even though acknowledgments are optional to include and do not add anything to the actual science that I will ultimately be judged on. I guess, that after devoting my last few years to writing scientific pieces of work, the creative and emotive freedom does take a bit of a backseat (I could not go around calling lions a hard-core killer cat or penguins a bloated bird of awesomeness in my chapters – even though they obviously are!). And yet there are just so many credible people that deserve a befitting mention and I really wanted to do justice with their acknowledgment, because this thesis is a by-product of their support, guidance, trust and friendship.

Firstly, starting with the head honcho himself - Prof. Rory Wilson. There is probably nothing I could say that has not already been said before by his previous students (all positive of course), and certainly nothing that I could say that would justify the level of gratitude that I have towards him. He is an amazing human being and one hell of a charismatic scientist. I can safely say that without him, I would not be submitting this thesis. Having suspended right at the start with an intention to quit science all together, he was the reason I came back and got me believing in myself and my science again. The lessons that I have learned from him, both in a scientific and personal context, I will hold on to for the rest of my life. Even with the Covid situation, he was always a WhatsApp-come-Signal voice message away, whatever the time, whatever the day, no matter where or how busy he was (and he is an in-demand guy!), he was always there for me. From the bottom of my heart, thank you Roar! I definitely feel that I am a much-improved scientist from your mentoring and whilst I cannot promise that split infinitives and verb tense errors are a thing of the past, I can promise that I will be forever grateful – You're a walking, talking legend!

I would also like to give Prof. Emily Shepard a special mention. I have been at Swansea for eight years now, having previously undertaken my undergraduate Zoology- and Master of Research degree here. Emily was my undergraduate second- and third year tutor and she saw something in me right from the start and essentially opened the doors for me to spend my third-year summer in Norway collecting data on beavers (my first fieldwork experience) with the awesome Prof. Frank Rosell and from thereon, partner up with Rory as my undergraduate thesis supervisor. The rest as they say, is history, and without Emily's trust and support, things could have ended up very differently for me.

I have been very fortunate to have been involved in various fieldworks during my PhD, from Africa to Argentina, I have collaborated with some amazing people and renowned scientists. The list of people that deserve a mention is endless, though I would like to single out Dr. Mike Scantlebury, Dr. Flavio Quintana and Dr. Agustina Gómez-Laich – You have all been incredibly supportive and I have become a much more rounded scientist both in- and out of the field because of your expertise and guidance.

I would like to thank all the students that have been part of the SLAM lab journey with me, including, Baptise, Alexis, Alex, Llyod, Sophie, James, Will, Hannah, Manos, Emma, Kiki and Ewan. You are all incredible people and the blend of different backgrounds and research interests made for a vibrant, interesting, fun and supportive working environment. A special shoutout to James (Jimmy, Jimmybob) Redcliffe who, besides being a true bro, has been a key influence to this work. I would also like to extend a shoutout to the Irish Holly English(!). Again, besides being a key influence to this work, she has been a great friend and kept me sane during the height of lockdown with our weekly zoom meets.

I have the uttermost respect and gratitude towards Dr. Mark Holton, who supplies the biotech (DD's) and software (DDMT) used throughout this thesis. He is one of the hardest working people I have ever met and just a genuinely nice guy. He has always been there for me (literally 24/7 – he never sleeps!), whether its sharing ideas,

teaching me complex concepts, helping me with fieldwork prep, or just recommending what film to watch - Mark your awesome! I would also like to thank Phil Hopkins. Phil is a crazy hard grafter – he provided me with the tag housings and attachment methods for all my fieldworks, no matter how tight the deadlines were, he got it done! Moreover, Phil is one of the kindest people I have met. I have had many a memorable chat over a cup of coffee in his office, or beer at 6am as the case was in Africa after successful lion deployments. You have always been there for me, whether its offering sound advice and encouragement, or simply just listening to my random questions, rants and nonsense conversations - long may it continue!

I would also like to give an honourable mention to my 'old' school friends 'back home' – Adam, Zoe and Doug. You have been both encouraging and sarcastic in equal fun-sized measures. Here is to many more years of epic comradery (cue metaphorical toast). An extended thanks is also required to some more of my past- and present Swansea-based friends, Marcus, Mattdawg, Doogle, Emma, Ben and Big Al.

It would not sit right without giving a special thanks to Lottie Rees-Rodrick. What for? Everything! I do not know what I would do without you. In my brightest and darkest moments, you have always been there for me, and no words could justify how much I cherish our companionship. Lastly, of course I save acknowledging my family till last. You have been incredibly supportive throughout my life, and I would not be in this position of submitting a PhD if not for your encouragement and understanding. I am especially indebted to my parents; I honestly could not have achieved what I have done during this PhD without their morale (and financial) support - this thesis is dedicated to you guys (so you have to read it now 😊).

Ethics statement and approvals

All fieldwork procedures involving interventions with live animals that I participated in were undertaken in accordance with approval from the Swansea University College of Science Ethics Committee (SU) and the Animal Welfare Ethical Review Body (AWERB) group. These, along with ethical and/or permit approvals obtained for pre-collected data and/or collaborative institutions also involved with the field work are detailed in the table below.

Field work I was involved in is denoted with ✓. The column, 'Year' denotes when the fieldwork was conducted.

Animal	Chapter(s) used in	Study site	Ethics and approvals	Year
Loggerhead turtle (<i>Caretta caretta</i>)	2, 3	Southern beaches of Boa Vista, Cabo (Cape) Verde (15°58'22" N, 22°47'56" W)	Ethical approval was obtained from the Oceanographic Animal Care & Welfare Committee (OCE-16-18) for the captive turtles and authorisations were obtained from the Direcção Geral do Ambiente (DGA 30/2013) for the wild turtles.	2014
African lion (<i>Panthera leo</i>)	4, 5, 6, 9	Kgalagadi Transfrontier Park wildlife preserve and conservation area (26°28'43" N, 20°36'45" W)	SU-Ethics-Student-260919/1229 Conditions and approvals for lion fieldwork were also granted by the Animals Scientific Procedures Act (ASPA) at Queens University of Belfast (QUB-BS-AREC-18-006) and Pretoria University (NAS061-19), permit authorisation was given by South African National Parks (Permit Number SCAM 1550).	2019 ✓
Magellanic penguin (<i>Spheniscus magellanicus</i>)	5, 6, 7, 8, 9	Punte Norte penguin colony, located within the San Lorenzo Gulf, Peninsula Valdes, Chubut, Argentina (42°4'48" N, 63°51'36" W)	SU-Ethics-Student: 260919/1894. AWERB approval: IP-1819-30. Permit for field work were granted by the Conservation Agency from the Chubut Province (Disp N° 047/19-SsCyAP; No. 060/19-DFyFS-MP). All penguin handling procedures were approved by the Dirección de Fauna y Flora Silvestre y el Ministerio de Turismo y Áreas Protegidas de la Provincia de Chubut.	2019 ✓
Imperial cormorant (<i>Leucocarbo atriceps</i>)	5, 6, 9	Punta León cormorant colony, located within the Peninsula Valdes, Chubut, Argentina (43°3'55" N, 64°27'32" W)	SU-Ethics-Student: 260919/1894. AWERB approval: IP-1819-30. Permit for field work were granted by the Conservation Agency from the Chubut Province (Disp N° 047/19-SsCyAP; No. 047-SsCy/19). All cormorant handling procedures were approved by the Dirección de Fauna y Flora Silvestre y el Ministerio de Turismo y Áreas Protegidas de la Provincia de Chubut.	2019 ✓
Red-tailed tropic bird (<i>Phaethon rubricauda</i>)	6	Round Island, Mauritius (19°50'51" N, 58°47'20" W)	SU-Ethics-Student: 040118/39. AWERB approval: IP-1617-9. All fieldwork was conducted in collaboration with the Durrell Wildlife Conservation Trust, Mauritius and the Mauritius Wildlife Foundation	2017

Contributing authors and funding

In addition to the candidate submitting this thesis, the following authors that assisted in the data collection, research and/or manuscript revision presented in this thesis are detailed in the table below.

Names listed in order of chapter appearances. Each authors role is specified in the text below the table, referenced with their initials.

Name	Primary institution/Organisation	Chapter(s) contributed to
Rory P. Wilson	Swansea University College of Science	1, 2, 3, 4, 5, 6, 7, 8, 9
Mark D. Holton	Swansea University College of Science	2, 3, 4, 5, 6, 7, 8
Phil Hopkins	Swansea University College of Science	2, 3, 4, 5, 6, 7, 8
Carlos M. Duarte	Abdullah University of Science and Technology	2, 3, 4, 5, 6, 7, 8
Flavio Quintana	Instituto de Biología de Organismos Marinos (IBIOMAR), CONICET	5, 6, 7, 8
Ken Yoda	Nagoya University Graduate School of Environmental Studies: Nagoya Daigaku Daigakuin Kankyogaku Kenkyuka	5, 6, 7, 8
Takashi Yamamoto	Organization for the Strategic Coordination of Research and Intellectual Properties, Meiji University	5, 6, 7, 8
Mike D. Scantlebury	Queen's University Belfast School of Biological	4, 5, 6
Nigel C. Bennett	University of Pretoria Department of Zoology and Entomology	4, 5, 6
Sam Ferreira	SANParks: South African National Parks	4, 5, 6
Danny Govender	SANParks: South African National Parks	4, 5, 6
Pauli Viljoen	SANParks: South African National Parks	4, 5, 6
Angela Bruns	SANParks: South African National Parks	4, 5, 6
Louis van Schalkwyk	SANParks: South African National Parks	4, 5, 6
Stephen H. Bell	Queen's University Belfast School of Biological Sciences	4, 5, 6
Nikki J. Marks	Queen's University Belfast School of Biological Sciences	4, 5, 6
Martin C. van Rooyen	University of Pretoria Department of Zoology and Entomology	4, 5, 6
Mads F. Bertelsen	Center for Zoo and Wild Animal Health, Copenhagen Zoo	4, 5, 6
Craig J. Tambling	University of Fort Hare Department of Zoology and Entomology	4, 5, 6
Mariano H. Tonini	Instituto Andino Patagónico de Tecnologías Biológicas y Geoambientales, Grupo GEA, IPATEC-UNCO-CONICET	5, 6, 8
Rebecca Scott	GEOMAR Helmholtz Centre for Ocean Research	2, 3
Agustina Gómez-Laich	Departamento de Ecología, Genética y Evolución & Instituto de Ecología, Genética y Evolución de Buenos Aires (IEGEB), CONICET	5, 6
Luca Börger	Swansea University College of Science	5, 6
James Redcliffe	Swansea University College of Science	5, 6
Holly H. English	University College Dublin School of Biology and Environmental Science	5, 6
Luca Börger	Swansea University College of Science	5, 6
Hannah J. Williams	Max Planck Institute of Animal Behaviour	5, 6
Fabian Gabelli	Cátedra de Biología del Comportamiento, Facultad de Psicología. Universidad de Buenos Aires	7, 8
Christophe Eizaguirre	Mary University of London School of Biological and Chemical Sciences	3
Marie Ulrich	Linköping Universitet, Institutionen för fysik kemi och biologi (IFM)	3
Andreas Fahlman	L'Oceanogràfic, Ciutat de les Arts i de les Ciències	3
Alex Arkwright	Swansea University College of Science	3
Emily L.C. Shepard	Swansea University College of Science	6
Adam J. Fell	Stirling University. Biological and Environmental Sciences	6
Baptiste Garde	Swansea University College of Science	6
Nik C. Cole	Durrell Wildlife Conservation Trust, Channel Islands	6
Vikash Tatayah	Mauritian Wildlife Foundation, Vacoas	6
Martin Brogger	Instituto de Biología de Organismos Marinos (IBIOMAR), CONICET	7

Author contributions

RMG and RPW conceptualised the studies, RMG carried out the data analysis and wrote the initial drafts, and RPW supported data curation and manuscript revisions. All co-authors (see table above) contributed suggestions of manuscript edits in preparation for journal submission. PH was involved in designing and constructed tag housings for all model species used. Data collection for the captive turtles in L'Oceanogràfic was carried out by AA and MU, and RS led the fieldwork in the Cabo Verde archipelago on wild inter-nesting turtles under supervision from CE. Data collection for the Kalahari lions was led by SF, DG, PV, LVS and AB and assisted by CJT, MFB, DMS, SB, MVR, PH and RMG. Data collection at Peninsula Valdes for the penguins was led by FQ and data collection for the cormorants was led by AG-L, with both fieldworks being assisted by KY, TY, FG and RMG. MHT supplied data for the instantaneous tidal currents of the San Lorenzo region. MB supplied data for the different habitats within the Punte Norte penguin colony. Data collection at Round Island for the tropic birds were carried out by NCC, VT and AJF. MDH conceived and regularly updated the Daily Diary Multi Trace software (DDMT; <http://www.wildbytetechnologies.com>) used throughout this thesis as part of the data processing. LB, HJW, HME, AG-L and LVS contributed to the testing of R syntax developed by RMG in Chapter 5.

Funding contributions

All research in this thesis contributes to the Coupled Animal and Artificial Sensing of the Environment (CAASE) project funded by King Abdullah University of Science and Technology (KAUST) under the KAUST Sensor Initiative, led by CMD. Fieldwork in the Cabo Verde archipelago was funded by a grant (CP1217) awarded to RS from the Cluster of Excellence 80 'The Future Ocean'. 'The Future Ocean' was funded within the framework of the Excellence Initiative by the Deutsche Forschungsgemeinschaft (DFG) on behalf of the German federal and state governments. This work was part of the Turtle Project created by CE and partly funded by National Geographic (GEFNE69-13), The Whitley Wildlife Conservation Trust and 'The Future Ocean' through a

Capacity Building grant to CE. Fieldwork in the Kgalagadi Transfrontier Park was supported in part by a Department for Economy Global Challenges Research Fund grant to MS. Fieldwork within the Chubut Province was supported in part by the National Agency for Scientific and Technological Promotion of Argentina (PICT 2017 - 1996 and PICT 2018 - 1480) awarded to FQ, and the Grants-in-Aid for Scientific Research from the Japan Society for the Promotion of Science (16K18617) awarded to KY. Fieldwork at Round Island, Mauritius, was supported by the European Research Council under the European Union's Horizon 2020 research and innovation programme grant (715874), awarded to ELCS.

Additional contributions and acknowledgments

I would like to acknowledge the engineers from the Technical and Logistical centre (TLZ) at GEOMAR that were also involved in constructing the tag housings for the wild turtles and the support from the Direção Nacional do Ambiente Cabo Verde. I thank South African National Parks and the Department of Wildlife and National Parks, Botswana for allowing our research in the Kgalagadi Transfrontier Park. I am grateful to support and kind assistance of the staff and Rangers at the Kgalagadi National Park who were involved with this work, especially Steven Smith, Christa von Elling, Wayne Oppel and Corera Links. Pertaining to the field work carried out in Argentina, I express my gratitude to Andrea Benvenuti, Monserrat Del Caño, La Chola, Miguel, Estancia El Pedral and Estancia San Lorenzo for assistance in various aspects of the research. I also appreciate the Instituto de Biología de Organismos Marinos (IBIOMAR-CONICET) for logistical support. Lastly, I thank the National Parks and Conservation Service, Government of Mauritius for their permission to conduct research on the movement behaviour of Red-tailed tropicbirds.

List of Tables and Figures

Chapter 1: Introduction	Summary	Page no.
Figure 1	Schematic diagram of the Daily Diary (DD) coordinate system	15
Chapter 2: Measuring angular velocity to determine activity		
Table 1	Metrics derived from accelerometer and magnetometer outputs	53
Figure 1	Association between various metrics of body rotation	54
Figure 2	Association between yaw rotation and VeDBA	55
Figure 3	Correlation between values of AVeY and number of turns	55
Figure 4	Time series of depth, acceleration and select body rotation derivatives comprising two flat U-dives similar in duration and differing in activity extent	57
Figure 5	Various examples of activity-specific patterns as resolved by examination of body rotations	58
Figure 6	Time series of mean values of VeDBA and AVeY	59
Figure 7	Cumulative frequency of VeDBA and AAV across the duration of 100 random U-dives	60
Chapter 3: Measuring angular velocity to determine activity		
Figure 1	Decision tree showing how deep dives were characterised	80
Figure 2	Time series of depth and select body rotation derivatives across a continuous bout of diving behaviour	81
Table 1	Descriptive statistics of type 1a dives	83
Figure 3	Time budget of depth use	83
Figure 4	Relationship between absolute values of angular velocity on all 3 axes	84
Figure 5	Breakdown of individual activity-budgets	85
Figure 6	Relationship between absolute angular velocity and dive duration	86
Figure 7	Estimated metabolic costs associated with variation in absolute angular velocity	86
Chapter 4: Filtering high-resolution GPS tracks		
Figure 1	Schematic diagram of the derivation of the movement verified filtering (MVF) protocol	108
Table 1	Contingency table documenting the mean accuracy and misclassification rate of the MVF method	109
Figure 2	Time series of select DD- and GPS-derived data showing intermittent periods of moving and stationary behaviours	110
Figure 3	Example of the movement-based thresholds involved with the MVF protocol	111
Figure 4	Relative frequency distributions of collar postural (pitch and roll) offsets according to MVF thresholds	112
Figure 5	Boxplot of mean hourly summed distance moved according to MVF values	113
Figure 6	Schematic diagram of the factors related to animal behaviour that can change the quality of GPS fixes	117
Chapter 5: Animal dead-reckoning in R		
Table 1	Possible system errors involved in the dead-reckoning process	132
Figure 1	Schematic diagram representation of a current low vector being integrated to a travel vector	136
Table 2	<i>Gundog.Tracks</i> input fields and description of their role	140-141
Figure 2	Schematic diagram of the conceptual workflow involved when dead-reckoning using <i>Gundog.Tracks</i>	142

Figure 3	Dead-reckoned movement path of lion as provided by <i>Gundog.Tracks</i> summary plots	144
Table 3	<i>Gundog.Tracks</i> data frame output names and their parameters	145-146
Figure 4	Net error between (GPS-corrected) dead-reckoned and GPS positions for a track from 5 African lions	147
Figure 5	Dead-reckoned lion track using variant estimates of speed	154
Figure 6	Dead-reckoned penguin track at sea, with and without current flow integration	155
Figure 7	Dead-reckoned penguin tracks walking to and from their nests using variant estimates of speed	156
Figure 8	Dead-reckoned cormorant tracks of Imperial cormorants foraging at sea	157
Figure 9	Schematic diagram demonstrating the order of fixes used when calculating the Distancecorr.factor and Headingcorr.factor	176
Chapter 6: How often to correct dead-reckoned paths?		
Table 1	Experimental protocol for each species	208
Figure 1	Boxplots demonstrating the magnitude of net error according to the VP correction rate per species	209
Figure 2	Boxplots demonstrating the total distance moved (km) during the tag deployment period according to VP correction rate for the study species	210
Figure 3	Dead-reckoned lion track using variant estimates of speed and associated net error	212
Figure 4	Dead-reckoned movements of lions in the Kgalagadi Transfrontier Park	213
Figure 5	Time series of select DD- and GPS-derived data from a section of a tropicbird's foraging flight at sea, also plotted in 3-D	214
Figure 6	Time series of select DD- and GPS-derived data from a section of a penguin foraging at sea, also plotted in 3-D	214
Figure 7	Dead-reckoned tropicbird flight using variant estimates of speed	215
Figure 8	Net error of dead-reckoned tracks at sea, with and without current flow integration	216
Figure 9	Schematic diagram of the various elements that modulate VP and VP corrected dead-reckoning accuracy	229
Chapter 7: Navigational ability of Magellanic Penguins on land		
Figure 1	Schematic diagram of a topographic cross-section of the Magellanic penguin colony	244
Figure 2	Schematic diagram demonstrating the 'actual' track of a returning bird in relation to the shortest theoretical 'line-of-sight' track and the ToF	252
Figure 3	Dead-reckoned penguin tracks walking to and from their nests	255
Figure 4	Assessments of heading-related metrics and pauses according to status and vegetation density	256
Table 1	Descriptive statistics of various metrics relating to heading and pauses	257
Table 2	Descriptive statistics of various metrics linked with energy expenditure	258
Figure 5	Relationship between distance travelled as a function of distance into the return trip (standardised to a proportion per bird; 0-1) and the track of familiarity (ToF)	260
Figure 6	Relationship between distance travelled as a function of distance into the return trip (standardised to a proportion per bird; 0-1), vegetation type and the track of familiarity (ToF).	261
Figure 7	Smooth GAM line fits denoting the trends in various response variables across the proportion of distance travelled (0-1)	263
Figure 8	Extent of turns made during incoming paths	264

Figure 9	Schematic diagram of the most common return strategies that penguins adopted when being appreciably displaced from their ToF	268
Chapter 8: Navigational ability of Magellanic Penguins at sea		
Figure 1	Representation of the five vectors calculated for analysis	284
Figure 2	Dead-reckoned penguin track at sea, relative to the grid of available current data	286
Figure 3	Distribution of the difference between the actual bird heading and 'line of Sight' heading according to current strength and contour plots highlighting the effect of current magnitude and direction on bird heading with respect to the 'line of Sight' heading	288
Figure 4	Contour plots to show the strategy shown by the real birds, relative to current flow and the 'theoretical' best heading required to achieve 'line of Sight' travel	289
Figure 5	Ease of transport of actual bird resultant- and 'theoretical' best resultant heading against the proportion of return distance to the colony	290
Chapter 9: Synopsis		
Figure 1	Time-depth profile of a penguin dive and a cormorant dive	304
Figure 2	Comparison of recognised penguin types plotted in 2-D and 3-D, highlighting differences in values of VeDBA and AVeY	306
Figure 3	Metrics of putative penguin prey capture examined in space in the dead-reckoned tracks	307
Figure 4	Examination of heading-based metrics in a cormorant dead-reckoned track	309
Figure 5	<i>Relationship between AVeY and VeDBA according to diving behaviour in cormorants</i>	311
Figure 6	Dead-reckoned hunt of two female lions	312
Figure 7	Dive depths and bottom phase tortuosity between male and female cormorants	313
Appendices		
Chapter 2: Supplementary Information		
Figure S1	Visualisations of yaw during bottom phase of type 1a dives	322
Figure S2	Yaw plotted in 3-D space during a bout of circling behaviour	322
Figure S3	Patterns of CuHe across 100 random U-dives (bottom phase)	323
Chapter 3: Supplementary Information		
Table S1	Step selection function analysis	324
Figure S1	Bathymetry estimates around the southern coast of Boa vista	324
Figure S2	Density estimates for raw values of yaw (°), pitch (°) and roll (°) per turtle	325
Figure S3	Mean values of VeDBA per turtle, aggregated as a function of dive status	326
Chapter 4: Supplementary Information		
Figure S1. 1	LiteTrack (Iridium) GPS collar	331
Figure S2. 1	Magnitude of acceleration and GPS speed during a period of predominantly traveling movement	333
Figure S2. 2	Relationship between VeDBA and GPS speed during a period of predominantly traveling movement	334
Figure S2. 3	Time series of DD- and GPS-derived data showing two different movement scenarios, each over 1 hour	336
Figure S2. 4	GPS speed~VeDBA relationships for all lions with linear regression	336
Figure S2. 5	GPS tracks for the entire data acquisition period of ~14 days, plotted according to MVF value	337
Table S3. 1	Summary parameters of fix success rate during the data acquisition period	338
Figure S3. 1	Relative cumulative frequency of missing locational data duration (%)	338

Figure S3. 2	Relative frequency of the four possible combinations of movement thresholds that result in zero MVF values	339
Table S3. 2	DD- and GPS derived summary metrics for MVF values of zero and one	340
Figure S4. 1	Relationship between DD- and GPS-derived heading for MVF values of zero and one	344
Chapter 5: Supplementary Information		
Figure S2. 1	Schematic diagram of the aerospace north-east-down (NED) coordinate system (top) and the Daily diary north-west-up (NWU) coordinate system (bottom)	351
Figure S3. 1	Output summary plot from <i>Gundog.Compass</i>	355
Figure S4. 1	Output plot from <i>Gundog.Peaks</i>	359
Figure S6. S1	Elapsed system time (s) to execute <i>Gundog.Tracks</i> according to various scenarios	365
Chapter 6: Supplementary Information		
Figure S1. 1	Boxplots demonstrating the magnitude of net error (top panel) and distance moved (bottom panel), per VP correction rate, per species	367
Figure S1. 2	Mean VeDBA (column/bar) and net error (line & symbol) per hour over the duration of three individual lion (top panel) and three penguin (bottom panel) VP corrected dead-reckoned tracks	368
Chapter 7: Supplementary Information		
Figure S1. 1	Time series of DD- and GPS-derived data during a bout of penguin walking	372
Table S1. 1	Acceleration- and GPS-based metrics used for identifying single stride cycles within the LoCoD method	373
Figure S2. 1	Output plot from <i>Gundog.Tracks</i>	376
Figure S2. 2	Example of the matchstick approach of deriving the ToF	376
Table S3. 1	Significant terms of the linear mixed effect- and generalised liner mixed effect models employed	377
Table S3. 2	GAM output for pause duration	377
Table S3. 3	Generalised additive model output for tortuosity, travelling speed and 'number of significant' turns	378
Table S3. 4	Generalised additive model output for pause number, extent of 'significant' turns and extent of turn following a pause	379
Case-studies S4	Eight individual penguin dead-reckoned tracks superimposed on to google maps with vegetation density polygons, with various metrics of movement	380-387
Chapter 8: Supplementary Information		
Figure S1. 1	Tidal elevations and components (U and V) in a period of 40 days	389
Figure S1. 2	Determining the start of a penguins return journey	389
Figure S1. 3	Distribution of the difference between the actual bird heading and 'theoretical' best heading with respect to the 'line of Sight' heading	390
Figure S1. 4	Relative frequencies of actual bird speed and the theoretical 'best' resultant speed pre- and post- current integration)	380
Figure S1. 5	Mean absolute difference between actual bird heading and 'Line of Sight' heading as a function of distance to the colony	391
Figure S1. 6	Mean penguin ease of for the actual bird resultant trajectory and the theoretical 'best' trajectory	391
Figure S1. 7	Mean dive depth per 0.01 proportion of total distance travelled	391

Chapter 1

Introduction

Richard M. Gunner



Photo taken by Richard M. Gunner

Why is it important to study animal behaviour?

Behavioural ecology embraces the theoretical and empirical considerations of how everything an animal does is purported to be adapted to the environment it inhabits. This field integrates concepts of internal state, behavioural plasticity, locomotion, energy expenditure and ecosystem functioning (Manning, Manning & Dawkins 1998; Nathan *et al.* 2008; Davies, Krebs & West 2012; Liedvogel *et al.* 2013). All species in the kingdom Animalia, whether they are sessile or motile, are considered to enhance their personal or inclusive fitness (their own life-time reproductive success or that of related individuals (*cf.* Dugatkin 2007; Anthes *et al.* 2010)), by being able to respond behaviourally, according to their physiological state and environmental circumstance (West & Gardner 2013). All behaviours relate to energy expenditure, however, and thus specific behaviours should only be selected for if resultant fitness improves (either directly or indirectly), relative to cost (van der Werf *et al.* 2009). Generally, a measure of a genotype's fitness involves the ability to survive, find mates and reproduce (Orr 2009) and it is the numerous selective pressures for developing adaptive survival and fitness mechanisms that have shaped the demographics of animals today (Pimentel 1961; Hutchinson 1991; van der Werf *et al.* 2009; Mori, Mazza & Lovari 2017; Silk *et al.* 2019).

At the crux of the matter, all animals must acquire and ingest food to survive (or more specifically, to respire, which fuels physiological processes *via* energy conversion and release) (*cf.* Altman & Dittmer 1971), with the ultimate goal of transmitting genes to future generations (Dawkins 2016). In addition to food, the majority of animals also require a combination of sunlight, oxygen, water, shelter, space and essential minerals (*cf.* Schmidt-Nielsen & Randall 1997). Such resources are rarely ubiquitous within a single defined area, but rather their distribution changes in time and space across the globe (Grant 1993; Johnson *et al.* 2002; Peng, Maldonado-Chaparro & Farine 2019). It is not surprising therefore, that most animals have evolved the capacity to locomote (move throughout their environment) with a plethora of convergent evolution strategies in locomotory patterns across both terrestrial and

fluid media (e.g., Gleiss *et al.* 2011; Bale *et al.* 2015). Motility enables animals to express more definitive behavioural responses to sensory stimuli and to adjust the ways by which they actively exploit and interact with their ecosystem in line with their requirements (Morales *et al.* 2010; Gingras *et al.* 2011; Rendueles & Velicer 2017; Biewener & Patek 2018). Examples include how animals encounter prey or escape predators (Brodie, Formanowicz & Brodie 1991; Richardson *et al.* 2018), move as a function of resource availability and habitat quality (Johnson *et al.* 2002; Mitchell & Powell 2004), find, attract/compete for and reproduce with conspecifics (Grammer *et al.* 2003; Reudink *et al.* 2009) and care for young (Trivers 1972).

Taken together, much of animal behaviour has been defined *via* body and limb movement as observed directly and as a consequence, the terms, ‘movement’ and ‘behaviour’ are often synonymously used, since movement of a whole organism elicits a behaviour response and a behavioural response (at least as measured *ex vivo*), requires movement to elicit (*cf.* Owen-Smith, Fryxell & Merrill 2010; Davies, Krebs & West 2012; Brown *et al.* 2013). Nikolaas Tinbergen was one of three pioneers of ethology (the discipline of animal behaviour - along with Konrad Lorenz and Karl von Frisch) and set out the ‘four problems’ concept, designed to facilitate a complete understanding of a given behavioural trait (Tinbergen 1963). These were; causation (how does it work?), ontogeny (how did it develop during the individual’s lifetime?), survival value (what is its purpose?) and evolution (how has it evolved over the species’ history?). Despite these names having been adapted with various authors over the years (*cf.* Dewsbury 1999), nearly six decades on, their general applicability remains relevant for directing the key considerations involved when assessing behaviour (*cf.* Bateson & Laland 2013) – and much boils down to energy. In essence, by measuring energy-specific movement behaviours in time and space, the ultimate- (why it exists) and proximate- (how it works) mechanisms and underlying causes can be elucidated to explain animal motivations, life history strategies and broader ecological concepts (Tinbergen 1963; Scott-Phillips, Dickins & West 2011). But why is it important to study this?

The behavioural ecology of many animal systems has a direct importance to humans (Mathews 2010). To name just a few examples, pollinators (such as some bat, bird, butterfly, beetle and bee species) facilitate plant reproduction and this is vital for maintaining plant diversity – required in global agriculture (Ollerton 2017). Grazing herbivores are effective mediators of nutrient cycling (Harrison & Bardgett 2008) and their movements are critical for maintaining ecological succession - preserving grasslands worldwide (Ellison 1960; Luken 1990). Knowledge of animal life history traits were key in the domestication and selective breeding processes (Jensen 2006), enabling humans to exploit various species for food, labour, companionship, experimentation and secondary products (Swart 2004; Zeder 2012). Moreover, we have a better understanding and subsequent ability to control for the spread of zoonotic diseases (Fèvre *et al.* 2006; Sekar *et al.* 2011) - although we are currently not shining in this field (*cf.* Carlo *et al.* 2020) - we do at least now appreciate that predators are a valuable top-down regulator (Ostfeld & Holt 2004).

Studying the demographics of animals is not just driven by the economic value it adds to human life. Animals have fascinated humans for centuries (*cf.* Shepard 1997). How many viewers have finished a wildlife documentary, such as an episode of Blue Planet or Planet Earth, with a greater appreciation of the natural world (*cf.* Hughes 2013; Nelson & Fijn 2013)? Arguably, applications of this discipline have never been more important as we proceed into a man-made sixth extinction event (Wake & Vredenburg 2008; Ceballos *et al.* 2015; Raven & Wagner 2021). The ability of animals to modify their behaviour to adapt to (and ultimately survive) environmental change, and the subsequent impact this has on other ecological interactions and biological communities is at the forefront of conservation study (Nagelkerken & Munday 2016). Conjointly, reasons such as the important roles that animals have in ecosystem functioning (and thus sustainability) and the intrinsic right for animals to coexist with humans are at the forefront of conservation support (Donaldson & Kymlicka 2011).

Human-induced behavioural changes can be investigated at various ecological levels, to help inform governing agencies of the impact that certain practices are having (e.g., culling or exceeding fishing quotas) (Darling 2008; Riordan *et al.* 2011).

Behavioural research enables us to apply better practices to conserve endangered species (Sutherland 1998; Martin-Wintle *et al.* 2015), improve animal husbandry techniques (Vaarst *et al.* 2004; Meyer, Puppe & Langbein 2010) and plan for or mitigate against deleterious human-wildlife interactions (Woodroffe *et al.* 2005; Macdonald 2016; Wilson *et al.* 2019; Pătru-Stupariu *et al.* 2020). In essence, the specifics of animal movement, the ‘what’, ‘where’, ‘why’, ‘when’ and ‘how’ (*cf.* Nathan *et al.* 2008) underpins a species interaction with its environment and by studying this, we can develop a greater understanding of aspects pertaining to an animal’s evolutionary history, ecological role, behavioural plasticity and sensitivity to human-induced impacts (Sutherland 1998; Caro & Sherman 2013; Schweiger *et al.* 2019). Such knowledge, whilst purposive as theory, can be pragmatically applied to help sustain ecosystems (Szaro, Sexton & Malone 1998; Schweiger *et al.* 2019) and enhance animal welfare and conservation practices (Swaisgood 2007; Greggor *et al.* 2016; Papastavrou, Leaper & Lavigne 2017).

How can we measure movement-specific behaviours?

This is unquestionably the golden era of ethology: Simultaneous advancements in the miniaturisation of data storage and analytical methodologies have enabled animal behaviour to be quantified with unprecedented resolution (*cf.* Brown *et al.* 2013; Nowacek *et al.* 2016; Whitford & Klimley 2019b; Börger *et al.* 2020), and the resultant information is more freely accessible than ever before (*cf.* McNeely & Wolverton 2008; Kranstauber *et al.* 2011; Newman *et al.* 2012). As previously alluded to, direct observation has been the foundation of measuring animal behaviour. The theory of evolution, first posited in Darwin’s ‘On the Origin of Species’ in 1859, heavily involved *ad libitum* behavioural observations of wild species to formulate the concept of natural selection (Darwin 1909; Swisher 1967). Today though, behavioural observations are typically standardised to a consistent sampling regime and documented within carefully designed ethograms to aid in objectively classifying focal species’ activity budgets (e.g., Powell *et al.* 2013), although, by definition, this

approach is restricted by visual ability and the continuity of measurement (Altmann 1974; Hall & Roshier 2016).

The level of detail that humans perceive about an animal's behaviour depends on how close we are (*cf.* Brown *et al.* 2013). Highly mobile and naturally reclusive free-ranging animals can be difficult to monitor closely (Hughey *et al.* 2018). The constraints of topography (e.g., dunes, cliffs, mountains, swamps, burrows, and dens), habitat heterogeneity (e.g., wooded land and areas of dense shrubbery), darkness and weather conditions can also impair visibility, whilst many wild animals operate in environments that preclude observation entirely (chiefly, within water and air) (Altmann 1974; Dawkins 2007; Cagnacci *et al.* 2010; Hall & Roshier 2016). Even when viable, human presence can bias behavioural responses (the 'observer effect', e.g., Crofoot *et al.* 2010), whilst sampling rate is completely contingent on the amount of time and effort devoted by the observer - typically a fraction of an animal's daily behavioural budget (*cf.* Brown *et al.* 2013). Moreover, human perception is naturally subjective (for instance, when does a slow walk turn into a fast walk?) and thus there is an inevitable degree of misclassification (human error, Tuytens *et al.* 2014). Enhanced digital imaging techniques, as measured *ex situ* can expediate behavioural observations to some extent though (*cf.* Nelson & Fijn 2013). For instance, high-definition cameras with telephoto lenses that enable magnification of distant objects can extend the line-of-sight, whilst integrating motion- and/or infrared-light detection sensors (e.g., camera traps) can permit autonomous surveillance and provide key insights into the behavioural repertoires of nocturnal and cryptic species (Trolliet *et al.* 2014; Alexander *et al.* 2016). Video-tracking also archives empirical evidence for later reassessments (*cf.* Xue & Henderson 2006).

It is the ever-evolving assortment of *in situ* biologging and telemetry however, that has ultimately shifted the paradigm of behavioural ecology (Bograd *et al.* 2010; Heylen & Nachtsheim 2018; Hughey *et al.* 2018). Biologging is the practise of using miniaturised animal-attached electronic tags to record data relating to an animal's behavioural-specific movements, physiology and/or the surrounding environment (Bograd *et al.* 2010; Wilson *et al.* 2015; Wurtz *et al.* 2019). A diverse array of on-board

sensors has permitted numerous environmental measurements, including: light (e.g., Coelho, Fernandez-Carvalho & Santos 2015), temperature (e.g., Thorrold *et al.* 2014), sound (e.g., Baumgartner *et al.* 2008; Blumstein *et al.* 2011), pressure (e.g., Hochscheid 2014; Williams *et al.* 2015), conductivity (e.g., Lydersen *et al.* 2002) and oxygen concentration (e.g., Coffey & Holland 2015). Direct quantification of body trunk or limb movements can be obtained *via* accelerometers (e.g., Yoda *et al.* 2001; Brown *et al.* 2013), magnetometers (e.g., Williams *et al.* 2017) and gyroscopes (e.g., Noda *et al.* 2012), typically using an orthogonal tri-axial set up for three-dimensional measurement (*cf.* Wilson, Shepard & Liebsch 2008; Noda *et al.* 2014). Swim speed can be approximated *via* sensors that measure flow rate (*cf.* Wilson *et al.* 2007) or resistance (*cf.* Allynay *et al.* 2019). Aspects of internal state are typically measured with implantable devices such as heart rate monitors (e.g., Ditmer *et al.* 2015), electroencephalogram systems (EEG, e.g., Vysotski *et al.* 2006), pH sensors (e.g., Papastamatiou, Meyer & Holland 2007) and stomach temperature loggers (e.g., Wilson *et al.* 1998), whilst various chemical and blood samplers have also been developed (*cf.* Whitford & Klimley 2019a). Passive integrated transponder (PIT) tags can be administered subcutaneously to enable life-long individual identification using radio frequency identification (RFID) readers (Bonter & Bridge 2011). Such tags have also been used to investigate conspecific proximity at sites frequented by the implanted individuals (Bandivadekar *et al.* 2018). An alternative proximity system is the use of (externally attached) ultra-high frequency (UHF) radio transmitters, which detect nearby devices within a Wireless Sensor Network (WSN, e.g., Handcock *et al.* 2009).

The conventional 'older' practice of locating an animal's whereabouts, involves physically triangulating (*cf.* Saltz 1994) an emitted signal from animal-borne acoustic- (e.g., Zeh *et al.* 2015) or Very High Frequency- (VHF) (e.g., Guthrie *et al.* 2011; Kays *et al.* 2011) transmitters. This technique is also relevant for recovering logging devices that are designed to automatically release from the animal, either remotely (Buil *et al.* 2019), or *via* an on-board timed drop-off mechanism (Rafiq *et al.* 2019), enabling non-invasive data retrieval (Evans, Lea & Patterson 2013). 'Newer' satellite tracking

technologies such as Global Positioning Systems (GPSs) have permitted remote recording of locational data at higher precision, accuracy, and continuity than ever before (*cf.* Tomkiewicz *et al.* 2010). Lastly, animal-borne video cameras, whilst useful on their own, can also provide crucial ground-truthing to the inferences made from simultaneously logged environmental-, motion- and/or physiological sensor data (*cf.* Seminoff, Jones & Marshall 2006; Watanabe & Takahashi 2013). Ultimately, biologging and transmission telemetry have provided researchers with a means to investigate and integrate paradigms in species-specific behavioural ecology, with unparalleled definition and data acquisition duration, juxtaposed with direct observation (*cf.* Kooyman 2004; Wilson, Shepard & Liebsch 2008; Brown *et al.* 2013; Evans, Lea & Patterson 2013; Wilson *et al.* 2015; Hughey *et al.* 2018; Williams *et al.* 2020).

GPS technology is arguably the most popular method for determining estimates of free-ranging animal movement (across all media of travel) (Hebblewhite & Haydon 2010; Latham *et al.* 2015; Patel *et al.* 2017). Part of this is because of the continuous improvements in the underlying tracking software, design, power consumption and battery size reductions, which has permitted longer-term and more continuous spatial monitoring of wild animals, independent of human disturbance (Clark *et al.* 2006; Recio *et al.* 2011; Wilmers *et al.* 2015). In addition, data output from GPS (or indeed, other satellite tracking systems, such as ARGOS, *e.g.*, Costa *et al.* 2010) is generally less computationally complex and time-consuming to process, compared to other biologging regimes (*e.g.*, inertial sensors, *cf.* Berger, Dettki & Urbano 2014). Important facets of animal demography have been revealed with remote-tracking technologies, including (though not limited to) home ranges (*e.g.*, Stark *et al.* 2017), patterns of resource selection (*e.g.*, Owen-Smith & Goodall 2014) and associated activity budgets (*e.g.*, Schlecht *et al.* 2004). Indeed, some recent studies now opt to record at frequencies ≥ 1 Hz and have used the resultant detailed space-use estimates to underpin their analysis of fine-scale behaviour (*e.g.*, Bouten *et al.* 2013; Riaboff *et al.* 2020). Nevertheless, accuracy of measurement is limited according to the dual proficiency of satellite-receiver signal propagation and reception and thus estimates

of movement can be biased according to the behaviour of the focal species and the heterogeneity of environment (e.g., thick forests) with which it interacts (Frair *et al.* 2010; Hofman *et al.* 2019). Furthermore, satellite signals cannot propagate meaningfully through water or underground, precluding assessment of space-use in such environments (Tomkiewicz *et al.* 2010).

Multi-channel data loggers have proven to be particularly effective at maximising the possibilities for behavioural inference, independent of human disturbance and the vagaries of the environment, and accordingly their utility within behavioural studies has proliferated in recent years (*cf.* Brown *et al.* 2013; Wassmer *et al.* 2020 [and references therein]). As its name suggests, a multitude of sensors are integrated within a single motherboard, collecting and storing on-board various inertial, magnetic and/or environmental parameters simultaneously (Gleiss, Gruber & Wilson 2010; Noda *et al.* 2014). Concurrent advances in solid state technology and battery size reductions, have enabled such parameters to be recorded continuously, with high accuracy and precision (*cf.* Wilson, Shepard & Liebsch 2008), at sub-second frequency (*cf.* Bäckman *et al.* 2017), on animals with masses ranging across nearly four orders of size magnitude (e.g., López-Calleja & Bozinovic 2003; Zimmer *et al.* 2003). Certainly, multi-channel data logger measurements provide a means to study behaviour that would otherwise be left unresolved or less defined using remote tracking systems (or direct observation) alone (*cf.* Ropert-Coudert & Wilson 2005; Wilson *et al.* 2007; Brown *et al.* 2013; Walker *et al.* 2015).

The relevance of magnetic and inertial measurements for elucidating behaviour

The Magnetic and Inertial Measurement Unit (MIMU; though commonly umbrellaed under the general term 'IMU') is a branch of multi-channel loggers, designed to measure a body's orientation, angular velocity and specific- ('non-gravitational') force. IMUs are typically composed of tri-axial magnetometers, gyroscopes and accelerometers, and this arrangement of sensors makes them extraordinarily powerful for resolving fine-scale 3-D movements (Fourati *et al.* 2011; Noda *et al.*

2014; Fan *et al.* 2017). For example, relative to tag placement, stylised patterns in the periodicity, amplitude and/or direction of raw values or select derivatives (*cf.* Eikelboom 2020) from one or more channels/sensor-type, has been demonstrated to effectively elucidate various step gait- (e.g., de Passillé *et al.* 2010), wing beat- (e.g., Van Walsum *et al.* 2020), flipper beat- (e.g., Battaile *et al.* 2015), tail beat- (e.g., Martín López *et al.* 2015) mandible- (Robert-Coudert *et al.* 2004a) and head- (Wilson *et al.* 2020c) frequencies/patterns of movement.

Specifically, each channel of a tri-axial accelerometer records acceleration due to gravity ($1\ g = 9.81\ \text{m/s}^2$ - the 'static' component), with instantaneous changes in velocity in the sensor itself (the 'dynamic' component) due to animal movement superimposed on to these values (Gleiss, Wilson & Shepard 2011). Assuming an accelerometer is positioned near an animal's Centre of Mass (CoM), body posture (typically expressed as Euler angles; pitch and roll) can be derived from the static component, since these values reflect the device's inclination with respect to the Earth's frame of reference (Bidder *et al.* 2015; Williams *et al.* 2015) (*cf.* Fig. 1). In contrast, the dynamic component reflects body movements arising from the spine (*cf.* Whitney *et al.* 2021), limbs (Yoda *et al.* 2001; Shepard *et al.* 2008a) and/or external force vectors (e.g., tidal/air currents, *cf.* Robert-Coudert & Wilson 2004). Nominally, the greater the extent of movement, the more energy is required for muscular contraction and the greater the inertial displacement of the attached sensor (with respect to an animal's CoM) (Wilson *et al.* 2006; Gleiss, Wilson & Shepard 2011). Based on this premise, it not surprising that various acceleration-based proxies for activity, traveling speed and activity-specific energy expenditure have been validated (Wilson *et al.* 2006; Halsey *et al.* 2008; Halsey, Shepard & Wilson 2011; Bidder *et al.* 2012; Qasem *et al.* 2012; Wilson *et al.* 2020a).

On the other hand, tri-axial magnetometers define the direction and intensity of the surrounding Earth's magnetic field across all three spatial dimensions, from which angular rotations can be resolved (Wilson *et al.* 2006; Williams *et al.* 2017) with 1-2° accuracy range (Painter *et al.* 2016). Unaffected by acceleration, they can act as a compliment alongside accelerometers in helping define behaviour, not least because

simultaneous readings from both sensors permit the third dimension of body orientation to be resolved; yaw (or 'heading'), *via* the tilt-compensated compass method (*cf.* Ozyagcilar 2012; Pedley 2012). Combining the above two sensor systems provide six degrees of freedom (DoF) forces to define movement in three-dimensional space (*cf.* Fig. 1). The three degrees of dynamic change are, surge ('forward and back', or, 'anterior-posterior'), sway ('side to side', or, 'medio-lateral') and heave ('up and down', or, 'dorsal-ventral') and the three degrees of attitude change are, pitch (rotation about the sway axis), roll (rotation about the surge axis) and yaw (rotation about the heave axis) (*cf.* Noda *et al.* 2012; Bidder *et al.* 2015).

IMU gyroscopes comprise of an oscillating mass which, when subjected to a directional force, elicits a fictitious Coriolis effect and this 'pattern of deflection' is used to measure angular velocity, providing stability in rotation measurements between two coordinate frames - that of the gyroscope itself, relative to the IMU body within which it situated (Liu *et al.* 2009; Bergamini *et al.* 2014). Gyroscopes have appreciable benefits in that they accurately reconstruct gravity-based acceleration and attitude (Wen 2019), which is not always possible when using the accelerometer-magnetometer method alone, particularly at times of high centripetal acceleration (Noda *et al.* 2012; Williams *et al.* 2015). However, gyroscopes are subject to drift over time (Fong, Ong & Nee 2008; Bergamini *et al.* 2014) and require high sampling rates (e.g., 100 Hz to 1 kHz, Noda *et al.* 2012) and coupled with relatively high power consumption (in part to power these rates) and the associated power to write data into the memory, means that overall current consumption is much higher when gyroscopes are used within animal-mounted IMUs (Katevas, Haddadi & Tokarchuk 2016; Martín López *et al.* 2016). This explains why, within a biologging context, integrating accelerometers and magnetometers within multi-channel data loggers is typically the favoured combination, both over the accelerometer-gyroscope approach and, indeed, integration of all three IMU sensors (particularly concerning free-ranging, longer-term studies, *cf.* Johnson 2011; Gerencsér *et al.* 2013; Bidder *et al.* 2015; Chakravarty *et al.* 2019b).

Choice of sensor with respect to the animal in question and questions being asked

Ultimately, the drive to develop and implement biologging and transmission telemetry was fuelled by our dual determination and physical limitation to observe and ultimately understand animal behaviour (Evans, Lea & Patterson 2013; Wilmers *et al.* 2015; Williams *et al.* 2020). This is the prime reason why the quantity and diversity of tag deployments (both past and present) have been biased towards the marine environment, because physical monitoring at sea is, at best, limited to 'snapshots' such as infrequent porpoising events (*cf.* Hastie *et al.* 2004). Given the acknowledged importance of the 3 R's in animal welfare (replace, reduce and refine, Rollin 2010), choice of sensors, sampling rate, and associated battery and accompanying housing have to be considered against the information gains for the questions being asked and the adverse effects on the animal in question (e.g., due to increased isometric stress and conspicuousness, *cf.* Hawkins 2004; Nuijten *et al.* 2020; Williams *et al.* 2020; Holton *et al.* 2021). In line with Archimedes' Principle, objects weigh less when submerged in water than in air (Mohazzab 2017) which has conveniently allowed primitive (larger/heavier) animal-borne technology to remain close to/within the 3-5 % remit of select aquatic species' overall mass (*cf.* Goulet *et al.* 2019) - the conventional 'ethical rule of thumb' used for many animal taxa (*cf.* Casper 2009). Indeed, device bulk is likely the primary reason why deployments have been historically less on species moving on land and in air (where in many cases, direct and/or *ex situ* digital observations are possible with greater capacity anyway). Nevertheless (and as mentioned), improvements in the size, weight, memory capacity, power consumption, design (and associated attachment methods) of electronic devices, partnered with the miniaturisation of batteries, have in recent years, expanded biologging and telemetry practices across all environments (e.g., Cooke *et al.* 2013; Hussey *et al.* 2015; Toledo 2015).

Alongside this expansion though, and with respect to the 3 R's, there has been an ever-growing assortment of studies demonstrating the detriment that encapsulated devices have on animals (even when tag weight is less than 3-5 % that of the animal's

weight, *cf.* Vandenabeele *et al.* 2015; Kay *et al.* 2019; Dickinson *et al.* 2020; Wilson *et al.* 2020b). Tagged animals are now acknowledged as having to be subject to an increase in one or more of the following:

- Inertia force (e.g., due to behaviour-induced start-stop momentum of biologging collars - Wilson *et al.* 2020b).
- Pressure and associated friction (*cf.* Krausman *et al.* 2004).
- Aero-/hydrodynamic forces (within fluid media, e.g., buoyancy and drag - Kay *et al.* 2019).

Such tag-induced force effects can have a negative impact on body condition (e.g., Hopkins & Milton 2016), kinematic capacity (and thus behaviour, e.g., Brooks, Bonyongo & Harris 2008; Broell, Burnell & Taggart 2016) and associated energy costs (e.g., Lefrançois, Odion & Claireaux 2001). The critical modulator of tag detriment is the accompanying power source, given that batteries are typically the largest and heaviest component (*cf.* Toledo 2015), which modulates housing design and extent of (potentially 'weighty') material required. Generally, there is a proportional relationship between device longevity (and sampling rate) and device weight (*cf.* Yoda, 2019). Lithium-ion batteries are the most efficient, having one of the highest energy densities (Kim *et al.* 2019) and are currently the most frequently used battery type within biologging studies (Markham 2008). However, with 'next generation' advancements in battery technologies (e.g., Hwang, Myung & Sun 2017; Gummow *et al.* 2018; Kwak *et al.* 2020) likely still some years away from commercialisation, it appears as though we have hit a 'technological wall'. For now, primary power sources are typically the limiting factor dictating sensor choice, associated sampling resolution and recording duration, with respect to the animal under investigation (*cf.* Cooke *et al.* 2013; Holton *et al.* 2021).

The Daily Diary (DD) & the GiPSy

Multi-channel data loggers (excl. gyroscopes), such as the Daily Diary (DD) unit (*cf.* Wilson, Shepard & Liebsch 2008), deployed on all study animals within this thesis (*cf.* Fig. 1), are typically much less power-hungry and much more efficient at writing large quantities of data to memory relative to other biologging systems, including animal-borne video cameras (*cf.* Huck & Watson 2019) and remote tracking systems (*cf.* Sherub *et al.* 2017). For instance, DD logging units measure tri-axial acceleration, tri-axial magnetometry and various environmental cues, including light, temperature and barometric pressure, and (under standard operating conditions) requires < 1.5 mA to power its on-board sensor system with a default logging frequency ratio of (approx.) 40-13-4-4 Hz. On the other hand, the GiPSy-5 techno-smart GPS devices [see, <https://www.technosmart.eu>] (one of the GPS units used within in this thesis), is approx. 20 mA, when recording at 1 Hz. Unlike the GiPSy-5, the DD (magnetism and acceleration) can be set to record at frequencies as high as 160 Hz (although if only acceleration is required, it can be logged at 800 Hz).

To come full circle, behavioural responses are fundamentally movement driven, and multi-channel data loggers, such as Daily Diary (DD) units, are powerful 'low power cost' tools which allow us to resolve (Wilson, Shepard & Liebsch 2008; Evans, Lea & Patterson 2013; Walker *et al.* 2015; Wilmers *et al.* 2015; Heylen & Nachtsheim 2018; Whitford & Klimley 2019a). Importantly though, simultaneous deployment with satellite transmission telemetry is required to superimpose elucidated movement-specific behaviours accurately, in time and space, relative to the environment (e.g., Laplanche, Marques & Thomas 2015; Walker *et al.* 2015).

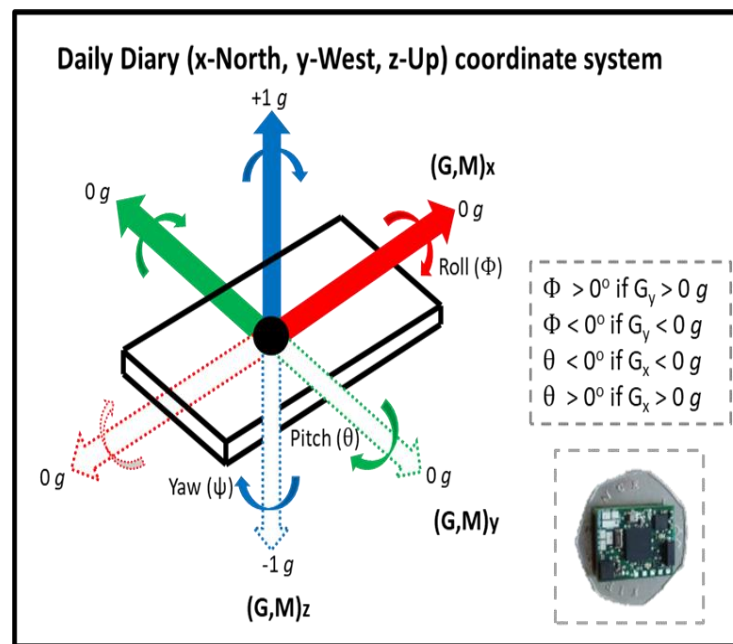


Figure 1. Illustration of the Daily Diary (DD) coordinate system. For all study animals analysed in this thesis, DDs were set to record tri-axial acceleration with respect to gravity ($1g = 9.81 \text{ m/s}^2$: range 0-32 g) and tri-axial magnetometry (Gauss - G) at 40 Hz. Note here, each channel's static (or gravitational) acceleration is referred to as 'G' and magnetometry is referred to as 'M'. In the case of this orientation, the x-axis represents the surge plane, the y-axis represents the sway plane, and the z-axis represents the heave plane of movement. A calibrated accelerometer measures +1 g when facing directly upwards, -1 g when facing directly downwards and 0 g when orientated parallel to the earth's surface. Readings of the magnetometer x- and y-axis are at a maximum and minimum when pointed at magnetic North and South, respectively. Assuming the orientation of the encapsulated DD (positioned flat on a table) starts at North, readings of the y-axis will be at a maximum and minimum when the device is rotated 90° East and 90° West, respectively, with the z-axis remaining constant. Yaw can thus be obtained by measuring the two orthogonal components of the $M_{x,y}$ magnetic vector, subsequent to correcting for device tilt (pitch and roll offsets). Note the latest variant of the DD (the 'thumb nail' - no batteries soldered to the board) is smaller than a 50 pence coin (18x14x5 mm), weighing 1.7 g (incl. microSD card). Dimensions of the DD models used within this thesis ranged between 27x26x10 mm and 26x17x5 mm (excl. batteries) and weighed 2-3 g (incl. microSD card and excl. batteries and additional compatible sensor types, e.g., external depth sensors). Dimensions of the GiPSy-5 model used within this thesis were 23x12.5x5 mm and the unit weighed 1.5 g (excl. batteries). This figure is adapted from Chapter 4, supplementary information. Text S2: Fig. S1.

The purpose of this thesis

My PhD concentrates on developing novel metrics and updating existing analytical approaches from multi-sensor data (DD's and GPS) to facilitate greater insights into the behaviour-specific movements and activity-time budgets of select animals. Dynamic acceleration is only one dimension of movement (Costello & Jitpraphai 2002; Mathie *et al.* 2002; Brown *et al.* 2013) and has been examined extensively (e.g., Halsey *et al.* 2008; Laich *et al.* 2008; Brown *et al.* 2013; DuBois *et al.* 2015; Chakravarty *et al.* 2019a; Ward *et al.* 2019; Williams *et al.* 2019; Wilson *et al.* 2020a [and refereces therein]), however another critical dimension of movement, and a fundamental aspect of animal behaviour, is body rotation, which can also be represented tri-axially (Williams *et al.* 2017). Unlike rotations about the pitch and roll axis, which can be resolved using accelerometers (*cf.* Marshall & Landman 2000; Shepard *et al.* 2008a; Zihajehzadeh *et al.* 2014), and have been discussed at some length (e.g., Whitney *et al.* 2010; Willener *et al.* 2015; Ciancio *et al.* 2016; Thompson *et al.* 2016), calculation of the yaw (hereafter termed 'heading') requires the tandem use of tri-axial accelerometers and tri-axial magnetometers (because accelerometers are insensitive to rotations about the gravity vector) and is generally overlooked as a behavioural identification parameter (Williams *et al.* 2017). Intrigued by the minimalist attention given to yaw in animal behaviour and its interaction with pitch and roll, in this thesis I set out to examine the application and relevance of body rotation within the framework of animal behaviour ecology. My overarching question was; ***What does animal rotation tell us about behaviour?*** Rather than being species-specific, with the obvious constraints that come with it, my PhD considers a diverse group of animals operating across scales of size and movement, including, mammals (lions - *Panthera leo*), reptiles (turtles - *Caretta caretta*) and birds (penguins - *Spheniscus magellanicus*, cormorants - *Leucocarbo atriceps*, tropic birds - *Phaethon rubricauda*), hoping that cross-cutting elements might emerge, and therefore be of most value to the community.

This thesis is comprised of three main components.

Firstly, I provide an overview of the value and use of angular velocity as an important element for assessing activity extent and exemplifying behaviours, particularly in scenarios where acceleration metrics have limited value, such as in slow-moving animal (*cf.* Wilson *et al.* 2020a). Secondly, I go on to look at how body rotation (focussing primarily on animal heading and acceleration-based metrics), can help us examine concepts relating to animal navigation. One powerful, yet sparingly utilised technique is ‘dead-reckoning’ (*cf.* Wilson & Wilson 1988; Elkaim *et al.* 2006; Wilson *et al.* 2007; Bidder *et al.* 2015), which integrates estimated vectors of travel (heading and speed), derived from sensor-borne estimates in 2-D or 3-D (pressure/pitch) space (Walker *et al.* 2015). This method can reveal fine-scale animal movement data in both space and time and has been shown to resolve movement so finely that even behaviour can be inferred (Bidder *et al.* 2015; Andrzejaczek *et al.* 2019). Extrapolated travel vectors nearly always comprise some degree of error, however, no matter how minuscule, and thus vector integration suffers from cumulative errors (Wensveen, Thomas & Miller 2015; Dewhirst *et al.* 2016).

As such, to maintain the accuracy of reconstructed movement in time, relative to the environment, periodic ground-truthing by a secondary source (e.g., GPS) is required (Walker *et al.* 2015; Dewhirst *et al.* 2016). I provide a reappraisal of the dead-reckoning process including improvements and extensions of the analytical procedure. In conjunction to this, and with respect to the third component of my thesis, I provide important insights into GPS performance (the most common method for attempting to determine an animal’s location) and suggest a novel protocol for filtering inaccurate fixes obtained (terrestrially) at high frequency, by combining both acceleration- and GPS-derived information. To this end, I suggest how to maximise the value of both multi-sensor- and GPS-borne assessments of movement within one dead-reckoning oriented framework. Throughout this thesis I demonstrate the value that these methodological advancements have in assessing the proximate and ultimate facets of animal behaviour. These components are detailed in the following chapters.

The layout of my data chapters

Chapter 2

There is a bias towards using acceleration metrics to elucidate animal behaviour within the biologging community (e.g., Shepard *et al.* 2008b; Wilson, Shepard & Liebsch 2008; Gleiss, Wilson & Shepard 2011; Halsey, Shepard & Wilson 2011; Brown *et al.* 2013; Graf *et al.* 2015; Miwa *et al.* 2015; Williams *et al.* 2015; Fehlmann *et al.* 2017), with the potential of tri-axial magnetism as a tool to distil out behaviour only being highlighted very recently (e.g., Painter *et al.* 2016; Williams *et al.* 2017; Chakravarty *et al.* 2019b). Whilst rotational metrics from gyroscopes have been used to show variations in movement (e.g., Kawabe *et al.* 2003; Noda *et al.* 2014), equivalent measurements (specifically, angular velocity) obtained from magnetometers have not, to my knowledge, been used within behavioural studies. Heading is a key variable obtained from the tandem use of accelerometers and magnetometers (Ozyagcilar 2012), however few field investigations have looked into its worth for helping differentiate animal behaviour (beyond its application in the general dead-reckoning procedure, e.g., Bidder *et al.* 2015), even though movement about this rotational axis should be at least as important as rotations in the other two (commonly assessed) axes; pitch and roll.

My first data chapter provides the mathematical and conceptual protocol for deriving rotation-based metrics with an overview of the value and use of angular velocity about the yaw axis (AVEY), as an important element for assessing activity extent and behaviours. I used free-ranging Loggerhead turtles as a model species for this work. Fundamentally, the concept of animal behaviour is broad (McFarland 1993; Manning & Dawkins 1998) and essentially refers to everything animals 'do', with this ranging from being immobile (resting/sleeping) to actions involving substantial body kinematics. 'Levels' of 'activity' emerge as a consequence of this. If such activity is predominately manifest in changes about the yaw axis, then the degree of activity extent can be assessed *via* indices of angular velocity. Specific behaviours that are

consistent in their magnitude and pattern of elicited body rotation may also be elucidated from estimates of the rate of change of yaw. Crucially however, even 'noisy' variations in AVEY can indicate more notable differences between supposed behaviours which may not be picked up by acceleration estimates (*cf.* Williams *et al.* 2017). This is an important concept which I promote within this chapter which then goes on to discuss the implications that the energy requirements of turns have (*cf.* Wilson *et al.* 2013). To my knowledge, this has not been properly assessed to date using sensor data and is likely to be an important concept for people studying animal behaviour.

Chapter 3

My second data chapter expands on the methodological protocols conceived from my first chapter and uses a new approach, integrating indices of angular rotation about the principal axes to deduce activity (integrating the magnitude of angular velocity of the pitch, roll and yaw rotations). This new metric, termed; 'Absolute Angular Velocity' (AAV), is used to assess the extent of resting behaviour in wild turtles. To my knowledge, assessing activity extent from angular velocities derived from the three axes of rotation has not been explored (with respect to the accelerometer-magnetometer approach). I advocate that the magnitude of rotations of animal bodies can inform biologists of animal activity, particularly in scenarios where standard acceleration metrics have limited value, such as in slow-moving animal groups.

The Loggerhead turtle is an endangered species although, because they spend most of their lives underwater, their activity budgets are poorly understood, being mostly derived from speculation based on 'dive profiles' (a graphic representation of depth on the y-axis *versus* time on the x-axis; Minamikawa, Naito & Uchida 1997; Hochscheid *et al.* 1999; Houghton *et al.* 2002; Hochscheid 2014). The Type 1a (flat U-shaped) dive is an easily identifiable and most commonly expressed dive type and is often labelled as the 'resting' dive on the seabed (e.g., Hays *et al.* 2002). My results

demonstrate that many ‘type 1a dives’ are episodic in nature, comprised of intermittent bouts of rest and activity, and show high inter-individual plasticity in depth utilisation, as well as in the frequency and intensity of activity. This implies that, far from simply resting and generating new eggs, as has been postulated for inter-nesting turtles (e.g., Houghton *et al.* 2002; Schofield *et al.* 2009), these animals probably actively forage.

Chapter 4

Accurate estimation of animal movement at fine temporal scales has proved a persistent challenge that is not resolved using conventional GPS because GPS performance is not perfect (although it is often implicitly assumed to be) (Cagnacci *et al.* 2010; Latham *et al.* 2015). In fact, locational accuracy can easily vary by a few metres or more depending upon the propagation of signal quality and/or receiver reception capability (Frair *et al.* 2010; Forin-Wiart *et al.* 2015). Such constraints can result in surprisingly variable assessments of deduced animal movement if GPS data are used alone (*cf.* Ryan *et al.* 2004; Poulin, Clermont & Berteaux 2021) and a host of studies have documented this error for low resolution datasets and offered methods to screen GPS anomalies (e.g., Apps & Kinley 2000; Lewis *et al.* 2007; Bjørneraas *et al.* 2010; Ironside *et al.* 2017). For high frequency datasets however, the extent to which species-specific movements can be misinterpreted because of additive GPS error, is far less explored, as are appropriate screening solutions. In this data chapter, I report how the use of motion sensor systems in tandem with GPS, can provide us with an important independent comparator for assessing the genuine incidence and extent of traveling movement. In particular, I present a Movement Verified Filtering (MVF) protocol to identify travelling behaviour and filter high-res GPS data - removing appreciable positional noise (which I term ‘jitter’). I demonstrate how its implementation provides substantially improved (and different) fine-scale movement and activity patterns than are apparent when using GPS data alone. I provide the conceptual and practical methodology for implementing this method, using the lion as a model species and emphasise its utility (and acknowledged

limitations) for different terrestrial species and within other movement analysis techniques - principally the dead-reckoning procedure. Results reveal the importance that MVF has for avoiding inaccurate movement estimates and I thus call into question the accuracy of findings from previous high-frequency GPS studies. As a product of this, I document some important parameters of lion movement, including daily movement trends and the top estimated speed obtained across a two-week period of free-ranging behaviour.

Chapter 5

The cumulative drift in dead-reckoning protocols requires periodic ground-truthing (Verified Positions (VPs)) if the data are to be placed in an environmentally correct context (such as in Google Earth) (Dewhirst *et al.* 2016). Importantly, with suitable correction, dead-reckoning is the only current method for resolving such fine-scale, continuous and accurate, free-ranging 2- or 3-D space use, which far out-weighs the definition of space-use interpolation derived from alternative methods (e.g., Mitani *et al.* 2004; Bidder *et al.* 2015; Laplanche, Marques & Thomas 2015; Dewhirst *et al.* 2016; Andrzejczek *et al.* 2019). Despite this, relatively few biologging studies have adopted this approach. I argue that this is due to the apparent complexity of the analytical processes involved which has led to studies utilising dead-reckoning to rely upon complex bespoke specialist software applications (e.g., Walker *et al.* 2015). In this data chapter, I present step-by-step instructions for implementing Verified Position Correction (VPC) dead-reckoning in R using the tilt-compensated compass method. R is a powerful open-source programming language, often used with statistics and mapping/visualisation of large data and is now commonly taught amongst university settings with a large range of supporting help sites, books and package repositories (58 of which have been specifically developed to deal with tracking data, Joo *et al.* 2020). I regarded this as an excellent opportunity to provide researchers with a comprehensive, easy-to-use process which would allow them to dead-reckon their animal movements. I outline improvements to the procedure and highlight important considerations to improve dead-reckoning accuracy. In line with

this, I developed a user-friendly VPC dead-reckoning R function; *Gundog.Tracks*, to reconstruct animal movement paths across terrestrial, aquatic, and aerial systems. This chapter involved the African lion, the Magellanic penguin, and the imperial cormorant to demonstrate the points being made.

Chapter 6

With suitable VPC, dead reckoning can by-pass the inaccuracies associated with VP performance (e.g., 'jitter') and sampling rate (e.g., due to constraints of power consumption or attenuation of signal), when reconstructing fine-scale movement paths. How often should one undertake VP correction though? Essentially there is a complex trade-off between dead-reckoning accuracy and VP rate (itself, primarily modulated *via* power consumption) and important considerations include:

- (i) The scales and mode(s) of movement elicited by the study animal
- (ii) The quality of motion sensor-derived data and VP acquisition
- (iii) Initial user-defined track scaling (principally speed allocation - pre-VP correction)
- (iv) Initial screening and filtering of VP inaccuracy

In this data chapter, I delve more deeply into how measurement error can arise using the dead-reckoning method and how to maximise its accuracy, including ensuring appropriate behavioural identification, speed allocation, VP error screening and correction rate. To demonstrate points being made, I used four model species (walkers, swimmers and fliers) as case-studies; the African lion, the Magellanic penguin, the imperial cormorant and the red-tailed tropic bird. Simulations were performed to examine the extent of dead-reckoning error, relative to VPs (obtained from GPS) as a function of VP correction rate and the effect of this on estimates of distance moved. I also showed how dead-reckoning can highlight specific behaviours and the intricacies of space-use within 'energy landscapes' (Shepard *et al.* 2013).

My results showed that the extent of obtainable dead-reckoning accuracy is primarily modulated by the lifestyle of the animal in question, with animals traveling in air and water being subjected to greater drift from true location per given VP correction rate. In line with the above, I argue that the required level of accuracy is dependent on the scale of movement being addressed (e.g., investigating 'general areas' of resource allocation over multiple days vs defining exact step lengths and turn extents over a matter of minutes). More generally, I highlight the current advantages, limitations and advancements with the dead-reckoning technique put forward, integrating considerations outlined in Chapter 4 and 5.

Chapter 7

How do central place foragers navigate between their foraging sites and central places in visual cluttered environments? Magellanic penguins nesting far from the sea at a highly vegetated colony in San Lorenzo, Argentina made for an interesting examination of this, particularly since they cannot fly and have a low profile that is generally lower than the surrounding shrubbery. The current consensus of how penguins navigate on land is divided, with some studies suggesting the use of a time-compensated sun compass (e.g., Emlen & Penney 1966) and others suggesting the use of environmental cues (e.g., Nesterova *et al.* 2010). I reconstructed the movement paths of these birds navigating between their nests and the sea at San Lorenzo, using the dead-reckoning protocols described in Chapter 5 and 6. This was conducted with a view to assessing how these birds may be navigating on land in habitats varying in vegetation density, The effort- (e.g., time and energy) and mechanisms of navigation (e.g., sight) involved are far less studied than 'at sea' trajectories and this made for an excellent opportunity to demonstrate the value of assessing rotation- and acceleration-based metrics in tandem to delineate movement with high detail. Specifically, I derived individual steps and pauses in travelling movement from acceleration measures. Additionally, from the computed dead-reckoned tracks, I derived metrics of step lengths, travel speed, turn extent, track tortuosity and horizontal displacement between outgoing and incoming tracks.

Results showed that outgoing birds essentially took a straight line to the sea edge, following their own well-used Track of Familiarity (ToF). On the other hand, incoming trajectories, which generally started at beach landing points displaced from the ToF, were rarely straight-line courses. Instead, it appeared that penguins actively corrected for such displacements by travelling at more acute angles with respect to the shoreline in favour of their ToF, and/or where possible, choosing routes that coincide with lower shrubbery extent. The reported trends support the notion that penguins use vision-based navigation during on-land navigation.

Chapter 8

One pivotal point about use of magnetometers and derivation of animal heading angles is that it allows researchers to determine the direction of travel of animals travelling in fluid media exposed to environmental currents. Movement within fluid media (water or air) may subject animals to external current vectors and this alters their vector of travel which, if left uncorrected, can have negative energetic and navigational consequences (Chapman *et al.* 2011). Few studies have investigated how birds deal with tidal currents, even though a strong selective pressure is presumed to have evolved to provide adaptive strategies to deal with drift. In order to examine such phenomena, studies should ideally use a species that travels within an environment that has a defined current profile in time and space and have individuals for which the destination is precisely known. Magellanic penguins breeding at Peninsula Valdes, Argentina, fulfil these criteria well because they are central place foragers (Orians & Pearson 1979) and range extensive distances (10s of km) at sea exploiting areas where the current streams are precisely known before returning to their nest. I assessed how penguins navigated back to their colony using dead-reckoning protocols (outlined in Chapter 5) and the well-defined (in time and space), currents of the region (Tonini & Palma 2017). I hypothesised that return trajectories would be highly directed, and based on navigation mechanisms that mitigated drift: Inability to correct for drift would incur time delays and additional energetic costs, thus diminishing the overall rate of food acquisition for their dependent chick(s)

(Ropert-Coudert *et al.* 2004b). Results indicated that penguins operating within high current regimes are able to perceive and react to currents. Specifically, penguins spent a disproportionate amount of the time moving perpendicular, or at lesser angles, to the current. I noted that due to the oscillating nature of tidally based cross-currents, penguins would be subject to changing, opposing current conditions for the majority of their return trajectories (at each point along their reconstructed movement paths) if they were to travel directly 'home' or choose a heading that when incorporating current flow, enabled this. Instead, penguins travelled at angle to their home-bound route, to capitalise on current conditions; a phenomenon known as 'flow assisted movement' (Chapman *et al.* 2011). This enabled them to travel faster, which I conjectured would help them with opportunistic foraging during the return leg. As a consequence, the return journey time and distance increased – characterised by S-shaped paths as the birds were subjected to ebb and flood changes in cross-current intensity and direction, which I investigated further within an energetic context, using variant Cost of Transport (CoT) formulae.

Chapter 9

Using new perspectives gained throughout my thesis, I summarise the wider significance of how I perceive that body rotation assessed at different temporal scales can reveal important movement strategies. Specifically, I use the penguin and cormorant as example species to demonstrate how the investment of time and heading in energies and space-use provide insights into their foraging strategy. Lastly, I go on to speculate the value of the analytical procedures developed throughout my PhD - primarily focussing on animal heading, angular velocity, and dead-reckoning - for exploring different biological phenomena pertaining to fitness.

References

- Alexander, J.S., Zhang, C., Shi, K. & Riordan, P. (2016) A granular view of a snow leopard population using camera traps in Central China. *Biological Conservation*, **197**, 27-31.
- Altman, P.L. & Dittmer, D.S. (1971) Respiration and circulation. Federation of American Societies for Experimental Biology Bethesda MD.
- Altmann, J. (1974) Observational Study of Behavior: Sampling Methods. *Behaviour*, **49**, 227-266.
- Altynay, K., Khan Mohammed, A., Marengo, M., Swanepoel, L., Przybysz, A., Muller, C., Fahlman, A., Buttner, U., Geraldini, N.R., Wilson, R.P., Duarte, C.M. & Kosel, J. (2019) Wearable multifunctional printed graphene sensors. *NPJ Flexible Electronics*, **3**.
- Andrzejczek, S., Gleiss, A.C., Lear, K.O., Pattiaratchi, C.B., Chapple, T.K. & Meekan, M.G. (2019) Biologging Tags Reveal Links Between Fine-Scale Horizontal and Vertical Movement Behaviors in Tiger Sharks (*Galeocerdo cuvier*). *Frontiers in Marine Science*, **6**.
- Anthes, N., Kappeler, P.M., Bergmüller, R., Blanckenhorn, W., Brockmann, H.J., Fichtel, C., Fromhage, L., Frommen, J., Goymann, W. & Heinze, J. (2010) *Animal Behaviour: Evolution and Mechanisms*. Springer Berlin Heidelberg.
- Apps, C. & Kinley, T. (2000) Mountain caribou habitat use, movements, and factors associated with GPS location bias in the Robson Valley, British Columbia.
- Bäckman, J., Andersson, A., Pedersen, L., Sjöberg, S., Tøttrup, A.P. & Alerstam, T. (2017) Actogram analysis of free-flying migratory birds: new perspectives based on acceleration logging. *Journal of comparative physiology. A, Neuroethology, sensory, neural, and behavioral physiology*, **203**, 543-564.
- Bale, R., Neveln, I.D., Bhalla, A.P.S., MacIver, M.A. & Patankar, N.A. (2015) Convergent Evolution of Mechanically Optimal Locomotion in Aquatic Invertebrates and Vertebrates. *PLOS Biology*, **13**, e1002123.
- Bandivadekar, R.R., Pandit, P.S., Sollmann, R., Thomas, M.J., Logan, S.M., Brown, J.C., Klimley, A.P. & Tell, L.A. (2018) Use of RFID technology to characterize feeder visitations and contact network of hummingbirds in urban habitats. *PLOS ONE*, **13**, e0208057.
- Bateson, P. & Laland, K.N. (2013) Tinbergen's four questions: an appreciation and an update. *Trends in Ecology & Evolution*, **28**, 712-718.
- Battaile, B.C., Sakamoto, K.Q., Nordstrom, C.A., Rosen, D.A.S. & Trites, A.W. (2015) Accelerometers Identify New Behaviors and Show Little Difference in the Activity Budgets of Lactating Northern Fur Seals (*Callorhinus ursinus*) between Breeding Islands and Foraging Habitats in the Eastern Bering Sea. *PLOS ONE*, **10**, e0118761.
- Baumgartner, M.F., Freitag, L., Partan, J., Ball, K.R. & Prada, K.E. (2008) Tracking Large Marine Predators in Three Dimensions: The Real-Time Acoustic Tracking System. *IEEE Journal of Oceanic Engineering*, **33**, 146-157.
- Bergamini, E., Ligorio, G., Summa, A., Vannozzi, G., Cappozzo, A. & Sabatini, A.M. (2014) Estimating Orientation Using Magnetic and Inertial Sensors and Different Sensor Fusion Approaches: Accuracy Assessment in Manual and Locomotion Tasks. *Sensors*, **14**, 18625-18649.
- Berger, A., Dettki, H. & Urbano, F. (2014) Deciphering Animals' Behaviour: Joining GPS and Activity Data. *Spatial Database for GPS Wildlife Tracking Data: A Practical Guide to Creating a Data Management System with PostgreSQL/PostGIS and R* (eds F. Urbano & F. Cagnacci), pp. 231-244. Springer International Publishing, Cham.

- Bidder, O.R., Soresina, M., Shepard, E.L.C., Halsey, L.G., Quintana, F., Gómez-Laich, A. & Wilson, R.P. (2012) The need for speed: testing acceleration for estimating animal travel rates in terrestrial dead-reckoning systems. *Zoology*, **115**, 58-64.
- Bidder, O.R., Walker, J.S., Jones, M.W., Holton, M.D., Urge, P., Scantlebury, D.M., Marks, N.J., Magowan, E.A., Maguire, I.E. & Wilson, R.P. (2015) Step by step: reconstruction of terrestrial animal movement paths by dead-reckoning. *Movement Ecology*, **3**, 23.
- Biewener, A. & Patek, S. (2018) *Animal Locomotion*. OUP Oxford.
- Bjørneraas, K., Van Moorter, B., Rolandsen, C.M. & Herfindal, I. (2010) Screening Global Positioning System Location Data for Errors Using Animal Movement Characteristics. *The Journal of Wildlife Management*, **74**, 1361-1366.
- Blumstein, D.T., Mennill, D.J., Clemins, P., Girod, L., Yao, K., Patricelli, G., Deppe, J.L., Krakauer, A.H., Clark, C., Cortopassi, K.A., Hanser, S.F., McCowan, B., Ali, A.M. & Kirschel, A.N.G. (2011) Acoustic monitoring in terrestrial environments using microphone arrays: applications, technological considerations and prospectus. *Journal of Applied Ecology*, **48**, 758-767.
- Bograd, S.J., Block, B.A., Costa, D.P. & Godley, B.J. (2010) Biologging technologies: new tools for conservation. Introduction. *Endangered Species Research*, **10**, 1-7.
- Bonter, D.N. & Bridge, E.S. (2011) Applications of radio frequency identification (RFID) in ornithological research: a review. *Journal of Field Ornithology*, **82**, 1-10.
- Börger, L., Bijleveld, A.I., Fayet, A.L., Machovsky-Capuska, G.E., Patrick, S.C., Street, G.M. & Vander Wal, E. (2020) Biologging Special Feature. *Journal of Animal Ecology*, **89**, 6-15.
- Bouten, W., Baaij, E.W., Shamoun-Baranes, J. & Camphuysen, K.C.J. (2013) A flexible GPS tracking system for studying bird behaviour at multiple scales. *Journal of Ornithology*, **154**, 571 - 580.
- Brodie, E.D., Formanowicz, D.R. & Brodie, E.D. (1991) Predator avoidance and antipredator mechanisms: distinct pathways to survival. *Ethology Ecology & Evolution*, **3**, 73-77.
- Broell, F., Burnell, C. & Taggart, C.T. (2016) Measuring abnormal movements in free-swimming fish with accelerometers: implications for quantifying tag and parasite load. *The Journal of Experimental Biology*, **219**, 695-705.
- Brooks, C., Bonyongo, C. & Harris, S. (2008) Effects of Global Positioning System Collar Weight on Zebra Behavior and Location Error. *The Journal of Wildlife Management*, **72**, 527-534.
- Brown, D.D., Kays, R., Wikelski, M., Wilson, R. & Klimley, A.P. (2013) Observing the unwatchable through acceleration logging of animal behavior. *Animal Biotelemetry*, **1**, 20.
- Buil, J.M.M., Peckre, L.R., Dörge, M., Fichtel, C., Kappeler, P.M. & Scherberger, H. (2019) Remotely releasable collar mechanism for medium-sized mammals: an affordable technology to avoid multiple captures. *Wildlife Biology*, **2019**, 1-7, 7.
- Cagnacci, F., Boitani, L., Powell, R.A. & Boyce, M.S. (2010) Animal ecology meets GPS-based radiotelemetry: a perfect storm of opportunities and challenges. *Philosophical Transactions of the Royal Society B: Biological Sciences*, **365**, 2157-2162.
- Carlo, C., Mariachiarra Di, N., Nicole, B., Aurora, B., Roberto De, G., Mauro, T. & Salvatore, R. (2020) The novel zoonotic COVID-19 pandemic: An expected global health concern. *The Journal of Infection in Developing Countries*, **14**.
- Caro, T. & Sherman, P.W. (2013) Eighteen reasons animal behaviourists avoid involvement in conservation. *Animal Behaviour*, **85**, 305-312.

- Casper, R.M. (2009) Guidelines for the instrumentation of wild birds and mammals. *Animal Behaviour*, **78**, 1477-1483.
- Ceballos, G., Ehrlich, P.R., Barnosky, A.D., García, A., Pringle, R.M. & Palmer, T.M. (2015) Accelerated modern human-induced species losses: Entering the sixth mass extinction. *Science Advances*, **1**, e1400253.
- Chakravarty, P., Cozzi, G., Ozgul, A. & Aminian, K. (2019a) A novel biomechanical approach for animal behaviour recognition using accelerometers. *Methods in Ecology and Evolution*, **10**, 802-814.
- Chakravarty, P., Maalberg, M., Cozzi, G., Ozgul, A. & Aminian, K. (2019b) Behavioural compass: animal behaviour recognition using magnetometers. *Movement Ecology*, **7**, 28.
- Chapman, Jason W., Klaassen, Raymond H.G., Drake, V.A., Fossette, S., Hays, Graeme C., Metcalfe, Julian D., Reynolds, Andrew M., Reynolds, Don R. & Alerstam, T. (2011) Animal Orientation Strategies for Movement in Flows. *Current Biology*, **21**, R861-R870.
- Ciancio, J.E., Venerus, L.A., Trobbiani, G.A., Beltramino, L.E., Gleiss, A.C., Wright, S., Norman, B., Holton, M. & Wilson, R.P. (2016) Extreme roll angles in Argentine sea bass: Could refuge ease posture and buoyancy control of marine coastal fishes? *Marine Biology*, **163**, 90.
- Clark, P.E., Johnson, D.E., Kniep, M.A., Jermann, P., Huttash, B., Wood, A., Johnson, M., McGillivan, C. & Titus, K. (2006) An Advanced, Low-Cost, GPS-Based Animal Tracking System. *Rangeland Ecology & Management*, **59**, 334-340.
- Coelho, R., Fernandez-Carvalho, J. & Santos, M.N. (2015) Habitat use and diel vertical migration of bigeye thresher shark: Overlap with pelagic longline fishing gear. *Marine Environmental Research*, **112**, 91-99.
- Coffey, D.M. & Holland, K.N. (2015) First autonomous recording of in situ dissolved oxygen from free-ranging fish. *Animal Biotelemetry*, **3**, 47.
- Cooke, S.J., Midwood, J.D., Thiem, J.D., Klimley, P., Lucas, M.C., Thorstad, E.B., Eiler, J., Holbrook, C. & Ebner, B.C. (2013) Tracking animals in freshwater with electronic tags: past, present and future. *Animal Biotelemetry*, **1**, 5.
- Costa, D.P., Robinson, P.W., Arnould, J.P.Y., Harrison, A.-L., Simmons, S.E., Hassrick, J.L., Hoskins, A.J., Kirkman, S.P., Oosthuizen, H., Villegas-Amtmann, S. & Crocker, D.E. (2010) Accuracy of ARGOS Locations of Pinnipeds at-Sea Estimated Using Fastloc GPS. *PLOS ONE*, **5**, e8677.
- Costello, M. & Jitpraphai, T. (2002) Determining Angular Velocity and Angular Acceleration of Projectiles Using Triaxial Acceleration Measurements. *Journal of Spacecraft and Rockets*, **39**, 73-80.
- Crofoot, M.C., Lambert, T.D., Kays, R. & Wikelski, M.C. (2010) Does watching a monkey change its behaviour? Quantifying observer effects in habituated wild primates using automated radiotelemetry. *Animal Behaviour*, **80**, 475-480.
- Darling, F.F. (2008) *A herd of red deer: a study in animal behaviour*. Luath Press Ltd, Edinburgh.
- Darwin, C. (1909) *The origin of species*. PF Collier & son New York.
- Davies, N.B., Krebs, J.R. & West, S.A. (2012) *An Introduction to Behavioural Ecology*. John Wiley & Sons.
- Dawkins, M.S. (2007) *Observing Animal Behaviour: Design and Analysis of Quantitative Data*. OUP Oxford.
- Dawkins, R. (2016) *The Selfish Gene*. Oxford University Press.

- de Passillé, A.M., Jensen, M.B., Chapinal, N. & Rushen, J. (2010) Technical note: Use of accelerometers to describe gait patterns in dairy calves. *Journal of Dairy Science*, **93**, 3287-3293.
- Dewhurst, O.P., Evans, H.K., Roskilly, K., Harvey, R.J., Hubel, T.Y. & Wilson, A.M. (2016) Improving the accuracy of estimates of animal path and travel distance using GPS drift-corrected dead reckoning. *Ecology and Evolution*, **6**, 6210-6222.
- Dewsbury, D.A. (1999) The proximate and the ultimate: past, present, and future. *Behavioural Processes*, **46**, 189-199.
- Dickinson, E.R., Stephens, P.A., Marks, N.J., Wilson, R.P. & Scantlebury, D.M. (2020) Best practice for collar deployment of tri-axial accelerometers on a terrestrial quadruped to provide accurate measurement of body acceleration. *Animal Biotelemetry*, **8**, 9.
- Ditmer, Mark A., Vincent, John B., Werden, Leland K., Tanner, Jessie C., Laske, Timothy G., laizzo, Paul A., Garshelis, David L. & Fieberg, John R. (2015) Bears Show a Physiological but Limited Behavioral Response to Unmanned Aerial Vehicles. *Current Biology*, **25**, 2278-2283.
- Donaldson, S. & Kymlicka, W. (2011) *Zoopolis: A Political Theory of Animal Rights*. OUP Oxford.
- DuBois, C., Zakrajsek, E., Haley, D.B. & Merckies, K. (2015) Validation of triaxial accelerometers to measure the lying behaviour of adult domestic horses. *Animal*, **9**, 110-114.
- Dugatkin, L.A. (2007) Inclusive Fitness Theory from Darwin to Hamilton. *Genetics*, **176**, 1375-1380.
- Eikelboom, J. (2020) Inferring an animal's environment through biologging: quantifying the environmental contribution to animal movement. Wageningen University & Research.
- Elkaim, G.H., Decker, E.B., Oliver, G. & Wright, B. (2006) Marine Mammal Marker (MAMMARK) dead reckoning sensor for In-Situ environmental monitoring. *Proceedings of IEEE/ION PLANS 2006*, pp. 976-987. San Diego, CA.
- Ellison, L. (1960) Influence of Grazing on Plant Succession of Rangelands. *Botanical Review*, **26**, 1-78.
- Emlen, J.T. & Penney, R.L. (1966) The navigation of penguins. *Scientific American*, **215**, 104-113.
- Evans, K., Lea, M.A. & Patterson, T.A. (2013) Recent advances in bio-logging science: Technologies and methods for understanding animal behaviour and physiology and their environments. *Deep Sea Research Part II: Topical Studies in Oceanography*, **88-89**, 1-6.
- Fan, B., Li, Q., Wang, C. & Liu, T. (2017) An Adaptive Orientation Estimation Method for Magnetic and Inertial Sensors in the Presence of Magnetic Disturbances. *Sensors (Basel, Switzerland)*, **17**, 1161.
- Fehlmann, G., O'Riain, M.J., Hopkins, P.W., O'Sullivan, J., Holton, M.D., Shepard, E.L.C. & King, A.J. (2017) Identification of behaviours from accelerometer data in a wild social primate. *Animal Biotelemetry*, **5**, 6.
- Fèvre, E.M., Bronsvoort, B.M.d.C., Hamilton, K.A. & Cleaveland, S. (2006) Animal movements and the spread of infectious diseases. *Trends in Microbiology*, **14**, 125-131.
- Fong, W.T., Ong, S.K. & Nee, A.Y.C. (2008) Methods for in-field user calibration of an inertial measurement unit without external equipment. *Measurement Science and Technology*, **19**, 085202.

- Forin-Wiart, M.-A., Hubert, P., Sirguy, P. & Poulle, M.-L. (2015) Performance and Accuracy of Lightweight and Low-Cost GPS Data Loggers According to Antenna Positions, Fix Intervals, Habitats and Animal Movements. *PLOS ONE*, **10**, e0129271.
- Fourati, H., Manamanni, N., Afilal, L. & Handrich, Y. (2011) Posture and body acceleration tracking by inertial and magnetic sensing: Application in behavioral analysis of free-ranging animals. *Biomedical Signal Processing and Control*, **6**, 94-104.
- Frair, J.L., Fieberg, J., Hebblewhite, M., Cagnacci, F., DeCesare, N.J. & Pedrotti, L. (2010) Resolving issues of imprecise and habitat-biased locations in ecological analyses using GPS telemetry data. *Philosophical Transactions of the Royal Society B: Biological Sciences*, **365**, 2187-2200.
- Gerencsér, L., Vászárhelyi, G., Nagy, M., Vicsek, T. & Miklósi, A. (2013) Identification of Behaviour in Freely Moving Dogs (*Canis familiaris*) Using Inertial Sensors. *PLOS ONE*, **8**, e77814.
- Gingras, M., Hagadorn, J.W., Seilacher, A., Lalonde, S.V., Pecoits, E., Petrash, D. & Konhauser, K.O. (2011) Possible evolution of mobile animals in association with microbial mats. *Nature Geoscience*, **4**, 372-375.
- Gleiss, A., Gruber, S. & Wilson, R. (2010) Multi-Channel Data-Logging: Towards Determination of Behaviour and Metabolic Rate in Free-Swimming Sharks. pp. 211-228.
- Gleiss, A.C., Jorgensen, S.J., Liebsch, N., Sala, J.E., Norman, B., Hays, G.C., Quintana, F., Grundy, E., Campagna, C., Trites, A.W., Block, B.A. & Wilson, R.P. (2011) Convergent evolution in locomotory patterns of flying and swimming animals. *Nature Communications*, **2**, 352.
- Gleiss, A.C., Wilson, R.P. & Shepard, E.L.C. (2011) Making overall dynamic body acceleration work: on the theory of acceleration as a proxy for energy expenditure. *Methods in Ecology and Evolution*, **2**, 23-33.
- Goulet, P., Guinet, C., Swift, R., Madsen, P.T. & Johnson, M. (2019) A miniature biomimetic sonar and movement tag to study the biotic environment and predator-prey interactions in aquatic animals. *Deep Sea Research Part I: Oceanographic Research Papers*, **148**, 1-11.
- Graf, P.M., Wilson, R.P., Qasem, L., Hackländer, K. & Rosell, F. (2015) The Use of Acceleration to Code for Animal Behaviours; A Case Study in Free-Ranging Eurasian Beavers *Castor fiber*. *PLOS ONE*, **10**, e0136751.
- Grammer, K., Fink, B., Møller, A.P. & Thornhill, R. (2003) Darwinian aesthetics: sexual selection and the biology of beauty. *Biological Reviews*, **78**, 385-407.
- Grant, J.W.A. (1993) Whether or not to defend? The influence of resource distribution. *Marine Behaviour and Physiology*, **23**, 137-153.
- Greggor, A.L., Berger-Tal, O., Blumstein, D.T., Angeloni, L., Bessa-Gomes, C., Blackwell, B.F., St Clair, C.C., Crooks, K., de Silva, S., Fernández-Juricic, E., Goldenberg, S.Z., Mesnick, S.L., Owen, M., Price, C.J., Saltz, D., Schell, C.J., Suarez, A.V., Swaisgood, R.R., Winchell, C.S. & Sutherland, W.J. (2016) Research Priorities from Animal Behaviour for Maximising Conservation Progress. *Trends in Ecology & Evolution*, **31**, 953-964.
- Gummow, R.J., Vamvounis, G., Kannan, M.B. & He, Y. (2018) Calcium-Ion Batteries: Current State-of-the-Art and Future Perspectives. *Advanced Materials*, **30**, 1801702.
- Guthrie, J.D., Byrne, M.E., Hardin, J.B., Kochanny, C.O., Skow, K.L., Snelgrove, R.T., Butler, M.J., Peterson, M.J., Chamberlain, M.J. & Collier, B.A. (2011) Evaluation of a Global Positioning System backpack transmitter for wild turkey research. *The Journal of Wildlife Management*, **75**, 539-547.

- Hall, C. & Roshier, A. (2016) Getting the measure of behavior... is seeing believing? *Interactions*, **23**, 42-46.
- Halsey, L.G., Shepard, E.L.C., Hulston, C.J., VENABLES, M.C., White, C.R., Jeukendrup, A.E. & Wilson, R.P. (2008) Acceleration versus heart rate for estimating energy expenditure and speed during locomotion in animals: Tests with an easy model species, *Homo sapiens*. *Zoology*, **111**, 231-241.
- Halsey, L.G., Shepard, E.L.C. & Wilson, R.P. (2011) Assessing the development and application of the accelerometry technique for estimating energy expenditure. *Comparative Biochemistry and Physiology Part A: Molecular & Integrative Physiology*, **158**, 305-314.
- Handcock, R.N., Swain, D.L., Bishop-Hurley, G.J., Patison, K.P., Wark, T., Valencia, P., Corke, P. & O'Neill, C.J. (2009) Monitoring Animal Behaviour and Environmental Interactions Using Wireless Sensor Networks, GPS Collars and Satellite Remote Sensing. *Sensors*, **9**, 3586-3603.
- Harrison, K.A. & Bardgett, R.D. (2008) Impacts of Grazing and Browsing by Large Herbivores on Soils and Soil Biological Properties. *The Ecology of Browsing and Grazing* (eds I.J. Gordon & H.H.T. Prins), pp. 201-216. Springer Berlin Heidelberg, Berlin, Heidelberg.
- Hastie, G.D., Wilson, B., Wilson, L.J., Parsons, K.M. & Thompson, P.M. (2004) Functional mechanisms underlying cetacean distribution patterns: hotspots for bottlenose dolphins are linked to foraging. *Marine Biology*, **144**, 397-403.
- Hawkins, P. (2004) Bio-logging and animal welfare : practical refinements. *Mem. Natl. Inst. Polar Res.*, 58-68.
- Hays, G.C., Glen, F., Broderick, A.C., Godley, B.J. & Metcalfe, J.D. (2002) Behavioural plasticity in a large marine herbivore: contrasting patterns of depth utilisation between two green turtle (*Chelonia mydas*) populations. *Marine Biology*, **141**, 985-990.
- Hebblewhite, M. & Haydon, D.T. (2010) Distinguishing technology from biology: a critical review of the use of GPS telemetry data in ecology. *Philosophical Transactions of the Royal Society B: Biological Sciences*, **365**, 2303-2312.
- Heylen, B.C. & Nachtsheim, D.A. (2018) Bio-telemetry as an Essential Tool in Movement Ecology and Marine Conservation. pp. 83-107. Springer International Publishing, Cham.
- Hochscheid, S. (2014) Why we mind sea turtles' underwater business: A review on the study of diving behavior. *Journal of Experimental Marine Biology and Ecology*, **450**, 118-136.
- Hochscheid, S., Godley, B.J., Broderick, A.C. & Wilson, R.P. (1999) Reptilian diving: highly variable dive patterns in the green turtle *Chelonia mydas*. *Marine Ecology Progress Series*, **185**, 101-112.
- Hofman, M.P.G., Hayward, M.W., Heim, M., Marchand, P., Rolandsen, C.M., Mattisson, J., Urbano, F., Heurich, M., Mysterud, A., Melzheimer, J., Morellet, N., Voigt, U., Allen, B.L., Gehr, B., Rouco, C., Ullmann, W., Holand, Ø., Jørgensen, N.H., Steinheim, G., Cagnacci, F., Kroeschel, M., Kaczensky, P., Buuveibaatar, B., Payne, J.C., Palmegiani, I., Jerina, K., Kjellander, P., Johansson, Ö., LaPoint, S., Bayrakcismith, R., Linnell, J.D.C., Zaccaroni, M., Jorge, M.L.S., Oshima, J.E.F., Songhurst, A., Fischer, C., Mc Bride, R.T., Jr., Thompson, J.J., Streif, S., Sandfort, R., Bonenfant, C., Drouilly, M., Klapproth, M., Zinner, D., Yarnell, R., Stronza, A., Wilmott, L., Meisingset, E., Thaker, M., Vanak, A.T., Nicoloso, S., Graeber, R., Said, S., Boudreau, M.R., Devlin, A., Hoogesteijn, R., May-Junior, J.A., Nifong, J.C., Odden, J., Quigley, H.B., Tortato, F., Parker, D.M., Caso, A., Perrine, J., Tellaeche, C., Zieba, F., Zwijacz-Kozica, T., Appel,

- C.L., Axsom, I., Bean, W.T., Cristescu, B., Périquet, S., Teichman, K.J., Karpanty, S., Licoppe, A., Menges, V., Black, K., Scheppers, T.L., Schai-Braun, S.C., Azevedo, F.C., Lemos, F.G., Payne, A., Swanepoel, L.H., Weckworth, B.V., Berger, A., Bertassoni, A., McCulloch, G., Šustr, P., Athreya, V., Bockmuhl, D., Casaer, J., Ekori, A., Melovski, D., Richard-Hansen, C., van de Vyver, D., Reyna-Hurtado, R., Robardet, E., Selva, N., Sergiel, A., Farhadinia, M.S., Sunde, P., Portas, R., Ambarli, H., Berzins, R., Kappeler, P.M., Mann, G.K., Pyritz, L., Bissett, C., Grant, T., Steinmetz, R., Swedell, L., Welch, R.J., Armenteras, D., Bidder, O.R., González, T.M., Rosenblatt, A., Kachel, S. & Balkenhol, N. (2019) Right on track? Performance of satellite telemetry in terrestrial wildlife research. *PLOS ONE*, **14**, e0216223.
- Holton, M.D., Wilson, R.P., Teilmann, J. & Siebert, U. (2021) Animal tag technology keeps coming of age: an engineering perspective. *Philosophical Transactions of the Royal Society*.
- Hopkins, M.E. & Milton, K. (2016) Adverse Effects of Ball-Chain Radio-Collars on Female Mantled Howlers (*Alouatta palliata*) in Panama. *International Journal of Primatology*, **37**, 213-224.
- Houghton, J.D., Broderick, A.C., Godley, B.J., Metcalfe, J.D. & Hays, G.C. (2002) Diving behaviour during the internesting interval for loggerhead turtles *Caretta caretta* nesting in Cyprus. *Marine Ecology Progress Series*, **227**, 63-70.
- Huck, M. & Watson, S. (2019) The use of animal-borne cameras to video-track the behaviour of domestic cats. *Applied Animal Behaviour Science*, **217**, 63-72.
- Hughes, K. (2013) Measuring the impact of viewing wildlife: do positive intentions equate to long-term changes in conservation behaviour? *Journal of Sustainable Tourism*, **21**, 42-59.
- Hughey, L.F., Hein, A.M., Strandburg-Peshkin, A. & Jensen, F.H. (2018) Challenges and solutions for studying collective animal behaviour in the wild. *Philosophical Transactions of the Royal Society B: Biological Sciences*, **373**, 20170005.
- Hussey, N.E., Kessel, S.T., Aarestrup, K., Cooke, S.J., Cowley, P.D., Fisk, A.T., Harcourt, R.G., Holland, K.N., Iverson, S.J., Kocik, J.F., Mills Flemming, J.E. & Whoriskey, F.G. (2015) Aquatic animal telemetry: A panoramic window into the underwater world. *Science*, **348**, 1255642.
- Hutchinson, G.E. (1991) Population studies: Animal ecology and demography. *Bulletin of Mathematical Biology*, **53**, 193-213.
- Hwang, J.-Y., Myung, S.-T. & Sun, Y.-K. (2017) Sodium-ion batteries: present and future. *Chemical Society Reviews*, **46**, 3529-3614.
- Ironside, K.E., Mattson, D.J., Arundel, T.R. & Hansen, J.R. (2017) Is GPS telemetry location error screening beneficial? *Wildlife Biology*, **2017**.
- Jensen, P. (2006) Domestication—From behaviour to genes and back again. *Applied Animal Behaviour Science*, **97**, 3-15.
- Johnson, D.D.P., Kays, R., Blackwell, P.G. & Macdonald, D.W. (2002) Does the resource dispersion hypothesis explain group living? *Trends in Ecology & Evolution*, **17**, 563-570.
- Johnson, M. (2011) Measuring the orientation and movement of marine animals using inertial and magnetic sensors—a tutorial. Hobart.
- Joo, R., Boone, M.E., Clay, T.A., Patrick, S.C., Clusella-Trullas, S. & Basille, M. (2020) Navigating through the R packages for movement. *Journal of Animal Ecology*, **89**, 248-267.

- Katevas, K., Haddadi, H. & Tokarchuk, L. (2016) SensingKit: Evaluating the Sensor Power Consumption in iOS Devices. *2016 12th International Conference on Intelligent Environments (IE)*, pp. 222-225.
- Kawabe, R., Kawano, T., Nakano, N., Yamashita, N., Hiraishi, T. & Naito, Y. (2003) Simultaneous measurement of swimming speed and tail beat activity of free-swimming rainbow trout *Oncorhynchus mykiss* using an acceleration data-logger. *Fisheries science*, **69**, 959-965.
- Kay, W.P., Naumann, D.S., Bowen, H.J., Withers, S.J., Evans, B.J., Wilson, R.P., Stringell, T.B., Bull, J.C., Hopkins, P.W. & Börger, L. (2019) Minimizing the impact of biologging devices: Using computational fluid dynamics for optimizing tag design and positioning. *Methods in Ecology and Evolution*, **10**, 1222-1233.
- Kays, R., Tilak, S., Crofoot, M., Fountain, T., Obando, D., Ortega, A., Kuemmeth, F., Mandel, J., Swenson, G., Lambert, T., Hirsch, B. & Wikelski, M. (2011) Tracking Animal Location and Activity with an Automated Radio Telemetry System in a Tropical Rainforest. *The Computer Journal*, **54**, 1931-1948.
- Kim, T., Song, W., Son, D.-Y., Ono, L.K. & Qi, Y. (2019) Lithium-ion batteries: outlook on present, future, and hybridized technologies. *Journal of Materials Chemistry A*, **7**, 2942-2964.
- Kooyman, G.L. (2004) Genesis and evolution of bio-logging devices: 1963-2002. *Memoirs of National Institute of Polar Research. Special issue*, 15-22.
- Kranstauber, B., Cameron, A., Weinzerl, R., Fountain, T., Tilak, S., Wikelski, M. and Kays, R. (2011) The Movebank data model for animal tracking. *Environmental Modelling & Software*, **26**(6), pp.834-835.
- Krausman, P.R., Bleich, V.C., Cain III, J.W., Stephenson, T.R., DeYoung, D.W., McGrath, P.W., Swift, P.K., Pierce, B.M. & Jansen, B.D. (2004) From the Field: Neck lesions in ungulates from collars incorporating satellite technology. *Wildlife Society Bulletin*, **32**, 987-991.
- Kwak, W.-J., Rosy, Sharon, D., Xia, C., Kim, H., Johnson, L.R., Bruce, P.G., Nazar, L.F., Sun, Y.-K., Frimer, A.A., Noked, M., Freunberger, S.A. & Aurbach, D. (2020) Lithium–Oxygen Batteries and Related Systems: Potential, Status, and Future. *Chemical Reviews*, **120**, 6626-6683.
- Laich, A.G., Wilson, R.P., Quintana, F. & Shepard, E.L. (2008) Identification of imperial cormorant *Phalacrocorax atriceps* behaviour using accelerometers. *Endangered Species Research*, **10**, 29-37.
- Laplanche, C., Marques, T.A. & Thomas, L. (2015) Tracking marine mammals in 3D using electronic tag data. *Methods in Ecology and Evolution*, **6**, 987-996.
- Latham, A.D.M., Latham, M.C., Anderson, D.P., Cruz, J., Herries, D. & Hebblewhite, M. (2015) The GPS craze: six questions to address before deciding to deploy GPS technology on wildlife. *New Zealand Journal of Ecology*, **39**, 143-152.
- Lefrançois, C., Odion, M. & Claireaux, G. (2001) An experimental and theoretical analysis of the effect of added weight on the energetics and hydrostatic function of the swimbladder of European sea bass (*Dicentrarchus labrax*). *Marine Biology*, **139**, 13-17.
- Lewis, J.S., Rachlow, J.L., Garton, E.O. & Vierling, L.A. (2007) Effects of habitat on GPS collar performance: using data screening to reduce location error. *Journal of Applied Ecology*, **44**, 663-671.
- Liedvogel, M., Chapman, B.B., Muheim, R. & Åkesson, S. (2013) The behavioural ecology of animal movement: reflections upon potential synergies. *Animal Migration*, **1**, 39-46.

- Liu, K., Zhang, W., Chen, W., Li, K., Dai, F., Cui, F., Wu, X., Ma, G. & Xiao, Q. (2009) The development of micro-gyroscope technology. *Journal of Micromechanics and Microengineering*, **19**, 113001.
- López-Calleja, M.V. & Bozinovic, F. (2003) Dynamic energy and time budgets in hummingbirds: a study in *Sephanoides sephaniodes*. *Comparative Biochemistry and Physiology Part A: Molecular & Integrative Physiology*, **134**, 283-295.
- Luken, J.O. (1990) *Directing Ecological Succession*. Springer Netherlands.
- Lydersen, C., Nøst, O.A., Lovell, P., McConnell, B.J., Gammelsrød, T., Hunter, C., Fedak, M.A. & Kovacs, K.M. (2002) Salinity and temperature structure of a freezing Arctic fjord—monitored by white whales (*Delphinapterus leucas*). *Geophysical Research Letters*, **29**, 34-31-34-34.
- Macdonald, D.W. (2016) Animal behaviour and its role in carnivore conservation: examples of seven deadly threats. *Animal Behaviour*, **120**, 197-209.
- Manning, P.A. & Dawkins, M.S. (1998) *An Introduction to Animal Behaviour*. Cambridge University Press.
- Manning, P.A., Manning, A. & Dawkins, M.S. (1998) *An Introduction to Animal Behaviour*. Cambridge University Press.
- Marshall, R. & Landman, D. (2000) An improved method for determining pitch and roll angles using accelerometers. *21st Aerodynamic Measurement Technology and Ground Testing Conference*.
- Martin-Wintle, M.S., Shepherdson, D., Zhang, G., Zhang, H., Li, D., Zhou, X., Li, R. & Swaisgood, R.R. (2015) Free mate choice enhances conservation breeding in the endangered giant panda. *Nature Communications*, **6**, 10125.
- Martín López, L.M., Aguilar de Soto, N., Miller, P. & Johnson, M. (2016) Tracking the kinematics of caudal-oscillatory swimming: a comparison of two on-animal sensing methods. *The Journal of Experimental Biology*, **219**, 2103-2109.
- Martín López, L.M., Miller, P.J.O., Aguilar de Soto, N. & Johnson, M. (2015) Gait switches in deep-diving beaked whales: biomechanical strategies for long-duration dives. *The Journal of Experimental Biology*, **218**, 1325-1338.
- Mathews, F. (2010) Wild animal conservation and welfare in agricultural systems. *Animal Welfare*, **19**, 159-170.
- Mathie, M.J., Lovell, N.H., Coster, A.C.F. & Celler, B.G. (2002) Determining activity using a triaxial accelerometer. *Proceedings of the Second Joint 24th Annual Conference and the Annual Fall Meeting of the Biomedical Engineering Society* [Engineering in Medicine and Biology, pp. 2481-2482 vol.2483.
- McFarland, D. (1993) *Animal behaviour: Psychobiology, ethology, and evolution, 2nd ed.* John Wiley & Sons, Oxford, England.
- McNeely, I.F. & Wolverson, L. (2008) *Reinventing Knowledge: From Alexandria to the Internet*. W. W. Norton.
- Meyer, S., Puppe, B. & Langbein, J. (2010) [Cognitive enrichment in zoo and farm animals--implications for animal behaviour and welfare]. *Berliner und Munchener tierärztliche Wochenschrift*, **123**, 446-456.
- Minamikawa, S., Naito, Y. & Uchida, I. (1997) Buoyancy control in diving behavior of the loggerhead turtle, *Caretta caretta*. *Journal of Ethology*, **15**, 109-118.
- Mitani, Y., Watanabe, Y., Sato, K., Cameron, M.F. & Naito, Y. (2004) 3D diving behavior of Weddell seals with respect to prey accessibility and abundance. *Marine Ecology Progress Series*, **281**, 275-281.
- Mitchell, M.S. & Powell, R.A. (2004) A mechanistic home range model for optimal use of spatially distributed resources. *Ecological Modelling*, **177**, 209-232.

- Miwa, M., Oishi, K., Nakagawa, Y., Maeno, H., Anzai, H., Kumagai, H., Okano, K., Tobioka, H. & Hirooka, H. (2015) Application of Overall Dynamic Body Acceleration as a Proxy for Estimating the Energy Expenditure of Grazing Farm Animals: Relationship with Heart Rate. *PLOS ONE*, **10**, e0128042.
- Mohazzab, P. (2017) Archimedes' Principle Revisited. *Journal of Applied Mathematics and Physics*, **Vol.05No.04**, 9.
- Morales, J.M., Moorcroft, P.R., Matthiopoulos, J., Frair, J.L., Kie, J.G., Powell, R.A., Merrill, E.H. & Haydon, D.T. (2010) Building the bridge between animal movement and population dynamics. *Philosophical Transactions of the Royal Society B: Biological Sciences*, **365**, 2289-2301.
- Mori, E., Mazza, G. & Lovari, S. (2017) Sexual dimorphism. *Encyclopedia of Animal Cognition and Behavior (J. Vonk, and T. Shakelford, Eds)*. Springer International Publishing, Switzerland, 1-7.
- Nagelkerken, I. & Munday, P.L. (2016) Animal behaviour shapes the ecological effects of ocean acidification and warming: moving from individual to community-level responses. *Global Change Biology*, **22**, 974-989.
- Nathan, R., Getz, W.M., Revilla, E., Holyoak, M., Kadmon, R., Saltz, D. & Smouse, P.E. (2008) A movement ecology paradigm for unifying organismal movement research. *Proceedings of the National Academy of Sciences*, **105**, 19052-19059.
- Nelson, X.J. & Fijn, N. (2013) The use of visual media as a tool for investigating animal behaviour. *Animal Behaviour*, **85**, 525-536.
- Nesterova, A.P., Le Bohec, C., Beaune, D., Pettex, E., Le Maho, Y. & Bonadonna, F. (2010) Do penguins dare to walk at night? Visual cues influence king penguin colony arrivals and departures. *Behavioral Ecology and Sociobiology*, **64**, 1145-1156.
- Newman, G., Wiggins, A., Crall, A., Graham, E., Newman, S. & Crowston, K. (2012) The future of citizen science: emerging technologies and shifting paradigms. *Frontiers in Ecology and the Environment*, **10**, 298-304.
- Noda, T., Kawabata, Y., Arai, N., Mitamura, H. & Watanabe, S. (2014) Animal-mounted gyroscope/accelerometer/magnetometer: In situ measurement of the movement performance of fast-start behaviour in fish. *Journal of Experimental Marine Biology and Ecology*, **451**, 55-68.
- Noda, T., Okuyama, J., Koizumi, T., Arai, N. & Kobayashi, M. (2012) Monitoring attitude and dynamic acceleration of free-moving aquatic animals using a gyroscope. *Aquatic Biology*, **16**, 265-276.
- Nowacek, D.P., Christiansen, F., Bejder, L., Goldbogen, J.A. & Friedlaender, A.S. (2016) Studying cetacean behaviour: new technological approaches and conservation applications. *Animal Behaviour*, **120**, 235-244.
- Nuijten, R.J.M., Gerrits, T., Shamoun-Baranes, J. & Nolet, B.A. (2020) Less is more: On-board lossy compression of accelerometer data increases biologging capacity. *Journal of Animal Ecology*, **89**, 237-247.
- Ollerton, J. (2017) Pollinator Diversity: Distribution, Ecological Function, and Conservation. *Annual Review of Ecology, Evolution, and Systematics*, **48**, 353-376.
- Orians, G.H. & Pearson, N.E. (1979) *On the theory of central place foraging*. Ohio State University Press, Columbus.
- Orr, H.A. (2009) Fitness and its role in evolutionary genetics. *Nature reviews. Genetics*, **10**, 531-539.
- Ostfeld, R.S. & Holt, R.D. (2004) Are predators good for your health? Evaluating evidence for top-down regulation of zoonotic disease reservoirs. *Frontiers in Ecology and the Environment*, **2**, 13-20.

- Owen-Smith, N., Fryxell, J.M. & Merrill, E.H. (2010) Foraging theory upscaled: the behavioural ecology of herbivore movement. *Philosophical Transactions of the Royal Society B: Biological Sciences*, **365**, 2267-2278.
- Owen-Smith, N. & Goodall, V. (2014) Coping with savanna seasonality: comparative daily activity patterns of African ungulates as revealed by GPS telemetry. *Journal of Zoology*, **293**, 181-191.
- Ozyagcilar, T. (2012) Implementing a tilt-compensated eCompass using accelerometer and magnetometer sensors. *Freescal semiconductor, Application Note*, **AN4248**, Austin, TX.
- Painter, M.S., Blanco, J.A., Malkemper, E.P., Anderson, C., Sweeney, D.C., Hewgley, C.W., Červený, J., Hart, V., Topinka, V., Belotti, E., Burda, H. & Phillips, J.B. (2016) Use of bio-loggers to characterize red fox behavior with implications for studies of magnetic alignment responses in free-roaming animals. *Animal Biotelemetry*, **4**, 20.
- Papastamatiou, Y.P., Meyer, C.G. & Holland, K.N. (2007) A new acoustic pH transmitter for studying the feeding habits of free-ranging sharks. *Aquat. Living Resour.*, **20**, 287-290.
- Papastavrou, V., Leaper, R. & Lavigne, D. (2017) Why management decisions involving marine mammals should include animal welfare. *Marine Policy*, **79**, 19-24.
- Patel, A., Stocks, B., Fisher, C., Nicolls, F. & Boje, E. (2017) Tracking the Cheetah Tail Using Animal-Borne Cameras, GPS, and an IMU. *IEEE Sensors Letters*, **1**, 1-4.
- Pătru-Stupariu, I., Nita, A., Mustățea, M., Huzui-Stoiculescu, A. & Fürst, C. (2020) Using social network methodological approach to better understand human-wildlife interactions. *Land Use Policy*, **99**, 105009.
- Pedley, M. (2012) eCompass-Build and Calibrate a Tilt-Compensating Electronic Compass. *Circuit Cellar-The Magazine For Computer Applications*, 1-6.
- Peng, H., Maldonado-Chaparro, A.A. & Farine, D.R. (2019) The role of habitat configuration in shaping social structure: a gap in studies of animal social complexity. *Behavioral Ecology and Sociobiology*, **73**, 9.
- Pimentel, D. (1961) Animal Population Regulation by the Genetic Feed-Back Mechanism. *The American Naturalist*, **95**, 65-79.
- Poulin, M.-P., Clermont, J. & Berteaux, D. (2021) Extensive daily movement rates measured in territorial arctic foxes. *Ecology and Evolution*, **00**, 1- 12.
- Powell, D., Speeg, B., Li, S., Blumer, E. & McShea, W. (2013) An ethogram and activity budget of captive Sichuan takin (*Budorcas taxicolor tibetana*) with comparisons to other Bovidae. *mammalia*, **77**, 391-401.
- Qasem, L., Cardew, A., Wilson, A., Griffiths, I., Halsey, L.G., Shepard, E.L.C., Gleiss, A.C. & Wilson, R. (2012) Tri-Axial Dynamic Acceleration as a Proxy for Animal Energy Expenditure; Should We Be Summing Values or Calculating the Vector? *PLOS ONE*, **7**, e31187.
- Rafiq, K., Appleby, R.G., Edgar, J.P., Jordan, N.R., Dexter, C.E., Jones, D.N., Blacker, A.R.F. & Cochrane, M. (2019) OpenDropOff: An open-source, low-cost drop-off unit for animal-borne devices. *Methods in Ecology and Evolution*, **10**, 1517-1522.
- Raven, P.H. & Wagner, D.L. (2021) Agricultural intensification and climate change are rapidly decreasing insect biodiversity. *Proceedings of the National Academy of Sciences*, **118**, e2002548117.
- Recio, M.R., Mathieu, R., Denys, P., Sirguy, P. & Seddon, P.J. (2011) Lightweight GPS-Tags, One Giant Leap for Wildlife Tracking? An Assessment Approach. *PLOS ONE*, **6**, e28225.

- Rendueles, O. & Velicer, G.J. (2017) Evolution by flight and fight: diverse mechanisms of adaptation by actively motile microbes. *The ISME Journal*, **11**, 555-568.
- Reudink, M.W., Marra, P.P., Kyser, T.K., Boag, P.T., Langin, K.M. & Ratcliffe, L.M. (2009) Non-breeding season events influence sexual selection in a long-distance migratory bird. *Proceedings of the Royal Society B: Biological Sciences*, **276**, 1619-1626.
- Riaboff, L., Couvreur, S., Madouasse, A., Roig-Pons, M., Aubin, S., Massabie, P., Chauvin, A., Bédère, N. & Plantier, G. (2020) Use of Predicted Behavior from Accelerometer Data Combined with GPS Data to Explore the Relationship between Dairy Cow Behavior and Pasture Characteristics. *Sensors*, **20**, 4741.
- Richardson, G., Dickinson, P., Burman, O.H.P. & Pike, T.W. (2018) Unpredictable movement as an anti-predator strategy. *Proceedings of the Royal Society B: Biological Sciences*, **285**, 20181112.
- Riordan, P., Delahay, R.J., Cheeseman, C., Johnson, P.J. & Macdonald, D.W. (2011) Culling-Induced Changes in Badger (*Meles meles*) Behaviour, Social Organisation and the Epidemiology of Bovine Tuberculosis. *PLOS ONE*, **6**, e28904.
- Robert-Coudert, Y. & Wilson, R.P. (2004) Subjectivity in bio-logging: do logged data mislead? *Memoirs of the National Institute of Polar Research: Special Issue*, **58**, 23-33.
- Rollin, B.E. (2010) Animal Research, Animal Welfare, and the Three R's. *The Journal of Philosophy, Science & Law*, **10**, 1-11.
- Robert-Coudert, Y., Kato, A., Liebsch, N., Wilson, R.P., Muller, G. & Baubet, E. (2004a) Monitoring jaw movements: a cue to feeding activity. *Game and Wildlife Science*, **21**, 1-20.
- Robert-Coudert, Y. & Wilson, R.P. (2005) Trends and perspectives in animal-attached remote sensing. *Frontiers in Ecology and the Environment*, **3**, 437-444.
- Robert-Coudert, Y., Wilson, R.P., Daunt, F. & Kato, A. (2004b) Patterns of energy acquisition by a central place forager: benefits of alternating short and long foraging trips. *Behavioral Ecology*, **15**, 824-830.
- Ryan, P.G., Petersen, S.L., Peters, G. & Grémillet, D. (2004) GPS tracking a marine predator: the effects of precision, resolution and sampling rate on foraging tracks of African Penguins. *Marine Biology*, **145**, 215-223.
- Saltz, D. (1994) Reporting Error Measures in Radio Location by Triangulation: A Review. *The Journal of Wildlife Management*, **58**, 181-184.
- Schlecht, E., Hülsebusch, C., Mahler, F. & Becker, K. (2004) The use of differentially corrected global positioning system to monitor activities of cattle at pasture. *Applied Animal Behaviour Science*, **85**, 185-202.
- Schmidt-Nielsen, K. & Randall, D.J. (1997) *Animal Physiology: Adaptation and Environment*. Cambridge University Press.
- Schofield, G., Bishop, C.M., Katselidis, K.A., Dimopoulos, P., Pantis, J.D. & Hays, G.C. (2009) Microhabitat selection by sea turtles in a dynamic thermal marine environment. *Journal of Animal Ecology*, **78**, 14-21.
- Schweiger, A.H., Boulangeat, I., Conradi, T., Davis, M. & Svenning, J.-C. (2019) The importance of ecological memory for trophic rewilding as an ecosystem restoration approach. *Biological Reviews*, **94**, 1-15.
- Scott-Phillips, T.C., Dickins, T.E. & West, S.A. (2011) Evolutionary Theory and the Ultimate-Proximate Distinction in the Human Behavioral Sciences. *Perspectives on Psychological Science*, **6**, 38-47.

- Sekar, N., Shah, N.K., Abbas, S.S., Kakkar, M. & on behalf of the Roadmap to Combat Zoonoses in India, I. (2011) Research Options for Controlling Zoonotic Disease in India, 2010–2015. *PLOS ONE*, **6**, e17120.
- Seminoff, J.A., Jones, T.T. & Marshall, G.J. (2006) Underwater behaviour of green turtles monitored with video-time-depth recorders: what's missing from dive profiles? *Marine Ecology Progress Series*, **322**, 269-280.
- Shepard, E.L., Wilson, R.P., Halsey, L.G., Quintana, F., Laich, A.G., Gleiss, A.C., Liebsch, N., Myers, A.E. & Norman, B. (2008a) Derivation of body motion via appropriate smoothing of acceleration data. *Aquatic Biology*, **4**, 235-241.
- Shepard, E.L., Wilson, R.P., Quintana, F., Laich, A.G., Liebsch, N., Albareda, D.A., Halsey, L.G., Gleiss, A., Morgan, D.T., Myers, A.E., Newman, C. & Macdonald, D.W. (2008b) Identification of animal movement patterns using tri-axial accelerometry. *Endangered Species Research*, **10**, 47-60.
- Shepard, E.L., Wilson, R.P., Rees, W.G., Grundy, E., Lambertucci, S.A. & Vosper, S.B. (2013) Energy Landscapes Shape Animal Movement Ecology. *The American Naturalist*, **182**, 298-312.
- Shepard, P. (1997) *The Others: How Animals Made Us Human*. Island Press.
- Sherub, S., Fiedler, W., Duriez, O. & Wikelski, M. (2017) Bio-logging, new technologies to study conservation physiology on the move: a case study on annual survival of Himalayan vultures. *Journal of Comparative Physiology A*, **203**, 531-542.
- Shiomi, K., Kokubun, N., Shimabukuro, U. & Takahashi, A. (2020) Homing Ability of Adélie Penguins Investigated with Displacement Experiments and Bio-Logging. *Ardea*, **107**, 333-339.
- Silk, M.J., Hodgson, D.J., Rozins, C., Croft, D.P., Delahay, R.J., Boots, M. & McDonald, R.A. (2019) Integrating social behaviour, demography and disease dynamics in network models: applications to disease management in declining wildlife populations. *Philosophical Transactions of the Royal Society B: Biological Sciences*, **374**, 20180211.
- Stark, D.J., Vaughan, I.P., Ramirez Saldivar, D.A., Nathan, S.K.S.S. & Goossens, B. (2017) Evaluating methods for estimating home ranges using GPS collars: A comparison using proboscis monkeys (*Nasalis larvatus*). *PLOS ONE*, **12**, e0174891.
- Sutherland, W.J. (1998) The importance of behavioural studies in conservation biology. *Animal Behaviour*, **56**, 801-809.
- Swaigood, R.R. (2007) Current status and future directions of applied behavioral research for animal welfare and conservation. *Applied Animal Behaviour Science*, **102**, 139-162.
- Swart, J.A.A. (2004) The Wild Animal as a Research Animal. *Journal of Agricultural and Environmental Ethics*, **17**, 181-197.
- Swisher, C.N. (1967) CHARLES DARWIN ON THE ORIGINS OF BEHAVIOR. *Bulletin of the History of Medicine*, **41**, 24-43.
- Szaro, R.C., Sexton, W.T. & Malone, C.R. (1998) The emergence of ecosystem management as a tool for meeting people's needs and sustaining ecosystems. *Landscape and Urban Planning*, **40**, 1-7.
- Thompson, R., Matheson, S.M., Plötz, T., Edwards, S.A. & Kyriazakis, I. (2016) Porcine lie detectors: Automatic quantification of posture state and transitions in sows using inertial sensors. *Computers and Electronics in Agriculture*, **127**, 521-530.
- Thorrold, S.R., Afonso, P., Fontes, J., Braun, C.D., Santos, R.S., Skomal, G.B. & Berumen, M.L. (2014) Extreme diving behaviour in devil rays links surface waters and the deep ocean. *Nature Communications*, **5**, 4274.

- Tinbergen, N. (1963) On aims and methods of Ethology. *Zeitschrift für Tierpsychologie*, **20**, 410-433.
- Toledo, S. (2015) Evaluating batteries for advanced wildlife telemetry tags. *IET Wireless Sensor Systems*, pp. 235-242. Institution of Engineering and Technology.
- Tomkiewicz, S.M., Fuller, M.R., Kie, J.G. & Bates, K.K. (2010) Global positioning system and associated technologies in animal behaviour and ecological research. *Philosophical Transactions of the Royal Society B: Biological Sciences*, **365**, 2163-2176.
- Tonini, M.H. & Palma, E.D. (2017) Tidal dynamics on the North Patagonian Argentinean Gulfs. *Estuarine, Coastal and Shelf Science*, **189**, 115-130.
- Trivers, R. (1972) Parental investment and sexual selection. *Sexual Selection & the Descent of Man, Aldine de Gruyter, New York*, 136-179.
- Trolliet, F., Huynen, M.-C., Vermeulen, C. & Hambuckers, A. (2014) Use of camera traps for wildlife studies. A review. *Biotechnologie, Agronomie, Société et Environnement*, **18**, 446-454.
- Tuytens, F.A.M., de Graaf, S., Heerkens, J.L.T., Jacobs, L., Nalon, E., Ott, S., Stadig, L., Van Laer, E. & Ampe, B. (2014) Observer bias in animal behaviour research: can we believe what we score, if we score what we believe? *Animal Behaviour*, **90**, 273-280.
- Vaarst, M., Lund, V., Roderick, S. & Lockeretz, W. (2004) *Animal Health and Welfare in Organic Agriculture*. CABI.
- van der Werf, J., Graser, H.-U., Frankham, R. & Gondro, C. (2009) Adaptation and fitness in animal populations : evolutionary and breeding perspectives on genetic resource management. Dordrecht ; London : Springer.
- Van Walsum, T.A., Perna, A., Bishop, C.M., Murn, C.P., Collins, P.M., Wilson, R.P. & Halsey, L.G. (2020) Exploring the relationship between flapping behaviour and accelerometer signal during ascending flight, and a new approach to calibration. *Ibis*, **162**, 13-26.
- Vandenabeele, S.P., Shepard, E.L.C., Grémillet, D., Butler, P.J., Martin, G.R. & Wilson, R.P. (2015) Are bio-telemetric devices a drag? Effects of external tags on the diving behaviour of great cormorants. *Marine Ecology Progress Series*, **519**, 239-249.
- Vyssotski, A.L., Serkov, A.N., Itskov, P.M., Dell'Omo, G., Latanov, A.V., Wolfer, D.P. & Lipp, H.-P. (2006) Miniature Neurologgers for Flying Pigeons: Multichannel EEG and Action and Field Potentials in Combination With GPS Recording. *Journal of Neurophysiology*, **95**, 1263-1273.
- Wake, D.B. & Vredenburg, V.T. (2008) Are we in the midst of the sixth mass extinction? A view from the world of amphibians. *Proceedings of the National Academy of Sciences*, **105**, 11466-11473.
- Walker, J.S., Jones, M.W., Laramée, R.S., Holton, M.D., Shepard, E.L.C., Williams, H.J., Scantlebury, D.M., Marks, N.J., Magowan, E.A., Maguire, I.E., Bidder, O.R., Di Virgilio, A. & Wilson, R.P. (2015) Prying into the intimate secrets of animal lives; software beyond hardware for comprehensive annotation in 'Daily Diary' tags. *Movement Ecology*, **3**, 29.
- Ward, C.R.E., Bouyoucos, I.A., Brooks, E.J. & O'Shea, O.R. (2019) Novel attachment methods for assessing activity patterns using triaxial accelerometers on stingrays in the Bahamas. *Marine Biology*, **166**, 53.
- Wassmer, T., Murray, D., Boutin, S., Fahlman, A. & Jensen, F.H. (2020) *Ecology and Behaviour of Free-Ranging Animals Studied by Advanced Data-Logging and Tracking Techniques*. Frontiers Media SA.

- Watanabe, Y.Y. & Takahashi, A. (2013) Linking animal-borne video to accelerometers reveals prey capture variability. *Proceedings of the National Academy of Sciences*, **110**, 2199-2204.
- Wen, H. (2019) *Toward Inertial-Navigation-on-Chip: The Physics and Performance Scaling of Multi-Degree-of-Freedom Resonant MEMS Gyroscopes*. Springer International Publishing.
- Wensveen, P.J., Thomas, L. & Miller, P.J.O. (2015) A path reconstruction method integrating dead-reckoning and position fixes applied to humpback whales. *Movement Ecology*, **3**, 31.
- West, Stuart A. & Gardner, A. (2013) Adaptation and Inclusive Fitness. *Current Biology*, **23**, R577-R584.
- Whitford, M. & Klimley, A.P. (2019a) An overview of behavioral, physiological, and environmental sensors used in animal biotelemetry and biologging studies. *Animal Biotelemetry*, **7**, 1-24.
- Whitford, M. & Klimley, A.P. (2019b) An overview of behavioral, physiological, and environmental sensors used in animal biotelemetry and biologging studies. *Animal Biotelemetry*, **7**, 26.
- Whitney, N.M., Pratt Jr, H.L., Pratt, T.C. & Carrier, J.C. (2010) Identifying shark mating behaviour using three-dimensional acceleration loggers. *Endangered Species Research*, **10**, 71-82.
- Whitney, N.M., White, C.F., Smith, B.J., Cherkiss, M.S., Mazzotti, F.J. & Hart, K.M. (2021) Accelerometry to study fine-scale activity of invasive Burmese pythons (*Python bivittatus*) in the wild. *Animal Biotelemetry*, **9**, 1-13.
- Willener, A.S.T., Handrich, Y., Halsey, L.G. & Strike, S. (2015) Effect of walking speed on the gait of king penguins: An accelerometric approach. *Journal of Theoretical Biology*, **387**, 166-173.
- Williams, H., Shepard, E., Duriez, O. & Lambertucci, S.A. (2015) Can accelerometry be used to distinguish between flight types in soaring birds? *Animal Biotelemetry*, **3**, 1-11.
- Williams, H.J., Holton, M.D., Shepard, E.L.C., Largey, N., Norman, B., Ryan, P.G., Duriez, O., Scantlebury, M., Quintana, F., Magowan, E.A., Marks, N.J., Alagaili, A.N., Bennett, N.C. & Wilson, R.P. (2017) Identification of animal movement patterns using tri-axial magnetometry. *Movement Ecology*, **5**, 6.
- Williams, H.J., Taylor, L.A., Benhamou, S., Bijleveld, A.I., Clay, T.A., de Grissac, S., Demšar, U., English, H.M., Franconi, N., Gómez-Laich, A., Griffiths, R.C., Kay, W.P., Morales, J.M., Potts, J.R., Rogerson, K.F., Rutz, C., Spelt, A., Trevail, A.M., Wilson, R.P. & Börger, L. (2020) Optimizing the use of biologgers for movement ecology research. *Journal of Animal Ecology*, **89**, 186-206.
- Williams, L.R., Bishop-Hurley, G.J., Anderson, A.E. & Swain, D.L. (2019) Application of accelerometers to record drinking behaviour of beef cattle. *Animal Production Science*, **59**, 122-132.
- Wilmers, C.C., Nickel, B., Bryce, C.M., Smith, J.A., Wheat, R.E. & Yovovich, V. (2015) The golden age of bio-logging: How animal-borne sensors are advancing the frontiers of ecology. *Ecology*, **96**, 1741-1753.
- Wilson, A.D., Wikelski, M., Wilson, R.P. & Cooke, S.J. (2015) Utility of biological sensor tags in animal conservation. *Conservation Biology*, **29**, 1065-1075.
- Wilson, R., Griffiths, I., Legg, P., Friswell, M., Bidder, O., Halsey, L., Lambertucci, S.A. & Shepard, E. (2013) Turn costs change the value of animal search paths. *Ecology Letters*, **16**, 1145-1150.

- Wilson, R., Peters, G., Regel, J., Grémillet, D., Pütz, K., Kierspel, M., Weimerskirch, H. & Cooper, J. (1998) Short retention times of stomach temperature loggers in free-living seabirds: is there hope in the spring? *Marine Biology*, **130**, 559-566.
- Wilson, R. & Wilson, M.-P. (1988) Dead reckoning: a new technique for determining penguin movements at sea. *Meeresforschung (Hamburg)*, **32**, 155-158.
- Wilson, R.P., Börger, L., Holton, M.D., Scantlebury, D.M., Gómez-Laich, A., Quintana, F., Rosell, F., Graf, P.M., Williams, H., Gunner, R., Hopkins, L., Marks, N., Gerdali, N.R., Duarte, C.M., Scott, R., Strano, M.S., Robotka, H., Eizaguirre, C., Fahlman, A. & Shepard, E.L.C. (2020a) Estimates for energy expenditure in free-living animals using acceleration proxies: A reappraisal. *Journal of Animal Ecology*, **89**, 161-172.
- Wilson, R.P., Holton, M., Wilson, V.L., Gunner, R., Tysse, B., Wilson, G.I., Quintana, F., Duarte, C. & Scantlebury, D.M. (2019) Towards informed metrics for examining the role of human-induced animal responses in tag studies on wild animals. *Integrative Zoology*, **14**, 17-29.
- Wilson, R.P., Liebsch, N., Davies, I.M., Quintana, F., Weimerskirch, H., Storch, S., Lucke, K., Siebert, U., Zankl, S., Müller, G., Zimmer, I., Scolaro, A., Campagna, C., Plötz, J., Bornemann, H., Teilmann, J. & McMahon, C.R. (2007) All at sea with animal tracks; methodological and analytical solutions for the resolution of movement. *Deep Sea Research Part II: Topical Studies in Oceanography*, **54**, 193-210.
- Wilson, R.P., Rose, K.A., Gunner, R., Holton, M., Marks, N.J., Bennett, N.C., Bell, S.H., Twining, J.P., Hesketh, J., Duarte, C.M., Bezodis, N. & Scantlebury, D.M. (2020b) Forces experienced by instrumented animals depend on lifestyle. *bioRxiv*, 2020.2008.2020.258756.
- Wilson, R.P., Shepard, E. & Liebsch, N. (2008) Prying into the intimate details of animal lives: use of a daily diary on animals. *Endangered Species Research*, **4**, 123-137.
- Wilson, R.P., White, C.R., Quintana, F., Halsey, L.G., Liebsch, N., Martin, G.R. & Butler, P.J. (2006) Moving towards acceleration for estimates of activity-specific metabolic rate in free-living animals: the case of the cormorant. *Journal of Animal Ecology*, **75**, 1081-1090.
- Wilson, R.P., Williams, H.J., Holton, M.D., di Virgilio, A., Börger, L., Potts, J.R., Gunner, R., Arkwright, A., Fahlman, A., Bennett, N.C., Alagaili, A., Cole, N.C., Duarte, C.M. & Scantlebury, D.M. (2020c) An "orientation sphere" visualization for examining animal head movements. *Ecology and Evolution*, **10**, 4291-4302.
- Woodroffe, R., Thirgood, S., Rabinowitz, A. & Corporation, E. (2005) *People and Wildlife, Conflict Or Co-existence?* Cambridge University Press.
- Wurtz, K., Camerlink, I., D'Eath, R.B., Fernández, A.P., Norton, T., Steibel, J. & Siegford, J. (2019) Recording behaviour of indoor-housed farm animals automatically using machine vision technology: A systematic review. *PLOS ONE*, **14**, e0226669.
- Xue, X. & Henderson, T.C. (2006) Video-based Animal Behavior Analysis From Multiple Cameras. *2006 IEEE International Conference on Multisensor Fusion and Integration for Intelligent Systems*, pp. 335-340.
- Yoda, K., Naito, Y., Sato, K., Takahashi, A., Nishikawa, J., Ropert-Coudert, Y., Kurita, M. & Le Maho, Y. (2001). A new technique for monitoring the behaviour of free-ranging Adelie penguins. *Journal of Experimental Biology*, **204**, 685-690.
- Yoda, K.. (2019). Advances in bio-logging techniques and their application to study navigation in wild seabirds. *Advanced Robotics*, **33**(3-4), pp.108-117.
- Zeder, M.A. (2012) The Domestication of Animals. *Journal of Anthropological Research*, **68**, 161-190.

- Zeh, D.R., Heupel, M.R., Limpus, C.J., Hamann, M., Fuentes, M.M.P.B., Babcock, R.C., Pillans, R.D., Townsend, K.A. & Marsh, H. (2015) Is acoustic tracking appropriate for air-breathing marine animals? Dugongs as a case study. *Journal of Experimental Marine Biology and Ecology*, **464**, 1-10.
- Zihajehzadeh, S., Loh, D., Lee, M., Hoskinson, R. & Park, E.J. (2014) A cascaded two-step Kalman filter for estimation of human body segment orientation using MEMS-IMU. *2014 36th Annual International Conference of the IEEE Engineering in Medicine and Biology Society*, pp. 6270-6273.
- Zimmer, W.M.X., Johnson, M.P., Amico, A.D. & Tyack, P.L. (2003) Combining data from a multisensor tag and passive sonar to determine the diving behavior of a sperm whale (*Physeter macrocephalus*). *IEEE Journal of Oceanic Engineering*, **28**, 13-28.

Chapter 2

A new direction for differentiating animal activity based on measuring angular velocity about the yaw axis

Richard M. Gunner



Photo taken by Richard M. Gunner

This work was published in *Ecology and evolution* as:

Gunner, R.M., Wilson, R.P., Holton, M.D., Scott, R., Hopkins, P. and Duarte, C.M., 2020. A new direction for differentiating animal activity based on measuring angular velocity about the yaw axis. *Ecology and evolution*, 10(14), pp.7872-7886, DOI: <https://doi.org/10.1002/ece3.6515>

Abstract

The use of animal-attached data loggers to quantify animal movement has increased in popularity and application in recent years. High-resolution tri-axial acceleration and magnetometry measurements have been fundamental in elucidating fine-scale animal movements, providing information on posture, traveling speed, energy expenditure and associated behavioural patterns. Heading is a key variable obtained from the tandem use of magnetometers and accelerometers, although few field investigations have explored fine-scale changes in heading to elucidate differences in animal activity (beyond the notable exceptions of dead-reckoning). This paper provides an overview of the value and use of animal heading and a prime derivative, angular velocity about the yaw axis, as an important element for assessing activity extent with potential to allude to behaviours, using 'free-ranging' Loggerhead turtles (*Caretta caretta*) as a model species. I also demonstrate the value of yaw rotation for assessing activity extent, which varies over the time scales considered and show that various scales of body rotation, particularly rate of change of yaw, can help resolve differences between fine-scale behaviour-specific movements. For example, oscillating yaw movements about a central point of the body's arc implies bouts of foraging while unusual circling behaviour, indicative of conspecific interactions, could be identified from complete revolutions of the longitudinal axis. I believe this approach should help identification of behaviours and 'space-state' approaches to enhance our interpretation of behaviour-based movements, particularly in scenarios where acceleration metrics have limited value, such as for slow-moving animals.

Background

Animals can enhance their fitness by responding behaviourally according to their physiological state and environmental circumstance (Nathan *et al.* 2008; Shepard *et al.* 2013; Wilmers *et al.* 2015). At its inception, animal behaviour was defined by direct observation of body posture and limb movement (Patterson *et al.* 2008; Brown *et al.* 2013). More recently, however, researchers have realised that animal-attached tags can help define behaviour using tri-axial acceleration data, which resolves both animal posture and the dynamism of movement (Yoda *et al.* 2001; Shepard *et al.* 2008; Zimmer *et al.* 2011; Wilson *et al.* 2015). Indeed, animal-attached accelerometers are now widespread and common for both short-term and long-term continuous monitoring of the behaviour of wild animals (Brown *et al.* 2013; Wilmers *et al.* 2015). Methods used to identify animal behaviours in sensor data include random forests (e.g., Fehlmann *et al.* 2017), neural networks (Samarasinghe 2016) and support vector machines (e.g., Martiskainen *et al.* 2009) and generally tease out accelerometer-derived data streams using both raw accelerometer data and derivatives, such as VeDBA (e.g., Patterson *et al.* 2019; Benoit *et al.* 2020), to find some combination of values that characterise specific behaviours.

Not all behaviours can be accurately resolved from accelerometers though (Williams *et al.* 2017) because slow-moving animals, such as some reptiles (Wyneken 1997; Walker & Westneat 2000), may produce negligible changes in the recorded dynamic acceleration (for definition see Wilson *et al.* (2020a)). Similar issues arise during bouts of gliding behaviour, as exhibited by many marine and aerial species that can maintain relatively constant velocity for long periods of time (Eckert 2002; Williams *et al.* 2015). In addition, external forces acting on the animal, such as current vectors in air or water, can decrease the signal-to-noise ratio of measured acceleration, confounding the interpretation of data (*cf.* Ropert-Coudert & Wilson 2004; Halsey, Shepard & Wilson 2011). Animal posture derived from acceleration also becomes problematic when animals are subject to high centripetal acceleration (e.g. when a bird banks sharply (Clark 2009; Williams *et al.* 2015)) or when substrate beneath the

study animal varies in declination (Wilson *et al.* 2018). Finally, a critical limitation of accelerometers, is that they cannot resolve rotation about the yaw axis (typically referred to as; ‘heading’) even though movement in this axis is at least as important (or more) as rotations in the other two axes; pitch and roll (Noda *et al.* 2012; Kano *et al.* 2018).

Both Williams *et al.* (2017) and Chakravarty *et al.* (2019) have suggested that tri-axial magnetometers could be used as behavioural identification sensors in manner analogous to tri-axial accelerometers. Certainly, magnetometers have appreciable advantages over accelerometers because they are unaffected by both gravitational and dynamic components of acceleration (Noda *et al.* 2014; Martín López *et al.* 2016) and, unlike gyroscopes, are not subject to drift over larger time intervals (Fong, Ong & Nee 2008), also requiring less electric current and can be usefully sampled at lower frequencies (Caruso 2000). I note though, that gyroscopes have been used in a suite of biologging studies to determine angular velocity (e.g., Noda *et al.* 2012; Gerencsér *et al.* 2013; Noda *et al.* 2013; Noda *et al.* 2014). Tri-axial magnetometers react to variations in magnetic field orientation and intensity in all three spatial dimensions (Wilson *et al.* 2007; Martín López *et al.* 2016). Orientation about the yaw axis of an animal-attached tag is accessed by consideration of the animal’s pitch and roll (from accelerometers) in relation to the output of the tri-axial magnetic field sensors and is described in detail by Bidder *et al.* (2015). This approach normally allows the animal heading to be defined to within about 1–2° (Wilson, Shepard & Liebsch 2008; Painter *et al.* 2016).

Importantly, derivation of heading, and associated metrics (see later), should provide additional important measurements to define activity and with which behaviours may be identified using techniques such as machine learning (Wang *et al.* 2015) and time-based decision-trees (Rutkowski, Jaworski & Duda 2020) as well as being important in dead-reckoning studies (Laplanche, Marques & Thomas 2015; Walker *et al.* 2015). Crucially, magnetometers reveal patterns in movement at various scales of rotation along the yaw axis that are not always evident in acceleration data (Martín López *et al.* 2015; Williams *et al.* 2015; Martín López *et al.* 2016; Williams *et al.* 2017),

which should prove particularly informative for behaviours that produce no definitive acceleration-based pattern and for animals that generate negligible dynamic acceleration signal.

This paper examines the value and use of animal heading and a prime derivative, angular velocity about the yaw axis (hereafter termed 'AVeY'), as an element for quantifying activity and ultimately aspiring to help differentiate animal behaviour using the Loggerhead turtle (*Caretta caretta*) as a model species. Firstly, I propose several metrics derived from AVeY and discuss how various temporal scales over which AVeY (and derivatives) is calculated, in some cases, can be a sensitive indicator of to some types of movement beyond those which acceleration alone can detail. Secondly, I outline the wider implications of using such AVeY metrics to aid in examining fine-scale behaviours. Lastly, I assess the relationship between AVeY and the commonly used DBA-based proxy for energy expenditure; vectorial dynamic body acceleration (VeDBA) (*cf.* Miwa *et al.* 2015) to see how the two metrics scale. The general aims of this research are to examine the potential importance in AVeY for enhancing our understanding of animal movement and to provide a framework for deriving and utilising indices of AVeY for researchers investigating proximate and ultimate aspects of animal behaviour using the technology outlined above.

Materials and methods

Subjects, study area and tagging

The attachment of data loggers was carried out between July-August 2014 on five mature female loggerhead turtles, intercepted and tagged immediately post egg-laying on the Southern beaches of Boa Vista, Cape Verde Islands (15°58'22" N, 22°47'56" W). Daily diary (DD) logging units (Wilson, Shepard & Liebsch 2008) were used in this study. Acceleration measurements were logged as acceleration with respect to gravity (1 g = 9.81 m/s) from each of the three orthogonally mounted sensor axes (measuring within the range of $\pm 16 g$). Orthogonal magnetometry

measurements were recorded in Gauss (G) (magnetic intensity recorded within the range of ± 0.88 G at 0.73 mG/LSB resolution). Both accelerometry and magnetometry data were logged at 40 Hz. The DD's also recorded temperature ($^{\circ}\text{C}$) and pressure (mbar). Data were stored on a 2 GB removable microSD card. The DDs were enclosed in an oval-cylinder water-tight nylon casing and powered with one A-cell battery. Tags were attached onto the second dorsal scute of the turtle carapace, using a two-component epoxy resin glue, to ensure tag housings (and thus sensors) were placed as close as possible to the horizontal. Tags were positioned so that the x, y and z axes of both the accelerometer and magnetometer sensors were aligned to the anterior-posterior (surge), medio-lateral (sway) and dorsal-ventral (heave) axes of the animal, respectively. Tags were retrieved after a single inter-nesting interval (approximately 2 weeks after initial deployment).

Derivation of VeDBA

Vectorial dynamic body acceleration (VeDBA) is a single integrated measure of the vector sum of dynamic acceleration from the three spatial dimensions during a given inertial frame (Qasem *et al.* 2012). To calculate VeDBA, a 2-second running mean was applied to each of the acceleration axes to approximate the static acceleration (Shepard *et al.* 2008; McClune *et al.* 2014). The static acceleration from each axis was subtracted from the raw acceleration values from each axis to derive the dynamic acceleration (Gleiss, Wilson & Shepard 2011; Shepard *et al.* 2013). VeDBA was determined by taking the vectorial sum of the dynamic acceleration using:

$$\text{VeDBA} = \sqrt{(x^2 + y^2 + z^2)} \quad (1)$$

where x, y & z are the derived dynamic acceleration values from each axis.

Derivation of angular velocity

The static component of acceleration (due to gravity, which amounts to 1 g) is used in the computation of rotation about the three axes and is typically achieved by

passing a moving average of a given window size w (2 seconds used in this study) through a given sample (S_i) of each orthogonal channel's acceleration *via*;

$$S_i = \frac{1}{w} \sum_{j=i-\frac{w}{2}}^{i+\frac{w}{2}} S_j \quad (2)$$

Pitch and roll are computed via;

$$Pitch (\beta) = (atan2(S_x, \sqrt{S_y \cdot S_y + S_z \cdot S_z}) \cdot \frac{180}{\pi}) \quad (3)$$

$$Roll (Y) = (atan2(S_y, \sqrt{S_x \cdot S_x + S_z \cdot S_z}) \cdot \frac{180}{\pi}) \quad (4)$$

where $S_{x,y,z}$ refer to the static components of acceleration from the x, y and z channels of the accelerometer, respectively (Bidder *et al.* 2015).

For review of all stages and mathematical components involved in the derivation of compass heading (H) (yaw), see Bidder *et al.* (2015) and Walker *et al.* (2015). In brief however, the magnetometer is typically calibrated by rotating the tag so that all orientations of roll, pitch and yaw are covered (Williams *et al.* 2017). In the absence of distortions to the local magnetic field, the normalised data from each axis (of this calibration period), forms a sphere when plotted on a tri-axial magnetic field intensity scatter-plot (the 'm-sphere'; Williams *et al.* 2017). This process essentially provides a reference frame of the vectorial sum of magnetometry data across all three spatial-dimensions and enables subsequent compensation for 'hard' and 'soft iron' errors. Soft iron deposits distort the magnetic field around the device, causing the sphere to take on an ovoid/ellipsoid form (Gebre-Egziabher *et al.* 2006; Ozyagcilar 2012). Hard iron deposits introduce a constant bias, shifting the position of the magnetic field and thus position of the sphere away from its true origin (Gebre-Egziabher *et al.* 2006; Ozyagcilar 2012).

An ellipsoid-fitting algorithm and correction factor are used to correct such distortions and re-form uniform spherical fields about the true origin (Renaudin, Afzal & Lachapelle 2010). Angular rotations about the pitch and roll axes, derived from the

static component of acceleration are subsequently used in the tilt correction procedure on each orthogonal magnetometer channel. Compass data is first normalised and then each orthogonal channel is rotated according to the pitch and roll. This ensures magnetometer outputs are compensated, according to the inclination and declination angles caused by postural offsets, with outputs corrected to give a horizontal co-ordinate frame (Pedley 2012; Bidder *et al.* 2015). Finally, compass heading (H) with respect to magnetic North, is achieved *via*:

$$H = \text{mod} \left(360 + (\text{atan2}(-m_y, m_x) \cdot \frac{180}{\pi}), 360 \right) \quad (5)$$

where m_{xy} refer to the normalised, ellipse fitted and co-ordinate frame-adjusted x and y channels of the magnetometer, respectively (Bidder *et al.* 2015) and *mod* refers to the modulo operator. The heading output uses a scale of 0° to 360°, with Magnetic North equating to a heading of 0° or 360°, South to 180° and thus East and West to 90° and 270°, respectively.

Data analysis

All data analysis was performed in the custom designed software; Daily Diary Multi Trace (DDMT, <http://www.wildbytetechologies.com>), R (open source statistical programming software, <http://www.R-project.org>), Origin pro 2016 (OriginLab Corporation, <http://www.originlab.com>) and Microsoft Excel 2016. Only flat U-shaped dives (type 1a) greater than or equal to 3 meters in depth (*cf.* Houghton *et al.* 2002) were used in the analysis to illustrate points being made.

DDMT enables 2-D visualisations of infra-second variation per sensor axis output (visualised as waveforms over time) and includes built-in features for; quantifying and exporting channel subsets, calculating channel differentials and derivatives (including VeDBA), altering channel smoothing windows, producing multi-dimensional plots and an interface for searching for behaviours and bookmarking them using a Boolean time-based approach (Wilson *et al.* 2018). DDMT also provides the platform to

correct for iron distortions and tilt offsets from calibration data, before computing compass heading. All three indices of derived body rotation (pitch, roll and yaw) were pre-smoothed using a rolling window of 2 seconds to reduce small deviations due to noise (i.e., small deviations manifest by the flipper beat cycle). Pitch and roll values ranged from -90° to $+90^\circ$. The arithmetic mean of the yaw axis is problematic due to the periodic nature of circular data (range from 0° to 360° ; both of which define the exact same point on the circumference of the unit circle - magnetic North, *cf.* Pewsey, Neuhäuser & Ruxton 2013). Therefore, a circular mean was used; units were converted from degrees to cartesian coordinates, before calculating the arithmetic mean of the individual angles from sample trigonometric moments and finally, restoring resultant units back to degrees via;

$$\bar{\theta}_p = \text{atan2}\left(\frac{1}{n} \sum_{j=i}^n \sin\left(H_j \cdot \frac{\pi}{180}\right), \frac{1}{n} \sum_{j=i}^n \cos\left(H_j \cdot \frac{\pi}{180}\right)\right) \quad (6)$$

$$\bar{H} = \text{mod}\left(360 + \left(\bar{\theta}_p \cdot \frac{180}{\pi}\right), 360\right) \quad (7)$$

Each dataset was subsequently sub-sampled to 1 Hz (selected values at $i = 40$) to make the data more manageable and because turtles are generally slow-moving anyway (as manifest by extremely low VeDBA values, typically lower than $0.08 g$). Differentials were then calculated from the smoothed values of each axis, using a stepping range of 1 second ($^\circ/s$) and termed; 'AVeP', 'AVeR' and 'AVeY' (Angular Velocity about the Pitch, Roll and Yaw axis, respectively). AVeY was also calculated over two larger temporal scales; 5 seconds (AVeY ($^\circ/5_s$)) and 10 seconds (AVeY ($^\circ/10_s$)).

Since compass heading is circular, with no true zero and any designation of low or high values being arbitrary, a logical expression was implemented on the derivative AVeY to ensure rate of change never exceeded $180^\circ/s$, whereby 360 was added to AVeY values less than -180 and 360 was subtracted from AVeY values greater than 180 . This makes biological sense as long as the time interval over which the angular velocity is calculated is restricted because it is far more likely that an animal that caused the compass heading to change from 10° to 350° , turned 20° anticlockwise,

rather than 330° clockwise. Careful consideration of the animal in question must be made when choosing the sampling period of AVeY, to avoid inaccurate rates of change. Ideally, this should be less than the time it takes the animal to rotate through half a revolution.

The maximum angle that could be yielded from any given axis per second was therefore 180°. A metric termed ‘absolute angular velocity’ (AAV) was derived from the integration of each of the rotational axes’ absolute instantaneous angular velocity measurement;

$$AAV = \sqrt{(AVeP^2 + AVeR^2 + AVeY^2)} \quad (8)$$

Conditional running cumulative sum functions in R were implemented on AVeY (°/s) to document each time a turn (or multitude of turns) in either direction, totalled/surpassed 20°, 45°, 90° and 180° with respect to a particular starting orientation, resetting each time the condition (angle of specified yaw rotation to exceed) was met. The degree of yaw rotation in either direction with respect to the starting orientation and the specified turn angle with which it was equated, was expressed as a percentage coverage over time (0 to ± 100 %; ‘+’ representing clockwise, ‘-’ representing anticlockwise). A final new metric, termed ‘cumulative heading’ (CuHe), also implemented on AVeY (°/s), assessed the percentage coverage (0 to 100 %) about the yaw axis from the culmination of angular rotations in both directions, resetting each time the animal had (at least once), rotated through all 360°. R code for computing these metrics is available at <https://github.com/Richard6195/Dead-reckoning-animal-movements-in-R>.

A Linear mixed model (LMM) was performed utilising the ‘lmer’ function in R, from the ‘lme4’ package (Bates *et al.* 2015); to determine the relationship between mean values of AVeY (°/s) and VeDBA per dive. Turtle ID was included as a random factor in the model (Kuznetsova, Brockhoff & Christensen 2017). Three outliers were removed from the model following diagnostic plots of residuals. A Random slope model (including random intercepts) was also constructed to examine whether there

was a significant difference between the slope coefficients, as given from the interaction of AVeY by turtle ID. The model simplification method was employed using likelihood ratio tests, with AIC values also assessed. The interclass correlation (ICC) was computed for the best performing model. Spearman rank correlation coefficients (r_s) were derived to determine the association of ranks between various metrics of body rotation (detailed in Table 1) and VeDBA.

Table 1. Description of the metrics derived from accelerometer and magnetometer outputs.

Metric	Abbreviation	Description	Smoothing	Unit
Angular velocity about the yaw axis	AVeY	$AVeY (^{\circ}/s^{-1}) = x_{i+1} - x_i$, $AVeY (^{\circ}/5s) = x_{i+5} - x_i$, $AVeY (^{\circ}/10s) = x_{i+10} - x_i$, where x is the i_{th} value of heading	Yaw pre-smoothed by 2 seconds (circular mean) prior to calculating differentials	$^{\circ}/s$ $^{\circ}/5s$ $^{\circ}/10s$
Angular velocity about the pitch axis	AVeP	$AVeP = x_{i+1} - x_i$, where x is the i_{th} value of pitch	Pitch pre-smoothed by 2 seconds prior to calculating differential	$^{\circ}/s$
Angular velocity about the roll axis	AVeR	$AVeR = x_{i+1} - x_i$, where x is the i_{th} value of roll	Roll pre-smoothed by 2 seconds prior to calculating differential	$^{\circ}/s$
Absolute angular velocity	AAV	$AAV = \sqrt{(AVeY^2 + AVeP^2 + AVeR^2)}$	N/A	$^{\circ}/s$
Vectorial dynamic body acceleration	VeDBA	$VeDBA = \sqrt{(x^2 + y^2 + z^2)}$, where x , y & z are the derived dynamic acceleration values from each axis	2 seconds	g

Results

There were strong positive significant correlations between the three differentials of body rotation, with higher angular velocities of body orientation being apparent across all three axes of rotation (pitch, roll and yaw) (Fig. 1). Of the three rotational axes though, AVeY had the strongest correlation with AAV, signifying that yaw was the predominant axis of rotation during activity (for this study species at least).

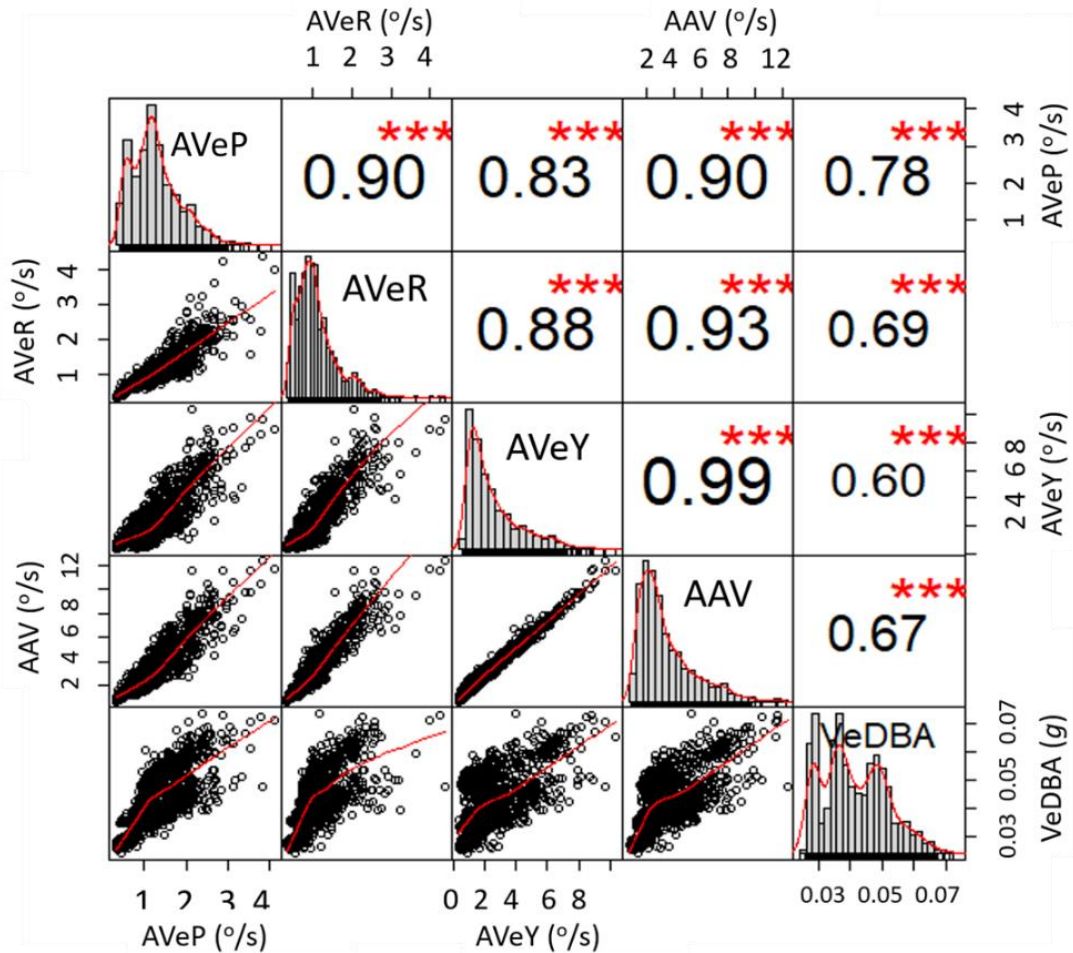


Figure 2. Association between the various metrics of body rotation (outlined in table 1) and VeDBA, with strength of correlation coefficients (spearman rank) and significance level detailed (***) = 0.01 significance level). Each data point represents the mean value per flat U-dive (bottom phase duration).

Model simplification and AIC values detailed the model incorporating both random slopes and random intercepts best improved goodness of fit; AVeY significantly affected VeDBA (LMM: $\chi^2(1) = 15.82$, $p < 0.01$), with every 1 unit increase in AVeY increasing VeDBA by approximately 0.029 g (est. = 0.0029 ± 0.00027 (se), $t = 4.92$, 95 % CI[0.0022, 0.0035], $p < 0.001$) (Fig. 2A). Incorporating random effects greatly improved the variance explained (marginal $R^2 = 0.33$; conditional $R^2 = 0.84$). In addition, the ICC was high at 0.79, indicating a high account of correlation among observations within groups. Typically, mean values of VeDBA were higher (and encompassed greater range) during faster turn rates (Fig. 2B).

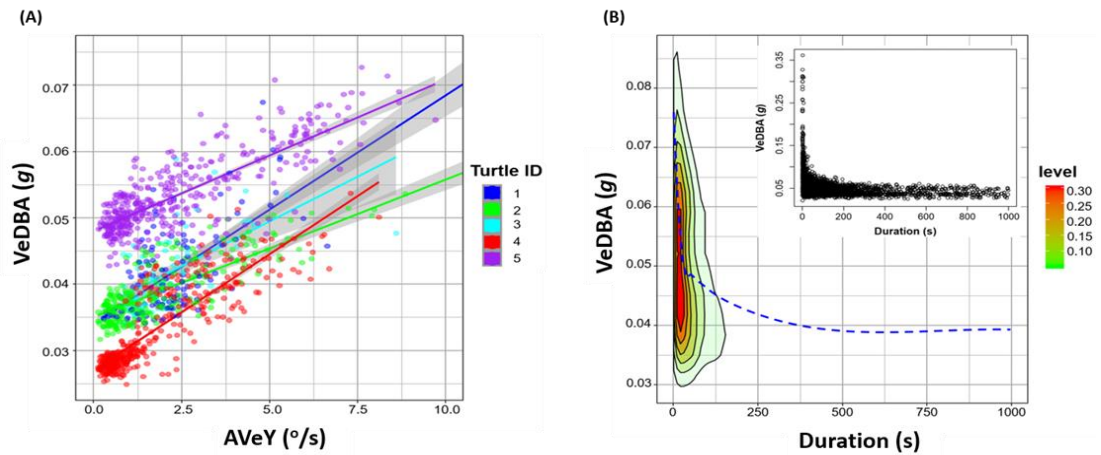


Figure 2. Association between yaw rotation and VeDBA, each data point represents the mean value per flat U-dive (bottom phase duration). Relationship between AVeY (°/s) and VeDBA with implemented linear regressions and 95 % confidence intervals (grey shading around each regression) (A). Data points and regression lines coloured according to turtle ID. Contour plot showing the kernel density level of VeDBA as a function of the time it took to complete 90° turns, with ‘loess smooth’ line (blue dashed) fitted (inset shows the raw x-y data) (B).

Generally, greater values of AVeY corresponded in a linear fashion with the number of (specified) turn angles. This was particularly evident for 45° turns (Fig. 3A). However, the relationship became weaker as the extent of the turn increased (Fig. 3B), indicating that as the angle of a turn increased the chances of the animal turning back also increased.

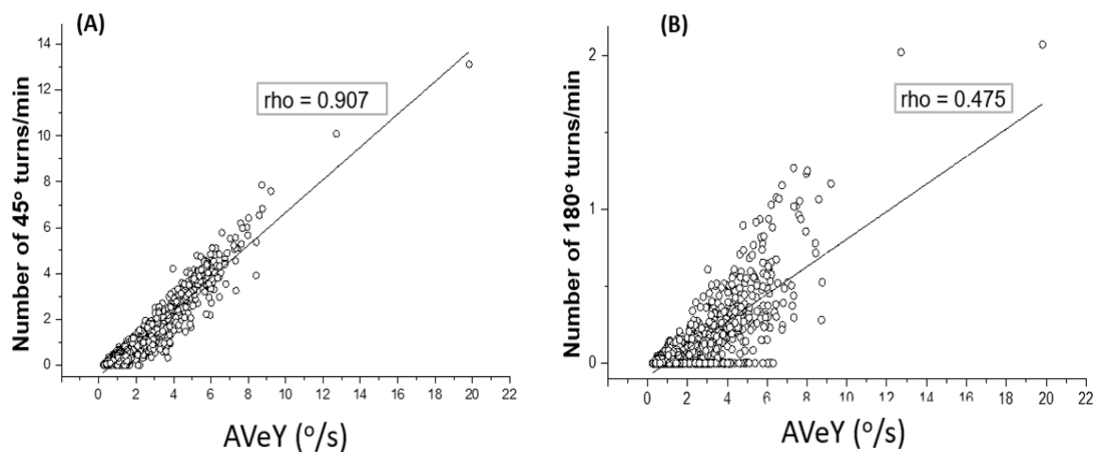


Figure 3. Correlation between values of AVeY (°/s) and the corresponding number of 45° turns (A) and 180° turns (B) per minute. Each data point represents the mean value per flat U-dive (bottom phase duration).

I recognised that the bottom phase of turtle dives showed appreciable variability in recorded parameters, but that they could be broadly divided into apparently 'active' and 'inactive' (or 'quiescent') according to changes in yaw (*cf.* Supplementary Information (SI): Fig. S1). Both types involved little or no change in depth but in the quiescent dives, there were no definitive changes in either the acceleration or geomagnetism traces throughout the duration of the bottom phase, with yaw and VeDBA values also showing marked consistency (Fig. 4A₁). In such cases, CuHe remained static, showing that no 'new' orientation was adopted following the initial descent (with only three 20° turn angles being surpassed during this period for the example in Fig. 4A₁). Frequency distributions were also similar between the three scales of AVeY, indicating changes in directionality were monotonous over time (Fig. 4B₁).

Conversely, 'active' dives showed greater fluctuations in the geomagnetism traces and associated values of yaw, even though the depth, acceleration and VeDBA values showed similar patterns to apparently quiescent bottom phases of dives (*cf.* Fig. 4A₂). Full rotations about the yaw axis as depicted by CuHe, were completed at a relatively consistent rate, as detailed by the percentage coverage of 90° and 180° turns and were nearly exclusively carried out in the clockwise direction, depicting a type of 'circling' behaviour (*cf.* SI: Fig. S2).

There was greater variation between the frequency distributions of the various rates of AVeY (Fig. 4B₂), all of which portrayed a greater spread and skewness compared to the quiescent dives (Fig. 4B₁), signifying a greater variability of turn rates, primarily carried out in one direction.

Measuring angular velocity to determine activity

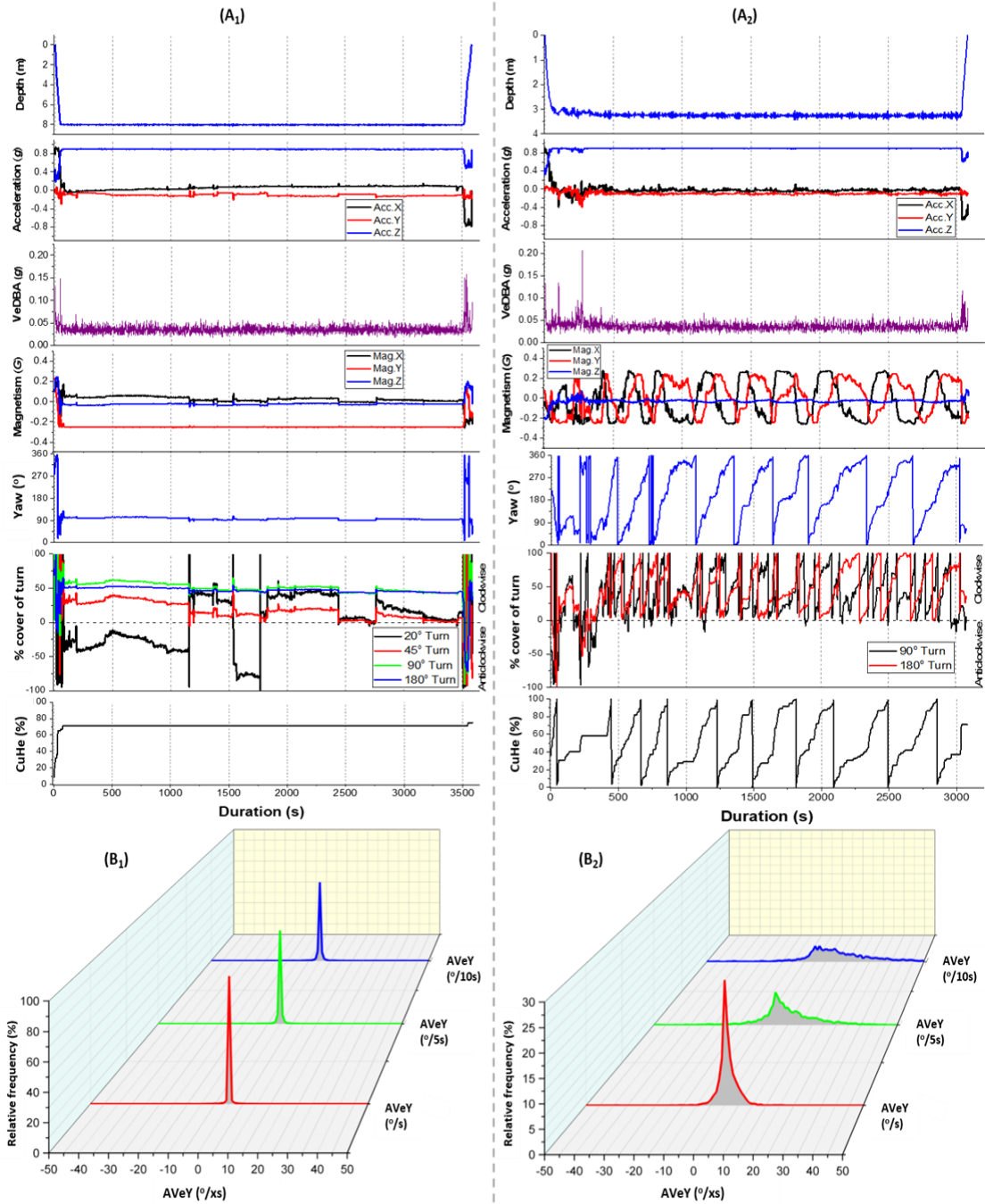


Figure 4. Two flat U-dives similar in duration and differing in activity extent. Stacked line graphs detailing differences between acceleration- and magnetism-based metrics plotted against dive duration. From top to bottom; depth profile, dynamic acceleration and derived VeDBA, magnetism and derived yaw, percentage coverage of various turn extents and CuHe (A). Frequency distribution of AVEY of both dives, calculated at three temporal scales (B).

Calculating AVeY over different intervals and ‘post-smoothing’ at various window lengths highlighted behaviour-specific patterns in signal minima and maxima of AVeY, such as clear alternating fluctuations in heading, even when there seemed no clear pattern observed from acceleration data (e.g., Fig. 5A₁). In the example shown in Fig. 5A₁, changes in heading resulted in 45° turns in both directions, yet 180° turns were never achieved, indicating an activity-specific behaviour with an overall directionality (Fig. 5A₂).

Conversely, patterns apparent in the acceleration data could be further investigated with respect to AVeY to enhance information of the behaviour-specific movement taking place. For example, Fig. 5B Shows relatively consistent deviations recorded from the surge axis (Acc. X), manifest as in spikes of pitch, a pattern which coincided with acute anti-clockwise turns although changes in orientation did not necessarily correspond with clear changes to dynamic acceleration estimates (Fig. 5C).

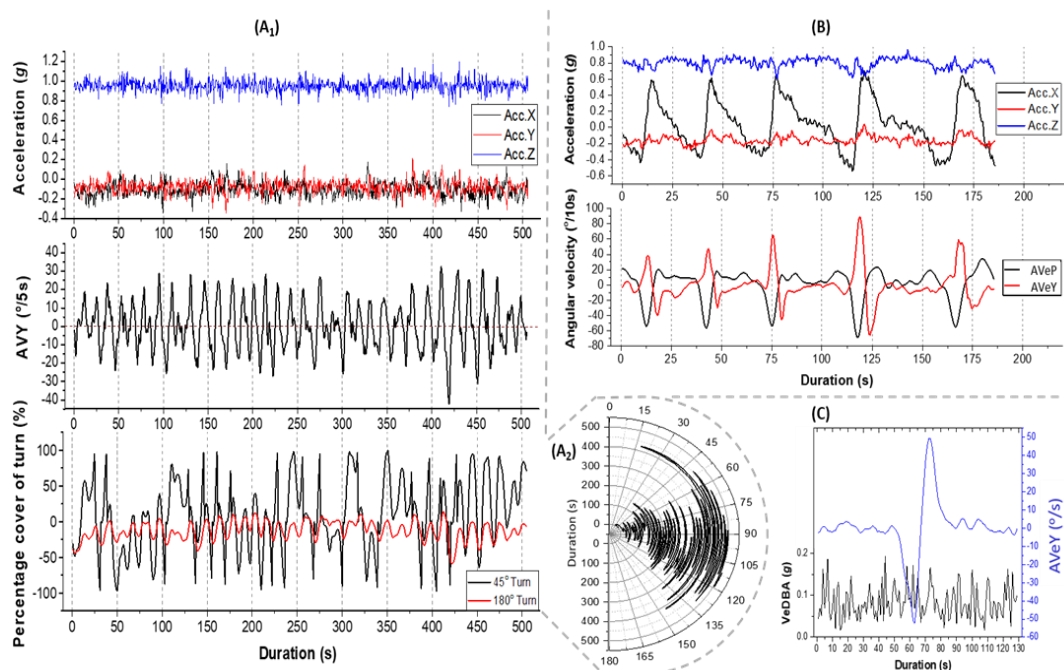


Figure 5. Various examples of activity-specific patterns as resolved by examination of body rotations at various temporal scales and smoothing windows. Stacked line graphs showing the variation in acceleration, AVeY (°/5s) (smoothing window; 3 seconds) and percentage coverage of 45° and 180° turns over an eight-minute period (A₁). Polar theta chart detailing the changes in heading (from A₁) over time (A₂). Stacked line graphs showing the variation in acceleration, AVeP and AVeY (°/s) (smoothing window; 5 seconds) over a three-minute period (B). Changes in VeDBA and AVeY (°/s) (smoothing window; 3 seconds) during a segment of acute turning behaviour (C).

In the turtle data, the different yaw-based metrics were often complementary, showing clear patterns in activity. For example, AVeY (and VeDBA) could show similar changes over a 24-hour period (Fig. 6A) even though higher turn rates did not necessarily correspond with turn extent (Fig. 6B), indicating that different processes were at work over the sample period.

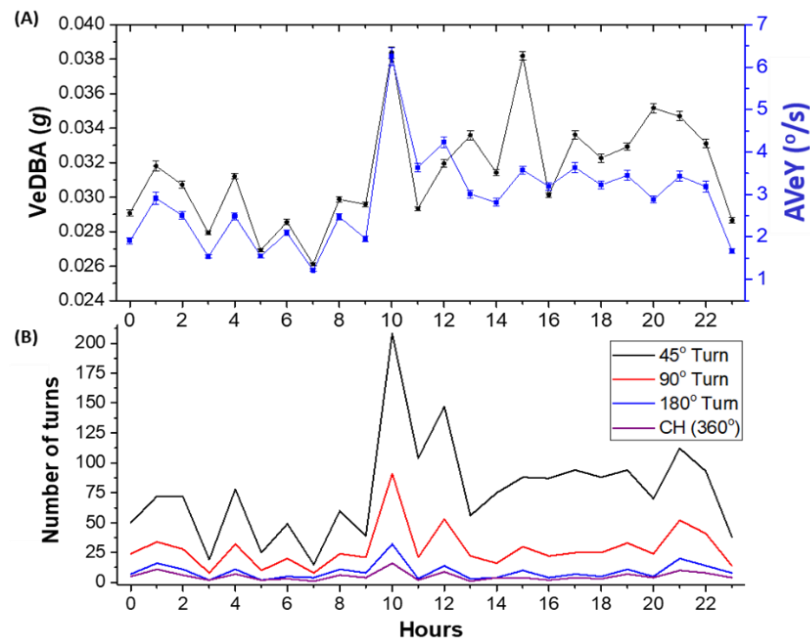


Figure 6. Time series plot of mean values of VeDBA and AVeY (\pm se) per hour over a 24-hour period (A) and the corresponding number of 45°, 90°, 180° turns and complete rotations about the yaw axis (CuHe) (B).

Accumulating (absolute) values of angular rotation across duration of 100 random U-dives demonstrated the variability both within and between dives (Fig. 7). Such a spread of accumulated distributions was less pronounced for acceleration indices. Moreover, the frequency distribution of cumulated AAV gradients was less obviously monomodal than the equivalent VeDBA gradients. CuHe was another diverse yaw-based metric, reflecting the degree and intensity of directionality involved in movement. Behaviours that were manifest by restricted, or no change in direction, resulted in a lower accumulation of unique angles attained around the body's circumference, which was reflected in the small step ranges of CuHe and fewer resets to zero (when 100 % of angles have been covered at least once). Conversely, other,

ostensibly more active behaviours with little overall directionality (i.e., searching) resulted in frequent revolutions. Here, a distinct tri-modal distribution of CuHe frequencies (from same 100 random U-dives mentioned above) was apparent, inferring a distinction between activity/behaviour types (SI: Fig. S3).

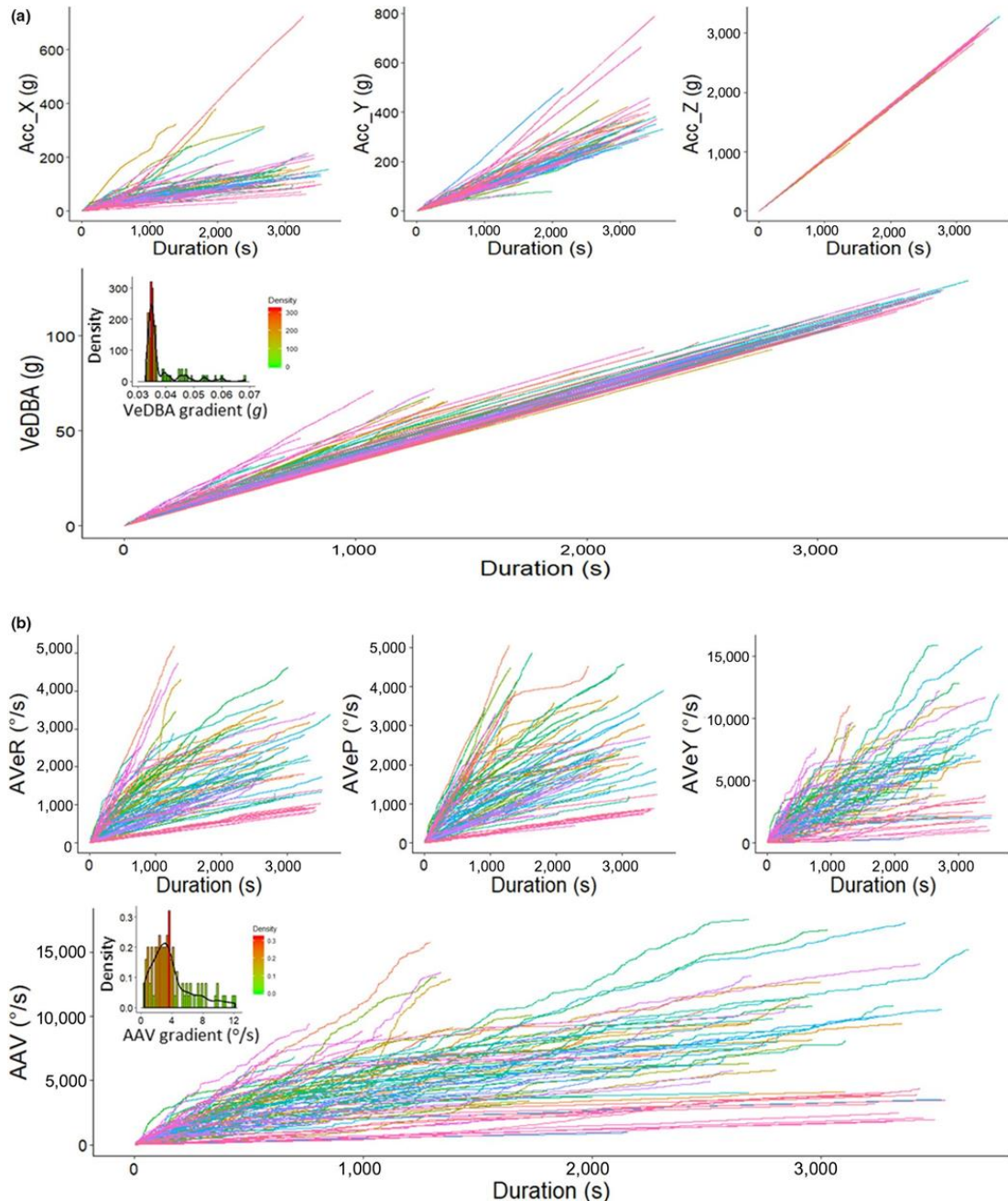


Figure 7. Cumulative frequency of VeDBA (g) (A) and AAV (°/s) (B) across the duration of 100 random U-dives (bottom phase), including their precursor measurements; raw absolute values of acceleration (including both dynamic and static components) from the x- (surge), y- (sway) and z- (heave) channels (A) and absolute values of AVeR, AVeP and AVeY (B). Frequency histogram distribution inlets given for cumulative VeDBA and AAV gradients per dive. Note the much larger spread and variability of patterns when cornering indices of angular rotation.

Discussion

Angular velocity as a metric for animal movement

Movement of the body trunk, nearly always involves some degree of angular rotation (*cf.* Martín López *et al.* 2016), which is perhaps why rotational indices were suggested as a potential activity index two decades ago (*cf.* Hochscheid & Wilson 1999). I was able to show a link between activity extent (as manifest by VeDBA) and angular velocity about all three dimensions of rotation, indicating that movement, in this example animal at least, was rarely confined to a specific axis (Fig. 1). However, the rate of change of yaw was much higher than the equivalent in pitch and roll (Fig. 7). This is not surprising, not least because full rotation about the pitch and roll axes necessitates body inversion whereas in yaw it does not. In addition, turning about the yaw axis is an important component of behaviour for most animals, particularly during navigation, escape, search, foraging and hunting strategies (Ballerini *et al.* 2008; Wilson *et al.* 2013b). For ostensibly technical reasons however, yaw metrics seem to have been largely overlooked in animal activity and behaviour studies (excepting studies using gyroscopes, e.g., Kawabata *et al.* (2014)).

The extent to which yaw angle changes compared to pitch or roll (metrics for angular turn extent are about 4 times higher for yaw than pitch or roll in these turtles – *cf.* Fig. 1) indicates that yaw likely has greater scope and range than pitch or roll as a behaviour identifier (and at the very least, should complement them). This will be particularly the case as the extent of any angular turns decreases so that recorded changes impinge on the resolution capacity of the sensors, as may particularly be the case in very slow-moving animals. For these reasons, I have primarily focused on the yaw dimension of rotation to demonstrate its utility for assessing both general-scale differences in activity extent and fine-scale behaviour-specific movements. Care should be taken to determine that this is the case for the study species though, since animals engage in a variety of rotational movement about their principle axes (*cf.* Tinbergen 1963). Indeed, a more sophisticated approach could consider pitch-, roll- and yaw-specific rotations together as signatures of particular behaviours (*cf.* Fig. 5B).

In a similar manner, consideration of multiple metrics for angular changes in yaw over time are complimentary. For example, periods of high AVEY do not necessarily correspond with high turn extent (*cf.* Fig. 3), but indicate rapid, but non-extensive, changes in heading. This can be symptomatic of a particular behaviour such as searching by an animal following environmental cues (*cf.* Basil & Atema 1994). Indeed, these turtles often exhibited activities consisting of high AVEY, signifying quick transitions between small turn extents, with such oscillating yaw movements accompanied by a high degree of directionality likely resulting from benthic surveying (Fig. 5A₁). By contrast, great turn extents in a particular directional plane shows circling behaviour (*cf.* Fig. 4A₂, SI: Fig. S2), important for a suite of situations (Narazaki *et al.* 2021) ranging from birds soaring on thermals (Williams *et al.* 2018) to turtle courtship (Schofield *et al.* 2007). Importantly though, the lack of any rotation about the yaw axis can equally be used (in conjunction with other sensor outputs) to define resting behaviour more appropriately than can be done using accelerometers alone (Fig. 4). This is especially the case in slow-moving species where yaw metrics are of particular value for much longer-term investigations (Fig. 6). Thus, aggregation of mean epochs of, for example, hourly AVEY estimates in relation to the accumulation of the number of various turn extents, can highlight minimal, but important, activity and provide detailed changes of activity over days. Such a broad approach is particularly relevant for reptiles (*cf.* Shine 2005) and many invertebrates (*cf.* McLeese 1973) where body orientation changes can occur over much longer time periods than is normal for mammals or birds and for which acceleration data serve well to define activity.

Tri-axial magnetometers have two main drawbacks though: Firstly, being a vector field sensor, only two rotational degrees of freedom are measured at any one time and so angular rotation cannot be resolved should one sensor axis align with respect to the Earth's magnetic inclination lines (*cf.* Johnson & Tyack 2003; Martín López *et al.* 2016). Secondly, the derivation procedure of pitch and roll (required in the computation of heading) breaks down during bouts of fast, erratic behaviour (e.g.,

during rapid cornering; (e.g., during rapid cornering; *cf.* McNarry *et al.* 2017), because it can be difficult to separate the static from the dynamic component of acceleration at such times, which can cause subsequent inaccuracies of all three rotational axes' derivatives (Noda *et al.* 2012). Choice of study animal, tag attachment method, animal location on Earth and the period over which any differential is calculated, are key parameters to consider when assessing the likelihood and extent of such limitations

Relationship between AVeY and VeDBA

VeDBA has been used extensively as an acceleration-based proxy for activity-specific energy expenditure (e.g., Stothart *et al.* 2016; Jeanniard-du-Dot *et al.* 2017; Wilson *et al.* 2020a). This is based on the theoretical understanding that movement of most vertebrates is the main factor in modulating energy expenditure (Gleiss, Wilson & Shepard 2011; Qasem *et al.* 2012). The more vigorous the movement, the more energy is expended in muscular contraction, with any change in measured body acceleration being proportional to the muscular forces that displaced the animal's body (and therefore the attached sensor - according to Newton's first law, Miwa *et al.* 2015). Consequently, the integrated measure of dynamic acceleration from each of the three spatial dimensions has been proposed to reflect the mechanical equivalent to energy expenditure involved in movement. I documented a clear relationship between VeDBA and AVeY across each turtle (Fig. 2A) and this is presumably because turning comprises an appreciable fraction of overall movement costs (McNarry *et al.* 2017; Wilson *et al.* 2020b). Specifically, a body that moves in a circular motion (of radius r) at constant speed (v) is always being accelerated at right angles to the direction of motion (towards the centre of the circle of magnitude v^2 / r). Given that Force = mass \times acceleration ($F = m * (v^2 / r)$) and it is typically the animal that supplies the force through muscular contraction (Halsey *et al.* 2011), more acute and higher frequency turns are associated with greater energy expenditure (Wilson *et al.* 2013a; Wilson *et al.* 2013b; McNarry *et al.* 2017; Wilson *et al.* 2020b; Fig. 2A, Fig. 2B). Taken together then, assessing the frequency and extent of turns can be

helpful for understanding aspects of animal energy expenditure and the motivations behind behaviour (however identified), since the degree and associated cost of angular rotation is modulated by movement decisions (Vásquez, Ebensperger & Bozinovic 2002). It is worth noting however, that turn costs increase non-linearly with speed and thus it is far more efficient to turn while stationary/slow-moving, in order to minimise the perpendicular forces and duration of a turn (*cf.* McNarry *et al.* 2017; Wilson *et al.* 2020b). This may partially explain the spread of VeDBA values during acute turns (Fig. 2B), and why AVeY does not necessarily scale nicely with VeDBA over time (Fig. 4B₂, Fig. 5C, Fig. 6A).

Advantages of AVeY over acceleration estimates

Acceleration measured by animal-attached tags is susceptible to the specific site of tag placement, so that data from tags that are deployed on, for example, animal carapaces that vary in morphology (including some reptiles, crustaceans and gastropod species), are particularly likely to incur this problem, making DBA-type metrics difficult to compare between individuals (*cf.* Wilson *et al.* 2020a). The problem is also likely to be manifest to some extent even when animals are morphologically similar, simply because the researchers do not place the tags identically on all individuals. Yaw metrics such as those proposed here (AVeY and angular extent) do not suffer from this problem because they are corrected in their derivation (see methods). In fact, the difference in susceptibility to tag orientation between accelerometer- and magnetometer-derived metrics appears within these turtle datasets, which showed markedly different VeDBA *versus* AVeY relationships for the different individuals (Fig. 2A). Note though, that the derivation of pitch and roll becomes problematic when they approach $\pm 90^\circ$, when x, y and z values can become inversed. As such, large offsets in position would be problematic, since it restricts the range for accurate measurements of pitch and roll to be made (consequently affecting the accuracy of yaw). This assumption, therefore, breaks down for animals that change orientations frequently at angles greater than

perpendicular from their longitudinal and lateral axes of 'normal' posture. However, this is less problematic for slow-moving animals (such as the turtle).

The broad use of DBA metrics as a measure of movement and energy use for many vertebrates to date indicates their utility. However, for turtles, the narrower operational range of VeDBA increases the contribution of relative error from discrepancies in tag placement, which, in turn, can make separation of energy-specific behaviours between individuals more challenging. This was the case in these datasets, with an extremely low range of VeDBA estimates and notable offsets between turtles (Fig. 2A). Furthermore, various scales of AVeY reported here revealed repetitive patterns in rotational movement that were not evident in acceleration data during short-term behavioural bouts (Fig. 4A₂, Fig. 5A₁). I suggest that, in its simplest form, fine temporal responses of orientation may indicate a change in 'state', presumably from an underlying sensory input or physiological demand and this may not always be reflected from the culmination of dynamic movement as manifest by accelerometers (Fig. 5c). Crucially, since angular velocity about the three axes of rotation is not affected by discrepancies of tag placements (though see above), it provides a standardised comparator of movement between individuals.

Changes in the recorded acceleration, may not always result from movement arising from the limbs. These may, for example, arise from external forces acting on the animal, such as current vectors in the water (Ropert-Coudert & Wilson 2004) which will tend to translate the body rather than rotate it. I suggest that AVeY and AAV should be used as a measure for activity that is complimentary to DBA, being particularly valuable when DBA-type metrics are weak and when behaviours can be exemplified according to the scale (or lack of) and pattern of angular rotation exerted. Lastly, whilst this study does not provide specific ground-truthing of the exact 'type' of behaviour involved, clear patterns emerge using this approach that would otherwise be left unresolved if only acceleration estimates were considered (Fig. 7). The advantages of animal-attached logging systems include to pry more deeply into the movement ecology of animals independent of direct observation, especially

when observer monitoring is difficult, such is the case with free-ranging turtles. However, inference without ground-truthing does not determine the finding irrelevant (Collins *et al.* 2015). Previous studies have made subjective behavioural assignments using prior knowledge and an objective intuition of what acceleration-based measures infer (*cf.* Laich *et al.* 2008; Collins *et al.* 2015; Williams *et al.* 2015). With regards to turtles, underwater behaviour has mostly been inferred from speculation based on 'dive profiles' (2-D representation of depth versus time). The fact that trends of movement can be resolved more finely using indices of angular velocity, especially during slow scales of movement (pertinent in this study), only aids in objectively quantifying behavioural differences. I suggest that variation of heading in a specified time frame is intrinsically linked to the functional behaviour motivation exhibited. Estimates that are consistent in the magnitude and pattern of change reveal a behaviour that is consistent in its vector of imparted motion (or rotation) (*cf.* Fig. 5, SI: Fig. S3). Crucially however, even 'noisy' variations in AVeY may indicate more notable differences between activity-specific behaviours that acceleration estimates do not (Fig. 7).

Conclusion

This work assessed the value of animal heading (body orientation) and associated metrics for quantifying animal activity and for helping define behaviours. My results show that incorporating the frequency and extent of yaw axis rotations at various temporal scales aids in resolving patterns of movement beyond that which acceleration-based metrics alone can detail. I suggest that yaw-based metrics should help identify animal behaviour and as indices of general activity over both short- and long-term periods, especially (within an energetic context) for slow-moving animals. It would be useful to have AVeY and AAV metrics compared to oxygen consumption to check their validity as a potential proxy of energy expenditure. Further work should assess the value of AVeY on a suite of terrestrial, aquatic and volant animals, varying in activity extent and behaviour. Judicious choice of sampling intervals and smoothing windows will be important considerations in this.

References

- Ballerini, M., Cabibbo, N., Candelier, R., Cavagna, A., Cisbani, E., Giardina, I., Orlandi, A., Parisi, G., Procaccini, A. & Viale, M. (2008) An empirical study of large, naturally occurring starling flocks: a benchmark in collective animal behaviour. *arXiv preprint arXiv:0802.1667*.
- Basil, J. & Atema, J. (1994) Lobster orientation in turbulent odor plumes: simultaneous measurement of tracking behavior and temporal odor patterns. *The Biological Bulletin*, **187**, 272-273.
- Bates, D., Mächler, M., Bolker, B. & Walker, S. (2015) Fitting Linear Mixed-Effects Models Using lme4. *2015*, **67**, 48.
- Benoit, L., Hewison, A.J.M., Coulon, A., Debeffe, L., Grémillet, D., Ducros, D., Cargnelutti, B., Chaval, Y. & Morellet, N. (2020) Accelerating across the landscape: The energetic costs of natal dispersal in a large herbivore. *Journal of Animal Ecology*, **89**, 173-185.
- Bidder, O.R., Walker, J.S., Jones, M.W., Holton, M.D., Urge, P., Scantlebury, D.M., Marks, N.J., Magowan, E.A., Maguire, I.E. & Wilson, R.P. (2015) Step by step: reconstruction of terrestrial animal movement paths by dead-reckoning. *Movement Ecology*, **3**, 23.
- Brown, D.D., Kays, R., Wikelski, M., Wilson, R. & Klimley, A.P. (2013) Observing the unwatchable through acceleration logging of animal behavior. *Animal Biotelemetry*, **1**, 20.
- Caruso, M.J. (2000) Applications of magnetic sensors for low cost compass systems. *IEEE 2000. Position Location and Navigation Symposium (Cat. No.00CH37062)*, pp. 177-184.
- Chakravarty, P., Maalberg, M., Cozzi, G., Ozgul, A. & Aminian, K. (2019) Behavioural compass: animal behaviour recognition using magnetometers. *Movement Ecology*, **7**, 28.
- Clark, C.J. (2009) Courtship dives of Anna's hummingbird offer insights into flight performance limits. *Proceedings of the Royal Society B: Biological Sciences*, **276**, 3047-3052.
- Collins, P.M., Green, J.A., Warwick-Evans, V., Dodd, S., Shaw, P.J.A., Arnould, J.P.Y. & Halsey, L.G. (2015) Interpreting behaviors from accelerometry: a method combining simplicity and objectivity. *Ecology and Evolution*, **5**, 4642-4654.
- Eckert, S.A. (2002) Swim speed and movement patterns of gravid leatherback sea turtles (*Dermochelys coriacea*) at St Croix, US Virgin Islands. *Journal of Experimental Biology*, **205**, 3689-3697.
- Fehlmann, G., O'Riain, M.J., Hopkins, P.W., O'Sullivan, J., Holton, M.D., Shepard, E.L.C. & King, A.J. (2017) Identification of behaviours from accelerometer data in a wild social primate. *Animal Biotelemetry*, **5**, 6.
- Fong, W.T., Ong, S.K. & Nee, A.Y.C. (2008) Methods for in-field user calibration of an inertial measurement unit without external equipment. *Measurement Science and Technology*, **19**, 085202.
- Gebre-Egziabher, D., Elkaim, G.H., Powell, D.J. & Parkinson, B.W. (2006) Calibration of Strapdown Magnetometers in Magnetic Field Domain. *Journal of Aerospace Engineering*, **19**, 87-102.
- Gerencsér, L., Vásárhelyi, G., Nagy, M., Vicsek, T. & Miklósi, A. (2013) Identification of Behaviour in Freely Moving Dogs (*Canis familiaris*) Using Inertial Sensors. *PLOS ONE*, **8**, e77814.

- Gleiss, A.C., Wilson, R.P. & Shepard, E.L.C. (2011) Making overall dynamic body acceleration work: on the theory of acceleration as a proxy for energy expenditure. *Methods in Ecology and Evolution*, **2**, 23-33.
- Halsey, L.G., Jones, T.T., Jones, D.R., Liebsch, N. & Booth, D.T. (2011) Measuring Energy Expenditure in Sub-Adult and Hatchling Sea Turtles via Accelerometry. *PLOS ONE*, **6**, e22311.
- Halsey, L.G., Shepard, E.L.C. & Wilson, R.P. (2011) Assessing the development and application of the accelerometry technique for estimating energy expenditure. *Comparative Biochemistry and Physiology Part A: Molecular & Integrative Physiology*, **158**, 305-314.
- Hochscheid, S. & Wilson, R.P. (1999) A new method for the determination of at-sea activity in sea turtles. *Marine Ecology Progress Series*, **185**, 293-296.
- Houghton, J.D., Broderick, A.C., Godley, B.J., Metcalfe, J.D. & Hays, G.C. (2002) Diving behaviour during the internesting interval for loggerhead turtles *Caretta caretta* nesting in Cyprus. *Marine Ecology Progress Series*, **227**, 63-70.
- Jeanniard-du-Dot, T., Guinet, C., Arnould, J.P.Y., Speakman, J.R. & Trites, A.W. (2017) Accelerometers can measure total and activity-specific energy expenditures in free-ranging marine mammals only if linked to time-activity budgets. *Functional Ecology*, **31**, 377-386.
- Johnson, M.P. & Tyack, P.L. (2003) A digital acoustic recording tag for measuring the response of wild marine mammals to sound. *IEEE Journal of Oceanic Engineering*, **28**, 3-12.
- Kano, F., Walker, J., Sasaki, T. & Biro, D. (2018) Head-mounted sensors reveal visual attention of free-flying homing pigeons. *Journal of Experimental Biology*, **221**.
- Kawabata, Y., Noda, T., Nakashima, Y., Nanami, A., Sato, T., Takebe, T., Mitamura, H., Arai, N., Yamaguchi, T. & Soyano, K. (2014) Use of a gyroscope/accelerometer data logger to identify alternative feeding behaviours in fish. *Journal of Experimental Biology*, **217**, 3204-3208.
- Kuznetsova, A., Brockhoff, P. & Christensen, R. (2017) lmerTest Package: Tests in Linear Mixed Effects Models. *Journal of Statistical Software*, **82**, 1-26.
- Laich, A.G., Wilson, R.P., Quintana, F. & Shepard, E.L. (2008) Identification of imperial cormorant *Phalacrocorax atriceps* behaviour using accelerometers. *Endangered Species Research*, **10**, 29-37.
- Laplanche, C., Marques, T.A. & Thomas, L. (2015) Tracking marine mammals in 3D using electronic tag data. *Methods in Ecology and Evolution*, **6**, 987-996.
- Martín López, L.M., Aguilar de Soto, N., Miller, P. & Johnson, M. (2016) Tracking the kinematics of caudal-oscillatory swimming: a comparison of two on-animal sensing methods. *The Journal of Experimental Biology*, **219**, 2103-2109.
- Martín López, L.M., Miller, P.J.O., Aguilar de Soto, N. & Johnson, M. (2015) Gait switches in deep-diving beaked whales: biomechanical strategies for long-duration dives. *Journal of Experimental Biology*, **218**, 1325-1338.
- Martiskainen, P., Järvinen, M., Skön, J.-P., Tiirikainen, J., Kolehmainen, M. & Mononen, J. (2009) Cow behaviour pattern recognition using a three-dimensional accelerometer and support vector machines. *Applied Animal Behaviour Science*, **119**, 32-38.
- McClune, D.W., Marks, N.J., Wilson, R.P., Houghton, J.D.R., Montgomery, I.W., McGowan, N.E., Gormley, E. & Scantlebury, M. (2014) Tri-axial accelerometers quantify behaviour in the Eurasian badger (*Meles meles*): towards an automated interpretation of field data. *Animal Biotelemetry*, **2**, 5.

- McLeese, D.W. (1973) Orientation of Lobsters (*Homarus americanus*) to Odor. *Journal of the Fisheries Research Board of Canada*, **30**, 838-840.
- McNarry, M.A., Wilson, R.P., Holton, M.D., Griffiths, I.W. & Mackintosh, K.A. (2017) Investigating the relationship between energy expenditure, walking speed and angle of turning in humans. *PLOS ONE*, **12**, e0182333.
- Miwa, M., Oishi, K., Nakagawa, Y., Maeno, H., Anzai, H., Kumagai, H., Okano, K., Tobioka, H. & Hirooka, H. (2015) Application of Overall Dynamic Body Acceleration as a Proxy for Estimating the Energy Expenditure of Grazing Farm Animals: Relationship with Heart Rate. *PLOS ONE*, **10**, e0128042.
- Narazaki, T., Nakamura, I., Aoki, K., Iwata, T., Shiomi, K., Luschi, P., Suganuma, H., Meyer, C.G., Matsumoto, R., Bost, C.A., Handrich, Y., Amano, M., Okamoto, R., Mori, K., Ciccione, S., Bourjea, J. & Sato, K. (2021) Similar circling movements observed across marine megafauna taxa. *iScience*, 102221.
- Nathan, R., Getz, W.M., Revilla, E., Holyoak, M., Kadmon, R., Saltz, D. & Smouse, P.E. (2008) A movement ecology paradigm for unifying organismal movement research. *Proceedings of the National Academy of Sciences*, **105**, 19052-19059.
- Noda, T., Kawabata, Y., Arai, N., Mitamura, H. & Watanabe, S. (2013) Monitoring Escape and Feeding Behaviours of Cruiser Fish by Inertial and Magnetic Sensors. *PLOS ONE*, **8**, e79392.
- Noda, T., Kawabata, Y., Arai, N., Mitamura, H. & Watanabe, S. (2014) Animal-mounted gyroscope/accelerometer/magnetometer: In situ measurement of the movement performance of fast-start behaviour in fish. *Journal of Experimental Marine Biology and Ecology*, **451**, 55-68.
- Noda, T., Okuyama, J., Koizumi, T., Arai, N. & Kobayashi, M. (2012) Monitoring attitude and dynamic acceleration of free-moving aquatic animals using a gyroscope. *Aquatic Biology*, **16**, 265-276.
- Ozyagcilar, T. (2012) Implementing a tilt-compensated eCompass using accelerometer and magnetometer sensors. *Freescale semiconductor, Application Note, AN4248*, Austin, TX.
- Painter, M.S., Blanco, J.A., Malkemper, E.P., Anderson, C., Sweeney, D.C., Hewgley, C.W., Červený, J., Hart, V., Topinka, V., Belotti, E., Burda, H. & Phillips, J.B. (2016) Use of bio-loggers to characterize red fox behavior with implications for studies of magnetic alignment responses in free-roaming animals. *Animal Biotelemetry*, **4**, 20.
- Patterson, A., Gilchrist, H.G., Chivers, L., Hatch, S. & Elliott, K. (2019) A comparison of techniques for classifying behavior from accelerometers for two species of seabird. *Ecology and Evolution*, **9**, 3030-3045.
- Patterson, T.A., Thomas, L., Wilcox, C., Ovaskainen, O. & Matthiopoulos, J. (2008) State-space models of individual animal movement. *Trends in Ecology & Evolution*, **23**, 87-94.
- Pedley, M. (2012) eCompass-Build and Calibrate a Tilt-Compensating Electronic Compass. *Circuit Cellar-The Magazine For Computer Applications*, 1-6.
- Pewsey, A., Neuhäuser, M. & Ruxton, G.D. (2013) *Circular Statistics in R*. OUP Oxford.
- Qasem, L., Cardew, A., Wilson, A., Griffiths, I., Halsey, L.G., Shepard, E.L.C., Gleiss, A.C. & Wilson, R. (2012) Tri-Axial Dynamic Acceleration as a Proxy for Animal Energy Expenditure; Should We Be Summing Values or Calculating the Vector? *PLOS ONE*, **7**, e31187.
- Renaudin, V., Afzal, M.H. & Lachapelle, G. (2010) Complete Triaxis Magnetometer Calibration in the Magnetic Domain. *Journal of Sensors*, **2010**, 967245.

- Ropert-Coudert, Y. & Wilson, R.P. (2004) Subjectivity in bio-logging: do logged data mislead? *Memoirs of the National Institute of Polar Research: Special Issue*, **58**, 23-33.
- Rutkowski, L., Jaworski, M. & Duda, P. (2020) *Stream data mining: Algorithms and their probabilistic properties*, 1 edn. Springer, Cham, Switzerland.
- Samarasinghe, S. (2016) *Neural Networks for Applied Sciences and Engineering: From Fundamentals to Complex Pattern Recognition*. CRC Press.
- Schofield, G., Katselidis, K.A., Pantis, J.D., Dimopoulos, P. & Hays, G.C. (2007) Female–female aggression: structure of interaction and outcome in loggerhead sea turtles. *Marine Ecology Progress Series*, **336**, 267-274.
- Shepard, E.L., Wilson, R.P., Halsey, L.G., Quintana, F., Laich, A.G., Gleiss, A.C., Liebsch, N., Myers, A.E. & Norman, B. (2008) Derivation of body motion via appropriate smoothing of acceleration data. *Aquatic Biology*, **4**, 235-241.
- Shepard, E.L., Wilson, R.P., Rees, W.G., Grundy, E., Lambertucci, S.A. & Vosper, S.B. (2013) Energy Landscapes Shape Animal Movement Ecology. *The American Naturalist*, **182**, 298-312.
- Shine, R. (2005) Life-History Evolution in Reptiles. *Annual Review of Ecology, Evolution, and Systematics*, **36**, 23-46.
- Stothart, M.R., Elliott, K.H., Wood, T., Hatch, S.A. & Speakman, J.R. (2016) Counting calories in cormorants: dynamic body acceleration predicts daily energy expenditure measured in pelagic cormorants. *Journal of Experimental Biology*, **219**, 2192-2200.
- Tinbergen, N. (1963) On aims and methods of Ethology. *Zeitschrift für Tierpsychologie*, **20**, 410-433.
- Vásquez, R.A., Ebensperger, L.A. & Bozinovic, F. (2002) The influence of habitat on travel speed, intermittent locomotion, and vigilance in a diurnal rodent. *Behavioral Ecology*, **13**, 182-187.
- Walker, J.A. & Westneat, M.W. (2000) Mechanical performance of aquatic rowing and flying. *Proceedings of the Royal Society of London. Series B: Biological Sciences*, **267**, 1875-1881.
- Walker, J.S., Jones, M.W., Laramee, R.S., Holton, M.D., Shepard, E.L.C., Williams, H.J., Scantlebury, D.M., Marks, N.J., Magowan, E.A., Maguire, I.E., Bidder, O.R., Di Virgilio, A. & Wilson, R.P. (2015) Prying into the intimate secrets of animal lives; software beyond hardware for comprehensive annotation in 'Daily Diary' tags. *Movement Ecology*, **3**, 29.
- Wang, Y., Nickel, B., Rutishauser, M., Bryce, C.M., Williams, T.M., Elkaim, G. & Wilmers, C.C. (2015) Movement, resting, and attack behaviors of wild pumas are revealed by tri-axial accelerometer measurements. *Movement Ecology*, **3**, 1-12.
- Williams, H., Shepard, E., Duriez, O. & Lambertucci, S.A. (2015) Can accelerometry be used to distinguish between flight types in soaring birds? *Animal Biotelemetry*, **3**, 1-11.
- Williams, H.J., Duriez, O., Holton, M.D., Dell'Omo, G., Wilson, R.P. & Shepard, E.L.C. (2018) Vultures respond to challenges of near-ground thermal soaring by varying bank angle. *Journal of Experimental Biology*, **221**.
- Williams, H.J., Holton, M.D., Shepard, E.L.C., Largey, N., Norman, B., Ryan, P.G., Duriez, O., Scantlebury, M., Quintana, F., Magowan, E.A., Marks, N.J., Alagaili, A.N., Bennett, N.C. & Wilson, R.P. (2017) Identification of animal movement patterns using tri-axial magnetometry. *Movement Ecology*, **5**, 6.
- Wilmers, C.C., Nickel, B., Bryce, C.M., Smith, J.A., Wheat, R.E. & Yovovich, V. (2015) The golden age of bio-logging: How animal-borne sensors are advancing the frontiers of ecology. *Ecology*, **96**, 1741-1753.

- Wilson, A.D., Wikelski, M., Wilson, R.P. & Cooke, S.J. (2015) Utility of biological sensor tags in animal conservation. *Conservation Biology*, **29**, 1065-1075.
- Wilson, J.W., Mills, M.G., Wilson, R.P., Peters, G., Mills, M.E., Speakman, J.R., Durant, S.M., Bennett, N.C., Marks, N.J. & Scantlebury, M. (2013a) Cheetahs, *Acinonyx jubatus*, balance turn capacity with pace when chasing prey. *Biology Letters*, **9**, 20130620.
- Wilson, R., Griffiths, I., Legg, P., Friswell, M., Bidder, O., Halsey, L., Lambertucci, S.A. & Shepard, E. (2013b) Turn costs change the value of animal search paths. *Ecology Letters*, **16**, 1145-1150.
- Wilson, R.P., Börger, L., Holton, M.D., Scantlebury, D.M., Gómez-Laich, A., Quintana, F., Rosell, F., Graf, P.M., Williams, H., Gunner, R., Hopkins, L., Marks, N., Geraldi, N.R., Duarte, C.M., Scott, R., Strano, M.S., Robotka, H., Eizaguirre, C., Fahlman, A. & Shepard, E.L.C. (2020a) Estimates for energy expenditure in free-living animals using acceleration proxies: A reappraisal. *Journal of Animal Ecology*, **89**, 161-172.
- Wilson, R.P., Holton, M.D., di Virgilio, A., Williams, H., Shepard, E.L.C., Lambertucci, S., Quintana, F., Sala, J.E., Balaji, B., Lee, E.S., Srivastava, M., Scantlebury, D.M. & Duarte, C.M. (2018) Give the machine a hand: A Boolean time-based decision-tree template for rapidly finding animal behaviours in multisensor data. *Methods in Ecology and Evolution*, **9**, 2206-2215.
- Wilson, R.P., Liebsch, N., Davies, I.M., Quintana, F., Weimerskirch, H., Storch, S., Lucke, K., Siebert, U., Zankl, S., Müller, G., Zimmer, I., Scolaro, A., Campagna, C., Plötz, J., Bornemann, H., Teilmann, J. & McMahan, C.R. (2007) All at sea with animal tracks; methodological and analytical solutions for the resolution of movement. *Deep Sea Research Part II: Topical Studies in Oceanography*, **54**, 193-210.
- Wilson, R.P., Rose, K.A.R., Metcalfe, R.S., Holton, M.D., Redcliffe, J., Gunner, R.M., Börger, L., Loison, A., Miloš, J., Painter, M.S., Silovský, V., Marks, N., Garel, M., Toigo, C., Marchand, P., Bennett, N.C., McNarry, M.A., Mackintosh, K.A., Brown, M.R. & Scantlebury, D.M. (2020b) Path tortuosity changes the transport cost paradigm in terrestrial animals. *bioRxiv*, 2020.2008.2020.259390.
- Wilson, R.P., Shepard, E. & Liebsch, N. (2008) Prying into the intimate details of animal lives: use of a daily diary on animals. *Endangered Species Research*, **4**, 123-137.
- Wyneken, J. (1997) *Sea turtle locomotion: mechanics, behavior, and energetics*. CRC Press, Boca Raton.
- Yoda, K., Naito, Y., Sato, K., Takahashi, A., Nishikawa, J., Ropert-Coudert, Y., Kurita, M. & Le Maho, Y. (2001) A new technique for monitoring the behaviour of free-ranging Adelie penguins. *Journal of Experimental Biology*, **204**, 685-690.
- Zimmer, I., Ropert-Coudert, Y., Kato, A., Ancel, A. & Chiaradia, A. (2011) Does Foraging Performance Change with Age in Female Little Penguins (*Eudyptula minor*)? *PLOS ONE*, **6**, e16098.

Chapter 3

Activity of loggerhead turtles during the U-shaped dive: insights using angular velocity metrics

Richard M. Gunner



Photo taken by Dr Rebecca Scott

This work was published in *Endangered Species Research* as:

Gunner, R.M., Wilson, R.P., Holton, M.D., Scott, R., Arkwright, A., Fahlman, A., Ulrich, M., Hopkins, P., Duarte, C. and Eizaguirre, C., 2021. Activity of loggerhead turtles during the U-shaped dive: insights using angular velocity metrics. *Endangered Species Research*, 45, pp.1-12, DOI: <https://doi.org/10.3354/esr01125>

Abstract

Understanding the behavioural ecology of endangered taxa can inform conservation strategies. The activity budgets of the loggerhead turtle *Caretta caretta* are still poorly understood because many tracking methods show only horizontal displacement and ignore dives and associated behaviours. However, time-depth recorders have enabled researchers to identify flat, U-shaped dives (or type 1a dives) and these are conventionally labelled as resting dives on the seabed because they involve no vertical displacement of the animal during the bottom phase. Video- and acceleration-based studies have demonstrated this is not always true. Focusing on sea turtles nesting on the Cabo Verde archipelago, I describe a new metric derived from magnetometer data, absolute angular velocity, that integrates indices of angular rotation in the horizontal plane to infer activity. Using this metric, I evaluated the variation in putative resting behaviours during the bottom phase of type 1a dives for 5 individuals over 13 to 17 d at sea during a single inter-nesting interval (over 75 turtle d in total). I defined absolute resting within the bottom phase of type 1a dives as periods with no discernible acceleration or angular movement. Whilst absolute resting constituted a significant proportion of each turtle's time budget for this 1a dive type, turtles allocated 16–38 % of their bottom time to activity, with many dives being episodic, comprised of intermittent bouts of rest and rotational activity. This implies that previously considered resting (and/or vigilance) behaviours are complex and need to be accounted for in energy budgets, particularly since energy budgets may impact conservation strategies.

Background

Sea turtles spend almost all of their lives at sea, which creates logistic difficulties in collecting data that may be relevant to their conservation (Gilman, Moth-Poulsen & Bianchi 2007; Hochscheid 2014; Wallace, Zolkewitz & James 2015; Butt, Whiting & Dethmers 2016; Mingozi *et al.* 2016). This is particularly true with respect to behaviours associated with space-use and energy expenditure (López-Sepulcre 2007; Greggor *et al.* 2016). However, animal-attached logging devices have provided researchers with a powerful tool to record patterns of behaviour, even when turtles are underwater. A tag commonly used for this is the time depth recorder (TDR, Hays, Marshall & Seminoff 2007; Hart *et al.* 2010; Wilson *et al.* 2017; Dodge *et al.* 2018), which provides information on depth use over time, from which dive profiles can be reconstructed (Eckert *et al.* 1986; Hays *et al.* 2002b; Rice & Balazs 2008). These dive profiles have been broadly classified into five or six distinguishable types through their marked repetition and consistent patterns (Minamikawa, Naito & Uchida 1997; Hochscheid *et al.* 1999; Hays *et al.* 2000; Houghton *et al.* 2002; Hochscheid 2014; Wilson *et al.* 2017).

Different dive types are hypothesised to reflect changes in behavioural motivation and associated activity levels (Hochscheid 2014). For example, 'type 1a' dives, flat U-shaped dives, are very common among sea turtles (Hochscheid *et al.* 2007; Cheng 2009), and are typically associated with resting (Hays *et al.* 2000; Seminoff, Jones & Marshall 2006; Hays 2008; Cheng 2009; Okuyama *et al.* 2012). These dives are more prevalent between nesting events, at times when turtles are reported to be minimizing energy expenditure so as to allocate resources to developing eggs. Indeed, classification of these dives as resting behaviour is important, particularly because of their potential role in saving energy for turtles, which are considered to be primarily 'capital' breeders (Jönsson 1997; Bonnet, Bradshaw & Shine 1998; Plot *et al.* 2013). But evidence that type 1a dive types in inter-nesting female turtles are genuinely just resting dives is equivocal: Hochscheid *et al.* (1999) suggested that turtles might forage during the dive, and Myers and Hays (2006) explicitly noted beak

movements in inter-nesting leatherback turtles (*Dermochelys coriacea*) during various dives that also implied foraging in nesting areas. There is thus a need for further information on the activities of female turtles during the inter-nesting phase to determine the extent to which type 1a dives might be associated with foraging in nesting areas. Such information may be important for conservation initiatives, which may have to consider protecting the space used by inter-nesting females rather than considering it energetically barren.

TDRs, however, lack the resolution to detect specific behaviours beyond changes in depth and therefore the ability to determine the extent to which turtles may be foraging is limited using this approach. Seminoff, Jones and Marshall (2006) addressed this issue using video recorders integrated with TDR technology (VTDRs) mounted onto the carapaces of (non-nesting) green turtles (*Chelonia mydas*). From their observations, they concluded that a suite of behaviours can be expressed within a single dive profile, noting that time-depth plots for determining underwater behaviours should therefore be treated with caution. Type 1a dives, for instance, consisted of both continuous and episodic resting behaviour. Furthermore, horizontal movements and stationary- and active benthic feeding were prevalent during the bottom phase of this dive type. Although illuminating, animal-attached video recording systems are power and memory hungry and so can only operate continuously for a few hours during daylight (Park *et al.* 2019).

Another approach to elucidate turtle behaviour is the deployment of high frequency tri-axial accelerometers which can be used over extended period (e.g., Narazaki *et al.* 2009; Hussey *et al.* 2015; Wilmers *et al.* 2015). Accelerometers have been used to link dive profiles with underwater activities in the context of buoyancy regulation, depth utilisation and the dynamism of movement (Hays, Marshall & Seminoff 2007; Fossette *et al.* 2010; Parlin *et al.* 2018). However, turtles can spend large portions of their behavioural time budget gliding at relatively constant velocity (Wyneken 1997; Walker & Westneat 2000; Martin 2003), especially during the bottom phase of type 1a dives, which produces little or no change in the acceleration, making interpretation of behaviours problematic (Eckert 2002; Wilson *et al.* 2020a).

The lack of dynamism in some turtle activities can be addressed, in part, by examining various scales of angular body rotations over time, which can reveal patterns of movement (Noda *et al.* 2012) beyond those imparted by the dynamism in body acceleration (*cf.* Chapter 2). This concept was introduced by Hochscheid and Wilson (1999), who quantified activity patterns *via* a compass system using a miniature, fluid-filled ship's compass with two magnetic field (Hall) sensors on the sphere's equator. These sensors are particularly sensitive to changes in individuals' horizontal orientation (changes in animal yaw) and Hochscheid *et al.* (1999) demonstrated how this approach could be used to produce an activity index for two free-living green turtles. Although their system did not allow for precise calculation of angular velocities or defined angular extents, it is, to my knowledge, the only study that quantifies the behavioural time budget of common type 1a dives over whole inter-nesting intervals.

Here, I assess the extent to which angular rotation can quantify the activity of five wild loggerhead turtles *Caretta caretta* engaged in type 1a dives between nesting events. Specifically, tags were deployed which recorded tri-axial acceleration and tri-axial magnetic field intensity, both of which can be recorded over periods of many days (*cf.* Brown *et al.* 2013). These allowed us to estimate the angular velocity of all three axes of rotation (pitch, roll and yaw), and combine them into an overall absolute angular velocity (AAV) proxy to infer activity. I also used three captive loggerhead turtles to ground-truth the wild turtle data. Beyond indicating that turtles might be feeding, angular velocity is relevant to nesting turtles because body rotation is energetically expensive (Wilson *et al.* 2020a; Wilson *et al.* 2020b), with the power costs projected to rise with increasing angular extent and velocity (*cf.* Wilson *et al.* 2013a; Wilson *et al.* 2013b). Precise quantification of the extent of activities should therefore help us understand power and energy management in turtles during this critical phase of their lives.

Materials and methods

Subjects, study area and tagging

Five mature female loggerhead turtles were equipped with Daily diary (DD) logging units (Wilson, Shepard & Liebsch 2008) enclosed in a square silicone casing and attached, using an epoxy resin, by placing them flat against the shell, usually between the first and second scute. Tri-axial acceleration (range, $\pm 16 g$) and tri-axial magnetic field intensity (recorded in Gauss (G) at 0.73 mG/LSB (Milligauss/least significant bit, *cf.* Tuck 2010) resolution, range; $\pm 0.88 G$) data were recorded at 40 Hz, while pressure was recorded at 4 Hz to provide depth information. Devices were deployed only on nesting turtles after egg deposition, to minimise disruption and stress. All devices were deployed on a single beach in the south of Boa Vista island, Cabo Verde (Cameron *et al.* 2019), over a period of 8 nights starting on 22 July 2014. Turtles also received a passive integrated transponder to identify them in case they were seen again without the DD units. All tags were retrieved when the turtles returned after a single inter-nesting interval, either on the beach of deployment or on adjacent beaches.

Three female adult captive turtles housed at the Arca del Mar rehabilitation centre in Oceanografic in Valencia were also fitted with DD loggers intermittently between June and August 2018. Data was recorded at 20 Hz. Turtles undergoing rehabilitation were housed in separate circular tanks, 6 m in diameter, with a water depth of 0.95 m. These turtles were observed at intervals (between 10 and 60 min) and results obtained were used solely to ground-truth an absolute angular velocity metric (see later) by ascertaining that high values of absolute angular velocity corresponded to periods when turtles exhibited high turning rates.

Custom-designed software; Daily Diary Multi Trace (DDMT, <http://www.wildbytetechologies.com>), was used to visualise DD data, create the appropriate channel smoothing windows, extract differentials and implement Boolean-type, time-based behavioural expressions linked to the dive depths at which

type 1a dives occurred. R (version 3.51, <https://www.r-project.org>) and Origin pro 2016 (OriginLab Corporation, <https://www.originlab.com>) were used for further statistical and graphical analysis. Google earth (<https://earth.google.com>) was used to perform polygon transects to approximate the seabed elevation profile as a function of distance from the coastline of the nesting beach.

Derivation of angular velocity

All stages involved in the derivation of pitch, roll and compass heading (using tri-axial accelerometers and magnetometers) are detailed in Ozyagcilar (2012); Pedley (2012); Pedley (2013); and Chapter 2.

All three indices of derived body rotation (pitch, roll and yaw) were pre-smoothed using a rolling window of two seconds to eliminate small deviations due to noise stemming from the flipper beat cycle. A circular mean was used for yaw (Pewsey, Neuhäuser & Ruxton 2013). Each complete set of data taken from an individual turtles was subsequently subsampled to 1 Hz to facilitate computation.

AAV was derived using data from both the accelerometers and magnetometers (Chapter 2). AAV is calculated from the integration of each rotational axis' instantaneous angular velocity measurement and given by

$$AAV = \sqrt{(AVeP^2 + AVeR^2 + AVeY^2)} \quad (1)$$

where the differentials AVeP, AVeR and AVeY (angular velocity about the pitch, roll and yaw axis, respectively) were calculated in °/s using a stepping range of 1 s (Chapter 2). A logical expression was implemented on the derivative AVeY to ensure rate of change never exceeded 180°/s (*cf.* Wilson, Shepard & Liebsch 2008) to determine whether the rotation was clockwise or anti-clockwise.

The vectorial dynamic body acceleration (VeDBA) was also calculated following the protocols outlined by Qasem *et al.* (2012). To calculate VeDBA, the dynamic acceleration of each axis was derived by subtracting the smoothed (static)

acceleration from the raw data before taking the vectorial sum of the dynamic accelerations.

Depiction of type 1a dives and activity

The DD also records pressure (mbar), which was used to determine diving depth in m (see equations in Wilson *et al.* 1992). Baseline offsets of recorded pressure were accounted for and a further 10 cm buffer depth offset was implemented, less than or equal to the corrected depth at the surface (essentially 10 cm less than or equal to 0 m depth), before depth was computed. Only dives with (at least part of) a bottom phase greater than or equal to 3 m, (termed 'deep dives'; Fig. 1) were considered for analysis (Fig. 1) were categorised by dive type, because relative variation in depth at shallower depths was higher due to the effect of waves (*cf.* Houghton *et al.* 2002).

Type 1a dives were identified based on three criteria:

- (1) The general shape of the dive profile consisted of steep descent and ascent phases with a flat bottom between (*cf.* Fig. 2);
- (2) the pressure differential (calculated over 10 s; pressure pre-smoothed by 2 s) exceeded a defined threshold of ± 0.03 mbar during periods of descent and ascent (~ 0.03 m/s differential depth [vertical speed], as previously determined and proposed by Hays *et al.* (2000)), and;
- (3) over the duration of the bottom phase, change in depth did not exceed 1 m from the base line.

Only the bottom phase of type 1a dives were assessed. Video recordings of captive turtles were taken to ground-truth whether AAV was an accurate reflection of activity extent observed directly. To stimulate appreciable activity, turtles were provided with a food source (jellyfish). Despite relatively restricted movements due to tank confinement, clear differences were noted between actively swimming, manoeuvring along the bottom and complete rest periods. Activity resulted in periods of AAV exceeding $5^\circ/\text{s}$, while only continuous bouts of rest coincided with

constant values of AAV below $3^\circ/s$ (the limit of resolution of the system). The contrasting pattern was apparent during visual inspection of the sensor data from free-ranging turtles (*cf.* Fig. 2).

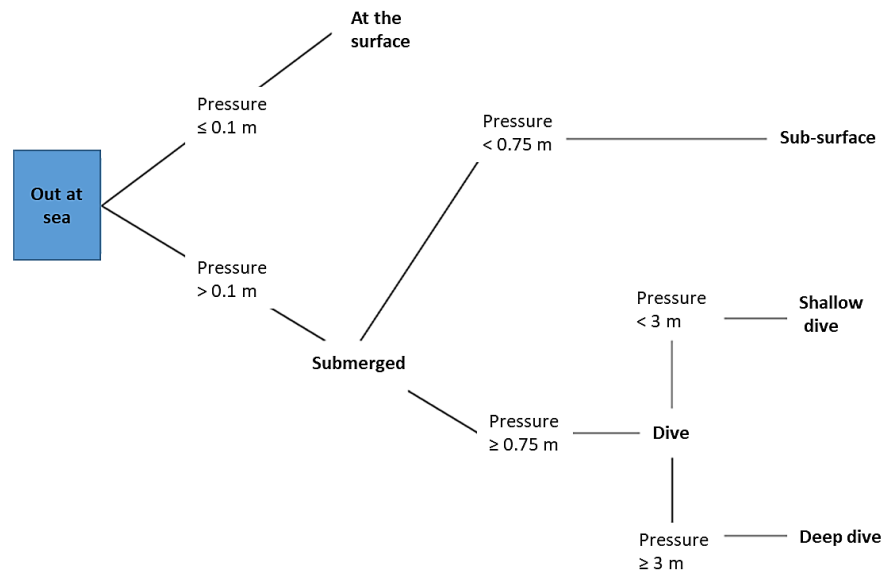


Figure 1. Decision tree showing how deep dives were characterised.

The topographic conditions associated with wild turtles resting were taken into consideration. Turtles do not always rest on a hard substrate; they have also been reported to rest on fauna (corals), flora (algae) and in the open with no apparent holdfasts. Thus, they are subject to motion from current vectors (Okuyama *et al.* 2010). To account for this additional degree of possible sensor noise a slightly higher threshold of $5^\circ/s$ was implemented for AAV, below which the animals were considered to be at absolute rest. However, even during periods of low activity, e.g., stationary foraging or slow rates of movement, intermittent values above the threshold were apparent. To account for those effects, two time-based criteria were implemented, both of which had to be met for a resting bout to be marked as such:

- (1) AAV had to remain below $5^\circ/s$ for a minimum of 30 s
- (2) During a rolling window of 30 s, the extent of a turn could not exceed 45° .

Periods not marked as resting were active. Finally, depending on the proportion of bottom phase attributed to periods of marked rest, type 1a dives were subclassified as being predominantly resting (resting $\geq 80\%$), episodic-resting (resting between 20 and 80%) or active (resting $\leq 20\%$). This subclassification is referred to hereafter as dive status.

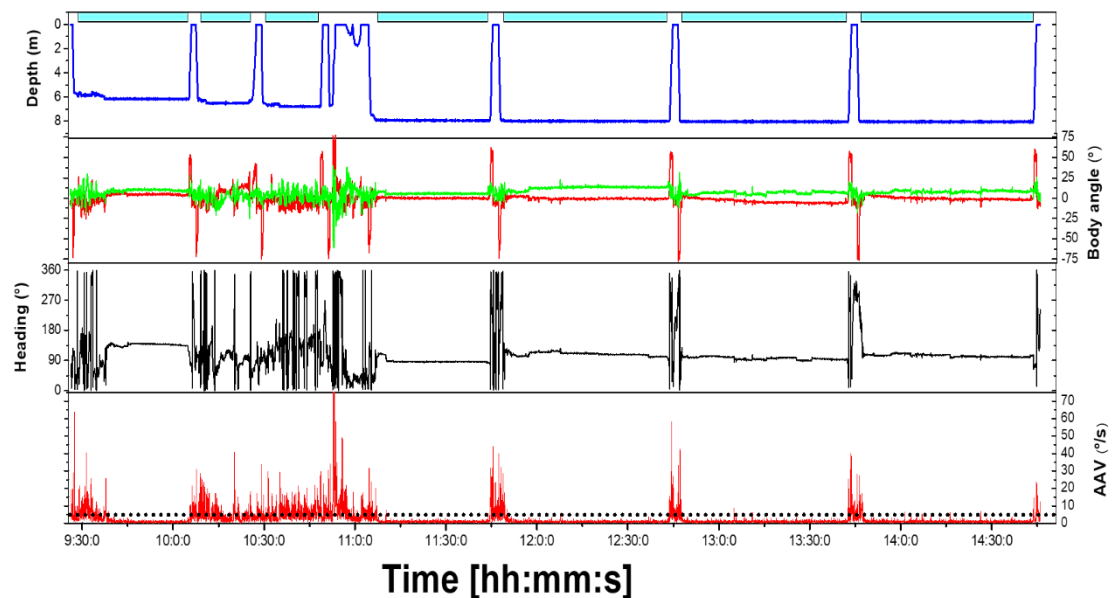


Figure 2. An example of a continuous bout of diving behaviour (approx. 5.5 hours) from a wild loggerhead turtle. Bottom phase of type 1a dive denoted with cyan blocks (top). Rest periods are inferred by continuous bouts of relatively unchanging body rotation (red: pitch, green: roll, black: yaw [heading]). Note, heading is plotted in a different panel to pitch and roll because its range of measurement range is higher. Absolute angular velocity (AAV) periods during bouts of active swimming and remains consistently low during rest periods. The threshold of 5°/s for AAV is denoted with a back dotted line.

Statistical analyses

A Linear mixed model (LMM) was performed using the lmer function in R, from the lme4 package (Bates *et al.* 2015), to determine the extent to which dive duration correlated with AAV and dive depth (mean values per type 1a dive pooled into one grand mean value for each turtle). Turtle ID was set as a random factor. Diagnostic plots of the residuals revealed a departure from linearity and homoscedasticity. As such, box-cox transformation analysis from the MASS package was used to assess the appropriate exponent ($\lambda = 1$) with which to transform data; the natural log of the independent variables (AAV and depth) was used. The model simplification method (backward selection) was employed using likelihood ratio tests with an ANOVA

function. Due to the apparent non-linear relationship between untransformed variables, a generalised additive mixed effects model (GAM; mgcv package, using thin plate regression splines ($k = 7$) and a smoothing function) was also constructed for comparison. To infer the metabolic costs associated with dives and angular velocity, I used the approximation that zero AAV corresponded to resting metabolic rate (RMR). Under the condition that zero AAV approximately corresponds to RMR, dives with zero angular velocity throughout the bottom phase were approximately 40 min in duration (see Fig. 6A). Based on this approximation, I constructed the putative curve of metabolic costs associated with AAV (expressed as a multiple of RMR) by dividing 40 min by the dive duration predicted based on AAV (using the predict.gam function in R).

Results

Overall, I analysed a total of 75 turtle d, with individuals spending between 13 and 17 d at sea (mean (\pm SD) 15 ± 1.6 d). Weather conditions during the study (as reported every 3 h by a nearby station in Curral Velho) varied appreciably, such as wind (9–39 km/h, typically coming from the northeast), rain (0–1.4 mm/3 h), humidity (77–92 %) and pressure (1012–1018 mb), though temperature remained relatively constant (23–25°C).

There were large inter-individual differences in the proportion of time spent at different depths (Fig. 3A). Type 1a dives were frequent and represented between 40 and 61 % of the total number of deep dives (> 3 m, Fig. 3A,B), despite the total number of deep dives differing substantially among turtles (Table 1). Depths during type 1a dives were generally quite shallow, with only one turtle exceeding a depth of 11 m (Fig. 3C, Table 1, see supplementary information (SI) for approximate bathymetry estimates around the nesting site). The duration of this dive type varied considerably for each turtle (Table 1).

I noted large variations in the mean VeDBA estimates (mean value per type 1a dive pooled into one grand mean value for each turtle) between turtles, ranging from

0.037 to 0.096 g , with a coefficient of variation (CV) of 36.95 %. Equivalent AAV offsets appeared much lower, ranging from 2.851 to 3.902 $^{\circ}/s$, with a CV of 13.05 %.

Table 1. Number of type 1a dives (vs. total number of deep dives in parentheses) and mean (\pm SD) number per day, maximum depth and duration of this dive type for each tracked turtle.

Turtle ID	Count (Total count of deep dives)	Daily mean	Depth (m)	Duration (min)
1	122 (280)	8.13 \pm 5.15	5.48 \pm 1.93	34.43 \pm 18.05
2	255 (415)	17.0 \pm 6.75	5.24 \pm 0.79	31.67 \pm 16.05
3	76 (184)	5.85 \pm 3.83	3.65 \pm 0.61	22.01 \pm 14.71
4	419 (684)	23.28 \pm 10.62	4.32 \pm 0.84	27.65 \pm 16.20
5	400 (758)	25.0 \pm 10.39	4.26 \pm 1.11	25.52 \pm 17.96

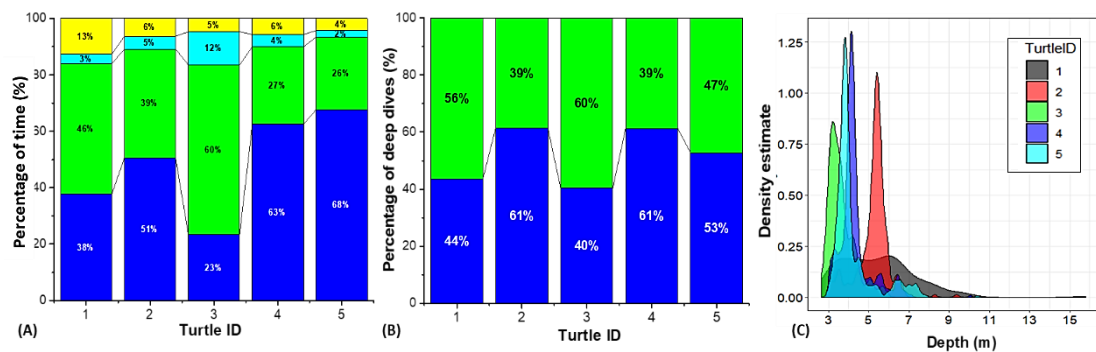


Figure 3. (A) Time-budget of depth use by five female loggerhead turtles while out at sea [blue: deep dive, green: shallow dive, cyan: sub-surface swimming, yellow: surface]. (B) Percentage of deep dives defined as type 1a [blue: type 1a, green: other]. (C) Relative density of depths obtained during type 1a dive bottom phase, coloured according to turtle ID.

In terms of angular velocity, higher rates of activity were indicated by higher estimates of AVer, AVeP and AVeY and typically included appreciable components from all three rotation axes (Fig. 4). However, the rate change along the yaw axis was substantially greater than the other two, approximately 2.5 times higher than the equivalent in pitch and roll (Fig. 4). I also noted, in a tri-axial plot of the extent of the three rotation metrics, how different individual turtles tended to occupy different sections of the envelope (Fig. 4).

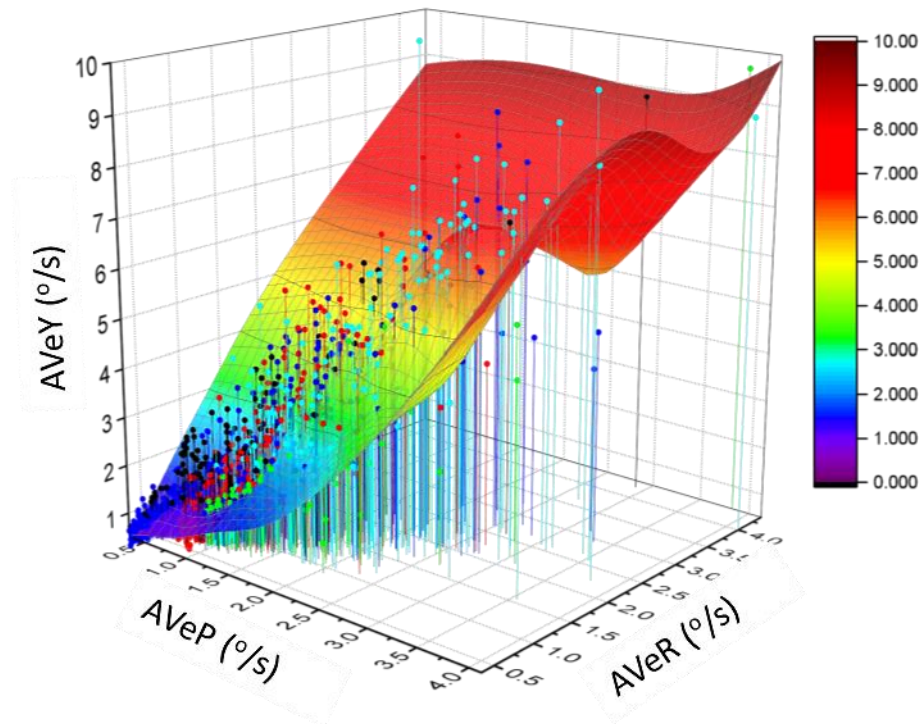


Figure 4. Relationship between the absolute values of angular velocity on all three axes (see Eq. 1). Each data point represents the mean value per dive. 3-D colour map surface (coloured by AVeY) using a thin plated spline (smoothing of 1), constructed from a 3-D gridding matrix. Projection of data points coloured according to turtle ID.

The majority of time spent at the bottom was associated with resting, with individual values ranging from 62 to 84 % (Fig. 5A). However, resting behaviour was rarely continuous over the duration of a single dive, with the bulk of dives incorporating intermittent bouts of rest and activity (Fig. 5C). Subclassification of dives into predominantly resting, active or episodic demonstrated this, with a high proportion of the dives (mean (\pm SD) 50 ± 22.5 %) showing patterns of activity lasting over 20 % of the dive duration (Fig. 5B). There were also notable inter-individual differences in the proportion of time allocated to each dive status (Fig. 5B). The relative distribution of raw pitch, roll and yaw values differed between aggregated periods of rest and activity, with the latter generally showing greater variability (SI: Fig. S2). There were, however, considerable offset differences between turtles in the unimodal peaks of density estimates for roll and pitch values (SI: Fig. S2).

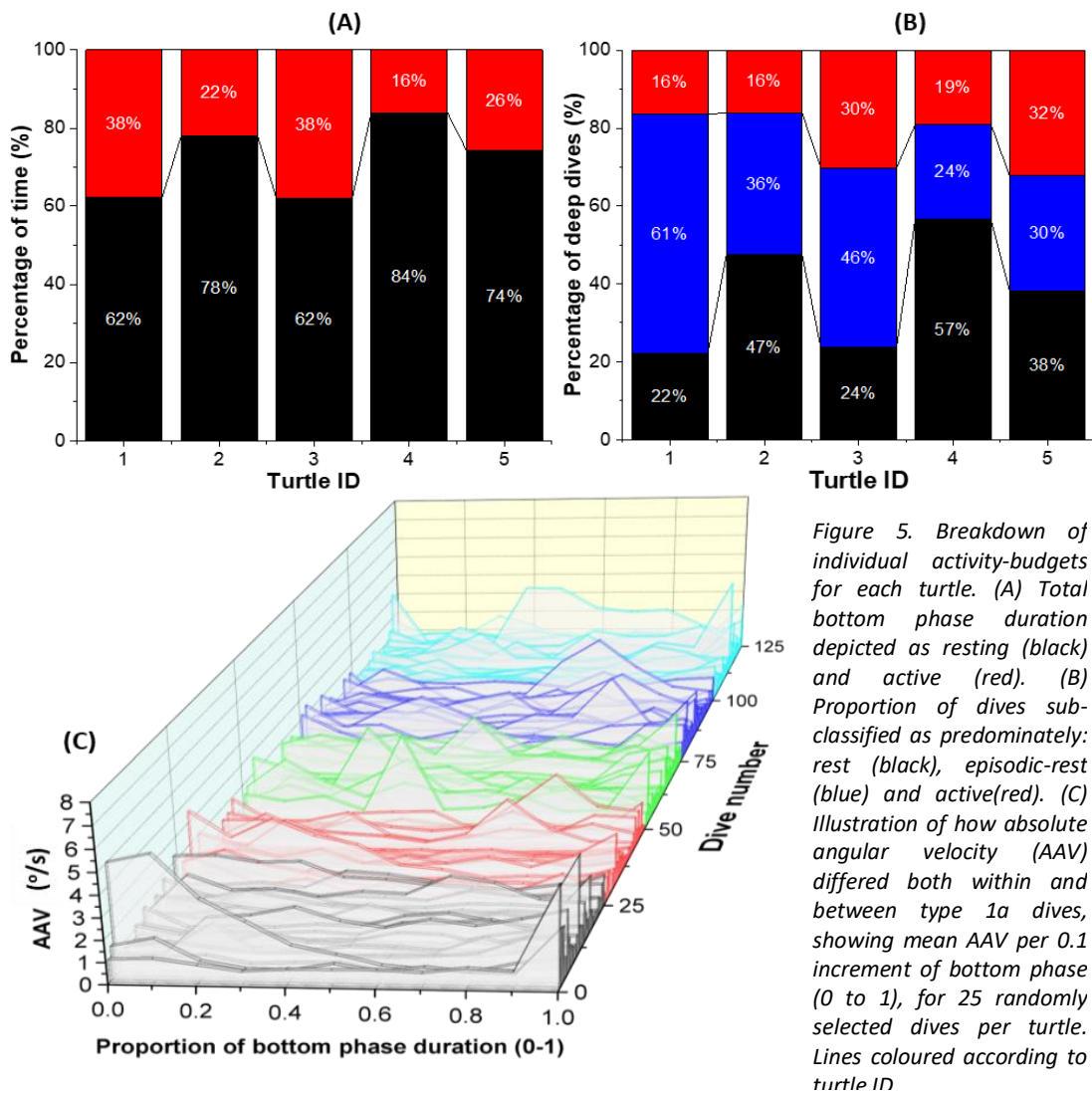


Figure 5. Breakdown of individual activity-budgets for each turtle. (A) Total bottom phase duration depicted as resting (black) and active (red). (B) Proportion of dives sub-classified as predominately: rest (black), episodic-rest (blue) and active (red). (C) Illustration of how absolute angular velocity (AAV) differed both within and between type 1a dives, showing mean AAV per 0.1 increment of bottom phase (0 to 1), for 25 randomly selected dives per turtle. Lines coloured according to turtle ID

There was a significant negative relationship between (log-transformed) AAV and bottom phase dive duration (LMM: $\chi^2_{(1)} = 1147$, $p < 0.01$) (Fig. 6): for every 1 % increase in AAV, dive duration decreased by 0.25 minutes (estimate (\pm SE) = -24.86 ± 0.58 , $t = -43.20$, $p < 0.001$), suggesting that rotational activity resulted in shorter dives. Similarly, there was a significant negative relationship between (log-transformed) AVeY and bottom phase dive duration (LMM: $\chi^2_{(1)} = 1102$, $p < 0.01$; estimate (\pm SE) = -17.49 ± 0.42 , $t = -42.01$, $p < 0.001$) although the strength of the relationship was lower: AIC values were higher, and coefficient of determination (R^2 values) were lower than for AAV (AIC = 9576 and 9530 respectively; $R^2 = 0.63$ and 0.66, respectively).

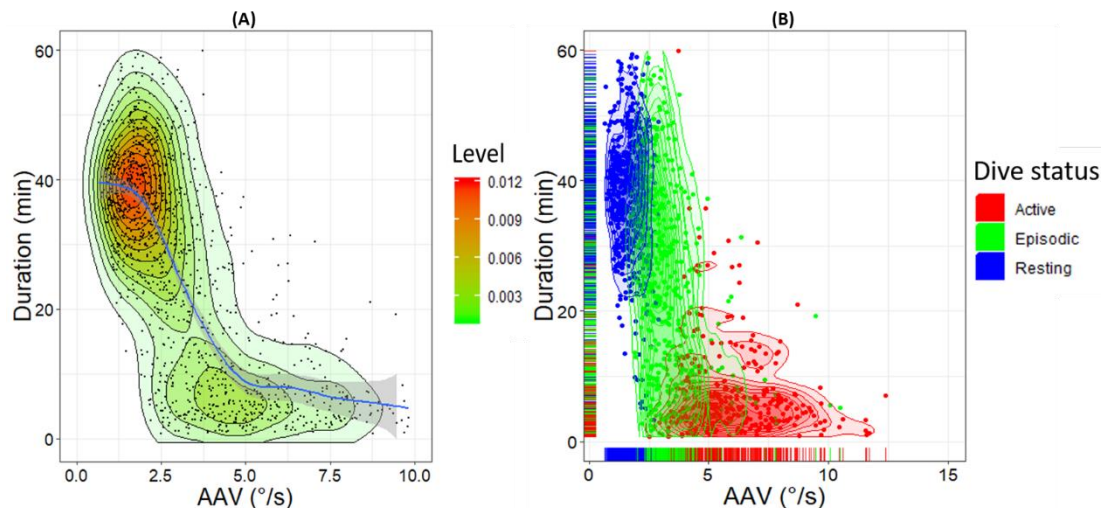


Figure 6. (A) Relationship between absolute angular velocity (AAV) and dive duration; each data point represents the mean AAV value per dive. Contour plot showing the kernel density level of aggregated points and fitted with a line of best fit obtained from GAM smoothing (grey shading around line represents 95 % confidence level interval). (B) Clustered polygon plot; points coloured according to the activity level of the dive (rest: red, episodic-rest: green and active: blue) and fitted with two 1-dimensional marginal rugs displaying individual case distributions.

The significance of the AAV model was echoed by data fitted with a GAM model. Predicted multiples of RMR appeared to increase in a linear fashion relative to AAV (Fig. 7). Depth was not correlated with dive duration (estimate $[\pm SE] = 1.28 \pm 1.43$, $t = 0.90$, $p = 0.37$) and the interactive effect between depth and dive duration was also non-significant (estimate $[\pm SE] = -2.24 \pm 2.30$, $t = -0.97$, $p = 0.33$). See SI: Table S1 for all model parameters.

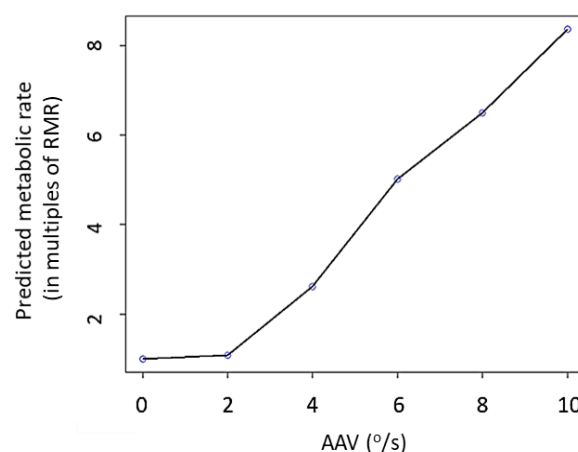


Figure 7. Estimated metabolic costs (expressed as a multiple of resting metabolic rate [RMR]) associated with variation in absolute angular velocity (AAV). Estimated dive duration derived from GAM model (cf. Fig. 6A), divided by 40 min per 2-step increase in AAV (°/s).

Discussion

AAV and its ability to infer activity in turtles

Comparison between acceleration- and angular velocity-derived metrics

Measures of acceleration are useful for quantifying animal activity (Brown *et al.* 2013; Wilmers *et al.* 2015). Indeed, dynamic body acceleration seems a reliable proxy for movement costs (Wilson *et al.* 2006; Qasem *et al.* 2012; Wilson *et al.* 2020a). However, for slow-moving animals, acceleration can be negligible for extended periods (*cf.* Williams *et al.* 2017; Chapter 2), making dynamic acceleration a poor metric for activity (Wilson *et al.* 2020a). Despite this, and the extremely low VeDBA estimates in these turtles generally, mean values of VeDBA did increase over the three categories of resting, episodic-resting and active dives for each turtle (SI: Fig. S3). However, the large offsets in VeDBA estimates between turtles, presumed to be due to differing tag placements on the animals (Wilson *et al.* 2020a), makes inter-individual comparisons problematic. In contrast, and critically, angular rotation across all three axes is not affected by site of placement of the tag on the carapace (within limits; see SI: Text S1), so that angular velocity is a more standardised metric than dynamic body acceleration for inter-individual comparisons (Wilson *et al.* 2020a). A further advantage of AAV as a general activity metric is that it considers all three rotation axes equally, providing a relative magnitude of rotation per s that offers information about any sort of rotation.

AAV values are, however, not always due to rotations instigated by the animal (*cf.* Halsey *et al.* 2011). In the marine environment, for example, waves at the sea surface, as well as variations in underwater current vectors, probably apply rotational forces to animals. Similarly, passive descents of the water column, such as ‘drift dives’ by northern elephant seals *Mirounga angustirostris*, can result in body rotations (Mitani *et al.* 2010) and a similar process may operate in species that have passive ascents. However, although such things need to be borne in mind when considering AAV metrics, the effects are likely to be small compared to animal-instigated body rotations.

Potential for AAV metrics to elucidate turtle behaviour

Overall, the AAV metric resulting from combining the angular rotation about all three axes seems to be a sensitive proxy for depicting changes between active and inactive states in species that have low dynamism in their movement. Beyond this, I expect the contribution of the angular velocity from each rotational axis to vary (Fig. 4) according to behaviour-specific movements. For example, axis-linked angular velocity should vary between turtles changing heading while travelling (or not) along the seabed vs. animals travelling up and down the water column and this may have accounted, in part, for the variation in the position of individual turtles in the AVeY/AVeP/AVeR envelope (Fig. 4). In future work, detailed studies of behaviour using video systems (e.g., Seminoff, Jones & Marshall 2006; Jeantet *et al.* 2018; Jeantet *et al.* 2020) combined with DD-type tags, could code observed behaviours in terms of axis-specific angular rotations. The findings could then be used to differentiate behaviours for individuals not equipped with video systems over much longer periods and at night.

However, even using AAV as a summary metric for general turtle activity seems to have appreciable value, not least due to the fine temporal scales over which angular rotation can be calculated. In this study, increased rotational activity is probably related, to some degree, to foraging. However, based on my findings, I suggest that the utility of AAV could be expanded to investigate turtle activity levels across different dive types (see, for example, those detailed by Hochscheid (2014)). This metric may prove particularly useful for slow-moving animals in general because small variations in AAV can provide the resolution required to distinguish activity from inactivity, itself an important biomarker for understanding energy expenditure and even health (*cf.* Arkwright *et al.* 2020).

*Behaviour during dives**Depth use*

Sea turtles show complex diving patterns, each characteristic dive pattern associated with specific behaviours. Type 1a dives are generally considered important for facilitating bouts of benthic rest, most particularly in nesting females that have to manage energy reserves in order to maximise egg development (e.g., Wallace *et al.* 2005; Walcott, Eckert & Horrocks 2012).

Bathymetry estimates at Boa Vista beach showed that bottom depth can be < 8 m at distances greater than 3 km from the nesting beach (SI: Fig. S1). Given the relatively low percentage of time that turtles dived deeper than 3 m, the shallow depths obtained during type 1a dives and the relatively high occurrence of this dive type throughout the inter-nesting interval (Fig. 3B, Table 1), it is highly probable that the turtles spent the bulk of their time close to the coast, or at least within shallow areas out at sea. This is similar to the results of previous studies, which have documented turtles often preferring to be near topographic features in shallow water. These features provide important microsites for cover, reducing susceptibility to predation (Heithaus, Frid & Dill 2002) and decreasing energetic costs by minimising current vectors which could otherwise disrupt motionless rest (Seminoff, Jones & Marshall 2006). My results also seem to mirror those found for loggerhead turtles in Greece, where nesting females spend the most time in shallow waters that are likely to be warmer, to enhance incubation (Schofield *et al.* 2009).

Activity extent of type 1a dives

Given the focus on shallow depths in this study (Table 1) (and only one dive type assessed), it is not surprising that I did not find a relationship between dive duration and depth, which has been repeatedly confirmed by multiple authors (e.g., Minamikawa, Naito & Uchida 1997; Hochscheid *et al.* 1999; Hays *et al.* 2000; Minamikawa *et al.* 2000; Hays, Metcalfe & Walne 2004). However, the consistency of dive depth shown by the turtles does make a case for them loading similar amounts

of oxygen for their type 1a dives (Minamikawa *et al.* 2000). This helps minimise depth as a confounding effect in the data set. Specifically, assuming that turtles diving to a set depth do indeed submerge with comparable amounts of oxygen, when they are more active underwater, it should deplete oxygen stores faster, resulting in shorter dives. Indeed, this reasoning is why it has been suggested that dive duration can sometimes be used to infer metabolic rate (Hays *et al.* 2000; Enstipp *et al.* 2011). In the current study I found that dive duration decreased with increasing rotational movement (mean AAV) over the bottom phase of type 1a dives (Fig. 6A). This agrees with past studies showing that energetic cost is related to activity and indicates that greater amounts of movement are indeed associated with higher power use (Enstipp *et al.* 2011; Halsey *et al.* 2011; Fahlman *et al.* 2013; Wilson *et al.* 2013b; Zamparo *et al.* 2019). What my study adds that is new to this framework is the idea that rotational movement, rather than just linear acceleration as exemplified by DBA metrics (Enstipp *et al.* 2011; Halsey *et al.* 2011), appears to be a major modulator of oxygen consumption. As projected, it seems higher power use associated with rotation depletes oxygen stores at a faster rate, causing dives to be correspondingly curtailed. I estimated that turtles could increase their metabolic rate by up to eight times RMR during the bottom phase of type 1a dives in times of their most extreme AAV activity (Fig. 7).

This predicted increase in RMR presumably has general energetic consequences at a time when females are considered to be under strong selection pressure to be judicious with their reserves during initial egg gestation. Displaying appreciable activity would seem to conflict with the argument that energy conservation should be a prime modulator of fitness for female sea turtles (Hays *et al.* 2002a; Hopkins-Murphy, Owens & Murphy 2003; Schofield *et al.* 2006). Such an increase in energy expenditure could be justified, however, if it were to result in a net gain of energy *via* local feeding around the nesting sites. Based on this, I suggest that, although turtles may rotate for a number of reasons, such as to react to predators (Heithaus, Frid & Dill 2002) or conspecifics (Schofield *et al.* 2007), the AAV metrics from this study predominantly indicate local supplementary foraging of those nesting turtles. This

inference is supported to some extent (1) by results obtained *via* animal-borne video cameras and movement-based sensors deployed elsewhere (e.g., Hochscheid & Wilson 1999; Schofield *et al.* 2006; Seminoff, Jones & Marshall 2006; Houghton *et al.* 2008; Fossette *et al.* 2010), and (2) indirectly by known change in stable isotope values over the nesting season in this population (Cameron *et al.* 2019). Certainly, captive Loggerheads rotate their bodies appreciably during feeding (Wilson *et al.* 2020c) as they deal with their prey which for wild animals consists primarily of crustaceans, gastropods and echinoids (Bjorndal 2003), and the peaks I observed in AAV (Fig. 5C) may be due to this. These predominantly benthic food items would require turtles to maintain a constant depth, a critical criterion for type 1a dives. All this ties in with Hochscheid *et al.*'s (1999) study, where they noted appreciable angular body movement in two inter-nesting green turtles off Cyprus, from which they deduced that 34 % of the time budget of these animals was spent foraging. A notable point made in the Hochscheid *et al.* (1999) study was that the inter-nesting area frequented by their animals was extensively covered by sea grass, the primary food of green turtles (Hays *et al.* 2002b; Lemons *et al.* 2011; Heithaus *et al.* 2014), so there was ample opportunity to feed.

Although, my results coupled with those of Hochscheid *et al.* (1999) only amount to data from 7 animals (of two different species), they do suggest that female turtles may forage between nesting events. If true, this has implications for area management. For example, it may indicate that protection of resources, e.g., by minimizing exploitation around the nesting site, is important to allow females to maintain body condition at this critical time.

Conclusion

Here, I show that a metric resulting from combining the angular rotation about all three axes (AAV) seems to be a sensitive proxy for depicting changes between active and inactive states. I also note the benefit of using derivatives of rotation (rate of change) to overcome the limitations associated with discrepancies of tag placement between individuals. I show that, although resting behaviour contributed a significant portion of the loggerhead turtle behaviour-time budget, supporting the notion that energy saving is a major driver during the inter-nesting period, these five tagged animals showed appreciable activity which, after consideration of other studies, I suggest is due largely to foraging. Given that all seven species of turtle are considered to be capital breeders, this requires urgent examination in order to understand the energetic constraints on these animals that are renowned for their long migrations between feeding and breeding sites.

References

- Arkwright, A.C., Archibald, E., Fahlman, A., Holton, M.D., Crespo-Picazo, J.L., Cabedo, V.M., Duarte, C.M., Scott, R., Webb, S., Gunner, R.M. & Wilson, R.P. (2020) Behavioral Biomarkers for Animal Health: A Case Study Using Animal-Attached Technology on Loggerhead Turtles. *Frontiers in Ecology and Evolution*, **7**.
- Bates, D., Mächler, M., Bolker, B. & Walker, S. (2015) Fitting Linear Mixed-Effects Models Using lme4. *2015*, **67**, 48.
- Bjorndal, K.A. (2003) *Roles of loggerhead sea turtles in marine ecosystems*. Smithsonian Books, Washington, DC.
- Bonnet, X., Bradshaw, D. & Shine, R. (1998) Capital versus Income Breeding: An Ectothermic Perspective. *Oikos*, **83**, 333-342.
- Brown, D.D., Kays, R., Wikelski, M., Wilson, R. & Klimley, A.P. (2013) Observing the unwatchable through acceleration logging of animal behavior. *Animal Biotelemetry*, **1**, 20.
- Butt, N., Whiting, S. & Dethmers, K. (2016) Identifying future sea turtle conservation areas under climate change. *Biological Conservation*, **204**, 189-196.
- Cameron, S.J.K., Baltazar-Soares, M., Stiebens, V.A., Reischig, T., Correia, S.M., Harrod, C. & Eizaguirre, C. (2019) Diversity of feeding strategies in loggerhead sea turtles from the Cape Verde archipelago. *Marine Biology*, **166**, 130.
- Cheng, I. (2009) Changes in diving behaviour during the internesting period by green turtles. *Journal of Experimental Marine Biology and Ecology*, **381**, 18-24.
- Dodge, K.L., Kukulya, A.L., Burke, E. & Baumgartner, M.F. (2018) TurtleCam: A “Smart” Autonomous Underwater Vehicle for Investigating Behaviors and Habitats of Sea Turtles. *Frontiers in Marine Science*, **5**.
- Eckert, S.A. (2002) Swim speed and movement patterns of gravid leatherback sea turtles (*Dermochelys coriacea*) at St Croix, US Virgin Islands. *Journal of Experimental Biology*, **205**, 3689-3697.
- Eckert, S.A., Nellis, D.W., Eckert, K.L. & Kooyman, G.L. (1986) Diving Patterns of Two Leatherback Sea Turtles (*Dermochelys coriacea*) during Internesting Intervals at Sandy Point, St. Croix, U.S. Virgin Islands. *Herpetologica*, **42**, 381-388.
- Enstipp, M.R., Ciccione, S., Gineste, B., Milbergue, M., Ballorain, K., Ropert-Coudert, Y., Kato, A., Plot, V. & Georges, J.-Y. (2011) Energy expenditure of freely swimming adult green turtles (*Chelonia mydas*) and its link with body acceleration. *The Journal of Experimental Biology*, **214**, 4010-4020.
- Fahlman, A., Svärd, C., Rosen, D.A.S., Wilson, R.P. & Trites, A.W. (2013) Activity as a proxy to estimate metabolic rate and to partition the metabolic cost of diving vs. breathing in pre- and post-fasted Steller sea lions. *Aquatic Biology*, **18**, 175-184.
- Fossette, S., Gleiss, A.C., Myers, A.E., Garner, S., Liebsch, N., Whitney, N.M., Hays, G.C., Wilson, R.P. & Lutcavage, M.E. (2010) Behaviour and buoyancy regulation in the deepest-diving reptile: the leatherback turtle. *The Journal of Experimental Biology*, **213**, 4074-4083.
- Gilman, E., Moth-Poulsen, T. & Bianchi, G. (2007) *Review of measures taken by intergovernmental organizations to address sea turtle and seabird interactions in marine capture fisheries*. Food and Agriculture Organization of the United Nations, Rome.
- Greggor, A.L., Berger-Tal, O., Blumstein, D.T., Angeloni, L., Bessa-Gomes, C., Blackwell, B.F., St Clair, C.C., Crooks, K., de Silva, S., Fernández-Juricic, E., Goldenberg, S.Z.,

- Mesnick, S.L., Owen, M., Price, C.J., Saltz, D., Schell, C.J., Suarez, A.V., Swaisgood, R.R., Winchell, C.S. & Sutherland, W.J. (2016) Research Priorities from Animal Behaviour for Maximising Conservation Progress. *Trends in Ecology & Evolution*, **31**, 953-964.
- Halsey, L.G., Jones, T.T., Jones, D.R., Liebsch, N. & Booth, D.T. (2011) Measuring Energy Expenditure in Sub-Adult and Hatchling Sea Turtles via Accelerometry. *PLOS ONE*, **6**, e22311.
- Hart, K.M., Zawada, D.G., Fujisaki, I. & Lidz, B.H. (2010) Inter-nesting habitat-use patterns of loggerhead sea turtles: enhancing satellite tracking with benthic mapping. *Aquatic Biology*, **11**, 77-90.
- Hays, G., Hochscheid, S., Broderick, A., Godley, B. & Metcalfe, J. (2000) Diving behaviour of green turtles: dive depth, dive duration and activity levels. *Marine Ecology Progress Series*, **208**, 297-298.
- Hays, G.C. (2008) Sea turtles: A review of some key recent discoveries and remaining questions. *Journal of Experimental Marine Biology and Ecology*, **356**, 1-7.
- Hays, G.C., Broderick, A.C., Glen, F., Godley, B.J., Houghton, J.D.R. & Metcalfe, J.D. (2002a) Water temperature and internesting intervals for loggerhead (*Caretta caretta*) and green (*Chelonia mydas*) sea turtles. *Journal of Thermal Biology*, **27**, 429-432.
- Hays, G.C., Glen, F., Broderick, A.C., Godley, B.J. & Metcalfe, J.D. (2002b) Behavioural plasticity in a large marine herbivore: contrasting patterns of depth utilisation between two green turtle (*Chelonia mydas*) populations. *Marine Biology*, **141**, 985-990.
- Hays, G.C., Marshall, G.J. & Seminoff, J.A. (2007) Flipper beat frequency and amplitude changes in diving green turtles, *Chelonia mydas*. *Marine Biology*, **150**, 1003-1009.
- Hays, G.C., Metcalfe, J.D. & Walne, A.W. (2004) The implications of lung-regulated buoyancy control for dive depth and duration. *Ecology*, **85**, 1137-1145.
- Heithaus, M., Frid, A. & Dill, L. (2002) Shark-inflicted injury frequencies, escape ability, and habitat use of green and loggerhead turtles. *Marine Biology*, **140**, 229-236.
- Heithaus, M.R., Alcoverro, T., Arthur, R., Burkholder, D.A., Coates, K.A., Christianen, M.J.A., Kelkar, N., Manuel, S.A., Wirsing, A.J., Kenworthy, W.J. & Fourqurean, J.W. (2014) Seagrasses in the age of sea turtle conservation and shark overfishing. *Frontiers in Marine Science*, **1**.
- Hochscheid, S. (2014) Why we mind sea turtles' underwater business: A review on the study of diving behavior. *Journal of Experimental Marine Biology and Ecology*, **450**, 118-136.
- Hochscheid, S., Bentivegna, F., Bradai, M.N. & Hays, G.C. (2007) Overwintering behaviour in sea turtles: dormancy is optional. *Marine Ecology Progress Series*, **340**, 287-298.
- Hochscheid, S., Godley, B.J., Broderick, A.C. & Wilson, R.P. (1999) Reptilian diving: highly variable dive patterns in the green turtle *Chelonia mydas*. *Marine Ecology Progress Series*, **185**, 101-112.
- Hochscheid, S. & Wilson, R.P. (1999) A new method for the determination of at-sea activity in sea turtles. *Marine Ecology Progress Series*, **185**, 293-296.
- Hopkins-Murphy, S., Owens, D. & Murphy, T. (2003) *Ecology of immature loggerheads on foraging grounds and adults in internesting habitat in the eastern United States*. Smithsonian Institution Press, Washington, DC.
- Houghton, J.D., Broderick, A.C., Godley, B.J., Metcalfe, J.D. & Hays, G.C. (2002) Diving behaviour during the internesting interval for loggerhead turtles *Caretta caretta* nesting in Cyprus. *Marine Ecology Progress Series*, **227**, 63-70.

- Houghton, J.D.R., Doyle, T.K., Davenport, J., Wilson, R.P. & Hays, G.C. (2008) The role of infrequent and extraordinary deep dives in leatherback turtles (*Dermochelys coriacea*). *Journal of Experimental Biology*, **211**, 2566-2575.
- Hussey, N.E., Kessel, S.T., Aarestrup, K., Cooke, S.J., Cowley, P.D., Fisk, A.T., Harcourt, R.G., Holland, K.N., Iverson, S.J., Kocik, J.F., Mills Flemming, J.E. & Whoriskey, F.G. (2015) Aquatic animal telemetry: A panoramic window into the underwater world. *Science*, **348**, 1255642.
- Jeantet, L., Dell'Amico, F., Forin-Wiart, M.-A., Coutant, M., Bonola, M., Etienne, D., Gresser, J., Regis, S., Lecerf, N., Lefebvre, F., de Thoisy, B., Le Maho, Y., Brucker, M., Châtelain, N., Laesser, R., Crenner, F., Handrich, Y., Wilson, R. & Chevallier, D. (2018) Combined use of two supervised learning algorithms to model sea turtle behaviours from tri-axial acceleration data. *The Journal of Experimental Biology*, **221**, jeb177378.
- Jeantet, L., Planas-Bielsa, V., Benhamou, S., Geiger, S., Martin, J., Siegwalt, F., Lelong, P., Gresser, J., Etienne, D., Hiélard, G., Arque, A., Regis, S., Lecerf, N., Frouin, C., Benhalilou, A., Murgale, C., Mailliet, T., Andreani, L., Campistron, G., Delvaux, H., Guyon, C., Richard, S., Lefebvre, F., Aubert, N., Hibold, C., le Maho, Y. & Chevallier, D. (2020) Behavioural inference from signal processing using animal-borne multi-sensor loggers: a novel solution to extend the knowledge of sea turtle ecology. *Royal Society Open Science*, **7**, 200139.
- Jönsson, K.I. (1997) Capital and Income Breeding as Alternative Tactics of Resource Use in Reproduction. *Oikos*, **78**, 57-66.
- Lemons, G., Lewison, R., Komoroske, L., Gaos, A., Lai, C.-T., Dutton, P., Eguchi, T., LeRoux, R. & Seminoff, J.A. (2011) Trophic ecology of green sea turtles in a highly urbanized bay: Insights from stable isotopes and mixing models. *Journal of Experimental Marine Biology and Ecology*, **405**, 25-32.
- López-Sepulcre, A.s. (2007) *The evolutionary ecology of space use and its conservation consequences*. University of Jyväskylä.
- Martin, C. (2003) The Behaviour of Free-living Marine Turtles: Underwater Activities, Migrations and Seasonal Occurrences. PhD Thesis, University of Wales Swansea.
- Minamikawa, S., Naito, Y., Sato, K., Matsuzawa, Y., Bando, T. & Sakamoto, W. (2000) Maintenance of neutral buoyancy by depth selection in the loggerhead turtle *Caretta caretta*. *Journal of Experimental Biology*, **203**, 2967-2975.
- Minamikawa, S., Naito, Y. & Uchida, I. (1997) Buoyancy control in diving behavior of the loggerhead turtle, *Caretta caretta*. *Journal of Ethology*, **15**, 109-118.
- Mingozzi, T., Mencacci, R., Cerritelli, G., Giunchi, D. & Luschi, P. (2016) Living between widely separated areas: Long-term monitoring of Mediterranean loggerhead turtles sheds light on cryptic aspects of females spatial ecology. *Journal of Experimental Marine Biology and Ecology*, **485**, 8-17.
- Mitani, Y., Andrews, R.D., Sato, K., Kato, A., Naito, Y. & Costa, D.P. (2010) Three-dimensional resting behaviour of northern elephant seals: drifting like a falling leaf. *Biology Letters*, **6**, 163-166.
- Myers, A.E. & Hays, G.C. (2006) Do leatherback turtles *Dermochelys coriacea* forage during the breeding season? A combination of data-logging devices provide new insights. *Marine Ecology Progress Series*, **322**, 259-267.
- Narazaki, T., Sato, K., Abernathy, K., Marshall, G. & Miyazaki, N. (2009) Sea turtles compensate deflection of heading at the sea surface during directional travel. *Journal of Experimental Biology*, **212**, 4019-4026.

- Noda, T., Okuyama, J., Koizumi, T., Arai, N. & Kobayashi, M. (2012) Monitoring attitude and dynamic acceleration of free-moving aquatic animals using a gyroscope. *Aquatic Biology*, **16**, 265-276.
- Okuyama, J., Kataoka, K., Kobayashi, M., Abe, O., Yoseda, K. & Arai, N. (2012) The regularity of dive performance in sea turtles: a new perspective from precise activity data. *Animal Behaviour*, **84**, 349-359.
- Okuyama, J., Shimizu, T., Abe, O., Yoseda, K. & Arai, N. (2010) Wild versus head-started hawksbill turtles *Eretmochelys imbricata*: post-release behavior and feeding adaptations. *Endangered Species Research*, **10**, 181-190.
- Ozyagcilar, T. (2012) Implementing a tilt-compensated eCompass using accelerometer and magnetometer sensors. *Freescale semiconductor, Application Note, AN4248*, Austin, TX.
- Park, S., Aschenbach, K.H., Ahmed, M., Scott, W.L., Leonard, N.E., Abernathy, K., Marshall, G., Shepard, M. & Martins, N.C. (2019) Animal-borne wireless network: Remote imaging of community ecology. *Journal of Field Robotics*, **36**, 1141-1165.
- Parlin, A.F., Nardone, J.A., Kelly Dougherty, J., Rebein, M., Safi, K. & Schaeffer, P.J. (2018) Activity and movement of free-living box turtles are largely independent of ambient and thermal conditions. *Movement Ecology*, **6**, 12.
- Pedley, M. (2012) eCompass-Build and Calibrate a Tilt-Compensating Electronic Compass. *Circuit Cellar-The Magazine For Computer Applications*, 1-6.
- Pedley, M. (2013) Tilt sensing using a three-axis accelerometer. *Freescale semiconductor. Application Note 2461*, **1**, 1-22.
- Pewsey, A., Neuhäuser, M. & Ruxton, G.D. (2013) *Circular Statistics in R*. OUP Oxford.
- Plot, V., Jenkins, T., Robin, J.-P., Fossette, S. & Georges, J.-Y. (2013) Leatherback Turtles Are Capital Breeders: Morphometric and Physiological Evidence from Longitudinal Monitoring. *Physiological and Biochemical Zoology*, **86**, 385-397.
- Qasem, L., Cardew, A., Wilson, A., Griffiths, I., Halsey, L.G., Shepard, E.L.C., Gleiss, A.C. & Wilson, R. (2012) Tri-Axial Dynamic Acceleration as a Proxy for Animal Energy Expenditure; Should We Be Summing Values or Calculating the Vector? *PLOS ONE*, **7**, e31187.
- Rice, M.R. & Balazs, G.H. (2008) Diving behavior of the Hawaiian green turtle (*Chelonia mydas*) during oceanic migrations. *Journal of Experimental Marine Biology and Ecology*, **356**, 121-127.
- Schofield, G., Bishop, C.M., Katselidis, K.A., Dimopoulos, P., Pantis, J.D. & Hays, G.C. (2009) Microhabitat selection by sea turtles in a dynamic thermal marine environment. *Journal of Animal Ecology*, **78**, 14-21.
- Schofield, G., Katselidis, K.A., Dimopoulos, P., Pantis, J.D. & Hays, G.C. (2006) Behaviour analysis of the loggerhead sea turtle *Caretta caretta* from direct in-water observation. *Endangered Species Research*, **2**, 71-79.
- Schofield, G., Katselidis, K.A., Pantis, J.D., Dimopoulos, P. & Hays, G.C. (2007) Female-female aggression: structure of interaction and outcome in loggerhead sea turtles. *Marine Ecology Progress Series*, **336**, 267-274.
- Seminoff, J.A., Jones, T.T. & Marshall, G.J. (2006) Underwater behaviour of green turtles monitored with video-time-depth recorders: what's missing from dive profiles? *Marine Ecology Progress Series*, **322**, 269-280.
- Tuck, K. (2010) How many bits are enough? The trade-off between high resolution and low power using oversampling modes. Technical Report, Freescale Semiconductor Inc. Tempe, Arizona.

- Walcott, J., Eckert, S. & Horrocks, J. (2012) Tracking hawksbill sea turtles (*Eretmochelys imbricata*) during inter-nesting intervals around Barbados. *Marine Biology*, **159**, 927-938.
- Walker, J.A. & Westneat, M.W. (2000) Mechanical performance of aquatic rowing and flying. *Proceedings of the Royal Society of London. Series B: Biological Sciences*, **267**, 1875-1881.
- Wallace, B.P., Williams, C.L., Paladino, F.V., Morreale, S.J., Lindstrom, R.T. & Spotila, J.R. (2005) Bioenergetics and diving activity of internesting leatherback turtles *Dermochelys coriacea* at Parque Nacional Marino Las Baulas, Costa Rica. *Journal of Experimental Biology*, **208**, 3873-3884.
- Wallace, B.P., Zolkewitz, M. & James, M.C. (2015) Fine-scale foraging ecology of leatherback turtles. *Frontiers in Ecology and Evolution*, **3**.
- Williams, H.J., Holton, M.D., Shepard, E.L.C., Largey, N., Norman, B., Ryan, P.G., Duriez, O., Scantlebury, M., Quintana, F., Magowan, E.A., Marks, N.J., Alagaili, A.N., Bennett, N.C. & Wilson, R.P. (2017) Identification of animal movement patterns using tri-axial magnetometry. *Movement Ecology*, **5**, 6.
- Wilmers, C.C., Nickel, B., Bryce, C.M., Smith, J.A., Wheat, R.E. & Yovovich, V. (2015) The golden age of bio-logging: How animal-borne sensors are advancing the frontiers of ecology. *Ecology*, **96**, 1741-1753.
- Wilson, A.M., Lowe, J., Roskilly, K., Hudson, P.E., Golabek, K. & McNutt, J. (2013a) Locomotion dynamics of hunting in wild cheetahs. *Nature*, **498**, 185-189.
- Wilson, J.W., Mills, M.G., Wilson, R.P., Peters, G., Mills, M.E., Speakman, J.R., Durant, S.M., Bennett, N.C., Marks, N.J. & Scantlebury, M. (2013b) Cheetahs, *Acinonyx jubatus*, balance turn capacity with pace when chasing prey. *Biology Letters*, **9**, 20130620.
- Wilson, M., Tucker, A.D., Beedholm, K. & Mann, D.A. (2017) Changes of loggerhead turtle (*Caretta caretta*) dive behavior associated with tropical storm passage during the inter-nesting period. *Journal of Experimental Biology*, **220**, 3432-3441.
- Wilson, R.P., Börger, L., Holton, M.D., Scantlebury, D.M., Gómez-Laich, A., Quintana, F., Rosell, F., Graf, P.M., Williams, H., Gunner, R., Hopkins, L., Marks, N., Geraldi, N.R., Duarte, C.M., Scott, R., Strano, M.S., Robotka, H., Eizaguirre, C., Fahlman, A. & Shepard, E.L.C. (2020a) Estimates for energy expenditure in free-living animals using acceleration proxies: A reappraisal. *Journal of Animal Ecology*, **89**, 161-172.
- Wilson, R.P., Hustler, K., Ryan, P.G., Burger, A.E. & Noldeke, E.C. (1992) Diving birds in cold water: do Archimedes and Boyle determine energetic costs? *The American Naturalist*, **140**, 179-200.
- Wilson, R.P., Rose, K.A.R., Metcalfe, R.S., Holton, M.D., Redcliffe, J., Gunner, R.M., Börger, L., Loison, A., Miloš, J., Painter, M.S., Silovský, V., Marks, N., Garel, M., Toigo, C., Marchand, P., Bennett, N.C., McNarry, M.A., Mackintosh, K.A., Brown, M.R. & Scantlebury, D.M. (2020b) Path tortuosity changes the transport cost paradigm in terrestrial animals. *bioRxiv*, 2020.2008.2020.259390.
- Wilson, R.P., Shepard, E. & Liebsch, N. (2008) Prying into the intimate details of animal lives: use of a daily diary on animals. *Endangered Species Research*, **4**, 123-137.
- Wilson, R.P., White, C.R., Quintana, F., Halsey, L.G., Liebsch, N., Martin, G.R. & Butler, P.J. (2006) Moving towards acceleration for estimates of activity-specific metabolic rate in free-living animals: the case of the cormorant. *Journal of Animal Ecology*, **75**, 1081-1090.
- Wilson, R.P., Williams, H.J., Holton, M.D., di Virgilio, A., Börger, L., Potts, J.R., Gunner, R., Arkwright, A., Fahlman, A., Bennett, N.C., Alagaili, A., Cole, N.C., Duarte, C.M. &

- Scantlebury, D.M. (2020c) An “orientation sphere” visualization for examining animal head movements. *Ecology and Evolution*, **10**, 4291-4302.
- Wyneken, J. (1997) *Sea turtle locomotion: mechanics, behavior, and energetics*. CRC Press, Boca Raton.
- Zamparo, P., Pavei, G., Monte, A., Nardello, F., Otsu, T., Numazu, N., Fujii, N. & Minetti, A.E. (2019) Mechanical work in shuttle running as a function of speed and distance: Implications for power and efficiency. *Human movement science*, **66**, 487-496.

Chapter 4

Decision rules for determining terrestrial movement and the consequences for filtering high-resolution GPS tracks – A case study using the African Lion (*Panthera leo*)

Richard M. Gunner



Photo taken by Richard M. Gunner

This work is currently in review in *Movement Ecology* as:

Gunner, R.M., Wilson, R.P., Holton, M.D., Hopkins, P., Bell, S.H., Nikki, M.J., Bennett, N.C., Ferreira, S., Govender, D., Viljoen, P., Bruns, A., van Schalkwyk, O.L., Bertelsen, M.F., Duarte, C.M., van Rooyen, M.C., Tambling, C.J., Goppert, A., Diesel, D. and Scantlebury M.D., in review. Decision rules for determining terrestrial movement and the consequences for filtering high-resolution GPS tracks – A case study using the African Lion (*Panthera leo*). *Movement Ecology*, DOI: 10.21203/rs.3.rs-600317/v1

Abstract

The combined use of Global Positioning System (GPS) technology and motion sensors within the discipline of movement ecology has increased over recent years. This is particularly the case for instrumented wildlife, with many studies now opting to record parameters at high (infra-second) sampling frequency. However, the detail with which GPS loggers can elucidate fine-scale movement depends on the precision and accuracy of fixes, with accuracy (specifically, location error and fix success rate) being affected by signal reception. I hypothesised that animal behaviour was the main factor affecting fix inaccuracy (particularly for collar-mounted tags sampling at high frequency). In conjunction to this, inherent GPS positional noise ('jitter'), would be most apparent during GPS fixes for non-moving locations, thereby producing disproportionate error during rest periods. A Movement Verified Filtering (MVF) protocol was constructed to compare GPS-derived speed data to dynamic body acceleration (DBA). This was collected by a simultaneously deployed tri-axial accelerometer, to provide a computationally quick method for identifying genuine travelling movement. This method was tested on 11 free-ranging lions (*Panthera leo*) within the Kgalagadi Transfrontier park in the Kalahari Desert, fitted with collar-mounted GPS units and tri-axial motion sensors (Daily Diary; DD) recording at 1 and 40 Hz, respectively. The findings support the hypothesis and show that distance moved estimates were, on average, overestimated by > 80 % prior to GPS screening. I present the conceptual and mathematical protocols for screening fix inaccuracy within high resolution GPS datasets. I demonstrate the importance that MVF has for avoiding inaccurate and biased estimates of movement and caution the accuracy of findings from previous studies that employed minimal GPS pre-processing. Throughout, I address the applicability of comparing fine-scale indices of GPS- and motion sensor-borne data in tandem to qualify animal behaviour.

Background

A popular method to determine terrestrial animal movement uses Global Positioning Systems (GPS), which enables long-term continuous spatial monitoring of wild animals without disturbing them (for reviews see: Nathan *et al.* 2008; Cagnacci *et al.* 2010; Latham *et al.* 2015; Hofman *et al.* 2019; Dore *et al.* 2020). This approach has led to broad applications, including examination of home ranges (Pfeiffer & Meyburg 2015; Christiansen *et al.* 2016), migratory routes (Galanti *et al.* 2000; García-Ripollés, López-López & Urios 2010; Yamaç & Bilgin 2012), habitat use (Skarin *et al.* 2008; Nielson *et al.* 2009), resource allocation (Rumble *et al.* 2001; McDuie *et al.* 2019), activity budgets (Ungar *et al.* 2005; Owen-Smith & Goodall 2014; Cristescu, Stenhouse & Boyce 2015) as well as social interactions (Hacker, Horback & Miller 2015). Since their inception, animal-borne GPS's have reduced considerably in mass and size, whilst data storage capacity, battery longevity and affordability have improved (Recio *et al.* 2013; Liu *et al.* 2017; Dore *et al.* 2020). Consequently, scientists can now track animals as small as *ca.* 20 g songbirds (*Seiurus aurocapilla*) (Hallworth & Marra 2015) at frequencies as high as 10 Hz (e.g., Gibb *et al.* 2017), providing so much detail of animal movement that even animal behaviour can often be inferred (Blecha & Alldredge 2015; de Weerd *et al.* 2015; Wang *et al.* 2015). Such inference is, however, limited by fix precision, regardless of fix accuracy, which can be particularly ambiguous when the distance travelled of the focal species is less than the spatial resolution of the GPS fixes (Ryan *et al.* 2004). Species-specific resampling strategies and correction factors can go some way to redressing this (*cf.* Ryan *et al.* 2004; Humphries, Weimerskirch & Sims 2013; Edelhoff, Signer & Balkenhol 2016).

Many factors affect GPS performance including habitat type and heterogeneity (Janeau *et al.* 2004; Swanepoel, Dalerum & Van Hoven 2010; Smith *et al.* 2018; Cochrane, Brown & Moen 2019), topography of the terrain (Cain *et al.* 2005; Ironside *et al.* 2017), view of the sky availability (Adams *et al.* 2013), weather conditions (Swanepoel, Dalerum & Van Hoven 2010), submersion in water (Quaglietta *et al.* 2012; Justicia, Rosell & Mayer 2018), time of day (Heard, Ciarniello & Seip 2008), vegetation cover/type (Cain *et al.* 2005; Hansen & Riggs 2008), GPS orientation

(D'eon & Delparte 2005), fix acquisition rate (Forin-Wiart *et al.* 2015; McGavin *et al.* 2018), in addition to the number of available satellites and their orbiting geometry with respect to one another (Lewis *et al.* 2007; Vance *et al.* 2017). All these elements affect the propagation of signal quality and/or receiver reception capability and thus increase triangulation error (see Hofman *et al.* (2019) for review), with the latter two factors often assessed *via* the dilution of precision (DOP) values (Dussault *et al.* 2001; Vance *et al.* 2017).

Species-specific movements can be misinterpreted because GPS error often exaggerates the extent of movement, with error associated with distance measures being additive over time, and particularly germane at higher sampling frequencies (given that higher rates of error are incorporated per unit time, Ganskopp & Johnson 2007; McGavin *et al.* 2018). Indeed, although a number of authors have attempted to resolve the accuracy of GPS performance by quantifying the fix success rate and location error over various scenarios (*cf.* Bjørneraas *et al.* 2010; Frair *et al.* 2010), the critical modulator of GPS performance is animal behaviour (*cf.* D'eon & Delparte 2005; Jiang *et al.* 2008; Mattisson *et al.* 2010; Brown *et al.* 2012; Jung & Kuba 2015). For example, Heard, Ciarniello and Seip (2008) demonstrated that fix success rate for GPSs on grizzly bears (*Ursus arctos*) followed a bimodal circadian pattern, which was paralleled to the activity time-budgets of the bear, with higher forest density cover and variability in collar orientation being attributed to declines in fix rate. Similarly, after collaring both Eurasian lynx (*Lynx lynx*) and wolverine (*Gulo gulo*) in similar habitat, Mattisson *et al.* (2010) suggested that high discrepancy in fix rate between the two species could be explained by differences in their behavioural repertoire. In essence, the specifics of animal movement, the 'what', 'where', 'why', 'when' and 'how' (*cf.* Nathan *et al.* 2008), underpins the species interaction with its environment and consequently the dual proficiency of signal propagation and reception between satellites and receiver. Resting is the most common behaviour for most terrestrial animals (particularly carnivores) and critically affects fix accuracy, because resting is typically associated with a change of body position (e.g., resting on the collar) and/or coverage within/near 'signal obstructing' environmental features (e.g., sleeping

under trees or in caves/ burrows), thus decreasing the available sky for the GPS receiver (Cain *et al.* 2005; Vance *et al.* 2017; Smith *et al.* 2018; Cochrane, Brown & Moen 2019). This issue is compounded for collar-mounted GPS devices, because behaviours variously affect the position of the GPS antenna even though many collars are designed to be bottom-weighted to minimise this problem (Cain *et al.* 2005; Jiang *et al.* 2008; Belant 2009).

Despite the well-documented issues of locational error and numerous mitigation strategies being proposed (Frair *et al.* 2004; Visscher 2006; Patel *et al.* 2017; Joo *et al.* 2020), there has been no 'gold standard' solution to identify inaccurate fixes. For example, Lewis *et al.* (2007) emphasised using DOP values, removing fixes with values > 5 and only keeping positions where ≥ 3 satellites were registered to eliminate potentially large location errors. This recommendation was based on the premise that a wider geometry of satellite spacing, results in lower recorded DOP values and this along with a higher number of registered satellites, is associated with minimising triangulation error. The relationship between spatial precision and increasing DOP values, whilst generally accepted, is noisy however, and this approach can reduce datasets considerably, whilst still leaving notably anomalous fixes intact (Buerkert & Schlecht 2009; Ironside *et al.* 2017). Juxtaposed to this, Bjørneraas *et al.* (2010) developed a method that focused on the movement characteristics of the focal species to identify large locational errors with minimal data reduction. This included screening for unrealistic distances travelled, speeds and turn angles between successive locations. However, this can become complicated and arbitrary at high sampling frequencies and is computationally intensive for large data sets.

To my knowledge, a specific solution for screening inaccurate locations from high resolution GPS data (e.g., ≥ 1 Hz) has not yet been proposed. The difficulty is that, whilst shorter fix intervals are typically associated with higher fix accuracy (Jiang *et al.* 2008; Forin-Wiart *et al.* 2015; McGregor *et al.* 2016), locational error is, within the wider context of daily movement, relatively small and so harder to identify accurately. Disentangling this error is particularly relevant because GPS units with

high fix rates used on animals are deployed with fine-scale analysis of movement trends in mind (*cf.* Ryan *et al.* 2004).

I note that since GPS 'jitter' (a term I use to define fixes inaccurately fluctuating around a central location) is disproportionately high during stationary periods when GPS signal is most compromised (Ganskopp & Johnson 2007; Forin-Wiart *et al.* 2015; Justicia, Rosell & Mayer 2018), the viability of deriving accurate movement from high resolution GPS trajectories depends on the ability to determine when an animal is moving or not in a manner that is independent of the GPS-derived movement. Studies have already used acceleration to activate GPS units only during movement, both as a means to increase battery longevity and avoid the fix inaccuracy prevalent during periods of inactivity (Brown *et al.* 2012; Wilson *et al.* 2013). Properly coupled GPS-acceleration systems are uncommon however, whilst a moving animal (as discerned from the accelerometer), does not necessarily correspond with a working GPS (e.g., due to signal obstruction, and because cold start 'blind' satellite searches are associated with lower fix success rates (Forin-Wiart *et al.* 2015)). For highly resolved animal tracks, I advocate the importance of recording fixes continuously, in part to mitigate performance issues associated with cold starts between fix interval (Ryan *et al.* 2004; Forin-Wiart *et al.* 2015; Moriarty & Epps 2015) and also because fine-scale GPS estimates can be compared alongside acceleration data to aid in differentiating between non-travelling movements from travelling movements (*cf.* Watanabe *et al.* 2005). Beyond this, identifying 'hotspots' of GPS jitter may be useful for discerning GPS performance (*cf.* Fig. 6) according to habitat type and/or behaviour. As part of this, I propose a new method for screening raw, high-resolution GPS data by accounting for the amount of activity using accelerometers and equating their outputs with an estimate of speed to evaluate the likelihood of movement per unit time. This is based on the observation that dynamic body acceleration (DBA - for definition see Wilson *et al.* (2020)) increases approximately linearly with speed in terrestrial animals (Bidder *et al.* 2012; Bidder *et al.* 2015; Dewhirst *et al.* 2016). Thus, any GPS-derived speed should co-vary with DBA.

Here, I propose a decision tree-based framework in which user-defined thresholds of i) GPS speed, ii) DBA and iii) time, are implemented to screen GPS fixes and remove those that do not equate to genuine travelling movement. I also suggest an initial method for screening extreme anomalous fixes using distance estimates between the raw GPS track and the median filtered equivalent. I illustrate this using data from collar-fitted free-ranging lions (*Panthera leo*) within the Kgalagadi Transfrontier Park in the Kalahari Desert. The aims of this study are to provide both the conceptual and methodological protocol for screening high resolution GPS data using a Movement Verified Filtering (MVF) protocol and to discuss the broader applicability this method has for discerning animal movement. I provide a step-by step R script for implementing this MVF method and an example lion dataset (containing DD and GPS data files) on GitHub [available at, <https://github.com/Richard6195/Dead-reckoning-animal-movements-in-R>] to allow others to trial the MVF method.

Materials and methods

The procedure relates to 14 days of data derived from 11 wild lions (5 males and 6 females) in the Kgalagadi Transfrontier Park, South Africa, during February-March 2019. Lions were equipped with a LiteTrack GPS collar (Lotek Wireless Inc. <https://www.lotek.com>), to which a Gypsy_5 Techno-smart GPS unit (Technosmart s.r.l. <https://www.technosmart.eu>) set to record at 1 Hz and a 'Daily Diary' (DD) [containing *inter alia* tri-axial accelerometers and tri-axial magnetometers] (*cf.* Wilson, Shepard & Liebsch 2008) recording at 40 Hz, were attached. The GPS units were encased in a thick 3-D printed Acrylonitrile butadiene styrene (ABS) plastic oval housing and DDs were enclosed in a water-tight aluminium housing (*cf.* supplementary information (SI): Text S1. Fig. S1).

There were two collar sizes; small collars weighed 1.24 kg and large collars weighed 1.33 kg (attached with all devices), which constituted < 2 % and < 1 % of the body mass of the lightest equipped female and male animals, respectively. Data were retrieved from the collars approximately two weeks after the tag deployment.

Intermittent behavioural observations of each pride took place at dawn and dusk, and occasionally during the day and night, for approximately 2-3 hours. During these periods, ethograms of the collared individual's various activities were recorded to document movement for comparison with the acceleration and GPS speed estimates to verify the accuracy of the MVF thresholds (Table 1). These observations were also performed to check for any potential negative side effects of the collars - none were apparent. See SI: Text S1 for more information on the study site, capture protocol and devices used. All analyses were performed in Daily Diary Multi Trace (DDMT, <http://www.wildbytetechnologies.com>), R (version 3.51, <http://www.R-project.org>) and OriginPro 2019 (<http://www.originlab.com>).

The Movement Verified Filtering (MVF) method

The MVF protocol (illustrated in Fig. 1) primarily involves deriving DBA from tri-axial accelerometry data, computing speed from GPS data, and evaluating how both scale with each other during traveling movement. Specifically, the step-by-step method (used for lions) involves:

- 1) Derivation of DBA

Vectorial dynamic body acceleration (VeDBA, Qasem *et al.* 2012) was the DBA metric used for activity (Wilson *et al.* 2020) and as a proxy for speed (Bidder *et al.* 2012). VeDBA is the vectorial sum of the dynamic body acceleration in a tri-axial acceleration signal (*cf.* SI: Text S2). A rolling mean was applied to raw VeDBA values (a 2 s centre-aligned window was used for lions) to ensure that both acceleration and deceleration components of an animal's stride cycle were incorporated together within any particular time period (Wilson *et al.* 2020).

- 2) Derivation of GPS speed

The trigonometric Haversine formula (Chopde & Nichat 2013; Harja & Sarno 2018) was used to calculate the shortest distance between fixes of an appropriate stepping range (*cf.* SI: Text S2). I define a stepping range as the interval between each retained

fix - a 5-fix stepping range was used for lions (distance computed between every 5th fix). Each successive distance estimate was divided by its time period (between retained fixes) to convert to GPS speed (m/s). A rolling mean was applied to GPS speed, (5 s centre-aligned rolling mean used for lions) for greater interpolation purposes with respect to acceleration estimates (*cf.* discussion and SI: Text S2, detailing the importance of a suitable stepping/post-smoothing range). Missing fixes were not included in the computation of GPS speed.

3) Time synchronising GPS speed and DBA data

Both VeDBA and GPS speed data were time-synchronised and sub-sampled to 1 Hz to make the data more manageable for analysis and because differentiating between fine-scale behaviours was not a prime objective of this study. Missing locational data were expressed as 'NA'.

4) Using GPS-derived distance to identify extreme outliers – Distance threshold (Z)

Missing locational data were replaced by linearly interpolating between fixes (RF). To identify extreme outliers, a median rolling filter was applied to both the longitude and latitude coordinates of the RF (MeFF). The Haversine method was then used to calculate the distance (units in metres) between the two sets of coordinates (RF vs MeFF) per unit time. Locational data (RF) above the Z threshold were deemed outliers (and thus failed the first step of the MVF protocol). By applying a rolling median using a suitable window length, large distance estimates reflecting either a single or multiple 'batched' outlier(s) could be distinguished from fixes deemed 'accurate' but highly separated in space due to large gaps in locational data. The window length size and Z threshold should be chosen according to the animal in question due to the scales of movement undertaken by different species (median filter window length of 60 s and a lenient threshold of 100 m used for lions). The window length should be large enough so that the calculated median is not affected by a potential batch of consecutive anomalies at any one time. When plotted against time, the distance between RF vs MeFF shows relatively consistent variation about a given range

(dependent on the window size set), though large obvious spikes indicate outliers, and the extent of this disparity can give an indication of the Z threshold to set.

5) Movement thresholds (X & Y)

The second stage for screening the GPS data were the thresholds of VeDBA (X_{VeDBA}) and GPS speed (Y_{GPS}) that infer moving behaviour. I set the protocol for fixes to fail the MVF protocol when;

- (i) **VeDBA < X & GPS speed > Y** (likely resultant from locational error)
- (ii) **VeDBA > X & GPS speed < Y** (likely resultant from a stationary behaviour)

where X and Y were given defined thresholds.

For the lions, after initial inspection of data with respect to ground-truthed behavioural observations, the threshold X was determined as 0.11 *g* and the threshold Y was determined as 0.35 m/s (see below). These thresholds were lenient, incorporating even slow movement and accounting for discrepancies of the relative magnitude of acceleration estimates between individuals (*cf.* Williams *et al.* 2017; Wilson *et al.* 2020).

6) Time threshold (T)

The final stage of validating movement was to implement a minimum time threshold (T), over which uninterrupted movement had to occur before it was classified as such. This was implemented to discern travelling movement (where the animal location changed) from non-travelling movement (e.g., when the animal rolled over) for periods when both X_{VeDBA} and Y_{GPS} thresholds were met. MVF values were assigned a value of one, for every GPS fix that was time-matched to periods where the above thresholds (X_{VeDBA} and Y_{GPS}) were met for a minimum duration of T (5 s was used for lions in the current study). MVF periods encoded as 1, occurring ≤ 2 s from one another were merged. A MVF value of zero represented either missing locational

data, extreme outliers (identified by Z threshold) or periods when the data indicated the animal was non-moving.

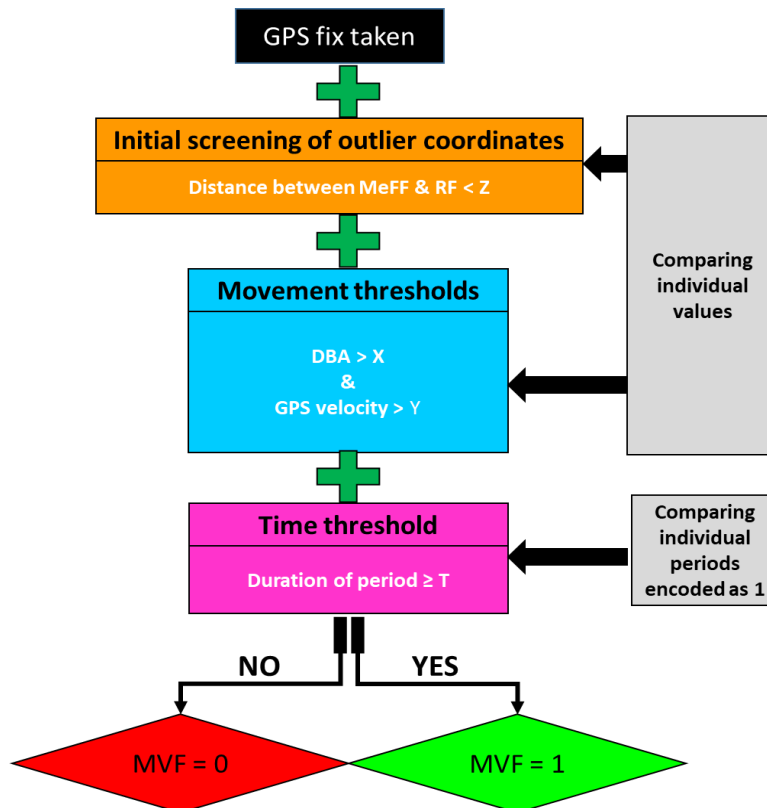


Figure 1. Schematic diagram of the movement verified filtering (MVF) procedure. GPS fixes with a MVF value of 1 are considered to be more accurate given the data indicates travelling. Note values used at each stage (including the stepping range and post-smoothing windows in the prior derivations of GPS speed and VeDBA) are user-defined and must be adapted for the study species.

Data analyses

Various movement-derived metrics were compared between periods when animals were deemed to be moving ('travelling' movement) (MVF = 1) and periods when they were deemed to be non-moving ('non-travelling'/stationary movement; MVF = 0). Such metrics include estimates of pitch, roll, heading, distance travelled, speed and tortuosity estimates (see SI: Text S4 for procedures and references therein). Here, unless otherwise stated, data ascribed as non-moving do not include data when GPS positions were missing or were extreme outliers (the latter, determined by the Z threshold as described above). Results presented as percentages are given as 'x' with variance as one standard deviation (SD) and range in the format; [$\bar{x} \pm 1$ SD (range_{min} - range_{max})].

Results

Across 25 hours of behavioural observations, the MVF method using the thresholds outlined above registered an average accuracy of 97 % (Table. 1; data correctly assigned as moving). This protocol was determined to have a high true negative rate (> 99 %) and low false positive rate (< 1 %), indicating that data that surpassed the MVF protocol indeed showed that the animal was moving with a high degree of certainty. True positive rate was slightly lower (c. 95 %) and was perceived to have been primarily modulated according to the variability in fix latency, which (irrespective of stepping/post-smoothing range) can result in a time delay, uncoupling estimates of GPS speed from the instantaneous and definitive expression of DBA estimates. It thus occasionally results in the beginning or end of periods that animals were moving being misclassified as ‘non-moving’ (MVF = 0).

Table 1. Contingency table documenting the mean accuracy and misclassification rate of the MVF method from ~ 25 hours of behavioural observations (ethograms) between eight individuals.

		Test data (actual)		Accuracy (TP + TN / TP + TN + FP + FN)
		Positive (Moving)	Negative (Non-moving)	
Predicted (MVF method)	Positive (MVF = 1 = Moving)	True Positive Rate (TPR) $TPR = \frac{TP}{(TP+FN)} \cdot 100 =$ 95.21 %	False Positive Rate (FPR) $FPR = \frac{FP}{(FP+TN)} \cdot 100 =$ 0.35 %	97.43%
	Negative (MVF = 0 = Non-moving)	False Negative Rate (FNR) = $FNR = \frac{FN}{(FN+TP)} \cdot 100 =$ 4.79 %	True Negative Rate (TNR) $TNR = \frac{TN}{(TN+FP)} \cdot 100 =$ 99.65 %	
Test data (actual)	Time spent moving / non-moving	19.37 %	80.63 %	
	VeDBA (± 1 SD)	0.198 ± 0.058	0.039 ± 0.012	

Fix success rate for the GPS varied between 89 % and 97 % across different animals. There was no indication of systematic drop-out (variability of fix success rate) being modulated according to time over the 14-day monitoring periods (SI: Text S3: Table S1 & Fig. S1). Generally, GPS-derived speed correlated well with VeDBA ($\bar{x} r^2 = 0.74 \pm 0.04$ (0.67 – 0.81), SI: Text S2: Fig. S4), especially during periods that were defined by the MVF protocol as ‘movement’ (Fig. 3A & C, SI: Text S2: Fig. S1:3). Discrepancies between GPS-speed and VeDBA were associated with location error (Fig. 2, SI: Text S2: Fig. S3), with the MVF approach highlighting that the position of the collar depended on the animal’s behaviour (Fig. 4, SI: Text S3: Table S2) and that this was a prime modulator of GPS performance (*cf.* Fig. 2, Fig. 3B, SI: Text S2: Fig. S3).

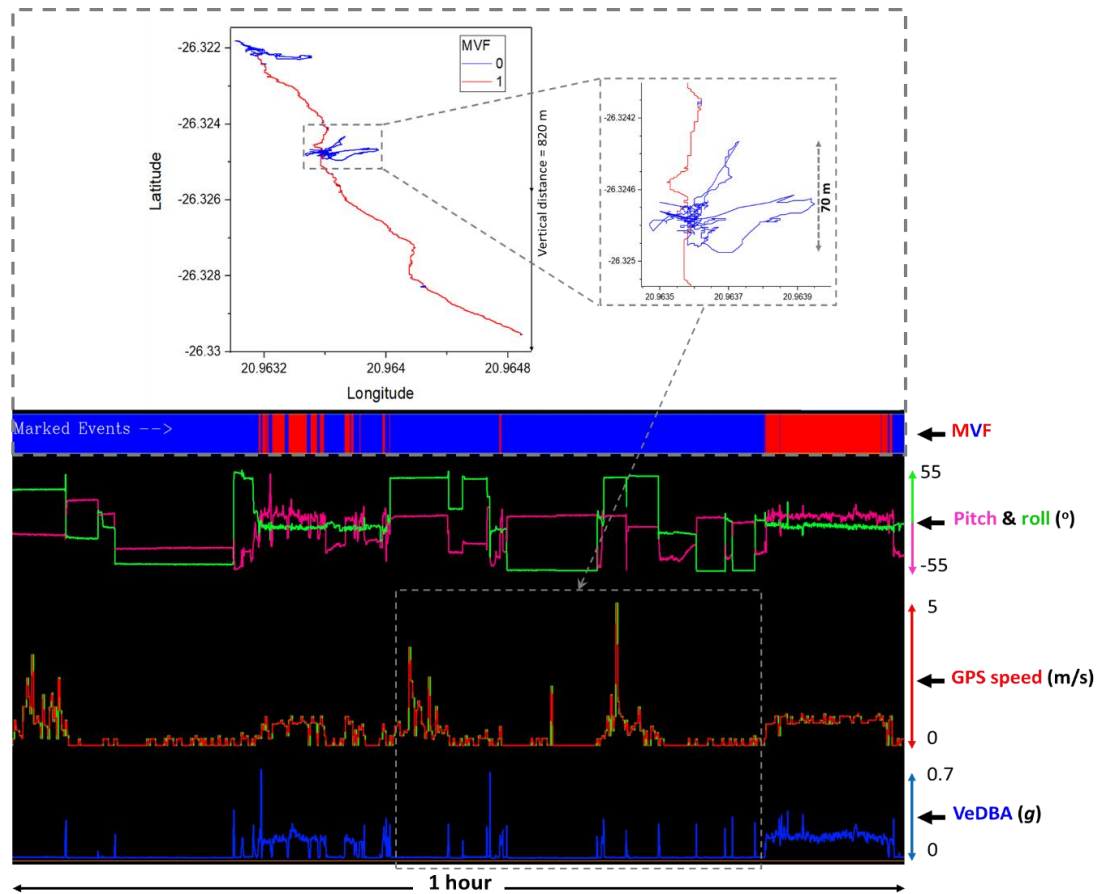


Figure 2. DD- and GPS-derived data showing intermittent periods of moving (MVF = 1: red) and stationary behaviours (MVF = 0: blue) [lower panel]. Note how many of the periods determined as non-moving high estimates of GPS speed (green = unsmoothed) due to large locational errors and this was often followed by sharp peaks in VeDBA, coinciding with a postural change (non-travelling behaviour). Note also how closely GPS speed estimates follow the VeDBA trace during periods of predominantly moving and the consistency of pitch and roll values (with intermittent bouts of stationary behaviour associated with a change in collar angle. The GPS fixes (upper panel) are coloured according to MVF values and exemplify high vertical straight-line distance between track coordinates due to GPS jitter.

On average, $13.3\% \pm 3.3$ (8.3 - 19.5) of data acquisition passed the MVF protocol (SI: Text S3: Table S2). The majority of data deemed to be non-moving, was due to both X_{VeDBA} and Y_{GPS} thresholds not being met; $70.4\% \pm 3.6$ (65 - 77). However, an appreciable proportion of non-moving data was due to the Y_{GPS} threshold being met, but not the X_{VeDBA} being met; $12.4\% \pm 3.0$ (9 - 18) or both Y_{GPS} and X_{VeDBA} thresholds being met, but not for the duration of T_{time} ; $12.5\% \pm 2.9$ (8 - 18). Data where X_{VeDBA} was met, but not Y_{GPS} , comprised $4.85\% \pm 1.3$ (3 - 7) (SI: 3: Fig. S2). The additive nature of errors associated with GPS jitter was significant and exemplified within cumulative distances moved (between fixes) (Fig. 5, SI: Text S3: Table S2) and apparent even at the broadest scales of movement (SI: Text S2: Fig. S5). It was clear that GPS jitter was much more prominent when lions were resting and unless these data were filtered, use of these raw unfiltered GPS data resulted in biased and erroneous speed, distance and tortuosity of movement estimates (SI: Text S3: Table S2). Following the MVF method, there appeared to be a greater correlation between DD- and GPS-derived heading estimates (SI: Text S4: Fig. S1).

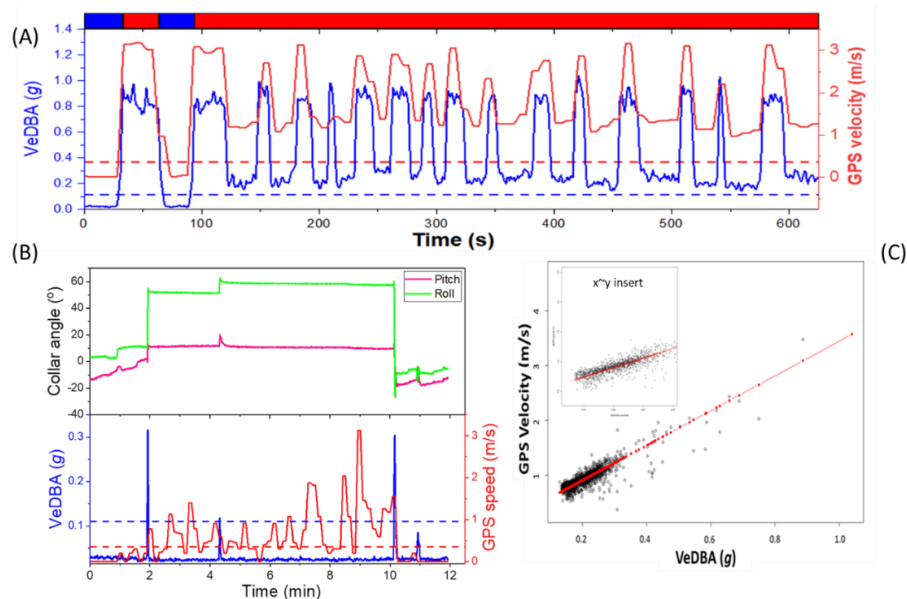


Figure 3. Example of the movement-based thresholds. (A) A period of predominately continuous movement (coloured rug at the top of plot denotes MVF values (1 = moving: red, 0 = non-moving: blue)). The peaks of both $VeDBA$ and GPS velocity are due to bouts of running, interspaced by either non-moving or walking bouts. (B) Relationship between $VeDBA$ and GPS speed during a rest period, whereby the individual carried out a transitional roll while lying prone (at approx. the 2-minute mark, as discerned by the pitch and roll angles), after which, GPS jitter became more apparent (as demonstrated by the higher variance in GPS speed estimates). (C) GPS speed \sim $VeDBA$ relationship for a given lion with linear regression ($y = a + bx$ and zoomed in the inset). Data from (C) are taken only from marked moving periods following the MVF method. Each data point represents the mean value per moving period, taken from ca. two weeks of data acquisition.

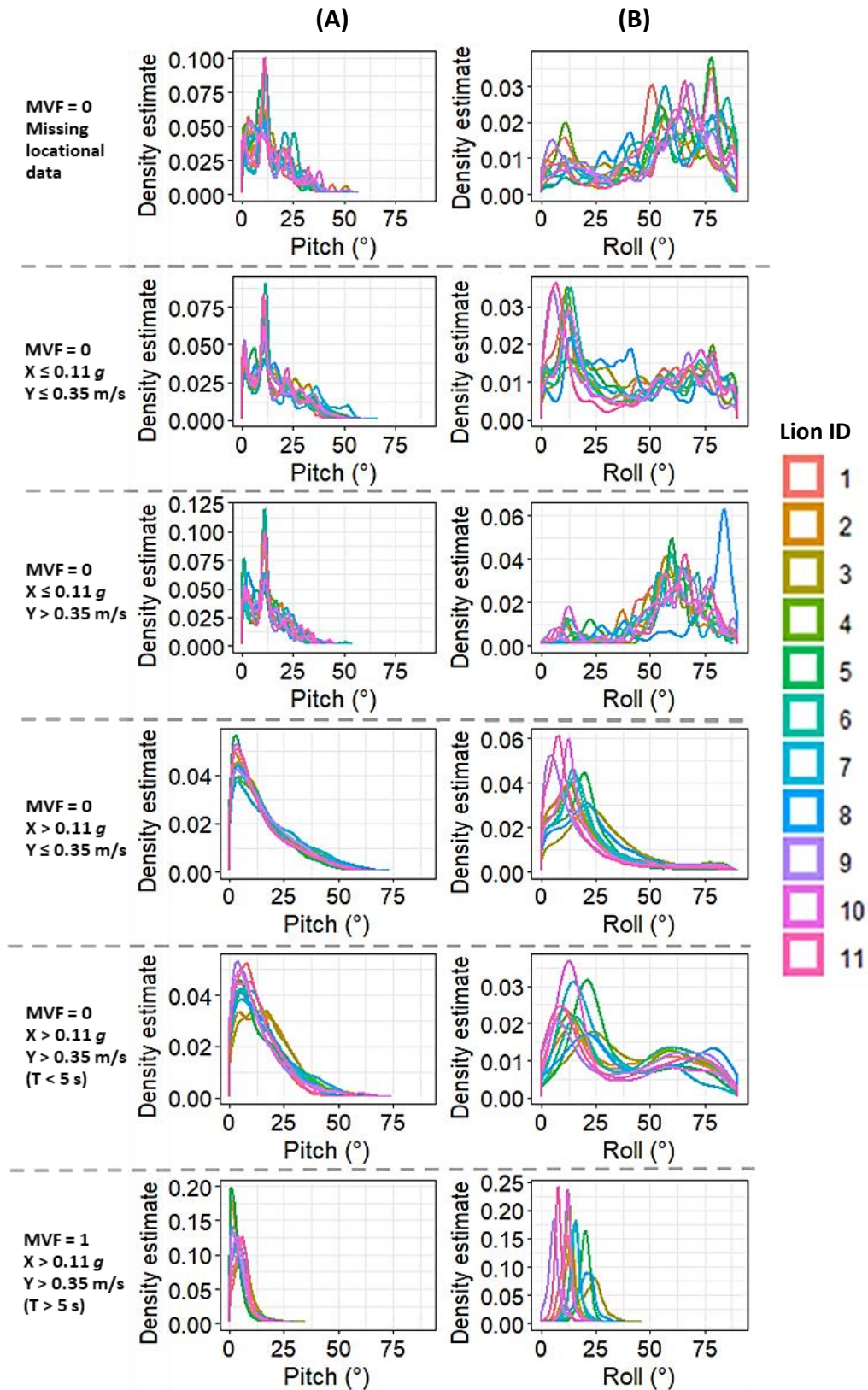


Figure 4. Indices of collar postural offsets per lion, assessed via density estimates of absolute values of; (A) pitch and (B) roll. Plots are faceted row-wise according to 5 scenarios as described to the left of each plot row. The distributions become tighter and more 'bell-shaped' at higher levels of activity.

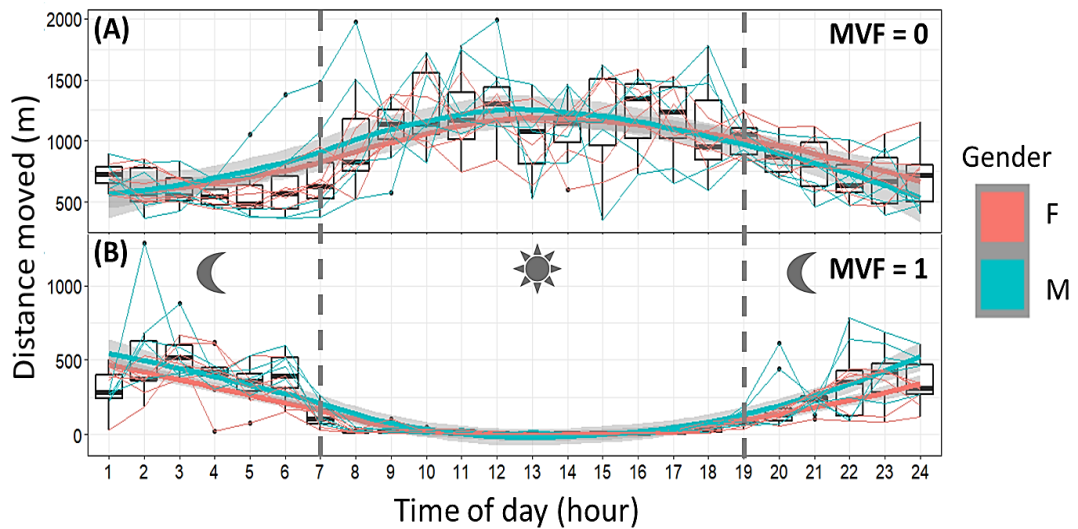


Figure 5. Mean summed distance moved (m) per hour per individual (cf. SI: Text S4 for full description of methods). Individual's hourly mean values are linearly connected across time (lines coloured according to gender; female: red, male: blue). Plots are fitted with a line of best fit according to gender, using a 'gam smoothing' (grey shading around line represents the 95 % confidence level interval). This procedure was applied independently for non-moving (MVF = 0: A) and moving (MVF = 1: B). Note the disparity in distance estimates, with non-moving bouts demonstrating high values during sunlight hours (approximately between 7 am to 7 pm [grey bars]).

Discussion

Evaluation of the MVF protocol

This work demonstrates the value of using both DBA and GPS data to discern moving behaviours from stationary behaviours with a computationally quick protocol which effectively filters inaccurate fixes from high frequency GPS data (e.g., ≥ 1 Hz, though possibly lower - cf. SI: Text S2: Fig. S1 & S2). The central premise is that when the magnitude of GPS speed and VeDBA both indicate movement (*via* pre-set thresholds, using ground-truthed data), then movement is indeed likely (Table. 1, Fig. 2, Fig. 3A, SI: Text S2: Fig S1 & S3). This highlights the problem of GPS jitter when VeDBA does not correspond to movement even though the GPS indicates otherwise. Conversely, (relatively energetic) non-travelling behaviours are flagged up when the magnitude of VeDBA infers movement while data of GPS speed does not.

Results reaffirm the importance of screening GPS inaccuracies within high frequency independently collected datasets of animal movements, due to the additive nature

of GPS jitter - most prevalent during rest periods (Fig. 2, SI: Text S3: Table S2 & Fig. S3). This was particularly relevant in the current study because of the high proportion of data allocated to non-moving behaviours (SI: Text S3: Table S2) (reflecting the energy-conservation strategy that Kalahari lions adopt, *cf.* Hill *et al.* 2004). Indices of collar/postural offsets (evaluated using absolute values of pitch and roll) showed high variability during times when GPS units did not acquire fixes (Fig. 4), even when fix success rate could not be attributed to battery longevity (SI: Text S3: Table S1, Fig. S1). Animal behaviour (including habitat selection) thus seems to be a primary factor affecting fix success rate and quality. Clear mono-modal peaks in the indices of posture were only witnessed when all thresholds of the MVF approach were met (Fig. 4). Whilst there were slight differences in the tightness of these distributions between lions (presumably due to discrepancies between collar fit), this does suggest that the optimum collar-body position for acquiring satellite signals occurred during travelling movement. In contrast, distributions were much more varied during times of non-moving, again highlighting the interplay between animal behaviour, collar orientation and GPS performance.

My results highlight how, in the absence of appropriate filtering, inappropriate conclusions about a species' movement can be made. Here, there were stark contrasts of tortuosity, speed and most notably, distance travelled estimates between sets of data that both passed and failed the MVF method (SI: Text S3: Table S2). This method may therefore have particular value for distinguishing true small-scale area-restricted search (ARS) behaviour (Weimerskirch *et al.* 2007) by removing spurious turn angles caused by jitter (DeCesare, Squires & Kolbe 2005; Hurford 2009) (*cf.* SI: Text S4: Fig. S1). Here, cumulative distance from non-moving data was 80 % higher than their actual moving periods for some lions and this highly inflated index of movement was exemplified when measured as hourly averages (Fig. 5), apparently showing that lions travelled greater distances during the hottest parts of the day, something that is extremely unlikely (*cf.* Packer *et al.* 2011). Furthermore, the MVF protocol reduced the apparent maximum speed of any lion from >150 to 48 km/h. This critical issue highlights the drawbacks of assessing GPS data sampled at high

frequency (despite necessary post-resampling strategies (SI.2)), which intensifies erroneous location estimates (*cf.* Fig. 2, SI: Text S2: Fig. S3), even at macro-scales of movement (SI: Text S2: Fig. S5).

Utility of the MVF protocol according to species-specific and environmental circumstance

The Haversine method for determination of animal speed and location using GPS positional fixes can estimate distances travelled with high precision, however for datasets containing many points collected at high frequencies, distance estimates are unreliable at small stepping ranges due to the interplay between location error and the precision of longitude and latitude coordinates that produce additive errors (Ryan *et al.* 2004; Laube & Purves 2011). Most commercial GPS units record fixes to five decimal places, with the fifth digit of the decimal place giving approximately 1.1 m resolution. Further, the computation time for a device to record a GPS fix can vary, reducing the synchronisation of time between both GPS and the accelerometer logger. Given that many terrestrial animals maintain relatively low travel speeds for extended periods (*cf.* Perry *et al.* 1988), I note that appropriate choice of stepping range and smoothing window are critical for deducing reasonable step length estimates per unit time (SI: Text S2: Fig. S1 & S2), with this being dependent upon the (species-specific) scales of movement being assessed (*cf.* Bidder, Qasem & Wilson 2012; Bidder *et al.* 2012).

Essentially, there is a trade-off between incorporating higher rates of error and increasing the lag of change relative to the properly time-synchronised acceleration data. This means that accurate fine-scale estimates of GPS-derived speed are not possible and so the relationship with body movement measurements such as VeDBA will never be succinct given the disparity of resolution from both measures. In addition, inter- and intra-specific variations of acceleration estimates can arise due to discrepancies of: morphology (Bidder *et al.* 2012), locomotion mechanisms (e.g., change in gait to facilitate higher speeds (Halsey *et al.* 2008)), extrinsic factors (e.g.,

moving over a deformable substrate / changeable grade (Kerdok *et al.* 2002; Bidder, Qasem & Wilson 2012)), tag placement (Wilson *et al.* 2020) and collar roll (Silvy, Lopez & Peterson 2005; Shepard *et al.* 2008), thereby altering the relationship between VeDBA and mechanical power (and thus speed) (Gleiss, Wilson & Shepard 2011; Bidder, Qasem & Wilson 2012).

Alongside GPS resampling, MVF user-defined thresholds are expected to change according to the study species and scales of movement in question. For example, DBA estimates (specifically ODBA - Wilson *et al.* 2020) of African elephants (*Loxodonta africana*) typically ranged between 0.15 and 0.3 *g* during periods of walking (Soltis *et al.* 2016) and this is comparable to that reported from Eurasian beavers (*Castor fiber*) (0.265 ± 0.029 - Graf *et al.* 2015), though notably, both species have different leg lengths and move with very different gaits which gives very different DBA-dependent speed estimates, as demonstrated by Bidder *et al.* (2012) for multiple species.

It is notable here that I have focussed on terrestrial movement, and this is primarily because the relationship between DBA and speed can break down substantially for many aquatic and aerial species. This occurs because, for example, birds can glide at a variety of ground speeds (depending on e.g., wind vectors and glide angle) without changing DBA, and air compression with depth affects the buoyancy of many marine animals, which complicates the DBA~speed relationship depending on swim angle (Wilson *et al.* 1992; Williams *et al.* 2015; Chapter 5). Furthermore, GPS is restricted to (potentially infrequent) resurfacing events for diving animals and so scaling DBA with GPS-derived speed is problematic for extended periods of time during underwater movements. Taken together, whilst I do not rule out extensions of the MVF method for use in such environments, I advocate that in its current form, it is most suitable for evaluating movements on land.

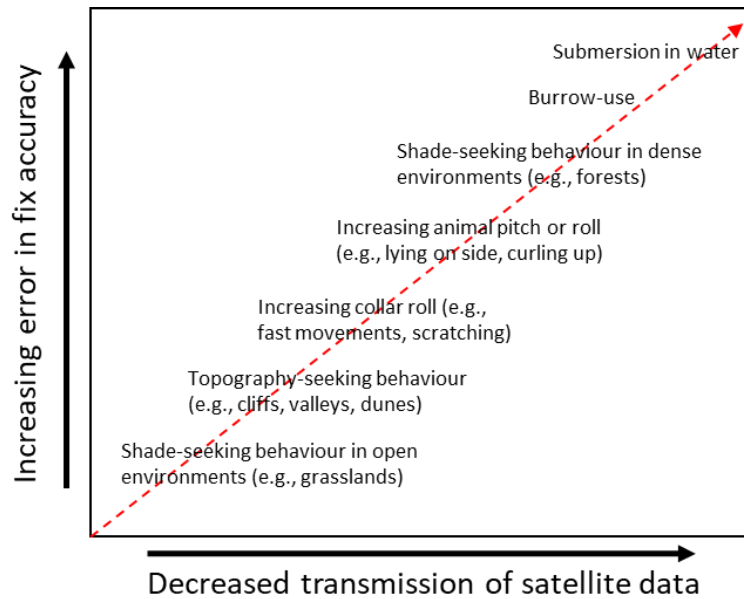


Figure 6. Schematic diagram of the factors related to animal behaviour that can change the quality of GPS fixes.

Importantly, the validity of this method is dependent on the interaction between a focal species' behaviour and where it inhabits - the critical limitation being the assumption that fixes are accurate during periods of moving. This is demonstrably not always the case (*cf.* Fig. 6), even in this study area, the Kgalagadi Transfrontier Park, which is open, with relatively sparse vegetation. Since vegetation type and density are key modulators of GPS accuracy (Lewis *et al.* 2007; Hansen & Riggs 2008; Heard, Ciarniello & Seip 2008; Frair *et al.* 2010; Adams *et al.* 2013), the viability of my method needs to be tested within other (e.g., more vegetated) environments.

Nevertheless, for the study species in question, I have highlighted the effectiveness of this method and, in line with the above considerations, have demonstrated that a general correlation does exist between the magnitudes of both DBA and GPS speed during movement periods (Fig. 3, SI: Text S2: Fig. S1:S3). As such, I suggest that this approach could be used further to discern reliable events of high performance (e.g., hunt chases) and implemented within the dead-reckoning framework (*cf.* Bidder *et al.* 2015; Walker *et al.* 2015), both as a corollary to the DBA-speed relationship (required for the speed coefficient, Bidder *et al.* 2015) and the GPS screening protocol

prior to the correction process of dead-reckoned tracks (Dewhirst *et al.* 2016). At the very least, I demonstrate the utility for GPS speed to be included as a useful parameter for identifying behaviours and may be of value to more complex approaches (e.g., machine learning (*cf.* Bidder *et al.* 2014; Samarasinghe 2016; Fehlmann *et al.* 2017; Goodall *et al.* 2019), the lowest common denominator (LoCoD) method, (*cf.* Wilson *et al.* 2018), and space-state models, (*cf.* Fleming *et al.* 2020; Jonsen *et al.* 2020)) for precluding certain behaviours from movement and screening for location error. Indeed, applying this method as a validator of movement extent within behaviour-based studies over finely resolved space and time, may facilitate the powers of inference, such as when considering animal responses to human barriers (*cf.* Jacobson *et al.* 2016). Lastly, I theorise that high fix frequency will help elucidate fix inaccuracy within areas of high canopy cover, possibly *via* extensions to this method such as including upper threshold limits and comparing variation in GPS speed juxtaposed to DBA estimates and GPS- and DD-derived heading estimates (*cf.* SI: Text S4).

Conclusion

Here I reaffirm the importance of initial GPS screening so to avoid inaccurate movement estimates. Animal behaviour seems to be a major modulator of GPS performance, and this is particularly germane in collared species due to the interaction between behaviour and collar orientation. The proposed Movement Verified Filtering method provides a basis for high-resolution GPS-screening, which is user-friendly, computationally quick and focuses on identifying behaviour to filter GPS data. Movement-defined thresholds can be modelled according to the focal species in question, whilst further differences between motion sensor and GPS derivatives can be incorporated into this MVF foundation to resolve fix inaccuracy during movement. Movement-based outputs comparing MVF values from lion data, exemplified the degree of inaccuracy associated with GPS jitter and the importance of removing such additive error prior to assessing fine-scale trends of movement,

particularly step length. My results show that consideration of data from both GPS units and motion sensors greatly helps validate true movement patterns and reaffirms the caution required when interpreting fine-scale GPS sampling such as during ARS analysis. Further work could assess the value of MVF for other species with different activities and habitat selections, particularly those that move within highly vegetated areas. The consequences of the errors introduced by GPS inaccuracies are broad, ranging from erroneous inferences of behaviour, movement, speed and energy budgets. The approach proposed here avoids these errors and enables accurate assessments of these traits.

References

- Adams, A.L., Dickinson, K.J.M., Robertson, B.C. & van Heezik, Y. (2013) An Evaluation of the Accuracy and Performance of Lightweight GPS Collars in a Suburban Environment. *PLOS ONE*, **8**, e68496.
- Belant, J.L. (2009) Effects of Antenna Orientation and Vegetation on Global Positioning System Telemetry Collar Performance. *Northeastern Naturalist*, **16**, 577-584, 578.
- Bidder, O.R., Campbell, H.A., Gómez-Laich, A., Urgé, P., Walker, J., Cai, Y., Gao, L., Quintana, F. & Wilson, R.P. (2014) Love Thy Neighbour: Automatic Animal Behavioural Classification of Acceleration Data Using the K-Nearest Neighbour Algorithm. *PLOS ONE*, **9**, e88609.
- Bidder, O.R., Qasem, L.A. & Wilson, R.P. (2012) On Higher Ground: How Well Can Dynamic Body Acceleration Determine Speed in Variable Terrain? *PLOS ONE*, **7**, e50556.
- Bidder, O.R., Soresina, M., Shepard, E.L.C., Halsey, L.G., Quintana, F., Gómez-Laich, A. & Wilson, R.P. (2012) The need for speed: testing acceleration for estimating animal travel rates in terrestrial dead-reckoning systems. *Zoology*, **115**, 58-64.
- Bidder, O.R., Walker, J.S., Jones, M.W., Holton, M.D., Urge, P., Scantlebury, D.M., Marks, N.J., Magowan, E.A., Maguire, I.E. & Wilson, R.P. (2015) Step by step: reconstruction of terrestrial animal movement paths by dead-reckoning. *Movement Ecology*, **3**, 23.
- Bjørneraas, K., Van Moorter, B., Rolandsen, C.M. & Herfindal, I. (2010) Screening Global Positioning System Location Data for Errors Using Animal Movement Characteristics. *The Journal of Wildlife Management*, **74**, 1361-1366.
- Blecha, K.A. & Alldredge, M.W. (2015) Improvements on GPS Location Cluster Analysis for the Prediction of Large Carnivore Feeding Activities: Ground-Truth Detection Probability and Inclusion of Activity Sensor Measures. *PLOS ONE*, **10**, e0138915.
- Brown, D.D., LaPoint, S., Kays, R., Heidrich, W., Kümmeth, F. & Wikelski, M. (2012) Accelerometer-informed GPS telemetry: Reducing the trade-off between resolution and longevity. *Wildlife Society Bulletin*, **36**, 139-146.
- Buerkert, A. & Schlecht, E. (2009) Performance of three GPS collars to monitor goats' grazing itineraries on mountain pastures. *Computers and Electronics in Agriculture*, **65**, 85-92.
- Cagnacci, F., Boitani, L., Powell, R.A. & Boyce, M.S. (2010) Animal ecology meets GPS-based radiotelemetry: a perfect storm of opportunities and challenges. *Philosophical Transactions of the Royal Society B: Biological Sciences*, **365**, 2157-2162.
- Cain, J.W., Krausman, P.R., Jansen, B.D. & Morgart, J.R. (2005) Influence of topography and GPS fix interval on GPS collar performance. *Wildlife Society Bulletin*, **33**, 926-934.
- Chopde, N.R. & Nichat, M.K. (2013) Landmark based shortest path detection by using A* and Haversine formula. *International Journal of Innovative Research in Computer and Communication Engineering*, **1**, 298-302.
- Christiansen, F., Esteban, N., Mortimer, J.A., Dujon, A.M. & Hays, G.C. (2016) Diel and seasonal patterns in activity and home range size of green turtles on their foraging grounds revealed by extended Fastloc-GPS tracking. *Marine Biology*, **164**, 10.
- Cochrane, M.M., Brown, D.J. & Moen, R.A. (2019) GPS Technology for Semi-Aquatic Turtle Research. *Diversity*, **11**, 34.
- Cristescu, B., Stenhouse, G.B. & Boyce, M.S. (2015) Predicting multiple behaviors from GPS radiocollar cluster data. *Behavioral Ecology*, **26**, 452-464.

- D'eon, R.G. & Delparte, D. (2005) Effects of radio-collar position and orientation on GPS radio-collar performance, and the implications of PDOP in data screening. *Journal of Applied Ecology*, **42**, 383-388.
- de Weerd, N., van Langevelde, F., van Oeveren, H., Nolet, B.A., Kölzsch, A., Prins, H.H.T. & de Boer, W.F. (2015) Deriving Animal Behaviour from High-Frequency GPS: Tracking Cows in Open and Forested Habitat. *PLOS ONE*, **10**, e0129030.
- DeCesare, N.J., Squires, J.R. & Kolbe, J.A. (2005) Effect of forest canopy on GPS-based movement data. *Wildlife Society Bulletin*, **33**, 935-941.
- Dewhurst, O.P., Evans, H.K., Roskilly, K., Harvey, R.J., Hubel, T.Y. & Wilson, A.M. (2016) Improving the accuracy of estimates of animal path and travel distance using GPS drift-corrected dead reckoning. *Ecology and Evolution*, **6**, 6210-6222.
- Dore, K.M., Hansen, M.F., Klegarth, A.R., Fichtel, C., Koch, F., Springer, A., Kappeler, P., Parga, J.A., Humle, T., Colin, C., Raballand, E., Huang, Z.-P., Qi, X.-G., Di Fiore, A., Link, A., Stevenson, P.R., Stark, D.J., Tan, N., Gallagher, C.A., Anderson, C.J., Campbell, C.J., Kenyon, M., Pebsworth, P., Sprague, D., Jones-Engel, L. & Fuentes, A. (2020) Review of GPS collar deployments and performance on nonhuman primates. *Primates*, **61**, 1-15.
- Dussault, C., Courtois, R., Ouellet, J.-P. & Huot, J. (2001) Influence of Satellite Geometry and Differential Correction on GPS Location Accuracy. *Wildlife Society Bulletin (1973-2006)*, **29**, 171-179.
- Edelhoff, H., Signer, J. & Balkenhol, N. (2016) Path segmentation for beginners: an overview of current methods for detecting changes in animal movement patterns. *Movement Ecology*, **4**, 21.
- Fehlmann, G., O'Riain, M.J., Hopkins, P.W., O'Sullivan, J., Holton, M.D., Shepard, E.L.C. & King, A.J. (2017) Identification of behaviours from accelerometer data in a wild social primate. *Animal Biotelemetry*, **5**, 6.
- Fleming, C.H., Drescher-Lehman, J., Noonan, M.J., Akre, T.S.B., Brown, D.J., Cochrane, M.M., Dejid, N., DeNicola, V., DePerno, C.S., Dunlop, J.N., Gould, N.P., Hollins, J., Ishii, H., Kaneko, Y., Kays, R., Killen, S.S., Koeck, B., Lambertucci, S.A., LaPoint, S.D., Medici, E.P., Meyburg, B.-U., Miller, T.A., Moen, R.A., Mueller, T., Pfeiffer, T., Pike, K.N., Roulin, A., Safi, K., Séchaud, R., Scharf, A.K., Shephard, J.M., Stabach, J.A., Stein, K., Tonra, C.M., Yamazaki, K., Fagan, W.F. & Calabrese, J.M. (2020) A comprehensive framework for handling location error in animal tracking data*. *bioRxiv*, 2020.2006.2012.130195.
- Forin-Wiart, M.-A., Hubert, P., Sirguy, P. & Poulle, M.-L. (2015) Performance and Accuracy of Lightweight and Low-Cost GPS Data Loggers According to Antenna Positions, Fix Intervals, Habitats and Animal Movements. *PLOS ONE*, **10**, e0129271.
- Frair, J.L., Fieberg, J., Hebblewhite, M., Cagnacci, F., DeCesare, N.J. & Pedrotti, L. (2010) Resolving issues of imprecise and habitat-biased locations in ecological analyses using GPS telemetry data. *Philosophical Transactions of the Royal Society B: Biological Sciences*, **365**, 2187-2200.
- Frair, J.L., Nielsen, S.E., Merrill, E.H., Lele, S.R., Boyce, M.S., Munro, R.H.M., Stenhouse, G.B. & Beyer, H.L. (2004) Removing GPS collar bias in habitat selection studies. *Journal of Applied Ecology*, **41**, 201-212.
- Galanti, V., Tosi, G., Rossi, R. & Foley, C. (2000) The use of GPS radio-collars to track elephants (*Loxodonta africana*) in the Tarangire National Park (Tanzania). *Hystrix, the Italian Journal of Mammalogy*, **11**.
- Ganskopp, D.C. & Johnson, D.D. (2007) GPS Error in Studies Addressing Animal Movements and Activities. *Rangeland Ecology & Management*, **60**, 350-358.

- García-Ripollés, C., López-López, P. & Urios, V. (2010) First description of migration and wintering of adult Egyptian Vultures *Neophron percnopterus* tracked by GPS satellite telemetry. *Bird Study*, **57**, 261-265.
- Gibb, R., Shoji, A., Fayet, A.L., Perrins, C.M., Guilford, T. & Freeman, R. (2017) Remotely sensed wind speed predicts soaring behaviour in a wide-ranging pelagic seabird. *Journal of The Royal Society Interface*, **14**, 20170262.
- Gleiss, A.C., Wilson, R.P. & Shepard, E.L.C. (2011) Making overall dynamic body acceleration work: on the theory of acceleration as a proxy for energy expenditure. *Methods in Ecology and Evolution*, **2**, 23-33.
- Goodall, V.L., Ferreira, S.M., Funston, P.J. & Maruping-Mzileni, N. (2019) Uncovering hidden states in African lion movement data using hidden Markov models. *Wildlife Research*, **46**, 296-303.
- Graf, P.M., Wilson, R.P., Qasem, L., Hackländer, K. & Rosell, F. (2015) The Use of Acceleration to Code for Animal Behaviours; A Case Study in Free-Ranging Eurasian Beavers *Castor fiber*. *PLOS ONE*, **10**, e0136751.
- Hacker, C.E., Horback, K.M. & Miller, L.J. (2015) GPS technology as a proxy tool for determining relationships in social animals: An example with African elephants. *Applied Animal Behaviour Science*, **163**, 175-182.
- Hallworth, M.T. & Marra, P.P. (2015) Miniaturized GPS Tags Identify Non-breeding Territories of a Small Breeding Migratory Songbird. *Scientific Reports*, **5**, 11069.
- Halsey, L.G., Shepard, E.L.C., Hulston, C.J., Venables, M.C., White, C.R., Jeukendrup, A.E. & Wilson, R.P. (2008) Acceleration versus heart rate for estimating energy expenditure and speed during locomotion in animals: Tests with an easy model species, *Homo sapiens*. *Zoology*, **111**, 231-241.
- Hansen, M.C. & Riggs, R.A. (2008) Accuracy, Precision, and Observation Rates of Global Positioning System Telemetry Collars. *The Journal of Wildlife Management*, **72**, 518-526.
- Harja, Y.D. & Sarno, R. (2018) Determine the best option for nearest medical services using Google maps API, Haversine and TOPSIS algorithm. *2018 International Conference on Information and Communications Technology (ICOIACT)*, pp. 814-819.
- Heard, D.C., Ciarniello, L.M. & Seip, D.R. (2008) Grizzly Bear Behavior and Global Positioning System Collar Fix Rates. *The Journal of Wildlife Management*, **72**, 596-602.
- Hill, R.W., Wyse, G.A., Anderson, M. & Anderson, M. (2004) *Animal physiology*. Sinauer Associates Sunderland, MA.
- Hofman, M.P.G., Hayward, M.W., Heim, M., Marchand, P., Rolandsen, C.M., Mattisson, J., Urbano, F., Heurich, M., Mysterud, A., Melzheimer, J., Morellet, N., Voigt, U., Allen, B.L., Gehr, B., Rouco, C., Ullmann, W., Holand, Ø., Jørgensen, N.H., Steinheim, G., Cagnacci, F., Kroeschel, M., Kaczensky, P., Buuveibaatar, B., Payne, J.C., Palmegiani, I., Jerina, K., Kjellander, P., Johansson, Ö., LaPoint, S., Bayrakcismith, R., Linnell, J.D.C., Zaccaroni, M., Jorge, M.L.S., Oshima, J.E.F., Songhurst, A., Fischer, C., Mc Bride, R.T., Jr., Thompson, J.J., Streif, S., Sandfort, R., Bonenfant, C., Drouilly, M., Klapproth, M., Zinner, D., Yarnell, R., Stronza, A., Wilmott, L., Meisingset, E., Thaker, M., Vanak, A.T., Nicoloso, S., Graeber, R., Said, S., Boudreau, M.R., Devlin, A., Hoogsteijn, R., May-Junior, J.A., Nifong, J.C., Odden, J., Quigley, H.B., Tortato, F., Parker, D.M., Caso, A., Perrine, J., Tellaeche, C., Zieba, F., Zwijacz-Kozica, T., Appel, C.L., Axsom, I., Bean, W.T., Cristescu, B., Périquet, S., Teichman, K.J., Karpanty, S., Licoppe, A., Menges, V., Black, K., Scheppers, T.L., Schai-Braun, S.C., Azevedo, F.C., Lemos, F.G., Payne, A., Swanepoel, L.H., Weckworth, B.V., Berger, A., Bertassoni, A., McCulloch, G., Šustr, P., Athreya, V., Bockmuhl, D., Casaer, J., Ekori, A., Melovski, D.,

- Richard-Hansen, C., van de Vyver, D., Reyna-Hurtado, R., Robardet, E., Selva, N., Sergiel, A., Farhadinia, M.S., Sunde, P., Portas, R., Ambarli, H., Berzins, R., Kappeler, P.M., Mann, G.K., Pyritz, L., Bissett, C., Grant, T., Steinmetz, R., Swedell, L., Welch, R.J., Armenteras, D., Bidder, O.R., González, T.M., Rosenblatt, A., Kachel, S. & Balkenhol, N. (2019) Right on track? Performance of satellite telemetry in terrestrial wildlife research. *PLOS ONE*, **14**, e0216223.
- Humphries, N.E., Weimerskirch, H. & Sims, D.W. (2013) A new approach for objective identification of turns and steps in organism movement data relevant to random walk modelling. *Methods in Ecology and Evolution*, **4**, 930-938.
- Hurford, A. (2009) GPS Measurement Error Gives Rise to Spurious 180° Turning Angles and Strong Directional Biases in Animal Movement Data. *PLOS ONE*, **4**, e5632.
- Ironside, K.E., Mattson, D.J., Arundel, T.R. & Hansen, J.R. (2017) Is GPS telemetry location error screening beneficial? *Wildlife Biology*, **2017**.
- Jacobson, S.L., Bliss-Ketchum, L.L., de Rivera, C.E. & Smith, W.P. (2016) A behavior-based framework for assessing barrier effects to wildlife from vehicle traffic volume. *Ecosphere*, **7**, e01345.
- Janeau, G., Adrados, C., Joachim, J., Gendner, J.-P. & Pépin, D. (2004) Performance of differential GPS collars in temperate mountain forest. *Comptes Rendus Biologies*, **327**, 1143-1149.
- Jiang, Z., Sugita, M., Kitahara, M., Takatsuki, S., Goto, T. & Yoshida, Y. (2008) Effects of habitat feature, antenna position, movement, and fix interval on GPS radio collar performance in Mount Fuji, central Japan. *Ecological Research*, **23**, 581-588.
- Jonsen, I.D., Patterson, T.A., Costa, D.P., Doherty, P.D., Godley, B.J., Grecian, W.J., Guinet, C., Hoenner, X., Kienle, S.S., Robinson, P.W., Votier, S.C., Whiting, S., Witt, M.J., Hindell, M.A., Harcourt, R.G. & McMahon, C.R. (2020) A continuous-time state-space model for rapid quality control of argos locations from animal-borne tags. *Movement Ecology*, **8**, 31.
- Joo, R., Boone, M.E., Clay, T.A., Patrick, S.C., Clusella-Trullas, S. & Basille, M. (2020) Navigating through the R packages for movement. *Journal of Animal Ecology*, **89**, 248-267.
- Jung, T.S. & Kuba, K. (2015) Performance of GPS collars on free-ranging bison (*Bison bison*) in north-western Canada. *Wildlife Research*, **42**, 315-323.
- Justicia, L.S., Rosell, F. & Mayer, M. (2018) Performance of GPS units for deployment on semiaquatic animals. *PLOS ONE*, **13**, e0207938.
- Kerdok, A.E., Biewener, A.A., McMahon, T.A., Weyand, P.G. & Herr, H.M. (2002) Energetics and mechanics of human running on surfaces of different stiffnesses. *Journal of Applied Physiology*, **92**, 469-478.
- Latham, A.D.M., Latham, M.C., Anderson, D.P., Cruz, J., Herries, D. & Hebblewhite, M. (2015) The GPS craze: six questions to address before deciding to deploy GPS technology on wildlife. *New Zealand Journal of Ecology*, **39**, 143-152.
- Laube, P. & Purves, R.S. (2011) How fast is a cow? Cross-Scale Analysis of Movement Data. *Transactions in GIS*, **15**, 401-418.
- Lewis, J.S., Rachlow, J.L., Garton, E.O. & Vierling, L.A. (2007) Effects of habitat on GPS collar performance: using data screening to reduce location error. *Journal of Applied Ecology*, **44**, 663-671.
- Liu, D., Zhang, G., Jiang, H., Chen, L., Meng, D. & Lu, J. (2017) Seasonal dispersal and longitudinal migration in the Relict Gull *Larus relictus* across the Inner-Mongolian Plateau. *PeerJ*, **5**, e3380.

- Mattisson, J., Andrén, H., Persson, J. & Segerström, P. (2010) Effects of Species Behavior on Global Positioning System Collar Fix Rates. *The Journal of Wildlife Management*, **74**, 557-563.
- McDuie, F., Casazza, M.L., Overton, C.T., Herzog, M.P., Hartman, C.A., Peterson, S.H., Feldheim, C.L. & Ackerman, J.T. (2019) GPS tracking data reveals daily spatio-temporal movement patterns of waterfowl. *Movement Ecology*, **7**, 6.
- McGavin, S.L., Bishop-Hurley, G.J., Charmley, E., Greenwood, P.L. & Callaghan, M.J. (2018) Effect of GPS sample interval and paddock size on estimates of distance travelled by grazing cattle in rangeland, Australia. *The Rangeland Journal*, **40**, 55-64.
- McGregor, H.W., Legge, S.M., Jones, M.E. & Johnson, C.N. (2016) GPS collars are more efficient when collecting high-frequency data. *Australian Mammalogy*, **38**, 237-240.
- Moriarty, K.M. & Epps, C.W. (2015) Retained satellite information influences performance of GPS devices in a forested ecosystem. *Wildlife Society Bulletin*, **39**, 349-357.
- Nathan, R., Getz, W.M., Revilla, E., Holyoak, M., Kadmon, R., Saltz, D. & Smouse, P.E. (2008) A movement ecology paradigm for unifying organismal movement research. *Proceedings of the National Academy of Sciences*, **105**, 19052-19059.
- Nielson, R.M., Manly, B.F.J., McDonald, L.L., Sawyer, H. & McDonald, T.L. (2009) Estimating habitat selection when GPS fix success is less than 100%. *Ecology*, **90**, 2956-2962.
- Owen-Smith, N. & Goodall, V. (2014) Coping with savanna seasonality: comparative daily activity patterns of African ungulates as revealed by GPS telemetry. *Journal of Zoology*, **293**, 181-191.
- Packer, C., Swanson, A., Ikanda, D. & Kushnir, H. (2011) Fear of darkness, the full moon and the nocturnal ecology of African lions. *PLOS ONE*, **6**, e22285.
- Patel, A., Stocks, B., Fisher, C., Nicolls, F. & Boje, E. (2017) Tracking the Cheetah Tail Using Animal-Borne Cameras, GPS, and an IMU. *IEEE Sensors Letters*, **1**, 1-4.
- Perry, A.K., Blickhan, R., Biewener, A.A., Heglund, N.C. & Taylor, C.R. (1988) Preferred speeds in terrestrial vertebrates: are they equivalent? *Journal of Experimental Biology*, **137**, 207-219.
- Pfeiffer, T. & Meyburg, B.-U. (2015) GPS tracking of Red Kites (*Milvus milvus*) reveals fledgling number is negatively correlated with home range size. *Journal of Ornithology*, **156**, 963-975.
- Qasem, L., Cardew, A., Wilson, A., Griffiths, I., Halsey, L.G., Shepard, E.L.C., Gleiss, A.C. & Wilson, R. (2012) Tri-Axial Dynamic Acceleration as a Proxy for Animal Energy Expenditure; Should We Be Summing Values or Calculating the Vector? *PLOS ONE*, **7**, e31187.
- Quaglietta, L., Martins, B.H., de Jongh, A., Mira, A. & Boitani, L. (2012) A Low-Cost GPS GSM/GPRS Telemetry System: Performance in Stationary Field Tests and Preliminary Data on Wild Otters (*Lutra lutra*). *PLOS ONE*, **7**, e29235.
- Recio, M.R., Mathieu, R., Latham, M.C., Latham, A.D.M. & Seddon, P.J. (2013) Quantifying fine-scale resource selection by introduced European hedgehogs (*Erinaceus europaeus*) in ecologically sensitive areas. *Biological Invasions*, **15**, 1807-1818.
- Rumble, M.A., Benkobi, L., Lindzey, F. & Gamo, R.S. (2001) Evaluating elk habitat interactions with GPS collars. *Tracking animals with GPS*, pp. 11-17. Macaulay Land Use Research Institute, Aberdeen, UK: Macaulay Institute.
- Ryan, P.G., Petersen, S.L., Peters, G. & Grémillet, D. (2004) GPS tracking a marine predator: the effects of precision, resolution and sampling rate on foraging tracks of African Penguins. *Marine Biology*, **145**, 215-223.
- Samarasinghe, S. (2016) *Neural Networks for Applied Sciences and Engineering: From Fundamentals to Complex Pattern Recognition*. CRC Press.

- Shepard, E.L., Wilson, R.P., Halsey, L.G., Quintana, F., Laich, A.G., Gleiss, A.C., Liebsch, N., Myers, A.E. & Norman, B. (2008) Derivation of body motion via appropriate smoothing of acceleration data. *Aquatic Biology*, **4**, 235-241.
- Silvy, N.J., Lopez, R.R. & Peterson, M.J. (2005) *Wildlife marking techniques*. The Wildlife Society: Bethesda, MD.
- Skarin, A., Danell, Ö., Bergström, R. & Moen, J. (2008) Summer habitat preferences of GPS-collared reindeer *Rangifer tarandus tarandus*. *Wildlife Biology*, **14**, 1-15.
- Smith, B.J., Hart, K.M., Mazzotti, F.J., Basille, M. & Romagosa, C.M. (2018) Evaluating GPS biologging technology for studying spatial ecology of large constricting snakes. *Animal Biotelemetry*, **6**, 1.
- Soltis, J., King, L., Vollrath, F. & Douglas-Hamilton, I. (2016) Accelerometers and simple algorithms identify activity budgets and body orientation in African elephants *Loxodonta africana*. *Endangered Species Research*, **31**, 1-12.
- Swanepoel, L.H., Dalerum, F. & Van Hoven, W. (2010) Factors affecting location failure of GPS collars fitted to African leopards (*Panthera pardus*). *African Journal of Wildlife Research*, **40**, 10-15.
- Ungar, E.D., Henkin, Z., Gutman, M., Dolev, A., Genizi, A. & Ganskopp, D. (2005) Inference of animal activity from GPS collar data on free-ranging cattle. *Rangeland Ecology & Management*, **58**, 256-266.
- Vance, J.A., Jachowski, D.S., Boynton, A.C. & Kelly, M.J. (2017) Importance of evaluating GPS telemetry collar performance in monitoring reintroduced populations. *Wildlife Society Bulletin*, **41**, 729-735.
- Visscher, D.R. (2006) GPS measurement error and resource selection functions in a fragmented landscape. *Ecography*, **29**, 458-464.
- Walker, J.S., Jones, M.W., Laramee, R.S., Holton, M.D., Shepard, E.L.C., Williams, H.J., Scantlebury, D.M., Marks, N.J., Magowan, E.A., Maguire, I.E., Bidder, O.R., Di Virgilio, A. & Wilson, R.P. (2015) Prying into the intimate secrets of animal lives; software beyond hardware for comprehensive annotation in 'Daily Diary' tags. *Movement Ecology*, **3**, 29.
- Wang, Y., Nickel, B., Rutishauser, M., Bryce, C.M., Williams, T.M., Elkaim, G. & Wilmers, C.C. (2015) Movement, resting, and attack behaviors of wild pumas are revealed by tri-axial accelerometer measurements. *Movement Ecology*, **3**, 1-12.
- Watanabe, S., Izawa, M., Kato, A., Ropert-Coudert, Y. & Naito, Y. (2005) A new technique for monitoring the detailed behaviour of terrestrial animals: A case study with the domestic cat. *Applied Animal Behaviour Science*, **94**, 117-131.
- Weimerskirch, H., Pinaud, D., Pawlowski, F. & Bost, C.A. (2007) Does Prey Capture Induce Area-Restricted Search? A Fine-Scale Study Using GPS in a Marine Predator, the Wandering Albatross. *The American Naturalist*, **170**, 734-743.
- Williams, H., Shepard, E., Duriez, O. & Lambertucci, S.A. (2015) Can accelerometry be used to distinguish between flight types in soaring birds? *Animal Biotelemetry*, **3**, 1-11.
- Williams, H.J., Holton, M.D., Shepard, E.L.C., Largey, N., Norman, B., Ryan, P.G., Duriez, O., Scantlebury, M., Quintana, F., Magowan, E.A., Marks, N.J., Alagaili, A.N., Bennett, N.C. & Wilson, R.P. (2017) Identification of animal movement patterns using tri-axial magnetometry. *Movement Ecology*, **5**, 6.
- Wilson, A.M., Lowe, J., Roskilly, K., Hudson, P.E., Golabek, K. & McNutt, J. (2013) Locomotion dynamics of hunting in wild cheetahs. *Nature*, **498**, 185-189.
- Wilson, R.P., Börger, L., Holton, M.D., Scantlebury, D.M., Gómez-Laich, A., Quintana, F., Rosell, F., Graf, P.M., Williams, H., Gunner, R., Hopkins, L., Marks, N., Geraldi, N.R., Duarte, C.M., Scott, R., Strano, M.S., Robotka, H., Eizaguirre, C., Fahlman, A. &

- Shepard, E.L.C. (2020) Estimates for energy expenditure in free-living animals using acceleration proxies: A reappraisal. *Journal of Animal Ecology*, **89**, 161-172.
- Wilson, R.P., Holton, M.D., di Virgilio, A., Williams, H., Shepard, E.L.C., Lambertucci, S., Quintana, F., Sala, J.E., Balaji, B., Lee, E.S., Srivastava, M., Scantlebury, D.M. & Duarte, C.M. (2018) Give the machine a hand: A Boolean time-based decision-tree template for rapidly finding animal behaviours in multisensor data. *Methods in Ecology and Evolution*, **9**, 2206-2215.
- Wilson, R.P., Hustler, K., Ryan, P.G., Burger, A.E. & Noldeke, E.C. (1992) Diving birds in cold water: do Archimedes and Boyle determine energetic costs? *The American Naturalist*, **140**, 179-200.
- Wilson, R.P., Shepard, E. & Liebsch, N. (2008) Prying into the intimate details of animal lives: use of a daily diary on animals. *Endangered Species Research*, **4**, 123-137.
- Yamaç, E. & Bilgin, C.C. (2012) Post-fledging movements of Cinereous Vultures *Aegypius monachus* in Turkey revealed by GPS telemetry. *Ardea*, **100**, 149-156.

Chapter 5

Dead-reckoning animal movements in R: a reappraisal using *Gundog.Tracks*

Richard M. Gunner



Photo taken by Martin C. van Rooyen

This work was published in *Animal Biotelemetry* as:

Gunner, R.M., Holton, M.D., Scantlebury M.D., van Schalkwyk, O.L., English, H.M., Williams, H.J., Hopkins, P., Quintana, F., Gómez-Laich, A., Börger, L., Redcliffe, J., Yoda, K., Yamamoto, T., Ferreira, S., Govender, D., Viljoen, P., Bruns, A., Bell, S.H., Nikki, M.J., Bennett, N.C., Mariano, T.M., Duarte, C.M., van Rooyen, M.C., Bertelsen, M.F., Tambling, C.J. and Wilson, R.P., 2021. Dead-reckoning animal movements in R: a reappraisal using *Gundog.Tracks*. *Animal Biotelemetry*, DOI: 10.1186/s40317-021-00245-z

Abstract

Fine-scale data on animal position are increasingly enabling us to understand the details of animal movement ecology and dead-reckoning, a technique integrating motion sensor-derived information on heading and speed, can be used to reconstruct fine-scale movement paths at sub-second resolution, irrespective of the environment. On its own however, the dead-reckoning process is prone to cumulative errors, so that position estimates quickly become uncoupled from true location. Periodic ground-truthing with aligned location data (e.g., from global positioning technology) can correct for this drift between Verified Positions (VPs). I present step-by-step instructions for implementing Verified Position Correction (VPC) dead-reckoning in R using the tilt-compensated compass method, accompanied by the mathematical protocols underlying the code and improvements and extensions of this technique to reduce the trade-off between VPC rate and dead-reckoning accuracy. These protocols are all built into a user-friendly, fully-annotated VPC dead-reckoning R function; *Gundog.Tracks*, with multi-functionality to reconstruct animal movement paths across terrestrial, aquatic, and aerial systems, provided within the supplementary information as well as online (GitHub). The *Gundog.Tracks* function is demonstrated on three contrasting model species (the African lion *Panthera leo*, the Magellanic penguin *Spheniscus magellanicus*, and the Imperial cormorant *Leucocarbo atriceps*) moving on land, in water and in air. I show the effect of uncorrected errors in speed estimations, heading inaccuracies and infrequent VPC rate and demonstrate how these issues can be addressed. The function provided will allow anyone familiar with R to dead-reckon animal tracks readily and accurately, as the key complex issues are dealt with by *Gundog.Tracks*. This will help the community to consider and implement a valuable, but often overlooked method of reconstructing high-resolution animal movement paths across diverse species and systems without requiring a bespoke application.

Background

Reconstructing animal movement paths is an important tool in ecology, providing insights into animal space-use, behaviour and habitat selection (Browning *et al.* 2018; McClune 2018; Schlägel *et al.* 2019). However, accurate estimation of paths at fine temporal scales has proved a persistent challenge (Cagnacci *et al.* 2010; Williams *et al.* 2020b). Dead-reckoning is a method used to reconstruct animal movement paths, based on sequentially integrating the vector of travel from a predetermined position using estimates of heading (also termed ‘bearing’ or ‘yaw’) and speed (and displacement about the vertical axis for 3-D movements), over an elapsed time interval (Cotter 1978; Levi & Judd 1996; Beauregard & Haas 2006; Walker *et al.* 2015). In its most advanced form, it can provide positional data with sub-second resolution, irrespective of the environment (e.g., Bidder *et al.* 2015; Wensveen, Thomas & Miller 2015; Andrzejczek *et al.* 2019) and it therefore has huge potential for providing data that can elucidate many fundamental behavioural and ecological issues related to space-use.

The concept of dead-reckoning (also termed ‘track integration’) originated to aid nautical navigation (Cotter 1978; Bowditch 2002), though its utility to reconstruct uninterrupted fine-scale (in time and space) animal movement paths by integrating different sensors in animal-attached tags was suggested over three decades ago (Wilson & Wilson 1988; Wilson *et al.* 1991). Today, this typically involves the simultaneous deployment of tri-axial accelerometers and magnetometers (e.g., Mitani *et al.* 2004; Elkaim *et al.* 2006; Wilson *et al.* 2007; Wilson, Shepard & Liebsch 2008; Bidder *et al.* 2015; Walker *et al.* 2015; Wilson *et al.* 2015), utilising the tilt-compensated compass method (Li, Li & Wang 2009; Ozyagcilar 2012; Pedley 2012; Gheorghe & Bodea 2018) [see glossary for a definition of dead-reckoning related terminology used throughout].

The utility of dead-reckoning depends on the accuracy of speed and heading estimates (see Table. 1) and, due to the nature of vector integration, dead-reckoned tracks accumulate errors (commonly termed ‘drift’) over time (Wilson *et al.* 1991; Liu

et al. 2015; Dewhirst *et al.* 2016). As a result, periodic ground-truthing by a secondary source is important for maintaining the accuracy of animal paths with all its underlying scales and tortuosity of movement (Mitani *et al.* 2003; Bidder *et al.* 2015; Walker *et al.* 2015). For this reason, dead-reckoning data is normally enhanced by combining it with other methods for providing Verified Positions (VPs). These are primarily: direct observation (e.g., Whitney *et al.* 2010), light intensity-based geolocation (e.g., Lisovski *et al.* 2012), VHF- (e.g., Miller *et al.* 2009), acoustic- (e.g., Baumgartner *et al.* 2008) and GPS telemetry (e.g., Dewhirst *et al.* 2016). Other, less utilised, systems that may also have merit at sites frequented by the tagged animals, include radio frequency identification (RFID) stations (*cf.* Williams *et al.* 2019), camera traps (*cf.* Alexander *et al.* 2016) and video footage, such as closed-circuit television (CCTV) surveillance (e.g., English *et al.* (in review)). Although all these systems are subject to a number of issues that can make their positional fixes temporally widely spaced (e.g., Fancy *et al.* 1988; Soutullo *et al.* 2007; Cagnacci *et al.* 2010), inaccurate (e.g., Catipovic 1990; Newey *et al.* 2015; Hofman *et al.* 2019) or impossible (e.g., Leonardo *et al.* 2005; Lewis *et al.* 2007; Kaur *et al.* 2011), they can be critical in providing ground-truthed positions, even infrequently, with which to reset accumulated drift (Walker *et al.* 2015; Dewhirst *et al.* 2016).

Of the above VP options, GPS-corrected dead-reckoning is the most widely used and there is a marked bias towards marine studies (e.g., Wilson *et al.* 1991; Davis *et al.* 2001; Wilson 2002; Johnson & Tyack 2003; Mitani *et al.* 2003; Mitani *et al.* 2004; Wilson *et al.* 2007; Shiomi *et al.* 2008; Narazaki *et al.* 2009; Ware, Friedlaender & Nowacek 2011; Aoki *et al.* 2012; Benoit-Bird *et al.* 2013; Bidder *et al.* 2015; Laplanche, Marques & Thomas 2015; Wensveen, Thomas & Miller 2015; Wilson *et al.* 2015; Adachi *et al.* 2017; Bras, Jouma'a & Guinet 2017; Wright *et al.* 2017; Andrzejaczek *et al.* 2018; Andrzejaczek *et al.* 2019; Wensveen *et al.* 2019). This is likely for logistical reasons, with many aquatic animals being larger (and thus can carry larger/more devices) than their terrestrial counterparts (Ropert-Coudert & Wilson 2005), whilst the utility of transmission telemetry is restricted to periodic resurfacing events (Francisco, Nührenberg & Jordan 2020). Moreover, speed can be more easily

measured or approximated in water, with previous studies obtaining estimates *via* acoustic flow noise (e.g., Goldbogen *et al.* 2006), passive sonar (e.g., Zimmer *et al.* 2005), pitch and change in depth (e.g., Wensveen, Thomas & Miller 2015) and speed sensors (*cf.* Wilson, Ropert-Coudert & Kato 2002; Wilson *et al.* 2007; Gabaldon *et al.* 2019). The efficacy of such techniques diminishes within the aerial environment, principally, due to the marked difference between water and air density (*cf.* Denny 1993) and the current speed and volatility of wind (*cf.* Williams *et al.* 2015; Altnay *et al.* 2019). Indeed, this may explain why, in part, (to my knowledge) only one study to date has dead-reckoned a volant species (Williams *et al.* 2020a). More recently, dynamic body acceleration (DBA, see Wilson *et al.* (2020a), for recent review) has been validated as a proxy of speed for terrestrial animals (Bidder, Qasem & Wilson 2012; Bidder *et al.* 2012) although there are still very few studies that use the dead-reckoning method in terrestrial animals (e.g., Bidder *et al.* 2015; Walker *et al.* 2015; Dewhurst *et al.* 2016; di Virgilio *et al.* 2018; Markovska & Svensson 2019; English *et al.* (in review)).

I suggest that another reason that Verified Position Correction (VPC) dead-reckoning has been little used relates to the apparent difficulty and poor accessibility of the analytical processes involved. With this in mind, the primary aim of this paper is to provide potential users with a clear, concise roadmap for implementing dead-reckoning protocols. Specifically, I revisit the dead-reckoning methodology, from calibrating magnetometry data and deriving heading (tilt-compensated compass method), to VPC dead-reckoning within both terrestrial and fluid media. I provide simplistic conceptual explanations and mathematical protocols and describe the pitfalls within the procedure that can increase error. I also translate the relevant equations into complementary R code (<https://www.r-project.org>) throughout the text, with fully annotated scripts deposited in the supplementary information (SI) files and GitHub available at, <https://github.com/Richard6195/Dead-reckoning-animal-movements-in-R>.

Table 1. Possible system errors that can affect the utility of animal dead-reckoning within the ‘tilt-compensated compass’ framework. ‘SI’ refers to Supplementary information.

System error	Reasons for error	Underlying causes	References	Possible mitigation measures
Derived Heading	Errors in deriving static acceleration (postural) estimates	During bouts of high centripetal (turning) acceleration. Free-falling behaviour	(Shepard <i>et al.</i> 2008) (Noda <i>et al.</i> 2012) (Wilson <i>et al.</i> 2013a) (Williams <i>et al.</i> 2015) (McNarry <i>et al.</i> 2017)	Gyro-integrated data (<i>cf.</i> Kaniewski & Kazubek 2009; Noda <i>et al.</i> 2014)
	Using Euler angles (angle of rotation about each axis of a given coordinate system)	The orientation of the device with respect to the earth’s frame of reference (<i>cf.</i> SI.1: Text S2) can only be defined reasonably at angles less than perpendicular or less than a 180° inversion (dependent on pitch & roll equations used - <i>cf.</i> “VPC dead-reckoning procedure in R” section) from their longitudinal and lateral axes of ‘normal’ posture (otherwise, unstable measures arise from the Gimbal lock singularity complex (<i>cf.</i> Patonis <i>et al.</i> 2018), whilst x, y and z values can become inversed and/or represent different ‘surge’, ‘sway’ and ‘heave’ planes)	(Diebel 2006) (Han & Wang 2011) (Säll & Merkel 2011) (Pedley 2012) (Alaimo <i>et al.</i> 2013)	Quaternion-estimated heading (<i>cf.</i> Valenti, Dryanovski & Xiao 2015; Feng <i>et al.</i> 2017; Chiella, Teixeira & Pereira 2019)
	Tag placement/dislodgment	In line with the above - range for accurate angular (pitch & roll) measures are restricted in one or more dimensions Heading will be biased according to the degree of displacement about the z-axis	(Wilson <i>et al.</i> 2015) (Chapter 2 and 3)	Ensure tag orientation is noted during deployment and retrieval operations (and subsequently used in corrections)
	Variations in the strength and declination of magnetic fields	Animals that undertake long journeys (regionally/globally) Environmental and man-made magnetic noise (iron distortions)	(Wiltchko 2012)	Ensure at least one magnetic calibration procedure is carried out (see SI. 1: Text S3 for details) and apply magnetic declination offset to heading values where required
Derived Speed	Deviations of the DBA~speed relationship	Load bearing Moving over a deformable substrate / changeable incline Changing gait Moving within fluid media Gliding/thermalling behaviour	(Sequeira <i>et al.</i> 1995) (Kerdok <i>et al.</i> 2002) (Halsey <i>et al.</i> 2008) (Bidder, Qasem & Wilson 2012) (Bidder <i>et al.</i> 2012) (Miwa <i>et al.</i> 2015) (Andrzejczek <i>et al.</i> 2019) (Williams <i>et al.</i> 2015)	Iteratively modulate the gradient and/or intercept within the DBA~speed linear regression according to environmental circumstance and mode of movement (<i>cf.</i> Bidder, Qasem & Wilson 2012). By-pass DBA (e.g., use speed/acoustic sensors, step/tail-/wing beat frequency, vertical speed etc. (e.g., Laplanche, Marques & Thomas 2015))
Both	External forces (e.g., current vectors in air- and water flow)	Decreases the signal-to-noise ratio of motion sensor data. Affects the relationship between an animal’s (longitudinal axis) direction of travel from their true vector of travel Some animals do not always move in the same direction as their anterior-posterior axis	(Wilson <i>et al.</i> 1991) (Shiomi <i>et al.</i> 2008) (Chapman <i>et al.</i> 2011) (Wensveen, Thomas & Miller 2015)	Smooth postural (and pre-derivative data) / DBA estimates (<i>cf.</i> Wilson <i>et al.</i> 2020a) Incorporate current flow vectors within the dead-reckoning procedure

In addition to the above, I outline recent advances to the VPC dead-reckoning technique. For use in terrestrial environments, this includes implementing step counts as a distance measure, by-passing dynamic body acceleration (DBA) as a proxy of speed, and assessing the value of ‘reverse dead-reckoning’ (useful when VPs are concentrated to the latter end of an animal’s trajectory). For marine and aerial environments, I demonstrate the value of integrating tidal-/air current data with dead-reckoned vectors (hereafter termed ‘current integration’) to reduce errors attributed to drift (*cf.* Shiomi *et al.* 2008; Chapman *et al.* 2011). Across all three media of travel (land, water and air), I show the value of incorporating different speed coefficients according to behaviour types. In addition, I provide examples of the various methods by which VP data can be under-sampled (relevant for high-res GPS datasets) prior to correcting dead-reckoned tracks and discuss the scales at which users should consider VP correction (which depend on the details of species-specific movement and length of data acquisition).

I specifically demonstrate the above using my R-functions (*Gundog.Tracks* being the primary function for dead-reckoning), providing examples of its utility across various scenarios. Lastly, I highlight the relevance of heading and distance correction factors (derived from the VPC procedure), which can also be used to interrogate the animal-environment interaction and biases stemming from animal tag performance. To illustrate my approach, I used three model species (the African lion *Panthera leo*, the Magellanic penguin *Spheniscus magellanicus* and the Imperial cormorant *Leucocarbo atriceps*) that cover almost two orders of size magnitude in body mass and that operate in markedly different environments and at different scales of movement. To make this review more broadly applicable to researchers of varying dead-reckoning and R knowledge, I have departed from a traditional article format and instead, split this body of work into two distinct sections: Firstly, I provide an overview of the critical *Gundog.Tracks* function and provide a brief review of the conceptual workflow (“Implementation of *Gundog.Tracks*” section). With respect to this, I discuss the relevant strengths and limitations of the current dead-reckoning framework and the key considerations involved. Secondly, I detail each ‘potential’

stage of the VPC dead-reckoning procedure with exemplar mathematical equations and R syntax (“VPC dead-reckoning procedure in R” section).

Implementation of *Gundog.Tracks*

I refer to mathematical equations as ‘E_x’ and R syntax as ‘R_x’, where _x is the reference number. To simplify concepts, I use base R syntax (wherever possible) and typically use vectors to demonstrate points made, though ‘df\$’ directly before the variable name indexes data retained within data frame columns (assuming data frame is called ‘df’). I note, however, that more efficient code implementations are possible (e.g., *data.table* (Dowle *et al.* 2019) and *lapply()*) than presented here, especially for large data, but here wanted to make the code as readable as possible in this manuscript, especially to persons not familiar with complex coding. More efficient code will be implemented through updated GitHub versions of the functions. I expand on key concepts in SI. 1 and provide complimentary R scripts (outlined below) in SI. 2, 3, 4 and 5. I also supply an example data set of a Magellanic penguin walking through the colony on its way to the sea in SI. 6, which can be used to trial each of the provided R scripts and perform the full dead-reckoning process. SI’s 2:6 are deposited in GitHub (<https://github.com/Richard6195/Dead-reckoning-animal-movements-in-R>). See SI. 1: Text S1 for the model species’ device set up and capture protocol and the glossary for a definition of dead-reckoning related terminology.

The order and content of SI’s are listed below:

- SI. 1) Methods expanded (.doc file). This contains:
 - Text S1. Device set up and capture protocol.
 - Text S2. The importance of having the correct coordinate system and axis alignment
 - Text S3. Magnetometer calibration, rotation correction and deriving yaw (heading) - *Gundog.Compass()* explained
 - Text S4. Step counts as a distance estimate - *Gundog.Peaks()* explained
 - Text S5. Time Data in R (POSIXct)
 - Text S6. VPC dead-reckoning – *Gundog.Tracks()* - explained

- SI 2) *Gundog.Compass()* (.R file)
- SI 3) *Gundog.Peaks()* (.R file)
- SI 4) *Gundog.Tracks()* (.R file)
- SI 5) *Step by step guide of using Gundog.Tracks (.R file) (to use in conjunction with below).*
- SI 6) Raw sensor and GPS data frame (.txt) of a penguin walking through the colony on its way to the sea.

User functionality

Gundog.Tracks is an all-encompassing dead-reckoning function that can be used to dead-reckon animal paths travelling terrestrially or through fluid media. Table 2 details all the function's input requirements/options.

Reverse dead-reckoning

Dead-reckoning backwards is useful when the start position is unknown, but the finishing coordinates are known. For example, central-place foraging, diving animals returning to land from the sea may not acquire a satellite fix for an appreciable period of time following submersion in water which can make determining the start position difficult. So, when VPs are skewed to the latter part of the track, it may be beneficial to start the iterative dead-reckoning process from that end. This involves reversing the order of data to be dead-reckoned and changing heading values by 180 degrees prior to dead-reckoning.

Integrating current vectors

Wind or ocean currents can change the relationship between an animal's (longitudinal axis) bearing and speed of travel from their true vector of travel (Shiomi *et al.* 2008; Chapman *et al.* 2011). This drift can be incorporated within movement paths by advancing each iterated dead-reckoned vector according to the direction and speed of the current at that point in space and time (*cf.* Fig. 1).

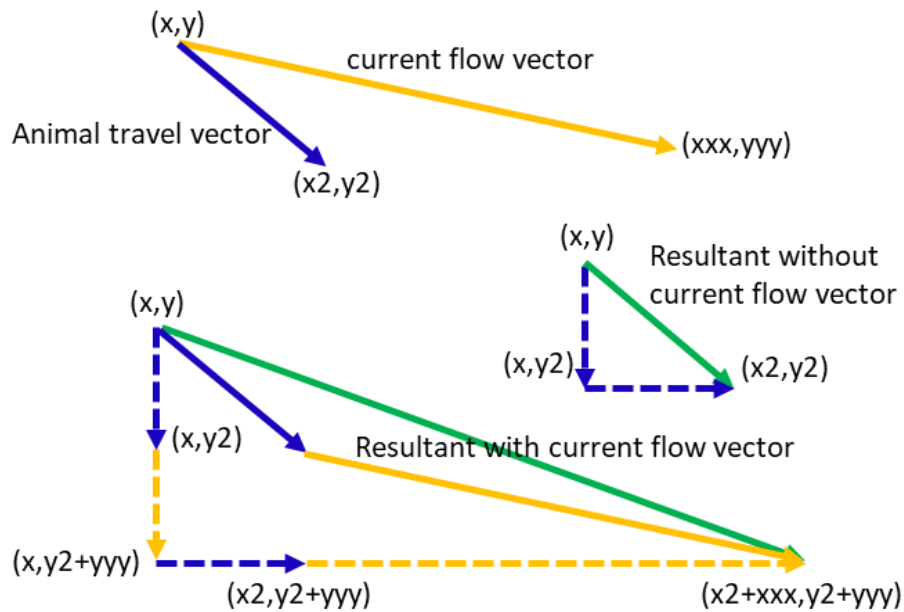


Figure 1. Schematic representation of a current flow vector (orange) (due to its speed and direction) being integrated to a given travel vector (blue). The x,y reflects the initial location of a dead-reckoned track, x_2 and y_2 are the resultant location following the integration of a travel vector (prior to current integration) and xxx and yyy advance these x_2 and y_2 values a step further in the direction of the current flow vector. The dashed lines indicate the magnitude of the x and y dimensions of travel (both pre- and post-current flow integration) and the green line reflects the actual travel vector.

DBA~speed derivation

Given the approximate linear relationship between DBA (*sensu* Wilson *et al.* 2020a) and terrestrial animal speed [$speed = (DBA \cdot m) + c$], DBA estimates can be multiplied by a gradient, m (the multiplicative coefficient) and summed with an intercept, c (the constant) to derive speed (Bidder *et al.* 2015; Dewhirst *et al.* 2016). These values are typically substituted with results from DBA~speed linear regression estimates, such as from treadmill tests or using GPS-derived speed (Bidder *et al.* 2012; Dewhirst *et al.* 2016; Dunford *et al.* 2020; Chapter 4). The m -coefficient should be selected such that (uncorrected) dead-reckoned tracks accord with the apparent straight-line distance between VPs. Importantly, the DBA~speed relationship may be a function of terrain-type (e.g., sand vs concrete), animal state (e.g., weight variation) and mode of movement (e.g., running vs climbing) (*cf.* Bidder, Qasem & Wilson 2012). For instance, a condor gliding within a thermal would have high speeds, despite having negligible DBA, while an Ibex traversing across different substrate types and

gradients would impart varying magnitudes of acceleration that may scale non-linearly with a change in stride gait. It may be of value, therefore, to iteratively change the supplied m (and possibly c) values between VPs according to behaviour and environment. The user may also opt to supply a ‘marked events’ (ME) vector (a marked event is a term I use that refers to a number of sequential (in time) data points within a dataset coded by integer values) to ensure dead-reckoned tracks are not advanced with non-animal movement behaviours. Within *Gundog.Tracks*, ME values of one or greater reflect progressive movement, and zero values code for stationary behaviour - dead-reckoned tracks are not advanced when $ME = 0$ (irrespective of the allocated speed). For example, in its simplest form, ME could be filled with binary 0’s and 1’s as governed by a DBA threshold (labelling the ME vector 0 in sleep and resting behaviour).

Pre-determining speed

For terrestrial species (specifically bipeds and quadrupeds), the interplay between peak heave acceleration amplitude and periodicity may be a useful indicator for the movement gait adopted (Wilson *et al.* 2020b), which may help decide the m -coefficient in the DBA~speed relationship (Bidder *et al.* 2012). There may be times, however, when DBA is an unreliable proxy of terrestrial speed (*cf.* Bidder, Qasem & Wilson 2012). At this time, given that the stride cycle can be easily detected by cyclic peaks in a given acceleration channel (e.g., Rong *et al.* 2007; Willener *et al.* 2015; Wilson *et al.* 2018), peak periodicity (and amplitude) may be used as a proxy of distance moved by providing a distance per step estimate (assuming constant distance travelled between step gaits if only concerning step periodicity - *cf.* “VPC dead-reckoning procedure in R” section and SI.1: Text S4).

DBA is a weak proxy of speed for many marine animals because overall body tissue density changes with depth when air is associated so that speed may be invariant of the movement kinematics (*cf.* Wilson *et al.* 1992; Aoki *et al.* 2011). DBA is also a weak proxy for flying animals that glide at constant velocity, use thermals or bank (*cf.*

Williams *et al.* 2017). One of the most common methods for determining animal speed in water is *via* devices that estimate flow or resistance rate (Wilson *et al.* 2007; Wilson *et al.* 2015; Altynay *et al.* 2019; Whitford & Klimley 2019). These often have appreciable limitations, with currents, biofouling, blockage and turbulence affecting performance (Altynay *et al.* 2019), and many of these issues are applicable to volant species, so that bird speed measures are typically restricted to GPS-derived estimates of ground speed (*cf.* Shamoun-Baranes *et al.* 2012). In the absence of a reliable motion sensor-derived speed proxy, previous reported approximated speed estimates according to movement modes and/or topological whereabouts can be used (*cf.* Miller *et al.* 2009). For example, for various diving animals such as penguins, a simple depth threshold may prove effective to differentiate between various previous reported modal ‘surface-resting’ and ‘underwater-commuting’ speeds (Wilson 1985; Culik *et al.* 1991; Bethge *et al.* 1997; Wilson, Ropert-Coudert & Kato 2002). For volant species, whilst wingbeat frequency or amplitude does not scale reliably with air speed (*cf.* Tobalske & Dial 1996), the interplay between both can decipher various flight modes (e.g., ‘cruising speed’ vs taking off/landing, Sato *et al.* 2009; Williams *et al.* 2015). Furthermore, tail beat frequency has been shown to be a good predictor of swimming speed for various fish species (Scharold *et al.* 1989; Kawabe *et al.* 2003; Steinhausen, Steffensen & Andersen 2005). For diving animals, a proxy for horizontal speed can be obtained based on animal pitch and rate of change of depth (Miller *et al.* 2004; Wensveen, Thomas & Miller 2015). Specifically, the rate change of depth is divided by the tangent of the body pitch.

In any case, when high resolution VP data is available (e.g., 0.01-10 Hz GPS), for instance, during short-term trial deployments, speed estimates can be compared alongside those derived between VPs and approximated according to behaviour type (elucidated from, for example, accelerometry- (e.g., Laich *et al.* 2008; Chakravarty *et al.* 2019a), magnetometry- (e.g., Williams *et al.* 2017; Chakravarty *et al.* 2019b), depth- (e.g., Hochscheid 2014) or altitude- (e.g., Williams *et al.* 2015) data), and uncorrected dead-reckoned tracks can be compared alongside VPs to determine where biases may occur visually. Furthermore, the correction factors obtained from

the VPC process are viable comparators for detecting consistent under- or over-estimations of speed and/or heading offsets (e.g., due to tag placement). Essentially, when empirical speed evidence is unavailable, the user can *ad hoc* iteratively adjust allocated speed values or the underlying DBA~speed coefficients until uncorrected dead-reckoned track segments scale proportionately to their aligned ground-truthed positions (pre-VPC). Within *Gundog.Tracks*, the user can modulate m , c and ME values to switch between pre-determined speed ($m = 1, c = 0$), DBA-derived speed ($m > 0, c \geq 0$) and stationary behaviour ($ME = 0$).

VPC procedure

Ground-truthing dead-reckoned tracks typically involves the linear drift correction method (*cf.* Shiomi *et al.* 2008; Dewhurst *et al.* 2016), outlined in Constandache *et al.* (2010) & Symington and Trigoni (2012). In essence, a shift vector aligns the starting dead-reckoned path segment with the VP at time point one, after which the difference between the VP and dead-reckoned path segment at time point two is calculated to provide a correction vector that is applied linearly between time point one and time point two. This method follows the protocols outlined by Walker *et al.* (2015), whereby the underlying correction coefficients (hereafter termed ‘factors’) for both heading and (radial) distance are calculated - adjusting the length and heading at each dead-reckoned path segment until the end points align to each VP along the path. This process requires the trigonometric ‘as the crow flies’ Haversine formulae (Robusto 1957; Bullock 2007; Harja & Sarno 2018) which allows one to translate a distance across the curvature of the Earth’s surface (detailed within “VPC dead-reckoning procedure in R” section). The advantage of this method is that, whilst correction factors are constant between VPs, it does not assume that the dead-reckoned path deviates linearly over time from the true path because (radial) distance is multiplied by the distance correction factor. This ensures that parts of track where the animal is determined to be stationary (e.g., $ME = 0$) are left unaltered. The function’s method of VPC, automatically handles NaN and Infinite (*Inf*) values

which can arise during the derivation of the distance correction factors (when no dead-reckoned movement occurs between successive VPs - detailed within the “VPC dead-reckoning procedure in R” Section). It is worth noting that even animals that travel in 3-D can be subject to the 2-D dead-reckoning formulae and Haversine computation of distance correction factors because we typically assume that both dead-reckoned- and VP positions are aligned in vertical space (assuming reliable pressure- [60]/ depth [13] data) and attempt to control for the horizontal component of speed (e.g., “VPC dead-reckoning procedure in R” section – E_{25,27}) pre-correction. Although not covered here, I acknowledge that various state-space modelling techniques have also been developed to georeference dead-reckoned tracks (e.g., Laplanche, Marques & Thomas 2015; Wensveen, Thomas & Miller 2015).

Table 2. Gundog.Tracks input fields and description of their role. Ref refers to the default value when no input is stated. Red shading represents required user inputs and green and orange shading reflect optional inputs (the latter change when using VPC). Note that if speed estimates (v) are directly inputted into the function then m and c (and possibly ME) defaults should not be changed. If either one of the VP.lon, VP.lat or method inputs is specified as NULL, then no VPC will occur.

Function input	Description	Ref
TS	Timestamp - POSIXct object. No missing data (NA's) permitted	-
h	Heading (0° to 360°) - No missing data (NA's) permitted	-
v	DBA (g or m/s ²) or speed (m/s) - No missing data (NA's) permitted	-
elv	Elevation / depth data (m) - No missing data (NA's) permitted	0
p	Pitch (°) – Only supply if user wants radial distance modulated according to pitch (cf. “VPC dead-reckoning procedure in R” section – E ₂₇). No missing data (NA's) permitted	NULL
cs	Current speed (m/s) - Supplied as a single value or vector/column of changeable values. NAs are replaced with the most recent non-NA prior to it (observations carried forward)	NULL
ch	Current heading (0° to 360°) - Supplied as a single value or vector/column of changeable values. NAs are replaced with the most recent non-NA prior to it (observations carried forward)	NULL
m	Multiplicative coefficient (gradient) - If speed (m/s) supplied for v, then m must be 1. Supplied as a single value or vector/column of changeable values	1
c	Constant (y-intercept) – If speed supplied for v, then c must be 0. Supplied as a single value or vector/column of changeable values	0

ME	Marked Events – 0 denotes periods of stationary behaviour and 1 (or any integer number > 0) denotes periods of traversing movement. ME overrides initial speed input / DBA-derived speed (calculated within the function itself). NA's and character values are replaced with zero	1
lo	Starting longitude coordinate to advance dead-reckon track from – Decimal format, e.g., 26.31989	0
la	Starting latitude coordinate to advance dead-reckon track from – Decimal format e.g., -06.11995	0
VP.lon	VP longitude coordinates – Decimal format. Missing relocation data expressed as either NA's or 0's. First (or last if reverse dead-reckoning) element/row allocated as lo within the function	NULL
VP.lat	VP latitude coordinates – Decimal format. Missing relocation data expressed as either NA's or 0's. First (or last if reverse dead-reckoning) element/row allocated as la within the function	NULL
VP.ME	TRUE = Supplied VPs removed at times when ME = 0 (relevant for high-res VP datasets, when location error is high during rest). Note, this does not remove the element/row allocated as lo/la	FALSE
method	How the function under-samples VPs prior to correction (subsequent to the VP.ME subset, if set to TRUE) – "divide" = Fix kept every x (<i>thresh</i>) segments of supplied VPs, based on row number. The first and last fixes are always included "time" (s) = Fix kept every x (<i>thresh</i>) accumulated seconds (or the next available fix after a period of missing locational data (\geq <i>thresh</i>)). The first and last fixes are always included "distance" = Fix kept every x (<i>thresh</i>) proportional segments of the total accumulated distance (m) between supplied VPs (using the stepping interval 'dist.step'). The first and last fixes are always included "all" = Every supplied VP kept (irrespective of thresh value)	NULL
thresh	Threshold - Degree of VP under-sampling prior to dead-reckon correction. The frequency of under sampling depends on the method selected	1
dist.step	The stepping interval used for calculating distance between VPs, both within the VP summary distance metrics (see Table. 3) and within the 'method = distance' VP under-sampling protocol prior to VPC. For example, dist.step = 5 computes distance between every 5th VP (irrespective of the time difference between them)	1
bound	TRUE = VPC dead-reckoning is bounded by the first and last VP present FALSE = VPC dead-reckoning is unbounded by the last available VP. The last dead-reckoned track segment inherits the previous correction factors	TRUE
Outgoing	TRUE = 'normal' dead-reckoning procedure FALSE = Reverse dead-reckoning. Note la and lo positions should now be the finishing longitude and latitude coordinates, respectively	TRUE
Plot	FALSE = No summary plots TRUE = R graphics window initialised: VPC = 4 summary plots / no VPC = 1 summary plot (cf. top left) Top left) Uncorrected dead-reckoned track (blue) and VP track (red). If currents are supplied, the blue track has currents integrated and an additional green track with no current integration is plotted Top right) VPC dead-reckoned track (blue) in relation to VP track (red) Bottom left) Net error (m) between VPs and dead-reckoned positions (un-corrected = red and corrected = black). If currents are supplied, then uncorrected with no current integration = green and uncorrected with current integration = red Bottom right) VPC corrected dead-reckoned track	TRUE

Default inputs for calculations and outputs

Gundog.Tracks default input takes the form:

Gundog.Tracks(*TS, h, v, elv = 0, p = NULL, cs = NULL, ch = NULL, m = 1, c = 0, ME = 1, lo = 0, la = 0, VP.lon = NULL, VP.lat = NULL, VP.ME = FALSE, method = NULL, thresh = 1, dist.step = 1, bound = TRUE, Outgoing = TRUE, plot = FALSE*)

, with input modulated according to the animal in question and data available (see Fig. 2).

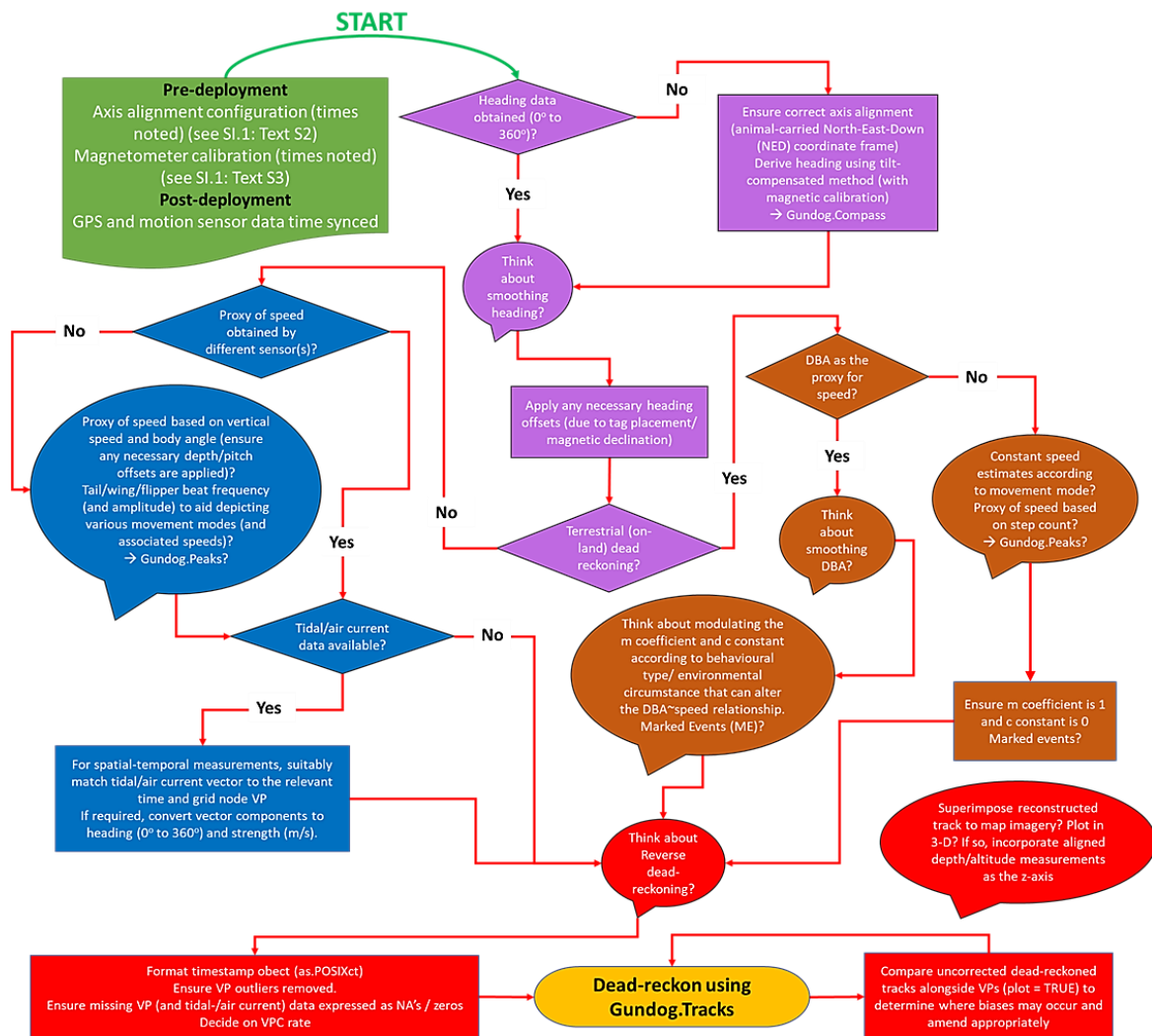


Figure 2. Schematic diagram of the conceptual workflow involved when dead-reckoning using Gundog.Tracks – elaborated within section 3. Note Gundog.Peaks is a peak finder function that locates peaks based on local signal maxima and Gundog.Compass is a function to correct iron distortions from tri-axial magnetometry data and subsequently compute tilt-compensated heading. Both functions are elaborated within “VPC dead-reckoning procedure in R” section and SI. 1. The direction of workflow and key questions asked follow from green- (pre-processing and data alignment) to purple- (computing heading) sections, before splitting into blue- (air/water) and brown- (land) sections (computing speed) and culminating at the red section (final pre-dead reckoning checks/data formats & post-dead-reckoning checks/plots) in conjunction with the process of using Gundog.Tracks in R (yellow).

The function outputs a data frame containing various descriptive columns which, depending on the input, includes (but is not limited to):

- The correction factors used
- Heading and radial distance estimates (both pre- and post-current integration and/or VPC)
- Distance moved and speed estimates (both in 2-D and 3-D when elevation/depth data supplied)
- Net error between dead-reckoned positions and VPs (both pre- and post-correction)
- Various VP summaries including notation of when VPs are present and which fixes were used in the correction process.

When specified, 2-D summary plots demonstrating the relationship between dead-reckoned positions and VPs (both pre- and post-current integration and/or VPC) are provided (e.g., Fig. 3). Table 3 details all the function's available outputs (modulated according to input). *Gundog.Tracks* uses the *na.locf()* function from the 'zoo' package (Zeileis *et al.* 2020) and the *slice()* function from the 'dplyr' package (Jockers & Thalken 2020) (both are checked as dependencies and installed when required within this function). Output 2-D distance/speed estimates are calculated with the Haversine formula. When depth/elevation data is supplied (and changes between sets of coordinates) 3-D distance/speed estimates are calculated with a variant of the Euclidean Formula - converting x, y, z from polar to Cartesian coordinates, and incorporating the Earth's oblate spheroid (*cf.* World Geodetic System (WGS84)), *via* conversion from Geodetic- to Geocentric-latitude (*cf.* Cross 2019).

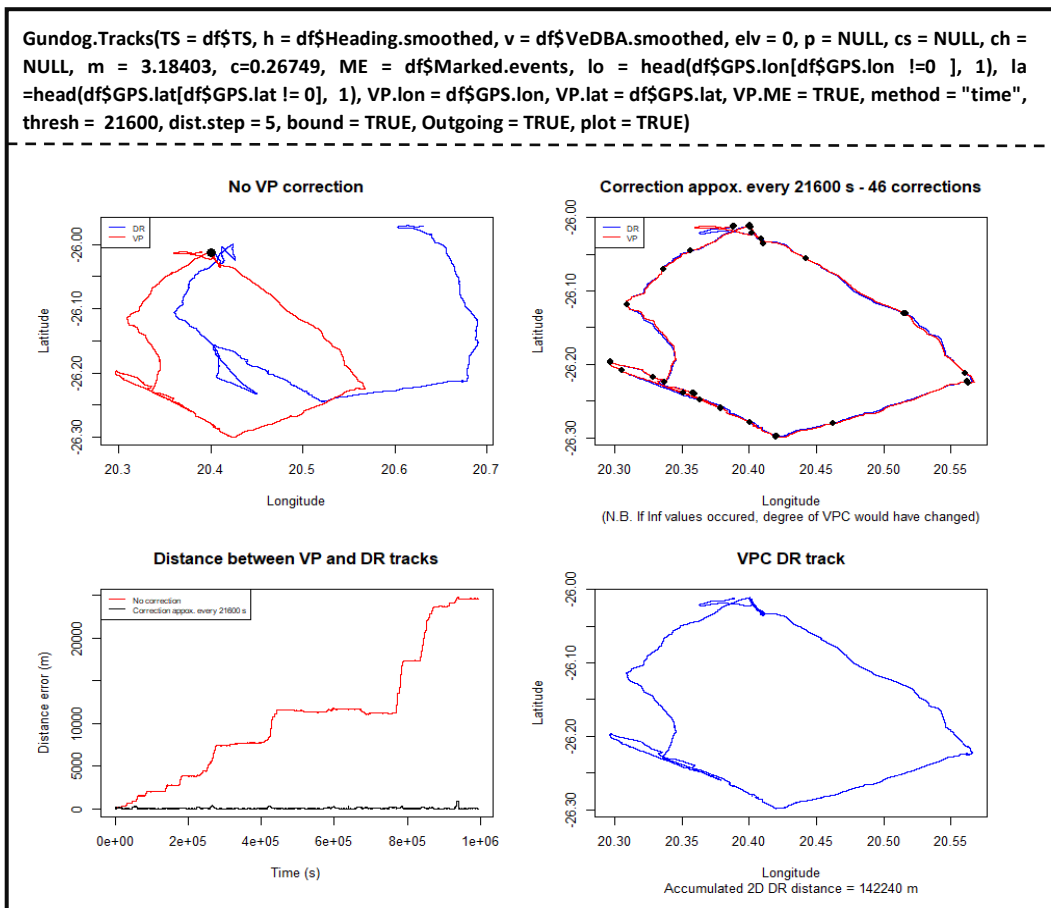


Figure 3. Dead-reckoned (DR) movement path of lion as provided by Gundog.Tracks summary plots (within the initialised R graphics window). This is an approximate two-week trajectory over an approximated total travel (DR) distance of > 142 km. (Pre-filtered) GPS (red) was sampled at 1 Hz and derived heading and speed measurements were sub-sampled to 1 Hz (initial acceleration/magnetometry data were recorded at 40 Hz). The VPC dead-reckoned track (blue) was constructed using DBA~GPS-derived speed regression estimates and corrected approx. every 6 hours. Note, for dead-reckoning within fluid media, an additional green dead-reckoned track with current integration and its associated distance estimates are also plotted (pre-correction) when wind/ocean currents are supplied (cf. Fig. 6). Accumulated 3-D DR distance is shown when elevation/depth data is supplied.

Table 3. Gundog.Tracks data frame output names and their parameters. The shading of Ref refers to when the outputs occur; red shading = always, purple shading = when pitch data is supplied, green shading = when elevation/depth data is supplied, blue = when current data is supplied and orange = when the user opts to undertake VPC. The symbol * demonstrates that the metrics will be derived from VPC tracks when correction is initialised. Note that, subsequent to reverse dead-reckoning, the data frame is reverted (back to original time order), though as a result, observations appear to be carried backwards in some instances, indicated by ↑. Due to the nature of reverse dead-reckoning (cf. SI. 1: Text S6), some input fields are shifted forward one row following the initial inversion of data. As such, fields indicated by #, are one row further forward in time (this is important when relating Head.corr.factor and Heading.corr output to the equivalent (uncorrected) Heading output. However, when currents are integrated, the Head.corr.factor and Heading.corr outputs refer to Heading.current.integrated and these are synchronised row-wise. All heading related data are rotated back 180 degrees following reverse dead-reckoning.

Function output	Description	Ref
Row.number	Row number	
Timestamp	Supplied timestamp - POSIXct object	
DR.seconds	Accumulated time (s) based on the supplied timestamp	
Heading	Supplied heading (0° to 360°)	
Marked.events	Supplied Marked events (or replicated default)	
DBA.or.speed	Supplied DBA (g or m/s ²) or speed (m/s)	
Pitch	Supplied pitch (°)	
Radial.distance	The calculated q-coefficient (prior to VPC) (see Sector 3 – E ₂₆)	#
Elevation	Supplied elevation / depth (m)	
Elevation.diff	Rate change of supplied elevation/depth (m/s) - (elevation difference / time difference between rows)	
Current.strength	Supplied current speed (m/s)	
Current.heading	Supplied current heading (0° to 360°)	
Heading.current.integrated	Updated heading (0° to 360°) following addition of current vectors (prior to VPC)	#
Radial.distance.current.integrated	Updated q-coefficient following addition of current vectors (prior to VPC)	#
DR.longitude	Dead-reckoned longitude coordinates – Decimal format (prior to VPC)	
DR.latitude	Dead-reckoned latitude coordinates – Decimal format (prior to VPC)	
DR.longitude.corr	Corrected dead-reckoned longitude coordinates – Decimal format (post VPC)	
DR.latitude.corr	Corrected dead-reckoned latitude coordinates – Decimal format (post VPC)	
Dist.corr.factor	Distance correction factor (observations carried forward)	↑ #
Head.corr.factor	Heading correction factor (0° to 360°) (observations carried forward)	↑ #
Heading.corr	Corrected heading (0° to 360°) (post VPC)	#
Radial.distance.corr	Corrected q-coefficient (post VPC)	#

Distance.error.before.correction	Distance (m) between uncorrected dead-reckoned positions and VPs (observations carried forward), subsequent to sub-sampling according to ME, if VP.ME = TRUE	↑
Distance.error.after.correction	Distance (m) between corrected dead-reckoned positions and VPs (observations carried forward), subsequent to sub-sampling according to ME, if VP.ME = TRUE	↑
DR.distance.2D	Two-dimensional distance moved (m) between dead-reckoned fixes	*
DR.distance.3D	Three-dimensional distance moved (m) between dead-reckoned fixes	*
DR.cumulative.distance.2D	Accumulated two-dimensional distance moved (m) between dead-reckoned fixes	*
DR.cumulative.distance.3D	Accumulated three-dimensional distance moved (m) between dead-reckoned fixes	*
DR.distance.from.start.2D	Two-dimensional (straight-line) distance moved (m) from starting position	*
DR.distance.from.start.3D	Three-dimensional (straight-line) distance moved (m) from the starting position	*
DR.speed.2D	Horizontal speed (m/s) (DR.distance.2D / time difference between rows)	*
DR.speed.3D	Total speed (m/s) (DR.distance.3D / time difference between rows)	*
VP.seconds	Accumulated time (s) between supplied VPs (observations carried forward)	
VP.longitude	Supplied VP longitude values (observations carried forward), sub-sampled according to ME, if VP.ME = TRUE	↑
VP.latitude	Supplied VP latitude values (observations carried forward), sub-sampled according to ME, if VP.ME = TRUE	↑
VP.fix.present	Denotes when a fix was present (1) or absent (0), subsequent to sub-sampling according to ME, if VP.ME = TRUE	
VP.used.to.correct	Denotes which VPs were used to correct (1) and which VPs were ignored (0)	
Number.of.VPCs	Increments by 1 each time a VP was used to correct (observations carried forward)	↑
VP.thresh	Replicates the thresh value set (or default) or warns the user that additional VP under-sampling was required if 'Inf' values produced	
VP.distance.2D	Two-dimensional distance moved (m) between VPs, subsequent to sub-sampling according to ME, if VP.ME = TRUE and using the stepping interval 'dist.step'	
VP.cumulative.distance.2D	Accumulated two-dimensional distance moved (m) between VPs, subsequent to sub-sampling according to ME, if VP.ME = TRUE and using the stepping interval 'dist.step'	

The interplay between numerical precision in R, correction rate and net error can make more than one round of adjustment necessary for dead-reckoning fixes to accord exactly with ground-truthed locations (*cf.* Fig. 4a), particularly given that slight discrepancies accumulate over time. Each iteration of the correction process produces a tighter adherence between estimated and ground-truthed positions (*cf.* Walker *et al.* 2015). Typically, this does not involve more than two rounds of VPC to achieve a maximum net error of .01 m (the threshold used within *Gundog.Tracks*)

across a *ca.* (1 Hz) 2 week-long track. For an indication of processing times see SI. 1: Text S6: Fig. 1; for example, dead-reckoning a lion at 1 Hz for 7 (continuous) days (with `plot = TRUE`, `dist.step = 5`, `VP.ME = TRUE`, `method = "time"` and `thresh = 3600`) took 25 seconds to compute (on a MSI GP72 7RD Leopard laptop with intel core i7 processor). Logically, the net error between VPs and (corrected) dead-reckoned positions is positively correlated to the time between corrections (*cf.* Fig. 4b, *cf.* Shiomi *et al.* 2008), although the rate of net error 'drop-off' is dependent on the accuracy of the initial (uncorrected) dead-reckoned track (*cf.* Fig. 5), itself, modulated by the extent of system errors (Table. 1) and initial user-defined track scaling.

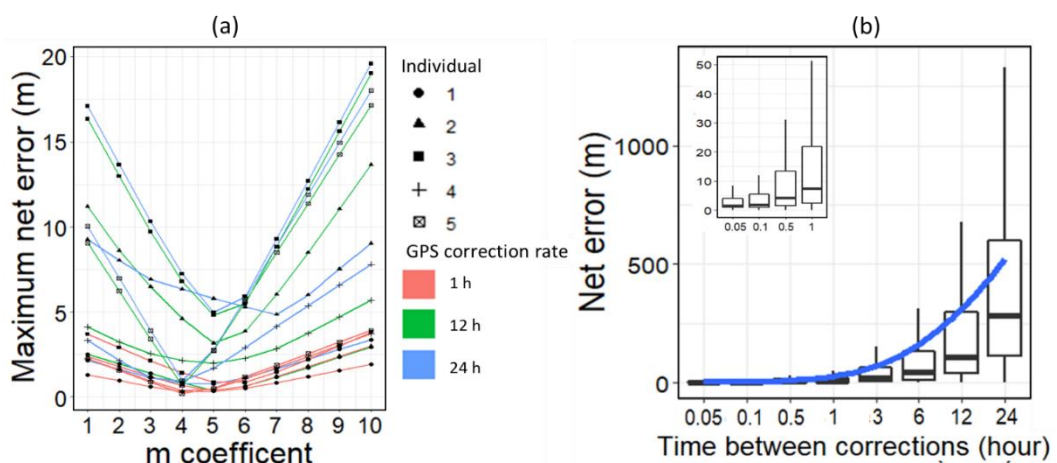


Figure 4. Net error between (GPS-corrected) dead-reckoned and GPS positions for a track from 5 African lions. (a) Maximum net error (m) between ground-truthed GPS and time-matched dead-reckoned positions after one iteration of correction, both as a function of GPS correction rate (one correction per 1- (red), 12- (green) and 24- (blue) hours) and underlying m -coefficient used to determine the DBA-derived speed. Data from 5 lions (individual denoted by symbol shape) over a period of 12 days. Note that the difference in error varies according to individual, initial speed estimate and the rate of correction. (b) Net error between dead-reckoned positions and all available GPS fixes, according to correction rate (data from the same 5 lions), subsequent to the iterative procedure of GPS correction (maximum distance between GPS fix used in correction procedure and according dead-reckoned position $< .01$ m). Boxes denote the median and 25-75 % interquartile range with a blue 'loess' smooth line. Whiskers extend to $1.5 * \text{Interquartile range}$ in both directions.

Within this process, people assume VPs to be perfect, however, across all VP determining methods, the rate and accuracy of data acquisition is highly moderated according to the permissiveness of the environment, such as high-density shrub or submersion in water (e.g., Hancock *et al.* 2009; Gužvica *et al.* 2014; Hofman *et al.* 2019). GPS technology is arguably the most popular and widely used method for determining estimates of free-ranging animal movement (*cf.* Hebblewhite & Haydon 2010; Latham *et al.* 2015; Patel *et al.* 2017). This is because inspection of data is less

complex and time-consuming than some of the alternatives, whilst improvements in design and battery longevity have enabled GPS units to be attached to a plethora of animals (up to almost four orders of magnitude in size and mass, *cf.* Wensveen, Thomas & Miller 2015; Gibb *et al.* 2017) and record at high frequencies (e.g., ≥ 1 Hz, Swain, Wark & Bishop-Hurley 2008; Patel *et al.* 2017). Consequently, GPS units are unparalleled for providing such detailed quantification of space-use outside of the VPC dead-reckoning framework, and are the most utilised VPC method within (including the case study datasets within this study). However, locational accuracy (excepting precision error radius (*cf.* Ryan *et al.* 2004) and variable latency (*cf.* Bouvet & Garcia 2000)) can vary by a few metres or be appreciably more depending upon the propagation of signal quality and/or receiver reception capability (Frair *et al.* 2010; Hofman *et al.* 2019; Péron *et al.* 2020). As such, VP error becomes more relevant at smaller scales of assessed movement and this is the reason why VP distance-moved estimates can go from being typically underestimated at low frequencies (due to linear interpolation of tortuous movements, Marcus Rowcliffe *et al.* 2012; Dewhirst *et al.* 2016; Poulin, Clermont & Berteaux 2021) to overestimated at high frequencies (Ryan *et al.* 2004; Chapter 4) and result in highly variable correction factors within the VPC dead-reckoning process (*cf.* Bidder *et al.* 2015). Indeed, judicious selection of VPC rate is critical in maximizing dead-reckoned track accuracy when relocation data is taken at fine spatial- and temporal resolutions (Dewhirst *et al.* 2016) (*cf.* Table. 2 – ‘VP.ME’, ‘method’, ‘thresh’ and ‘dist.step’ inputs to aid in modulating VPC rate). Likewise, the initial screening for location anomalies, across all VP methods and sampling intervals, is important to prevent incorrect distortion of tracks. Put simply, the higher the quality of VP data input, the greater the robustness of the VPC dead-reckoning output.

It was suggested by Bidder *et al.* (2015), that the next stage in this work is to derive a standardised set of rules to maximise the value of both GPS (though this applies to any VP method) and dead-reckoned data in line with the questions being asked. I argue that consistent trends in the magnitude and/or bias of correction factors can

be used as a diagnostic tool for elucidating; (i) VP inaccuracy (e.g., possibly manifested by extremely high distance and heading correction factors), (ii) required alterations to the DBA~speed relationship (e.g., due to traversing across different substrates (e.g., Fig. 5)) and (iii) drift due to current vectors (*cf.* Wilson *et al.* 2007; Shiomi *et al.* 2008, e.g., Fig. 6).

The case-studies

An important question to address is how often to do VP correction. This is obviously dependent upon the scales of movement elicited and the medium in/on which the animal in question navigates. Put simply, one should VP correct as little as possible, but as much as is necessary and I elaborate on this using my model species operating in different media. Within Fig. 5, the 1 Hz GPS track (blue) is plotted alongside two different dead-reckoned tracks; ((a) = uncorrected & (b) = corrected approx. every 30 mins (method = “time”)) from twelve days of data acquisition of one lion. There were two variations in the method of scaling the dead-reckoned tracks; a track based on a Vectorial Dynamic Body Acceleration (VeDBA) threshold (red), and a track advanced based on periods of identified movement (purple). The *m*-coefficient and *c*-constant values were determined from the VeDBA~GPS speed relationship [Fig. 5, insert a₁] and the Movement Verified Filtering (MVF) protocol (outlined in Chapter 4), was used to depict movement and anomalous GPS fixes (green) and to compute reasonable GPS-derived speed estimates. This case study demonstrates three important points. Firstly, on its own, dead-reckoning is subject to substantial drift and so VPC is essential for resetting this error. The more frequent a user corrects, the more accurate the dead reckon track becomes (relative to VPs), though VP error can also be substantial, especially during rest behaviour (see Chapter 4 for demonstration of this). For collared animals, heading measurements can become inaccurate at times of erratic collar roll (*cf.* Table. 1) and conjointly, GPS performance is also reduced when antenna position becomes compromised (e.g., Belant 2009).

Secondly, and in conjunction to the above, irrespective of VPC rate, the initial allocation of speed is important. Here, only dead-reckoning identified movement periods resulted in greater accuracy than just advancing tracks based on a VeDBA threshold. This is because even stationary behaviours can impart appreciable DBA (e.g., Graf *et al.* 2015) (beyond the threshold), and thus wrongly advance tracks. The false patterns of tortuosity created from this, whilst scaled and possibly rotated with VPC (*cf.* “VPC dead-reckoning procedure in R” section), remain incorporated to some degree. Whilst not illustrated here, advancing tracks without a VeDBA threshold would incur greater error still. Lastly, in this section, the distance correction factor was consistently high [Fig. 5, insert b₁] as the lion travelled along the Botswana fence boundary, perhaps as a result of the animal walking on the compact dirt road at this location [Fig. 5, insert a₂], altering the VeDBA~speed relationship. Such patterns in correction factors (whether consistent or highly variable) can highlight issues with the underlying track scaling.

Where animals move in water or air, obtaining accurate estimates of speed is more difficult without the use of speed sensors. Naturally, the resolution and accuracy of initial dead-reckoning track scaling (pre-VPC) reduces when speed has to be approximated using constant values according to behaviour type (a strategy used here). There is a balance between initial dead-reckoning accuracy and required VPC. The lower the initial track accuracy, the more frequent it should be corrected, and additional drift caused by external-force vectors compounds this issue. Within Fig. 6, I illustrate the value that current correction, dependent on current information, brings to the VPC procedure if the derived track is to be superimposed on the environment. Here, one Magellanic penguin was dead-reckoned with and without tidal vector integration (instantaneous tidal currents were deduced from a 3-D numerical model validated in the region (Tonini & Palma 2017), at hourly, 1 km² grid nodes). Commuting speed was allocated 2.1 m/s (*cf.* Wilson, Ropert-Coudert & Kato 2002; Wilson *et al.* 2004) and changed according to “VPC dead-reckoning procedure in R” section - R₄₁. Surface period ‘rest’ speed were allocated 0.416 m/s (*cf.* Wilson

1985). VP accuracy improved considerably both pre- and post- VPC when currents were integrated which points to the value of acquiring current data if possible, particularly if VPs are sparse. Notably the combination of dead-reckoning and VP estimation of both movements relative to the ground and fluid, may detail specific orientation strategies used and thus can have value for assessing the ability of drift compensation in aquatic or volant animals (Shiomi *et al.* 2008; Chapman *et al.* 2011)

For all my case study animals, GPS units were set to record at 1 Hz. With this temporal resolution (which is not always possible anyway due to the high-power requirements of the GPS), the value of dead-reckoning would seem questionable. However, dead-reckoning can; (i) work when GPS cannot – such as when an animal is underwater (e.g., Elkaim *et al.* 2006) or in thick forest (*cf.* McClune 2018) and it can (ii) by-pass the issues arising from GPS inaccuracies such as ‘jitter’ (*cf.* Chapter 4), allowing for more accurate and finer scale delineations of movement. This is illustrated in Fig. 7, in which twelve outgoing (green) and incoming (blue) dead-reckoned trajectories from Magellanic penguins walking to and from their nest are plotted. Incoming tracks were reverse-dead-reckoned (Outgoing = FALSE, bound = FALSE), because the GPS did not always register fixes for minutes after birds left the water and because nest coordinates were known [Fig. 7, insert]. This explains why the blue tracks extend into the sea rather than encroach further inland when speed was over-estimated. What is evident is that even ‘accurate’ GPS paths are coarsely resolved due to precision errors. Indeed, even with little or no GPS error, this can greatly compromise movement estimates (*cf.* Ryan *et al.* 2004). Conversely, the precision of the dead-reckoned tracks is only limited by the amount of initial motion sensor data under-sampling (usually required in some capacity to make datasets more manageable and less computationally expensive). Such fine-scale estimates can therefore (with suitable VPC) allow users to define movement in space with unprecedented resolution. The benefit of this is that such resolution can resolve important metrics of movement, such as step duration (*cf.* Wilson *et al.* 2013b) and the number and extent of turns made (*cf.* Potts *et al.* 2018); useful parameters for investigating

navigation and foraging strategies according to environmental circumstance - though, such parameters are also useful without superimposing on the environment. Moreover, even dead-reckoned tracks that are sparsely corrected or never corrected can detail important movement-specific behaviours (Andrzejaczek *et al.* 2019), for example, circling behaviour (Narazaki *et al.* 2021).

Ultimately, the higher the frequency at which dead-reckoning is undertaken, the better the resolution and detail of reconstructed tracks. However, accuracy only improves up to a point because extrapolated travel vectors (heading and speed estimates) nearly always comprise some degree of error (no matter how small) and so, with very high frequencies (> 1 Hz), more error is accumulated per unit time (*cf.* Wilson 2002; Wilson *et al.* 2007). In particular, when the temporal resolution of dead-reckoning results in a spatial resolution dominated more by sensor noise than by 'actual' movement of the animal in question, dead-reckoning accuracy will begin to decrease (at least pre-VPC). The extent of this will depend on the size, speed and lifestyle of the animal in question. For example, the benefits of dead-reckoning a lion at 40 Hz rather than 1 Hz are questionable (how often does a lion turn substantially within a second?), particularly given the additional computation time (*cf.* SI.1: Text S6) and possible error (relative to VPs). As such, and akin with VP under-sampling, choice of under-sampling data to be dead-reckoned may have implications to the resultant accuracy, and this will be moderated according to the scales (and media) of movement elicited by the animal in question. Beyond this, Fig. 7 also demonstrates the importance of initial track advancement, with three variants used, including step counts instead of DBA.

Finally, obtaining accurate estimates of altitude or depth allow users to plot and investigate scales of continuous movement in three dimensions and at times when VP success rate fails completely (such as underwater). I demonstrate this using the Imperial cormorant in Fig. 8. After visual inspection of data, uncorrected tracks were scaled according to the following speeds: periods of flying allocated 12 m/s, surface

'rest' periods allocated 0.1 m/s, bottom phase of dives allocated 0.4 m/s and descent and ascent speeds modulated according to "VPC dead-reckoning procedure in R" section - E₂₅. Note that elevation was not resolved during flying periods (although flying periods were dead-reckoned). Regardless of the current limitations, the VPC dead-reckoning procedure represents a substantial advance for resolving, and thereby allowing investigation of, continuous, fine-scale, free-ranging 2- or 3-D space-use with all its underlying scales of tortuosity and distances moved (e.g., Fig. 7 & 8).

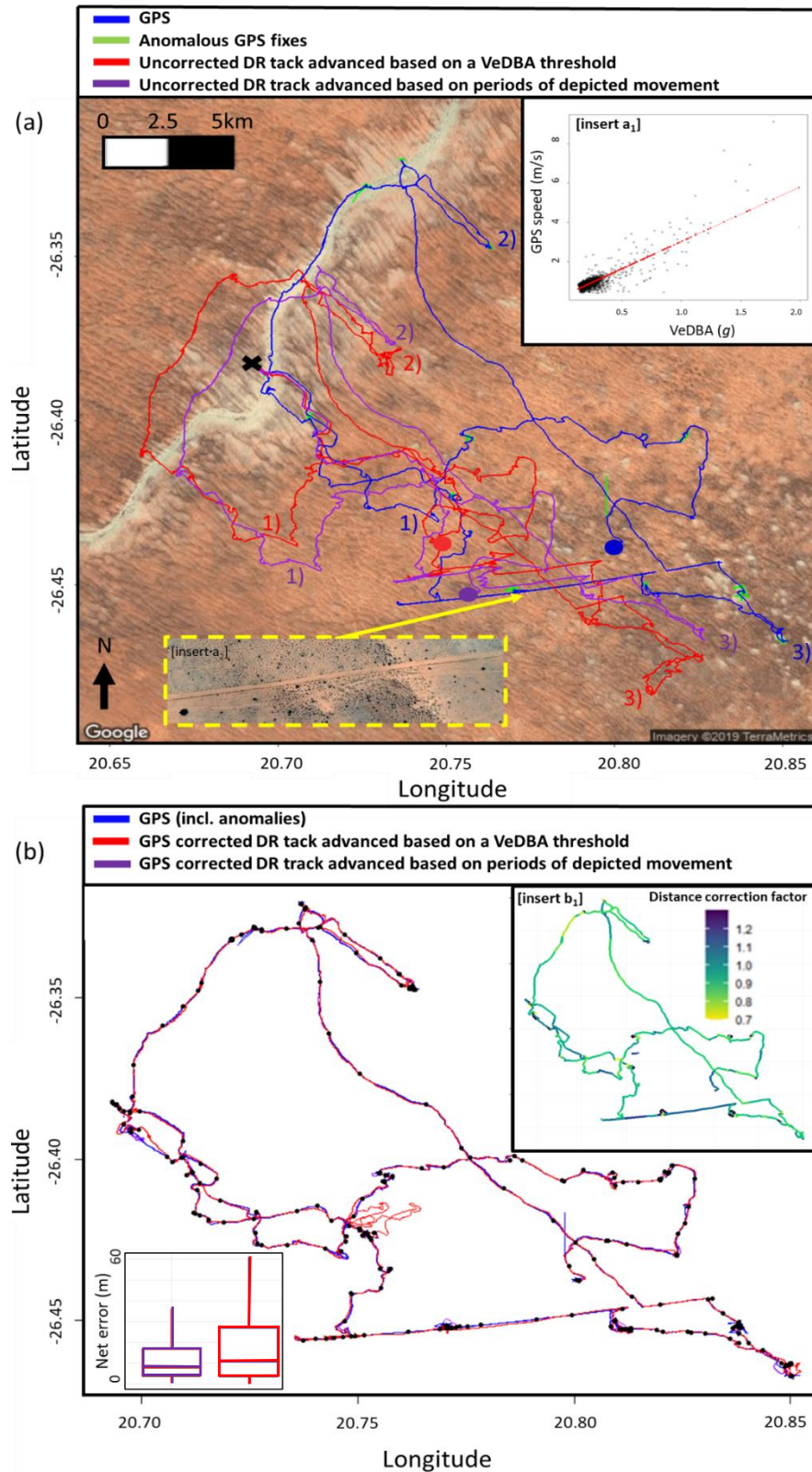


Figure 5. Dead reckoned lion track in relation to GPS positions ((a) = uncorrected & (b) = corrected – approx. every 30 mins (black circles)). The start of the track (lo and la) is denoted with a black x. Three corresponding sections of each track are denoted with the same number and the finishing positions denoted with a circle (coloured according to its reference track). Note that the horizontal straight-line sections (cf. yellow arrow) result from the lion following the Botswana boundary fence (which this individual eventually crossed). Mean net error between (corrected) dead-reckoned positions and all available GPS fixes was higher for tracks resolved using a VeDBA threshold (0.11 g), than for tracks advanced only at times of depicted movement using the MVF method.

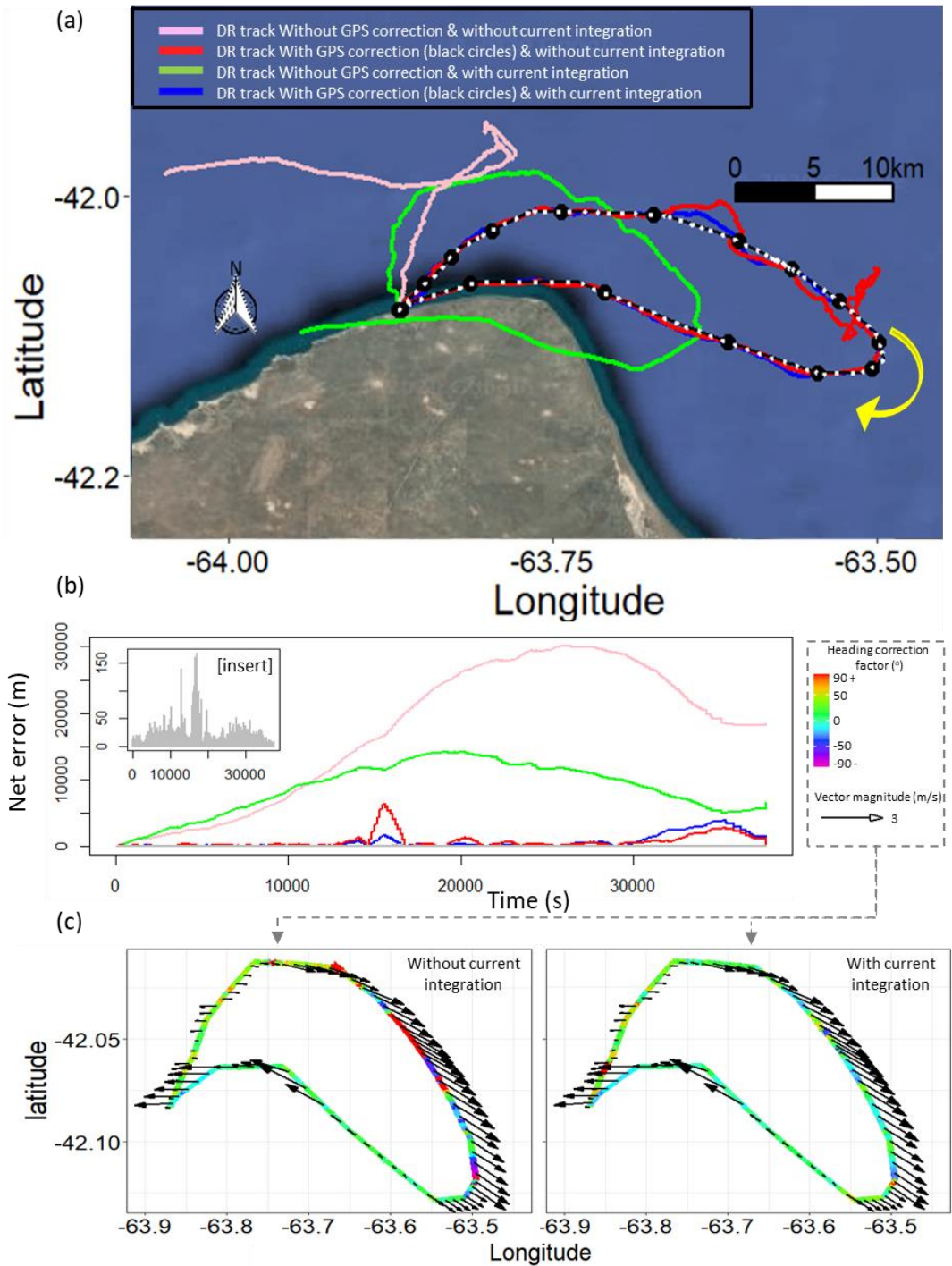


Figure 6. One Magellanic penguin's dead-reckoned foraging trip at sea, lasting approximately 9 hours (yellow arrow denotes the trajectory direction over time. Black track = GPS. Fifteen corrections (black circles) were made (method = "divide"). For comparison, the grey dotted track is the GPS corrected dead-reckoned track with current integration approx. every 1 min (where possible - method = "time") (a). Note the difference of net error between dead-reckoned positions and all available GPS fixes across the various tracks [insert = grey track] (b). Both uncorrected and corrected dead-reckoned tracks had less error after current integration (black arrows vector every 5 mins) and this was reflected in the direction and magnitude of heading correction factors required per unit time (c). Heading correction factors obtained from the track corrected approx. every 1 min; the colour of the scale bar indicates the extent of the heading correction factor required).

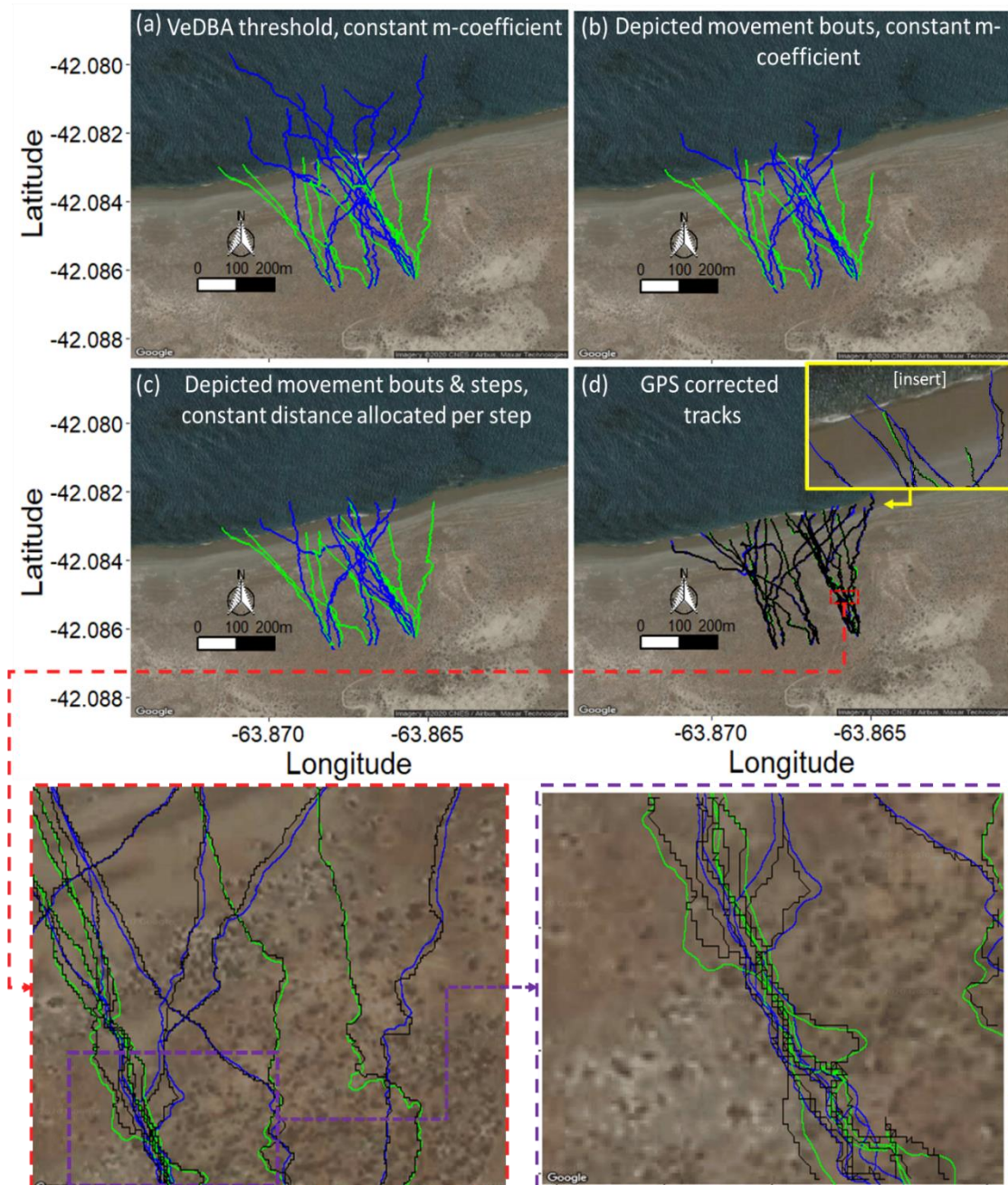


Figure 7. Twelve outgoing (green) and incoming (blue) dead-reckoned trajectories from Magellanic penguins walking to and from their nest. Three variants of track advancement were used; (a) A VeDBA threshold (0.1 g) and constant m -coefficient (1.4) (b), depicted movement periods using the LoCoD method to identify steps (cf. Wilson et al. 2018) and constant m -coefficient (1.4) and (c) depicted individual steps within depicted movement periods, from which a constant distance estimate (0.16 m) was multiplied by step frequency (\bar{x} no. steps/s) (full details within SI. 1: Text S4) (c). Note that the accuracy with respect to the radial distance can be evaluated by examining the track stops in relation to the shore-line. DBA-derived speed estimates were typically overestimated for incoming tracks, due to the birds being heavier (and thus impart greater DBA per stide cycle) after foraging. Tracks (from (c)) were GPS-corrected (d) (method = "distance", dist.step = 5, VP.ME = TRUE, thresh = between 8-15 (depending on track length) approx. every 50 m). A portion of the GPS-corrected dead-reckoned tracks (bottom panel) are magnified (2 iterations) to show the difference in resolution of movement tortuosity, between GPS and dead-reckoned tracks.

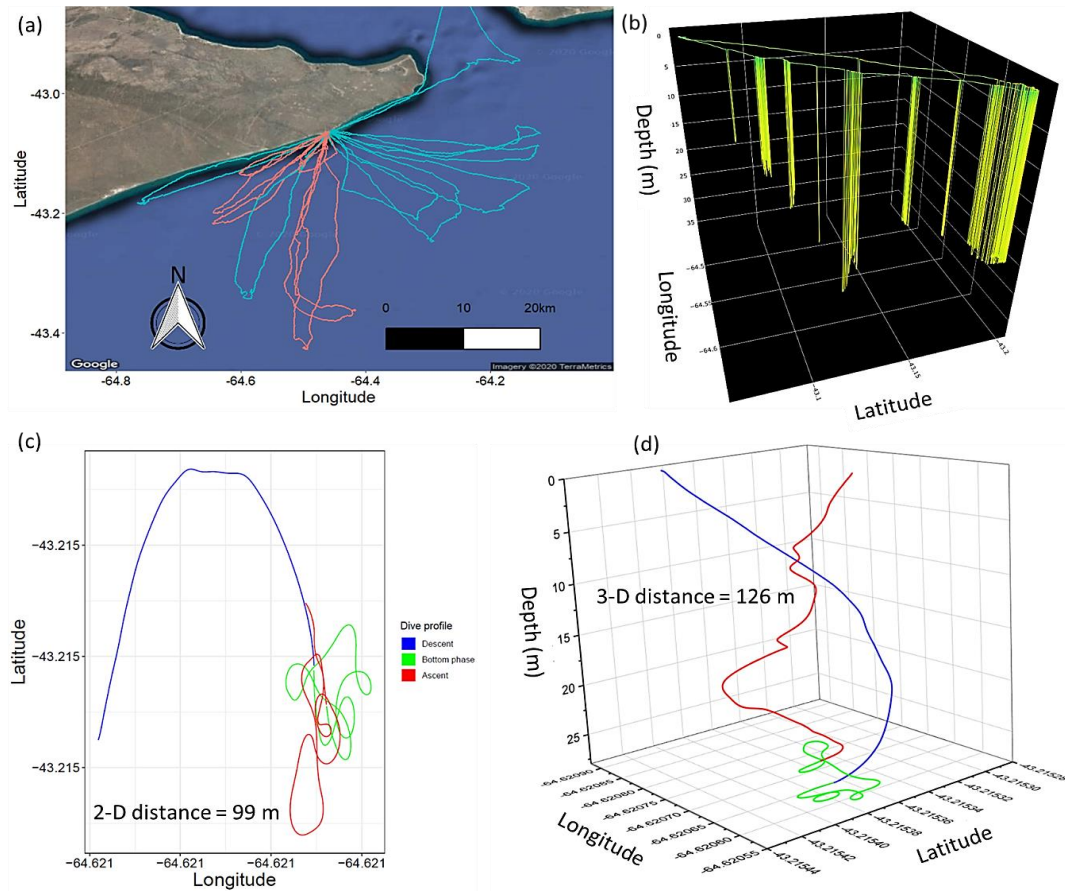


Figure 8. GPS-corrected dead-reckoned tracks of Imperial cormorants foraging at sea; (a) 15 birds (blue = male, red = female). (b) shows one of these tracks illustrated in 3-D. Note gaps between dives are either associated with current drift, while the bird is resting at the sea surface, or periods of flight. (c) and (d) show the descent, bottom phase and ascent of a given dive in both 2-D (c) and 3-D, respectively.

VPC dead-reckoning procedure in R

Preparing the three axes of rotation for derivation of heading

The tilt-compensated compass method is a well-known practice for deriving heading (e.g., Li, Li & Wang 2009; Säll & Merkel 2011; Pedley 2012). Correct coordinate system axis alignment and suitable calibration of tri-axial magnetometry data (*cf.* Kunčar, Sysel & Urbánek 2016) are crucial pre-processors, without which, heading estimates would likely incorporate substantial error (*cf.* Pedley 2012; Kunčar, Sysel & Urbánek 2016). The tilt-compensated compass method described below (following the framework outlined by Pedley (2012)), requires the aerospace (x-North, y-East, z-Down – ‘right-handed’) coordinate system, or ‘NED’ (*cf.* SI. 1: Text S2: Fig. S1). I provide examples of axis alignment, outline the importance of transforming between coordinate frames (relative to the Earths fixed frame) and recommend a universal configuration calibration procedure to aid correct axis alignment within SI. 1: Text S2.

Multiple mathematically sophisticated algorithms have been developed to correct distortions from each magnetometer channel’s output (e.g., Sodhi *et al.* 2008; Renaudin, Afzal & Lachapelle 2010; Ozyagcilar 2012; Tabatabaei, Gluhak & Tafazolli 2013; Kunčar, Sysel & Urbánek 2016). I provide an annotated R script - *Gundog.Compass* (SI. 2) that corrects both soft and hard iron distortions from tri-axial magnetometry data and subsequently computes tilt-compensated heading (0° to 360°). Within this function, there are two main methods of correction to choose from, based on the mathematical protocols outlined by Vitali (2016) - least-square error approximation (constructing an ellipsoid rotation matrix) and Winer (2017) - scale biases with simple orthogonal rescaling (avoiding matrices altogether). I expand on this user-defined functionality, as well as outlining the causes of soft and hard iron distortions and the initial calibration procedure required to correct such distortions within SI. 1: Text S3.

Tilt-compensated heading derivation

Device orientation is expressed in terms of a sequence of Euler angle (roll (Φ), pitch (θ), yaw (Ψ)) rotations about the x-,y- and z-axes, respectively, relative to the (inertial) Earth's fixed frame of reference (e.g., Earth-Centre, Earth-Fixed (ECEF) system, Premerlani & Bizard 2009). Being a vector field sensor with two degrees of rotational freedom, accelerometers are insensitive to rotations about the gravity vector and thus discerning heading requires the arctangent of the ratio between the x- and y-orthogonal magnetometer measurements (Grygorenko 2011). For the correct computation of heading, these two channels need to be aligned parallel to the earth's surface. This is achieved by correcting any orientation (de-rotation) according to pitch and roll angles (postural offsets) which can be deduced from acceleration. These angles are typically approximated by deriving gravity-based (static) acceleration (see Shepard *et al.* 2008; Gleiss, Wilson & Shepard 2011) from each channel by employing one of four approaches using; (i) a running mean (e.g., Shepard *et al.* 2008; Chapter 2), (ii) a Fast-Fourier transformation (e.g., Choi *et al.* 2014), (iii) a high-pass filter (e.g., Sato *et al.* 2003) or (iv) a Kalman-filter (e.g., Li & Wang 2013). Here, I use a computationally simple running mean over 2 seconds (Shepard *et al.* 2008) (E₁).

$$G_{x,y,z} = \frac{1}{w} \sum_{j=i-\frac{w}{2}}^{i+\frac{w}{2}} A_{x,y,z} \quad (\text{E}_1)$$

where, w is an integer specifying the window size and $G_{x,y,z}$ and $A_{x,y,z}$ represents the smoothed and raw components of acceleration, respectively. In the absence of linear (dynamic) acceleration (see Gleiss, Wilson & Shepard 2011; Pedley 2013), values of $G_{x,y,z}$ reflect the device orientation with respect to the earth's reference frame (though see Table. 1), reading approx. +1 g when orientated directly towards the gravity vector (down), -1 g against the gravity vector (up) and 0 g at perpendicular to it (horizontal). In R, the 'zoo' package (Zeileis *et al.* 2020) provides useful wrappers to apply arithmetic operations in a rolling fashion (R_{1:4}).

```
install.packages("zoo") ; library(zoo) (R1)
Gx = rollapply(Ax, width=w, FUN=mean, align="center", fill="extend") (R2)
Gy = rollapply(Ay, width=w, FUN=mean, align="center", fill="extend") (R3)
Gz = rollapply(Az, width=w, FUN=mean, align="center", fill="extend") (R4)
```

here, w should be replaced with the window width of choice (e.g., for 20 Hz data and a smoothing of 2 seconds required, replace w with 40). I use a centre-aligned index (compared to the rolling window of observations), with "extend" to indicate repetition of the leftmost or rightmost non-NA value (though fill can equally be set as NA, 0, etc.).

Importantly, for correct trigonometric formulae output within the tilt-compensated compass method, the vectorial sum of static acceleration ($G_{x,y,z}$) and calibrated magnetometry ($M_{x,y,z}$) measurements across all three spatial-dimensions must be normalised (to a unit vector) with a scaled magnitude (radius) of one (E2:3, R5:10). It was previously demonstrated that, for fast moving animals, high frequency of body posture changes could cause discrepancy between static acceleration data and magnetism data, which could consequently affect heading estimation (Shiomi *et al.* 2010). Although this effect would not change general shapes of movement paths, I suggest that prior to the normalisation process (and magnetic calibration procedure), it may be of value to initially smooth out (see E1, R1:4) small deviations within magnetometry data, both to avoid this type of error and to reduce the magnitude of anomalous spikes in magnetic inference. I used a smoothing window of 10 events for the 40 Hz datasets used in this study.

$$\begin{bmatrix} NG_x \\ NG_y \\ NG_z \end{bmatrix} = \frac{1}{\sqrt{G_x \cdot G_x + G_y \cdot G_y + G_z \cdot G_z}} \cdot \begin{bmatrix} G_x \\ G_y \\ G_z \end{bmatrix} \quad (E2) \quad \begin{bmatrix} NM_x \\ NM_y \\ NM_z \end{bmatrix} = \frac{1}{\sqrt{M_x \cdot M_x + M_y \cdot M_y + M_z \cdot M_z}} \cdot \begin{bmatrix} M_x \\ M_y \\ M_z \end{bmatrix} \quad (E3)$$

$$NG_x = G_x / \text{sqrt}(G_x^2 + G_y^2 + G_z^2) \quad (R5)$$

$$NG_y = G_y / \text{sqrt}(G_x^2 + G_y^2 + G_z^2) \quad (R6)$$

$$NG_z = G_z / \text{sqrt}(G_x^2 + G_y^2 + G_z^2) \quad (R7)$$

$$NM_x = M_x / \text{sqrt}(M_x^2 + M_y^2 + M_z^2) \quad (R8)$$

$$NM_y = M_y / \text{sqrt}(M_x^2 + M_y^2 + M_z^2) \quad (R9)$$

$$NM_z = M_z / \text{sqrt}(M_x^2 + M_y^2 + M_z^2) \quad (R10)$$

Depending on deployment position, the device-carried NED coordinate frame (the x,y,z axes) may not correspond with the animal's body-carried NED frame. When this occurs, prior to deriving animal orientation, the normalised gravity and magnetic vectors are required to be corrected so that their measurements are expressed relative to the body frame of the animal (Johnson & Tyack 2003). This requires three rotation sequences, using 3 by 3 rotation matrices (E4:6) and involves two intermediate frames. The aerospace sequence used here is as follows:

- 1) A right-handed rotation (C), about the z -axis axis of the device's frame (D), through angle Ψ (E4), to get to the first intermediate frame (F_1)
- 2) A right-handed rotation (C) about the y -axis at F_1 , through angle θ (E5), to get to the second intermediate frame (F_2)
- 3) A right-handed rotation (C) about the x -axis at F_2 , through angle Φ (E6), to get to the animal's body frame (B).

$$C_{F_1/D}^{(\Psi)} = \begin{bmatrix} \cos(\Psi) & \sin(\Psi) & 0 \\ -\sin(\Psi) & \cos(\Psi) & 0 \\ 0 & 0 & 1 \end{bmatrix} \quad (E_4)$$

$$C_{F_2/F_1}^{(\theta)} = \begin{bmatrix} \cos(\theta) & 0 & -\sin(\theta) \\ 0 & 1 & 0 \\ \sin(\theta) & 0 & \cos(\theta) \end{bmatrix} \quad (E_5)$$

$$C_{B/F_2}^{(\Phi)} = \begin{bmatrix} 1 & 0 & 0 \\ 0 & \cos(\Phi) & \sin(\Phi) \\ 0 & -\sin(\Phi) & \cos(\Phi) \end{bmatrix} \quad (E_6)$$

Note the right-handed rule of rotation; a positive Ψ reflects a clockwise rotation of the anterior-posterior axis (relative to North), a positive θ reflects a nose-upward tilt of this axis and a positive Φ reflects a bank angle tilt to the right about this axis. Reversing the direction of two axes causes a 180° inversion about the remaining axis and interchanging two axes (e.g., x with y) or reversing the direction of one or all three axes reverses the 'handedness' of rotation (right-handed – 'counter-clockwise' vs left-handed – 'clockwise' (when viewed from the tip of the z -axis)). Rotation matrices are orthogonal (unitary), with every row and column being linearly

independent and normal to every other row and column. The consequence of this is that the inverse of a rotation matrix is its transpose (Evans 2001) (which essentially reverses the direction of rotation, and within (E_{4:6}), this is achieved by negating the sign of the sines). Importantly, because rotation matrices are not symmetric, the order of matrix multiplication is important (Johnson & Tyack 2003 - otherwise Euler angles are without meaning for describing orientation). The product of the conventionally used aerospace rotation sequence outlined above (to get from the tag frame to the animal's body frame) can be expressed as (E₇).

$$C_{B/D}^{(\Phi, \theta, \Psi)} = C_{B/F_2}^{(\Phi)} \cdot C_{F_2/F_1}^{(\theta)} \cdot C_{F_1/D}^{(\Psi)} \quad (E_7)$$

When matrix multiplied out, this yields (E₈) - often referred to as a Direction Cosine Matrix (DCM). The composition of this DCM varies according the (six possible) orderings of the three rotation matrices (E_{4:6}) and the direction of intended rotation relative to the direction of measured *g* within the NED system (see SI.1: Text S2).

$$C_{B/D}^{(\Phi, \theta, \Psi)} = \begin{bmatrix} \cos(\Psi) \cdot \cos(\theta) & \sin(\Psi) \cdot \cos(\theta) & -\sin(\theta) \\ \cos(\Psi) \cdot \sin(\theta) \cdot \sin(\Phi) - \sin(\Psi) \cdot \cos(\Phi) & \sin(\Psi) \cdot \sin(\theta) \cdot \sin(\Phi) + \cos(\Psi) \cdot \cos(\Phi) & \cos(\theta) \cdot \sin(\Phi) \\ \cos(\Psi) \cdot \sin(\theta) \cdot \cos(\Phi) + \sin(\Psi) \cdot \sin(\Phi) & \sin(\Psi) \cdot \sin(\theta) \cdot \cos(\Phi) - \cos(\Psi) \cdot \sin(\Phi) & \cos(\theta) \cdot \cos(\Phi) \end{bmatrix} \quad (E_8)$$

Note the left-handed rule of reading the vectorial notation of ordered rotations, for example $C_{B/D}^{(\Phi, \theta, \Psi)}$ means going from the device frame to the animal's body frame, by first rotating about the z-axis (though angle Ψ), followed by the y-axis (though angle θ) and then lastly the x-axis (though angle Φ). The device offset can be estimated from direct observation or deduced using photographs or from the tag data itself. For example, assuming that 'normal animal posture' has no pitch and roll angle offset, then a tri-axial spherical plot of static acceleration (Wilson *et al.* 2016) would show a densely populated band of datapoints at the cross-sectional origin of 0 *g* about the x- and y-axes, respectively, when the tag and body NED axes are in alignment.

$NG_{x,y,z}$ and $NM_{x,y,z}$ are pre-multiplied by the DCM to compensate for offset. However, device offset is often parametrised by roll, pitch and/or yaw angles relative to the animal's body frame and thus, the device actually requires de-rotation (switching the 'handedness' of rotation) according to these values. For example, a +45° yaw offset requires an inverse rotation about the z-axis by -45°, rather than a further +45° rotation. This simply involves taking the transpose of the DCM (E₉), which is the same as the transpose of each of the individual rotation matrices (E_{10:11}).

$$C_{B/D}^{(\Phi,\theta,\Psi)T} = \begin{bmatrix} \cos(\Psi) \cdot \cos(\theta) & \cos(\Psi) \cdot \sin(\theta) \cdot \sin(\Phi) - \sin(\Psi) \cdot \cos(\Phi) & \cos(\Psi) \cdot \sin(\theta) \cdot \cos(\Phi) + \sin(\Psi) \cdot \sin(\Phi) \\ \sin(\Psi) \cdot \cos(\theta) & \sin(\Psi) \cdot \sin(\theta) \cdot \sin(\Phi) + \cos(\Psi) \cdot \cos(\Phi) & \sin(\Psi) \cdot \sin(\theta) \cdot \cos(\Phi) - \cos(\Psi) \cdot \sin(\Phi) \\ -\sin(\theta) & \cos(\theta) \cdot \sin(\Phi) & \cos(\theta) \cdot \cos(\Phi) \end{bmatrix} \quad (E_9)$$

$$\begin{bmatrix} NGb_x \\ NGb_y \\ NGb_x \end{bmatrix}^B = C_{B/F_2}^{(\Phi)T} \cdot C_{F_2/F_1}^{(\theta)T} \cdot C_{F_1/D}^{(\Psi)T} \cdot \begin{bmatrix} NG_x \\ NG_y \\ NG_x \end{bmatrix}^D \quad (E_{10})$$

$$\begin{bmatrix} NMb_x \\ NMb_y \\ NMb_x \end{bmatrix}^B = C_{B/F_2}^{(\Phi)T} \cdot C_{F_2/F_1}^{(\theta)T} \cdot C_{F_1/D}^{(\Psi)T} \cdot \begin{bmatrix} NM_x \\ NM_y \\ NM_x \end{bmatrix}^D \quad (E_{11})$$

where, T is the matrix transpose and resultant $NGb_{x,y,z}$ and $NMb_{x,y,z}$ vectors are expressed in the animal's body-carried NED frame. The input of these gravity and magnetic vectors are supplied as 3 by 1 column matrices for true matrix multiplication, and when expanding out (E₁₁), this results in (E₁₂) (substituting NM with NG expands out (E₁₀)).

$$\begin{bmatrix} NMb_x \\ NMb_y \\ NMb_x \end{bmatrix}^B = \begin{bmatrix} NM_x \cdot \cos(\Psi) \cdot \cos(\theta) + NM_y \cdot (\cos(\Psi) \cdot \sin(\theta) \cdot \sin(\Phi) - \sin(\Psi) \cdot \cos(\Phi)) + NM_z \cdot (\cos(\Psi) \cdot \sin(\theta) \cdot \cos(\Phi) + \sin(\Psi) \cdot \sin(\Phi)) \\ NM_x \cdot \sin(\Psi) \cdot \cos(\theta) + NM_y \cdot (\sin(\Psi) \cdot \sin(\theta) \cdot \sin(\Phi) + \cos(\Psi) \cdot \cos(\Phi)) + NM_z \cdot (\sin(\Psi) \cdot \sin(\theta) \cdot \cos(\Phi) - \cos(\Psi) \cdot \sin(\Phi)) \\ -NM_x \cdot \sin(\theta) + NM_y \cdot \cos(\theta) \cdot \sin(\Phi) + NM_z \cdot \cos(\theta) \cdot \cos(\Phi) \end{bmatrix}^D \quad (E_{12})$$

In R then, the alignment of device to body axes for both gravity and magnetic vectors can be performed using the following procedure (R_{11:22}).

```

RollSinAngle = sin(Roll * pi/180) (R11)
RollCosAngle = cos(Roll * pi/180) (R12)
PitchSinAngle = sin(Pitch * pi/180) (R13)
PitchCosAngle = cos(Pitch * pi/180) (R14)
YawSinAngle = sin(Yaw * pi/180) (R15)
YawCosAngle = cos(Yaw * pi/180) (R16)
NGbx = NGx * YawCosAngle * PitchCosAngle + NGy * (YawCosAngle *
PitchSinAngle * RollSinAngle - YawSinAngle * RollCosAngle) + NGz *
(YawCosAngle * PitchSinAngle * RollCosAngle + YawSinAngle * RollSinAngle)
NGby = NGx * YawSinAngle * PitchCosAngle + NGy * (YawSinAngle *
PitchSinAngle * RollSinAngle + YawCosAngle * RollCosAngle) + NGz *
(YawSinAngle * PitchSinAngle * RollSinAngle - YawCosAngle * RollSinAngle)
NGbz = -NGx * PitchSinAngle + NGy * PitchCosAngle * RollSinAngle +
NGz * PitchCosAngle * RollCosAngle (R19)
NMbx = NMx * YawCosAngle * PitchCosAngle + NMy * (YawCosAngle *
PitchSinAngle * RollSinAngle - YawSinAngle * RollCosAngle) + NMz *
(YawCosAngle * PitchSinAngle * RollCosAngle + YawSinAngle * RollSinAngle)
NMby = NMx * YawSinAngle * PitchCosAngle + NMy * (YawSinAngle *
PitchSinAngle * RollSinAngle + YawCosAngle * RollCosAngle) + NMz *
(YawSinAngle * PitchSinAngle * RollSinAngle - YawCosAngle * RollSinAngle)
NMbz = -NMx * PitchSinAngle + NMy * PitchCosAngle * RollSinAngle +
NMz * PitchCosAngle * RollCosAngle (R22)

```

here, *Roll*, *Pitch* and *Yaw* inputs denote the angular offset of the device, relative to the animal body frame. Note, standard trigonometric functions operate in radians, not degrees. In base R, $\pi = \text{pi}$. Multiplying values by $\text{pi}/180$ converts degrees into radians, whilst multiplying values by $180/\text{pi}$ does the reverse. This rotation correction procedure is implemented within *Gundog.Compass* when pitch, roll and/or yaw offsets are supplied (see SI.1: Text S3).

Following the alignment of device and body axes, pitch and roll of the animal are calculated from the DCM, and because there are multiple variations in the order that rotation sequences can be composed and applied, there are also different valid equations that output different pitch and roll angle estimates, for equivalent static acceleration input. The convention is to use formulae that have no dependence on yaw rotation and restrict either the pitch or the roll angles within the range -90° to $+90^\circ$ (but not both), with the other axis of rotation able to lie between -180° and 180° , thereby eliminating duplicate solutions at multiples of 360° . Multiplying (E_8) by the measured Earth's gravitational field vector (+1 g when initially aligned downwards along the z-axis) simplifies down to (E_{13}). The accelerometer output for this aerospace

rotation sequence is thus only dependent on the roll and pitch angles which can be solved (E_{14:15}), allowing roll angles the greater freedom (Pedley 2013). This is relevant for studies using collar-mounted tags, whereby collar may roll > 90° in either direction from default orientation.

$$\begin{aligned}
 NGB_{xyz} \begin{bmatrix} 0 \\ 0 \\ 1 \end{bmatrix} &= \\
 \begin{bmatrix} \cos(\Psi) \cdot \cos(\theta) & \sin(\Psi) \cdot \cos(\theta) & -\sin(\theta) \\ \cos(\Psi) \cdot \sin(\theta) \cdot \sin(\Phi) - \sin(\Psi) \cdot \cos(\Phi) & \sin(\Psi) \cdot \sin(\theta) \cdot \sin(\Phi) + \cos(\Psi) \cdot \cos(\Phi) & \cos(\theta) \cdot \sin(\Phi) \\ \cos(\Psi) \cdot \sin(\theta) \cdot \cos(\Phi) + \sin(\Psi) \cdot \sin(\Phi) & \sin(\Psi) \cdot \sin(\theta) \cdot \cos(\Phi) - \cos(\Psi) \cdot \sin(\Phi) & \cos(\theta) \cdot \cos(\Phi) \end{bmatrix} \cdot \\
 \begin{bmatrix} 0 \\ 0 \\ 1 \end{bmatrix} &= \begin{bmatrix} -\sin(\theta) \\ \cos(\theta) \cdot \sin(\Phi) \\ \cos(\theta) \cdot \cos(\Phi) \end{bmatrix}
 \end{aligned} \tag{E14}$$

$$\tan \theta_{xyz} = \left(\frac{-NGB_x}{\sqrt{NGB_y^2 + NGB_z^2}} \right) \Rightarrow \theta = \text{atan2} \left(-NGB_x, \sqrt{NGB_y \cdot NGB_y + NGB_z \cdot NGB_z} \right) \cdot \frac{180}{\pi}$$

$$\tan \Phi_{xyz} = \left(\frac{NGB_y}{NGB_z} \right) \Rightarrow \Phi = \text{atan2}(NGB_y, NGB_z) \cdot \frac{180}{\pi} \tag{E15}$$

The equation for roll (E₁₅) however, has a region of instability at obtuse pitch angles (e.g., for NED systems, the x-axis points directly up or down, with respect to the Earth's frame of reference). Whilst there is no 'gold standard' solution to this problem of singularity (using Euler angles), an attractive circumvention (detailed within (Pedley 2013)) is to modify (E₁₅) and add a very small percentage (μ) of the NGB_x reading into the denominator, preventing it ever being zero and thus driving roll angles to zero when pitch approaches $-/+ 90^\circ$ for stability (E₁₆).

$$\Phi = \text{atan2}(NGB_y, \text{sign}(NGB_z) \cdot \sqrt{NGB_z \cdot NGB_z + \mu \cdot NGB_x \cdot NGB_x}) \cdot \frac{180}{\pi} \tag{E16}$$

where, $\text{sign}(NGB_z)$ is allocated the value +1 when NGB_z is non-negative and -1, when NGB_z is negative (recovers directionality of NGB_z , subsequent to the square-root). Taken together then, in R, pitch and roll are computed according to, (R_{24:25}) with

outputs within the range of -90° to $+90^\circ$ for pitch and -180° to $+180^\circ$ for roll, and this is the formula I use in the tilt compensated method outlined below (and within SI.2).

$$\mu = 0.01 ; \text{sign} = \text{ifelse}(\text{NGbz} \geq 0, 1, -1) \quad (\text{R}_{23})$$

$$\text{Pitch} = \text{atan2}(-\text{NGbx}, \sqrt{\text{NGby}^2 + \text{NGbz}^2}) * 180/\text{pi} \quad (\text{R}_{24})$$

$$\text{Roll} = \text{atan2}(\text{NGby}, \text{sign} * \sqrt{\text{NGbz}^2 + \mu * \text{NGbx}^2}) * 180/\text{pi} \quad (\text{R}_{25})$$

here, prior to the derivation of pitch and roll, μ is allocated the value 0.01 and a vector termed 'sign' is created, containing 1's and -1's according to the direction of measured g from NGb_z (R₂₃).

The magnetic vector of the device is then de-rotated to the Earth frame (tilt-corrected) by pre-multiplying by the product of the inverse roll multiplied by inverse pitch rotation matrix (E₁₇), which when expanded out gives (E₁₈).

$$\begin{bmatrix} \text{NMbf}_x \\ \text{NMbf}_y \\ \text{NMbf}_z \end{bmatrix} = \begin{bmatrix} \cos(\theta) & \sin(\theta) \cdot \sin(\Phi) & \sin(\theta) \cdot \cos(\Phi) \\ 0 & \cos(\Phi) & -\sin(\Phi) \\ -\sin(\theta) & \cos(\theta) \cdot \sin(\Phi) & \cos(\theta) \cdot \cos(\Phi) \end{bmatrix} \cdot \begin{bmatrix} \text{NMb}_x \\ \text{NMb}_y \\ \text{NMb}_z \end{bmatrix} \quad (\text{E}_{17})$$

$$\begin{bmatrix} \text{NMbf}_x \\ \text{NMbf}_y \\ \text{NMbf}_z \end{bmatrix} = \begin{bmatrix} \text{NMb}_x \cdot \cos(\theta) + \text{NMb}_y \cdot \sin(\theta) \cdot \sin(\Phi) + \text{NMb}_z \cdot \sin(\theta) \cdot \cos(\Phi) \\ \text{NMb}_y \cdot \cos(\Phi) - \text{NMb}_z \cdot \sin(\Phi) \\ -\text{NMb}_x \cdot \sin(\theta) + \text{NMb}_y \cdot \cos(\theta) \cdot \sin(\Phi) + \text{NMb}_z \cdot \cos(\theta) \cdot \cos(\Phi) \end{bmatrix} \quad (\text{E}_{18})$$

here, $\text{NMbf}_{x,y,z}$ are the calibrated, normalised magnetometry data (expressed in the animal's body-carried NED frame) after tilt-correction. Finally, yaw (ψ) (heading – now defined by the compass convention, relative to magnetic North) can be computed from the NMbf_x and NMbf_y (E₁₉) via;

$$\psi = \text{atan2}(-\text{NMbf}_y, \text{NMbf}_x) \cdot \frac{180}{\pi} \quad (\text{E}_{19})$$

I outline the R code for this procedure below (R_{26:34}).

$$\text{RollSinAngle} = \sin(\text{Roll} * \text{pi}/180) \quad (\text{R}_{26})$$

$$\text{RollCosAngle} = \cos(\text{Roll} * \text{pi}/180) \quad (\text{R}_{27})$$

$$\text{PitchSinAngle} = \sin(\text{Pitch} * \text{pi}/180) \quad (\text{R}_{28})$$

$$\text{PitchCosAngle} = \cos(\text{Pitch} * \text{pi}/180) \quad (\text{R}_{29})$$

```

NMbfx = NMbx * PitchCosAngle + NMby * PitchSinAngle * RollSinAngle + (R30)
NMbz * PitchSinAngle * RollCosAngle
NMbfy = NMby * RollCosAngle - NMbz * RollSinAngle (R31)
NMbfz = -NMbx * PitchSinAngle + NMby * PitchCosAngle + RollSinAngle +
(R32) NMbz * PitchCosAngle * RollCosAngle
Yaw = atan2(-NMfy, NMfx) * 180/pi (R33)
Yaw = ifelse(Yaw < 0, Yaw + 360, Yaw) (R34)

```

Note, yaw output from (R₃₃) uses the scale -180° to + 180°. (R₃₄) converts to the scale 0° to 360° (specifically, 0° to 359°). This is also achieved by using a modulus (mod) operator (E₂₀, R₃₅), which in base R takes the form %%.

```

ψ = mod(360 + ψ, 360) (E20)
Yaw = (360 + Yaw) %% 360 (R35)

```

Magnetic declination is defined as the angle on the horizontal plane between magnetic north and true north (Caruso 2000). Prior to dead-reckoning, magnetic declination should be summed to heading values to convert from magnetic to true North (Boelter 2020). There are many online sources to calculate the magnetic declination of an area (e.g., http://www.geomag.bgs.ac.uk/data_service/models_compass/wmm_calc.html).

Notably, logical corrections may need to be performed to ensure data does not exceed either circular direction after applying magnetic declination (R₃₆).

```

h = ifelse(h < 0, h + 360, h) ; h = ifelse(h > 360, h - 360, h) (R36)

```

where h refers to the vector containing the heading data. Should the user not correct for axis alignment between the device and animal body frame (*cf.* E_{4:12}, R_{11:22}) then a reasonable post-correction for small discrepancies about the yaw axis would be to subtract the difference to h values at this point.

Preparing speed estimates

The vectorial dynamic body acceleration (VeDBA) (E₂₁) (cf. Qasem *et al.* 2012; Wilson *et al.* 2020a) was my choice of DBA-based speed proxy for terrestrial dead-reckoning purposes. This is given by;

$$v = \sqrt{(D_x^2 + D_y^2 + D_z^2)} \quad (\text{E}_{21})$$

where v represents VeDBA, D_x , D_y & D_z are the dynamic acceleration values from each axis, themselves obtained by subtracting each axis' static component of acceleration (cf. E₁, R_{1:4}) from their raw equivalent (R₃₇).

$$v = \text{sqrt}((Ax - Gx)^2 + (Ay - Gy)^2 + (Az - Gz)^2) \quad (\text{R}_{37})$$

where, Ax , Ay , Az and Gx , Gy , Gz are the raw and static (smoothed) values of each channel's recorded acceleration.

I recommend implementing a running mean (cf. E₁, R_{1:4}) to raw VeDBA values to ensure that both acceleration and deceleration components of a stride cycle are incorporated together per unit time and to reduce the magnitude of small temporal spikes, (likely not attributable to the scale of movement elicited. Choice of smoothing window size is dependent on the scale of movement being investigated, though as a basic rule, I suggest 1 to 2 seconds. For similar reasons, it is also worth post-smoothing raw pitch, roll and heading outputs, although heading requires a circular mean (E_{22:23}) (cf. Pewsey, Neuhäuser & Ruxton 2013).

$$\bar{\theta}_p = \text{atan2}\left(\frac{1}{n} \sum_{j=i}^n \sin\left(h_j \cdot \frac{\pi}{180}\right), \frac{1}{n} \sum_{j=i}^n \cos\left(h_j \cdot \frac{\pi}{180}\right)\right) \quad (\text{E}_{22})$$

$$\bar{h} = \text{mod}\left(360 + \left(\bar{\theta}_p \cdot \frac{180}{\pi}\right), 360\right) \quad (\text{E}_{23})$$

where h_j and \bar{h} are the unsmoothed and smoothed heading values, $\bar{\theta}_p$ the arithmetic mean after converting degrees to cartesian coordinates and *mod* refers to the modulo operator.

In R, the above formula can be made into a function (R₃₈), to be applied within the ‘*rollapply*’ wrapper (replacing ‘FUN = *mean*’ with ‘FUN = *Circ.Avg*’) (cf. R_{1:4}).

```
Circ.Avg = function(x){
  H.East = mean(sin(x * pi / 180))
  H.North = mean(cos(x * pi / 180))
  MH = (atan2(H.East, H.North)) * 180/pi
  MH = (360 + MH) %% 360
  return(MH)
}
```

(R₃₈)

Speed (*s*) can be estimated from VeDBA (*v*) via (E₂₄).

$$s = (v \cdot m) + c \quad (\text{E}_{24})$$

where *m* is the multiplicative coefficient and *c* is a constant (Bidder *et al.* 2012; Bidder *et al.* 2015). Here, a user can define various bouts of movement from motion sensor data (e.g., via various machine learning approaches (for review see Farrahi *et al.* (2019) or the Boolean-based LoCoD method (Wilson *et al.* 2018) and/or substrate condition (e.g., via GPS)), to be cross-referenced when allocating variants of the speed coefficients. As a simple example, in R, should walking (coded for as 1) and running (coded for as 2) be teased apart from all other (non-moving) data (coded for as 0) within a Marked Events vector (*ME*), then *ME* can be used to allocate various *m* (and if applicable, *c*) values using simple ‘*ifelse*’ statements (R_{39:40}).

```
m = ifelse(ME == 1, 1.5, ifelse(ME == 2, 3.5, 0))
```

(R₃₉)

```
c = ifelse(ME > 0, 0.1, 0)
```

(R₄₀)

Here, walking is given an arbitrary coefficient of 1.5 and running, 3.5 with a value of 0.1 for their constants. All other *ME* values are given a 0 coefficient and 0 constant, which results in no speed at such times, regardless of DBA magnitude.

By-passing DBA as a speed proxy

Dividing the number of steps detected within a given rolling window length (*cf.* R_{1:4}), by the window length (*s*) gives an estimated step count per second. This can be converted to speed by multiplying by a distance per step estimate (assuming constant distance travelled between step gaits). I review this further in SI. 1: Text S4, including a simple peak finder function – *Gundog.Peaks* (SI. 3) that locates peaks based on local signal maxima, using a given rolling window, with each candidate peak filtered according to whether it surpassed a threshold height (in conjunction with other potential user-defined thresholds). Note, this method can equally be applied to non-terrestrial species, using flipper/tail beats instead, where appropriate.

For diving animals, a proxy for horizontal speed can be obtained based on animal pitch and rate change in depth (Miller *et al.* 2004; Laplanche, Marques & Thomas 2015). Specifically, rate change of depth (Δd) (units in m/s) is divided by the tangent of pitch (θ) (converted from degrees to radians) (E₂₅).

$$s = \frac{\Delta d}{\tan(\theta \cdot \frac{\pi}{180})} \quad (\text{E}_{25})$$

here, resultant speed values need to be made absolute (positive). This calculation is only valid when the direction of movement is the same as the direction of the animal's longitudinal axis (equal pitch assumption) (*cf.* Laplanche, Marques & Thomas 2015) and thus should only be calculated at times when the animal is travelling 'ballistically' (at considerable vertical speed).

$$s = \text{ifelse}(\text{abs}(p) \geq 10, \text{abs}(RCD / \tan(p * \text{pi}/180)), s) \quad (\text{R}_{41})$$

In the above example (R₄₁), nominal speed values are overwritten with the trigonometric formula output (E₂₅) at times of 'appreciable' pitch (10°) (*cf.* Ropert-Coudert *et al.* 2001), where *RCD* is the rate change of depth and *p* is the pitch (in radians). An upper limit should be imposed on speed values derived in this way because values can become highly inflated when the pitch angle is particularly acute.

Converting speed to a distance coefficient

Speed (s) estimates are multiplied by the time difference between the values (TD) to give a distance estimate (units in metres) which, in turn, standardises coefficient comparisons across datasets sampled at different rates. These distance values are then divided by the approximate radius of the earth ($R = 6378137$ m) to give a radial distance coefficient (q ; see, <https://www.movable-type.co.uk/scripts/latlong.html>; E26).

$$q = \frac{s \cdot TD}{R} \quad (\text{E26})$$

Assuming that high resolution depth data is not available, but ‘absolute’ speed estimates have been obtained, then an alternative to (E25, in accordance with the equal pitch assumption) is to derive horizontal distance estimates by multiplying the absolute distance by the cosine of the pitch (θ , converted from degrees to radians), which can equally be performed on the radial distance (E27).

$$q = q \cdot \cos\left(\theta \cdot \frac{\pi}{180}\right) \quad (\text{E27})$$

In R, to determine accurate lengths of time between values, it is best to save date and time variables together as *POSIX* class (Grolemund & Wickham 2011). Creating timestamp (TS) objects with *POSIXct* class enables greater control and manipulation of time data. This makes computing the rolling time difference (TD ; units in seconds) between data points simple (R42)

$$TD = c(\theta, \text{difftime}(TS, \text{lag}(TS), \text{units} = "secs"))[-1]) \quad (\text{R42})$$

I detail how to create timestamp objects of *POSIXct* class within SI. 1: Text S5, including formatting with decimal seconds (important for infra-second datasets) and various codes useful for manipulating data to be dead-reckoned based on time.

In R then, following the computation of TD , q is obtained *via* (R43:44).

$$s = (v * m) + c \quad (\text{R43})$$

$$q = (s * TD) / 6378137 \quad (\text{R44})$$

Note, if a negative c intercept is used (e.g., to allow for some body movement without translation), then any negative speed values would need to be equated to zero as an additional step.

As previously mentioned, the ME vector (progressive movement coded by integer values greater than zero (e.g., 1) and stationary behaviour coded by zero) can be used to ensure q (essentially the distance moved) is zero when ME reads zero, ensuring dead-reckoned tracks are not advanced at such times, regardless of the computed speed (R₄₅).

```
q = ifelse(ME == 0, 0, q) (R45)
```

Derivation of co-ordinates

Once q and h are obtained, coordinates are advanced using (E_{28:29});

$$Lat_i = asin(\sin Lat_0 \cdot \cos q + \cos Lat_0 \cdot \sin q \cdot \cos h) \quad (E_{28})$$

$$Lon_i = Lon_0 + atan2((\sin h \cdot \sin q \cdot \cos Lat_0), (\cos q - \sin Lat_0 \cdot \sin Lat_i)) \quad (E_{29})$$

where Lat_0 , Lat_i and Lon_0 , Lon_i are the previous and present latitude and longitude coordinates, respectively (in radians), h is the (present) heading (in radians) and q is the (present) distance coefficient.

In R, the above can be performed iteratively within a for-loop (iteration of code repeated per consecutive i_{th} element of data; R₄₉). Initializing the output latitude ($DR.lat$) and longitude ($DR.lon$) variables to the required length (e.g., as governed by the vector length of other input data (heading, speed, etc.) speeds up processing time (R₄₆). Within the trigonometric dead-reckoning formulae, the starting latitude (la) and longitude (lo) coordinates and heading (h) values must be supplied in radians (R₄₇). The la and lo values are saved as the first elements of the $DR.lat$ and $DR.lon$ vectors to be advanced, respectively (R₄₈).

```

DR.lat = rep(NA, length(h)) ; DR.lon = rep(NA, length(h))           (R46)
la = la * pi/180 ; lo = lo * pi/180 ; h = h * pi/180              (R47)
DR.lat[1] = la ; DR.lon[1] = lo                                     (R48)
for(i in 2:length(DR.lat)) {                                       (R49)
  DR.lat[i] = asin(sin(DR.lat[i-1]) * cos(q[i]) + cos(DR.lat[i-1]) *
  sin(q[i]) * cos(h[i]))
  DR.lon[i] = DR.lon[i-1] + atan2(sin(h[i]) * sin(q[i]) *
  cos(DR.lat[i-1]), cos(q[i]) - sin(DR.lat[i-1]) * sin(DR.lat[i]))
}

```

Reverse dead-reckoning

For this, firstly, the time difference is computed as usual (R₅₀) and the dimensions of each vector required in the dead-reckoning calculation are reversed. I bind all relevant vectors into a data frame (df) (R₅₁), subsequent to reversing data frame dimensions (R₅₂); the last row becomes the first row, second to last row becomes the second etc. Note, this can equally be achieved by using the *rev()* function within base R, on each individual vector. These reversed columns are now restored as vectors (R₅₃) and shifted forward by one element (R₅₄). This is required for correct alignment in time so that dead-reckoning works in exactly the opposite manner to ‘forward’ dead-reckoning.

```

TD = c(0, difftime(TS, lag(TS), units = "secs")[-1])              (R50)
df = data.frame(TD, h, v, m, c, ME)                                (R51)
df = df[dim(df)[1]:1, ]                                           (R52)
TD = df[, 'TD'] ; h = df[, 'h'] ; v = df[, 'v'] ;                 (R53)
m = df[, 'm'] ; c = df[, 'c'] ; ME = df[, 'ME']
TD = c(NA, TD[-length(TD)]) ; h = c(NA, h[-length(h)]) ;         (R54)
v = c(NA, v[-length(v)]) ; m = c(NA, m[-length(m)]) ;
c = c(NA, c[-length(c)]) ; ME = c(NA, ME[-length(ME)])

```

The next step is to rotate heading 180° and correct for its circular nature (R₅₅).

```
h = h - 180 ; h = ifelse(h < 0, h + 360, h)                       (R55)
```

Lastly, *q* is determined and *DR.lon* and *DR.lat* are advanced based on the dead-reckoning formula (cf. R_{46:49}), except in this instance, the first element of *DR.lon* and *DR.lat* needs to be supplied by the ‘known’ last *lo* and *la* coordinates.

Integrating current vectors

In R, current vectors can be added according to (R_{56:60}). Current speed (*cs*) is in m/s (ensure values are absolute) and current heading (*ch*) uses the scale 0° to 360°. Note the use of ‘*yy*’ and ‘*xx*’ vectors, storing the previous *DR.lat* and *DR.lon* coordinates prior to implementing the next ‘current drift’ vector per iteration. The current speed is also standardised according to the time period length and Earth’s radius (analogous to the derivation of *q*). When reverse dead-reckoning, it is important to ensure that *cs* and *ch* are included in the steps outlined above (R_{50:55}).

```
DR.lat = rep(NA, length(h)) ; DR.lon = rep(NA, length(h)) (R56)
```

```
xx <- rep(NA, length(cs)) ; yy <- rep(NA, length(cs)) (R57)
```

```
la = la * pi/180 ; lo = lo * pi/180 ; (R58)
```

```
h = h * pi/180 ; ch = ch * pi/180
```

```
DR.lat[1] = la DR.lon[1] = lo (R59)
```

```
for(i in 2:length(DR.lat)) { (R60)
```

```
  DR.lat[i] = asin(sin(DR.lat[i-1]) * cos(q[i]) + cos(DR.lat[i-1]) *  
  sin(q[i]) * cos(h[i]))
```

```
  yy[i] = DR.lat[i]
```

```
  DR.lon[i] = DR.lon[i-1] + atan2(sin(h[i]) * sin(q[i]) *  
  cos(DR.lat[i-1]), cos(q[i]) - sin(DR.lat[i-1]) * sin(DR.lat[i]))
```

```
  xx[i] = DR.lon[i]
```

```
  DR.lat[i] = asin(sin(yy[i]) * cos((cs[i] * TD[i]) / 6378137) +  
  cos(yy[i]) * sin((cs[i] * TD[i]) / 6378137) * cos(ch[i]))
```

```
  DR.lon[i] = xx[i] + atan2(sin(ch[i]) * sin((cs[i] * TD[i]) /  
  6378137) * cos(yy[i]), cos((cs[i] * TD[i]) / 6378137) - sin(yy[i]) *  
  sin(DR.lat[i]))
```

```
}
```

VPC procedure

Specifically, this method entails calculating the difference of Haversine distance (net error) and bearing (from true North) between consecutive VPs and the corresponding time-matched dead-reckoned track positions. The trigonometric Haversine formulae (E_{30:31}) are used to calculate the great-circle distance (*d*) and great circular bearing (*b*) between consecutive VPs and consecutive (time-matched) dead-reckoned positions (note I use the term ‘bearing’ to differentiate between heading estimates from motion data – though they are essentially the same).

$$d = 2 \cdot R \cdot \sin^{-1} \left(\sqrt{\sin^2 \left(\frac{Lat_i - Lat_0}{2} \right) + \cos(Lat_0) \cdot \cos(Lat_i) \cdot \sin^2 \left(\frac{Lon_i - Lon_0}{2} \right)} \right) \quad (E_{30})$$

where, R is the Earth's radius and d , the output in metres.

$$b = \text{atan2} \left(\frac{\sin(\Delta Lon) \cdot \cos(Lat_i)}{\cos(Lat_0) \cdot \sin(\Delta Lat) \cdot \cos(Lat_i) \cdot \cos(\Delta Lon)} \right) \cdot \frac{180}{\pi} \quad (E_{31})$$

where, ΔLon represents $Lon_i - Lon_0$, ΔLat represents $Lat_i - Lat_0$ and b output is in the scale -180° to $+180^\circ$. To convert b to the conventional 0° to 360° scale, 360 should be added to values < 0 .

For each VP, the distance is divided by the dead-reckoned distance providing a distance correction factor (ratio; E_{32}). The heading correction factor is computed by subtracting the dead-reckoned bearing from the VP bearing (E_{33}). To ensure that difference does not exceed 180° in either circular direction, 360 should be added to values < -180 and 360 subtracted from values > 180 . A simple example of why this is relevant can be illustrated by subtracting a dead-reckoned bearing value of 359° from a VP bearing value of 1° – post correction, the difference is $+2^\circ$.

$$Distance_{corr.factor} = \frac{Distance_{VP}}{Distance_{DR}} \quad (E_{32})$$

$$Heading_{corr.factor} = Bearing_{VP} - Bearing_{DR} \quad (E_{33})$$

All intermediate q values are multiplied by the distance correction factor and the heading correction factor is added to all intermediate h values (ensuring that h values are in degrees). To ensure circular range is maintained between 0° and 360° , 360 should be subtracted from values > 360 and added to values < 0 .

Specifically, I follow the protocol illustrated within Figure 9 for intermediate values. Note the formulae to calculate both distance (d ; E_{30}) and bearing (b ; E_{31}) between two points, are also used to recalculate both the heading (h) and radial distance (q) between current-integrated dead-reckoned fixes (pre-VPC; *cf.* R_{60}). Note that the

Haversine distance is required to be converted back to radial distance by dividing by R ($R = 6378137$).

GPS fix	DR fix	Intermediate Correction order	ΔLon ΔLat
1*	1*	—	
	2	1	
	3	1	
	4	1	
2	5	1	
	6	2	
	7	2	
	8	2	
	9	2	
	10	2	
3	11	2	
	12	3	
	13	3	
4	14	3	
	15	4	
	16	4	
	17	4	
	18	4	
	19	4	
5	20	4	
	21	5	

Figure 9. Schematic diagram illustrating the order of fixes used when calculating the $Distance_{corr.factor}$ and $Heading_{corr.factor}$ (difference of both GPS and dead-reckoned (DR) positions between arrow heads). Note the discrepancy with the order at which these correction factors are applied to intermediate DR positions (as denoted by colour shading). Known starting position denoted with *.

In R, the formulae to calculate the great-circle distance and great circular bearing are saved within the $disty$ (R_{61}) and $beary$ (R_{62}) functions, respectively, where $lon1$, $lat1$, $long2$ and $lat2$ represent longitude and latitude positions (decimal format) at t_i and t_{i+1} , (t representing time).

```

disty = function(long1, lat1, long2, lat2) {                                     (R61)
  long1 = long1 * pi/180 ; long2 = long2 * pi/180 ; lat1 = lat1 *
  pi/180 ; lat2 = lat2 * pi/180
  a = sin((lat2 - lat1) / 2) * sin((lat2 - lat1) / 2) + cos(lat1) *
  cos(lat2) * sin((long2 - long1) / 2) * sin((long2 - long1) / 2)
  c = 2 * atan2(sqrt(a), sqrt(1 - a))
  d = 6378137 * c
  return(d)
}

```

```

beary = function(long1, lat1, long2, lat2) {                                     (R62)
  long1 = long1 * pi/180 ; long2 = long2 * pi/180 ; lat1 = lat1 *
  pi/180 ; lat2 = lat2 * pi/180
  a = sin(long2 - long1)*cos(lat2)
  b = cos(lat1) * sin(lat2) - sin(lat1) * cos(lat2) * cos(long2 - long
  1)
  c = ((atan2(a, b) / pi)*180)
  return(c)
}

```

Below, I outline an example of VPC in R and assume VP coordinates (decimal format) are aligned in the same length vectors/columns as motion sensor-derived data, e.g., heading, DBA/speed etc, with the corresponding indexed (element-/row-wise) time. Typically, motion sensor data is recorded at much higher frequency so that there are many dead-reckoned fixes between sequential VPs. As such, in the example below, I assume NAs are expressed in the VP longitude and latitude fields at times of missing locational data. This approach of synchronising VP- with motion sensor data also applies when integrating current data; assuming *ch* and *cs* are element/row-wise matched to the relevant VP grid node.

Firstly, an indexing row number (*Row.number*) vector, the length of the data used in the dead-reckoning operation (e.g., *h*) is created (R₆₃), which is relevant for merging full-sized and under-sampled data frames together (seen later). Together, the row number, (un-corrected) dead-reckoned longitude and latitude coordinates, VP longitude and latitude coordinates, heading and the radial distance vectors are inputted column-wise into a 'main' data frame, termed '*df*' (R₆₄; user-assigned column names of each vector are within quotation marks). This data frame is then filtered removing rows with missing VP data and stored as '*df.sub*' (R₆₅). This under-sampled data frame thus, row-wise, contains the time-matched dead-reckoned and ground-truthed positions. The VPC process is analogous for reverse dead-reckoned tracks – although *VP.lon* and *VP.lat* must also be reversed (*Row.number* remains in ascending order (not reversed)). The first element of *VP.lon* and *VP.lat* must be the *lo* and *la*, respectively (or for reverse dead-reckoning, the last element prior to reversing these vectors).

```
Row.number = rep(1:length(h)) (R63)
```

```
df = data.frame(Row.number, 'DR.longitude' = DR.lon, (R64)
  'DR.latitude' = DR.lat, 'VP.longitude' = VP.lon,
  'VP.latitude' = VP.lat, h, q)
```

```
df.sub = df[!with(df, is.na(VP.longitude) | is.na(VP.latitude)) ,] (R65)
```

Both sets of dead-reckoned and VP coordinates are shifted backwards one row within new columns termed: *'DR.loni'*, *'DR.lati'*, *'VP.loni'*, *'VP.lati'* (R66). Row-wise, these columns represent the consecutive fix at t_{i+1} with their originals being t_i . This provides the correct format for the inputs required within the *disty* (cf. R61) and *beary* (cf. R62) functions. The distances between consecutive dead-reckoned estimates are stored within the column termed *'DR.distance'* (R67) and the corresponding distances between VPs are stored within the column termed *'VP.distance'* (R68). The *VP.distance* is divided by the *DR.distance* to provide the distance correction factor, termed *'Dist.corr.factor'* (R69). Importantly here, an ifelse statement is incorporated so that *Dist.corr.factor* defaults to zero at times when both *VP.distance* and *DR.distance* are zero (otherwise dividing zero by zero in R produces NaNs).

```
df.sub$DR.loni = c(df.sub[-1, 'DR.longitude'], NA) (R66)
```

```
df.sub$DR.lati = c(df.sub[-1, 'DR.latitude'], NA)
```

```
df.sub$VP.loni = c(df.sub[-1, 'VP.longitude'], NA)
```

```
df.sub$VP.lati = c(df.sub[-1, 'VP.latitude'], NA)
```

```
df.sub$DR.distance= disty(df.sub$DR.longitude, (R67)
```

```
df.sub$DR.latitude, df.sub$DR.loni, df.sub$DR.lati)
```

```
df.sub$VP.distance= disty(df.sub$VP.longitude, (R68)
```

```
df.sub$VP.latitude, df.sub$VP.loni, df.sub$VP.lati)
```

```
df.sub$Dist.corr.factor = ifelse(df.sub$VP.distance == 0 & (R69)
```

```
df.sub$DR.distance == 0, 0, df.sub$VP.distance / df.sub$DR.distance)
```

Analogous to the distance correction, the bearings between consecutive dead-reckoned estimates are stored within the column termed *'DR.head'* (R70) and the corresponding bearings between VPs are stored within the column termed *'VP.head'* (R71). Logical corrections are performed to convert both to the 0° to 360° scale (R72), *DR.head* is subtracted from *VP.head* providing the heading correction factor, termed

'*Head.corr.factor*' (R₇₃) and further logical corrections are performed to ensure a minimum and maximum difference range between -180° to +180° (R₇₄).

```
df.sub$DR.head = beary(df.sub$DR.longitude, (R70)
df.sub$DR.latitude, df.sub$DR.loni, df.sub$DR.lati)
df.sub$VP.head = beary(df.sub$VP.longitude, (R71)
df.sub$VP.latitude, df.sub$VP.loni, df.sub$VP.lati)
df.sub$DR.head = ifelse(df.sub$DR.head < 0, (R72)
df.sub$DR.head + 360, df.sub$DR.head)
df.sub$VP.head = ifelse(df.sub$VP.head < 0,
df.sub$VP.head + 360, df.sub$VP.head)
df.sub$Head.corr.factor = df.sub$VP.head - df.sub$DR.head (R73)
df.sub$Head.corr.factor = ifelse(df.sub$Head.corr.factor < -180, (R74)
(df.sub$Head.corr.factor + 360), df.sub$Head.corr.factor)
df.sub$Head.corr.factor = ifelse(df.sub$Head.corr.factor > 180,
(df.sub$Head.corr.factor - 360), df.sub$Head.corr.factor)
```

Only the relevant columns: *Row.number*, *Dist.corr.factor* and *Head.corr.factor* are preserved (R₇₅) and merged back into the main data frame (*df*) based on the matching row numbers (R₇₆). Both *Dist.corr.factor* and *Head.corr.factor* express NA's between VPs. These are replaced with the most recent non-NA (observations carried forwards; R₇₇). *Dist.corr.factor* and *Head.corr.factor* values are shifted forward by one row (R₇₈) for correct alignment purposes with respect to *h* and *q* values to be adjusted (*cf.* Fig. 9; R_{79:80}). A logical correction is performed to ensure that a 0° to 360° circular scale is maintained after the heading correction (R₈₁). Note, the *na.locf()* function is required from the 'zoo' package, to replace NA values with the last non-NA value.

```
df.sub = df.sub[, c('Row.number', 'Dist.corr.factor', 'Head.corr.factor')] (R75)
df = merge(df, df.sub, by = "Row.number", all = TRUE)
df$Dist.corr.factor = na.locf(df$Dist.corr.factor) (R77)
df$Head.corr.factor = na.locf(df$Head.corr.factor)
df$Dist.corr.factor = c(NA, df$Dist.corr.factor[-nrow(df)]) (R78)
df$Head.corr.factor = c(NA, df$Head.corr.factor[-nrow(df)])
q = (df$q * df$Dist.corr.factor) (R79)
h = (df$h + df$Head.corr.factor) (R80)
h = ifelse(h > 360, h - 360, h) ; h = ifelse(h < 0, h + 360, h) (R81)
```

These updated coefficients are substituted into the dead-reckoning formula (cf. R46:49) and this process is repeated iteratively (using the updated dead-reckoned coordinates, heading and radial distance each time) until dead-reckoning fixes accord 'exactly' (*Gundog.Tracks* uses a threshold of .01 m) with ground-truthed locations. An important pitfall of the correction process to consider is that dividing 'any' value (e.g., > 0) by 0 results in infinite (*Inf*) values in R. This can arise during the correction process when there is a given distance between consecutive VPs, but no displacement between the according dead-reckoned positions. This can be a consequence of ground-truthing too frequently (typically relevant to high-res GPS studies), where positional noise is more apparent during rest periods (cf. Chapter 4) and/or wrongly assigned speed estimates/*ME* values. *Gundog.Tracks* automatically resamples VPC rate where necessary to avoid *Inf* values, essentially by changing the VPC-rate to avoid using successive VPs at times of no dead-reckoned track advancement. Lastly, *Gundog.Tracks* outputs messages to the user's console, detailing up to six stages of dead-reckoning progression, which includes reporting the maximum distance (units in metres) between dead-reckoned- and ground-truthed positions (used within the VPC procedure) at each iteration of correction and whether automatic VPC resampling due to *Inf* values occurred.

Conclusion

I have provided a comprehensive, fully integrated application of the dead-reckoning procedure within the framework of the programming language, R, from pre-processing raw tri-axial accelerometry and magnetometry data to VPC dead-reckoning. I have highlighted important considerations to increase the accuracy of the analytical procedure and to avoid misinterpretation of error. I have also supplied extensive supplementary information and supporting functions to aid the process of deriving fine-scale movement paths, including the protocols to correct magnetometry data and derive (tilt-compensated) heading. Importantly, I have demonstrated the value of *Gundog.Tracks*; a multi-functional and user-friendly tool to derive animal movement paths across all media of travel, with detailed input flexibility and output summaries. I suggest the next phase in advancing the utility of animal dead-reckoning includes looking for 'track signatures' that may signify a particular behaviour or reference a particular 'ground-truthed' location. Lastly to advance the utility of *Gundog.Tracks*, I aim to optimise future iterations of the online code to speed up computation time on larger datasets (e.g., sub-second data collected over many months).

References

- Adachi, T., Costa, D.P., Robinson, P.W., Peterson, S.H., Yamamichi, M., Naito, Y. & Takahashi, A. (2017) Searching for prey in a three-dimensional environment: hierarchical movements enhance foraging success in northern elephant seals. *Functional Ecology*, **31**, 361-369.
- Alaimo, A., Artale, V., Milazzo, C. & Ricciardello, A. (2013) Comparison between Euler and quaternion parametrization in UAV dynamics. *AIP Conference Proceedings*, **1558**, 1228-1231.
- Alexander, J.S., Zhang, C., Shi, K. & Riordan, P. (2016) A granular view of a snow leopard population using camera traps in Central China. *Biological Conservation*, **197**, 27-31.
- Altynay, K., Khan Mohammed, A., Marengo, M., Swanepoel, L., Przybysz, A., Muller, C., Fahlman, A., Buttner, U., Geraldi, N.R., Wilson, R.P., Duarte, C.M. & Kosel, J. (2019) Wearable multifunctional printed graphene sensors. *NPJ Flexible Electronics*, **3**.
- Andrzejczek, S., Gleiss, A.C., Lear, K.O., Pattiaratchi, C.B., Chapple, T.K. & Meekan, M.G. (2019) Biologging Tags Reveal Links Between Fine-Scale Horizontal and Vertical Movement Behaviors in Tiger Sharks (*Galeocerdo cuvier*). *Frontiers in Marine Science*, **6**.
- Andrzejczek, S., Gleiss, A.C., Pattiaratchi, C.B. & Meekan, M.G. (2018) First Insights Into the Fine-Scale Movements of the Sandbar Shark, *Carcharhinus plumbeus*. *Frontiers in Marine Science*, **5**.
- Aoki, K., Amano, M., Mori, K., Kourogi, A., Kubodera, T. & Miyazaki, N. (2012) Active hunting by deep-diving sperm whales: 3D dive profiles and maneuvers during bursts of speed. *Marine Ecology Progress Series*, **444**, 289-301.
- Aoki, K., Watanabe, Y.Y., Crocker, D.E., Robinson, P.W., Biuw, M., Costa, D.P., Miyazaki, N., Fedak, M.A. & Miller, P.J.O. (2011) Northern elephant seals adjust gliding and stroking patterns with changes in buoyancy: validation of at-sea metrics of body density. *Journal of Experimental Biology*, **214**, 2973-2987.
- Baumgartner, M.F., Freitag, L., Partan, J., Ball, K.R. & Prada, K.E. (2008) Tracking Large Marine Predators in Three Dimensions: The Real-Time Acoustic Tracking System. *IEEE Journal of Oceanic Engineering*, **33**, 146-157.
- Beauregard, S. & Haas, H. (2006) Pedestrian dead reckoning: A basis for personal positioning. *Proceedings of the 3rd Workshop on Positioning, Navigation and Communication*, pp. 27-35.
- Belant, J.L. (2009) Effects of Antenna Orientation and Vegetation on Global Positioning System Telemetry Collar Performance. *Northeastern Naturalist*, **16**, 577-584, 578.
- Benoit-Bird, K.J., Battaile, B.C., Nordstrom, C.A. & Trites, A.W. (2013) Foraging behavior of northern fur seals closely matches the hierarchical patch scales of prey. *Marine Ecology Progress Series*, **479**, 283-302.
- Bethge, P., Nicol, S., Culik, B.M. & Wilson, R.P. (1997) Diving behaviour and energetics in breeding little penguins (*Eudyptula minor*). *Journal of Zoology*, **242**, 483-502.
- Bidder, O.R., Qasem, L.A. & Wilson, R.P. (2012) On Higher Ground: How Well Can Dynamic Body Acceleration Determine Speed in Variable Terrain? *PLOS ONE*, **7**, e50556.
- Bidder, O.R., Soresina, M., Shepard, E.L.C., Halsey, L.G., Quintana, F., Gómez-Laich, A. & Wilson, R.P. (2012) The need for speed: testing acceleration for estimating animal travel rates in terrestrial dead-reckoning systems. *Zoology*, **115**, 58-64.
- Bidder, O.R., Walker, J.S., Jones, M.W., Holton, M.D., Urge, P., Scantlebury, D.M., Marks, N.J., Magowan, E.A., Maguire, I.E. & Wilson, R.P. (2015) Step by step:

- reconstruction of terrestrial animal movement paths by dead-reckoning. *Movement Ecology*, **3**, 23.
- Boelter, K.D.H. (2020) Aircraft Magnetic Declinator System. The Boeing Company , Chicago , IL (US)
- Bouvet, D. & Garcia, G. (2000) GPS latency identification by Kalman filtering. *Robotica*, **18**, 475-485.
- Bowditch, N. (2002) The American practical navigator, Bicentennial edition, National Imagery and Mapping Agency, Bethesda, Maryland, 879.
- Bras, Y.L., Jouma'a, J. & Guinet, C. (2017) Three-dimensional space use during the bottom phase of southern elephant seal dives. *Movement Ecology*, **5**, 18.
- Browning, E., Bolton, M., Owen, E., Shoji, A., Guilford, T. & Freeman, R. (2018) Predicting animal behaviour using deep learning: GPS data alone accurately predict diving in seabirds. *Methods in Ecology and Evolution*, **9**, 681-692.
- Bullock, R. (2007) Great circle distances and bearings between two locations. *MDT*.
- Cagnacci, F., Boitani, L., Powell, R.A. & Boyce, M.S. (2010) Animal ecology meets GPS-based radiotelemetry: a perfect storm of opportunities and challenges. *Philosophical Transactions of the Royal Society B: Biological Sciences*, **365**, 2157-2162.
- Caruso, M.J. (2000) Applications of magnetic sensors for low cost compass systems. *IEEE 2000. Position Location and Navigation Symposium (Cat. No.00CH37062)*, pp. 177-184.
- Catipovic, J.A. (1990) Performance limitations in underwater acoustic telemetry. *IEEE Journal of Oceanic Engineering*, **15**, 205-216.
- Chakravarty, P., Cozzi, G., Ozgul, A. & Aminian, K. (2019a) A novel biomechanical approach for animal behaviour recognition using accelerometers. *Methods in Ecology and Evolution*, **10**, 802-814.
- Chakravarty, P., Maalberg, M., Cozzi, G., Ozgul, A. & Aminian, K. (2019b) Behavioural compass: animal behaviour recognition using magnetometers. *Movement Ecology*, **7**, 28.
- Chapman, Jason W., Klaassen, Raymond H.G., Drake, V.A., Fossette, S., Hays, Graeme C., Metcalfe, Julian D., Reynolds, Andrew M., Reynolds, Don R. & Alerstam, T. (2011) Animal Orientation Strategies for Movement in Flows. *Current Biology*, **21**, R861-R870.
- Chiella, A.C.B., Teixeira, B.O.S. & Pereira, G.A.S. (2019) Quaternion-Based Robust Attitude Estimation Using an Adaptive Unscented Kalman Filter. *Sensors*, **19**, 2372.
- Choi, S., Youn, I.-H., LeMay, R., Burns, S. & Youn, J.-H. (2014) Biometric gait recognition based on wireless acceleration sensor using k-nearest neighbor classification. *2014 International Conference on Computing, Networking and Communications (ICNC)*, pp. 1091-1095.
- Constandache, I., Bao, X., Azizyan, M. & Choudhury, R.R. (2010) Did you see Bob? human localization using mobile phones. *Proceedings of the sixteenth annual international conference on Mobile computing and networking*, pp. 149–160. Association for Computing Machinery, Chicago, Illinois, USA.
- Cotter, C.H. (1978) Early Dead Reckoning Navigation. *Journal of Navigation*, **31**, 20-28.
- Cross (2019) Calculating Azimuth, Distance, and Altitude from a Pair of GPS Locations in JavaScript. GitHub repository, GitHub repository.
- Culik, B.M., Wilson, R.P., Dannfeld, R., Adelung, D., Spairani, H.J. & Coria, N.R.C. (1991) Pygoscelid penguins in a swim canal. *Polar Biology*, **11**, 277-282.
- Davis, R.W., Fuiman, L.A., Williams, T.M. & Le Boeuf, B.J. (2001) Three-dimensional movements and swimming activity of a northern elephant seal. *Comparative*

- Biochemistry and Physiology Part A: Molecular & Integrative Physiology*, **129**, 759-770.
- Denny, M. (1993) *Air and Water: The Biology and Physics of Life's Media*. Princeton University Press.
- Dewhurst, O.P., Evans, H.K., Roskilly, K., Harvey, R.J., Hubel, T.Y. & Wilson, A.M. (2016) Improving the accuracy of estimates of animal path and travel distance using GPS drift-corrected dead reckoning. *Ecology and Evolution*, **6**, 6210-6222.
- di Virgilio, A., Morales, J.M., Lambertucci, S.A., Shepard, E.L. & Wilson, R.P. (2018) Multi-dimensional Precision Livestock Farming: a potential toolbox for sustainable rangeland management. *PeerJ*, **6**, e4867.
- Diebel, J. (2006) Representing attitude: Euler angles, unit quaternions, and rotation vectors. *Technical Report*, pp. 1-35. Stanford University, Stanford.
- Dowle, M., Srinivasan, A., Gorecki, J., Chirico, M., Stetsenko, P., Short, T., Lianoglou, S., Antonyan, E., Bonsch, M. & Parsonage, H. (2019) Package 'data.table'. *Extension of 'data.frame'*.
- Dunford, C.E., Marks, N.J., Wilmers, C.C., Bryce, C.M., Nickel, B., Wolfe, L.L., Scantlebury, D.M. & Williams, T.M. (2020) Surviving in steep terrain: a lab-to-field assessment of locomotor costs for wild mountain lions (*Puma concolor*). *Movement Ecology*, **8**, 34.
- Elkaim, G.H., Decker, E.B., Oliver, G. & Wright, B. (2006) Marine Mammal Marker (MAMMARK) dead reckoning sensor for In-Situ environmental monitoring. *Proceedings of IEEE/ION PLANS 2006*, pp. 976-987. San Diego, CA.
- English, H.M., Harvey, L., Wilson, R.P., Gunner, R.M., Holton, M.D., Woodroffe, R. & Börger, L. ((in review)) Multi-sensor biologgers and innovative training allow data collection with high conservation and welfare value in zoos. *Journal of Zoo and Aquarium Research*.
- Evans, P. (2001) Rotations and rotation matrices. *Acta Crystallographica Section D*, **57**, 1355-1359.
- Fancy, S.G., Pank, L.F., Douglas, D.C., Curby, C.H. & Garner, G.W. (1988) Satellite telemetry: a new tool for wildlife research and management. Fish and Wildlife Service Washington DC, Washington, D.C.
- Farrahi, V., Niemelä, M., Kangas, M., Korpelainen, R. & Jämsä, T. (2019) Calibration and validation of accelerometer-based activity monitors: A systematic review of machine-learning approaches. *Gait & Posture*, **68**, 285-299.
- Feng, K., Li, J., Zhang, X., Shen, C., Bi, Y., Zheng, T. & Liu, J. (2017) A New Quaternion-Based Kalman Filter for Real-Time Attitude Estimation Using the Two-Step Geometrically-Intuitive Correction Algorithm. *Sensors*, **17**, 2146.
- Frair, J.L., Fieberg, J., Hebblewhite, M., Cagnacci, F., DeCesare, N.J. & Pedrotti, L. (2010) Resolving issues of imprecise and habitat-biased locations in ecological analyses using GPS telemetry data. *Philosophical Transactions of the Royal Society B: Biological Sciences*, **365**, 2187-2200.
- Francisco, F.A., Nührenberg, P. & Jordan, A. (2020) High-resolution, non-invasive animal tracking and reconstruction of local environment in aquatic ecosystems. *Movement Ecology*, **8**, 27.
- Gabaldon, J., Turner, E.L., Johnson-Roberson, M., Barton, K., Johnson, M., Anderson, E.J. & Shorter, K.A. (2019) Integration, Calibration, and Experimental Verification of a Speed Sensor for Swimming Animals. *IEEE Sensors Journal*, **19**, 3616-3625.
- Gheorghe, M.V. & Bodea, M.C. (2018) Calibration Optimization Study for Tilt-Compensated Compasses. *IEEE Transactions on Instrumentation and Measurement*, **67**, 1486-1494.

- Gibb, R., Shoji, A., Fayet, A.L., Perrins, C.M., Guilford, T. & Freeman, R. (2017) Remotely sensed wind speed predicts soaring behaviour in a wide-ranging pelagic seabird. *Journal of The Royal Society Interface*, **14**, 20170262.
- Gleiss, A.C., Wilson, R.P. & Shepard, E.L.C. (2011) Making overall dynamic body acceleration work: on the theory of acceleration as a proxy for energy expenditure. *Methods in Ecology and Evolution*, **2**, 23-33.
- Goldbogen, J.A., Calambokidis, J., Shadwick, R.E., Oleson, E.M., McDonald, M.A. & Hildebrand, J.A. (2006) Kinematics of foraging dives and lunge-feeding in fin whales. *Journal of Experimental Biology*, **209**, 1231-1244.
- Graf, P.M., Wilson, R.P., Qasem, L., Hackländer, K. & Rosell, F. (2015) The Use of Acceleration to Code for Animal Behaviours; A Case Study in Free-Ranging Eurasian Beavers *Castor fiber*. *PLOS ONE*, **10**, e0136751.
- Grolemund, G. & Wickham, H. (2011) Dates and times made easy with lubridate. *Journal of Statistical Software*, **40**, 1-25.
- Grygorenko, V. (2011) Sensing-magnetic compass with tilt compensation. *Cypress Perform, Semiconductor Application Notes*, **AN2272**.
- Gužvica, G., Bošnjak, I., Bielen, A., Babić, D., Radanović-Gužvica, B. & Šver, L. (2014) Comparative Analysis of Three Different Methods for Monitoring the Use of Green Bridges by Wildlife. *PLOS ONE*, **9**, e106194.
- Halsey, L.G., Shepard, E.L.C., Hulston, C.J., Venable, M.C., White, C.R., Jeukendrup, A.E. & Wilson, R.P. (2008) Acceleration versus heart rate for estimating energy expenditure and speed during locomotion in animals: Tests with an easy model species, *Homo sapiens*. *Zoology*, **111**, 231-241.
- Han, S. & Wang, J. (2011) A Novel Method to Integrate IMU and Magnetometers in Attitude and Heading Reference Systems. *The Journal of Navigation*, **64**, 727-738.
- Handcock, R.N., Swain, D.L., Bishop-Hurley, G.J., Patison, K.P., Wark, T., Valencia, P., Corke, P. & O'Neill, C.J. (2009) Monitoring Animal Behaviour and Environmental Interactions Using Wireless Sensor Networks, GPS Collars and Satellite Remote Sensing. *Sensors*, **9**, 3586-3603.
- Harja, Y.D. & Sarno, R. (2018) Determine the best option for nearest medical services using Google maps API, Haversine and TOPSIS algorithm. *2018 International Conference on Information and Communications Technology (ICOIACT)*, pp. 814-819.
- Hebblewhite, M. & Haydon, D.T. (2010) Distinguishing technology from biology: a critical review of the use of GPS telemetry data in ecology. *Philosophical Transactions of the Royal Society B: Biological Sciences*, **365**, 2303-2312.
- Hochscheid, S. (2014) Why we mind sea turtles' underwater business: A review on the study of diving behavior. *Journal of Experimental Marine Biology and Ecology*, **450**, 118-136.
- Hofman, M.P.G., Hayward, M.W., Heim, M., Marchand, P., Rolandsen, C.M., Mattisson, J., Urbano, F., Heurich, M., Mysterud, A., Melzheimer, J., Morellet, N., Voigt, U., Allen, B.L., Gehr, B., Rouco, C., Ullmann, W., Holand, Ø., Jørgensen, N.H., Steinheim, G., Cagnacci, F., Kroeschel, M., Kaczensky, P., Buuveibaatar, B., Payne, J.C., Palmegiani, I., Jerina, K., Kjellander, P., Johansson, Ö., LaPoint, S., Bayraksiz, R., Linnell, J.D.C., Zaccaroni, M., Jorge, M.L.S., Oshima, J.E.F., Songhurst, A., Fischer, C., Mc Bride, R.T., Jr., Thompson, J.J., Streif, S., Sandfort, R., Bonenfant, C., Drouilly, M., Klaproth, M., Zinner, D., Yarnell, R., Stronza, A., Wilmott, L., Meisingset, E., Thaker, M., Vanak, A.T., Nicoloso, S., Graeber, R., Said, S., Boudreau, M.R., Devlin, A., Hoogsteijn, R., May-Junior, J.A., Nifong, J.C., Odden, J., Quigley, H.B., Tortato, F., Parker, D.M., Caso, A., Perrine, J., Tellaeche, C., Zieba, F., Zwijacz-Kozica, T., Appel,

- C.L., Axsom, I., Bean, W.T., Cristescu, B., Périquet, S., Teichman, K.J., Karpanty, S., Licoppe, A., Menges, V., Black, K., Scheppers, T.L., Schai-Braun, S.C., Azevedo, F.C., Lemos, F.G., Payne, A., Swanepoel, L.H., Weckworth, B.V., Berger, A., Bertassoni, A., McCulloch, G., Šustr, P., Athreya, V., Bockmuhl, D., Casaer, J., Ekori, A., Melovski, D., Richard-Hansen, C., van de Vyver, D., Reyna-Hurtado, R., Robardet, E., Selva, N., Sergiel, A., Farhadinia, M.S., Sunde, P., Portas, R., Ambarli, H., Berzins, R., Kappeler, P.M., Mann, G.K., Pyritz, L., Bissett, C., Grant, T., Steinmetz, R., Swedell, L., Welch, R.J., Armenteras, D., Bidder, O.R., González, T.M., Rosenblatt, A., Kachel, S. & Balkenhol, N. (2019) Right on track? Performance of satellite telemetry in terrestrial wildlife research. *PLOS ONE*, **14**, e0216223.
- Jockers, M.L. & Thalken, R. (2020) Introduction to dplyr. *Text Analysis with R for Students of Literature*, pp. 121-132. Springer, Cham, Switzerland.
- Johnson, M.P. & Tyack, P.L. (2003) A digital acoustic recording tag for measuring the response of wild marine mammals to sound. *IEEE Journal of Oceanic Engineering*, **28**, 3-12.
- Kaniewski, P. & Kazubek, J. (2009) Integrated system for heading determination. *Acta Physica Polonica-Series A General Physics*, **116**, 325.
- Kaur, M., Sandhu, M., Mohan, N. & Sandhu, P.S. (2011) RFID technology principles, advantages, limitations & its applications. *International Journal of Computer and Electrical Engineering*, **3**, 151.
- Kawabe, R., Kawano, T., Nakano, N., Yamashita, N., Hiraishi, T. & Naito, Y. (2003) Simultaneous measurement of swimming speed and tail beat activity of free-swimming rainbow trout *Oncorhynchus mykiss* using an acceleration data-logger. *Fisheries science*, **69**, 959-965.
- Kerdok, A.E., Biewener, A.A., McMahon, T.A., Weyand, P.G. & Herr, H.M. (2002) Energetics and mechanics of human running on surfaces of different stiffnesses. *Journal of Applied Physiology*, **92**, 469-478.
- Kunčar, A., Sysel, M. & Urbánek, T. (2016) Calibration of low-cost triaxial magnetometer. *MATEC Web of Conferences 20th International Conference on Circuits, Systems, Communications and Computers (CSCC 2016)*. EDP Sciences.
- Laich, A.G., Wilson, R.P., Quintana, F. & Shepard, E.L. (2008) Identification of imperial cormorant *Phalacrocorax atriceps* behaviour using accelerometers. *Endangered Species Research*, **10**, 29-37.
- Laplanche, C., Marques, T.A. & Thomas, L. (2015) Tracking marine mammals in 3D using electronic tag data. *Methods in Ecology and Evolution*, **6**, 987-996.
- Latham, A.D.M., Latham, M.C., Anderson, D.P., Cruz, J., Herries, D. & Hebblewhite, M. (2015) The GPS craze: six questions to address before deciding to deploy GPS technology on wildlife. *New Zealand Journal of Ecology*, **39**, 143-152.
- Leonardo, M., Noss, A.J., Erika, C. & Damián, I.R. (2005) Ocelot (*Felis pardalis*) Population Densities, Activity, and Ranging Behaviour in the Dry Forests of Eastern Bolivia: Data from Camera Trapping. *Journal of Tropical Ecology*, **21**, 349-353.
- Levi, R.W. & Judd, T. (1996) Dead reckoning navigational system using accelerometer to measure foot impacts. pp. 8. Point Research Corporation, Santa Meijer, et al., Methods to Assess Physical Activity with Ana, Calif. .
- Lewis, J.S., Rachlow, J.L., Garton, E.O. & Vierling, L.A. (2007) Effects of habitat on GPS collar performance: using data screening to reduce location error. *Journal of Applied Ecology*, **44**, 663-671.

- Li, W. & Wang, J. (2013) Effective Adaptive Kalman Filter for MEMS-IMU/Magnetometers Integrated Attitude and Heading Reference Systems. *Journal of Navigation*, **66**, 99-113.
- Li, Z., Li, X. & Wang, Y. (2009) A calibration method for magnetic sensors and accelerometer in tilt-compensated digital compass. *2009 9th International Conference on Electronic Measurement & Instruments*, pp. 2-868-862-871.
- Lisovski, S., Hewson, C.M., Klaassen, R.H.G., Korner-Nievergelt, F., Kristensen, M.W. & Hahn, S. (2012) Geolocation by light: accuracy and precision affected by environmental factors. *Methods in Ecology and Evolution*, **3**, 603-612.
- Liu, Y., Battaile, B.C., Trites, A.W. & Zidek, J.V. (2015) Bias correction and uncertainty characterization of Dead-Reckoned paths of marine mammals. *Animal Biotelemetry*, **3**, 51.
- Marcus Rowcliffe, J., Carbone, C., Kays, R., Kranstauber, B. & Jansen, P.A. (2012) Bias in estimating animal travel distance: the effect of sampling frequency. *Methods in Ecology and Evolution*, **3**, 653-662.
- Markovska, M. & Svensson, R. (2019) Evaluation of drift correction strategies for an inertial based dairy cow positioning system. : A study on tracking the position of dairy cows using a foot mounted IMU with drift correction from ZUPT or sparse RFID locations. Independent thesis Advanced level (degree of Master (Two Years)) Student thesis.
- McClune, D.W. (2018) Joining the dots: reconstructing 3D environments and movement paths using animal-borne devices. *Animal Biotelemetry*, **6**, 5.
- McNarry, M.A., Wilson, R.P., Holton, M.D., Griffiths, I.W. & Mackintosh, K.A. (2017) Investigating the relationship between energy expenditure, walking speed and angle of turning in humans. *PLOS ONE*, **12**, e0182333.
- Miller, P.J.O., Johnson, M.P., Madsen, P.T., Biassoni, N., Quero, M. & Tyack, P.L. (2009) Using at-sea experiments to study the effects of airguns on the foraging behavior of sperm whales in the Gulf of Mexico. *Deep Sea Research Part I: Oceanographic Research Papers*, **56**, 1168-1181.
- Miller, P.J.O., Johnson, M.P., Tyack, P.L. & Terray, E.A. (2004) Swimming gaits, passive drag and buoyancy of diving sperm whales *Physeter macrocephalus*. *Journal of Experimental Biology*, **207**, 1953-1967.
- Mitani, Y., Sato, K., Ito, S., Cameron, M.F., Siniff, D.B. & Naito, Y. (2003) A method for reconstructing three-dimensional dive profiles of marine mammals using geomagnetic intensity data: results from two lactating Weddell seals. *Polar Biology*, **26**, 311-317.
- Mitani, Y., Watanabe, Y., Sato, K., Cameron, M.F. & Naito, Y. (2004) 3D diving behavior of Weddell seals with respect to prey accessibility and abundance. *Marine Ecology Progress Series*, **281**, 275-281.
- Miwa, M., Oishi, K., Nakagawa, Y., Maeno, H., Anzai, H., Kumagai, H., Okano, K., Tobioka, H. & Hirooka, H. (2015) Application of Overall Dynamic Body Acceleration as a Proxy for Estimating the Energy Expenditure of Grazing Farm Animals: Relationship with Heart Rate. *PLOS ONE*, **10**, e0128042.
- Narazaki, T., Nakamura, I., Aoki, K., Iwata, T., Shiomi, K., Luschi, P., Suganuma, H., Meyer, C.G., Matsumoto, R., Bost, C.A., Handrich, Y., Amano, M., Okamoto, R., Mori, K., Ciccione, S., Bourjea, J. & Sato, K. (2021) Similar circling movements observed across marine megafauna taxa. *iScience*, 102221.
- Narazaki, T., Sato, K., Abernathy, K., Marshall, G. & Miyazaki, N. (2009) Sea turtles compensate deflection of heading at the sea surface during directional travel. *Journal of Experimental Biology*, **212**, 4019-4026.

- Newey, S., Davidson, P., Nazir, S., Fairhurst, G., Verdicchio, F., Irvine, R.J. & van der Wal, R. (2015) Limitations of recreational camera traps for wildlife management and conservation research: A practitioner's perspective. *Ambio*, **44**, 624-635.
- Noda, T., Kawabata, Y., Arai, N., Mitamura, H. & Watanabe, S. (2014) Animal-mounted gyroscope/accelerometer/magnetometer: In situ measurement of the movement performance of fast-start behaviour in fish. *Journal of Experimental Marine Biology and Ecology*, **451**, 55-68.
- Noda, T., Okuyama, J., Koizumi, T., Arai, N. & Kobayashi, M. (2012) Monitoring attitude and dynamic acceleration of free-moving aquatic animals using a gyroscope. *Aquatic Biology*, **16**, 265-276.
- Ozyagcilar, T. (2012) Implementing a tilt-compensated eCompass using accelerometer and magnetometer sensors. *Freescale semiconductor, Application Note, AN4248*, Austin, TX.
- Patel, A., Stocks, B., Fisher, C., Nicolls, F. & Boje, E. (2017) Tracking the Cheetah Tail Using Animal-Borne Cameras, GPS, and an IMU. *IEEE Sensors Letters*, **1**, 1-4.
- Patonis, P., Patias, P., Tziavos, I.N., Rossikopoulos, D. & Margaritis, K.G. (2018) A Fusion Method for Combining Low-Cost IMU/Magnetometer Outputs for Use in Applications on Mobile Devices. *Sensors (Basel, Switzerland)*, **18**, 2616.
- Pedley, M. (2012) eCompass-Build and Calibrate a Tilt-Compensating Electronic Compass. *Circuit Cellar-The Magazine For Computer Applications*, 1-6.
- Pedley, M. (2013) Tilt sensing using a three-axis accelerometer. *Freescale semiconductor. Application Note 2461*, **1**, 1-22.
- Péron, G., Calabrese, J.M., Duriez, O., Fleming, C.H., García-Jiménez, R., Johnston, A., Lambertucci, S.A., Safi, K. & Shepard, E.L.C. (2020) The challenges of estimating the distribution of flight heights from telemetry or altimetry data. *Animal Biotelemetry*, **8**, 5.
- Pewsey, A., Neuhäuser, M. & Ruxton, G.D. (2013) *Circular Statistics in R*. OUP Oxford.
- Potts, J., Börger, L., Scantlebury, D.M., Bennett, N.C., Alagaili, A. & Wilson, R.P. (2018) Finding turning-points in ultra-high-resolution animal movement data. *Methods in Ecology and Evolution*, **9**, 2091-2101.
- Poulin, M.-P., Clermont, J. & Berteaux, D. (2021) Extensive daily movement rates measured in territorial arctic foxes. *Ecology and Evolution*, **00**, 1- 12.
- Premerlani, W. & Bizard, P. (2009) Direction cosine matrix imu: Theory. *Diy Drone: Usa*, 13-15.
- Qasem, L., Cardew, A., Wilson, A., Griffiths, I., Halsey, L.G., Shepard, E.L.C., Gleiss, A.C. & Wilson, R. (2012) Tri-Axial Dynamic Acceleration as a Proxy for Animal Energy Expenditure; Should We Be Summing Values or Calculating the Vector? *PLOS ONE*, **7**, e31187.
- Renaudin, V., Afzal, M.H. & Lachapelle, G. (2010) Complete Triaxis Magnetometer Calibration in the Magnetic Domain. *Journal of Sensors*, **2010**, 967245.
- Robusto, C.C. (1957) The Cosine-Haversine Formula. *The American Mathematical Monthly*, **64**, 38-40.
- Rong, L., Zhiguo, D., Jianzhong, Z. & Ming, L. (2007) Identification of Individual Walking Patterns Using Gait Acceleration. *2007 1st International Conference on Bioinformatics and Biomedical Engineering*, pp. 543-546.
- Ropert-Coudert, Y., Kato, A., Baudat, J., Bost, C.-A., Le Maho, Y. & Naito, Y. (2001) Time/depth usage of Adélie penguins: an approach based on dive angles. *Polar Biology*, **24**, 467-470.

- Ropert-Coudert, Y. & Wilson, R.P. (2005) Trends and perspectives in animal-attached remote sensing. *Frontiers in Ecology and the Environment*, **3**, 437-444.
- Ryan, P.G., Petersen, S.L., Peters, G. & Grémillet, D. (2004) GPS tracking a marine predator: the effects of precision, resolution and sampling rate on foraging tracks of African Penguins. *Marine Biology*, **145**, 215-223.
- Säll, J. & Merkel, J. (2011) Indoor Navigation Using Accelerometer and Magnetometer. Independent thesis Basic level (university diploma) Student thesis.
- Sato, K., Mitani, Y., Cameron, M.F., Siniff, D.B. & Naito, Y. (2003) Factors affecting stroking patterns and body angle in diving Weddell seals under natural conditions. *Journal of Experimental Biology*, **206**, 1461-1470.
- Sato, K., Sakamoto, K.Q., Watanuki, Y., Takahashi, A., Katsumata, N., Bost, C.-A. & Weimerskirch, H. (2009) Scaling of Soaring Seabirds and Implications for Flight Abilities of Giant Pterosaurs. *PLOS ONE*, **4**, e5400.
- Scharold, J., Lai, N.C., Lowell, W. & Graham, J. (1989) Metabolic rate, heart rate, and tailbeat frequency during sustained swimming in the leopard shark *Triakis semifasciata*. *Experimental biology*, **48**, 223-230.
- Schlägel, U.E., Signer, J., Herde, A., Eden, S., Jeltsch, F., Eccard, J.A. & Dammhahn, M. (2019) Estimating interactions between individuals from concurrent animal movements. *Methods in Ecology and Evolution*, **10**, 1234-1245.
- Sequeira, M.M., Rickenbach, M., Wietlisbach, V., Tullen, B. & Schutz, Y. (1995) Physical Activity Assessment Using a Pedometer and Its Comparison with a Questionnaire in a Large Population Survey. *American Journal of Epidemiology*, **142**, 989-999.
- Shamoun-Baranes, J., Bom, R., van Loon, E.E., Ens, B.J., Oosterbeek, K. & Bouten, W. (2012) From Sensor Data to Animal Behaviour: An Oystercatcher Example. *PLOS ONE*, **7**, e37997.
- Shepard, E.L., Wilson, R.P., Halsey, L.G., Quintana, F., Laich, A.G., Gleiss, A.C., Liebsch, N., Myers, A.E. & Norman, B. (2008) Derivation of body motion via appropriate smoothing of acceleration data. *Aquatic Biology*, **4**, 235-241.
- Shiomi, K., Narazaki, T., Sato, K., Shimatani, K., Arai, N., Ponganis, P.J. & Miyazaki, N. (2010) Data-processing artefacts in three-dimensional dive path reconstruction from geomagnetic and acceleration data. *Aquatic Biology*, **8**, 299-304.
- Shiomi, K., Sato, K., Mitamura, H., Arai, N., Naito, Y. & Ponganis, P.J. (2008) Effect of ocean current on the dead-reckoning estimation of 3-D dive paths of emperor penguins. *Aquatic Biology*, **3**, 265-270.
- Sodhi, R., Prunty, J., Hsu, G. & Oh, B. (2008) Automatic calibration of a three-axis magnetic compass. PNI Corporation (Santa Rosa, CA, US).
- Soutullo, A., Cadahía, L., Urios, V., Ferrer, M. & Negro, J.J. (2007) Accuracy of lightweight satellite telemetry: a case study in the Iberian Peninsula. *The Journal of Wildlife Management*, **71**, 1010-1015.
- Steinhausen, M.F., Steffensen, J.F. & Andersen, N.G. (2005) Tail beat frequency as a predictor of swimming speed and oxygen consumption of saithe (*Pollachius virens*) and whiting (*Merlangius merlangus*) during forced swimming. *Marine Biology*, **148**, 197-204.
- Swain, D.L., Wark, T. & Bishop-Hurley, G.J. (2008) Using high fix rate GPS data to determine the relationships between fix rate, prediction errors and patch selection. *Ecological Modelling*, **212**, 273-279.
- Symington, A. & Trigoni, N. (2012) Encounter based sensor tracking. *Proceedings of the thirteenth ACM international symposium on Mobile Ad Hoc Networking and*

- Computing*, pp. 15–24. Association for Computing Machinery, Hilton Head, South Carolina, USA.
- Tabatabaei, S.A.H., Gluhak, A. & Tafazolli, R. (2013) A Fast Calibration Method for Triaxial Magnetometers. *IEEE Transactions on Instrumentation and Measurement*, **62**, 2929-2937.
- Tobalske, B. & Dial, K. (1996) Flight kinematics of black-billed magpies and pigeons over a wide range of speeds. *Journal of Experimental Biology*, **199**, 263-280.
- Tonini, M.H. & Palma, E.D. (2017) Tidal dynamics on the North Patagonian Argentinean Gulfs. *Estuarine, Coastal and Shelf Science*, **189**, 115-130.
- Valenti, R.G., Dryanovski, I. & Xiao, J. (2015) Keeping a good attitude: A quaternion-based orientation filter for IMUs and MARGs. *Sensors*, **15**, 19302-19330.
- Vitali, A. (2016) Ellipsoid or sphere fitting for sensor calibration, Dt0059. *ST Microelectronics, Design Tip*.
- Walker, J.S., Jones, M.W., Laramée, R.S., Holton, M.D., Shepard, E.L.C., Williams, H.J., Scantlebury, D.M., Marks, N.J., Magowan, E.A., Maguire, I.E., Bidder, O.R., Di Virgilio, A. & Wilson, R.P. (2015) Prying into the intimate secrets of animal lives; software beyond hardware for comprehensive annotation in 'Daily Diary' tags. *Movement Ecology*, **3**, 29.
- Ware, C., Friedlaender, A.S. & Nowacek, D.P. (2011) Shallow and deep lunge feeding of humpback whales in fjords of the West Antarctic Peninsula. *Marine Mammal Science*, **27**, 587-605.
- Wensveen, P.J., Isojunno, S., Hansen, R.R., von Benda-Beckmann, A.M., Kleivane, L., van IJsselmuide, S., Lam, F.-P.A., Kvadsheim, P.H., DeRuiter, S.L., Curé, C., Narazaki, T., Tyack, P.L. & Miller, P.J.O. (2019) Northern bottlenose whales in a pristine environment respond strongly to close and distant navy sonar signals. *Proceedings of the Royal Society B: Biological Sciences*, **286**, 20182592.
- Wensveen, P.J., Thomas, L. & Miller, P.J.O. (2015) A path reconstruction method integrating dead-reckoning and position fixes applied to humpback whales. *Movement Ecology*, **3**, 31.
- Whitford, M. & Klimley, A.P. (2019) An overview of behavioral, physiological, and environmental sensors used in animal biotelemetry and biologging studies. *Animal Biotelemetry*, **7**, 1-24.
- Whitney, N.M., Pratt Jr, H.L., Pratt, T.C. & Carrier, J.C. (2010) Identifying shark mating behaviour using three-dimensional acceleration loggers. *Endangered Species Research*, **10**, 71-82.
- Willener, A.S.T., Handrich, Y., Halsey, L.G. & Strike, S. (2015) Effect of walking speed on the gait of king penguins: An accelerometric approach. *Journal of Theoretical Biology*, **387**, 166-173.
- Williams, H., Shepard, E., Duriez, O. & Lambertucci, S.A. (2015) Can accelerometry be used to distinguish between flight types in soaring birds? *Animal Biotelemetry*, **3**, 1-11.
- Williams, H.J., Holton, M.D., Shepard, E.L.C., Largey, N., Norman, B., Ryan, P.G., Duriez, O., Scantlebury, M., Quintana, F., Magowan, E.A., Marks, N.J., Alagaili, A.N., Bennett, N.C. & Wilson, R.P. (2017) Identification of animal movement patterns using tri-axial magnetometry. *Movement Ecology*, **5**, 6.
- Williams, H.J., Shepard, E., Holton, M.D., Alarcón, P., Wilson, R. & Lambertucci, S. (2020a) Physical limits of flight performance in the heaviest soaring bird. *Proceedings of the National Academy of Sciences*, **117**, 17884-17890.

- Williams, H.J., Taylor, L.A., Benhamou, S., Bijleveld, A.I., Clay, T.A., de Grissac, S., Demšar, U., English, H.M., Franconi, N. & Gómez-Laich, A. (2020b) Optimizing the use of biologgers for movement ecology research. *Journal of Animal Ecology*, **89**, 186-206.
- Williams, L.R., Fox, D.R., Bishop-Hurley, G.J. & Swain, D.L. (2019) Use of radio frequency identification (RFID) technology to record grazing beef cattle water point use. *Computers and Electronics in Agriculture*, **156**, 193-202.
- Wilson, A.D., Wikelski, M., Wilson, R.P. & Cooke, S.J. (2015) Utility of biological sensor tags in animal conservation. *Conservation Biology*, **29**, 1065-1075.
- Wilson, J.W., Mills, M.G., Wilson, R.P., Peters, G., Mills, M.E., Speakman, J.R., Durant, S.M., Bennett, N.C., Marks, N.J. & Scantlebury, M. (2013a) Cheetahs, *Acinonyx jubatus*, balance turn capacity with pace when chasing prey. *Biology letters*, **9**, 20130620.
- Wilson, R. (1985) The Jackass Penguin (*Spheniscus demersus*) as a pelagic predator. *Marine Ecology Progress Series*, **25**, 219-227.
- Wilson, R., Griffiths, I., Legg, P., Friswell, M., Bidder, O., Halsey, L., Lambertucci, S.A. & Shepard, E. (2013b) Turn costs change the value of animal search paths. *Ecology Letters*, **16**, 1145-1150.
- Wilson, R. & Wilson, M.-P. (1988) Dead reckoning: a new technique for determining penguin movements at sea. *Meeresforschung (Hamburg)*, **32**, 155-158.
- Wilson, R.P. (2002) Movements in Adélie Penguins foraging for chicks at Ardley Island, Antarctica: circles within spirals, wheels within wheels. *Polar Bioscience*, 75-87.
- Wilson, R.P., Börger, L., Holton, M.D., Scantlebury, D.M., Gómez-Laich, A., Quintana, F., Rosell, F., Graf, P.M., Williams, H., Gunner, R., Hopkins, L., Marks, N., Geraldi, N.R., Duarte, C.M., Scott, R., Strano, M.S., Robotka, H., Eizaguirre, C., Fahlman, A. & Shepard, E.L.C. (2020a) Estimates for energy expenditure in free-living animals using acceleration proxies: A reappraisal. *Journal of Animal Ecology*, **89**, 161-172.
- Wilson, R.P., Holton, M.D., di Virgilio, A., Williams, H., Shepard, E.L.C., Lambertucci, S., Quintana, F., Sala, J.E., Balaji, B., Lee, E.S., Srivastava, M., Scantlebury, D.M. & Duarte, C.M. (2018) Give the machine a hand: A Boolean time-based decision-tree template for rapidly finding animal behaviours in multisensor data. *Methods in Ecology and Evolution*, **9**, 2206-2215.
- Wilson, R.P., Holton, M.D., Walker, J.S., Shepard, E.L.C., Scantlebury, D.M., Wilson, V.L., Wilson, G.I., Tysse, B., Gravenor, M., Ciancio, J., McNarry, M.A., Mackintosh, K.A., Qasem, L., Rosell, F., Graf, P.M., Quintana, F., Gomez-Laich, A., Sala, J.-E., Mulvenna, C.C., Marks, N.J. & Jones, M.W. (2016) A spherical-plot solution to linking acceleration metrics with animal performance, state, behaviour and lifestyle. *Movement Ecology*, **4**, 22.
- Wilson, R.P., Hustler, K., Ryan, P.G., Burger, A.E. & Noldeke, E.C. (1992) Diving birds in cold water: do Archimedes and Boyle determine energetic costs? *The American Naturalist*, **140**, 179-200.
- Wilson, R.P., Kreye, J.M., Lucke, K. & Urquhart, H. (2004) Antennae on transmitters on penguins: balancing energy budgets on the high wire. *Journal of Experimental Biology*, **207**, 2649-2662.
- Wilson, R.P., Liebsch, N., Davies, I.M., Quintana, F., Weimerskirch, H., Storch, S., Lucke, K., Siebert, U., Zankl, S., Müller, G., Zimmer, I., Scolaro, A., Campagna, C., Plötz, J., Bornemann, H., Teilmann, J. & McMahon, C.R. (2007) All at sea with animal tracks; methodological and analytical solutions for the resolution of movement. *Deep Sea Research Part II: Topical Studies in Oceanography*, **54**, 193-210.
- Wilson, R.P., Ropert-Coudert, Y. & Kato, A. (2002) Rush and grab strategies in foraging marine endotherms: the case for haste in penguins. *Animal Behaviour*, **63**, 85-95.

- Wilson, R.P., Rose, K.A., Gunner, R., Holton, M., Marks, N.J., Bennett, N.C., Bell, S.H., Twining, J.P., Hesketh, J., Duarte, C.M., Bezodis, N. & Scantlebury, D.M. (2020b) Forces experienced by instrumented animals depend on lifestyle. *bioRxiv*, 2020.2008.2020.258756.
- Wilson, R.P., Shepard, E. & Liebsch, N. (2008) Prying into the intimate details of animal lives: use of a daily diary on animals. *Endangered Species Research*, **4**, 123-137.
- Wilson, R.P., Wilson, M.-P.T., Link, R., Mempel, H. & Adams, N.J. (1991) Determination of movements of African penguins *Spheniscus demersus* using a compass system: dead reckoning may be an alternative to telemetry. *Journal of Experimental Biology*, **157**, 557-564.
- Wiltschko, R. (2012) *Magnetic orientation in animals*. Springer Science & Business Media, Berlin Heidelberg.
- Winer (2017) Simple and Effective Magnetometer Calibration. *GitHub repository* (ed. G. repository).
- Wright, B.M., Ford, J.K., Ellis, G.M., Deecke, V.B., Shapiro, A.D., Battaile, B.C. & Trites, A.W. (2017) Fine-scale foraging movements by fish-eating killer whales (*Orcinus orca*) relate to the vertical distributions and escape responses of salmonid prey (*Oncorhynchus* spp.). *Movement Ecology*, **5**, 1-18.
- Zeileis, A., Grothendieck, G., Ryan, J.A., Andrews, F. & Zeileis, M.A. (2020) Package 'zoo'.
- Zimmer, W.M., Tyack, P.L., Johnson, M.P. & Madsen, P.T. (2005) Three-dimensional beam pattern of regular sperm whale clicks confirms bent-horn hypothesis. *The Journal of the Acoustical Society of America*, **117**, 1473-1485.

Glossary

Acceleration – The first derivative (rate of change) of an object’s velocity with respect to time. Units are expressed as metres per second squared (m/s^2) or in G-forces (g). A single G-force on Earth (though this does vary slightly with elevation) is $9.81 m/s^2$. Tri-axial accelerometers measure acceleration in three orthogonal planes (surge – ‘anterior-posterior’, sway – ‘medio-lateral’ and heave – ‘dorsal-ventral’). Under non-moving conditions, relative to gravity, the device tilt (pitch and roll) can be calculated directly from raw accelerometry values since they are composed entirely of the static force (gravity). Under linear acceleration, ‘moving’ forces applied to the device (e.g., due to the animal moving) are superimposed to static readings and as such measured animal acceleration is typically comprised of both a static and dynamic component.

Barometric pressure – pressure with the Earth’s atmosphere, that is a measure of force per unit area, often expressed as standard atmosphere (symbol: atm), defined as $101,325 Pa$ ($1,013.25 mbar$; $1 pascal = 1 N/m^2$). The Earth’s mean sea-level atmospheric pressure is approx. 1 atm. Barometric pressure decreases with elevation and increases with depth.

Centripetal acceleration – Inertial force caused by circular motion because an object is always accelerating when either its direction or magnitude (speed) changes, and in circular motion, the direction changes instantaneously. This can cause the animal to ‘pull g ’, such as at times of banking and cornering very fast.

Coordinate frame - In 3-D space, this is a set of three vectors (x,y,z axes) of unit length, perpendicular (orthogonal) to each other.

Current flow vectors – (or ‘external’ current flow vectors). The heading and speed of tidal-/air-currents

Current integration – Adding current flow vectors to dead-reckoned travel vectors.

De-rotation - Within the tilt-compensated compass framework, this is the conversion of the magnetic vector values through multiplying by the transpose (inverse) of the pitch and then roll rotation matrices.

Distance correction factor – The 2-D Haversine distance ratio between successive Verified positions (VPs) (used in the VP-correction procedure) and corresponding dead-reckoned positions. This is multiplied to all intermediate (between VPs) radial distance (q) values.

Drift – The accumulation of spatial errors relative to a Verified Position, arising from integrating incorrect dimensions of travel.

Dynamic Body Acceleration (DBA) – The dynamic component of acceleration which is typically induced by the limb and/or spine kinematics of the animal (and thus the attached accelerometer). Generally, more mechanical work (*via* muscular contraction), corresponds to higher metabolic rate and greater magnitudes in accelerometry readings (dependent on tag deployment site). Typically, dynamic values from each multi-axial channel are integrated into an overall metric, such as ‘Overall Dynamic Body Acceleration’ [$ODBA = |DBAx| + |DBAy| + |DBAz|$] or ‘Vectorial Dynamic Body Acceleration’ [$VeDBA = (DBAx^2 + DBAy^2 + DBAz^2)^{0.5}$]. Such derivatives have been demonstrated as useful proxies for movement-based power.

Earth-Centre, Earth-Fixed (ECEF) system – This defines a non-inertial reference coordinate frame that rotates with the Earth (this is often simplified to ‘Earth frame of reference’ or ‘Earth’s fixed frame’ in text). Its origin is fixed at the Earth’s centre (the x-axis points towards the intersection of the Earth’s Greenwich Meridian and equatorial plane, the y-axis pointing 90 degrees East of the x-axis and the z pointing north, along the Earth’s rotation axis). Note, this is different to the Earth-Centred Inertial (ECI) system, which is non-rotating (and the x-axis instead always points towards the vernal equinox).

Equal pitch assumption – The animal moves in the same direction and angle as its anterior-posterior axis (relative to North and the gravity vector, respectively).

Georeference – Within the dead-reckoning framework this is another term used for carrying out VPC-dead-reckoning, or drift-correction or GPS-corrected dead-reckoning.

Gimbal lock – This is the loss of a degree of freedom in 3-D, when two axes become parallel to each other (locked in the same attitude, reflecting the same rotation). For example if the anterior-posterior axis ('surge' or 'forward-back' - x-axis for NED coordinate frames) points in the plane of the gravity vector (pitched 90 degrees up or down), then the dorsal-ventral ('heave' or 'up-down' - z-axis for NED coordinate frames) and the medio-lateral axis ('sway' or 'side-to-side' – y-axis for NED coordinate frames) become parallel to each other, and changes about the yaw can no longer be compensated for (changes in the roll (or 'bank') is equivalent to changing the heading).

GPS-derived speed – The Haversine distance calculated between successive GPS coordinates, divided by the time taken between locations.

Ground-truthing - Empirical evidence (often information obtained by direct observation), as opposed to inference for validating something under investigation. Within the dead-reckoning framework, VPs such as GPS locations are used to periodically ground-truth an animal's position.

Haversine formula - Computes the great-circular distance (units in metres) between two locations (using their longitude and latitude coordinates) on a sphere, applying trigonometry to map a triangle to the surface of a unit sphere. This formula is only an approximation because the Earth is not a perfect sphere, with numerical errors also arising at the antipodal regions.

Heading correction factor – The difference of heading (or 'bearing') from true North between consecutive VPs (used in the VPC procedure) and temporally aligned dead-reckoned positions. This is summed to all intermediate (between VPs) heading (h) values.

Inf – Results from numerical calculations which are mathematically infinite (e.g., in R, dividing any value by zero results in Inf).

Linear drift correction method – At each path segment, the dead-reckoned path is shifted to the position of the first VP encounter using a shift vector. A correction vector then adds the difference between the VP and estimated dead-reckoned end points linearly over this path segment period.

Multiplicative (m)-coefficient – Within the dead-reckoning framework, this refers to the gradient of a linear regression, e.g., [speed = (VeDBA • m) + c], where m is the multiplicative factor of VeDBA, and c is the subsequently summed constant value (reflecting the y-intercept).

NaN – Non-numeric (un-defined) values (e.g., in R, diving zero by zero results in NaN).

Net error – Here, net error reflects the 2-D Haversine distance (units in metres) between VPs and temporally aligned dead-reckoned positions.

Non-movement behaviours – Behaviour performed while stationary, whereby the animal may be moving, e.g., feeding on the spot, but there is no locomotion (not moving to a different position in 3-D space).

North-East-Down (NED) system – Often used in flight mechanics, this defines a non-inertial 3-D coordinate frame, the origin affixed as the devices centre of gravity and its axes oriented along the geodetic directions defined by the Earth surface (the x- and y-axis pointing true north and East, respectively, parallel to the geoid surface and the z-axis pointing downwards towards the Earth's surface).

Pitch – The angle of device's anterior-posterior inclination or declination, relative to the horizontal plane of the Earth's surface. Pitch is often expressed as an Euler angle, which describe the attitude and rotations of a device *via* a given Euler angle sequence (yaw, pitch and roll) of rotations (using rotation matrices). Pitch can be derived from the static component of acceleration. Assuming an NED system, pitch defines the degree of rotation about the y-axis.

Radial distance (q) – Within the dead-reckoning framework, this refers to a progression distance accounting for the approximate curvature of the Earth (longlat projection approximating the geoid to a sphere; Radius (R) = 6378137).

Right-handed coordinates/rotations – The direction in which the fingers curl when pointing the right thumb along the positive direction (+ 1 *g*) of the z-axis (e.g., down for NED coordinates), reflect the direction of rotation to be applied about each axis (for a given Euler angle sequence), with the index finger representing the x axis and the middle finger representing the y-axis, respectively, when splayed out at right angles to the thumb.

Roll – The angle of rotation about the device’s anterior-posterior axis. Roll is often expressed as an Euler angle, which describe the attitude and rotations of a device *via* a given Euler angle sequence (yaw, pitch and roll) of rotations (using rotation matrices). Roll is thus derived after rotating by yaw and pitch and can be derived from the static component of acceleration. Assuming an NED system, roll defines the degree of rotation about the x-axis (also termed ‘bank angle’).

Static Body Acceleration (SBA) – The static component of acceleration, due to gravity. Apart from being used to calculate the angle of device tilt, increased inertial (centripetal) acceleration, e.g., when the animal ‘pulls *g*’, can be captured more fully with static measures (rather than DBA estimates), and analogous to VeDBA, the computation of the Vectorial Static Body Acceleration [$\text{VeSBA} = (\text{SBAX}^2 + \text{SBAY}^2 + \text{SBAZ}^2)^{0.5}$] has been considered as a proxy of power

Tilt-compensated compass method - The compass heading (estimated using the arctangent ratio between two orthogonal components of the magnetic vector) is only accurate if the magnetometer outputs (typically x,y channels - assuming the NED coordinate system is used (SI₂)) are taken when the compass is level. Assuming the accelerometer-magnetometer approach, static acceleration measures are used to calculate the angles between the tag’s gravity (and thus magnetic) vector and the Earths frame of reference (e.g., Earth-Centered, Earth-Fixed (ECEF) coordinate system). These angles are typically expressed as pitch and roll Euler angles which are

used to compensate for variations in the magnetometer output due to device tilt. The tilt-compensated compass method covers the procedures of adjusting the coordinate frame of the device to correspond with a level inclination and subsequently compute the compass heading from the adjusted magnetometry values.

Tortuosity – The straight-line distance between the start and end positions of the path segment divided by the sum of the consecutive intermediate individual distance steps that constituted the total path segment's length. Values closer to 0 (or conversely values closer to 1 if subtracting the resultant 'tortuosity' value from 1) reflect more twists and turns in the movement path.

Vector integration – Adding vectors (of travel) together. Assuming Cartesian coordinates, vector addition is performed by adding the corresponding components of the vectors together. E.g., $[A + B = (a_1 + b_1, a_2 + b_2, \dots, a_n + b_n)]$.

Vertical speed – Distance travelled vertically up (at altitude) or down (at depth) divided by the time period between values.

World Geodetic System 1984 (WGS-84) – The typical model of the Earth's shape (standard for maps and satellite navigation), defining a coordinate system that accounts for the oblate spheroid.

Yaw – The orientation of the device, generally, with respect to true North (assuming any required magnetic declination offset has been applied). Yaw, also termed 'heading' or 'bearing', is often expressed as an Euler angle, which describe the attitude and rotations of a device *via* a given Euler angle sequence (yaw, pitch and roll) of rotations (using rotation matrices). Yaw can be derived is calculated using the arctangent of the ratio between the x- and y- magnetometer channel measurements. But for the correct computation of heading, these two channels need to be aligned parallel to the earth's surface and so the magnetic vectors are required to de-rotated, or 'tilt-compensating' them, according to pitch and roll angles of the device. Assuming an NED system, yaw defines the degree of rotation about the z-axis.

Chapter 6

How often should dead-reckoned animal movement paths be corrected for drift?

Richard M. Gunner



Photo taken by Adam J. Fell

This work is currently in press in *Animal Biotelemetry* as:

Gunner, R.M., Holton, M.D., Scantlebury M.D., Hopkins, P., Shepard, E.L.C., Fell, A.J., Garde, B., Quintana, F., Gómez-Laich, A., Yoda, K., Yamamoto, T., English, H.M., Ferreira, S., Govender, D., Viljoen, P., Bruns, A., van Schalkwyk, O.L., Cole, N.C., Tatayah, V., Börger, L., Redcliffe, J., Bell, S.H., Nikki, M.J., Bennett, N.C., Mariano, T.M., Williams, H.J., Duarte, C.M., van Rooyen, M.C., Bertelsen, M.F., Tambling, C.J. and Wilson, R.P., in review. How often should dead-reckoned animal movement paths be corrected for drift? *Animal Biotelemetry*, DOI: 10.21203/rs.3.rs-587959/v1

Abstract

Understanding what animals do in time and space is important for a range of ecological questions, however accurate estimates of how animals use space is challenging. Within the use of animal-attached tags, radio telemetry (including the Global Positioning System, 'GPS') is typically used to verify an animal's location periodically. Straight lines are typically drawn between these 'Verified Positions' ('VPs') so the interpolation of space-use is limited by the temporal- and spatial resolution of the system's measurement. As such, parameters such as route-taken and distance travelled can be poorly represented when using VP systems alone. Dead-reckoning has been suggested as a technique to improve the accuracy and resolution of reconstructed movement paths, whilst maximising battery life of VP systems. This typically involves deriving travel vectors from motion sensor systems and periodically correcting path dimensions for drift with simultaneously deployed VP systems. How often paths should be corrected for drift, however, has remained unclear. Here, I review the utility of dead-reckoning across four contrasting model species using different forms of locomotion (the African lion *Panthera leo*, the Red-tailed tropicbird *Phaethon rubricauda*, the Magellanic penguin *Spheniscus magellanicus*, and the Imperial cormorant *Leucocarbo atriceps*). Simulations were performed to examine the extent of dead-reckoning error, relative to VPs, as a function of Verified Position correction (VP correction) rate and the effect of this on estimates of distance moved. Dead-reckoning error was greatest for animals travelling within air and water. We demonstrate how sources of measurement error can arise within VP corrected dead-reckoned tracks and propose advancements to this procedure to maximise dead-reckoning accuracy. I review the utility of VP corrected dead-reckoning according to movement type and consider a range of ecological questions that would benefit from dead-reckoning, primarily concerning animal-barrier interactions and foraging strategies.

Background

Much of animal behaviour is defined by movement patterns in environmental space (Morales *et al.* 2010; Edelhoff, Signer & Balkenhol 2016; Browning *et al.* 2018). Today, most researchers use transmission telemetry (e.g., VHF, GPS, and acoustic transmitters) to verify an animal's location periodically connecting these 'Verified Positions' (VPs) linearly in time to reconstruct movement paths (Coulombe, Massé & Côté 2006; Campbell *et al.* 2012; McDuie *et al.* 2019; Yuan *et al.* 2019). Using this approach, researchers can use the combination of step lengths and turn angles as indicative of behaviour, functional motivation, habitat quality, resource selection and networks of space-use (Benhamou 2004; Morales *et al.* 2004; Fortin *et al.* 2005; Henderson *et al.* 2018; Wiesel, Karthun-Strijbos & Jänecke 2019). While it is acknowledged that more positional fixes enhance our ability to define these metrics, approaches for interpolating space-use depend on the temporal- and spatial resolution of the system's measurement so that obtaining fine-scale, continuous and accurate estimates of animal space-use is not straight forward (Mills, Patterson & Murray 2006; Forin-Wiart *et al.* 2015; Hughey *et al.* 2018; Poulin, Clermont & Berteaux 2021). Specifically, the resolution of tortuosity – how convoluted an animal track is - in animal movement paths is compromised when consecutive VPs are temporally far apart (Swain, Wark & Bishop-Hurley 2008; Poulin, Clermont & Berteaux 2021), whilst all VP systems are subject to positional inaccuracy (Frair *et al.* 2010; Ironside *et al.* 2017; Hofman *et al.* 2019), which can lead to varying assessments of movement (Ryan *et al.* 2004; Marcus Rowcliffe *et al.* 2012).

GPS units are one of the most technologically advanced (and arguably the most popular) VP systems (cf. Cagnacci *et al.* 2010; Latham *et al.* 2015; Seidel *et al.* 2018), capable of recording with high frequency (e.g., 5 Hz) (Hubel *et al.* 2018) and for many months (although not both simultaneously for reasons of power draw) (Krop-Benesch *et al.* 2013). Yet, even with GPS, fix success rate can drop dramatically and locational accuracy can easily vary by a few metres or more, depending on the propagation of signal quality and/or receiver reception capability (D'eon & Delparte 2005; Lewis *et al.* 2007). In addition, these units can be subject to latency delays by

up to ~ 5 s (Farrell *et al.* 1997; Bouvet & Garcia 2000), whilst most commercial loggers are only precise to around 1 m (Ryan *et al.* 2004) and so, irrespective of fix accuracy, time-based positional error can accumulate (as a function of sampling rate) when the spatial resolution of animal movement is less than the precision error radius between consecutive readings.

Motion sensor systems (also called Inertial Measurement Units - IMUs) incorporating tri-axial accelerometers and magnetometers are increasingly being used in animal-attached tags to determine fine-scale (second to infra-second) movement of animals *via* dead-reckoning (Cotter 1978; Wilson *et al.* 1991), thereby allowing elucidation of movement-related behaviours (cf. Yoda *et al.* 2001; Rong *et al.* 2007; Wilson, Shepard & Liebsch 2008; Brown *et al.* 2013; Graf *et al.* 2015; Wilson *et al.* 2018). Dead-reckoning involves sequentially integrating travel vectors (heading and speed estimates), radially in time (Walker *et al.* 2015) (and 3-D space with aligned pressure/depth data). Compared to animal-borne video recorders and GPS units, motion sensors require far less current (cf. Bidder *et al.* 2015; Park *et al.* 2019) and operate at much higher recording frequencies and precision (Wilson, Shepard & Liebsch 2008; Brown *et al.* 2013; den Uijl *et al.* 2017; Barwick *et al.* 2018). Indeed, studies are increasingly demonstrating the value of motion sensors for resolving continuous and fine-scale movements in 2- or 3-D space, on/in terrestrial- (e.g., Bidder *et al.* 2015; Dewhirst *et al.* 2016), marine (e.g., Wensveen, Thomas & Miller 2015; Andrzejaczek *et al.* 2019) and aerial (e.g., Williams *et al.* 2020) environments – far beyond what would have been obtained using VP systems alone (f. Latham *et al.* 2015; Dewhirst *et al.* 2016; Poulin, Clermont & Berteaux 2021).

Crucially, inertial measurements, being unaffected by factors that modulate VP accuracy, provide an independent and higher resolution comparator for assessing the extent (and type) of movement undertaken (cf. Chapter 4), which can be localised in environmental space when paired with a VP system. Uncorrected dead-reckoned paths have been referred to as 'pseudo-tracks' (Walker *et al.* 2015; Andrzejaczek *et al.* 2018), because extrapolated travel vectors always incur some error, and being additive (Bidder *et al.* 2015), even small errors accumulate to have more substantial influences on path shape (conventionally termed 'drift' (Wilson *et al.* 1991; Fischer *et*

al. 2008; Dewhirst *et al.* 2016)). This means that, although the form of animal movement is maintained most accurately by adjacent track sections (e.g., Andrzejaczek *et al.* 2019; Narazaki *et al.* 2021), the relationship between animal path and the environment tends to deviate over time (Wilson *et al.* 2007). VPs obtained from a secondary source (e.g., GPS) can correct for this by periodically resetting accumulated drift (Walker *et al.* 2015; Dewhirst *et al.* 2016).

The fusion of VP systems and dead-reckoning involves a trade-off between dead-reckoning accuracy and VP correction rate (itself, usually constrained by power consumption). Dewhirst *et al.* (2016) were the first to review this, as they compared various scales of GPS-corrected dead-reckoned tracks, obtained from domestic dogs (*Canis lupus familiaris*). Unsurprisingly, position error (the distance between temporally aligned dead-reckoned and GPS positions) decreased as a function of correction rate and the authors concluded that a correction rate of one fix every five minutes resulted in highly accurate distance moved estimates. For similar results using GPS alone, they noted that it would have required 12 fixes per minute (assuming no GPS error) which would have reduced battery life from months to days. Dead-reckoning thus provides the means to extend battery life (or reduce battery size in any tag deployment, with the attendant benefits for animal wellbeing (cf. Kay *et al.* 2019; Wilson *et al.* 2020b)) and improve the accuracy and detail of behaviour-specific travelling movements between VPs (e.g., Mitani *et al.* 2004; Bidder *et al.* 2015; Walker *et al.* 2015). How this extends to wild animals and beyond the terrestrial movement medium, however, requires further investigation.

This study uses the dead-reckoning protocols and R functions described in Chapter 4 to examine the movement of VP corrected dead-reckoned animal paths for four wild species (a mammal (lions - *Panthera leo*) and three bird species (penguins - *Spheniscus magellanicus*, cormorants - *Leucocarbo atriceps*, tropicbirds - *Phaethon rubricauda*)), varying across greater than an order of magnitude in mass and travelling in the three major media (land, water and air) using walking, swimming and flying. I sub-sampled the scale of VP correction to examine the trends in net error and compared cumulative distance moved estimates between VP corrected dead-reckoned tracks and GPS paths alone according to VP correction rate and simulated

VP down-sampling, respectively. My goal was to demonstrate that the traditional trade-off between VP correction rate and dead-reckoning accuracy is more complex than simply 'the higher the rate, the greater the accuracy' (though this would be the case if VPs were perfect). Rather, the accuracy of both reconstructed paths is heavily dependent on the animal's lifestyle (including the specifics of location and the speeds and mode(s) of movement). Accordingly, I assess the importance of appropriate dead-reckoned track scaling, which is primarily based on speed estimates prior to VP correction. I also highlight the benefit of acquiring external air-/tidal flow vectors for animals traveling in fluid media (air and water), particularly when VPs are temporally widely spaced, and emphasize the danger of carrying out VP correction too frequently (irrespective of battery consumption) due to VP error. Lastly, in context of the above, I outline the utility of dead-reckoning across various scenarios and the key considerations for deciding VP correction frequency.

Materials and methods

Study species

I selected four free-living species, exemplifying almost two orders of magnitude of mass, which travel in three media. These were; 10 lions (mass *ca.* 130-190 kg; 'four-legged walkers'), 15 penguins (mass *ca.* 4 kg; 'two-legged walkers' & 'swimmers'), 15 cormorants (mass *ca.* 1.8-3.5 kg; 'flyers' & 'swimmers') and seven tropicbirds (mass *ca.* 0.6 kg; 'flyers'). Animals were equipped with Daily Diaries (DDs) [Wildbyte Technologies - <http://www.wildbytetechnologies.com/>], recording tri-axial acceleration, magnetic field intensity and pressure (either barometric- or hydrostatic pressure) (Wilson, Shepard & Liebsch 2008). Unencapsulated DD models ranged between 27x26x10 mm and 26x17x5 mm and weighed 2-3 g (incl. microSD card and excl. batteries). In tandem, animals were also equipped with GPS (Axytrek or Gipsy) units [<https://www.technosmart.eu/>], programmed to record at one fix every minute for tropicbirds and one fix every second for the other species. Both encapsulated devices (incl. batteries) always comprised < 3% of the average body mass of each species. Animals were left to roam freely, for periods ranging between 1 to 16 days before the devices were recovered (Table. 1).

VP-corrected dead-reckoning procedure

Tracks were reconstructed and drift corrected using the *Gundogs.Tracks()* function in R, based on the protocols outlined in Walker *et al.* (2015). See supplementary information (SI) for the VP correct dead-reckoning formulae. Pitch and roll (representing posture, expressed using Euler angles - *cf.* Johnson & Tyack 2003), were calculated from static acceleration estimates (Shepard *et al.* 2008b) and heading was derived using the tilt-compensated compass method (Pedley 2012), with any required magnetic declination offset applied. Pitch (used in the computation of speed for diving animals; see Table. 1) and heading were post-smoothed by 1-2 seconds (i.e., a rolling ‘circular’ mean used for heading values, *cf.* Pewsey, Neuhäuser & Ruxton 2013).

I used the Vector of the Dynamic Body Acceleration (VeDBA; see eqn 1) (Qasem *et al.* 2012; Wilson *et al.* 2020a) (smoothed by 2 seconds) as a speed proxy for terrestrial locomotion (Bidder *et al.* 2012).

$$VeDBA = \sqrt{(D_x^2 + D_y^2 + D_z^2)}, \quad (1)$$

where D_x , D_y & D_z are the dynamic acceleration values from each axis. The ‘linear’ VeDBA~speed relationships [$speed = (VeDBA \cdot m) + c$] were derived either by iteratively changing the m -coefficient (gradient) per individual until (uncorrected) dead-reckoned tracks were scaled according to the corresponding GPS tracks (using a zero c constant (intercept)), or by substituting m - and c values with GPS-derived speed *versus* VeDBA regression estimates (Dewhirst *et al.* 2016). For swimming and flying locomotion, where Dynamic Body Acceleration (DBA) is considered a weak proxy of speed (*cf.* Wilson *et al.* 1992; Williams *et al.* 2020), speed values were allocated according to; (i) behaviour type (itself, elucidated from motion sensor data (e.g., Wilson *et al.* 2018; Yu & Klaassen, 2020.) (ii) rate of change of depth *versus* dive angle-derived speed (Laplanche, Marques & Thomas 2015) or (iii) GPS-derived speed estimates (using the Haversine distance formula, Chopde & Nichat 2013) between GPS fixes (at defined fix intervals). Movement-specific behaviours were identified using one or a combination of; visual interpretation of stylised patterns in

acceleration data (*cf.* Rong *et al.* 2007; Willener *et al.* 2015; Williams *et al.* 2015), the Lowest Common Denominator Method (LoCoD) method (Wilson *et al.* 2018) and the Movement Verified Filtering (MVF) method (Chapter 4). Species' specific speed allocation details according to movement-specific behaviour and/or topological whereabouts, are given in Table. 1. Any required tag orientation offsets (e.g., due to imperfect tag placement along the longitudinal axis of the animal) as well as baseline pressure drift were accounted for by rotation correction of magnetic and acceleration vectors (Johnson & Tyack 2003; Chapter 5) and trend estimation with asymmetric least squares (*cf.* Peng *et al.* 2010), respectively.

VP correction rate and metrics of analysis

All tracks were dead-reckoned at periods between 1-10 Hz resolution (Table. 1). According to the duration of deployment and GPS fix rate, VP correction rate was thinned at scales of; 1 fix/24 h, 1 fix/12 h, 1 fix/6 h, 1 fix/3 h, 1 fix/1 h, 1 fix/30 min, 1 fix/15 min, 1 fix/5 min, 1 fix/min, 1 fix/30 s, and 1 fix/1 s. Net error and distance moved estimates (in metres) were calculated for each species, individual and VP correction rate. The Haversine distance formula (Chopde & Nichat 2013) was used to compute 2-D net error, which we define as the distance between every VP (irrespective of VP-correction rate) and the corresponding time-matched VP corrected dead-reckoned position. Distance moved was summed separately, both between consecutive dead-reckoned positions and consecutive GPS positions, the latter being down-sampled according to the VP correction rate (e.g., if the VP correction rate was approx. 1 fix/h, then GPS data was sub-sampled to this frequency prior to computing distance moved between retained positions). The Haversine formula was used to compute 2-D distance moved (terrestrial 'on-land' movement). For 3-D dead-reckoned movements (penguins and cormorants at depth and tropicbirds at altitude), positions were converted to Cartesian coordinates (x,y,z), incorporating the Earth's oblate spheroid shape (geodetic latitude) and the straight-line distance between sets of Cartesian coordinates were calculated using Pythagorean theorem. 3-D distance moved was not computed between VPs since

both the level of VP thinning (particularly at lower VP correction rates) and the periods of time where fix success rate dropped (e.g., under water) made this inappropriate. Altitude (in metres) was calculated using local coastal meteorological recordings of air pressure at 5-min resolution by a portable weather station (Kestrel 5500L, Kestrel instruments, USA) stationed at the highest point above sea-level (*ca.* 280 m) on Round Island, Mauritius (Garde *et al.* (in review)). Ocean current vectors were composed from a validated 3-D numerical model constructed for the region (Tonini & Palma 2017), with tidal currents deduced hourly at 1 km² resolution.

All VPs (filtering out obvious outliers visually) were used when making inter-specific comparisons of net error estimates across VP correction rates and given that, in this process, VPs are considered the benchmark upon which net error is assessed, net error zeros out when VP correction includes all VPs (VP correction rate = VP logging frequency; see Table. 1). In conjunction with the main findings, I report various applications of dead-reckoning and extensions to improve dead-reckoning accuracy, such as the importance of initial speed estimates and incorporation of external current flow vector estimates in fluid media, using various species-specific case-studies as examples.

How often to correct dead-reckoned paths?

Table 1. Experimental protocol for each species. Note, ' $\Delta d/\tan(\theta \cdot \pi/180)$ ' refers to the rate change of depth (m/s) divided by the tangent of the body pitch (converted from degrees to radians). DR =, dead-reckoning and DBA = dynamic body acceleration. m- and c values represent the (multiplicative) coefficient (gradient) and constant (intercept) of the $VeDBA \sim \text{speed}$ regression [$\text{speed} = VeDBA \cdot m + c$].

Animal (number (n) assessed)	Scheduled GPS frequency	DR frequency	Approx. DR length	Extrapolated speeds	Capture & Deployment method
Lion (n = 10)	1 Hz	1 Hz	2 weeks	DBA-based speed Due to high variability in step gaits, m- & c-values were computed per individual from $VeDBA \sim \text{GPS}$ -derived speed regression (cf. Chapter 4).	Prides were lured to bait using audio recordings and individuals were anaesthetised at night according to SANParks operational procedures - detailed in SANParks' 'Standard Operating Procedures for the Capture, Transportation and Maintenance in Holding Facilities of Wildlife' Units were mounted to a Litetrack collar [https://www.lotek.com]. Collars were loose enough to allow three fingers to pass through
Penguin on land (walking) (n = 15 – 2 DR paths per individual (out- & inbound))	1 Hz	10 Hz	30 mins	DBA-based speed Due to having a constant step gait, m-values were selected (c = 0) per individual based on the best scaling relative to GPS path pre-VP correction	Penguins were caught at the nest during the chick rearing season using the clipboard method (Wilson 1997) and cormorants were caught at the nest during the chick rearing season via a crook on the end of a long pole (cf. Sakamoto <i>et al.</i> 2009). Birds were blind folded and restrained on a researcher's knees Devices fitted longitudinally to the base of the spine using Tesa® tape (Wilson & Wilson 1989; Wilson 1997; Wilson <i>et al.</i> 1997; Wilson <i>et al.</i> 2005)
Penguin at sea (diving) (n = 15)	1 Hz	2 Hz	1.5 days	Change between constant values (according to behaviour-type) and vertical movement-based speed → speed = 0.416 m/s (cf. Wilson 1985) when depth ≤ 0.3 m (cf. Ropert-Coudert <i>et al.</i> 2001) → speed = 2.1 m/s (cf. Wilson, Ropert-Coudert & Kato 2002; Wilson <i>et al.</i> 2004) when depth > 0.3 m and absolute values of pitch were $< 10^\circ$ → speed = $\Delta d/\tan(\theta \cdot \pi/180)$ (upper cap of speed derived this way = 3 m/s) when depth > 0.3 m and absolute values of pitch were $\geq 10^\circ$	
Cormorant at sea (flying and diving) (n = 15)	1 Hz	10 Hz	8 hours	Change between constant values (according to behaviour-type) and vertical movement-based speed → speed = 12 m/s when flying (derived from the heave acceleration (cf. Williams <i>et al.</i> 2015)) → speed = 0.1 m/s when resting at the sea surface (derived from depth sensor and lack of dynamic acceleration) → speed = $\Delta d/\tan(\theta \cdot \pi/180)$ (upper cap of speed derived this way = 3 m/s) during the ascents and descents of dives → speed = 0.4 m/s during the bottom phase of dives	
Tropicbird at sea (flying) (n = 7)	1 fix every minute	10 Hz	3 hours	GPS-based speed → speed = Haversine distance between GPS fixes divided by the time period between values and linearly interpolated (cf. Feng & Timmermans 2013). Speed values overwritten as 0.1 m/s when birds were resting at sea surface	

Results

Net error decreased with increasing VP correction rate, although the species travelling in fluid media had much larger net error estimates for any given VP correction rate (Fig. 1). For example, considering a VP correction rate of 1 fix/h, the mean net error of penguins (at sea), cormorants and tropicbirds were approximately 28, 42 and 95 times greater, respectively, than lions. A visually obvious ‘plateau’ of net error drop (relative to the initial gradient) varied between species (with respect to magnitude of net error and level of VP correction rate).

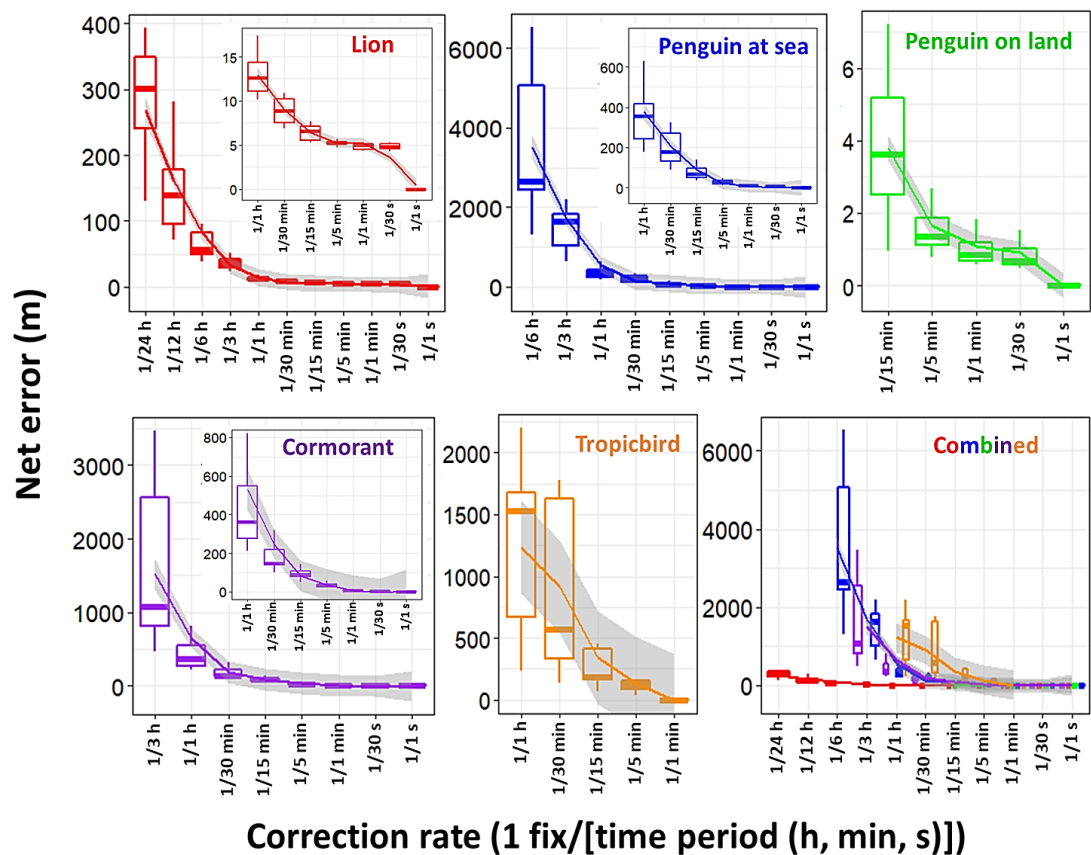


Figure 1. Boxplots demonstrating the magnitude of net error according to the VP correction rate per species. Mean values were aggregated per individual and VP correction rate. Boxes encompass the 25-75% interquartile range and horizontal bars denote the median value with 'loess' smooth line (grey shading shows the standard error and Whiskers extend to 1.5 * Interquartile range). Note net error drops to zero when the VP correction rate equates with GPS recording frequency (1 Hz for the lions, penguins and cormorants, and 1 fix/min for the tropicbirds). The inserts zoom in on the net error between VP correction rates of one fix per hour and one fix per second.

Across all species, estimates of overall distance moved were smaller when summed between GPS positions (thinned according to VP correction rate) than for dead-reckoned positions (Fig. 2). Dead-reckoned estimates of distance moved were generally more consistent across the VP correction rates, relative to the corresponding GPS-derived distance moved estimates (in which VP thinning is equivalent to VP correction rate). Although there are slight variations in the pattern of these trends between species, there was a notable increase when VP correction rate is highest.

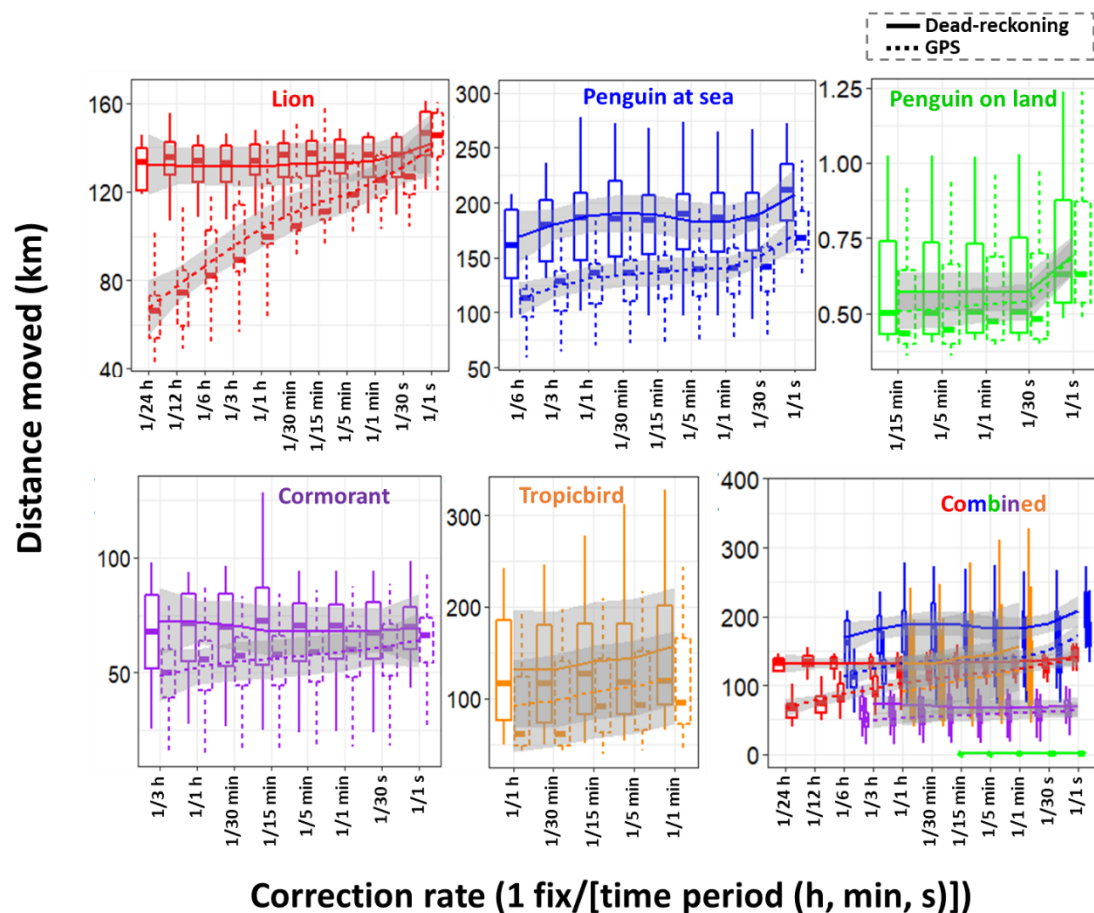


Figure 2.. Boxplots demonstrating the total distance moved (km) during the tag deployment period according to VP correction rate for the study species. Solid lines show the distance moved calculated using successive dead-reckoned positions (distance moved (see methods) was 3-D and computed for penguins and cormorants operating at varying depths and tropicbirds at varying altitudes, and 2-D computed for lions and penguins walking on land). Dashed lines reflect the distance moved calculated from successive GPS positions according to the level of VP under-sampling stated (only 2-D distances were computed). Mean values were aggregated per individual and per VP correction rate. Boxes encompass the 25-75 % interquartile range and horizontal bars denote the median value with 'loess' smooth line (grey shading shows the standard error and Whiskers extend to 1.5 * Interquartile range). Note that the high spread of each species boxplot is due to the high intra-specific variability of distances moved – e.g., with the tropicbirds, differences in foraging/distance roamed may be due to breeding vs. non-breeding status.

Estimates of net error and distance moved were standardized according to the mean time between corrections per VP correction rate and the duration of the movement path, respectively, per individual (Fig. S1), which further highlighted the trend between speed of movement and net error estimates. Beyond this, the rate of net error was relatively consistent between VP correction rates (Fig. S1), demonstrating that the 'plateaus' of net error drop observed in Fig. 1, are primarily the result of the non-linear scales of VP correction thinning (although there was a noticeable minor decreasing trend from lowest to highest VP correction rates for animals moving in fluid media). Alongside VP-correction rate, dead-reckoning accuracy was heavily affected by the initial scaling of dead-reckoning tracks (Fig. 3). This principally related to appropriate speed allocation, such as threshold values of DBA to estimate speed and only advancing tracks at times of known travelling movements, thus excluding DBA values due to movements which do not lead to a displacement of the body in space (e.g., self-grooming movements). Here, per given VP correction rate, tracks advanced only during times of depicted movement (using the MVF protocol, (Chapter 4); green) recorded the lowest net error, relative to using all data (red) and subset data using a VeDBA threshold (blue) (Fig. 3). Whilst net error generally did not vary strongly with activity level (of which VeDBA is a proxy) for lions, the variance was markedly higher at both high and low VeDBA values, indicating that correcting for VP error during inactivity may be just as important as the initial track scaling (Fig. S2).

VP corrected dead-reckoning provided the means to investigate behavioral responses with higher resolution, without incorporating the inaccuracies of positional noise associated with VPs obtained at high frequency (Fig. 4). For example, here, VP corrected dead-reckoning (using a VP correction rate of 1 fix/min) shows the various sites at which three female lions crossed the Kgalagadi Transfrontier Park fence line (into Botswana from South Africa), including patrolling behaviour of one female (purple) that became separated in time and space (Fig. 4).

How often to correct dead-reckoned paths?

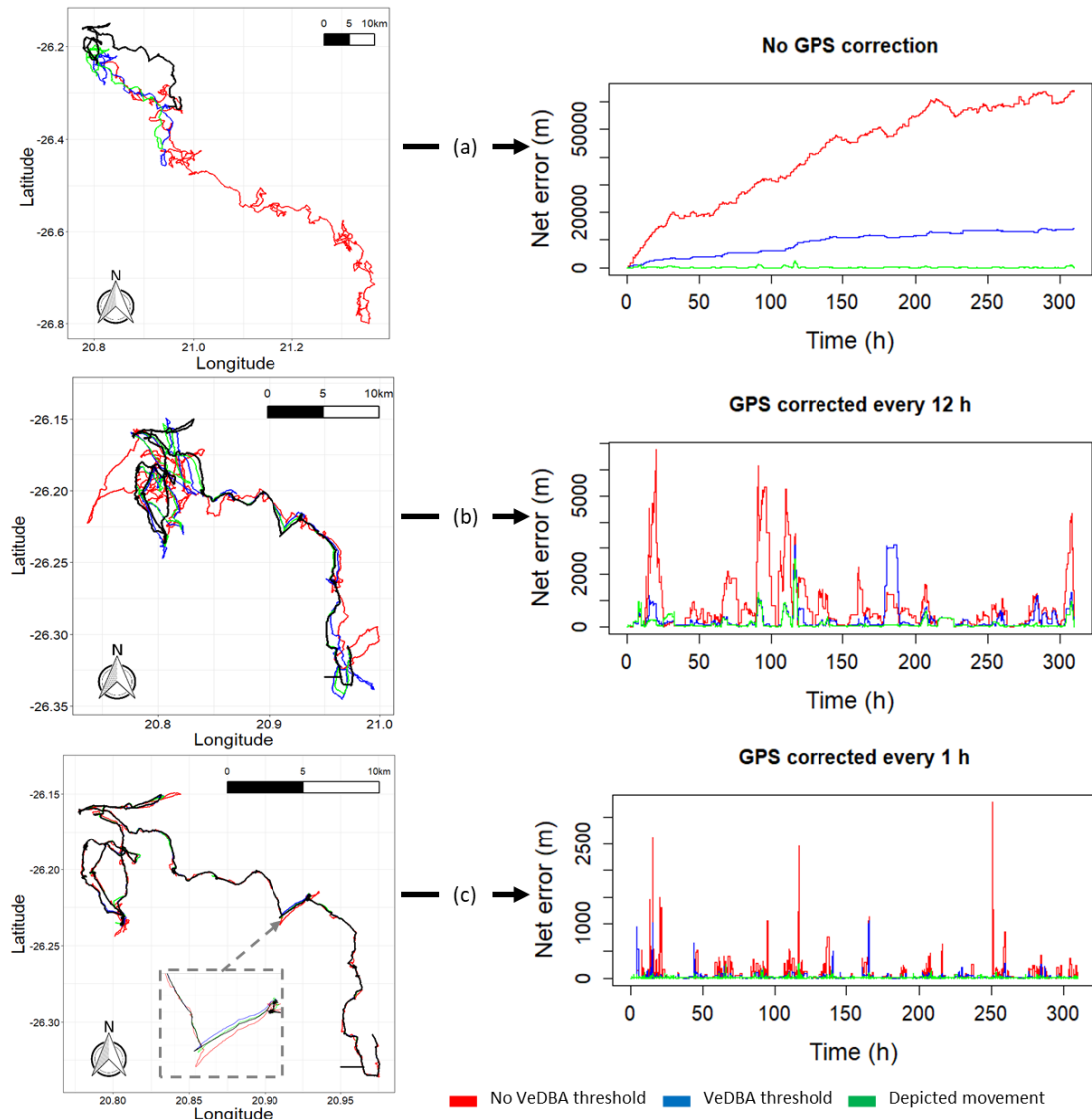


Figure 3. A lion's dead-reckoned movement path (approx. 12 days) in relation to (all) GPS positions (black), plotted both as a function of GPS correction rate ((a) = no correction, (b) = GPS corrected every 12 h, (c) = GPS corrected once every hour) and initial subset of data used to create the path (red = all data (no VeDBA threshold for speed), blue = only data that surpassed VeDBA threshold (> 0.1 g) used for speed, green = only data during periods depicted as proper movement (using the MVF protocol [23])). Note the difference in y-scales across the net error graphs.

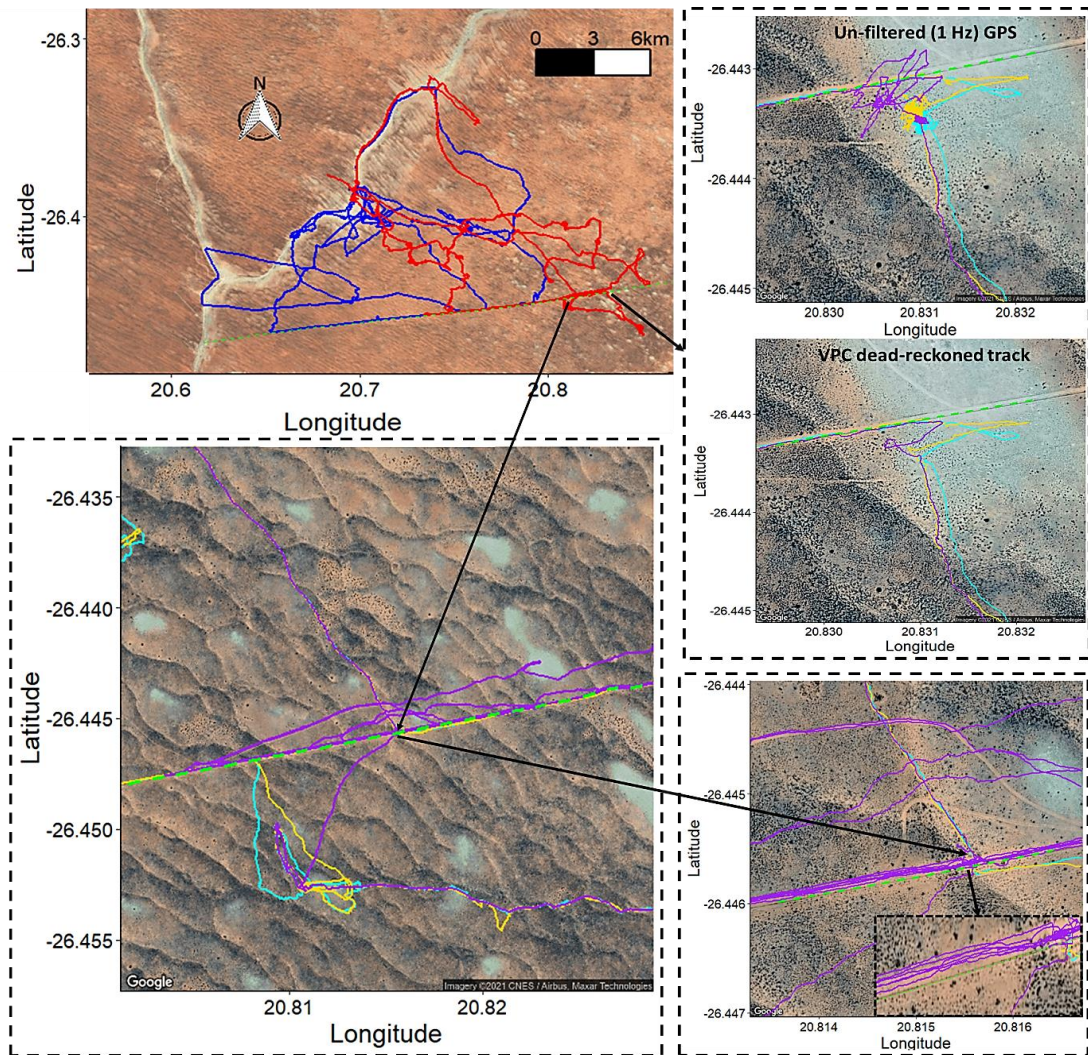


Figure 2. VP corrected dead-reckoned movements of lions in the Kgalagadi Transfrontier Park. The top left plots show a pride of 5 lions (2 Males – blue and 3 females – red). Both male and female movements abutted the Botswana fence boundary (dashed green line), although only the females crossed (illustrated in the dotted inserts, with yellow, cyan and purple tracks denoting individual females) The bottom right insert shows one female pacing along the fence line in an attempt to re-join the other two that crossed hours earlier. Note the extent of (unfiltered) GPS error that occurs (particularly during resting behaviours) (top right).

Even when dead-reckoned travel vectors likely incorporated appreciable error (e.g., due to low-resolution (constant) speed estimates), fine-scale movement-specific behaviours were apparent (beyond the capacity of the VP systems used), for example, soaring in thermals (Fig. 5) or the tortuosity of foraging (Fig. 6).

How often to correct dead-reckoned paths?

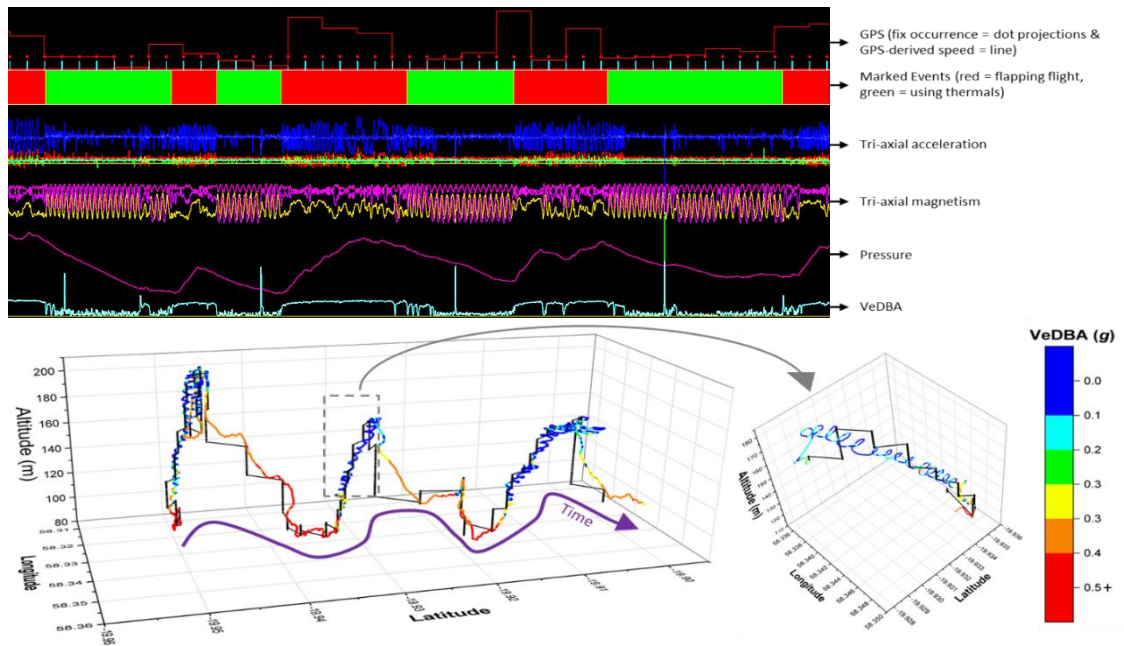


Figure 5. A 45-minute section of a tropicbird's foraging flight at sea, encompassing periods of thermal soaring. The top plot characterises stylised trends in the raw values and select derivatives from the motion sensor and GPS unit outputs (2-D waveforms vs time), including differentiating flapping flight from thermal soaring (Marked events - primarily based on magnetism data). The sine waves appearing in two of the magnetometer channels simultaneously reflects circling. The bottom plot graphs the dead-reckoned track (coloured according to VeDBA) in 3-D, relative to all available GPS fixes obtained (black) (including an insert of circling behaviour). Note periods of thermal soaring are not apparent with GPS at the recording frequency of 1 fix/1 min as used here. Note that climb rate increases a function of the inverse of pressure.

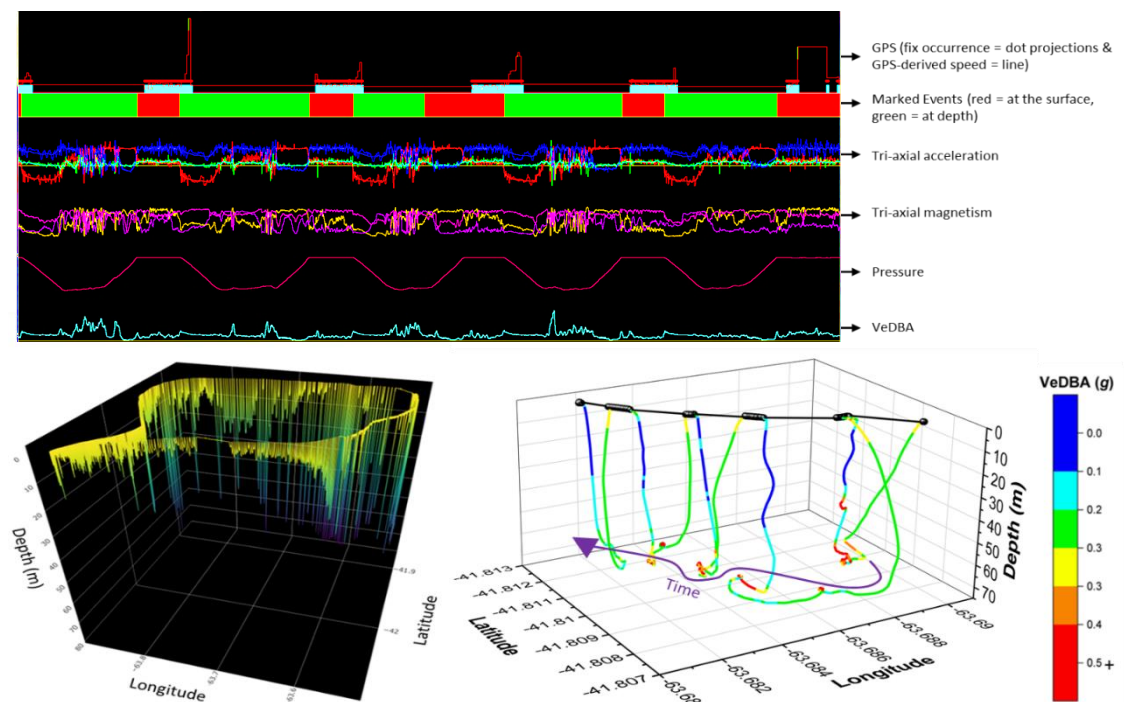


Figure 6. A 15-minute duration of a Magellanic penguin's foraging trip at sea. The top plot characterises stylised trends in the raw values and select derivatives from motion sensor and GPS unit output (2-D waveforms vs time), including differentiating between dives and surface periods (Marked events - primarily based on depth data). Note that pressure is inverted to reflect depth. The bottom left plot maps the entire (17 hour) VP-corrected dead-reckoned foraging trip. The bottom right plot graphs the resultant VP-corrected dead-reckoned track from the 15-minute section of data shown above (coloured according to VeDBA) in 3-D, relative to all available GPS fixes obtained (black). Note the latency delays in GPS recordings (as seen in the top plot), with a temporal offset of fixes (red dot projections) occurring at green marked events (at depth)). Fixes that occurred at depth were removed from the analysis.

I found that the interplay between the accuracy (and resolution) of speed estimates, animal behaviour and VP inaccuracy could result in correction factors (see discussion) that disproportionately (incorrectly) expanded sections of the dead-reckoned track (Fig. 7). For example, in Figure 7, clear scaling errors arose between the third and fourth VP (post-VP correction) during soaring in a thermal when VeDBA- and GPS-derived speeds were used. At this path segment, the distance correction factor required when using constant speed values differentiated according to behaviour (green) was 3, juxtaposed with 22 and 47 for the VeDBA- (blue) and GPS- (red) derived speeds, respectively.

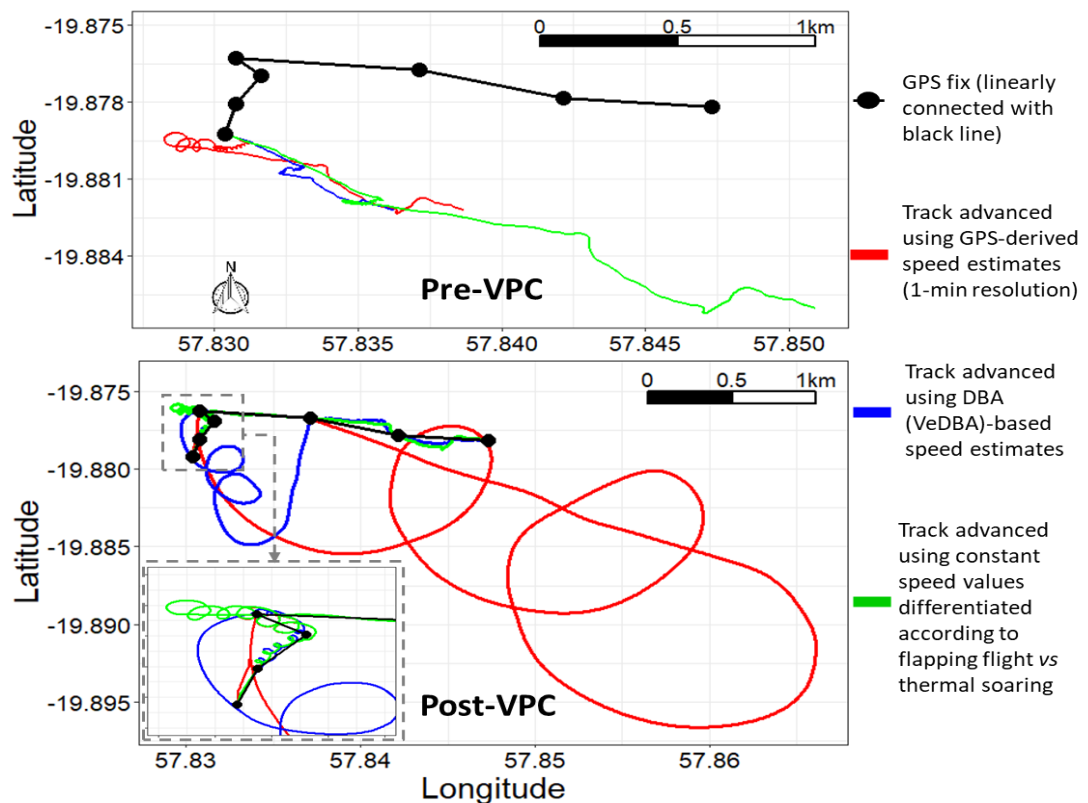


Figure 7. Seven minutes of tropicbird flight with dead-reckoned tracks advanced according to 3 different allocations of speed, plotted alongside GPS (1 fix/min) both pre- and post-VP-correction. This demonstrates the main error that can arise during the VP correction procedure (using heading and distance correction factors (see discussion)), when there is a large disparity in distance between consecutive VPs and consecutive dead-reckoned positions, primarily due to inaccurate speed allocation and/or VP error. Note how a segment of thermalling behaviour was disproportionately expanded during the VP correction process when using GPS-derived speeds and DBA-based estimates, because there was no differentiation between thermal soaring and flapping flight (cf. Fig. 5). Using a much lower speed value during thermal soaring value (a quarter of the magnitude allocated for flapping flight) greatly improved track estimates because the magnitude of linear drift correction works as a function of the underlying speed allocation.

The dead-reckoned tracks in air and water improved in general accuracy when suitably estimated external current flow vectors (tidal-/wind-speeds and direction per unit time and space) were incorporated (*via* travel vector and current flow vector addition - 'current integration', Fig. 8).

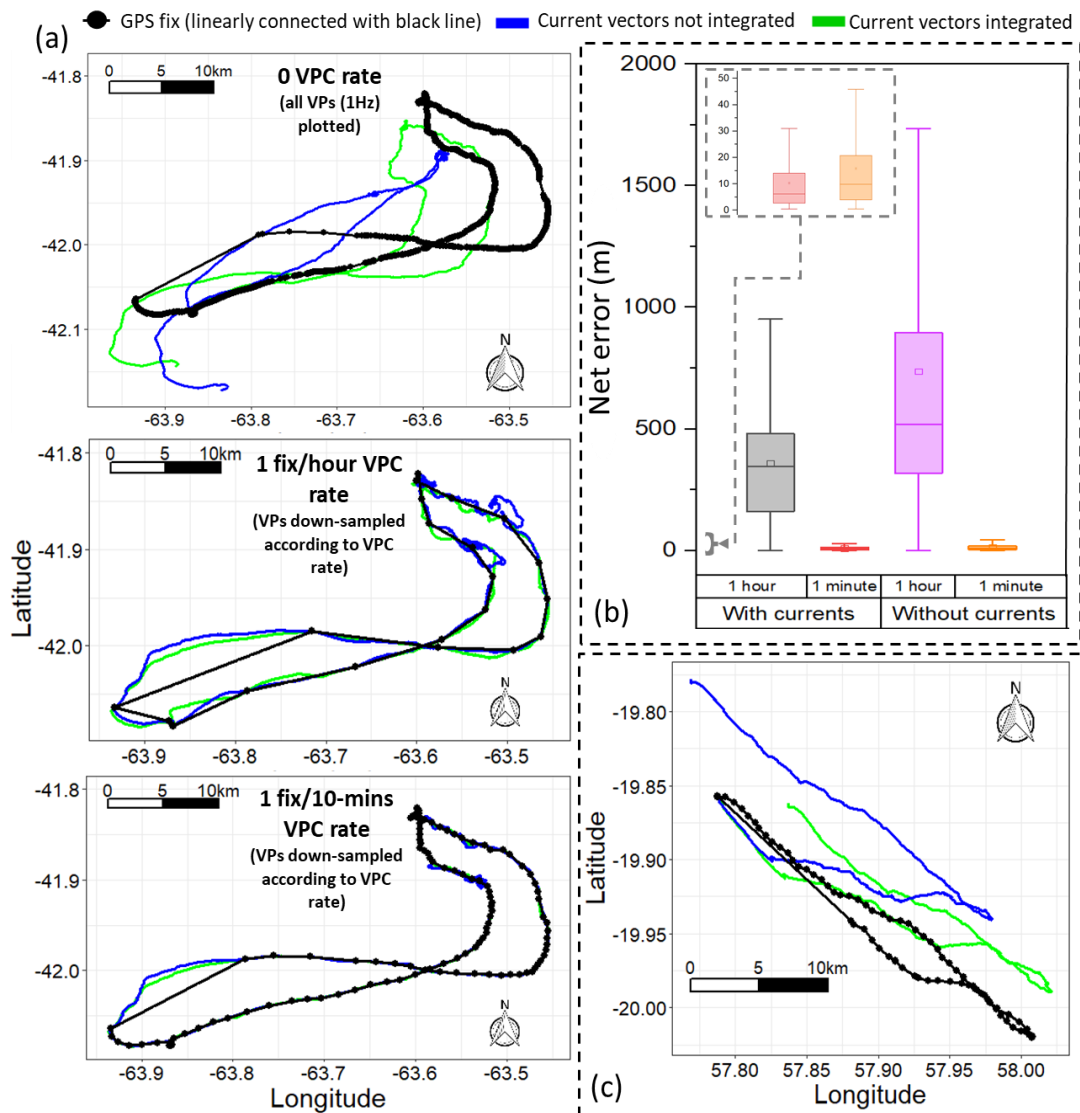


Figure 8. (a) One penguin's dead-reckoned track calculated with- (green) and without- (blue) current integration and 3 variant VP correction rates (left panel). (b) shows differences in net error when dead-reckoned tracks were iteratively integrated with space- and time-correction (net error estimates obtained from 5 penguin datasets). The boxes denote the median and 25-75 % interquartile range and whiskers extend to 1.5*IQR. (c) shows an uncorrected dead-reckoned tropicbird flight path, relative to GPS, both with (green) and without (blue) current integration. Note the clustering of fixes (e.g., due to animal not moving much for extended periods of time) that can occur when using temporal sub-sampling routines (a more refined method could include using a VP correction rate of 1 fix every x m moved (e.g., as estimated between VP's)).

Discussion

Speed inaccuracies and VP corrected dead-reckoning

It is notable that the calculated examples of animals travelling on land (lions and walking penguins), had far less net error per given VP correction rate than the animals travelling in fluid media (swimming penguins, cormorants and tropicbirds), confirming the accuracy of the method for the former medium. However, dead-reckoning is very valuable for animals moving in fluid media (particularly for 3-D movement and movements underwater, which cannot be monitored by GPS), even though the inaccuracy is greatest at such times. There are three reasons for the greater inaccuracy:

1. The DBA approach of deriving speed estimates is temporally highly resolved and more accurate than GPS-derived estimates (used for tropicbirds) and the constant values used for part of the paths calculated for penguins and cormorants.
2. Typically, terrestrial species move slower than aerial/marine equivalents and thus incorporate less spatial error per unit time (cf. Fig. S1).
3. External current flow vectors can cause the relationship between an animal's (longitudinal axis) powered direction of travel and their true vector of travel to deviate (Shiomi *et al.* 2008; Chapman *et al.* 2011). Indeed, in one of the earliest considerations of dead-reckoning for animals, Wilson *et al.* (1991) noted that ocean currents were likely to be the greatest source of inaccuracy for positional fixes because of this.

Although convenient and powerful, DBA-derived speed has its own inaccuracies. The proposed linear relationship between DBA and mechanical power (cf. Gleiss, Wilson & Shepard 2011; Wilson *et al.* 2020a) presumably changes when the animal is load-bearing (Sequeira *et al.* 1995; Miwa *et al.* 2015), moving over a deformable substrate, over varying incline (Kerdok *et al.* 2002; Halsey *et al.* 2008; Bidder, Qasem & Wilson 2012) or changing gait (Bidder *et al.* 2012), or the attached logger undergoes motion independent of the body frame (e.g., collar roll), whilst even stationary behaviours

can impart appreciable DBA, all of which may affect the relationship between DBA and speed (Bidder, Qasem & Wilson 2012; Bidder *et al.* 2015).

DBA-derived speed estimates can sometimes break down for species that hold appreciable quantities of air underwater (such as birds (Wilson *et al.* 1992)) due to the compression of the air that takes place with increasing depth, with consequent changes in upthrust and power allocation according to swim angle (Wilson *et al.* 2011) (cf. the difference of VeDBA magnitude between ascents and descents – Fig. 6). In addition, DBA does not scale reliably with speed for animals that glide, use thermals (cf. Fig. 5 & 7), or bank and turn sharply (Williams *et al.* 2015; McNarry *et al.* 2017) because the more a gliding bird pitches down, the faster it will travel, even though there is no change in DBA. The same is true of animals with a higher density than water, such as elasmobranchs (cf. Smith *et al.* 2004), although in both cases the speed can be determined using the rate of change of altitude/depth if the pitch angle is known and it is high enough (Wensveen, Thomas & Miller 2015)).

Most previous studies that have used in-water speed sensors have done so by counting rotation of an external propeller or paddlewheel (e.g., Mitani *et al.* 2003; Shiomi *et al.* 2008; Matsumura *et al.* 2011; Watanabe *et al.* 2011; Iwata *et al.* 2015). However, such systems have appreciable limitations with their ability to measure highly dynamic speed because (aside from environmental confounds such as blockage and turbulence (cf. Shepard *et al.* 2008c)) flow characteristics around the sensor can change radically as a function of speed, most particularly in proximity to the animal body where the sensors are situated (Kreye 2003). Recent research into fluid media speed sensors (e.g., Altynay *et al.* 2019) though, may eventually provide systems that could markedly enhance the dead-reckoning process for animals travelling in water or air. Beyond this, the principal low-resolution methods for determining a speed proxy involve GPS-derived speed estimates or constant/simulated values according to behaviour-type or topological whereabouts (the primary approach used here for aquatic/aerial movement). Clearly, using constant speed estimates (even if they are a mode of the true value) quickly give erroneous integrated travel vectors, which emphasises the importance of appropriately spaced VP correction, particularly when speed is highly variable.

Generally, environmental covariate maps are typically given with lower resolution in aerial and aquatic domains, so location errors seem less important because space-use is, anyway, typically considered at larger scales (cf. Wensveen *et al.* 2019). For example, foraging ‘hotspots’ can be obtained based from 3-D dive profiles and even if dead-reckoning accuracy had an approximate 500 m error radius (e.g., 1 fix/hour VP correction rate for penguins (Fig. 1)), such errors seem more acceptable in an apparently predominantly featureless ocean (although not necessarily - e.g., investigating disturbances to animal movements created by underwater turbines). The same reasoning applies to most flying species although, because so many fly over land, higher absolute resolution is often required in order to map out the specifics of land-based features, such as wind turbines (Rydell *et al.* 2010; Everaert 2014) or thermals (Harel *et al.* 2016), that are relevant for bird (or bat) movement. Airflows themselves represent dynamic environments and assessing fine-scale dead-reckoned tracks in 3-D may reveal important interactions between animal and aircscape and the energetic consequences involved (cf. Lempidakis *et al.* 2018; Williams *et al.* 2020; Lempidakis *et al.* 2021; Garde *et al.* (in review)). Most importantly, although dead-reckoning for fliers can incur substantial wind-based drift, GPS-based VP is usually accurate, because of the open sky which enhances signal transmission (Forin-Wiart *et al.* 2015), and this can help correct tracks accordingly.

Whilst the accuracy of current flow vectors may be imprecise, their integration (see Chapter 5 for method) can improve dead-reckoning estimates substantially (both pre- and post-VP correction, Fig. 8), which is especially important when VPs are scarce. It is worth noting however, that using GPS-derived speed and/or output from speed sensors estimating parameters of flow incorporates the speed of any current flow. Against this, assessing dead-reckoned travel vectors alongside VPs and external current flow vector estimates can provide insights into movement strategies of animals compensating for current drift (cf. Shiomi *et al.* 2008; Chapman *et al.* 2011).

The greater accuracy of VP corrected dead-reckoning in terrestrial movement compared to fluid media is important because covariates of interest on land are typically highly resolved with, for example, habitat use (Valeix *et al.* 2010; Tracey *et al.* 2013), conspecific interactions (Schlägel *et al.* 2019) and the effect of man-made

structures (Shepard *et al.* 2008a; Panzacchi *et al.* 2016) (e.g., roads, fences etc.) being of interest. Unlike most aquatic and aerial species, DBA can be continuously applied as the speed proxy for land animals, and the DBA~speed regressions (m and c values) can be modelled according to behaviour/terrain type, for higher resolution estimates (Bidder, Qasem & Wilson 2012). In this, a primary factor in maximising dead-reckoning accuracy in a speed context, is to ensure that only periods of genuine traveling movement are dead-reckoned, since even stationary behaviours (e.g., grooming, feeding, rolling over etc.) can impart appreciable DBA, which can inaccurately advance the vector of travel (cf. Fig. 3) (English *et al.* (in review)). Though notably, this is harder to achieve for animals in/on fluid media.

The VP correction procedure outlined in Walker *et al.* (2015) (and used here), divides the distance between consecutive VPs with the corresponding distance between temporally aligned dead-reckoned positions to obtain a distance correction factor (ratio) that is multiplied to all intermediate dead-reckoned distance moved estimates. This method has the advantage that the periods when the dead-reckoned vectors are not advanced (e.g., by allocating zero speed values for stationary behaviours, which can be determined from inertial data (e.g., Graf *et al.* 2015)), are not subsequently expanded out in the linear drift correction procedure (since multiplying by zero achieves a zero-correction factor). Notably though, this method of correction can inflate error, beyond the normal linear vector expansion or contraction (cf. Constandache *et al.* 2010). This is particularly problematic in small looping movements because if there is a disparity in the distance estimates between successive VPs and the corresponding dead-reckoned positions, path segments may be disproportionately expanded (and even inappropriately rotated) in order for the endpoints of both to align. Even though such path segments may simply be an artefact of VP inaccuracy, heading error or (as demonstrated in Fig. 7), wrongly assigned speed values. This has consequences for space-use estimates and thus drives home the importance of initial behavioural identification, speed allocation, and VP screening prior to the VP correcting dead-reckoning procedure, particularly during highly tortuous movement. Erroneous estimates of speed can occur, for example, due to the DBA~speed relationship changing as a function of behaviour (i.e.,

thermal soaring), or using low-resolution GPS-derived speed. Specifically, in Fig. 7, this was because, respectively, the GPS frequency was not high enough to resolve the tortuosity of movement involved between fixes accurately (and thus the distance travelled, from which GPS-derived speed is calculated), and because birds typically impart negligible DBA during soaring behaviour. The latter effect, along with the presence of external wind currents, can substantially alter the required coefficients (gradient and intercept) and/or linearity of the DBA~speed relationship in time and space.

Heading inaccuracies and VP-corrected dead-reckoning accuracy

Whilst not explicitly covered in these results, it is notable that because it is a vectorial operation, heading is the second major component in dictating dead-reckoning inaccuracy. Therefore, I clarify the potential causes of such error (first outlined in Chapter 5) below. Heading is calculated using the arctangent of the ratio between two orthogonal components of the magnetic vector when the magnetic field sensor is lying flat and parallel to the Earth's frame of reference (Grygorenko 2011). The tilt-compensated compass method rotates the attached tag's magnetic vector coordinates and subsequently converts values of each magnetic vector channel to the corresponding Earth's reference coordinate system, using the angles between the tag's magnetic- and the gravity vector. These angles are typically expressed as pitch and roll (Euler angles), which are resolved from the static component of acceleration (the gravity vector). The difficulty can be separating the static- (due to gravity) and dynamic (due to the animal's movement) components of acceleration (cf. Fourati *et al.* 2011). Although various methods have been proposed to do this (e.g., using a running mean (Shepard *et al.* 2008b; Gunner *et al.* 2020) or high-pass filter (Sato *et al.* 2003)), estimates are problematic during periods of high centripetal acceleration ('pulling g '; e.g., rapid cornering (McNarry *et al.* 2017)), free-falling (no discernible or low gravity-component) (Williams *et al.* 2015) and highly dynamic movements (Noda *et al.* 2014). Consequently, azimuth measurement error can be inflated at times when derived static acceleration estimates break down as a proxy of tag attitude relative to the Earth's fixed reference frame.

Incorporating gyroscopes can improve the accuracy of computed heading, since they accurately reconstruct gravity-based attitude, irrespective of acceleration (Wen 2019). However, gyroscopes suffer from drift, high-power requirements and rapid memory consumption (Fong, Ong & Nee 2008; Noda *et al.* 2012). Complex data processing makes them unappealing in most free-ranging bio-logging studies, particularly when information gains may be limited (cf. Martín López *et al.* 2016). Further work should assess the extent to which gyroscopes do improve (species-specific) VP corrected dead-reckoning accuracy, particularly at fine-scales (e.g., during fast, transient manoeuvres such as prey pursuit).

The usual method to derive Euler angles is to determine a set vectoral orientation with each orthogonal channel representing a particular body plane (anterior-posterior, medio-lateral and dorsal-ventral) with respect to the earth's frame of reference (Ozyagcilar 2012; Pedley 2012; Walker *et al.* 2015), and the order of these channels is pivotal for deriving correct estimates of body rotation about the three axes (Johnson & Tyack 2003 - for equations see Chapter 5). However, this assumption breaks down for animals (or attached tags) that change orientations frequently at angles greater than perpendicular from their longitudinal and lateral axes of 'normal' posture due to the singularity issues (Gimbal lock) that arise when using the Euler sequence of 3-D vector rotation (Pedley 2013). This problem can be mitigated by using a quaternion-based orientation filter (Valenti, Dryanovski & Xiao 2015; Chiella, Teixeira & Pereira 2019), however such an approach requires complex mathematical processing which may, in part, explain why Euler rotations are favoured (at least in biologging studies). I suggest that quaternion estimated heading should be compared with Euler angle-derived heading within the dead-reckoning framework, to assess the extent of error that occurs during times when the Euler sequence for determining attitude/orientation is likely to break down (e.g., during high centripetal acceleration). At the very least (when using Euler angles), inertial measurement coordinate frame adjustments of the tag frame (reflecting the body frame) relative to the Earth should be carried out (cf. Johnson & Tyack 2003) for animals that carry out $\geq 90^\circ$ body inversions (e.g., a penguin walking vs swimming).

Small discrepancies between the tag and animal body coordinate frames are not as vital to correct for deriving heading since the tilt-compensated compass only concerns the attitude of the tag relative to the Earth so any required heading offset between the tag and animal's body frame can be subsequently applied. In fact, consistent biases in tag heading are easily corrected for within the VP corrected dead-reckoning framework, with the difference in heading from true North between consecutive VPs and corresponding dead-reckoned positions being applied as the heading correction factor. However, there is no straight-forward solution to correcting heading from tags that move independently of the body (e.g., through partial dislodgment).

Animals that undertake long migrations can be subject to variations in the strength and declination of magnetic fields and this can be difficult to account for, because the magnetometry calibration procedure (Williams *et al.* 2017), required for correcting soft and hard iron distortions (Chi, Lv & Wang 2019), is typically performed prior to deployment and is therefore only relevant according to the specific magnetic conditions of that area. Even after sufficiently calibrating magnetometry data, local changes in the magnetic field (e.g., due to the presence of ferrous material) and temperature-induced offsets (Caruso 2000; Johnson & Tyack 2003) can introduce channel bias in measured magnetism, confounding heading output. Moreover, the horizontal components of the magnetic field become small when the magnetic-field inclination angle increase towards the poles, which can also result in heading measurement error (Johnson & Tyack 2003). Lastly, heading estimates assume the animal moves in the direction of its longitudinal axis, which is not always the case (Laplanche, Marques & Thomas 2015).

VP inaccuracies and VP-corrected dead-reckoning accuracy

Data collected from tags attached to neck collars generally shows more variation in acceleration and magnetic field intensity values than data obtained from loggers deployed near an animal's Centre of Mass (CoM). This is because collars can roll independently to that of the body frame. That our net error estimates plateaued for

(collared) lions at *ca.* 10 m, with a 1 fix/30 mins VP correction rate demonstrates though, the value that VP corrected dead-reckoning can have for constructing long-term, fine-scale terrestrial movement. Indeed, across all VP correction rates, distance moved estimates alone were more consistent (and higher) when estimated between dead-reckoned positions than VPs (Fig. 2). The sharp increase that occurs in distance moved estimates (at the highest VP correction rate) stems principally from incorporating all the VP locational error (Fig. 2). Notably, the temporal sub-sampling intervals of VP correction were not always exact because fix success can fail for periods longer than the set VP correction rate (e.g., during submersion in water) (Costa *et al.* 2010). As such, I advocate that the VP correction rate should not be treated literally between species with the number and regularity of VP correction generally lower for aquatic animals per set VP sampling rate. Indeed, dead-reckoned distance moved estimates were generally much higher than the equivalent VP distance in aquatic and flying species. This is because VPs can fail for extended periods while dead-reckoning is continuous.

It is worth reemphasizing that across all travel media, dead-reckoning accuracy as assessed *via* net error must not be taken literally (particularly at high VP correction rates), since VP error can also be appreciable (cf. Fig. 4, Fig. S2), whilst net error does not account for inaccuracies between VPs (cf. Fig. 7) and extremely high values at single points in time (likely due to VP error) may increase overall net error estimates (cf. Fig. 3). Only including fixes where genuine travelling movement occurred (e.g., as assessed from motion sensor data) can help remove GPS error that occurs when animals are stationary or extremely slow-moving (e.g., tortoises) where the disparity between VP error and genuine travelling movement become disentangled (even at low VP correction rates).

Deciding drift correction rates

The specific number of VPs that are required to drift correct are obviously species-specific and there are many confounds to this process that we outline above, including user-defined track-scaling and initial VP screening, that will change on a case-by-case basis. The scenarios outlined above should provide a general idea of the

required correction rates for the resolution that is required in aerial, aquatic and terrestrial domains. In essence, we suggest that VP correction should be undertaken as little as possible, but as much that is required. For investigating highly defined scales of movement (for example here, lion-fence boundary interactions or penguin navigation strategies on land) then 1 fix/15 mins or more may be required - particularly during highly dynamic and tortuous movements when net error is generally greatest (cf. Fig. S2) and when speed estimates may be unreliable (cf. Fig. 7). For longer-term studies (e.g., weeks to months) general movement networks and distance moved estimates, where net errors of *ca.* two hundred metres, may be deemed reasonable definition for the questions being asked, much lower VP correction rates could be used to preserve battery life, allowing animals to carry smaller tags. Importantly, even when high VP correction rate is possible (e.g., ≥ 0.1 Hz), corrections should only be carried out at times of genuine traveling movement, whereby distance moved between VPs exceeds the positional error radius stemming from the precision of their measurement.

The utility of dead-reckoning

The vast majority of animal tag studies investigating space-use have done so subject to the resolution of the VP system utilised (typically GPS), something that has generally resulted in low-aspect ratio location-based point density (cf. Fleming & Calabrese 2017) or diffusive straight-line movements (cf. Edelhoff, Signer & Balkenhol 2016). VP corrected dead-reckoning provides a means to incorporate all the various scales and directions of movement between VPs (rather than just linear interpolation (Poulin, Clermont & Berteaux 2021)) and thus has the capacity to map out movement patterns to a hitherto-unrealized degree (Dewhirst *et al.* 2016). Such expansion of the resolution of animal space-use into fine-scale, uninterrupted movement path networks can enhance insight into a number of fundamental concepts considered important in structuring movement paths and space-use by animals, including energy landscapes (Shepard *et al.* 2013), landscapes of fear (Gallagher *et al.* 2017) and accident landscapes (Wheatley *et al.* 2021). VP corrected dead-reckoning has particular relevance for marine underwater studies because 3-D movement can be

reconstructed (Wilson *et al.* 2007; Laplanche, Marques & Thomas 2015) at times when VPs cannot be obtained (Costa *et al.* 2010) (e.g., Fig. 6).

The immediate benefits of using VP corrected dead-reckoning are:

1. That it can reconstruct continuous, fine-scale 2-/3-D movement paths, irrespective of the environment and at higher resolution than any VP system (Bidder *et al.* 2015; Chapter 5)
2. That it provides a means to reduce the recording frequency of GPS locations, thus extending battery life and/or reducing deployment bulk/weight (Dewhirst *et al.* 2016)
3. That it prevents/limits positional noise ('jitter') of 'high-res' (e.g., ≥ 1 Hz) GPS datasets, which is most apparent during non-moving behaviours such as rest and in highly heterogenous environments where radio signal can be easily obstructed (*cf.* Ryan *et al.* 2004; Chapter 4)

In particular, the scales of tortuosity exhibited between VPs, as defined with VP corrected dead-reckoning, irrespective of the drift from true location (net error), can highlight behaviours that VPs alone cannot. For example, I demonstrate here that circling behaviour (Narazaki *et al.* 2021) can easily be distinguished in dead-reckoned tracks from tropicbirds (Fig. 5), even when the circling duration is as low as 10 s. VP corrected dead-reckoning can also greatly improve the accuracy of space-use estimates by limiting the inclusion of positional noise *via* advancing travel vectors and carrying out VP correction only at times when the animal is determined to be travelling (English *et al.* (in review)). In fact, we believe that a particular value of VP corrected dead-reckoning, is that it will provide important detail about the effects of humans and anthropogenic landscape features on animal movements, a topic that is increasingly germane (Rahel & McLaughlin 2018; Tucker *et al.* 2018; Suraci *et al.* 2019). For example, understanding the extent of the permeability of anthropogenic barriers (e.g., fences, roads) and the hazards that they pose to specific animals (Foley *et al.* 2017; Shi *et al.* 2018; Xu *et al.* 2021) is key to proper livestock and wildlife management (Hooten *et al.* 2017; Katzner & Arlettaz 2020; Chung, Lee & Lee 2021; Li *et al.* 2021). My work demonstrates that this approach details the intricacies of

animal-barrier interactions, including the locations of barrier transgression as well as movement paths pre-, during and post- barrier transgression. Moreover, VP corrected dead-reckoning should also elucidate animal foraging- and predator avoidance strategies as well as provide vital information that will help us understand how animals respond to, and navigate through (air/tidal) current flows (Chapman *et al.* 2011). Beyond this, dead-reckoning has been demonstrated to have high welfare value in zoos, by enabling continuous assessments of enclosure space-use relative to enrichment regimes and the possible occurrence of stereotypical behaviours such as pacing (English *et al.* (in review)).

Importantly, this approach has implications for informing conservation management. For instance, the impacts of free-ranging forest elephants depend largely on what they are doing at very specific localities (Ngene *et al.* 2010; Mills *et al.* 2018). At present, GPS is mostly used to reflect on where elephants move as a general response to the availability of resources such as food, water and safety (e.g., Blake, Douglas-Hamilton & Karesh 2001; Ott & Aarde 2010; Mills *et al.* 2018). Drift-corrected dead-reckoning can highlight the specifics of behaviours and localities, and therefore, for example, allow researchers to retrace elephant movements to determine what elephants feed on and where they do it, which has obvious management value. Lastly, alongside capturing under-water movements, dead-reckoning may prove effective for elucidating movement-specific behaviours in other habitats that have poor signal reception, such as within caves and burrows.

Key considerations governing the relationship between VP correction rate and dead-reckoning accuracy

To improve VP-corrected dead-reckoning estimates (assuming the accelerometer-magnetometer Euler angle approach) the minimum pre-routine should consider the following:

- 1) Screening for, and removal of, erroneous VP estimates
- 2) A suitable magnetometer calibration (Vitali 2016; Williams *et al.* 2017) with correction of acceleration and magnetometry data for any discrepancies between the tag coordinate frame and body coordinate frame, relative to the

Earth's fixed frame of reference (e.g., by visually taking note of the deployment angle offset and derotating using rotation matrices as outlined in Johnson & Tyack 2003)

- 3) Application of any required magnetic declination offsets (and approximate yaw offset if step 2 was not carried out)
- 4) Computation of suitable estimates of speed (possibly modulated according to identified behaviour and/or terrain type)
- 5) Integration of external current flow vectors where appropriate (and when reasonably modelled/measured)
- 6) Post-examination of dead-reckoned tracks (both pre- and post-VP correction), relative to VPs, visually to examine and readjust aspects of the initial track scaling.

Further advances could include additional limb-borne logger deployments that may decipher limb stride frequency *via* clearer stylised patterns of inertial measurement (Radeski & Ilijeski 2017; Wilson *et al.* 2018; Whitford & Klimley 2019). Such counts per unit time, may themselves be used as a speed proxy (*cf.* Chapter 5). Whilst not covered here, investigation of extremely high or biased distance (speed) and heading correction factors may be used to aid in identifying inaccuracies originating from tag performance (heading, speed and/or VP inaccuracy). Very low distance correction factors (< 1) either indicate inaccurately identified bouts of travelling movement or supplying inaccurately high-speed estimates. On the other hand, very high distance correction factors (> 1) again, could indicate inaccurately identified bouts of travelling movement, or supplying inaccurately low-speed estimates or, the most likely cause is due to VP error. Consistency in the direction of heading correction factors either indicate a yaw offset of the tag relative to the animal's coordinate frame, a hard iron offset in magnetic data (or a required summation of the magnetic declination), or due to external current flow drift.

Generally, the factors that affect dead-reckoning and VP accuracy are illustrated in Fig. 9, with the level of obtainable dead-reckoning accuracy depending on the user-defined initial track scaling, VP screening and the study species.

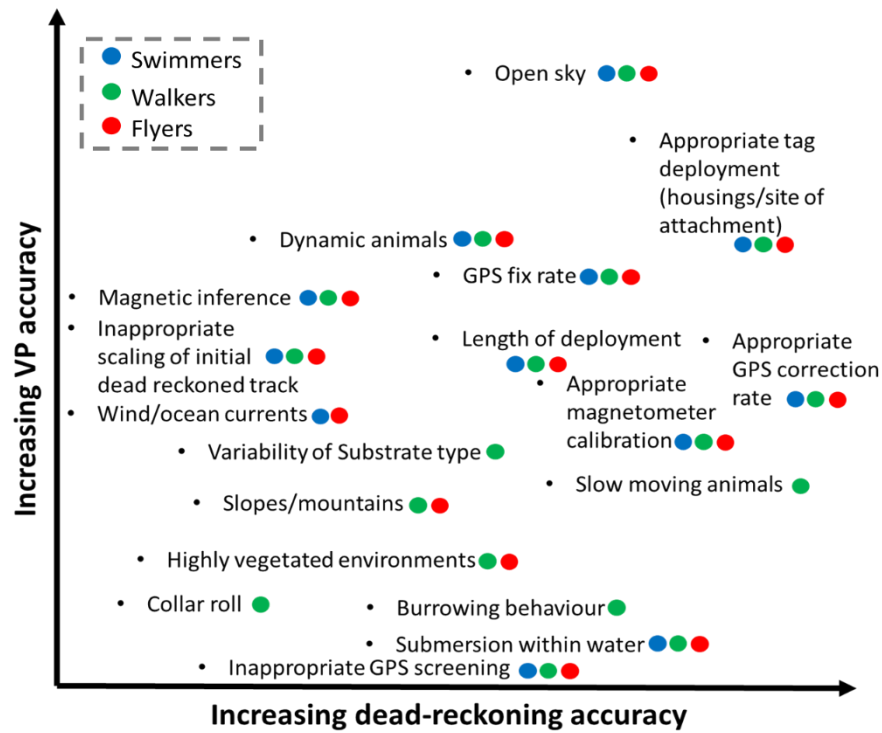


Figure 9. Schematic diagram to illustrate the various elements that modulate VP and VP corrected dead-reckoning accuracy. Black dots illustrate the element's graphical position.

Conclusion

Combining dead-reckoning and VPs (specifically, GPS) produces an extraordinarily powerful method for looking at animal movement. Under ideal conditions, VP-corrected dead-reckoning can enhance the resolution of animal movement from diffusive area-use to high resolution animal pathways. I have highlighted the main sources of inaccuracy within the dead-reckoning framework and considered the implications of such error across a diverse group of animals using different modes of movement and operating in the three main media. A major improvement to this approach necessitates accurate speed estimates (particularly in fluid media). Further work could build on these fundamentals and investigate the utility of VP-corrected dead-reckoning across a suite of animals and environments. Appropriate sharing of finding would provide a repository of species-specific rules for assessing movement-specific behaviours, VP inaccuracy, speed allocation and heading computation for the community to benefit from maximum resolution of animal movement.

References

- Altyntay, K., Khan Mohammed, A., Marengo, M., Swanepoel, L., Przybysz, A., Muller, C., Fahlman, A., Buttner, U., Geraldini, N.R., Wilson, R.P., Duarte, C.M. & Kosel, J. (2019) Wearable multifunctional printed graphene sensors. *NPJ Flexible Electronics*, **3**.
- Andrzejczek, S., Gleiss, A.C., Lear, K.O., Pattiaratchi, C.B., Chapple, T.K. & Meekan, M.G. (2019) Biologging Tags Reveal Links Between Fine-Scale Horizontal and Vertical Movement Behaviors in Tiger Sharks (*Galeocerdo cuvier*). *Frontiers in Marine Science*, **6**.
- Andrzejczek, S., Gleiss, A.C., Pattiaratchi, C.B. & Meekan, M.G. (2018) First Insights Into the Fine-Scale Movements of the Sandbar Shark, *Carcharhinus plumbeus*. *Frontiers in Marine Science*, **5**.
- Barwick, J., Lamb, D.W., Dobos, R., Welch, M. & Trotter, M. (2018) Categorising sheep activity using a tri-axial accelerometer. *Computers and Electronics in Agriculture*, **145**, 289-297.
- Benhamou, S. (2004) How to reliably estimate the tortuosity of an animal's path:: straightness, sinuosity, or fractal dimension? *Journal of Theoretical Biology*, **229**, 209-220.
- Bidder, O.R., Qasem, L.A. & Wilson, R.P. (2012) On Higher Ground: How Well Can Dynamic Body Acceleration Determine Speed in Variable Terrain? *PLOS ONE*, **7**, e50556.
- Bidder, O.R., Soresina, M., Shepard, E.L.C., Halsey, L.G., Quintana, F., Gómez-Laich, A. & Wilson, R.P. (2012) The need for speed: testing acceleration for estimating animal travel rates in terrestrial dead-reckoning systems. *Zoology*, **115**, 58-64.
- Bidder, O.R., Walker, J.S., Jones, M.W., Holton, M.D., Urge, P., Scantlebury, D.M., Marks, N.J., Magowan, E.A., Maguire, I.E. & Wilson, R.P. (2015) Step by step: reconstruction of terrestrial animal movement paths by dead-reckoning. *Movement Ecology*, **3**, 23.
- Blake, S., Douglas-Hamilton, I. & Karesh, W.B. (2001) GPS telemetry of forest elephants in Central Africa: results of a preliminary study. *African Journal of Ecology*, **39**, 178-186.
- Bouvet, D. & Garcia, G. (2000) GPS latency identification by Kalman filtering. *Robotica*, **18**, 475-485.
- Brown, D.D., Kays, R., Wikelski, M., Wilson, R. & Klimley, A.P. (2013) Observing the unwatchable through acceleration logging of animal behavior. *Animal Biotelemetry*, **1**, 20.
- Browning, E., Bolton, M., Owen, E., Shoji, A., Guilford, T. & Freeman, R. (2018) Predicting animal behaviour using deep learning: GPS data alone accurately predict diving in seabirds. *Methods in Ecology and Evolution*, **9**, 681-692.
- Cagnacci, F., Boitani, L., Powell, R.A. & Boyce, M.S. (2010) Animal ecology meets GPS-based radiotelemetry: a perfect storm of opportunities and challenges. *Philosophical Transactions of the Royal Society B: Biological Sciences*, **365**, 2157-2162.
- Campbell, H.A., Watts, M.E., Dwyer, R.G. & Franklin, C.E. (2012) V-Track: software for analysing and visualising animal movement from acoustic telemetry detections. *Marine and Freshwater Research*, **63**, 815-820.
- Caruso, M.J. (2000) Applications of magnetic sensors for low cost compass systems. *IEEE 2000. Position Location and Navigation Symposium (Cat. No.00CH37062)*, pp. 177-184.
- Chapman, Jason W., Klaassen, Raymond H.G., Drake, V.A., Fossette, S., Hays, Graeme C., Metcalfe, Julian D., Reynolds, Andrew M., Reynolds, Don R. & Alerstam, T. (2011) Animal Orientation Strategies for Movement in Flows. *Current Biology*, **21**, R861-R870.

- Chi, C., Lv, J.-W. & Wang, D. (2019) Calibration of triaxial magnetometer with ellipsoid fitting method. *IOP Conference Series: Earth and Environmental Science*, **237**, 032015.
- Chiella, A.C.B., Teixeira, B.O.S. & Pereira, G.A.S. (2019) Quaternion-Based Robust Attitude Estimation Using an Adaptive Unscented Kalman Filter. *Sensors*, **19**, 2372.
- Chopde, N.R. & Nichat, M.K. (2013) Landmark based shortest path detection by using A* and Haversine formula. *International Journal of Innovative Research in Computer and Communication Engineering*, **1**, 298-302.
- Chung, H., Lee, J. & Lee, W.Y. (2021) A Review: Marine Bio-logging of Animal Behaviour and Ocean Environments. *Ocean Science Journal*.
- Constandache, I., Bao, X., Azizyan, M. & Choudhury, R.R. (2010) Did you see Bob? human localization using mobile phones. *Proceedings of the sixteenth annual international conference on Mobile computing and networking*, pp. 149–160. Association for Computing Machinery, Chicago, Illinois, USA.
- Costa, D.P., Robinson, P.W., Arnould, J.P.Y., Harrison, A.-L., Simmons, S.E., Hassrick, J.L., Hoskins, A.J., Kirkman, S.P., Oosthuizen, H., Villegas-Amtmann, S. & Crocker, D.E. (2010) Accuracy of ARGOS Locations of Pinnipeds at-Sea Estimated Using Fastloc GPS. *PLOS ONE*, **5**, e8677.
- Cotter, C.H. (1978) Early Dead Reckoning Navigation. *Journal of Navigation*, **31**, 20-28.
- Coulombe, M.L., Massé, A. & Côté, S.D. (2006) Quantification and Accuracy of Activity Data Measured with VHF and GPS Telemetry. *Wildlife Society Bulletin*, **34**, 81-92.
- D'eon, R.G. & Delparte, D. (2005) Effects of radio-collar position and orientation on GPS radio-collar performance, and the implications of PDOP in data screening. *Journal of Applied Ecology*, **42**, 383-388.
- den Uijl, I., Gómez Álvarez, C.B., Bartram, D., Dror, Y., Holland, R. & Cook, A. (2017) External validation of a collar-mounted triaxial accelerometer for second-by-second monitoring of eight behavioural states in dogs. *PLOS ONE*, **12**, e0188481.
- Dewhirst, O.P., Evans, H.K., Roskilly, K., Harvey, R.J., Hubel, T.Y. & Wilson, A.M. (2016) Improving the accuracy of estimates of animal path and travel distance using GPS drift-corrected dead reckoning. *Ecology and Evolution*, **6**, 6210-6222.
- Edelhoff, H., Signer, J. & Balkenhol, N. (2016) Path segmentation for beginners: an overview of current methods for detecting changes in animal movement patterns. *Movement Ecology*, **4**, 21.
- English, H.M., Harvey, L., Wilson, R.P., Gunner, R.M., Holton, M.D., Woodroffe, R. & Börger, L. ((in review)) Multi-sensor biologgers and innovative training allow data collection with high conservation and welfare value in zoos. *Journal of Zoo and Aquarium Research*.
- Everaert, J. (2014) Collision risk and micro-avoidance rates of birds with wind turbines in Flanders. *Bird Study*, **61**, 220-230.
- Farrell, J., Djodat, M., Barth, M. & Grewal, M. (1997) Latency Compensation for Differential GPS. *NAVIGATION*, **44**, 99-107.
- Feng, T. & Timmermans, H.J.P. (2013) Transportation mode recognition using GPS and accelerometer data. *Transportation Research Part C: Emerging Technologies*, **37**, 118-130.
- Fischer, C., Muthukrishnan, K., Hazas, M. & Gellersen, H. (2008) Ultrasound-aided pedestrian dead reckoning for indoor navigation. *Proceedings of the first ACM international workshop on Mobile entity localization and tracking in GPS-less environments*, pp. 31–36. Association for Computing Machinery, San Francisco, California, USA.

- Fleming, C.H. & Calabrese, J.M. (2017) A new kernel density estimator for accurate home-range and species-range area estimation. *Methods in Ecology and Evolution*, **8**, 571-579.
- Foley, A.M., Goolsby, J.A., Ortega-S, A., Ortega-S, J.A., Pérez de León, A., Singh, N.K., Schwartz, A., Ellis, D., Hewitt, D.G. & Campbell, T.A. (2017) Movement patterns of nilgai antelope in South Texas: Implications for cattle fever tick management. *Preventive Veterinary Medicine*, **146**, 166-172.
- Fong, W.T., Ong, S.K. & Nee, A.Y.C. (2008) Methods for in-field user calibration of an inertial measurement unit without external equipment. *Measurement Science and Technology*, **19**, 085202.
- Forin-Wiart, M.-A., Hubert, P., Sirguy, P. & Poulle, M.-L. (2015) Performance and Accuracy of Lightweight and Low-Cost GPS Data Loggers According to Antenna Positions, Fix Intervals, Habitats and Animal Movements. *PLOS ONE*, **10**, e0129271.
- Fortin, D., Beyer, H.L., Boyce, M.S., Smith, D.W., Duchesne, T. & Mao, J.S. (2005) Wolves influence elk movements: behavior shapes a trophic cascade in Yellowstone National Park. *Ecology*, **86**, 1320-1330.
- Fourati, H., Manamanni, N., Afilal, L. & Handrich, Y. (2011) Posture and body acceleration tracking by inertial and magnetic sensing: Application in behavioral analysis of free-ranging animals. *Biomedical Signal Processing and Control*, **6**, 94-104.
- Frair, J.L., Fieberg, J., Hebblewhite, M., Cagnacci, F., DeCesare, N.J. & Pedrotti, L. (2010) Resolving issues of imprecise and habitat-biased locations in ecological analyses using GPS telemetry data. *Philosophical Transactions of the Royal Society B: Biological Sciences*, **365**, 2187-2200.
- Gallagher, A.J., Creel, S., Wilson, R.P. & Cooke, S.J. (2017) Energy Landscapes and the Landscape of Fear. *Trends in Ecology & Evolution*, **32**, 88-96.
- Garde, B., Fell, A., Lempidakis, E., de Grissac, S., Gunner, R.M., Tatayah, V., Cole, N.C. & Shepard, E.L.C. ((in review)) Ar density drives flight costs in a tropical seabird, suggesting additional impacts of rising temperatures. *Journal of Animal Ecology*.
- Gleiss, A.C., Wilson, R.P. & Shepard, E.L.C. (2011) Making overall dynamic body acceleration work: on the theory of acceleration as a proxy for energy expenditure. *Methods in Ecology and Evolution*, **2**, 23-33.
- Graf, P.M., Wilson, R.P., Qasem, L., Hackländer, K. & Rosell, F. (2015) The Use of Acceleration to Code for Animal Behaviours; A Case Study in Free-Ranging Eurasian Beavers *Castor fiber*. *PLOS ONE*, **10**, e0136751.
- Grygorenko, V. (2011) Sensing-magnetic compass with tilt compensation. *Cypress Perform, Semiconductor Application Notes*, **AN2272**.
- Halsey, L.G., Shepard, E.L.C., Hulston, C.J., VENABLES, M.C., White, C.R., Jeukendrup, A.E. & Wilson, R.P. (2008) Acceleration versus heart rate for estimating energy expenditure and speed during locomotion in animals: Tests with an easy model species, *Homo sapiens*. *Zoology*, **111**, 231-241.
- Harel, R., Duriez, O., Spiegel, O., Fluhr, J., Horvitz, N., Getz, W.M., Bouten, W., Sarrazin, F., Hatzofe, O. & Nathan, R. (2016) Decision-making by a soaring bird: time, energy and risk considerations at different spatio-temporal scales. *Philosophical Transactions of the Royal Society B: Biological Sciences*, **371**, 20150397.
- Henderson, T., Vernes, K., Körtner, G. & Rajaratnam, R. (2018) Using GPS Technology to Understand Spatial and Temporal Activity of Kangaroos in a Peri-Urban Environment. *Animals*, **8**, 97.
- Hofman, M.P.G., Hayward, M.W., Heim, M., Marchand, P., Rolandsen, C.M., Mattisson, J., Urbano, F., Heurich, M., Mysterud, A., Melzheimer, J., Morellet, N., Voigt, U., Allen, B.L., Gehr, B., Rouco, C., Ullmann, W., Holand, Ø., Jørgensen, N.H., Steinheim, G., Cagnacci, F., Kroeschel, M., Kaczensky, P., Buuveibaatar, B., Payne, J.C., Palmegiani,

- I., Jerina, K., Kjellander, P., Johansson, Ö., LaPoint, S., Bayrakcismith, R., Linnell, J.D.C., Zaccaroni, M., Jorge, M.L.S., Oshima, J.E.F., Songhurst, A., Fischer, C., Mc Bride, R.T., Jr., Thompson, J.J., Streif, S., Sandfort, R., Bonenfant, C., Drouilly, M., Klapproth, M., Zinner, D., Yarnell, R., Stronza, A., Wilmott, L., Meisingset, E., Thaker, M., Vanak, A.T., Nicoloso, S., Graeber, R., Said, S., Boudreau, M.R., Devlin, A., Hoogesteijn, R., May-Junior, J.A., Nifong, J.C., Odden, J., Quigley, H.B., Tortato, F., Parker, D.M., Caso, A., Perrine, J., Tellaeche, C., Zieba, F., Zwijacz-Kozica, T., Appel, C.L., Axsom, I., Bean, W.T., Cristescu, B., Périquet, S., Teichman, K.J., Karpanty, S., Licoppe, A., Menges, V., Black, K., Scheppers, T.L., Schai-Braun, S.C., Azevedo, F.C., Lemos, F.G., Payne, A., Swanepoel, L.H., Weckworth, B.V., Berger, A., Bertassoni, A., McCulloch, G., Šustr, P., Athreya, V., Bockmuhl, D., Casaer, J., Ekori, A., Melovski, D., Richard-Hansen, C., van de Vyver, D., Reyna-Hurtado, R., Robardet, E., Selva, N., Sergiel, A., Farhadinia, M.S., Sunde, P., Portas, R., Ambarli, H., Berzins, R., Kappeler, P.M., Mann, G.K., Pyritz, L., Bissett, C., Grant, T., Steinmetz, R., Swedell, L., Welch, R.J., Armenteras, D., Bidder, O.R., González, T.M., Rosenblatt, A., Kachel, S. & Balkenhol, N. (2019) Right on track? Performance of satellite telemetry in terrestrial wildlife research. *PLOS ONE*, **14**, e0216223.
- Hooten, M.B., Johnson, D.S., McClintock, B.T. & Morales, J.M. (2017) *Animal Movement: Statistical Models for Telemetry Data*. CRC Press.
- Hubel, T.Y., Golabek, K.A., Rafiq, K., McNutt, J.W. & Wilson, A.M. (2018) Movement patterns and athletic performance of leopards in the Okavango Delta. *Proceedings of the Royal Society B: Biological Sciences*, **285**, 20172622.
- Hughey, L.F., Hein, A.M., Strandburg-Peshkin, A. & Jensen, F.H. (2018) Challenges and solutions for studying collective animal behaviour in the wild. *Philosophical Transactions of the Royal Society B: Biological Sciences*, **373**, 20170005.
- Ironside, K.E., Mattson, D.J., Arundel, T.R. & Hansen, J.R. (2017) Is GPS telemetry location error screening beneficial? *Wildlife Biology*, **2017**.
- Johnson, M.P. & Tyack, P.L. (2003) A digital acoustic recording tag for measuring the response of wild marine mammals to sound. *IEEE Journal of Oceanic Engineering*, **28**, 3-12.
- Katzner, T.E. & Arlettaz, R. (2020) Evaluating Contributions of Recent Tracking-Based Animal Movement Ecology to Conservation Management. *Frontiers in Ecology and Evolution*, **7**.
- Kay, W.P., Naumann, D.S., Bowen, H.J., Withers, S.J., Evans, B.J., Wilson, R.P., Stringell, T.B., Bull, J.C., Hopkins, P.W. & Börger, L. (2019) Minimizing the impact of biologging devices: Using computational fluid dynamics for optimizing tag design and positioning. *Methods in Ecology and Evolution*, **10**, 1222-1233.
- Kerdok, A.E., Biewener, A.A., McMahon, T.A., Weyand, P.G. & Herr, H.M. (2002) Energetics and mechanics of human running on surfaces of different stiffnesses. *Journal of Applied Physiology*, **92**, 469-478.
- Kreye, J. (2003) Messung der Schwimmgeschwindigkeit und deren Konsequenzen für luftatmende marine Vertebraten. Diplom-Biologen, Universität des Saarlandes, Saarbrücken.
- Krop-Benesch, A., Berger, A., Hofer, H. & Heurich, M. (2013) Long-term measurement of roe deer (*Capreolus capreolus*) (Mammalia: Cervidae) activity using two-axis accelerometers in GPS-collars. *Italian Journal of Zoology*, **80**, 69-81.
- Laplanche, C., Marques, T.A. & Thomas, L. (2015) Tracking marine mammals in 3D using electronic tag data. *Methods in Ecology and Evolution*, **6**, 987-996.
- Latham, A.D.M., Latham, M.C., Anderson, D.P., Cruz, J., Herries, D. & Hebblewhite, M. (2015) The GPS craze: six questions to address before deciding to deploy GPS technology on wildlife. *New Zealand Journal of Ecology*, **39**, 143-152.

- Lempidakis, E., Ross, A.N., Börger, L. & Shepard, E.L. (2021) Airflow modelling predicts seabird breeding habitat across islands. *Authorea Preprints*.
- Lempidakis, E., Wilson, R.P., Luckman, A. & Metcalfe, R.S. (2018) What can knowledge of the energy landscape tell us about animal movement trajectories and space use? A case study with humans. *Journal of Theoretical Biology*, **457**, 101-111.
- Lewis, J.S., Rachlow, J.L., Garton, E.O. & Vierling, L.A. (2007) Effects of habitat on GPS collar performance: using data screening to reduce location error. *Journal of Applied Ecology*, **44**, 663-671.
- Li, W., Bakker, J.D., Li, Y., Zheng, S. & Li, F.Y. (2021) Applying a high-precision tracking system to distinguish the spatiotemporal patterns of animal movement in grassland ecology. *Biological Conservation*, **255**, 109016.
- Marcus Rowcliffe, J., Carbone, C., Kays, R., Kranstauber, B. & Jansen, P.A. (2012) Bias in estimating animal travel distance: the effect of sampling frequency. *Methods in Ecology and Evolution*, **3**, 653-662.
- Martín López, L.M., Aguilar de Soto, N., Miller, P. & Johnson, M. (2016) Tracking the kinematics of caudal-oscillatory swimming: a comparison of two on-animal sensing methods. *The Journal of Experimental Biology*, **219**, 2103-2109.
- McDuie, F., Casazza, M.L., Overton, C.T., Herzog, M.P., Hartman, C.A., Peterson, S.H., Feldheim, C.L. & Ackerman, J.T. (2019) GPS tracking data reveals daily spatio-temporal movement patterns of waterfowl. *Movement Ecology*, **7**, 6.
- McNarry, M.A., Wilson, R.P., Holton, M.D., Griffiths, I.W. & Mackintosh, K.A. (2017) Investigating the relationship between energy expenditure, walking speed and angle of turning in humans. *PLOS ONE*, **12**, e0182333.
- Mills, E.C., Poulsen, J.R., Fay, J.M., Morkel, P., Clark, C.J., Meier, A., Beirne, C. & White, L.J.T. (2018) Forest elephant movement and habitat use in a tropical forest-grassland mosaic in Gabon. *PLOS ONE*, **13**, e0199387.
- Mills, K.J., Patterson, B.R. & Murray, D.L. (2006) Effects of Variable Sampling Frequencies on GPS Transmitter Efficiency and Estimated Wolf Home Range Size and Movement Distance. *Wildlife Society Bulletin*, **34**, 1463-1469.
- Mitani, Y., Watanabe, Y., Sato, K., Cameron, M.F. & Naito, Y. (2004) 3D diving behavior of Weddell seals with respect to prey accessibility and abundance. *Marine Ecology Progress Series*, **281**, 275-281.
- Miwa, M., Oishi, K., Nakagawa, Y., Maeno, H., Anzai, H., Kumagai, H., Okano, K., Tobioka, H. & Hirooka, H. (2015) Application of Overall Dynamic Body Acceleration as a Proxy for Estimating the Energy Expenditure of Grazing Farm Animals: Relationship with Heart Rate. *PLOS ONE*, **10**, e0128042.
- Morales, J.M., Haydon, D.T., Frair, J., Holsinger, K.E. & Fryxell, J.M. (2004) Extracting more out of relocation data: building movement models as mixtures of random walks. *Ecology*, **85**, 2436-2445.
- Morales, J.M., Moorcroft, P.R., Matthiopoulos, J., Frair, J.L., Kie, J.G., Powell, R.A., Merrill, E.H. & Haydon, D.T. (2010) Building the bridge between animal movement and population dynamics. *Philosophical Transactions of the Royal Society B: Biological Sciences*, **365**, 2289-2301.
- Narazaki, T., Nakamura, I., Aoki, K., Iwata, T., Shiomi, K., Luschi, P., Suganuma, H., Meyer, C.G., Matsumoto, R., Bost, C.A., Handrich, Y., Amano, M., Okamoto, R., Mori, K., Ciccione, S., Bourjea, J. & Sato, K. (2021) Similar circling movements observed across marine megafauna taxa. *iScience*, 102221.
- Ngene, S.M., Van Gils, H., Van Wieren, S.E., Rasmussen, H., Skidmore, A.K., Prins, H.H.T., Toxopeus, A.G., Omondi, P. & Douglas-Hamilton, I. (2010) The ranging patterns of elephants in Marsabit protected area, Kenya: the use of satellite-linked GPS collars. *African Journal of Ecology*, **48**, 386-400.

- Noda, T., Kawabata, Y., Arai, N., Mitamura, H. & Watanabe, S. (2014) Animal-mounted gyroscope/accelerometer/magnetometer: In situ measurement of the movement performance of fast-start behaviour in fish. *Journal of Experimental Marine Biology and Ecology*, **451**, 55-68.
- Noda, T., Okuyama, J., Koizumi, T., Arai, N. & Kobayashi, M. (2012) Monitoring attitude and dynamic acceleration of free-moving aquatic animals using a gyroscope. *Aquatic Biology*, **16**, 265-276.
- Ott, T. & Aarde, R.J.v. (2010) Inferred Spatial use by Elephants is Robust to Landscape Effects on GPS Telemetry. *South African Journal of Wildlife Research*, **40**, 130-138, 139.
- Ozyagcilar, T. (2012) Implementing a tilt-compensated eCompass using accelerometer and magnetometer sensors. *Freescale semiconductor, Application Note, AN4248*, Austin, TX.
- Panzacchi, M., Van Moorter, B., Strand, O., Saerens, M., Kivimäki, I., St. Clair, C.C., Herfindal, I. & Boitani, L. (2016) Predicting the continuum between corridors and barriers to animal movements using Step Selection Functions and Randomized Shortest Paths. *Journal of Animal Ecology*, **85**, 32-42.
- Park, S., Aschenbach, K.H., Ahmed, M., Scott, W.L., Leonard, N.E., Abernathy, K., Marshall, G., Shepard, M. & Martins, N.C. (2019) Animal-borne wireless network: Remote imaging of community ecology. *Journal of Field Robotics*, **36**, 1141-1165.
- Pedley, M. (2012) eCompass-Build and Calibrate a Tilt-Compensating Electronic Compass. *Circuit Cellar-The Magazine For Computer Applications*, 1-6.
- Pedley, M. (2013) Tilt sensing using a three-axis accelerometer. *Freescale semiconductor. Application Note 2461*, **1**, 1-22.
- Peng, J., Peng, S., Jiang, A., Wei, J., Li, C. & Tan, J. (2010) Asymmetric least squares for multiple spectra baseline correction. *Analytica Chimica Acta*, **683**, 63-68.
- Pewsey, A., Neuhäuser, M. & Ruxton, G.D. (2013) *Circular Statistics in R*. OUP Oxford.
- Poulin, M.-P., Clermont, J. & Berteaux, D. (2021) Extensive daily movement rates measured in territorial arctic foxes. *Ecology and Evolution*, **00**, 1- 12.
- Qasem, L., Cardew, A., Wilson, A., Griffiths, I., Halsey, L.G., Shepard, E.L.C., Gleiss, A.C. & Wilson, R. (2012) Tri-Axial Dynamic Acceleration as a Proxy for Animal Energy Expenditure; Should We Be Summing Values or Calculating the Vector? *PLOS ONE*, **7**, e31187.
- Radeski, M. & Ilieski, V. (2017) Gait and posture discrimination in sheep using a tri-axial accelerometer. *Animal*, **11**, 1249-1257.
- Rahel, F.J. & McLaughlin, R.L. (2018) Selective fragmentation and the management of fish movement across anthropogenic barriers. *Ecological Applications*, **28**, 2066-2081.
- Rong, L., Zhiguo, D., Jianzhong, Z. & Ming, L. (2007) Identification of Individual Walking Patterns Using Gait Acceleration. *2007 1st International Conference on Bioinformatics and Biomedical Engineering*, pp. 543-546.
- Ropert-Coudert, Y., Kato, A., Baudat, J., Bost, C.-A., Le Maho, Y. & Naito, Y. (2001) Time/depth usage of Adélie penguins: an approach based on dive angles. *Polar Biology*, **24**, 467-470.
- Ryan, P.G., Petersen, S.L., Peters, G. & Grémillet, D. (2004) GPS tracking a marine predator: the effects of precision, resolution and sampling rate on foraging tracks of African Penguins. *Marine Biology*, **145**, 215-223.
- Rydell, J., Bach, L., Dubourg-Savage, M.-J., Green, M., Rodrigues, L. & Hedenström, A. (2010) Mortality of bats at wind turbines links to nocturnal insect migration? *European Journal of Wildlife Research*, **56**, 823-827.

- Sakamoto, K.Q., Sato, K., Ishizuka, M., Watanuki, Y., Takahashi, A., Daunt, F. & Wanless, S. (2009) Can Ethograms Be Automatically Generated Using Body Acceleration Data from Free-Ranging Birds? *PLOS ONE*, **4**, e5379.
- Sato, K., Mitani, Y., Cameron, M.F., Siniff, D.B. & Naito, Y. (2003) Factors affecting stroking patterns and body angle in diving Weddell seals under natural conditions. *Journal of Experimental Biology*, **206**, 1461-1470.
- Schlägel, U.E., Signer, J., Herde, A., Eden, S., Jeltsch, F., Eccard, J.A. & Dammhahn, M. (2019) Estimating interactions between individuals from concurrent animal movements. *Methods in Ecology and Evolution*, **10**, 1234-1245.
- Seidel, D.P., Dougherty, E., Carlson, C. & Getz, W.M. (2018) Ecological metrics and methods for GPS movement data. *International Journal of Geographical Information Science*, **32**, 2272-2293.
- Sequeira, M.M., Rickenbach, M., Wietlisbach, V., Tullen, B. & Schutz, Y. (1995) Physical Activity Assessment Using a Pedometer and Its Comparison with a Questionnaire in a Large Population Survey. *American Journal of Epidemiology*, **142**, 989-999.
- Shepard, D.B., Kuhns, A.R., Dreslik, M.J. & Phillips, C.A. (2008a) Roads as barriers to animal movement in fragmented landscapes. *Animal Conservation*, **11**, 288-296.
- Shepard, E.L., Wilson, R.P., Halsey, L.G., Quintana, F., Laich, A.G., Gleiss, A.C., Liebsch, N., Myers, A.E. & Norman, B. (2008b) Derivation of body motion via appropriate smoothing of acceleration data. *Aquatic Biology*, **4**, 235-241.
- Shepard, E.L.C., Wilson, R.P., Liebsch, N., Quintana, F., Gómez-Mez Laich, A. & Lucke, K. (2008c) Flexible paddle sheds new light on speed: a novel method for the remote measurement of swim speed in aquatic animals. *Endangered Species Research*, **4**, 157-164.
- Shepard, E.L.C., Wilson, R.P., Rees, W.G., Grundy, E., Lambertucci, S.A. & Vosper, S.B. (2013) Energy Landscapes Shape Animal Movement Ecology. *The American Naturalist*, **182**, 298-312.
- Shi, H., Shi, T., Yang, Z., Wang, Z., Han, F. & Wang, C. (2018) Effect of Roads on Ecological Corridors Used for Wildlife Movement in a Natural Heritage Site. *Sustainability*, **10**, 2725.
- Shiomi, K., Sato, K., Mitamura, H., Arai, N., Naito, Y. & Ponganis, P.J. (2008) Effect of ocean current on the dead-reckoning estimation of 3-D dive paths of emperor penguins. *Aquatic Biology*, **3**, 265-270.
- Smith, M.F., Marshall, A., Correia, J.P. & Rupp, J. (2004) Elasmobranch transport techniques and equipment. *Elasmobranch husbandry manual: captive care of sharks, rays, and their relatives. Columbus: The Ohio Biological Survey. p*, 105-132.
- Suraci, J.P., Clinchy, M., Zanette, L.Y. & Wilmers, C.C. (2019) Fear of humans as apex predators has landscape-scale impacts from mountain lions to mice. *Ecology Letters*, **22**, 1578-1586.
- Swain, D.L., Wark, T. & Bishop-Hurley, G.J. (2008) Using high fix rate GPS data to determine the relationships between fix rate, prediction errors and patch selection. *Ecological Modelling*, **212**, 273-279.
- Tonini, M.H. & Palma, E.D. (2017) Tidal dynamics on the North Patagonian Argentinean Gulfs. *Estuarine, Coastal and Shelf Science*, **189**, 115-130.
- Tracey, J.A., Zhu, J., Boydston, E., Lyren, L., Fisher, R.N. & Crooks, K.R. (2013) Mapping behavioral landscapes for animal movement: a finite mixture modeling approach. *Ecological Applications*, **23**, 654-669.
- Tucker, M.A., Böhning-Gaese, K., Fagan, W.F., Fryxell, J.M., Van Moorter, B., Alberts, S.C., Ali, A.H., Allen, A.M., Attias, N., Avgar, T., Bartlam-Brooks, H., Bayarbaatar, B., Belant, J.L., Bertassoni, A., Beyer, D., Bidner, L., van Beest, F.M., Blake, S., Blaum, N., Bracis, C., Brown, D., de Bruyn, P.J.N., Cagnacci, F., Calabrese, J.M., Camilo-

- Alves, C., Chamailé-Jammes, S., Chiaradia, A., Davidson, S.C., Dennis, T., DeStefano, S., Diefenbach, D., Douglas-Hamilton, I., Fennessy, J., Fichtel, C., Fiedler, W., Fischer, C., Fischhoff, I., Fleming, C.H., Ford, A.T., Fritz, S.A., Gehr, B., Goheen, J.R., Gurarie, E., Hebblewhite, M., Heurich, M., Hewison, A.J.M., Hof, C., Hurme, E., Isbell, L.A., Janssen, R., Jeltsch, F., Kaczensky, P., Kane, A., Kappeler, P.M., Kauffman, M., Kays, R., Kimuyu, D., Koch, F., Kranstauber, B., LaPoint, S., Leimgruber, P., Linnell, J.D.C., López-López, P., Markham, A.C., Mattisson, J., Medici, E.P., Mellone, U., Merrill, E., de Miranda Mourão, G., Morato, R.G., Morellet, N., Morrison, T.A., Díaz-Muñoz, S.L., Mysterud, A., Nandintsetseg, D., Nathan, R., Niamir, A., Odden, J., O'Hara, R.B., Oliveira-Santos, L.G.R., Olson, K.A., Patterson, B.D., Cunha de Paula, R., Pedrotti, L., Reineking, B., Rimmler, M., Rogers, T.L., Rolandsen, C.M., Rosenberry, C.S., Rubenstein, D.I., Safi, K., Saïd, S., Sapir, N., Sawyer, H., Schmidt, N.M., Selva, N., Sergiel, A., Shiilegdamba, E., Silva, J.P., Singh, N., Solberg, E.J., Spiegel, O., Strand, O., Sundaresan, S., Ullmann, W., Voigt, U., Wall, J., Wattles, D., Wikelski, M., Wilmers, C.C., Wilson, J.W., Wittemyer, G., Zięba, F., Zwijacz-Kozica, T. & Mueller, T. (2018) Moving in the Anthropocene: Global reductions in terrestrial mammalian movements. *Science*, **359**, 466-469.
- Valeix, M., Loveridge, A.J., Davidson, Z., Madzikanda, H., Fritz, H. & Macdonald, D.W. (2010) How key habitat features influence large terrestrial carnivore movements: waterholes and African lions in a semi-arid savanna of north-western Zimbabwe. *Landscape Ecology*, **25**, 337-351.
- Valenti, R.G., Dryanovski, I. & Xiao, J. (2015) Keeping a good attitude: A quaternion-based orientation filter for IMUs and MARGs. *Sensors*, **15**, 19302-19330.
- Vitali, A. (2016) Ellipsoid or sphere fitting for sensor calibration, Dt0059. *ST Microelectronics, Design Tip*.
- Walker, J.S., Jones, M.W., Laramée, R.S., Holton, M.D., Shepard, E.L.C., Williams, H.J., Scantlebury, D.M., Marks, N.J., Magowan, E.A., Maguire, I.E., Bidder, O.R., Di Virgilio, A. & Wilson, R.P. (2015) Prying into the intimate secrets of animal lives; software beyond hardware for comprehensive annotation in 'Daily Diary' tags. *Movement Ecology*, **3**, 29.
- Wen, H. (2019) *Toward Inertial-Navigation-on-Chip: The Physics and Performance Scaling of Multi-Degree-of-Freedom Resonant MEMS Gyroscopes*. Springer International Publishing.
- Wensveen, P.J., Isojunno, S., Hansen, R.R., von Benda-Beckmann, A.M., Kleivane, L., van IJsselmuide, S., Lam, F.-P.A., Kvadsheim, P.H., DeRuiter, S.L., Curé, C., Narazaki, T., Tyack, P.L. & Miller, P.J.O. (2019) Northern bottlenose whales in a pristine environment respond strongly to close and distant navy sonar signals. *Proceedings of the Royal Society B: Biological Sciences*, **286**, 20182592.
- Wensveen, P.J., Thomas, L. & Miller, P.J.O. (2015) A path reconstruction method integrating dead-reckoning and position fixes applied to humpback whales. *Movement Ecology*, **3**, 31.
- Wheatley, R., Buettel, J.C., Brook, B.W., Johnson, C.N. & Wilson, R.P. (2021) Accidents alter animal fitness landscapes. *Ecology Letters*, **24**, 920-934.
- Whitford, M. & Klimley, A.P. (2019) An overview of behavioral, physiological, and environmental sensors used in animal biotelemetry and biologging studies. *Animal Biotelemetry*, **7**, 1-24.
- Wiesel, I., Karthun-Strijbos, S. & Jänecké, I. (2019) The Use of GPS Telemetry Data to Study Parturition, Den Location and Occupancy in the Brown Hyaena. *African Journal of Wildlife Research*, **49**, 1-11, 11.

- Willener, A.S.T., Handrich, Y., Halsey, L.G. & Strike, S. (2015) Effect of walking speed on the gait of king penguins: An accelerometric approach. *Journal of Theoretical Biology*, **387**, 166-173.
- Williams, H., Shepard, E., Duriez, O. & Lambertucci, S.A. (2015) Can accelerometry be used to distinguish between flight types in soaring birds? *Animal Biotelemetry*, **3**, 1-11.
- Williams, H.J., Holton, M.D., Shepard, E.L.C., Largey, N., Norman, B., Ryan, P.G., Duriez, O., Scantlebury, M., Quintana, F., Magowan, E.A., Marks, N.J., Alagaili, A.N., Bennett, N.C. & Wilson, R.P. (2017) Identification of animal movement patterns using tri-axial magnetometry. *Movement Ecology*, **5**, 6.
- Williams, H.J., Shepard, E., Holton, M.D., Alarcón, P., Wilson, R. & Lambertucci, S. (2020) Physical limits of flight performance in the heaviest soaring bird. *Proceedings of the National Academy of Sciences*, **117**, 17884-17890.
- Wilson, R. (1985) The Jackass Penguin (*Spheniscus demersus*) as a pelagic predator. *Marine Ecology Progress Series*, **25**, 219-227.
- Wilson, R.P. (1997) A method for restraining penguins. *Marine Ornithology*, **25**, 72-73.
- Wilson, R.P., Börger, L., Holton, M.D., Scantlebury, D.M., Gómez-Laich, A., Quintana, F., Rosell, F., Graf, P.M., Williams, H., Gunner, R., Hopkins, L., Marks, N., Geraldini, N.R., Duarte, C.M., Scott, R., Strano, M.S., Robotka, H., Eizaguirre, C., Fahlman, A. & Shepard, E.L.C. (2020a) Estimates for energy expenditure in free-living animals using acceleration proxies: A reappraisal. *Journal of Animal Ecology*, **89**, 161-172.
- Wilson, R.P., Holton, M.D., di Virgilio, A., Williams, H., Shepard, E.L.C., Lambertucci, S., Quintana, F., Sala, J.E., Balaji, B., Lee, E.S., Srivastava, M., Scantlebury, D.M. & Duarte, C.M. (2018) Give the machine a hand: A Boolean time-based decision-tree template for rapidly finding animal behaviours in multisensor data. *Methods in Ecology and Evolution*, **9**, 2206-2215.
- Wilson, R.P., Hustler, K., Ryan, P.G., Burger, A.E. & Noldeke, E.C. (1992) Diving birds in cold water: do Archimedes and Boyle determine energetic costs? *The American Naturalist*, **140**, 179-200.
- Wilson, R.P., Kreye, J.M., Lucke, K. & Urquhart, H. (2004) Antennae on transmitters on penguins: balancing energy budgets on the high wire. *Journal of Experimental Biology*, **207**, 2649-2662.
- Wilson, R.P., Liebsch, N., Davies, I.M., Quintana, F., Weimerskirch, H., Storch, S., Lucke, K., Siebert, U., Zankl, S., Müller, G., Zimmer, I., Scolaro, A., Campagna, C., Plötz, J., Bornemann, H., Teilmann, J. & McMahan, C.R. (2007) All at sea with animal tracks; methodological and analytical solutions for the resolution of movement. *Deep Sea Research Part II: Topical Studies in Oceanography*, **54**, 193-210.
- Wilson, R.P., McMahan, C.R., Quintana, F., Frere, E., Scolaro, A., Hays, G.C. & Bradshaw, C.J.A. (2011) N-dimensional animal energetic niches clarify behavioural options in a variable marine environment. *Journal of Experimental Biology*, **214**, 646-656.
- Wilson, R.P., Pütz, K., Peters, G., Culik, B., Scolaro, J.A., Charrassin, J.-B. & Ropert-Coudert, Y. (1997) Long-Term Attachment of Transmitting and Recording Devices to Penguins and Other Seabirds. *Wildlife Society Bulletin (1973-2006)*, **25**, 101-106.
- Wilson, R.P., Ropert-Coudert, Y. & Kato, A. (2002) Rush and grab strategies in foraging marine endotherms: the case for haste in penguins. *Animal Behaviour*, **63**, 85-95.
- Wilson, R.P., Rose, K.A., Gunner, R., Holton, M., Marks, N.J., Bennett, N.C., Bell, S.H., Twining, J.P., Hesketh, J., Duarte, C.M., Bezodis, N. & Scantlebury, D.M. (2020b) Forces experienced by instrumented animals depend on lifestyle. *bioRxiv*, 2020.2008.2020.258756.
- Wilson, R.P., Scolaro, J.A., Grémillet, D., Kierspel, M.A.M., Laurenti, S., Upton, J., Gallelli, H., Quintana, F., Frere, E., Müller, G., Straten, M.T. & Zimmer, I. (2005) How do

- Magellanic Penguins cope with variability in their access to prey? *Ecological Monographs*, **75**, 379-401.
- Wilson, R.P., Shepard, E. & Liebsch, N. (2008) Prying into the intimate details of animal lives: use of a daily diary on animals. *Endangered Species Research*, **4**, 123-137.
- Wilson, R.P., Wilson, M.-P.T., Link, R., Mempel, H. & Adams, N.J. (1991) Determination of movements of African penguins *Spheniscus demersus* using a compass system: dead reckoning may be an alternative to telemetry. *Journal of Experimental Biology*, **157**, 557-564.
- Wilson, R.P. & Wilson, M.-P.T.J. (1989) Tape: A Package-Attachment Technique for Penguins. *Wildlife Society Bulletin (1973-2006)*, **17**, 77-79.
- Xu, W., Dejid, N., Herrmann, V., Sawyer, H. & Middleton, A.D. (2021) Barrier Behaviour Analysis (BaBA) reveals extensive effects of fencing on wide-ranging ungulates. *Journal of Applied Ecology*, **58**, 690-698.
- Yoda, K., Naito, Y., Sato, K., Takahashi, A., Nishikawa, J., Ropert-Coudert, Y., Kurita, M. & Le Maho, Y. (2001) A new technique for monitoring the behaviour of free-ranging Adelie penguins. *Journal of Experimental Biology*, **204**, 685-690.
- Yu, H. & Klaassen, M. (R package for animal behaviour classification from accelerometer data - rabc. *Authorea*. November 21, 2020.).
- Yuan, B.-d., Xie, S.-b., Liu, B., Xue, D.-d. & Sun, D.-m. (2019) Differential movement pattern of Père David's deer associated with the temporal rhythm using GPS collar fix. *Global Ecology and Conservation*, **18**, e00641.

Chapter 7

Magellanic Penguins navigate effectively on land in multiple landscapes

Richard M. Gunner



Photo taken by Richard M. Gunner

This work is currently being prepared for publication with authors:

Gunner, R.M., Quintana, F., Gómez Laich, A., Yoda, K., Yamamoto, T., Gabelli, F., Brogger, M., Del Omo, G. and Wilson, R. P.

Abstract

The navigation mechanisms that penguins use on land are unclear. A time-compensated sun compass is the most widely accepted theory because birds at sea returning from foraging to their nests, navigate back to specific localities across seemingly featureless expanses of ocean where landmark-type visual cues are normally absent. On land, studies also report straight-line travel between the nest and the sea, which could be explained by the sun-compass theory. Here, I assess the movements of 24 Magellanic penguins walking in well-defined landscapes varying in vegetation density, with infra-second resolution (40 Hz) using GPS-enabled dead-reckoning to resolve bird pathways in detail, elucidating step lengths, pauses, turns and turn extents. Results show that outgoing birds each followed their own well-used Track of Familiarity (ToF) which took them in a straight line essentially perpendicular to the sea edge. Against this, incoming trajectories, which generally started at beach landing points displaced from the ToF, were rarely straight-line courses: Instead, penguins moved at an angle to the shore, which led to them crossing their ToF whereupon they corrected their paths to follow the ToF. There were notable differences in the dynamism, extent of pausing and the directionality of movement between incoming and outgoing trips and I argue that this supports the notion that penguins use vision-based navigation during on-land navigation.

Introduction

The navigational ability of seabirds across extensive tracts of seemingly featureless ocean has long intrigued naturalists (Cooke 1984; Brooke 2020) and has been the subject of much study (e.g., Wehner 2001; Bonadonna, Benhamou & Jouventin 2003; Åkesson & Weimerskirch 2005; Bonadonna *et al.* 2005; Gill Jr *et al.* 2009; Chapman *et al.* 2011; Reynolds *et al.* 2015; Goto, Yoda & Sato 2017; Ballard *et al.* 2019; Yoda 2019; Putman 2020) with many concluding that a time-corrected sun compass is important (Alerstam & Pettersson 1991; Guilford & Taylor 2014; Padget *et al.* 2018). Less effort has been devoted to seabird navigation on land, even though many species have prolonged phases moving overland between feeding and breeding sites (e.g. Emlen & Penney 1964; Péron & Grémillet 2013; Pollonara *et al.* 2015; Yoda *et al.* 2017; Shiomi *et al.* 2019), travelling in static landscapes where object salience could be used to navigate (Able 2001; Holland 2003; Newton 2015; Atchoi, Mitkus & Rodríguez 2020). Indeed, the constant, accessible environment of land should facilitate studies of seabird navigation although such studies are few compared to those looking at movement at sea (e.g., Nesterova *et al.* 2010; Yoda *et al.* 2017; Shiomi *et al.* 2020).

Effective navigation is particularly relevant for breeding, central-place-foraging (Orians & Pearson 1979) seabirds because the ability to travel efficiently between the nest and the sea has fitness implications for both the provisioning adult and its brood (Boersma & Rebstock 2009; Phillips *et al.* 2017). For example, higher levels of track tortuosity (see Benhamou (2004), for review) manifest by higher turn frequencies and turn extents, increase both the overall distance travelled and the duration of the trip, whilst incurring a higher energetic cost associated with the turn processes (Wilson *et al.*, 2020a). Effective navigational strategies should, therefore, be highly directional to minimise transport and time costs (Lusseau 2004; Wilson *et al.* 2013; Lempidakis *et al.* 2018; Wilson *et al.* 2020a). Many believe that land-based navigation in seabirds is based on vision (e.g. Nesterova *et al.* 2010; Clark *et al.* 2016; Atchoi, Mitkus & Rodríguez 2020), with recent work by Yoda *et al.* (2017) noting that vision seems important in streaked shearwaters (*Calonectris leucomelas*) even at sea because these birds follow the coastline to arrive at their colonies. As a corollary,

Shiomi *et al.* (2019) showed that shearwaters prefer to travel back to their breeding colony during daylight hours, presumably because visual range is greatest at such times.

Penguins have well-developed vision, including at low light intensities (Howland & Sivak 1984; Martin & Young 1984; Sivak, Howland & McGill-Harelstad 1987; Suburo, Marcantoni & Scolaro 1988; Suburo & Scolaro 1990; Coimbra *et al.* 2012) and are reliant on vision for prey capture (Wilson *et al.* 1993; Thiebot *et al.* 2016). Theories about how penguins navigate using vision, range from a time-compensated sun compass (Emlen & Penney 1964; Emlen & Penney 1966) to the use of ‘landmarks’ (Mattern *et al.* 2007; Nesterova *et al.* 2010; Shiomi *et al.* 2020), although navigation studies on penguins are in their infancy, and typically in published studies no distinction is made between land and sea phases (though see Shiomi *et al.* 2020). I argue that navigation on land for penguins involves different mechanisms to navigation at sea and has different consequences. Firstly, penguins have a low profile at sea where they effectively disappear between wave troughs, which makes vision for navigation problematic, although this is generally not the case on land (Shiomi *et al.* 2020). But penguins travel much more efficiently at sea than on land, moving 4.6 times farther per unit energy (Pinshow, Fedak & Schmidt-Nielsen 1977; Griffin & Kram 2000; Shiomi *et al.* 2020) at a speed that is about four times faster (e.g. Kooyman *et al.* 1971; Dewasmes *et al.* 1980; Wilson & Wilson 1990; Wilson *et al.* 1991; Wilson 2004; Willener *et al.* 2015; Shiomi *et al.* 2020), so the consequences of inefficient navigation are less telling.

I examined on-land navigation in breeding Magellanic penguins (*Spheniscus magellanicus*) at the Punta Norte colony, San Lorenzo (-63.86°E, -42.08°N), Argentina, which has particularly challenging characteristics for navigation as birds move between the shoreline and their nests: The penguins here breed in a large (600,000 breeding pairs, Pozzi *et al.* 2015) densely populated colony and may walk distances of up to 700 m between their nests and the sea (Villanueva & Bertellotti 2014), having to navigate through different landscapes varying in vegetation density. The navigational challenge is particularly acute for birds returning to their broods from the sea since they have to locate the singular locality of their nests. The specifics of

the return trip at San Lorenzo involve arrival on the shore after foraging at distances typically ranging between 91 km (Boersma *et al.* 2009) and 231 km away (Sala *et al.* 2012). The arrival site is an ostensibly featureless (because it changes regularly by high tides) steep pebble beach, above which the penguin cannot see landmarks until they have climbed some 20-50 m, at which point they can see the landscape and colony beyond. At the top of the beach, the birds are presented with a flat, open pebble and low grass landscape some 100 m wide running parallel to the shore, over which landmarks at distance (low hilltops etc.) can be seen. Once this open expanse has been crossed, the penguins have to move through high-density shrub, with vegetation being typically much higher than an erect penguin's head, thus precluding all but the most proximate visual cues for navigation (see Fig. 1 for a schematic cross-section of the study site). This constellation of conditions forms a natural experiment within which to examine navigation in Magellanic penguins because their vision is compromised in a defined manner.

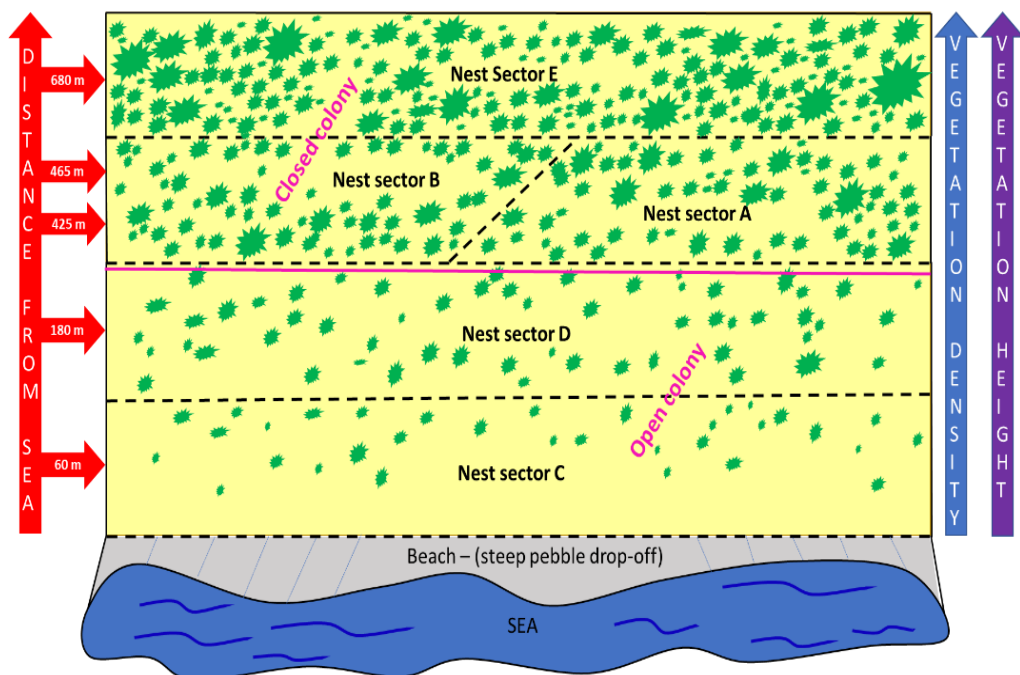


Figure 1. Simplified topographic cross-section of the Magellanic penguin colony at Punta Norte, San Lorenzo. The height and density of shrubbery generally increases with distance from the sea which can restrict the 'line-of-sight' to just a few metres. I refer to 'nest sector' as a particular area of the San Lorenzo colony within which study nests sites were located. The black dashed lines denote the boundaries between the nest sites. The purple line shows an approximate boundary between 'open colony' and 'closed colony', which reflects the greatest change in the extent of shrubbery, though see Fig. 2 for a detailed mapping of the different vegetation types.

Quintana *et al.* (in review) have described the outgoing and incoming terrestrial paths at this study site with high resolution based on 108 trajectories from penguins with nests in the closed colony – see Fig. 1. Eighty-nine of these tracks were derived from twenty-two birds which were instrumented with GPS (recording at 1 Hz), with the remaining 19 tracks coming from eight birds instrumented with dead-reckoning tags (recording at 40 Hz, e.g., Bidder *et al.* 2015). The authors found that outbound penguins essentially took a (presumed familiar by virtue of its consistency and frequency of use) route that took them in a virtually straight line to the closest point of the sea (which they defined as the ‘l-point’ and termed here their ‘Track of Familiarity’ (ToF)). In contrast, returning birds exhibited greater variability in path shape, and this typically depended on the extent of lateral displacement from their ToF upon their exit from the sea, presumed to be due to them moving across less familiar terrain (Quintana *et al.* in review). Many of the displaced journeys had a characteristic ‘Y-path’ shape, which was hypothesised to be a navigation strategy – specifically walking obliquely to the coastline until they intersected their ToF. Interestingly though, penguin navigation seemed unaffected by time of day or night and moon so the extent to which these birds rely on sight for navigation is still largely conjecture. Whilst the work by Quintana *et al.*, (in review) provided much new information, most tracks were GPS derived, precluding fine-scale (e.g., infra-second) assessments of turn extents and step lengths which may help understand navigation behaviour. In addition, Quintana *et al.*, (in review) did not define vegetation density and distribution, which I assume is likely to be important.

The aims of this study were to advance the resolution of on-land penguin navigation analysis, particularly to examine how movement patterns might vary with vegetation density. Here, I document the trajectories and behaviours of 24 Magellanic penguins from different nest sectors varying in distance from the sea and shrubbery extent (Fig. 1), as they moved between the nest and sea and back. Specifically, I reconstruct their terrestrial movement paths at 40 Hz using the verified position (VP) dead-reckoning protocol outlined in Chapter 5. As part of this, I could resolve individual step lengths, pauses, turns (including turn extent) and more generally, the speed, tortuosity, and extent of movement involved. I examine such metrics with respect to

the proximity of the penguins from their ToF and the level of vegetation density through which they were travelling.

I expect movement within open landscapes to be highly directed as birds should be able to use landmarks while the vegetated landscape should involve increased track tortuosity, most particularly in incoming trajectories that involve movement through vegetated sections away from the ToF. I examine whether 'significant' turns and pauses, are associated with homing corrections, irrespective of vegetation avoidance and 'rest-recovery' periods. Although this is primarily an exploratory analysis, working under the hypothesis that vision is important for navigation in Magellanic penguins, I would expect trends to become apparent between these various movement metrics and distance from the ToF as birds are forced to navigate through increasingly unfamiliar terrain. More generally though, I hypothesise that the tracks taken by returning birds within the different environments will show different properties, both in an energetics and time context, and the implications of this are discussed.

Materials and methods

Study site

Field work was undertaken during November and December 2020 at the Punte Norte Magellanic penguin colony, located within the San Lorenzo Gulf, Peninsula Valdes, Chubut, Argentina (-63.86°E, -42.08°N). All penguin handling procedures were approved by the Dirección de Fauna y Flora Silvestre y el Ministerio de Turismo y Áreas Protegidas de la Provincia de Chubut. Figure 1 illustrates a simplified topographic map of the San Lorenzo penguin colony.

Animal-attached tags and capture protocol

To determine route choice and activities in the penguins, I used animal-attached GPS (Axytrek, Technosmart, Italy; <https://www.technosmart.eu>) units and 'Daily diary' (DD) technology (cf. Wilson, Shepard & Liebsch 2008) (<http://www.wildbytetechologies.com>). DD technology consisted of tags that logged *inter alia* tri-axial acceleration ($1 g = 9.81 \text{ m/s}^{-2}$) at 40 Hz (16-bit resolution) and tri-axial magnetic field intensity (0.73 mG/LSB resolution). The DD was placed within a waterproof, elongated rounded acrylic housing. The dimensions (in cm) of the DD unit (connected to the battery, with SD card, within the housing) were 7.8L x 3W x 1.2H and it weighed 31.7 g. GPS units (integrated with a rechargeable battery) were made waterproof by setting them within flattened, angled resin. The dimensions (in cm) of the GPS unit (within the housing) were 6.4L x 3.9W x 1.9H and it weighed 55 g. These units were set to record fixes at 1 Hz and activated using a magnet. Both DD and GPS housings were designed to incorporate a streamlined hydro-dynamic profile following recommendations made in Bannasch, Wilson and Culik (1994). The combined weight of attached tags comprised < 1 % of the animal's mass.

For tag attachment, penguins were removed at their nest during the brooding season, using the clipboard method (cf. Wilson 1997). The devices were fitted longitudinally to the base of the spine using overlapping strips of Tesa® tape (cf. Wilson & Wilson 1989; Wilson *et al.* 2005). Birds were left to forage once at sea (a period that typically lasted between 24 and 48h) encompassing one outbound and one inbound terrestrial trip, before being re-caught at the nest to recover the devices. No tag-related detriment to the penguins was observed during device retrieval. Data were downloaded to a personal computer and GPS positions were time-synchronised with DD data.

Colony mapping

An unmanned aerial vehicle (UAV, DJI Mavic Pro) was used to reconstruct fine-resolution mapping of the various landscapes and shrub density. On a clear day, an automatic flight mission was performed using DJI Ground Station Pro Application (DJI GS Pro), at an altitude of approximately 125 m above ground altitude (3.9 cm per pixel), taking aerial photographs in the areas used by the instrumented penguins covering a total of ~58 ha. The images were captured at equal distance interval and using a course-aligned approach, with a front overlap ratio of 75 % and side overlap ratio of 60 % for each photo. The drone imagery was downloaded and processed using Structure-from-motion (SMF) available in Agisoft Photoscan version 1.4.3. The orthomosaic (i.e., orthophoto) and the Digital Elevation Model (DEM) of the colony were assembled and gridded with ~10 m by 10 m resolution. The I) beach landscape was decrypted by eye and the: II) non-vegetated- III) low vegetation-, IV) medium vegetation- and V) high vegetation density landscapes, were allocated based on estimates of pixel density per gridded cell (a proxy of shrubbery extent). Each ascribed landscape type was converted into polygon shape (.shp) files for subsequent analysis in the R environment (R Development Core Team 2021).

Track analysis

Pre-processing of GPS-integrated motion sensor data was carried out in custom software; Daily Diary Multi Trace (DDMT, <http://www.wildbytetechologies.com>) which enables 2-D time series visualisations of each sensor axis output (including derivatives) and a built-in search platform for finding behaviours using a Boolean 'lowest common denominator' (LoCoD) time-based approach (Wilson *et al.* 2018). Bird posture (pitch and roll) and heading were calculated using methods detailed in Chapter 5. A proxy of speed was derived from dynamic body acceleration (DBA; Bidder *et al.* 2012) - specifically, the vectorial dynamic body acceleration (VeDBA (smoothed by 2 s), Qasem *et al.* 2012; see Chapter 5 for calculation). The beginning of each penguin's outgoing journey was determined by inspection of an appreciable period of movement away from nest (e.g., when the bird left the nest area and moved towards the sea), characterised by waveform signatures in the acceleration

characteristic of walking (e.g. Willener *et al.* 2015; Wilson *et al.* 2018). The end of the outbound trip was made obvious by a substantial change in body posture (Shepard *et al.* 2008), from vertical walking to horizontal swimming and changes to the stylised patterns of acceleration (Wilson *et al.* 2010). Conversely, the beginning of each penguin's incoming land journey was apparent when the longitudinal body posture changed back from the horizontal to the vertical and acceleration signatures demonstrated walking. Once the start and finish time of each journey had been determined, the LoCoD method was used to identify each individual stride cycle, with pauses between walking bouts also discerned. Only pauses ≤ 60 s in duration with minimal associated DBA (indicating immobility of the body trunk, and thus not attributed to preening behaviour) were included in analysis (*cf.* supplementary information (SI): Text S1: Fig. S1). Specifically, a one-minute cut off was used because this represented the greatest clustering of data points and the ~ 95 % quantile of all pause durations with the remaining durations sporadically spread up to 1200 s. Further, only pauses that had a mean VeDBA ≤ 0.25 g were considered, because this magnitude typically represented < 25 % of the pause duration being attributed to sharp transitional movements. I detail the LoCoD method used for identifying walking within SI: Text S1. All analyses from this point onwards were conducted in the R environment (R Development Core Team 2021).

Each bird's trajectory was reconstructed using the *Gundog.Tracks* dead-reckoning function in R, based on the formulae outlined in Chapter 5. The dead-reckoned tracks were corrected for drift approximately every 50 m moved using GPS (See SI: Text S2 for information pertaining to how speed estimates and drift correction rates were decided within the dead-reckoning method).

For each GPS-corrected dead-reckoned track and associated DD data, the following parameters were assessed:

- I) VP-corrected track heading ($^{\circ}$)
- II) Percentage of time allocated to walking and pausing (%)
- III) Cumulative distance moved (m)
- IV) Straight-line distance moved towards or away from the the nest (m)
- V) Travelling speed (m/s)
- VI) Tortuosity (range 0-1, with higher values being more tortuous)

- VII) Number of pauses (per 10 metres) and the extent of a turn from the start of a pause to one second into the subsequent walking bout ($^{\circ}$). From here on, I refer to this as ‘the extent of turn following a pause’
- VIII) Number of ‘significant’ turns (per 10 metres) and their angular extent ($^{\circ}$)
- IX) Rate of change of heading during continuous walking ($^{\circ}/s$), hereafter termed ‘turn extents during walking’
- X) Distance from the track of familiarity (ToF) (m)

Distance and speed estimates were calculated using the trigonometric haversine formula (Harja & Sarno 2018) between consecutive (GPS corrected) dead-reckoned positions. Only speed during walking was assessed. Two elements were necessary to calculate tortuosity because I define tortuosity as the straight-line distance (SLD) divided by the sum of the consecutive distance steps (SDS) for the same period according to;

$$SLD = \sqrt{(\lambda_n - \lambda_1)^2 + (\varphi_n - \varphi_1)^2} \quad (1)$$

$$SDS = \sum_{i=1}^n \left(\sqrt{(\lambda_2 - \lambda_1)^2 + (\varphi_2 - \varphi_1)^2} \right) \quad (2)$$

$$T = 1 - \frac{SLD}{SDS} \quad (3)$$

where φ and λ are the latitude and longitude coordinates (decimal format), respectively. These were calculated to give one value per trip and one value per 10 m moved, respectively. All tortuosity values were subtracted from one (eq 3), so that zero values reflect straight-line movement and values closer to one reflect more ‘tortuous’ paths. Note that for the tortuosity calculated with 10 m resolution, only the shortest straight-line distance moved towards the goal-orientated destination was considered as the SLD value. For each bird, the goal-orientated destination was their last position before they entered the sea, and their nest location for outgoing- and incoming trips, respectively.

Given that penguins typically have a well-used outgoing route (Quintana et al., (in review)), this was presumed to be their ToF. Line transects were constructed using a match-stick approach, with the GPS positions used within the drift correction procedure being treated as breakpoints of the transect (thus accounting for potentially ‘curvilinear’ paths, cf. SI: Text S2: Fig. S2).

To help assess the penguin's incoming strategy, pseudo tracks were created in which the starting and finishing coordinates of the return journey were linearly interpolated (assuming constant travelling speed) to mimic the shortest course back to the nest. I define this as the 'line-of-sight' route (*cf.* Fig. 2). The most common vegetation type traversed per 10 m bin was calculated separately for the 'actual' and 'line-of-sight' tracks, and the relative percentage frequency of distance spent traveling through each vegetation density was computed. Alongside this, horizontal Haversine distance between each i) dead-reckoned position and ii) 'line-of-sight' position and the closest point on the ToF was computed. R code for drift-corrected dead-reckoning and calculating the distance from the ToF is available at <https://github.com/Richard6195/Dead-reckoning-animal-movements-in-R>.

The initial travel heading angle relative to the shore-line (perpendicular equating to 90° – directly South) was calculated for the actual route taken (the circular mean heading during first 25 m of travel) and for the 'line-of-sight' heading (which remained consistent throughout, *cf.* Fig. 2).

'Significant' turns were calculated based on the turning-point algorithm described by Potts *et al.* (2018). Briefly, the algorithm looks for changes in the heading by sliding a small window ($w = 40$ consecutive points (over 1s) and used here) across the path and observes the squared circular standard deviation (SCSD) across the window. Spikes in the SCSD indicates a turn and candidate turns are filtered according to whether they achieved a threshold turn angle (thresh = 30° used here). For an illustration of computed turn points superimposed onto tracks, see SI: Text S4.

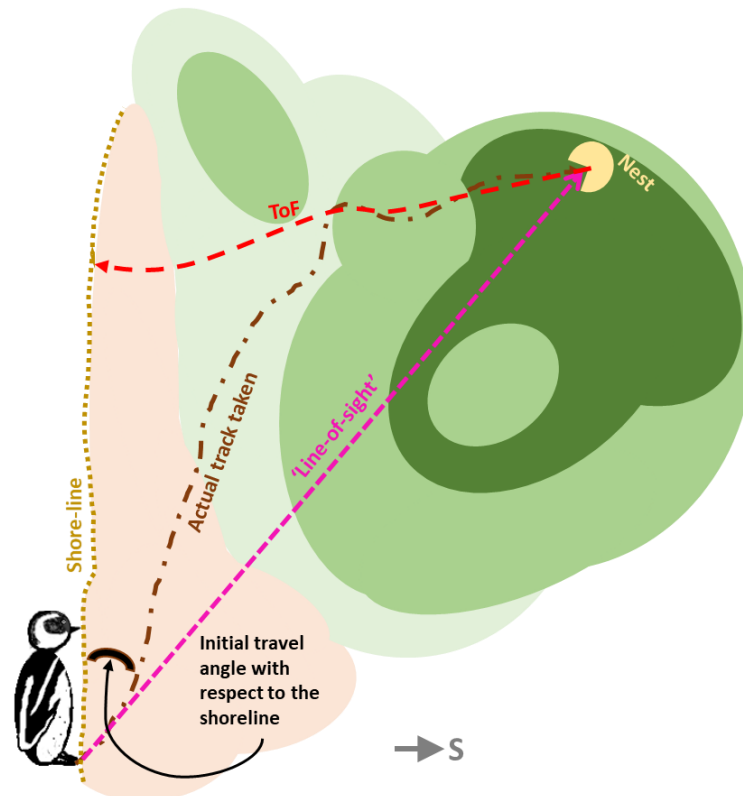


Figure 2. Schematic diagram demonstrating the 'actual' track of a returning bird in relation to the shortest theoretical 'line-of-sight' track and the ToF, (itself based on the bird's outgoing path). Vegetation density is reflected by the opaqueness of colour (from tan to greens increasing in darkness). Smaller (more acute) initial travel heading angles relative to the shoreline reflect more oblique angles relative to the nest.

Statistical Analysis

All data analysis was performed in the R core environment (R Development Core Team 2021). Linear mixed models (LMM) were undertaken using the lme package, (Zuur *et al.* 2009; Pinheiro *et al.* 2017). Generalised additive mixed effects model (GAMM) were constructed using the mgcv package (Wood 2007) and beta mixed effect models were performed using the glmmADMB and betareg packages (Bolker *et al.*, 2012). Unless otherwise stated, for all models, penguin ID was included as a random factor and the significance of model parameters was evaluated by using likelihood ratio tests (backward selection - assessing the effect of removing the parameter of interest on the fit of the model). Non-significant terms were discounted, and model parameters of the significant terms are given in SI: Text S3, Tables S1:S4. For all models, required residual fit assumptions were examined and appropriate family-wise transformations were made. All statistical tests were

performed using a significance level of $p < 0.05$. I define 'status' as either 'outgoing' or 'incoming' tracks, and 'vegetation density' as the grouping variable of 'none', 'medium' and 'high' vegetation types (no penguins traversed through 'low' vegetation, cf. Fig. 3).

1) A two-sample Kolmogorov-Smirnov test was used to compare the cumulative distribution function (CDF) of turn extents to determine if pauses were followed by greater changes in walking heading than changes in heading associated with continuous walking.

2) A Welch two sample paired t-test was used to determine if there was a significant difference in the tortuosity calculated over the entire trip as a function of 'status'. Another two-sample paired t-test was performed to assess if there was a significant difference in the tortuosity calculated with 10 m resolution (grand mean per trip used), according to status.

3) A linear mixed model was used to test if total distance travelled varied significantly between incoming and outgoing trips. For the incoming trips only, a linear model (LM) was fitted to test the relationship between the initial travel heading angle and the initial horizontal distance from the ToF, and a linear mixed models with nest sector (A, B, D or E – see Fig. 1) as the random effect, was fitted to test the relationship between total distance travelled and the initial horizontal distance from the ToF.

4) Tortuosity estimates of the entire track were compared against status, total distance travelled and initial distance from the ToF, with a beta mixed effect model (glmmADMB; family = "beta", link = "logit").

For all further analysis, variables of interest were aggregated (mean, or count used, depending on the variable) over 10 m distance travelled bins, per bird, per status, per vegetation density.

5) A Wallraff test was used to compare the angular dispersion of heading values adopted between incoming and outgoing journeys. The distributions of mean heading values were compared as a function of vegetation density, separately for outgoing and incoming trips, respectively, using the Watson's goodness of fit test.

6) GAMM models were constructed to assess the non-linear trends in: tortuosity [per 10 m], speed (m/s), number of 'significant' turns [per 10 m], extent of 'significant' turn angle ($^{\circ}$), number of pauses [per 10 m], extent of turn angle following a pause ($^{\circ}$) and duration of pauses (s), across the proportion of distance travelled accounting for the effect of status and vegetation density. All models were fitted with a smooth interaction term between the proportion of distance travelled and status to differentiate any potential patterns between outbound and inbound trips. The number of smooth term bases (k) was set at a moderate value of 9 (Wood 2017). Vegetation density and status was included as fixed factors to account for potentially varying intercepts, the latter being in conjunction with the smooth interaction, to evaluate whether the two conditions were different in overall means in addition to their smoothed patterns. The model involving tortuosity as the response variable was fitted with family = betar (link="logit") to account for the (left-skewed) bounded data. Both the number of 'significant' turns and the number of pauses were fitted with a zero-inflated Poisson regression family distribution (family = ziP). Lastly the extent of turn angle following a pause and extent of turn angle for 'significant' turns were modelled with family = Gamma(link="log") and pause duration with family = inverse.Gaussian(link="log), respectively. All GAM models used obtained full convergence and gam.check() was used to ascertain that residuals were randomly distributed and smooth terms were fitted with enough basis functions.

Results

In total, the tracks from 29 penguins from the five nest sectors (*cf.* Fig. 1) were dead-reckoned (Fig. 3). The shore-line colony penguins (n = 5) and the beach phase of navigation was excluded from all further analysis because penguins often spent extensive periods of time resting and preening on the beach (typically after foraging at sea, *cf.* SI: Text S1: Fig. S1) - unrelated to navigation.

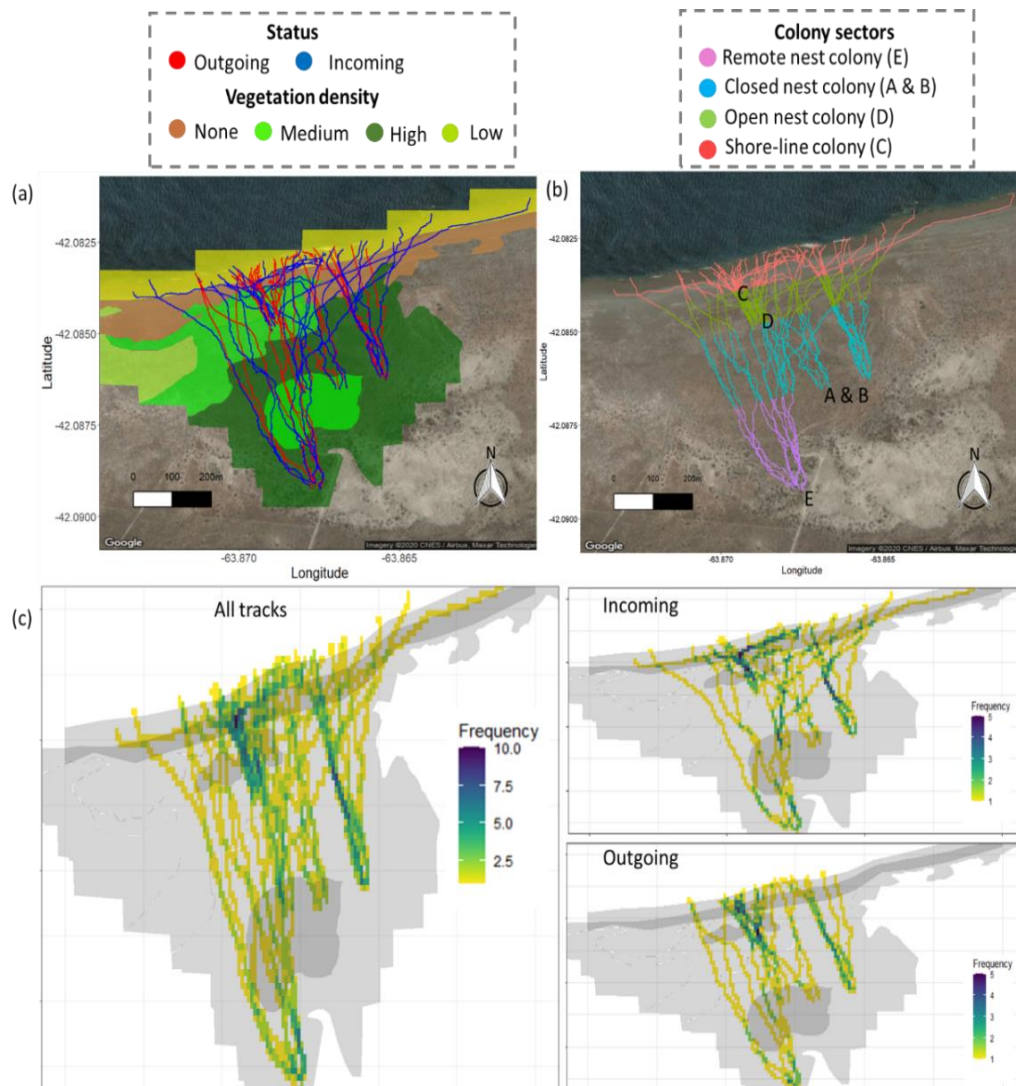


Figure 3. **Outgoing and incoming trips** - Fifty-seven dead-reckoned tracks constructed from the paths taken by 29 penguins, coloured according to (a) status and (b) colony sector. (c) Frequency of grid revisits using a 10 x 10 m resolution. Note in (a), that no penguin walked through the low vegetation density polygon (the jagged yellow polygon denotes the beach). Also note that whilst plotted here, no results include the shoreline sector (sector C).

Outgoing penguins headed approximately North to the sea, with the majority using relatively straight pathways (Fig. 3, Fig. 4a,b). There was a significant difference in the variance of the heading values adopted between incoming and outgoing journeys ($\chi^2 = 181.82(1)$ $p < 0.001$, cf. Table. 1, Fig. 4b,c). Furthermore, the distributions of mean heading values differed significantly between the varying vegetation densities during incoming trips ($F = 43.13(2)$ $p < 0.001$), though not for outgoing trips ($F = 1.10(2)$ $p = 0.332$).

Navigational ability of Magellanic Penguins on land

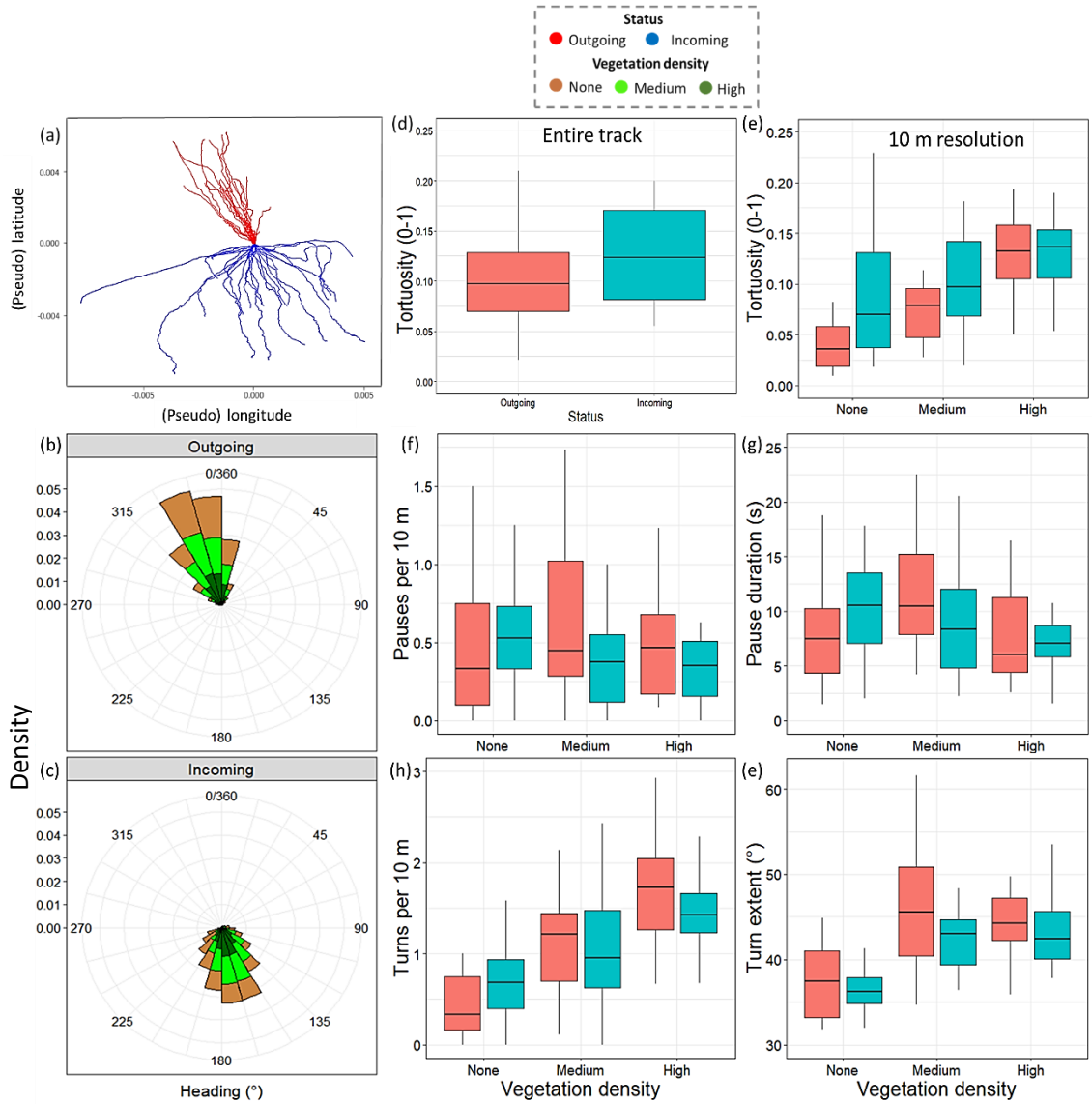


Figure 4. Outgoing and incoming trips - Assessments of heading-related metrics and pauses according to status and vegetation density. (a) shows the dead-reckoned tracks from Fig. 2, starting at a 0,0 origin (b) and (c) show radial plots of the relative heading frequency distributions per vegetation type. (d) and (e) indicate, using boxplots, the tortuosity calculated over the entire track (according to status) and over 10 m resolution (according to status and vegetation density), respectively. Boxplots are also given of; (f) pause number per 10 m, and (g) their duration, (h) number of 'significant' turns per 10 m and (i) their extents. All boxplots (boxes encompass the 25-75% interquartile range, horizontal bars reflect the median and whiskers extend to 1.5 * Interquartile range) were constructed using the mean values per bird, per status and (excepting (d)), per vegetation density.

Table 1. Descriptive statistics of various metrics relating to heading and pauses. Grand mean [± 1 SD] values were derived from all individual means, status, and vegetation type. The mean resultant length ($[R_{\text{mean resultant length}}]$) is a statistic between 0 and 1 that gives an index of the spread of heading values (values closer to 1 reflect a concentrated distribution and values closer to 0 reflect a large spread. A circular mean was used for heading values.

Vegetation density	Status	Heading ($^{\circ}$) [$R_{\text{mean resultant length}}$]	Pauses			'Significant' turns		Tortuosity (0-1) [per 10 m]	% of time spent walking	Speed (m/s)
			Number of pauses [per 10 m]	Pause duration (s)	Turn extent following a pause ($^{\circ}$)	Number of turns [per 10 m]	Turn extent ($^{\circ}$)			
None	Outgoing	345 \pm 23 [0.92]	0.55 \pm 0.59	8.1 \pm 5.2	14.2 \pm 9.4	0.51 \pm 0.55	39.1 \pm 6.9	0.05 \pm 0.06	84.1 \pm 21.1	0.414 \pm 0.092
	Incoming	186 \pm 47 [0.71]	0.60 \pm 0.44	10.3 \pm 5.2	13.6 \pm 5.9	0.69 \pm 0.43	38.0 \pm 5.3	0.10 \pm 0.09	64.7 \pm 29.9	0.384 \pm 0.065
Medium	Outgoing	342 \pm 21 [0.93]	0.68 \pm 0.62	10.3 \pm 4.5	22.9 \pm 19.9	1.20 \pm 0.70	50.1 \pm 12.5	0.10 \pm 0.14	74.6 \pm 23.2	0.389 \pm 0.080
	Incoming	159 \pm 39 [0.79]	0.36 \pm 0.29	10.7 \pm 8.8	21.3 \pm 17.6	1.05 \pm 0.61	43.6 \pm 5.7	0.12 \pm 0.09	80.6 \pm 18.1	0.422 \pm 0.064
High	Outgoing	342 \pm 23 [0.92]	0.58 \pm 0.51	8.0 \pm 4.1	32.4 \pm 15.2	1.73 \pm 0.59	48.1 \pm 7.7	0.14 \pm 0.06	80.6 \pm 17.9	0.404 \pm 0.082
	Incoming	169 \pm 29.8 [0.87]	0.33 \pm 0.20	8.9 \pm 7.3	34.8 \pm 29.3	1.46 \pm 0.40	45.3 \pm 6.1	0.13 \pm 0.04	86.6 \pm 13.0	0.417 \pm 0.063
Combined	Outgoing	343 \pm 23 [0.92]	0.60 \pm 0.57	8.7 \pm 4.7	23.0 \pm 16.7	1.08 \pm 0.79	45.6 \pm 10.4	0.10 \pm 0.10	80.2 \pm 20.9	0.404 \pm 0.085
	Incoming	170 \pm 38 [0.79]	0.44 \pm 0.35	10.0 \pm 7.0	22.2 \pm 20.6	1.03 \pm 0.57	42.0 \pm 6.4	0.12 \pm 0.08	76.0 \pm 24.2	0.405 \pm 0.065

There was no significant difference in the mean tortuosity (of the entire track or when considered over 10 m resolution) between outgoing- and incoming tracks (Table 1, Table 2, Fig. 4d,e; $t(23) = 1.58$, $p\text{-value} = 0.064$, and $t(23) = 1.69$, $p\text{-value} = 0.052$, respectively). There was a positive significant relationship between tortuosity (of the entire track) and total distance travelled (GLMMADMB: Deviance = 7.07, $p = 0.008$, Table 2), however status and the initial landing distance from the sea at the beach from the ToF did not have a significant effect on track tortuosity and did not improve model performance (GLMMADMB: Deviance = 1.63, $p = 0.202$ for status and GLMMADMB: Deviance = 0.56, $p = 0.453$ for the ToF, respectively), which supports the t-test pair-wise status comparison result.

Table 2. Descriptive statistics of various metrics linked with energy expenditure. Grand mean [± 1 SD] values were derived from all individual values, per colony nest sector and status. Note that nest sector is given in the order from straight-line distance from the sea edge.

Nest sector	Status	Trip duration (min)	Straight-line distance (m)	Cumulative distance travelled (m)	Tortuosity (0-1) [entire trip]	Distance from ToF (m)	
						Max	Average
D	Outgoing	11.757 \pm 3.061	180.044 \pm 30.669	192.856 \pm 38.909	0.062 \pm 0.034	4.856 \pm 2.751	1.367 \pm 0.417
	Incoming	34.745 \pm 9.813	333.640 \pm 213.118	393.770 \pm 223.186	0.154 \pm 0.114	246.140 \pm 235.693	146.572 \pm 147.658
B	Outgoing	25.575 \pm 18.957	405.183 \pm 23.018	471.810 \pm 72.732	0.130 \pm 0.091	11.586 \pm 8.390	2.288 \pm 1.361
	Incoming	35.501 \pm 11.747	405.459 \pm 22.550	454.987 \pm 40.413	0.107 \pm 0.035	72.791 \pm 40.335	36.031 \pm 27.359
A	Outgoing	40.955 \pm 28.965	412.201 \pm 29.940	473.506 \pm 46.231	0.126 \pm 0.065	11.245 \pm 6.672	2.916 \pm 2.325
	Incoming	45.679 \pm 12.862	446.397 \pm 34.408	590.854 \pm 136.373	0.215 \pm 0.157	232.908 \pm 79.933	124.156 \pm 57.304
E	Outgoing	48.028 \pm 20.436	686.504 \pm 15.986	773.683 \pm 39.116	0.112 \pm 0.028	9.220 \pm 1.191	1.989 \pm 0.489
	Incoming	57.647 \pm 17.166	727.459 \pm 75.175	830.326 \pm 100.201	0.122 \pm 0.025	154.192 \pm 171.364	69.646 \pm 80.763
Combined	Outgoing	31.579 \pm 23.637	420.983 \pm 184.908	477.964 \pm 215.197	0.108 \pm 0.062	9.22675 \pm 5.868	2.1400 \pm 1.411
	Incoming	43.393 \pm 15.52	478.239 \pm 186.477	567.484 \pm 216.213	0.150 \pm 0.102	176.508 \pm 58.851	94.101 \pm 94.994

The greater dispersion in the overall directionality of incoming tracks appeared to be primarily modulated by the degree of horizontal displacement from the ToF in birds landing on the beach when they returned from foraging (Table 1, Fig. 3, Fig. 4a). Generally, birds walked further during inbound than outgoing trips (Table 2; LME: $L_{\text{ratio}} = 6.05$, $p = 0.014$) and, for incoming trips, there was a significant relationship between distance travelled and the amount of initial horizontal displacement from the ToF (Table 2; LME: $L_{\text{ratio}} = 26.55$, $p < 0.001$; $r^2_{\text{m}} = 0.298$, $r^2_{\text{c}} = 0.904$). Of these, 29 % started within 50 m of the bird's ToF, 29 % were between 50 and 100 m, and the remaining 42 % ranged between 118-462 m.

Birds that arrived on the shoreline close to their ToF, tended to remain on/close to it during their return route (Fig. 5a). Generally, the greater the displacement from the ToF, the more acute the initial travel angle with respect to the shoreline (Fig. 5b; LM: $F(22) = 7.12$, $p = 0.014$), with birds walking more obliquely to the coastline at a more acute angle to the 'line-of-sight' heading in favour of reaching the ToF more quickly (Fig. 5c,d). As part of this, birds generally walked less, in terms of distance travelled through 'higher' vegetation density, substituting it with distance travelled in open landscapes compared to the situation that would have occurred had they taken the 'line-of-sight' route (Fig. 6a). Only three birds had a phase in their track > 15 m (the threshold used in (Quintana *et al.* in review) for classifying 'l-point' (ToF)) from the theoretical 'line-of-sight' track that was further away from the ToF than the 'line-of-sight' track would have entailed (*cf.* Fig. 5d). Typically, as the return path to the nest progressed, a greater percentage of birds achieved a position where they were within 15 m of their ToF than the theoretical birds taking a 'line-of-sight' trajectory (Fig. 6b).

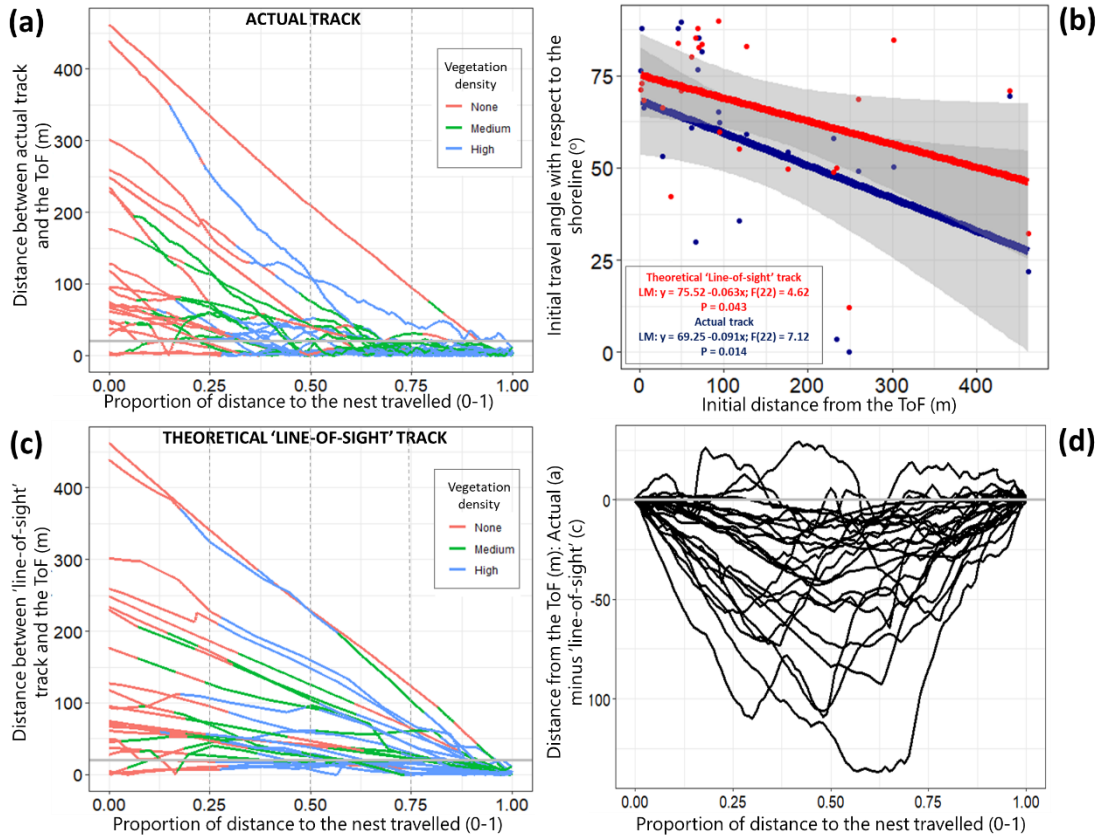


Figure 5 **Incoming trips** - Relationship between distance travelled as a function of distance into the return trip (standardised to a proportion per bird; 0-1) and the track of familiarity (ToF). (a) The distance between each penguin's ToF and the actual track taken. (b) The initial (absolute) angle of actual travel [blue] and theoretical 'line-of-sight' travel [red] relative to perpendicular from the coastline as a function of the initial displacement from the ToF with linear regression for both fitted (grey shading represents the standard error). (c) The distance between each penguin's ToF and the theoretical 'line-of-sight' track. (d) The difference in distance from the ToF between actual route taken and the 'line-of-sight' track, where negative values (below the horizontal grey line) reflect the penguin taking a closer course to their ToF than if they were to follow the theoretical 'line-of-sight' heading. The horizontal grey line in (a) and (c) denote 15 m from the ToF.

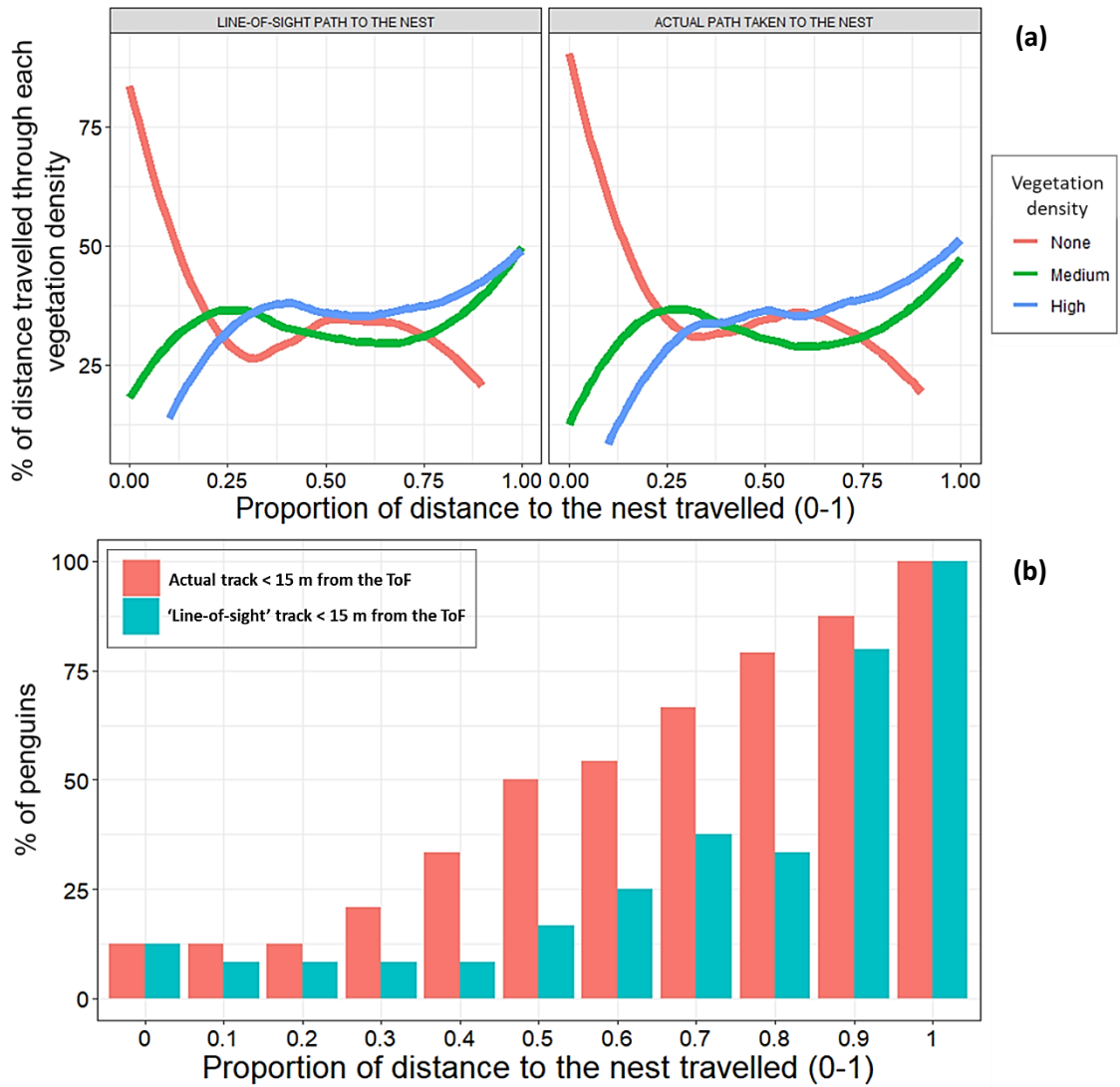


Figure 6. **Incoming trips** - Relationship between distance travelled as a function of distance into the return trip (standardised to a proportion per bird; 0-1), vegetation type and the track of familiarity (ToF). (a) Mean relative percentage of distance travelled through each vegetation density per 0.1 increment of the total distance travelled fitted with a GAM line ($k = 9$) for (left panel) birds taking a theoretical 'line-of-sight' heading to the nest and (right panel) the actual course taken by penguins to their nest. (b) The percentage of birds within 15 m of their ToF per 0.1 increment of total distance travelled, for the actual track taken and the theoretical 'line-of-sight' track. Note in (a), the relative frequency of each vegetation type moved through per bird, per 0.1 increment of total distance travelled was calculated prior to calculating a grand mean per 0.1 increment and converting back to a relative percentage (out of 100 %).

GAM models showed many contrasting non-linear relationships between the response variables tested across the proportion of distance travelled as predicted in interaction with status and partial effects of vegetation density (Fig. 7, for all GAM model parameter estimates, see SI: Text S3, Tables S2:S4). Both smooth terms and partial effects were significant for tortuosity [with 10 m resolution]. Tortuosity significantly increased as a function of increasing vegetation density (*cf.* Table 1, fig. 3e). Generally, tortuosity (Fig. 5a) was greatest at the start of outgoing trips and remained relatively consistent after about 40 % of the distance was travelled. Incoming trips were generally more tortuous in the first half of the distance travelled. Both smooth terms were significant for travelling speed (Fig. 7b) with incoming trips being much more variable across distance moved and on average, significantly higher than outgoing trips, although there were no significant differences according to vegetation density. Both smooth terms were significant for 'significant' turn number (Fig. 7c), with turn number being significantly higher in higher vegetated areas, though there were no significant differences in the overall means between incoming and outgoing. Both smooth terms for pause number (Fig. 7d) were significant and although on average, incoming trips had a significantly lower number of pauses, there were noticeably more pauses during the initial ~10 % of the distance travelled for incoming trips. Pause number did not significantly vary according to vegetation density. All smooth terms and partial effects were significant for the extent of 'significant' turn angle (Fig. 7e), with turn extent increasing as a function of vegetation density (*cf.* Table 1, Fig. 3h), being lower on average during incoming trips. The extent of turn angle following a pause (Fig. 7f) was significantly higher in 'high' vegetated density, although all other terms were non-significant. Lastly, there were no significant differences in the smooth terms or partial effects for pause duration.

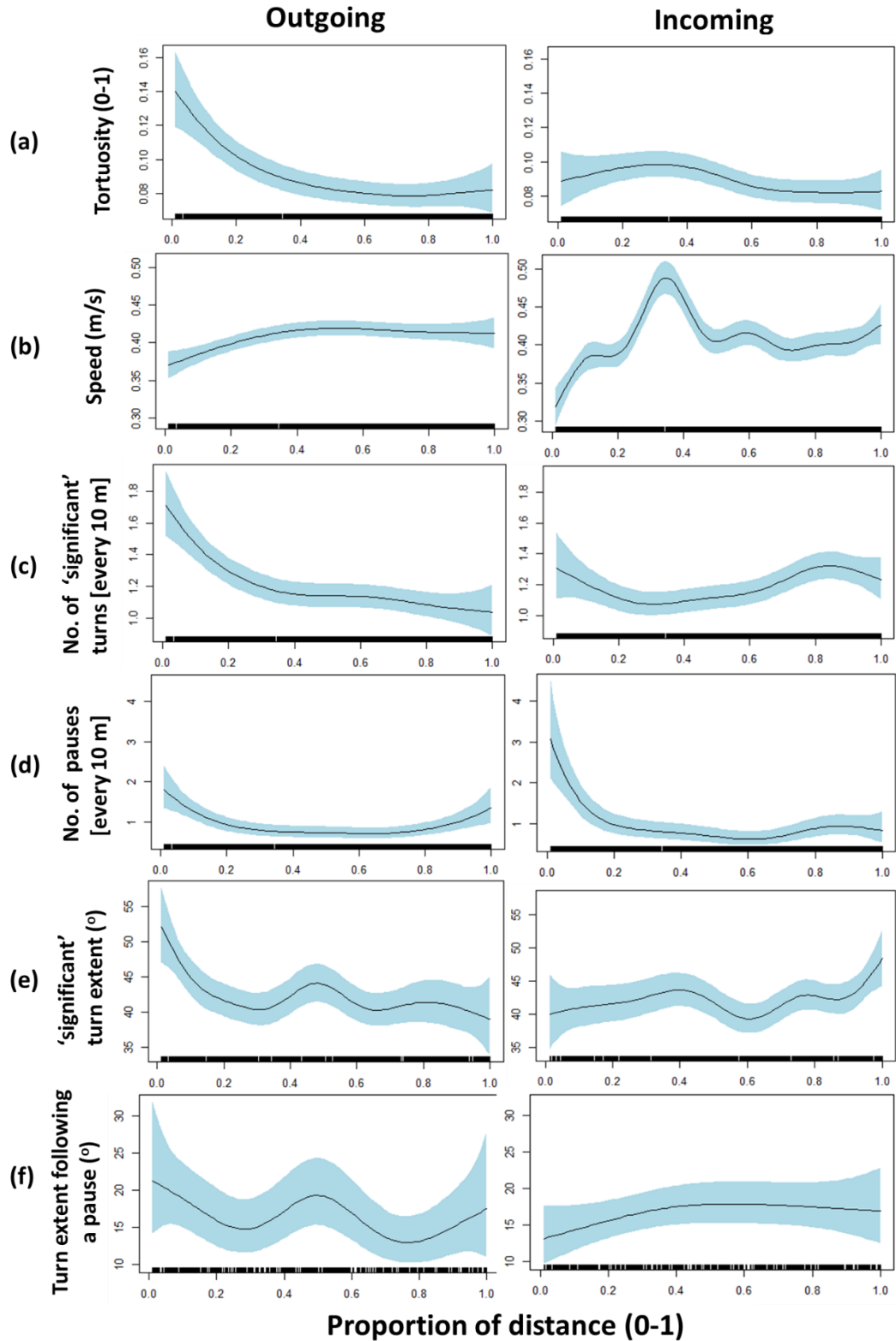


Figure 7. Smooth GAM line fits denoting the trends in various response variables across the proportion of distance travelled (0-1), as predicted by the additive component of the GAMM in interaction with status and partial effects of vegetation density. Blue shading denotes the standard errors (95 % confidence interval for the mean shape of the effect, which combines the partial effect terms with the standard errors of the model intercept).

The cumulative distribution function (CDF) of turn extents during walking ($^{\circ}/s$) differed significantly to turn extents following a pause ($D = 0.34$, $P < 0.001$, Fig. 8) and turn extents following a pause were generally higher across all three vegetation types than during continuous walking (Fig. 8c). Example individual bird cases-studies are provided in the SI: Text S4, showing expanded out dead-reckoned tracks of outgoing *versus* incoming trips, with vegetation type and fine-scale depiction of turns, and pauses superimposed to demonstrate the trends reported here).

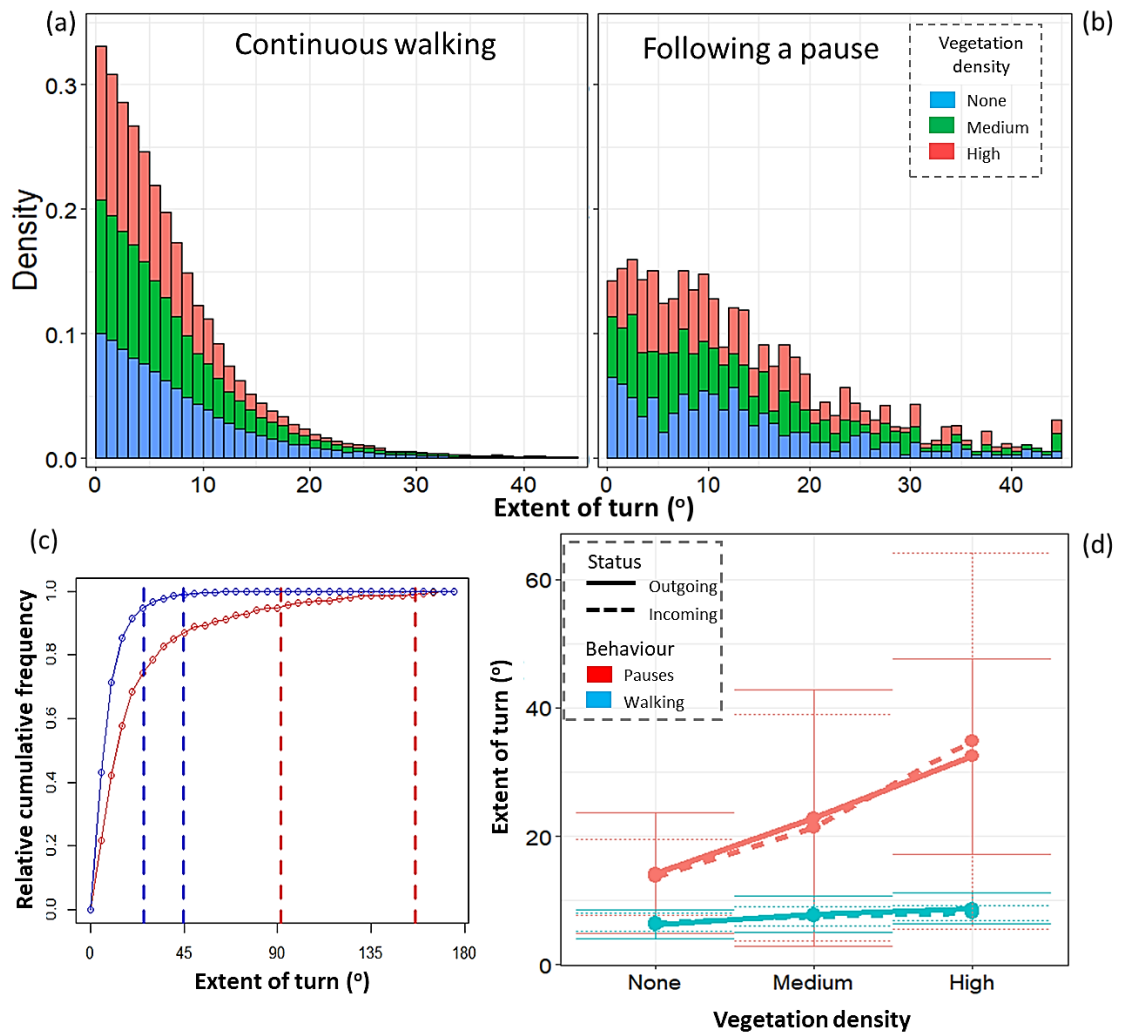


Figure 8. Extent of turns made during incoming paths – The relative frequency density of absolute heading change (extent of a turn, $^{\circ}$) between; (a) consecutive seconds during walking, and (b) between the start of a pause and one second into the following walking bout [coloured according to vegetation density]. (c) The 95 % and 99 % quantiles [vertical dashed lines] of the cumulative frequency distributions of change in heading following pausing [red] and during continuous walking [blue] for all vegetation densities. (d) Mean values of these turn extents per bird, per status [outgoing: solid line, incoming: dashed line], per vegetation density, with error bars showing ± 1 SD.

Discussion

The specific conditions that define the San Lorenzo Magellanic penguin colony should help clarify aspects of penguin navigation because the four defined landscapes (beach – (excluded in this analysis) and the variable vegetation densities) through which birds must travel, provide different types of information for animals reliant on vision. As a starting point, I suggest that the most efficient navigation course for the penguins walking from the nest to the sea at San Lorenzo is a straight-line path, with minor deviations for vegetation in the highly vegetated areas, because there are no varying energy landscape - (sensu Shepard *et al.* 2013) or predator conditions that would augur otherwise (Gallagher *et al.* 2017). In support of this, outgoing birds executed highly directional paths (*cf.* Table 1, Fig. 3, Fig. 4a,b) at constant travelling speeds (Fig. 7b). As part of this, there was a clear trend in all heading related metrics (tortuosity, number-, and extent of 'significant' turns, and the extent of turns following a pause) increasing as a function of vegetation density and generally being highest at the start of outgoing trips where the vegetation densities is highest (Table 1, Fig. 7). It is logical that higher vegetation density would relate to these metrics because higher bush numbers per unit area increase the probability that a bush will prohibit a straight-line path. Despite this, most outgoing birds managed to maintain a clear overall directionality (*cf.* Table 1, Fig. 4b) that did not significantly differ between vegetation types (juxtaposed with incoming trips that did), demonstrating the remarkable ability of these penguins to maintain what appears to be an optimum course despite necessary small-scale deviations around shrubbery.

Penguins at sea return primarily underwater, swimming at *ca.* 2-3 m depth (Wilson & Wilson 1990; Wilson & Wilson 1995) and so have no contact with the seabed (a mechanism suggested important for the supposedly visually guided navigation in Yellow-eyed penguins, *cf.* Mattern *et al.* 2007) nor, at this time, can they see the land. Even during the short breathing periods (typically a few seconds – Wilson & Wilson 1990) at the surface between dives, the low penguin profile, typically agitated sea of the region and low-lying topography of the colony means that visual cues will be minimal at best. Certainly, when Magellanic penguins initiate their return journey at sea, immediately post-feeding (some ~40 km or so away, *cf.* Chapter 8), land is not

visible at all, so much of the ‘at-sea’ navigation must be undertaken using a mechanism other than vision and landmarks, supporting the time-compensated sun-compass navigation strategy theory (*cf.* Emlen & Penney 1966). This, and possibly limited access to landmarks as returning penguins approach the coast, results in 88 % of birds at sea arriving at the beach within 300 m of their ToF: Considering the vast distances involved in the return leg at sea (Sala *et al.* 2012) in tidally-dominated current flows (Tonini & Palma 2017), this is impressive homing ability (*cf.* Chapter 8).

Assuming that penguins predominantly use a time-compensated sun compass mechanism both for homing at sea and on land during their return journeys, the expectation is that they should follow a ‘line-of-sight’ heading back to their nest in a manner similar to their directed outbound approach. This was not the case however, with many trends in the direction and dynamism of movement elicited being significantly different from outgoing trips, particularly during the early stages of return travel (Fig. 7), indicating that other processes are at work. Notably, many birds walked at an angle to their ‘line-of-sight’ heading in favour of their ToF (all but one individual undercut its ‘line-of-sight’ track, Fig. 5). As noted in Quintana *et al.* (in review), the angle of this homing correction seems to be modulated by the extent of initial displacement from the ToF on landing at the beach with, once penguins had bisected their ToF, them turning and immediately following it until they reached their nest (*cf.* Fig. 3, Text S4). The authors proposed that these individuals landing on the beach at distance from their ToF adopt this strategy because it allows them to move generally towards their nest (albeit at a slower rate than the theoretical ‘line-of-sight’ trajectory which puts them in unfamiliar areas) while giving them certitude that they will cross their ToF, which will provide certain travel back to the nest (*cf.* Fig. 9). However, my work shows that vegetation density also plays a role (Table 1, Fig. 4): Although penguins landing on the beach at distance from the ToF travelling at an angle that is not the ‘line-of-sight’ to their nest initially appear less efficient in terms of distance travelled, these more acute angles enable birds to remain in the ‘open’ colony for longer (*cf.* Fig. 6a), where they can benefit from walking in less vegetated areas with extended sightlines and no constraints in heading imposed by vegetation (they can choose from essentially a 360° arc). This is not only energetically favourable

but, in visually guided animals, it also enables the use of distant landmarks to facilitate travel decisions. This dovetails with the many studies that have hypothesised that path integration (essentially dead-reckoning) is an important mechanism used in a range of animal taxa including insects (Rolf *et al.* 1998), crustaceans (Patel & Cronin 2020), birds (Benhamou & Séguinot 1995) and mammals (Trapanese, Meunier & Masi 2019), to expediate movement from one place to another. Essentially, akin to the method described in Chapter 5, it is believed that some animals continuously update their records of their current direction and distance with respect to some 'waypoint' (Collett & Graham 2004). In this way, the inevitable errors that arise with path integration are minimised when animals travel in more familiar environments by use of recognisable landmarks, that essentially act as path integrator resets (Etienne *et al.* 2004).

By the time that the returning penguins are travelling in the highly vegetated areas, they have extremely limited sightlines, and they can only follow discreet (tortuous – see above) paths dictated by the bushes that diverge at junctions with a limited number of choices. In such situations, the closer the bird gets to the nest, the more a wrong turn leads to a subsequent proportionately disadvantageous course deviation because it must be corrected by a similarly substantive change in angle. It thus becomes increasingly costly (in both time and energy) to take incorrect headings, the further a bird progresses inland, and this is likely to be particularly problematic in unfamiliar areas. In short, the closer a bird gets to its nest, the shorter the sightlines become and the more 'appropriate' the travel decisions are required to be, which may explain why there was a general increase in the number of pauses, 'significant' turns and turn extents during the latter ~70-100 % of the distance travelled for incoming trips terminating in dense vegetation (Fig. 7). Critically, though, being near/on the ToF in such areas (*cf.* Fig. 6b), likely facilitates decision-making at critical junctions and this, in turn, may explain why there was also a general increase in

travelling speed (assuming that speed is a proxy of ‘certainty’) - comparable to the outgoing paths (Fig. 7b).

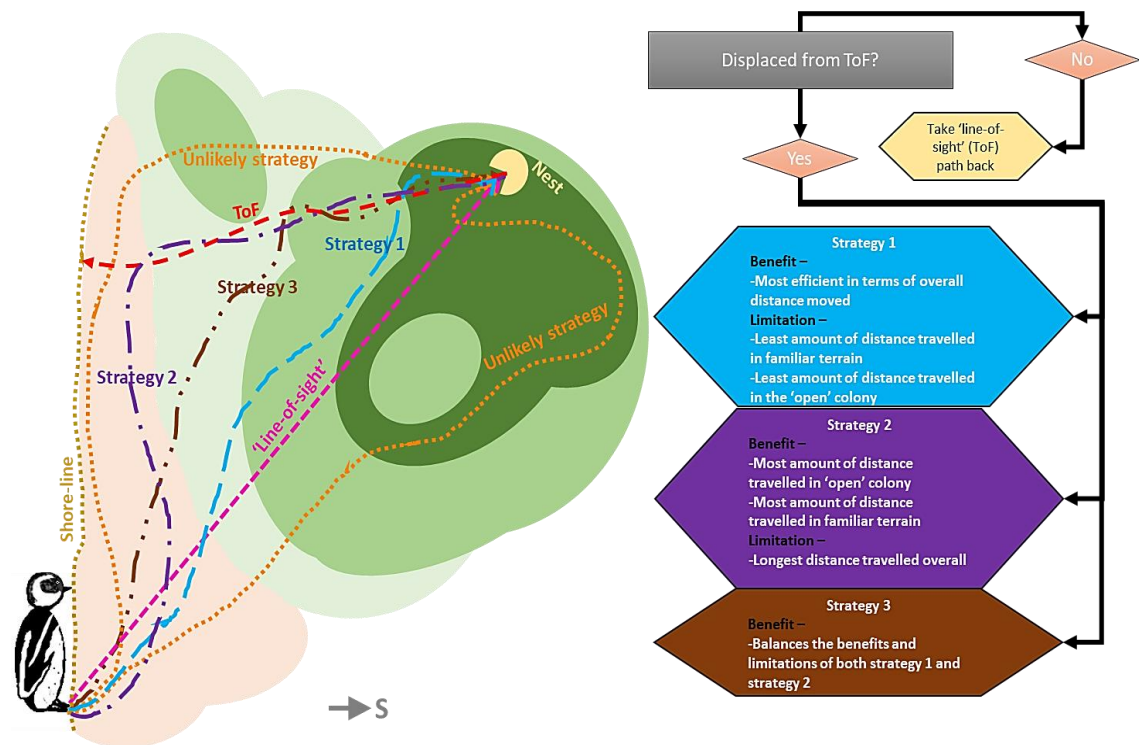


Figure 9. Schematic diagram of the most common return strategies that penguins adopted when being appreciably displaced from their ToF, with the potential limitations and/or benefits of each (elaborated in the main text below). Vegetation density is reflected by the opaqueness of colour (from tan to greens increasing in darkness). Unlikely strategies (not witnessed in this study) involve taking trajectories away from the ‘line-of-sight’ in an unfavourable direction to the ToF, and substantially ‘over-shooting’ the ToF after bisection. Note that this is just an illustration – cf. Fig. 3 for the actual vegetation densities.

The trends witnessed here support the idea that penguins travelling on land use a sight-based, dead-reckoning mechanism of navigation which particularly benefits from distant landmarks for course correction. That the incidence of pauses was highest and (pause-independent) travelling speed was lowest during the initial stage of the incoming trips (Fig. 7) may indicate a decision-making process that required time for birds to integrate such waypoints, not least because, by virtue of their separation relative to that of the penguin, they can induce greater error in estimation of their distance and bearing. That time is an important component of navigation in returning penguin tracks was emphasised by generally greater turn extents (and thus possible course deviations) following pauses than not (cf. Fig. 8), and I suggest that consideration of the details of pauses in animal movement may help reveal

navigational insights, such as bottlenecks in processing capacity of navigationally relevant information. This study also highlighted the role that variable vegetation played in penguin navigation strategies, and I propose that the preference of some returning birds to maintain a position outside dense vegetation before turning inland and moving perpendicular to the sea reflects advantageous enhanced contact with distant waypoints until the area becomes familiar. The above considerations support the notion that, despite travelling significantly greater distances than necessary during the incoming trips, birds use a sophisticated sight-based strategy to move quickly and efficiently to their nests in a cluttered and complex environment.

Conclusion

Magellanic penguins are effective at navigating on land and many finely resolved movement parameters examined here enhance our understanding of the decision-making processes used by these birds to navigate, most particularly in the highly heterogenous landscapes of the San Lorenzo colony. Specifically, movement trends differed significantly between inbound and outbound journeys, with this being principally affected according to how far away from the ToF birds landed on the beach. The work suggests that penguins actively correct for such displacements by travelling at angles in favour of their familiar paths, and/or where possible, choosing routes that coincide with lower shrubbery extent. The trends observed here suggest that penguins use visual information to both facilitate navigation and minimise energy associated with targeted movement. Lastly, I bring to attention the practicality of assessing fine-scale estimates of space-use with respect to pauses, turns and step lengths to qualify movement trends, which may prove informative for elucidating behaviour in other animals.

References

- Able, K.P. (2001) The concepts and terminology of bird navigation. *Journal of Avian Biology*, **32**, 174-183.
- Åkesson, S. & Weimerskirch, H. (2005) Albatross Long-Distance Navigation: Comparing Adults And Juveniles. *The Journal of Navigation*, **58**, 365-373.
- Alerstam, T. & Pettersson, S.-G. (1991) Orientation along great circles by migrating birds using a sun compass. *Journal of Theoretical Biology*, **152**, 191-202.
- Atchoi, E., Mitkus, M. & Rodriguez, A. (2020) Is seabird light-induced mortality explained by the visual system development? *Conservation Science and Practice*, **2**, e195.
- Ballard, G., Schmidt, A.E., Toniolo, V., Veloz, S., Jongsomjit, D., Arrigo, K.R. & Ainley, D.G. (2019) Fine-scale oceanographic features characterizing successful Adélie penguin foraging in the SW Ross Sea. *Marine Ecology Progress Series*, **608**, 263-277.
- Bannasch, R., Wilson, R. & Culik, B. (1994) Hydrodynamic aspects of design and attachment of a back-mounted device in penguins. *Journal of Experimental Biology*, **194**, 83-96.
- Benhamou, S. (2004) How to reliably estimate the tortuosity of an animal's path:: straightness, sinuosity, or fractal dimension? *Journal of Theoretical Biology*, **229**, 209-220.
- Benhamou, S. & Séguinot, V. (1995) How to find one's way in the labyrinth of path integration models. *Journal of Theoretical Biology*, **174**, 463-466.
- Bidder, O.R., Soresina, M., Shepard, E.L., Halsey, L.G., Quintana, F., Gómez-Laich, A. & Wilson, R.P. (2012) The need for speed: testing acceleration for estimating animal travel rates in terrestrial dead-reckoning systems. *Zoology*, **115**, 58-64.
- Bidder, O.R., Walker, J.S., Jones, M.W., Holton, M.D., Urge, P., Scantlebury, D.M., Marks, N.J., Magowan, E.A., Maguire, I.E. & Wilson, R.P. (2015) Step by step: reconstruction of terrestrial animal movement paths by dead-reckoning. *Movement Ecology*, **3**, 23.
- Boersma, P.D. & Rebstock, G.A. (2009) Foraging distance affects reproductive success in Magellanic penguins. *Marine Ecology Progress Series*, **375**, 263-275.
- Boersma, P.D., Rebstock, G.A., Frere, E. & Moore, S.E. (2009) Following the fish: penguins and productivity in the South Atlantic. *Ecological Monographs*, **79**, 59-76.
- Bonadonna, F., Bajzak, C., Benhamou, S., Igloi, K., Jouventin, P., Lipp, H. & Dell'Omo, G. (2005) Orientation in the wandering albatross: interfering with magnetic perception does not affect orientation performance. *Proceedings of the Royal Society B: Biological Sciences*, **272**, 489-495.
- Bonadonna, F., Benhamou, S. & Jouventin, P. (2003) Orientation in "featureless" environments: the extreme case of pelagic birds. *Avian migration*, pp. 367-377. Springer.
- Brooke, M. (2020) *Far from Land: The Mysterious Lives of Seabirds*. Princeton University Press.
- Chapman, J.W., Klaassen, R.H., Drake, V.A., Fossette, S., Hays, G.C., Metcalfe, J.D., Reynolds, A.M., Reynolds, D.R. & Alerstam, T. (2011) Animal orientation strategies for movement in flows. *Current Biology*, **21**, R861-R870.
- Clark, B., Votier, S., Hawkes, L., Witt, M., Miller, P. & Loveday, B. (2016) Sensory Processes Around Ocean Fronts: Insights from Seabird Bio-Logging in Three Dimensions. *AGUOS*, **2016**, ME24F-0770.
- Coimbra, J.P., Nolan, P.M., Collin, S.P. & Hart, N.S. (2012) Retinal ganglion cell topography and spatial resolving power in penguins. *Brain, Behavior and Evolution*, **80**, 254-268.
- Collett, T.S. & Graham, P. (2004) Animal Navigation: Path Integration, Visual Landmarks and Cognitive Maps. *Current Biology*, **14**, R475-R477.
- Cooke, P. (1984) How do birds find where they're going? *Science'84*, **5**, 26-27.

- Dewasmes, G., Le Maho, Y., Cornet, A. & Groscolas, R. (1980) Resting metabolic rate and cost of locomotion in long-term fasting emperor penguins. *Journal of Applied Physiology*, **49**, 888-896.
- Emlen, J. & Penney, R. (1964) Distance navigation in the Adelie Penguin. *Ibis*, **106**, 417-431.
- Emlen, J.T. & Penney, R.L. (1966) The navigation of penguins. *Scientific American*, **215**, 104-113.
- Etienne, A.S., Maurer, R., Boulens, V., Levy, A. & Rowe, T. (2004) Resetting the path integrator: a basic condition for route-based navigation. *Journal of Experimental Biology*, **207**, 1491-1508.
- Gallagher, A.J., Creel, S., Wilson, R.P. & Cooke, S.J. (2017) Energy landscapes and the landscape of fear. *Trends in Ecology & Evolution*, **32**, 88-96.
- Gill Jr, R.E., Tibbitts, T.L., Douglas, D.C., Handel, C.M., Mulcahy, D.M., Gottschalck, J.C., Warnock, N., McCaffery, B.J., Battley, P.F. & Piersma, T. (2009) Extreme endurance flights by landbirds crossing the Pacific Ocean: ecological corridor rather than barrier? *Proceedings of the Royal Society B: Biological Sciences*, **276**, 447-457.
- Goto, Y., Yoda, K. & Sato, K. (2017) Asymmetry hidden in birds' tracks reveals wind, heading, and orientation ability over the ocean. *Science Advances*, **3**, e1700097.
- Griffin, T.M. & Kram, R. (2000) Penguin waddling is not wasteful. *Nature*, **408**, 929-929.
- Guilford, T. & Taylor, G.K. (2014) The sun compass revisited. *Animal Behaviour*, **97**, 135-143.
- Harja, Y.D. & Sarno, R. (2018) Determine the best option for nearest medical services using Google maps API, Haversine and TOPSIS algorithm. *2018 International Conference on Information and Communications Technology (ICOIACT)*, pp. 814-819.
- Holland, R.A. (2003) The role of visual landmarks in the avian familiar area map. *Journal of Experimental Biology*, **206**, 1773-1778.
- Howland, H.C. & Sivak, J.G. (1984) Penguin vision in air and water. *Vision Research*, **24**, 1905-1909.
- Kooyman, G., Drabek, C., Elsner, R. & Campbell, W. (1971) Diving behavior of the emperor penguin, *Aptenodytes forsteri*. *The Auk*, 775-795.
- Lempidakis, E., Wilson, R.P., Luckman, A. & Metcalfe, R.S. (2018) What can knowledge of the energy landscape tell us about animal movement trajectories and space use? A case study with humans. *Journal of theoretical Biology*, **457**, 101-111.
- Lusseau, D. (2004) The Energetic Cost of Path Sinuosity Related to Road Density in the Wolf Community of Jasper National Park. *Ecology and Society*, **9**.
- Martin, G.R. & Young, S. (1984) The eye of the Humboldt penguin, *Spheniscus humboldti*: visual fields and schematic optics. *Proceedings of the Royal society of London. Series B. Biological sciences*, **223**, 197-222.
- Mattern, T., Ellenberg, U., Houston, D.M. & Davis, L.S. (2007) Consistent foraging routes and benthic foraging behaviour in yellow-eyed penguins. *Marine Ecology Progress Series*, **343**, 295-306.
- Nesterova, A.P., Le Bohec, C., Beaune, D., Pettex, E., Le Maho, Y. & Bonadonna, F. (2010) Do penguins dare to walk at night? Visual cues influence king penguin colony arrivals and departures. *Behavioral Ecology and Sociobiology*, **64**, 1145-1156.
- Newton, I. (2015) Navigation. *Flight and Motion*, pp. 384-389. Routledge.
- Orians, G.H. & Pearson, N.E. (1979) *On the theory of central place foraging*. Ohio State University Press, Columbus.
- Padget, O., Bond, S.L., Kavelaars, M.M., van Loon, E., Bolton, M., Fayet, A.L., Syposz, M., Roberts, S. & Guilford, T. (2018) In Situ Clock Shift Reveals that the Sun Compass Contributes to Orientation in a Pelagic Seabird. *Current Biology*, **28**, 275-279.e272.
- Patel, R.N. & Cronin, T.W. (2020) Path integration error and adaptable search behaviors in a mantis shrimp. *Journal of Experimental Biology*, **223**.

- Pedley, M. (2012) eCompass-Build and Calibrate a Tilt-Compensating Electronic Compass. *Circuit Cellar-The Magazine For Computer Applications*, 1–6.
- Péron, C. & Grémillet, D. (2013) Tracking through Life Stages: Adult, Immature and Juvenile Autumn Migration in a Long-Lived Seabird. *PLOS ONE*, **8**, e72713.
- Pewsey, A., Neuhäuser, M. & Ruxton, G.D. (2013) *Circular Statistics in R*. OUP Oxford.
- Phillips, R.A., Lewis, S., González-Solís, J. & Daunt, F. (2017) Causes and consequences of individual variability and specialization in foraging and migration strategies of seabirds. *Marine Ecology Progress Series*, **578**, 117-150.
- Pinheiro, J., Bates, D., DebRoy, S., Sarkar, D., Heisterkamp, S., Van Willigen, B. & Maintainer, R. (2017) Package 'nlme'. *Linear and nonlinear mixed effects models, version*, **3**.
- Pinshow, B., Fedak, M.A. & Schmidt-Nielsen, K. (1977) Terrestrial locomotion in penguins: it costs more to waddle. *Science*, **195**, 592-594.
- Pollonara, E., Luschi, P., Guilford, T., Wikelski, M., Bonadonna, F. & Gagliardo, A. (2015) Olfaction and topography, but not magnetic cues, control navigation in a pelagic seabird: displacements with shearwaters in the Mediterranean Sea. *Scientific reports*, **5**, 1-10.
- Potts, J.R., Börger, L., Scantlebury, D.M., Bennett, N.C., Alagaili, A. & Wilson, R.P. (2018) Finding turning-points in ultra-high-resolution animal movement data. *Methods in Ecology and Evolution*, **9**, 2091-2101.
- Pozzi, L.M., Borboroglu, P.G., Boersma, P.D. & Pascual, M.A. (2015) Population regulation in Magellanic penguins: what determines changes in colony size? *PloS one*, **10**, e0119002.
- Putman, N.F. (2020) Animal Navigation: Seabirds Home to a Moving Magnetic Target. *Current Biology*, **30**, R802-R804.
- Qasem, L., Cardew, A., Wilson, A., Griffiths, I., Halsey, L.G., Shepard, E.L.C., Gleiss, A.C. & Wilson, R. (2012) Tri-Axial Dynamic Acceleration as a Proxy for Animal Energy Expenditure; Should We Be Summing Values or Calculating the Vector? *PLOS ONE*, **7**, e31187.
- Quintana, F., Wilson, R.P., Gunner, R.M., Muzzio, R., Gabelli, F., Brogger, M., Dell'Omo, G., Duarte, C. & Gómez-Laich, A. (in review) Long walk home; strategies used by Magellanic penguins to find their nests. *Current Biology*.
- R Development Core Team (2021) R - A language and environment for statistical computing. R Foundation for Statistical Computing, Vienna, Austria.
- Reynolds, A.M., Cecere, J.G., Paiva, V.H., Ramos, J.A. & Focardi, S. (2015) Pelagic seabird flight patterns are consistent with a reliance on olfactory maps for oceanic navigation.
- Rolf, P., Bruce, B., Jean-Arcady, M. & Stewart, W.W. (1998) Modeling Ant Navigation with an Autonomous Agent. *From Animals to Animats 5: Proceedings of the Fifth International Conference on Simulation of Adaptive Behavior*, pp. 185-194. MIT Press.
- Sala, J., Wilson, R., Frere, E. & Quintana, F. (2012) Foraging effort in Magellanic penguins in coastal Patagonia, Argentina. *Marine Ecology Progress Series*, **464**, 273-287.
- Shepard, E.L., Wilson, R.P., Halsey, L.G., Quintana, F., Laich, A.G., Gleiss, A.C., Liebsch, N., Myers, A.E. & Norman, B. (2008) Derivation of body motion via appropriate smoothing of acceleration data. *Aquatic Biology*, **4**, 235-241.
- Shepard, E.L., Wilson, R.P., Rees, W.G., Grundy, E., Lambertucci, S.A. & Vosper, S.B. (2013) Energy Landscapes Shape Animal Movement Ecology. *The American Naturalist*, **182**, 298-312.
- Shiomi, K., Kokubun, N., Shimabukuro, U. & Takahashi, A. (2020) Homing Ability of Adélie Penguins Investigated with Displacement Experiments and Bio-Logging. *Ardea*, **107**, 333-339.

- Shiomi, K., Sato, K., Katsumata, N. & Yoda, K. (2019) Temporal and spatial determinants of route selection in homing seabirds. *Behaviour*, **156**, 1165-1183.
- Sivak, J., Howland, H. & McGill-Harestad, P. (1987) Vision of the Humboldt penguin (*Spheniscus humboldti*) in air and water. *Proceedings of the Royal Society of London. Series B. Biological sciences*, **229**, 467-472.
- Suburo, A.M., Marcantoni, M. & Scolaro, J.A. (1988) The structure of the eye in *Spheniscus magellanicus*: Dimensions of the cornea and lens in different age groups. *Colonial Waterbirds*, **11**, 227-233.
- Suburo, A.M. & Scolaro, J.A. (1990) The eye of the magellanic penguin (*Spheniscus magellanicus*): structure of the anterior segment. *American journal of anatomy*, **189**, 245-252.
- Thiebot, J.-B., Ito, K., Raclot, T., Poupart, T., Kato, A., Ropert-Coudert, Y. & Takahashi, A. (2016) On the significance of Antarctic jellyfish as food for Adélie penguins, as revealed by video loggers. *Marine Biology*, **163**, 108.
- Tonini, M.H. & Palma, E.D. (2017) Tidal dynamics on the North Patagonian Argentinean Gulfs. *Estuarine, Coastal and Shelf Science*, **189**, 115-130.
- Trapanese, C., Meunier, H. & Masi, S. (2019) What, where and when: spatial foraging decisions in primates. *Biological Reviews*, **94**, 483-502.
- Villanueva, C. & Bertellotti, M. (2014) Testing methods to estimate abundance of Magellanic Penguins *Spheniscus magellanicus*. *Bird Study*, **61**, 421-427.
- Wehner, R. (2001) Bird navigation--computing orthodromes. *Science*, **291**, 264-265.
- Willener, A.S., Handrich, Y., Halsey, L.G. & Strike, S. (2015) Effect of walking speed on the gait of king penguins: An accelerometric approach. *Journal of theoretical Biology*, **387**, 166-173.
- Wilson, R., Griffiths, I., Legg, P., Friswell, M., Bidder, O., Halsey, L., Lambertucci, S.A. & Shepard, E. (2013) Turn costs change the value of animal search paths. *Ecology Letters*, **16**, 1145-1150.
- Wilson, R., Rose, K.A., Metcalfe, R.S., Holton, M., Redcliffe, J., Gunner, R., Borger, L., Loison, A., Milos, J. & Painter, M.S. (2020a) Path tortuosity changes the transport cost paradigm in terrestrial animals. *bioRxiv*.
- Wilson, R.P. (1997) A method for restraining penguins. *Marine Ornithology*, **25**, 72-73.
- Wilson, R.P. (2004) Reconstructing the past using futuristic developments: trends and perspectives using logger technology on penguins. *Memoirs of the National Institute of Polar Research: Special Issue*, 34-49.
- Wilson, R.P., Börger, L., Holton, M.D., Scantlebury, D.M., Gómez-Laich, A., Quintana, F., Rosell, F., Graf, P.M., Williams, H. & Gunner, R. (2020b) Estimates for energy expenditure in free-living animals using acceleration proxies: A reappraisal. *Journal of Animal Ecology*, **89**, 161-172.
- Wilson, R.P., Culik, B., Adelung, D., Coria, N.R. & Spairani, H.J. (1991) To slide or stride: when should Adélie penguins (*Pygoscelis adeliae*) toboggan? *Canadian journal of zoology*, **69**, 221-225.
- Wilson, R.P., Holton, M.D., di Virgilio, A., Williams, H., Shepard, E.L., Lambertucci, S., Quintana, F., Sala, J.E., Balaji, B. & Lee, E.S. (2018) Give the machine a hand: A Boolean time-based decision-tree template for rapidly finding animal behaviours in multisensor data.
- Wilson, R.P., Puetz, K., Bost, C.A., Culik, B.M., Bannasch, R., Reins, T. & Adelung, D. (1993) Diel dive depth in penguins in relation to diel vertical migration of prey: whose dinner by candlelight? *Marine Ecology Progress Series*, **94**, 101-104.
- Wilson, R.P., Scolaro, J.A., Grémillet, D., Kierspel, M.A., Laurenti, S., Upton, J., Gallelli, H., Quintana, F., Frere, E. & Müller, G. (2005) How do Magellanic Penguins cope with variability in their access to prey? *Ecological Monographs*, **75**, 379-401.

- Wilson, R.P., Shepard, E. & Liebsch, N. (2008) Prying into the intimate details of animal lives: use of a daily diary on animals. *Endangered Species Research*, **4**, 123-137.
- Wilson, R.P., Shepard, E.L., Laich, A.G., Frere, E. & Quintana, F. (2010) Pedalling downhill and freewheeling up; a penguin perspective on foraging. *Aquatic Biology*, **8**, 193-202.
- Wilson, R.P. & Wilson, M.-P.T. (1990) *Foraging ecology of breeding Spheniscus penguins*. Academic Press, San Diego.
- Wilson, R.P. & Wilson, M.-P.T.J. (1989) Tape: A Package-Attachment Technique for Penguins. *Wildlife Society Bulletin (1973-2006)*, **17**, 77-79.
- Wood, S. (2007) The mgcv package. www.r-project.org.
- Wood, S.N. (2017) *Generalized additive models: an introduction with R*. CRC press.
- Yoda, K. (2019) Advances in bio-logging techniques and their application to study navigation in wild seabirds. *Advanced Robotics*, **33**, 108-117.
- Yoda, K., Yamamoto, T., Suzuki, H., Matsumoto, S., Müller, M. & Yamamoto, M. (2017) Compass orientation drives naïve pelagic seabirds to cross mountain ranges. *Current Biology*, **27**, R1152-R1153.
- Zuur, A., Ieno, E.N., Walker, N., Saveliev, A.A. & Smith, G.M. (2009) *Mixed effects models and extensions in ecology with R*. Springer Science & Business Media.

Chapter 8

Magellanic penguins react to current streams for efficient navigation

Richard M. Gunner



Photo taken by Richard M. Gunner

This work is currently being prepared for publication with authors:

Gunner, R.M., Quintana, F., Gómez Laich, A., Mariano, T.M., Yoda, K., Yamamoto, Gabelli, F., Del Omo, G. and Wilson, R. P.

Abstract

Animals that fly or swim must often deal with travelling through a moving medium. External current flow vectors can cause significant opposition, assistance, or lateral displacement (drift) to an animal's travelling movements, depending on the speed and direction that the animal chooses to adopt (its travel vector), relative to the speed and direction of the current flow through which it is travelling. Animals traveling within fluid media (air and water) are therefore expected to be able to detect and react to current flows in accordance with their preferred direction of travel, to reduce overall cost of transport (COT) during goal-orientated movements. Understanding the strategies that animals use to achieve this is challenging however, particularly for free-ranging animals where direct observation is limited. Here, I combine GPS and motion sensor units on Magellanic penguins returning back to their colony from foraging forays at sea. I assess how motion sensor derived heading estimates, alongside the drift-corrected dead-reckoning technique can elucidate strategies for drift compensation when compared against tidal-dominated currents of the region. Here, the ebb and flow of the tide rarely enabled penguins to adopt a travel vector, that when combined with currents, resulted in straight-line travel back to the colony, without being heavily subjected to opposing-directed flows. My results demonstrate that penguins are able to perceive and react to currents and travel back in manner that enables them to exploit favourable flow-assisted travel. However, this increased overall distance travelled as well as the overall energetic investment estimates of the return trip, juxtaposed with flow-incorporated straight-line travel. I hypothesise that the strategy adopted by these penguins facilitates opportunistic foraging during their return leg, by improving resultant travelling speeds which likely offsets the marginally higher energy costs from the optimum return path. This study represents the first step for utilising the dead-reckoning technique to detail specific orientation strategies within high current regimes.

Background

Animals moving within fluid media (water or air) may be subject to substantial current vectors relative to their own speed, that can cause substantial drift with appreciable energetic and navigational consequences, particularly when the movement is goal-oriented (see Chapman *et al.* 2011 for review). There is therefore presumed to be strong selection pressure for animals to deal with current vectors (Young & Braithwaite 1980; Åkesson & Hedenström 2007; Chapman *et al.* 2011; Shepard *et al.* 2013; Hays 2017). Accordingly, some animals respond either by only moving when flow vectors are favourable (Vogel 1978; Gibson, Barnes & Atkinson 2001) or by modulating their speed (Liechti, Hedenström & Alerstam 1994; Kelly & Klimley 2012) or heading to varying degrees (Shiomi *et al.* 2008; Klaassen *et al.* 2011; Goto, Yoda & Sato 2017; Cerritelli *et al.* 2019), which presupposes that they can detect current vectors (Chapman *et al.* 2011). While mechanisms for detecting current vectors have been proposed such as hairs on the wings of bats (Jones 2011) or reference to landmarks (Liechti 2006), animals navigating at sea at depths that give them no reference to the seabed (Bonadonna, Benhamou & Jouventin 2003) are considered to face particular challenges and it is unknown how goal-orientated behaviour might occur in this scenario. It has been shown, however, that sea turtles manifest appreciable track tortuosity during their migrations from feeding sites to breeding islands, suggesting imperfect information about their position, the position of their goal and/or the current vectors to which they are subject (Hays 2017). Similar sorts of findings have been noted for birds (Carter *et al.* 2016; Tarroux *et al.* 2016; Sánchez-Román *et al.* 2019).

Penguins are an excellent group with which to study the effects of current vectors on navigation strategies. During breeding, these birds are central place foragers (Boersma & Rebstock 2009; Sala *et al.* 2012; Rosciano, Polito & Raya Rey 2016) that must return regularly, efficiently and precisely to their colony from foraging far at sea (out of sight of land – a condition enhanced by their very low profiles at the sea surface and extensive time spent underwater - but see Mattern *et al.* 2007) to provision their brood (Williams & Busby 1995). Being unable to fly, the journey must be undertaken by swimming at speeds of *ca.* 2 m/s (Wilson, Ropert-Coudert & Kato

2002; Wilson *et al.* 2004), which compares to many ocean currents, particularly in areas exposed to substantial tides (Kantha *et al.* 1995; Kara, Metzger & Bourassa 2007). Importantly, for understanding how penguins react to currents, much animal-attached technology has been developed specifically for penguins, including dead-reckoning devices (Wilson 2004; Wilson *et al.* 2007), recording animal heading, depth and speed so as to be able to reconstruct bird tracks using vectors assuming no current drift (Shiomi *et al.* 2008).

I examined the navigation behaviour of Magellanic penguins *Spheniscus magellanicus* breeding at Peninsula Valdes, Chubut, Argentina while they were subject to well-defined, in time and space, currents of the region (Glorioso & Flather 1995) which can reach 2.5 m/s (see below). For this, I equipped birds with GPS-enhanced motion sensors recording location, depth, tri-axial acceleration, and tri-axial magnetic field intensity, from which the homebound (goal-orientated) tracks could be reconstructed. These were drift-corrected, by reference to the GPS, and considered with respect to the space- and time-corrected currents.

The aims of this study were three-fold. Firstly, to investigate the abilities of these birds to perceive the direction of their colony, secondly, to examine the extent to which birds react to currents when commuting back to the colony and finally, in tandem with the above, to evaluate the energetic and distance travelled consequences of their homing strategy.

Materials and methods

Study site, tags used and attachment method

Field work was undertaken between 22nd November and 1st December 2019 at the San Lorenzo Magellanic penguin colony (-63.86, -42.08) on birds brooding small chicks. Birds were fitted with GPS (Axytrek) units, programmed to record at 1 Hz and powered by a 3.6 V, Lithium Thionyl Chloride, 1,600 mAh battery and Daily Diary (DD) technology (Wilson, Shepard & Liebsch 2008) comprising a tri-axial accelerometer and tri-axial magnetometer recording at 40 Hz with 16-bit resolution and powered by a 3.6 V, Lithium Thionyl Chloride, 750 mAh battery. DDs were also integrated with a Keller pressure sensor, operating within the range of 0-30 bar with 24-bit resolution. DD units were fitted within an elongated rounded acrylic casing and GPS units within a flattened, angled resin mould, both housings being designed to be hydrodynamically streamlined following recommendations made in Bannasch, Wilson and Culik (1994). Combined device weight (85.7 g) comprised < 1 % of the penguin's body mass and represented < 1 % of the penguin's cross-sectional areas. Both units were attached to the base of the spine using Tesa[®] tape (Wilson *et al.* 1997), a process that typically took less than 5 minutes. Birds were left to undertake a single foraging trip at sea (typically lasting between 24 and 48h at this site) before being re-caught at the nest and the devices recovered.

Numerical ocean current model

The output simulations were performed using a numerical model called Regional Ocean Modelling System (ROMS, Shchepetkin & McWilliams 2005). In the vertical (depth) axis, the primitive equations are discretised over variable topography using stretched terrain-following coordinates. In the horizontal axes, the primitive equations were evaluated using orthogonal curvilinear coordinates on a staggered Arakawa C-grid. For the vertical mixing parameterization, the scheme developed by Mellor and Yamada (1982) was selected. The bathymetry is based on digitised nautical charts. The computational grid had three open boundaries (South, West and

North) where the tidal amplitudes and phases of 8 principal constituents (four semidiurnal; M 2 , S 2 , N 2 , K 2 , and four diurnal: K 1 , O 1 , P 1 and Q 1), two long-term constituents (M f and M m) and three higher harmonics (M 4 , MS 4 and MN 4) of the region were imposed, interpolated from a global tidal model (TPXO6, Egbert, Bennett & Foreman 1994). For more details in model setup simulations (grid, forcings, open boundaries, etc.) see Tonini and Palma (2017). The model was validated in the region using all *in-situ* data available from a long period of time (across > 10 years, see Tonini & Palma 2017 for details). The output instantaneous currents (3-D field) were used to perform a harmonic analysis of each tidal constituent in a 3-D and 2-D (depth averaged) field. After that, the most important current components that produced greatest variations of syzygy and quadrature (M2, S2 and N2) in the region were taken, with phase-adjustment using the free-to-use global xtide model (<https://flaterco.com>). From this, U and V components were assembled (*cf.* Pisoni *et al.* 2020). These are, respectively, the separate measures of flow speeds along two orthogonal axes: U represented the horizontal component in the East-West direction and V, the horizontal component in the North-South direction. Mean U and V components were calculated per grid node per hour (in m/s) (see supplementary information (SI): Text S1: Fig. S1). These were the averaged vertical currents because, in the case of instantaneous currents within the San Lorenzo gulf, there was no great variation from surface to bottom. Across all tracks, current strength averaged 0.6 ± 0.35 ($\pm 1SD$) (m/s) with peak syzygy being 2.5 m/s. In this study, the output model encompassed a sector covering 3.45×10^6 km² (which incorporated the majority of penguins foraging trips, *cf.* Fig. 1) at 1 km² resolution, starting from 22nd November at 1 am until 2nd December at 1 am (2019).

Speed estimates

I used 3 approaches to represent penguin swim speed.

- i. *Surface swimming* - When a bird was ≤ 0.3 m depth & absolute values of pitch (derived from the surge acceleration, Bidder *et al.* 2015) were $< 10^\circ$, it was considered to be travelling at 0.416 m/s (1.5 km/h based on the Wilson (1985)

- reported surface swimming speed of the congeneric African penguins (*Spheniscus demersus*).
- ii. *Underwater swimming with low body pitch* - When a bird was at > 0.3 m depth and absolute values of pitch were < 10°, it was deemed to be travelling at 2.1 m/s (the average of two reported Magellanic penguin modal commuting speeds of 2.0 m/s (Wilson, Ropert-Coudert & Kato 2002) and 2.2 m/s (Wilson *et al.* 2004)).
- iii. *Underwater swimming with high body pitch* - Following Ropert-Coudert *et al.* (2001), when a bird was > 0.3 m depth and absolute values of pitch were ≥ 10°, speed (s) was estimated using;

$$s = \frac{\Delta d}{\tan\left(\theta \cdot \frac{\pi}{180}\right)} \quad (1)$$

where speed is in m/s, Δd is the rate change of depth (m/s) and θ , the pitch angle (°). Speed values were capped at 5 m/s to ensure unrealistic speeds were not included. Prior to calculating speed, for equations deriving the three axes of rotation using the tilt-compensated compass method, see Pedley (2012); Bidder *et al.* (2015) and Chapter 5, offsets were applied to pitch and depth values to account for discrepancies of tag attitude relative to the body, and baseline pressure drift, respectively (SI: Text S2).

Dead-reckoning procedure

Bird heading during swimming was calculated using the *Gundogs.Tracks()* function in R, detailed in Chapter 5, before being integrated with speed and dive angle and finally being corrected using GPS fixes acquired when birds were at the surface (see SI: Text S2 for more information).

The beginning of each penguin's the return journey was determined by examining the shortest straight-line distance between the penguin and the colony over time during the period at sea, which I define as the 'line-of-sight' trajectory. When

graphed, this produced an inverted 'V', with the beginning of a continuous downward gradient highlighting the start of a penguin's homing trajectory (SI: Text S1: Fig. S2). All data from this point onwards (providing this coincided within the grid of available currents data (Fig. 2)) were included in the analysis. Data was sub-sampled to 1 Hz resolution with the time and position of each DR fix matched to the relevant grid node current vector (mean U and V components).

The travelling vectors and their derivation

To convert U and V components into strength/speed and direction estimates, or *vice versa*, see SI: Text S2.

In total, five 2-D vectors were calculated (*cf.* Fig. 2):

- (i) *Water current (see above)*
- (ii) *Bird heading and speed relative to the water* – This was derived from the estimated speed and heading derived during the DR process. I applied a 10 s running mean to all speed and heading values prior to converting it to U and V components (circular mean used for heading). Only the bird's estimated speed and heading estimates prior to GPS correction were used.
- (iii) *Bird resultant vector* - The U and V components of the bird were added to the U and V components of the current, respectively to compute the actual bird resultant vector (bird + current).
- (iv) *Theoretical 'best' heading* – At each point along the track, for the given bird's estimated travelling speed and exposure to current direction and speed, the heading required to provide the vector travel direction to return directly back along the 'line-of-sight' trajectory was calculated (following integration with currents; see SI: Text S1: Fig. S3, and SI: Text S2).
- (v) *Theoretical 'best' resultant vector* - The U and V components of the theoretical 'best' were added to the U and V components of the current, respectively, to compute the theoretical resultant vector (theoretical + current). In most cases, the direction of the theoretical resultant and 'line-of-sight' heading were the same.

Ease of transport (EOT)

I specified the inverse of cost of transport (COT - *cf.* Taylor, Caldwell & Rowntree 1972) as the Ease of transport (EOT in m/J) to highlight facilitated pathways by penguins exposed to the current landscape. For this, I calculated the power requirements for a penguin's chosen speed using the formula given in Luna-Jorquera and Culik (2000) relating mass-specific power to swim speed for congeneric Humboldt penguins (*Spheniscus humboldti*), a species morphologically and physiologically very similar to the Magellanic penguin (Wilson *et al.* 2004).

$$Power = 2.954 \cdot v^3 - 6.354 \cdot v^2 + 5.818 \cdot v + 5.9 \quad (2)$$

where v is velocity (penguin speed) and *Power* is in W/kg. Values were then multiplied by 4 (the average weight of Magellanic penguins is 4 kg (Williams & Busby 1995)) to convert the power costs to a rate of energy usage per animal and second (J/s).

At each point along the DR track, coordinates were advanced according to the speed and direction of the vector in question. This was done separately for actual bird resultant, theoretical 'best' resultant and actual bird options (pre-current integration - for comparison purposes). Finally, for each of the three progressed vectors, two variants of EOT (m/J) were calculated:

- (i) R1 (EOT transport in any direction) – Given by the distance moved per second divided by the power costs (*cf.* Fig. 1).
- (ii) R2 (Effective EOT) – Given by the distance covered along the effective 'line-of-sight' trajectory towards the colony per second divided by the power costs (*cf.* Fig. 1).

Negative EOT values for R2 (which could occur if the birds moved further away from the colony) were allocated as zero. This was another reason that EOT was explicitly used instead of COT, since descriptive stats incorporating joules per negative metre

made little mathematical sense and my approach sought to highlight distance covered by the birds.

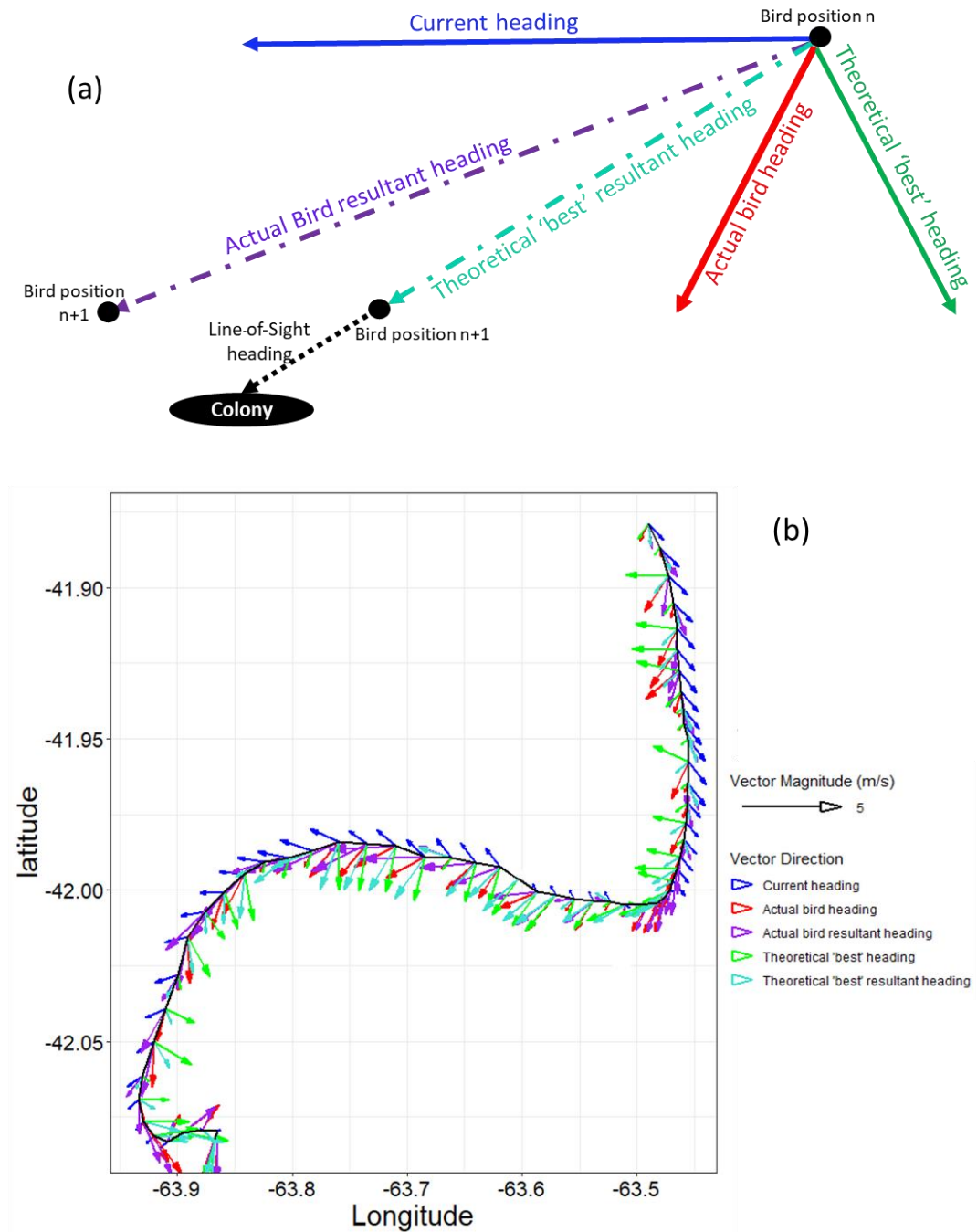


Figure 1. Representation of the five vectors calculated in this study. The schematic (top) diagram shows how vector addition of the current (solid blue) and either actual bird (solid red) or theoretical 'best' (solid green) options at bird position 'n', results in the actual bird resultant (dashed purple) or theoretical 'best' resultant (dashed turquoise), respectively, at bird position n+1. The dotted black lines reflect the magnitude and direction of the shortest straight-line distance ('line-of-sight') to the colony. The theoretical 'best' resultant always follows the direction of 'line-of-sight' heading except where penguin speed at any point was not high enough to correct for the current vector (SI: Text S2). In the lower panel, these vectors are calculated for the return journey of a penguin (plotted at 5-minute intervals along its dead-reckoned track (southerly trajectory)). Note that the theoretical 'best' (green) is sometimes directed against the current (> 90°) to achieve a theoretical 'best' resultant, directing the bird towards the colony. Note, R1 (EOT transport in any direction) is the distance progressed from bird position n to bird position n+1 and R2 (Effective EOT) is the difference between the 'line-of-sight' to the colony at bird position n and the bird position n+1.

Graphical and statistical analysis

The derivations of pitch, roll and heading were computed in the custom designed software; Daily Diary Multi Trace (DDMT, <http://www.wildbytetechologies.com>). All further work was performed in R (<http://www.R-project.org>). To control for unequal sample sizes between penguins, variables of interest (outlined below) were binned appropriately (sometimes 2-dimensionally) and a grand mean and standard error per bin was calculated from all 'pooled' mean/relative frequency values. For graphical purposes, when comparing variables as a function of proportion of total distance travelled (0-1), the calculated mean of a given variable per bin (0.01) per bird was pooled and in the case of comparing frequency distributions (of heading differences), the relative frequency per bin (into 5° or 10° epochs - range: -180° to +180°) per penguin was pooled prior to calculating a grand relative frequency across the bin range. For statistical analysis, data were binned into 1° epochs.

A boot-strap version of the two-sample Kolmogorov-Smirnov (KS) test was used to determine if the distribution of heading difference between actual bird heading and 'line-of-sight' heading was significantly different according to conditions of current strength. Data was subsetted between 'slack' current condition < 0.5 m/s (approx. half the relative distribution of current conditions and approximately a quarter of a Magellanic penguin's modal commuting speed, *cf.* SI: Text S1: Fig. S4) and 'appreciable' current condition ≥ 0.5 m/s. This was achieved using the 'ks.boot' function in R from the 'Matching' package (Sekhon & Sekhon 2020), in which the vertical distance between the empirical cumulative distributions functions from the two samples were compared using 1,000 bootstraps (Monte Carlo simulations) to determine the empirical p-value. Bootstrapping was chosen because of its robustness to integer ties. The null hypothesis was that the probability densities for both 'slack' and 'appreciable' current conditions were the same. Surface periods > 30 s were initially removed to include primarily 'commuting' movement rather than milling about at the water surface.

Four two-tailed Welch Two Sample paired t-tests were used to determine if there was a significant difference between the paired means of the theoretical 'best'

resultant EOT and the actual bird resultant EOT as well as the actual bird EOT and actual bird resultant EOT (using a grand mean from pooled mean EOT values per 0.01 epoch of total distance travelled per individual). This was computed for both R1 and R2 separately.

Results

In total, 15 birds were used for the analysis and the majority executed ‘looping pathways’ (*cf.* Weimerskirch *et al.* 1993), heading approximately North to forage and returning in a southerly direction to their colony, with most return tracks having an S-shape (Fig. 2). On average (± 1 SD), the beginning of the return trips started 38 ± 7.3 km from the colony.

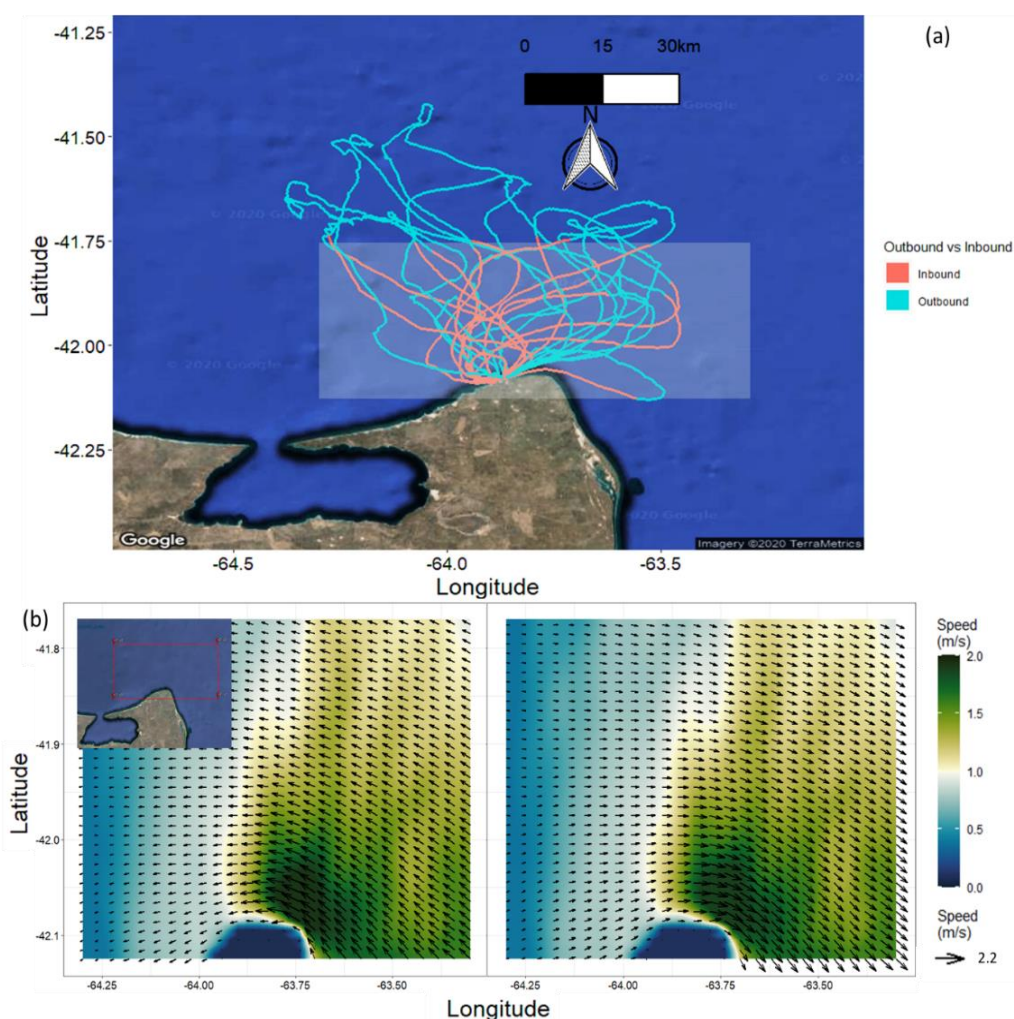


Figure 2. (a) The tracks at sea of 15 penguins, coloured according to outbound (blue) from inbound (red) phases (see text for details). The light grey shaded rectangle represents the grid for which current data is available. (b) The current conditions within this grid are visualised, showing peak syzygy (strength) as a function of the incoming (left panel) and outgoing (right panel) tides from a single day. Note that penguins are typically subject to cross-currents during their return phase.

Across individuals, penguin headings within both 'slack water' and 'appreciable current' conditions were centred about their 'line-of-sight' heading, rarely exceeding 90° from this and following a Gaussian distribution (Fig. 3a, SI: Text S1: Fig. S3). However, actual bird heading under 'slack water' conditions was less spread than during the 'appreciable current' conditions ($D = 0.106$, $p < 0.01$). It was not apparent though, that homing ability improved with decreasing 'line-of-sight' distance to the colony (SI: Text S1: Fig. S5). The variation in penguin heading around the 'line-of-sight' heading could be further expanded to examine the effect of current heading on bird strategy *via* contour plots that added the 'line-of-sight' heading minus the current heading for 'slack water' and 'appreciable current' conditions (Fig. 3). During 'slack water' conditions, actual bird heading was similar to line-of-sight heading (Fig. 3b), with variation around this to both the left and right of the mean as exemplified in Fig. 3a. However, during 'appreciable current' conditions, which were primarily manifest by currents that were perpendicular to line-of-sight travel due to the tide moving in and out of the gulf (*cf.* Fig. 2b), penguin heading minus 'line-of-sight' heading favoured swimming with the current, with greater deviation from the 'line-of-sight' heading (Fig. 3c).

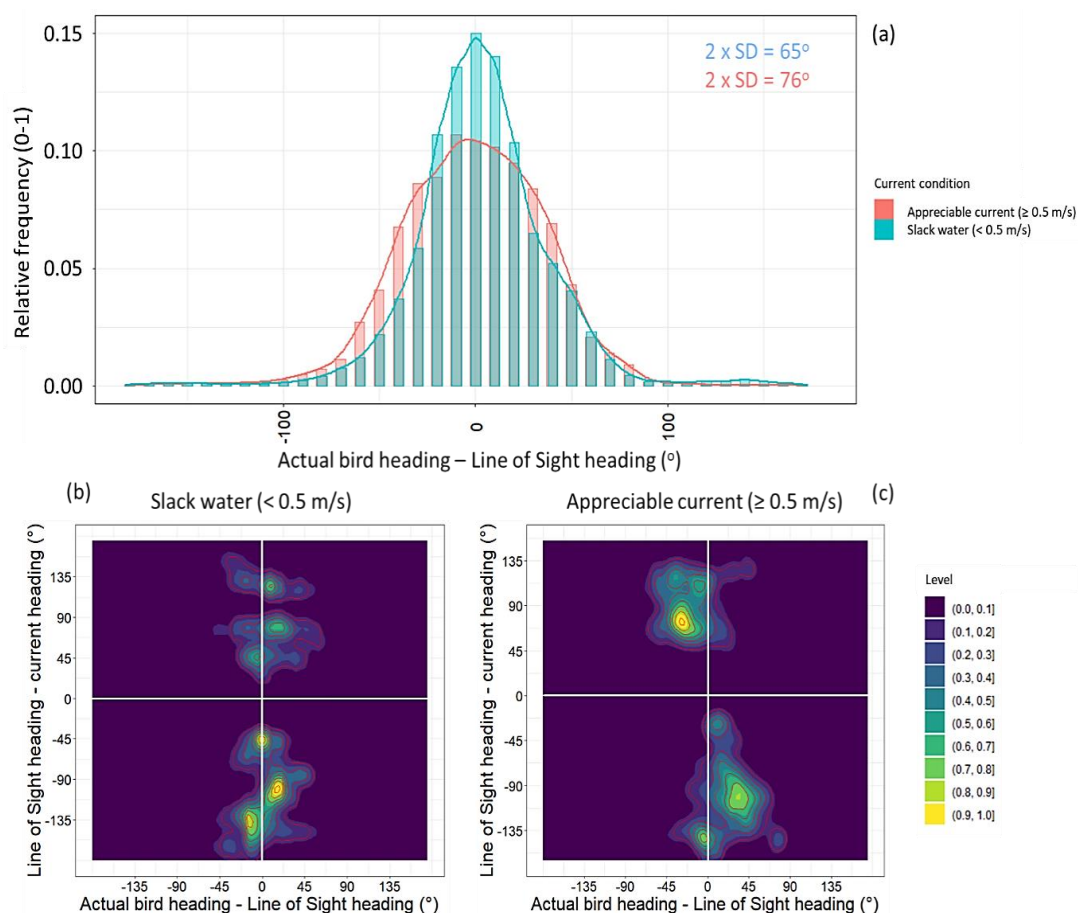


Figure 3. (a) Distribution of the difference between the actual bird heading and 'line of Sight' heading for both 'slack water' (< 0.5 m/s – green bars) and 'appreciable current' (≥ 0.5 m/s - red bars) conditions. Thus, values of 0° indicate that the birds were travelling directly towards the colony while 90° indicate that the birds were heading perpendicular to the colony. (b) and (c) expand plot (a) out into contour plots which highlight the effect of current magnitude and direction on bird heading with respect to the 'line of Sight' heading. (b) shows that the difference between 'line of Sight' heading and current heading (cf. 3a) does not substantially change with current heading under the (minimal) current conditions of 'slack water' (points centred around the 0° mark). However, under 'appreciable current' conditions (c), actual bird heading is skewed to the right of the 'line of Sight' heading when the 'line-of-Sight' heading minus the current heading is negative and skewed to the left when the 'line-of-Sight' heading minus the current heading is positive. This indicates that under high current conditions, birds deviate from the mid-point of their heading distributions following a 'line-of-sight' heading, to swim preferentially with the current.

Combining all data, the reaction of penguins to currents in general (cf. above) can be examined to see how the behaviour of the birds compares to putative optimal headings. Optimal headings are considered to be where penguins select headings that, after integration with current vectors, result in birds moving along a 'line-of-sight' trajectory (cf. Fig. 1), thereby minimizing distance travelled to the colony. The bird data show that the resultant bird headings (the actual headings minus the current headings) rarely involved penguins swimming against the current, instead resulting in birds swimming preferentially with the current, even if that led to them

deviating from a 'line-of-sight' trajectory back to the colony (Fig. 4a). By contrast, the theoretical 'best' heading would lead to penguins having to swim against the current (at an angle of $> 90^\circ$) for most of the time (Fig. 4b, SI: Text S1: Fig. S3).

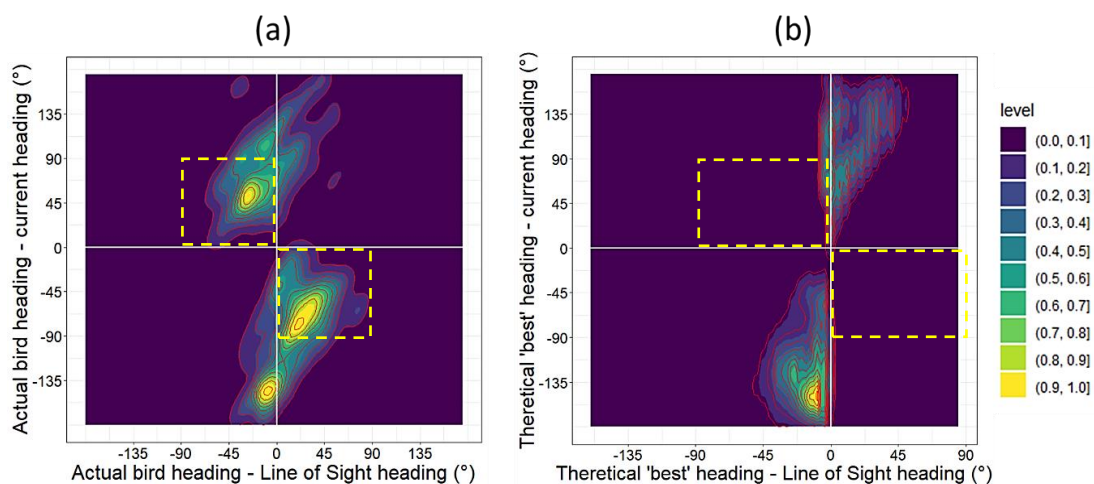


Figure 4. Contour plots (a) to show the strategy shown by the real birds, that have a diametrically opposed distribution with most time spent swimming with the current to some degree [inside the yellow boxes]. This is in stark contrast to the (b) theoretical 'best' heading by penguins (which would normally result in the birds navigating a 'line-of-sight' trajectory back to the colony – although not strictly in this visualisation since the speed cannot be incorporated) as a function of the current heading (y-axis), which results in displacement around the 'line-of-sight' heading (x-axis) with the birds spending most of their time swimming against the current [outside the yellow boxes]. There is, however, a notable peak located at the bottom section (a) where an appreciable proportion of time is spent swimming against the current. This is due, almost exclusively to penguins that had moved close to the colony but found themselves downstream and thus had to swim against the current for the last phase of the return journey.

Penguin heading with respect to current was calculated to have a substantial effect on the ease of transport. The ease of transport with respect to distance covered directly back to the colony (R2) indicated that of the theoretical 'best' heading produced significantly easier travel than that experienced by the penguins with their chosen headings ($t(14) = 2.186$, $p\text{-value} = 0.046$, $P < 0.05$) although in energetic terms the difference was marginal (Fig. 5a, SI: Text S1: Fig. S6). However, in terms of actual distance moved irrespective of direction, the mean ease of transport (R1) of the actual bird resultant vector of travel was significantly, and substantially, greater than the theoretical 'best' resultant ($t(14) = -7.582$, $p\text{-value} < 0.001$, Fig. 5b, SI: Text S1: Fig. S6).

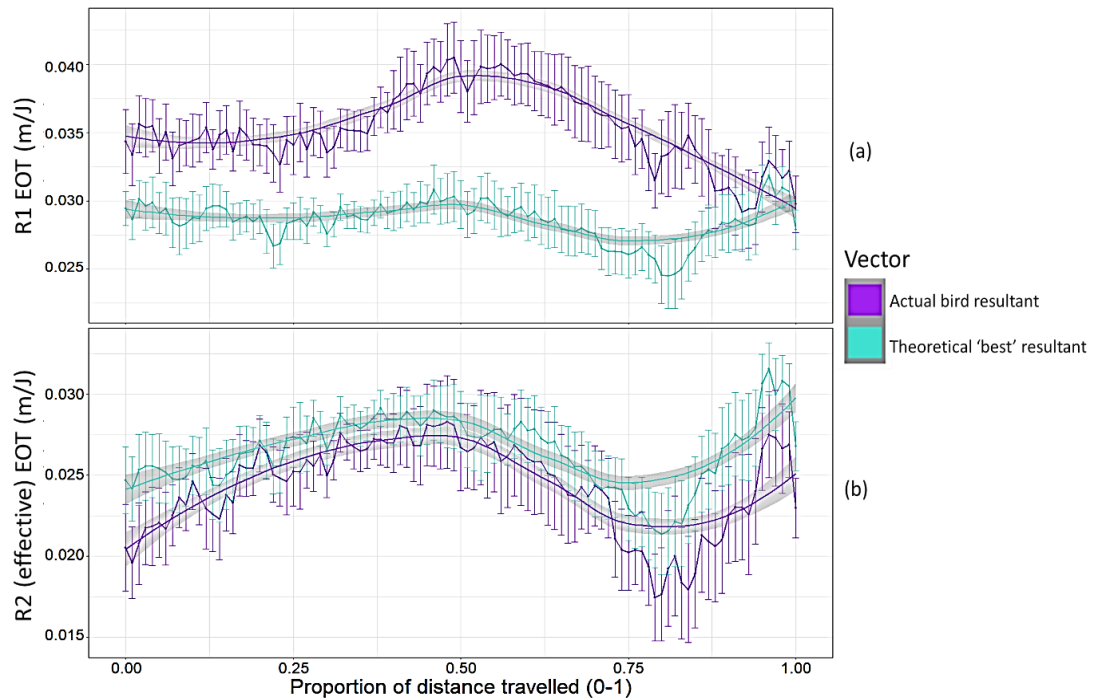


Figure 5. Mean (± 1 SE) penguin ease of transport (EOT - in metres travelled per joule) as a function of the proportion of the return distance to the colony for the (theoretical 'best' trajectory (turquoise) and the actual resultant trajectory (purple), linked with 'loess' smoothed lines. (a) shows the ease of transport in any direction (R1) while (b) shows ease of transport with respect to distance travelled towards the colony (R2) (for greater vector comparison, y-scales differ).

Discussion

Orientation strategy

My first aim, to investigate the abilities of the penguins to orientate themselves towards their colony, demonstrated that, with some (symmetrical) variation, they appeared to adopt a 'line-of-sight' heading (Fig. 3a). This is obviously most appropriate under conditions that I defined as 'slack water' (although even these usually had some minimal current flow) conditions. I suggest that the variation around the 'line-of-sight' heading at this time, stems from inaccuracies in the birds' navigational systems but are also due to deviations in the trajectory due to penguins occasionally pursuing prey. The important observation that the variation around the mean heading did not substantially change with distance to the colony (SI: Text S1: Fig. S3) suggests that the navigation process is not based on landmarks, which cannot be visible when birds start their return journey (at *ca.* 30 km) although they should

be when penguins are within a few km of the land, though, even when birds have line-of-sight, they do not improve, suggesting that sight is not important. Regardless, it appears that birds are not random in their return trajectories but rather have an overall ability to navigate at greater than 'approximate' cardinal directionality. The frequency distribution of 'line-of-sight' heading and current heading difference with respect to actual bird heading and 'line-of-sight' heading difference across the two current conditions, does suggest though, that they have a reasonable 'homing compass'. However, I do note that little or no current flow was sporadically and locally clustered along parts of a few penguin's return tracks. This was the reason for incorporating a relatively high current strength threshold between the two current conditions, and as such, I recommend that homing ability should be investigated further, in scenarios where current flow is predominantly lower and more variable in direction (current flow was rarely directly with or against 'line-of-sight' heading).

Secondly, the data suggest that the birds are able to determine when they are exposed to a current stream because the variance around the 'line-of-sight' heading increased under higher current flow conditions (Fig. 3a). Importantly, even without landmark references (*cf.* Emlen & Penney 1964; Shiomi *et al.* 2020), there is evidence that the penguins could determine current direction because an appreciable part of the variance around the 'line-of-sight' heading was due to the birds swimming preferentially with the current (Fig. 3b,c, Fig. 4a). Specifically, due to the nature of cross-currents across the majority of return legs (*cf.* Fig. 2), birds could choose between heading directly 'home' (or 'choosing' a heading [theoretical 'best' heading] that, when incorporated with current flow, enabled this [theoretical 'best' resultant heading' – *cf.* Fig. 1]) but at the expense of being greater exposed to opposing current conditions (Fig. 4b), or travelling at an angle to the 'line-of-sight' heading while capitalising on favourable current conditions, whilst still moving closer to the colony (Fig. 4a). That the penguins adopted the latter approach is a clear example of 'flow assisted movement' (*cf.* Chapman *et al.* 2011).

The success of any 'flow assisted movement' depends on the gain of energy imparted by the current vector and the extent to which it moves the navigating animal from its goal. The specific situation for the penguins navigating South within the San Mattias

Gulf depends on the alternating current regime due to the tidal cycle for the area. Here, there is an East-West and West-East current flow which will trend to push the birds, alternately, too far to the West and/or then too far to the East. Importantly though, since the return journey takes several hours (8 ± 2 h (± 1 SD)), this is enough time for the penguins to be exposed to elements of both current directions, and therefore for the currents to correct substantially for the unwanted lateral displacement. This can be demonstrated by a simple model. If we assume, during their return, that birds start at a position 38 km directly North of the colony, generally move in a southerly direction (Fig. 2a), that they are exposed to a perpendicular current of say 0.6 m/s (Fig. 2b) and that they generally adopt an actual heading that is centred around 25° off the 'line-of-sight' heading in favour of the current (*cf.* Fig. 4), swimming a mean speed of 1.5 m/s (accounting for surface periods, *cf.* Wilson 1985; Wilson, Ropert-Coudert & Kato 2002), they will be moving to the West or East of the colony at a rate of 1.23 m/s (and 1.35 m/s South). If the current were constant and not alternating, this would result in a displacement of 35.54 km to one side of the colony after a nominal 8 h return journey (and a slight 'overshoot' southbound, travelling 39.15 km). To swim directly against this current at the 'nominal commuting' speed of 2.1 m/s (*cf.* Wilson, Ropert-Coudert & Kato 2002) for 35.54 km would take 6.58 h, with an overall net speed of 1.5 m/s towards the 'line-of-sight' and require 1,654,006 additional joules. During an 8 h return journey, however, even if the penguins start their journey soon after the tide turns tide turns (nominally 6 hours per turn – SI: Text S1: Fig. S1) and were exposed to 5 h of current in one direction, followed by 3 hours in the opposite direction and the bird carried out the same strategy upon the turn tide (adopting an actual heading centred around 25° off the 'line-of-sight' heading in favour of the current, swimming at a mean speed of 1.5 m/s), then this approach would 'somewhat' cancel out and leave a smaller lateral displacement. In this scenario, the bird will be displaced 8.88 km to one side of the colony.

Assuming current direction is still in the favourable direction towards the 'line-of-sight', the bird would be required to take an additional correction trajectory, that (for commuting speed) would take 0.91 h (54.8 mins), with an overall net speed of 2.7

m/s and costing 229,613 additional joules. In fact, it is unlikely that any penguin will begin its return journey at exactly the point of a turning tide, so the displacement distance would nominally be less, whilst I am also excluding (amongst other things) the impact that variation in peak synergy (current strength) over time and across space would have). Nevertheless, if this second scenario is assumed to be the case, then the total energy usage for this return trajectory would amount to 1,842,735 joules and a median net speed of 1.84 m/s. All this suggests that the navigation strategy of Magellanic penguins actually capitalises on the alternating current directions generated by the San Matias Gulf tides, and that these are reflected in the typical 'S-shaped' movement patterns observed in these birds (Fig. 2a). However, the energetic benefits of this need to be considered with respect to a putative 'optimal' strategy, during which penguins adopt an 'actual bird heading' so that their 'theoretical 'best' resultant heading' (*cf.* Fig. 1a) accords with the 'line-of-sight' heading to the colony.

In accordance with the above scenario, if we now consider that the bird actually adopted the theoretical 'best' strategy, that is, the bird travelling at 1.5 m/s, would have to swim approximately 114° away from the current heading to obtain the 'line-of-sight' course, post current integration. This would necessitate a 1.37 m/s southbound speed and have the penguin back at the colony after 8 h (39.47 km), requiring 1,186,589 joules (only 64 % of that from the second scenario). In line with the actual data, the consequences of the penguin navigation strategy with respect to energy, my third aim, indicated that it was marginally (though significantly) energetically more efficient to move 'optimally' [theoretical 'best' heading] when the distance considered was the straight-line trajectory towards the colony (R2, Fig. 5, SI: Text S1: Fig. S6). Against this, the ease of transport for distance covered in any direction was substantially better for the headings taken by the penguins, and indeed better than they would be if the birds were swimming in slack waters because the penguins capitalise on the current strength (*cf.* SI: Text S1: Fig. S4), in a manner akin to the migrating birds flying with tailwinds (see Liechti 2006 for review). The specific advantage of this is that penguins can continue to search opportunistically for prey during their return journeys (as indicated by the depth of returning dives (SI: Text S1:

Fig. S7), which are much deeper than proposed 'travelling dives' (Wilson & Wilson 1995)) at low energetic cost. Further, whilst currently unexplored, resting periods, may be a low energetic opportunity (and/or necessity) to travel when currents are 'somewhat' favourable – this would rarely be possible when adopting the theoretical 'best' heading, given this nearly always involves some form of locomotion away from the 'line-of-sight' heading (*cf.* Fig. 4). Lastly, it is worth noting that my analyses were constrained to the GPS-corrected dead reckoned tracks and so the impact following the theoretical 'best' resultant vector of travel (in terms of departing from the track and thus subject to changeable current conditions) is currently unexplored.

Potential errors

I consider findings to be taken as general trends given that the nature of this study involved a degree of uncontrollable error. Firstly, with respect to currents, a depth-averaged field was used which does not take into account variations of syzygy with respect to depth (though the harmonic analysis used indicates that vertical variations in this area are minimal), or wind-generated waves at the sea surface, propagating chop through the top layers of the water column, whilst obviously current flow can vary within 1 km² grid resolution. Also, the model uses climatological external forcing (heating flux and wind stress), long-period averaged data (more than 10 years) based on satellite image sensors. This prevents the model from capturing events of particular years and high frequency variations. Secondly, heading derived from the tilt-compensated compass method can become inaccurate during periods of highly dynamic movement (Noda *et al.* 2012), whilst slight discrepancies in tag placement between birds and dislodgment of tag position during logging can introduce a constant source of bias to heading output. Moreover, variation between estimated and 'true' speed per unit time is inevitable. As such resultant vectors of travel incorporating both the magnitude and direction from both current and bird vectors, would have incorporated some degree of error. Nevertheless, I would expect such sources of error to be uniformly variable and thus conclude that the noticeable bias that exists between the direction a bird travels with respect to the colony and current direction is a true phenomenon.

Conclusion

I conclude from this study that penguins operating within high current regimes are able to perceive and react to currents and they do so in a manner that enables them to return home with a marginally greater effective cost than optimum, but at improved resultant speeds which, in the framework of dive performance and opportunistic foraging, makes for a sensible practice. This work provides a novel framework, merging both theoretical and practical aspects of movement within a dynamic medium for investigating animal-current interactions. I suggest that further work building on this approach should investigate 'homing' ability within environments where currents are minimal and have a multimodal directionality to further clarify the extent to which they 'know' where 'home' is.

References

- Åkesson, S. & Hedenström, A. (2007) How Migrants Get There: Migratory Performance and Orientation. *BioScience*, **57**, 123-133.
- Bannasch, R., Wilson, R. & Culik, B. (1994) Hydrodynamic aspects of design and attachment of a back-mounted device in penguins. *Journal of Experimental Biology*, **194**, 83-96.
- Bidder, O.R., Walker, J.S., Jones, M.W., Holton, M.D., Urge, P., Scantlebury, D.M., Marks, N.J., Magowan, E.A., Maguire, I.E. & Wilson, R.P. (2015) Step by step: reconstruction of terrestrial animal movement paths by dead-reckoning. *Movement Ecology*, **3**, 23.
- Boersma, P.D. & Rebstock, G.A. (2009) Foraging distance affects reproductive success in Magellanic penguins. *Marine Ecology Progress Series*, **375**, 263-275.
- Bonadonna, F., Benhamou, S. & Jouventin, P. (2003) Orientation in "Featureless" Environments: The Extreme Case of Pelagic Birds. pp. 367-377. Springer Berlin Heidelberg, Berlin, Heidelberg.
- Carter, M.I.D., Cox, S.L., Scales, K.L., Bicknell, A.W.J., Nicholson, M.D., Atkins, K.M., Morgan, G., Morgan, L., Grecian, W.J., Patrick, S.C. & Votier, S.C. (2016) GPS tracking reveals rafting behaviour of Northern Gannets (*Morus bassanus*): implications for foraging ecology and conservation. *Bird Study*, **63**, 83-95.
- Cerritelli, G., Bianco, G., Santini, G., Broderick, A.C., Godley, B.J., Hays, G.C., Luschi, P. & Åkesson, S. (2019) Assessing reliance on vector navigation in the long-distance oceanic migrations of green sea turtles. *Behavioral Ecology*, **30**, 68-79.
- Chapman, Jason W., Klaassen, Raymond H.G., Drake, V.A., Fossette, S., Hays, Graeme C., Metcalfe, Julian D., Reynolds, Andrew M., Reynolds, Don R. & Alerstam, T. (2011) Animal Orientation Strategies for Movement in Flows. *Current Biology*, **21**, R861-R870.
- Egbert, G.D., Bennett, A.F. & Foreman, M.G.G. (1994) TOPEX/POSEIDON tides estimated using a global inverse model. *Journal of Geophysical Research: Oceans*, **99**, 24821-24852.
- Emlen, J.T. & Penney, R.L. (1964) Distance navigation in the Adelie Penguin. *Ibis*, **106**, 417-431.
- Gibson, R., Barnes, M. & Atkinson, R. (2001) *Oceanography and Marine Biology, An Annual Review, Volume 39: An Annual Review: Volume 39*. CRC Press.
- Glorioso, P.D. & Flather, R.A. (1995) A barotropic model of the currents off SE South America. *Journal of Geophysical Research: Oceans*, **100**, 13427-13440.
- Goto, Y., Yoda, K. & Sato, K. (2017) Asymmetry hidden in birds' tracks reveals wind, heading, and orientation ability over the ocean. *Science Advances*, **3**, e1700097.
- Hays, G.C. (2017) Ocean currents and marine life. *Current Biology*, **27**, R470-R473.
- Jones, G. (2011) Sensory Biology: Bats Feel the Air Flow. *Current Biology*, **21**, R666-R667.
- Kantha, L.H., Tierney, C., Lopez, J.W., Desai, S.D., Parke, M.E. & Drexler, L. (1995) Barotropic tides in the global oceans from a nonlinear tidal model assimilating altimetric tides: 2. Altimetric and geophysical implications. *Journal of Geophysical Research: Oceans*, **100**, 25309-25317.
- Kara, A.B., Metzger, E.J. & Bourassa, M.A. (2007) Ocean current and wave effects on wind stress drag coefficient over the global ocean. *Geophysical Research Letters*, **34**.
- Kelly, J.T. & Klimley, A.P. (2012) Relating the swimming movements of green sturgeon to the movement of water currents. *Environmental Biology of Fishes*, **93**, 151-167.
- Klaassen, R.H., Hake, M., Strandberg, R. & Alerstam, T. (2011) Geographical and temporal flexibility in the response to crosswinds by migrating raptors. *Proceedings of the Royal Society B: Biological Sciences*, **278**, 1339-1346.
- Liechti, F. (2006) Birds: blowin' by the wind? *Journal of Ornithology*, **147**, 202-211.

- Liechti, F., Hedenström, A. & Ålerstam, T. (1994) Effects of Sidewinds on Optimal Flight Speed of Birds. *Journal of Theoretical Biology*, **170**, 219-225.
- Luna-Jorquera, G. & Culik, B.M. (2000) Metabolic rates of swimming Humboldt penguins. *Marine Ecology Progress Series*, **203**, 301-309.
- Mattern, T., Ellenberg, U., Houston, D.M. & Davis, L.S. (2007) Consistent foraging routes and benthic foraging behaviour in yellow-eyed penguins. *Marine Ecology Progress Series*, **343**, 295-306.
- Mellor, G.L. & Yamada, T. (1982) Development of a turbulence closure model for geophysical fluid problems. *Reviews of Geophysics*, **20**, 851-875.
- Noda, T., Okuyama, J., Koizumi, T., Arai, N. & Kobayashi, M. (2012) Monitoring attitude and dynamic acceleration of free-moving aquatic animals using a gyroscope. *Aquatic Biology*, **16**, 265-276.
- Pedley, M. (2012) eCompass-Build and Calibrate a Tilt-Compensating Electronic Compass. *Circuit Cellar-The Magazine For Computer Applications*, 1-6.
- Pisoni, J.P., Glembocki, N.G., Romero, S.I. & Tonini, M.H. (2020) Internal solitary waves from L-band SAR over the Argentine inner Patagonian shelf. *Remote Sensing Letters*, **11**, 525-534.
- Ropert-Coudert, Y., Kato, A., Baudat, J., Bost, C.-A., Le Maho, Y. & Naito, Y. (2001) Time/depth usage of Adélie penguins: an approach based on dive angles. *Polar Biology*, **24**, 467-470.
- Rosciano, N.G., Polito, M.J. & Raya Rey, A. (2016) Do penguins share? Evidence of foraging niche segregation between but not within two sympatric, central-place foragers. *Marine Ecology Progress Series*, **548**, 249-262.
- Sala, J., Wilson, R., Frere, E. & Quintana, F. (2012) Foraging effort in Magellanic penguins in coastal Patagonia, Argentina. *Marine Ecology Progress Series*, **464**, 273-287.
- Sánchez-Román, A., Gómez-Navarro, L., Fablet, R., Oro, D., Mason, E., Arcos, J.M., Ruiz, S. & Pascual, A. (2019) Rafting behaviour of seabirds as a proxy to describe surface ocean currents in the Balearic Sea. *Scientific Reports*, **9**, 17775.
- Sekhon, J.S. & Sekhon, M.J.S. (2020) Package 'Matching'. The Matching Package. R package documentation available from the Comprehensive R Archive: <http://cran.usthb.dz/web/packages/Matching/Matching.pdf>.
- Shchepetkin, A.F. & McWilliams, J.C. (2005) The regional oceanic modeling system (ROMS): a split-explicit, free-surface, topography-following-coordinate oceanic model. *Ocean Modelling*, **9**, 347-404.
- Shepard, E.L., Wilson, R.P., Rees, W.G., Grundy, E., Lambertucci, S.A. & Vosper, S.B. (2013) Energy Landscapes Shape Animal Movement Ecology. *The American Naturalist*, **182**, 298-312.
- Shiomi, K., Kokubun, N., Shimabukuro, U. & Takahashi, A. (2020) Homing Ability of Adélie Penguins Investigated with Displacement Experiments and Bio-Logging. *Ardea*, **107**, 333-339.
- Shiomi, K., Sato, K., Mitamura, H., Arai, N., Naito, Y. & Ponganis, P.J. (2008) Effect of ocean current on the dead-reckoning estimation of 3-D dive paths of emperor penguins. *Aquatic Biology*, **3**, 265-270.
- Tarroux, A., Weimerskirch, H., Wang, S.-H., Bromwich, D.H., Cherel, Y., Kato, A., Ropert-Coudert, Y., Varpe, Ø., Yoccoz, N.G. & Descamps, S. (2016) Flexible flight response to challenging wind conditions in a commuting Antarctic seabird: do you catch the drift? *Animal Behaviour*, **113**, 99-112.
- Taylor, C.R., Caldwell, S.L. & Rowntree, V. (1972) Running up and down hills: some consequences of size. *Science*, **178**, 1096-1097.
- Tonini, M.H. & Palma, E.D. (2017) Tidal dynamics on the North Patagonian Argentinean Gulfs. *Estuarine, Coastal and Shelf Science*, **189**, 115-130.

- Vogel, S. (1978) Organisms That Capture Currents. *Scientific American*, **239**, 128-139.
- Weimerskirch, H., Salamolard, M., Sarrazin, F. & Jouventin, P. (1993) Foraging strategy of wandering albatrosses through the breeding season: a study using satellite telemetry. *The Auk*, **110**, 325-342.
- Williams, T.D. & Busby, J. (1995) *Bird families of the world. 2. The Penguins: Spheniscidae*. Oxford University Press, Oxford.
- Wilson, R. (1985) The Jackass Penguin (*Spheniscus demersus*) as a pelagic predator. *Marine Ecology Progress Series*, **25**, 219-227.
- Wilson, R.P. (2004) Reconstructing the past using futuristic developments: trends and perspectives using logger technology on penguins. *Memoirs of the National Institute of Polar Research: Special Issue*, 34-49.
- Wilson, R.P., Kreye, J.M., Lucke, K. & Urquhart, H. (2004) Antennae on transmitters on penguins: balancing energy budgets on the high wire. *Journal of Experimental Biology*, **207**, 2649-2662.
- Wilson, R.P., Liebsch, N., Davies, I.M., Quintana, F., Weimerskirch, H., Storch, S., Lucke, K., Siebert, U., Zankl, S., Müller, G., Zimmer, I., Scolaro, A., Campagna, C., Plötz, J., Bornemann, H., Teilmann, J. & McMahon, C.R. (2007) All at sea with animal tracks; methodological and analytical solutions for the resolution of movement. *Deep Sea Research Part II: Topical Studies in Oceanography*, **54**, 193-210.
- Wilson, R.P., Pütz, K., Peters, G., Culik, B., Scolaro, J.A., Charrassin, J.-B. & Ropert-Coudert, Y. (1997) Long-Term Attachment of Transmitting and Recording Devices to Penguins and Other Seabirds. *Wildlife Society Bulletin (1973-2006)*, **25**, 101-106.
- Wilson, R.P., Ropert-Coudert, Y. & Kato, A. (2002) Rush and grab strategies in foraging marine endotherms: the case for haste in penguins. *Animal Behaviour*, **63**, 85-95.
- Wilson, R.P., Shepard, E. & Liebsch, N. (2008) Prying into the intimate details of animal lives: use of a daily diary on animals. *Endangered Species Research*, **4**, 123-137.
- Wilson, R.P. & Wilson, M.P.T. (1995) *The foraging behaviour of the African penguin Spheniscus demersus*. Surrey Beatty & Sons, Sydney.
- Young, C.M. & Braithwaite, L.F. (1980) Orientation and current-induced flow in the stalked ascidian *Styela montereyensis*. *The Biological Bulletin*, **159**, 428-440.

Chapter 9 Synopsis

Richard M. Gunner



Photo taken by Andrea Benvenuti

Why did my thesis take the direction it did?

One of the luxuries, for me, of undertaking a PhD, was the chance to pursue appealing avenues of research, and specifically ones that I felt would be of value to the community. It was clear that my work would involve animal-attached tags containing inertial measurement units (IMUs), but little was defined beyond that. The use of accelerometers within such tags, to quantify animal body posture and movement, has been examined extensively (Shepard *et al.* 2008a; Shepard *et al.* 2008b; Brown *et al.* 2013; McClune *et al.* 2014), providing information on travelling speed (Bidder *et al.* 2015; Walker *et al.* 2015), activity extent (Barwick *et al.* 2018; Fukasawa *et al.* 2018), mechanical energetic expenditure (Gleiss, Wilson & Shepard 2011; Wilson *et al.* 2020a) and associated behavioural patterns (Guo *et al.* 2006; Graf *et al.* 2015; Williams *et al.* 2015; Chakravarty *et al.* 2019a; Rodriguez-Baena *et al.* 2020). Beyond acceleration though, IMUs are often integrated with magnetometers, enabling animal heading to be resolved with high accuracy (Wilson, Shepard & Liebsch 2008; Fourati *et al.* 2011; Patel *et al.* 2017). Heading is a fundamental variable for characterising behaviour and although a few studies (using the accelerometer-magnetometer approach) have explored its utility for investigating various aspects of space-use (e.g., Bidder *et al.* 2015), behavioural time-budgets (e.g., Chakravarty *et al.* 2019b; Narazaki *et al.* 2021) and magnetic alignment responses (e.g., Painter *et al.* 2016), applications have been minimal compared to acceleration-based work.

In addition, work on the derivative of heading, the rate change of heading, or as defined in Chapter 2 - angular velocity about the yaw axis (AVeY) - is virtually absent in the biologging literature (excepting the odd gyroscopic study (e.g., Noda *et al.* 2014)), despite the interplay between step lengths and turn extents being important descriptors of behaviour-specific movements, as is referred to in navigation- (*cf.* Shiomi *et al.* 2020) and foraging strategies (*cf.* Weimerskirch *et al.* 2007). Many studies to date, have investigated such strategies using indices of tortuosity (*cf.* Li & Payandeh 2016) derived from interpolations between time-specific discrete verified positions (VPs; principally obtained using radio telemetry, *cf.* McLean & Skowron Volponi 2018) although, as highlighted with GPS in Chapter 4, 5 and 6, continuous measurements are not always possible and location estimates can be markedly

inaccurate anyway (Lewis *et al.* 2007; Frair *et al.* 2010; Forin-Wiart *et al.* 2015). For this reason, obtaining accurate fine-scale (e.g., infra-second) turn extents is simply not possible using this approach (*cf.* Hurford 2009), which compounds space-use and distance travelled estimates (McCann *et al.* 2021; Poulin, Clermont & Berteaux 2021). Furthermore, even coarsely resolved heading change requires consecutive VPs to be different and this precludes examination of orientation change (or lack of) when the animal is stationary (Swain, Wark & Bishop-Hurley 2008). Non-travelling orientations can be equally important to examine though, for example, to understand the impact of basking orientation on thermoregulation in ectotherms (e.g., Stanton-Jones, Parusnath & Alexander 2018). Indeed, one might speculate that patterns of angular rotation while stationary may have particular value for discerning behavioural state changes, for example, vigilance responses according to predator presence.

With the above considerations, the central theme of this thesis was to investigate how body rotation can help us understand biological phenomena, particularly movement strategies that they are considered to enhance fitness (Boggs 1992). My overarching question throughout was ‘What does animal rotation tell us about behaviour?’, and as my own PhD journey comes full circle (!), I now appreciate that different proximate and ultimate questions and explanations of behaviour arise according to the different scales over which rotation is assessed. I like to use the analogy of a jigsaw puzzle; the detail lies in the pieces, but the story requires the ‘complete picture’. Assessing body rotation at fine temporal scales can reveal important elements of behaviour and piecing them together in space and time can divulge important movement-specific behavioural strategies. I expand on this key concept here using the penguin and cormorant as example species to demonstrate my points and go on to speculate where I feel the direction of this work could usefully go in the future.

Piecing together the puzzle: the dive and foraging strategy

A critical consideration of Tinbergen’s ‘survival value’ concept is how behaviour is purported to maximise energy conservation and/or uptake (Nesse 2018). Turn rates are a key component of fitness because they have a direct link to energy expenditure

(Wilson *et al.* 2020b). The faster an animal changes its heading, the greater the energy investment and this is modulated according to its speed and medium of travel (Wilson *et al.* 2020b). Notably, in this, the time and energy that an animal allocates to different areas in space is a function of the time and speed that it adopts for given headings and turn angles, and this is a corollary of its behavioural response to internal motivation and environmental circumstance (e.g., Wilson *et al.* 2013a; Lempidakis *et al.* 2018).

Air-breathing diving marine vertebrates spend a large proportion of their lives underwater and make for excellent subjects for examination of investment of time and heading in energies and space-use, because they must balance the need to locate and capture food with the energy costs associated with swim speed and swim angle at depth (Sato *et al.* 2003; Wilson *et al.* 2010; Okuyama *et al.* 2012). Specifically, diving animals that hold appreciable volumes of air in their tissues (including lungs, air sacs and plumage, as is the case for both penguins and cormorants), are generally highly buoyant at the water surface and so have to invest appreciable energy to overcome this 'upward' buoyancy force during the initial descent (Wilson *et al.* 1992; Watanuki *et al.* 2003; Kato *et al.* 2006). Air compression increases with pressure (Wilson *et al.* 1992) and pressure increases with depth (Hays, Metcalfe & Walne 2004) so the deeper the dive, the lower the power costs associated with work done against buoyancy (Wilson *et al.* 2010). It is not surprising therefore, that a strong inverse relationship exists between dive duration and energy investment (Hays *et al.* 2000; Enstipp *et al.* 2011; Davis 2014). In addition, the power costs of swimming in water rise with the cube of the velocity (Wilson, Ropert-Coudert & Kato 2002; Langerhans & Reznick 2010) (excluding the effect of upthrust) so judicious management of speed is important in energy management. And then there are the power costs associated with turning underwater, which whilst unknown, are likely to be equivalent to, or higher than, the turn costs on land (which scale disproportionately with speed and angular velocity - Wilson *et al.* 2020b). This is because, to facilitate a turn in water (particularly at high speeds), the bank angle of the body must increase (which requires energy anyway), compromising the hydrodynamic profile of the animal and thus the wake momentum of the surrounding fluid velocity in a manner that is less

favourable to thrust and more favourable to drag (Drucker & Lauder 2000). In short, the dynamics of the dive descent and changing heading in diving birds critically modulate energy use and this affects dive duration. The ascent phase of a dive is far less energetically expensive than the descent and bottom phase (both in terms of speed and turn costs), because as the depth decreases, the upthrust increases, which helps increase speed (irrespective of the animal kinematics) (Wilson *et al.* 2010).

All the above boils down into two critical issues. Firstly, the functions of a given dive should govern its characteristics since changes in swim speed, body posture and/or heading at any given depth have energetic consequences. Secondly, if different dives (defined by their characteristics – *cf.* Wilson *et al.* 1996; Schreer, Hines & Kovacs 1998; Schreer, Kovacs & O'Hara Hines 2001) serve different purposes (as suggested by Wilson *et al.* (1991); Williams *et al.* (1992); Wilson *et al.* (1993); Peters *et al.* (1998) and others), then their appearance in space and time should reveal important strategies relating to space-use (e.g., Wilson 2002). Such thinking leads to questions such as; how do animals allocate their time and energy to areas? In the specific context of heading, why should animals turn unless the 'potential' benefit of doing so outweighs the cost? Such issues are directly relevant to optimal foraging theory (*cf.* Pyke 1984), though to my knowledge have never been incorporated, and relate critically to prey distribution in time and space (*cf.* Wilson 1985).

As highlighted in Chapter 3, researchers conventionally classify the functionality of a dive based on its time-depth profile – a representation of depth *versus* time (Halsey, Bost & Handrich 2007). Within this, Simeone and Wilson (2003) were amongst the first to demonstrate that undulations, or 'wiggles', during the bottom phase of penguin dives could be used to estimate prey consumption with reasonable accuracy (mean error: $10 \pm 6\%$) because each 'wiggle' corresponded to the capture of a single prey. The authors argued that this simple technique could be expanded to elucidate the foraging behaviour of other marine endotherm divers. Although illuminating, its utility is confined to animals that consistently have variation in depth associated with prey capture (such as Spheniscus penguins, which typically capture their prey from the underneath). However, this is not always the case in those species that display these patterns (Simeone & Wilson 2003) and serves virtually no purpose when

animals do not, such as in benthic feeders (e.g., most cormorant species, Quintana, Wilson & Yorio 2007; Cook *et al.* 2008; Laich *et al.* 2008; Kotzerka, Hatch & Garthe 2011). This is illustrated in Fig. 1.

In addition, the ‘effort’ underlying prey pursuit is hidden when just depth is assessed.

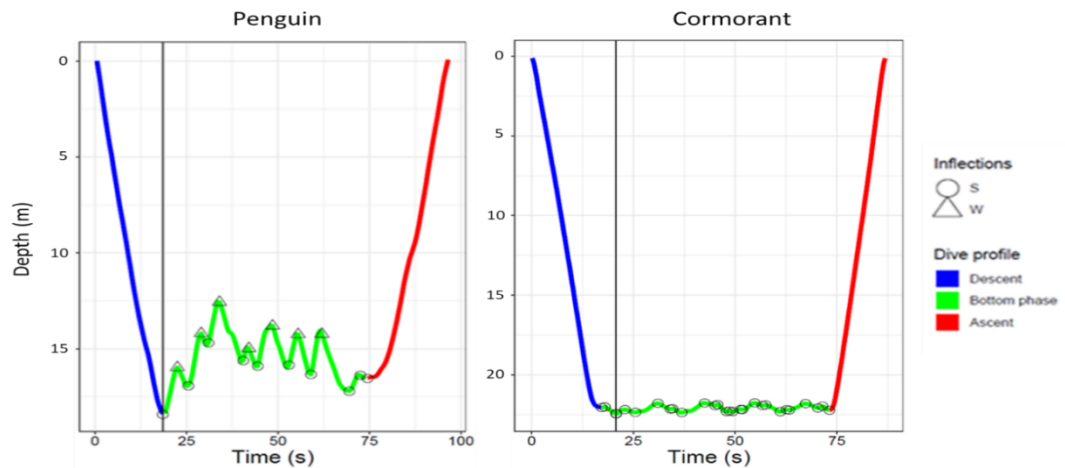


Figure 1. **Variation in depth may or may not indicate prey capture depending on diving bird lifestyle.** A dive profile of a Magellanic penguin [left] and Imperial cormorant [right] represented by depth (m) over time (s), coloured according to the 3 main components of a dive profile [descent = blue, bottom phase = green, ascent = red]. The vertical line demonstrates the point of maximum depth. Circles (S) represent ‘steps’ in depth - any time that the rate of change of depth changes from positive to negative or vice versa. Triangles (W) represent ‘wiggles’, which are supposedly indicative of prey capture (Simeone & Wilson 2003); steps are upgraded to wiggles when the difference in depth between steps ≥ 0.3 m and the differential of depth at any point during this candidate wiggle ≥ 0.3 m/s⁻¹ (Simeone & Wilson 2003). Note the absence of wiggles in the benthic-foraging cormorants.

Put simply, and seldom explicitly stated, the time-depth approach ignores space-use in 3-D, precluding potentially informative measures of effort, such as distance travelled, overall swim speed and the tortuosity of movement involved (Wilson *et al.* 2007). A primary reason for not stating this is that very few researchers have the necessary data to be able to examine it. Acceleration-based metrics do provide an extra layer of insight beyond simple changes in depth though. Dynamic body acceleration (DBA, and VeDBA is a variant of this), can provide an indication of the mechanical power involved in movement (Gómez-Laich *et al.* 2013), although it has never been assessed with respect to turns, and body posture (swim angle) derived from static acceleration (Shepard *et al.* 2008a) can be used to approximate the horizontal component of travel during descent and ascent by using trigonometry employing the rate of change of depth (Laplanche, Marques & Thomas 2015).

Importantly, the rate change of heading (AveY) can provide a useful independent metric of activity that should be at least as useful as acceleration-based metrics. In Chapter 2, I emphasise the utility of AveY for discerning activity in slow-moving animals, though it clearly should have value in dynamic animals. Throughout this thesis, I have acknowledged that heading measurements can become erroneous during periods of high centripetal acceleration (using the accelerometer-magnetometer approach; because the static acceleration, required to offset device tilt when deriving heading, can be difficult to resolve at such times). This would seem to negate the value of AveY for dynamic animals, however I do not think this is a problem. This is because high centripetal acceleration is always linked to high turn rates and so, although exact heading values may not be accurately resolved, the derivative of heading will still display high variation. In terms of AveY as an activity metric, this is nonetheless helpful because power costs increase disproportionately with turn rate (Wilson *et al.* 2020b) and thus high or erratic changes in directionality would act as an important marker for this.

An animal must change its heading to actively seek out and catch mobile prey during pursuit hunting (Wilson *et al.* 2013a; Hubel *et al.* 2016; Peterson, Soto & McHenry 2021). AveY, therefore, should be an invaluable metric to work alongside wiggle depiction and/or DBA when discerning dive function and performance. This is highlighted in Fig. 2, where there is clear disparity in the variation of AveY estimates between non-pursuit and pursuit dives. In fact, this disparity appears greater than that provided by VeDBA (Fig. 2D *versus* Fig. 2E), indicating that AveY may be a more sensitive measure of prey pursuit than either VeDBA or 'wiggles' in the depth profile. Importantly, what this figure makes clear, is that penguins have an astonishingly low rate of change of heading across all dive types except those associated with prey acquisition. Beyond this, and as alluded to in Chapter 5 and 6, the only method to date that can represent space-use under water in 3-D with fine resolution is dead-reckoning (Fig. 2B), and this can be examined with respect to prey acquisition metrics (wiggles, VeDBA and AveY) to construct prey-availability landscapes (Fig. 3).

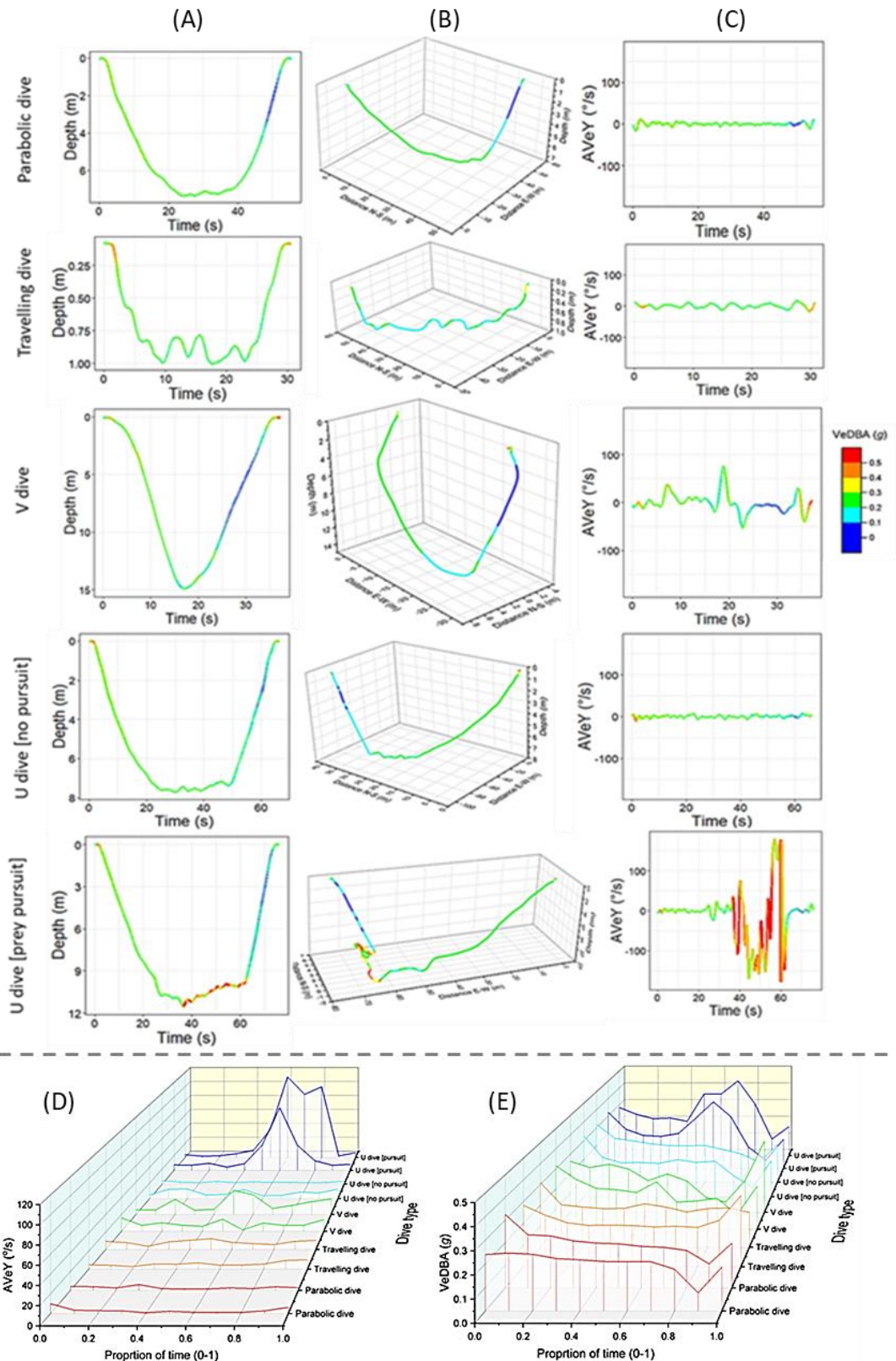


Figure 2. **Comparison of recognised penguin types based on the dive profile highlighting the value of AveY.** The five different Magellanic penguin dive types (e.g., Schreer et al. 1998) are represented as; (A) depth over time, (B) 3-D dead-reckoned paths and (C) AVEy ($^{\circ}/s$) over time, coloured according to VeDBA (g). The bottom panel shows mean absolute values of (D) angular velocity (AveY) and (E) VeDBA (E) per 0.1 increment of bottom phase (0 to 1), for each classified dive type (two dives per dive type).

Specifically, expanding out the scales of heading and rate of change in heading from individual dives to whole foraging trips can reveal how time and energy are allocated to space. For example, here aggregated mean (absolute) values of AVeY per given area of travelled movement (as ascertained *via* VP-corrected dead-reckoning - *cf.* Chapter 5) shows stark contrasts of rotation-related activity in space (Fig. 3B) which, at least visually, appear to also relate with the time spent in the area (Fig. 3A) and the incidence of ‘wiggles’; Fig. 3C).

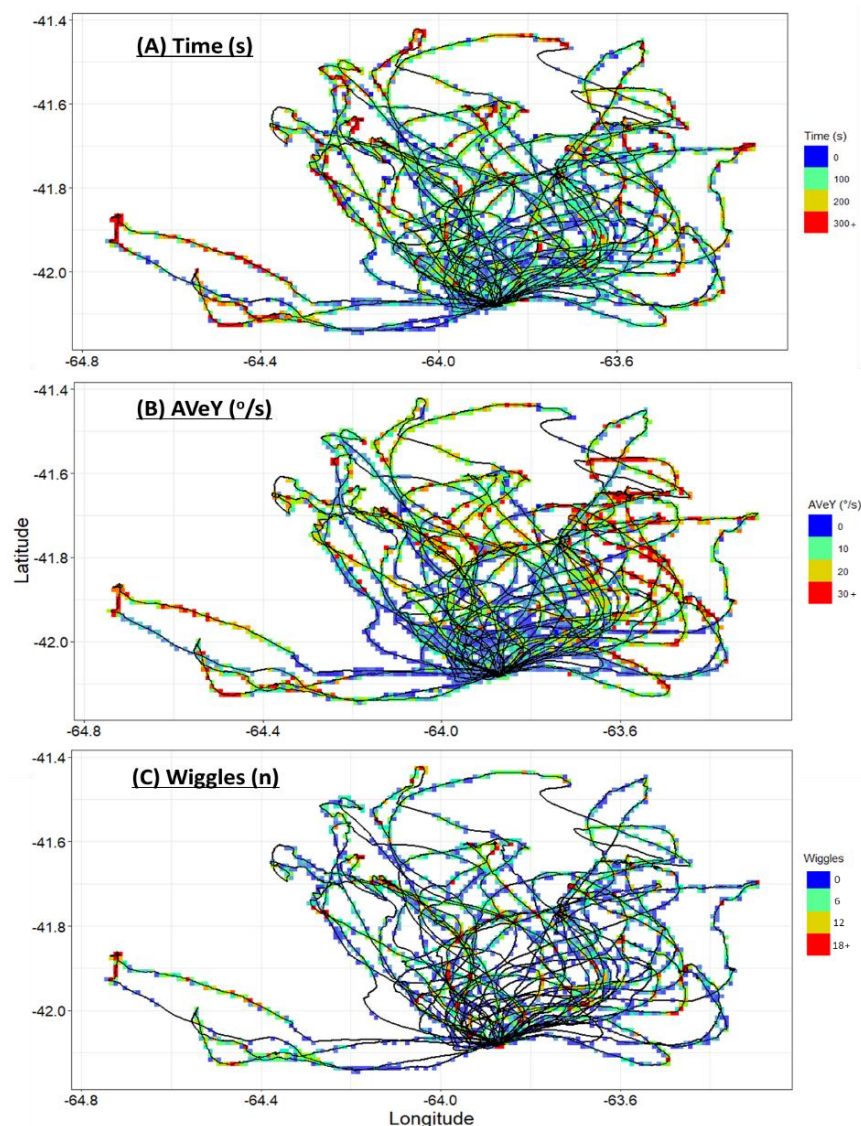


Figure 3. Metrics of putative prey capture can be examined in space in the dead-reckoned tracks of birds foraging underwater where normal tracking technologies fail. Mean values of; (A) time spent (s), (B) AVeY ($^{\circ}/s^{-1}$) and (C) the number of ‘wiggles’ (n) per ~ 1 km grid of travelled movement. Data taken from 29 Magellanic penguin dead-reckoned tracks during foraging trips. Only the bottom phases of dives > 0.5 m were assessed. Sections of track without a coloured grid indicates periods at or near the surface (≤ 0.5 m, which were classified as either resting bouts or travel dives).

Almost all diving birds are central place foragers during the breeding season (Elliott *et al.* 2009), having to commute appreciable distances between nest and food source. Most birds have facilitated commuting by using flight as an efficient mode of travel (Tucker 1975). Nevertheless, energy expenditure costs can still be appreciable because birds may spend significant amounts of time flying (Gómez-Laich *et al.* 2013), with the return leg typically being higher due to load-bearing as they transport food to the young (*cf.* Matyjasiak, Bazzi & Rubolini 2021). For minimizing cost of travel (COT; *sensu* Taylor, Caldwell & Rowntree 1972), ideal outgoing and incoming commutes should be highly directional and this is what is observed in the Imperial Cormorant data that I collected for parts of this thesis (*cf.* Chapter 5 and 6). Here, (Fig. 4), clear bimodality is seen in the radial plot of heading distribution during the flying phases, which is far less variable than non-flying periods (Fig. 4A [insert]), illustrating the value of heading data in examination of animal decision-making.

In terms of applying heading to diving strategy both *via* dead-reckoned paths and radial plots, I noticed that many birds foraged underwater using what appeared to be extensive line transects (e.g., Fig. 4B), rarely returning to a given area. This makes sense because, being bottom-foraging animals (Wilson & Wilson 1988) feeding primarily on stationary/slow-moving benthic prey (Punta, Saravia & Yorio 1993; Langerhans & Reznick 2010), they do not benefit by returning to a location recently visited. Confined tortuous movements did occasionally occur however (Fig. 4B [right]), and this likely relates to a high profitability in these areas, perhaps due to patchy prey (*cf.* Schoener 1971; Arditi & Dacorogna 1988; Foo *et al.* 2016). Further, whilst not shown here, some birds engaged in intermittent flights between dive bouts, presumably because, in contrast to area restricted searching (*cf.* Sims *et al.* 2006; Paiva *et al.* 2010; Reynolds 2012), this strategy likely indicates areas of low prey availability (*cf.* Weimerskirch 2007).

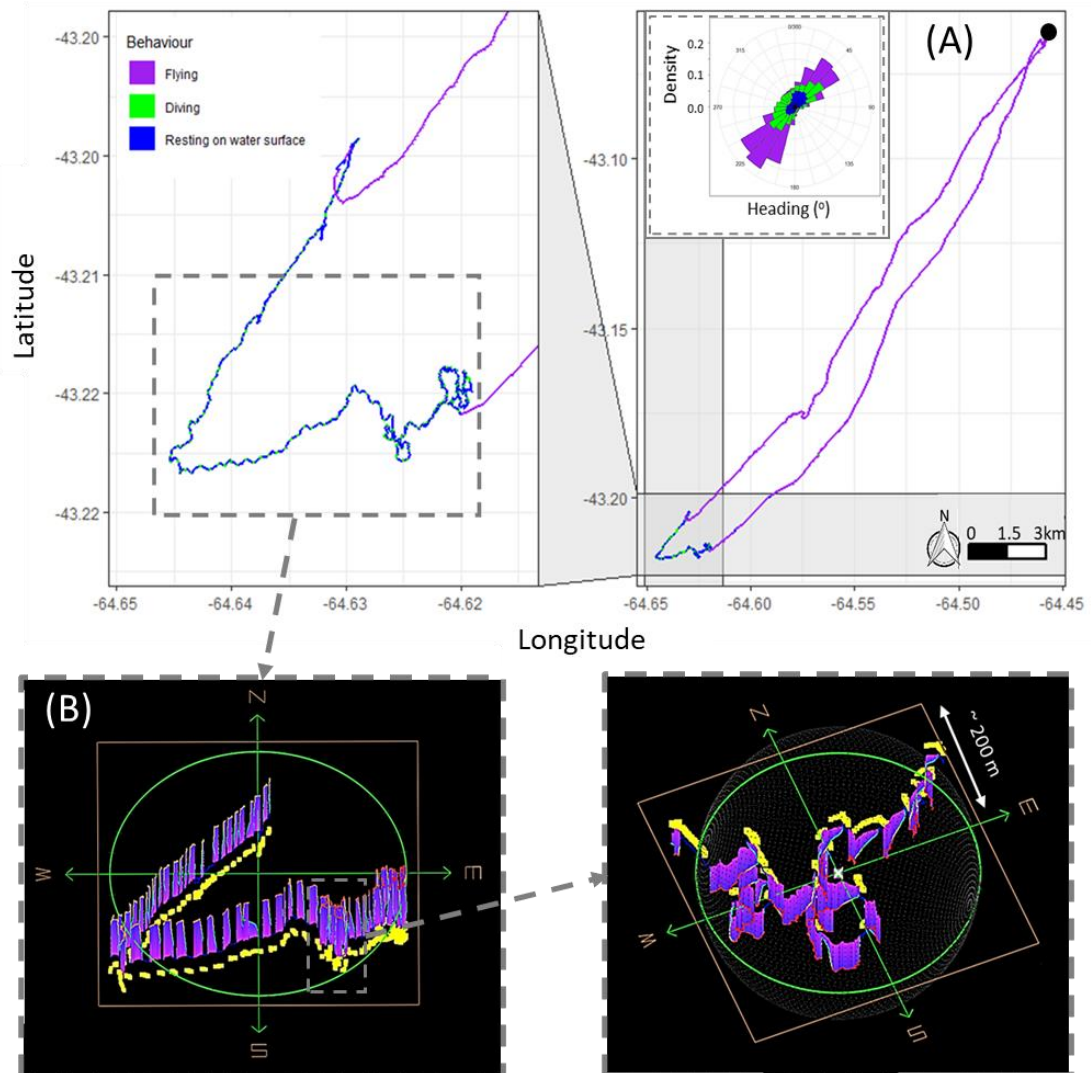


Figure 4. Examination of heading-based metrics reveals foraging patterns in a benthic foraging seabird. (A) One Imperial cormorant's foraging dead-reckoned track with an insert of a rose plot representing the relative frequency distribution of heading during flight [purple], dives [green] and resting on the water's surface [blue]. The intersection of the vertical and horizontal grey shading area shows the enlarged section in the left-hand panel. A section of the foraging phase of this track is magnified in (B) the bottom panel showing two different time periods and highlighting different path tortuosities. Note these two visualisations are inversely projected based on depth so that the bottom phase of dives appears to 'come out of the page'. Yellow markers denote GPS fixes (recording at 1 Hz).

The future

Throughout this PhD, I have become aware of the value that body rotation has for elucidating animal behavioural ecology and dead-reckoning is a fundamental component of this. I have left mention of dead-reckoning brief here as it constitutes large sections of my thesis, although its value, particularly when understanding human-wildlife disturbance is something I would like to continue to explore because I think that it could have genuine welfare, conservation and management

applications. Anthropogenetic alterations in habitat connectivity causes major disruption to the movement patterns of many free-ranging animals, and this can have deleterious consequences at various ecological levels (Clark *et al.* 2010; Marschall *et al.* 2011; Berger-Tal & Saltz 2019). Animal movement networks become fragmented and hazardous by works of deforestation and urbanisation (including the construction of roads, railways, fences, pipelines, dams and water diversion structures, Ito *et al.* 2013; Rahel & McLaughlin 2018). With respect to barriers, as an example, understanding where transgression occurs, including the conditions under which they occur and the effort involved by the transgressors, is critical to modelling the effect of the barriers on the issues they are designed to address (Hayward & Kerley 2009; Dupuis-Désormeaux *et al.* 2016). In contrast to the efforts of preventing passage, it may also be of value to examine the efforts of preserving connectivity, such as the utility of corridors (e.g., underpasses and overpasses) to facilitate safe movements between fragmented habitats (Panzacchi *et al.* 2016), such as adjacent sections of road (Lesbarrères & Fahrig 2012). In both scenarios, dead-reckoning may expedite the details of when, where, how and why transgression occurs by providing the necessary fine-scale movement trends pre- during- and post-transgression.

Clearly, rotation metrics provide vital information from individual behaviours to life history strategies, and further work should investigate their value (and how they can be applied) in machine-learning behavioural classifiers (e.g., Korpela *et al.* 2020), especially given its interplay with DBA. In fact, I would like to speculate (the joy of a synopsis), that there will be further value in exploring how AVeY scales with VeDBA (and other acceleration-based metrics), relative to behaviour. For example, if an animal must invest a lot of energy moving quickly, e.g., a lion chasing its prey, then straight-line travel would be energetically preferable than if high turn rates were also incorporated (Wilson *et al.* 2013b; Wilson *et al.* 2020b). This is supported to some extent by the contrasting differences between AVeY and VeDBA, apparent between flying and foraging periods in cormorants (Fig. 5).

In line with the above, there should therefore be important underlying reasons for both VeDBA and AVeY to scale together during travelling movements, such as the reward in catching high energy density prey (Wilson *et al.* 2013a). Indeed, combing dead-reckoning with metrics of high performance such as DBA and AVeY should be particularly informative for understanding the hunting strategies and performance in pack animals such the lion (Fig. 6).

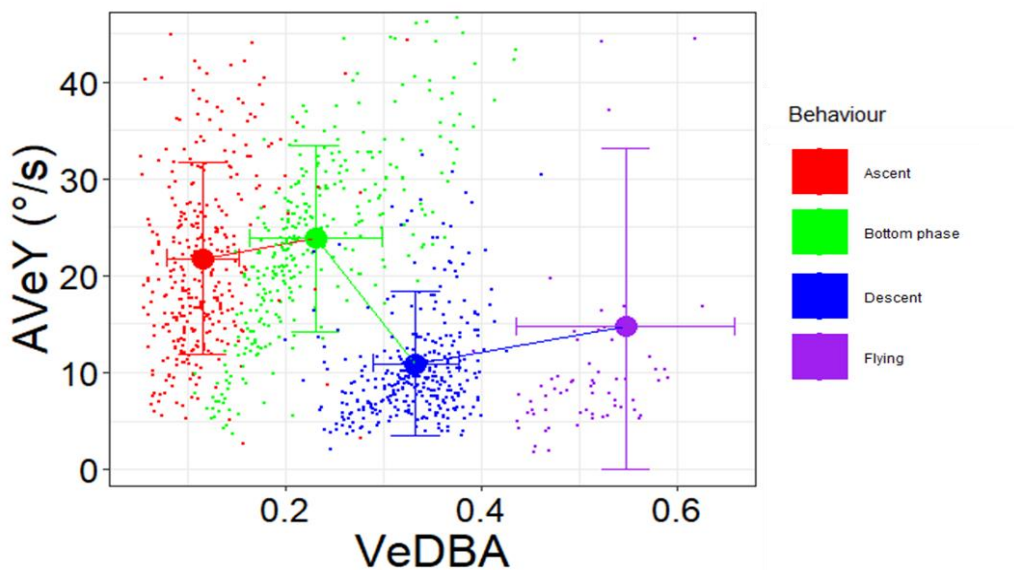


Figure 5. **Might AVeY scale with VeDBA according to behaviour.** Mean values aggregated per ascent (red), bottom phase (green) and descent (blue) per dive, and per flying (purple) period. Data taken from three individual Imperial cormorants across their entire foraging trips. Horizontal and vertical lines represent 1 SD (capped at $0\text{ }^\circ/\text{s}^{-1}$ for flying).

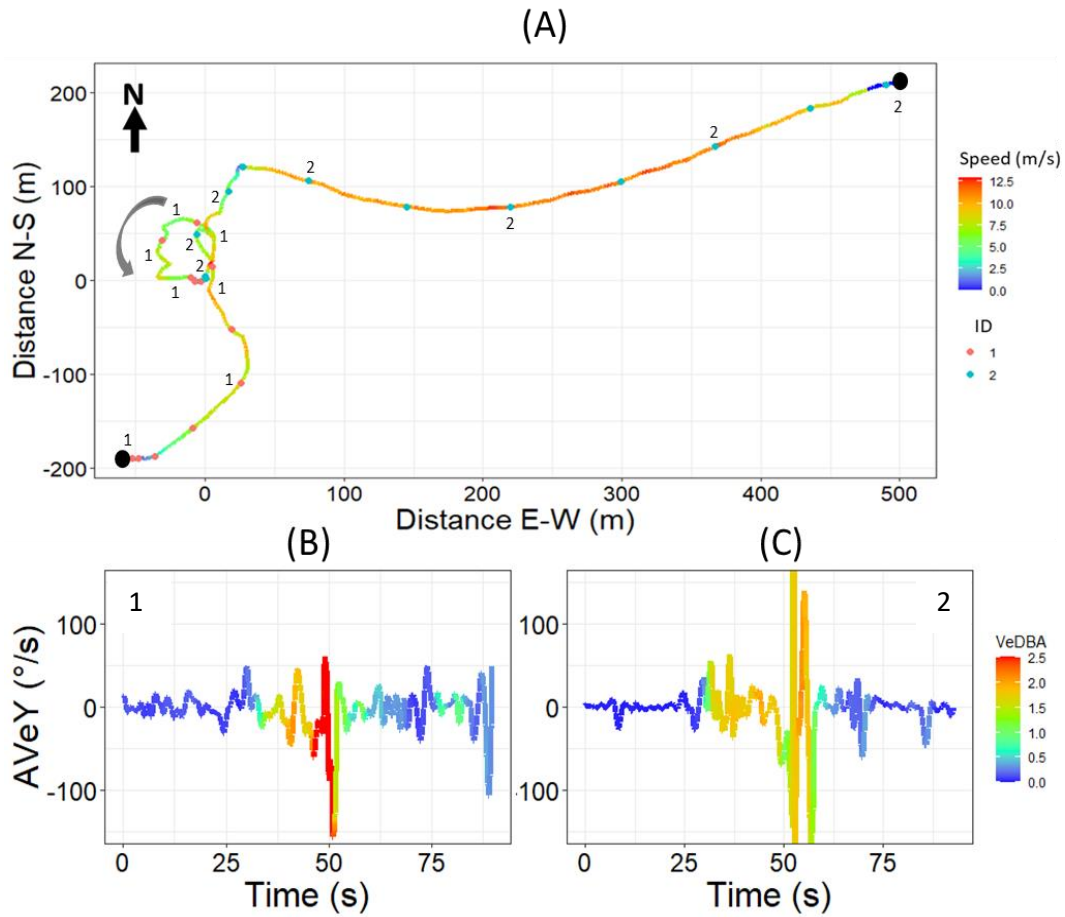


Figure 6. The movement strategy of two female lions during a hunt shows that high angular velocity is employed only in the closing stages of the capture of prey in a pincer movement. (A) The dead-reckoned tracks of two female lions during a high performance ~ 30 s chase coloured according to speed (m/s) estimated from the GPS-corrected dead-reckoned tracks. The circle symbols positioned ~ 2.5 s along the tracks are coloured according to the track ID with periodic ID numbers to help denote which track belongs to which individual. The females positioned themselves a dune apart (black circles) prior to initiating a chase, having separated some 40 mins beforehand, with the hunt terminating at the 0,0 m origin. (B) and (C) show the respective AVeY values over time profile associated with the two tracks, coloured according to VeDBA. This encompasses 30 s pre-chase (stationary-/slow stalking behaviour), the ~ 30 s chase and 30 s post-chase (stationary behaviour). This hunt was determined to be successful based on these two lions remaining at the 'kill site' for an extended period of time with characteristic oscillating patterns of acceleration indicating feeding.

Beyond this, rotation metrics may help elucidate how allometric scaling differences affect behaviour and associated activity budgets. For example, it is well known that the male Imperial cormorant, being slightly larger than the female, dives to greater depths than females benefitting in dive capacity due to its size (Laich *et al.* 2012 - *cf.* Fig. 7A). However, to date, very few people have the capacity to resolve gender-specific movement differences at depth such as 3-D tortuosity examined here (15 cormorants: 8 M, 7 F – 1495 dives) with a view to understanding how allometry affects performance. In my dataset, males had slightly more tortuous tracks (defined

as the straight-line distance divided by the sum of the distance travelled over the same period) in their 3-D dive profiles (Fig. 7B) which was determined to be significant (using two-sample t-tests), for the bottom phase ($t = 6.368$, $p < 0.001$ [\bar{x} : $M = 0.384$, $F = 0.291$]). Whether the higher levels of tortuosity exhibited in males during the bottom phase are an artifact of them having less time attributed to the bottom phase ($t = -3.161$, $p = 0.002$ [\bar{x} : $M = 72.486$ s, $F = 79.249$ s]) (cf. Laich *et al.* 2012) or attributed to higher dynamism in directionality remains to be seen.

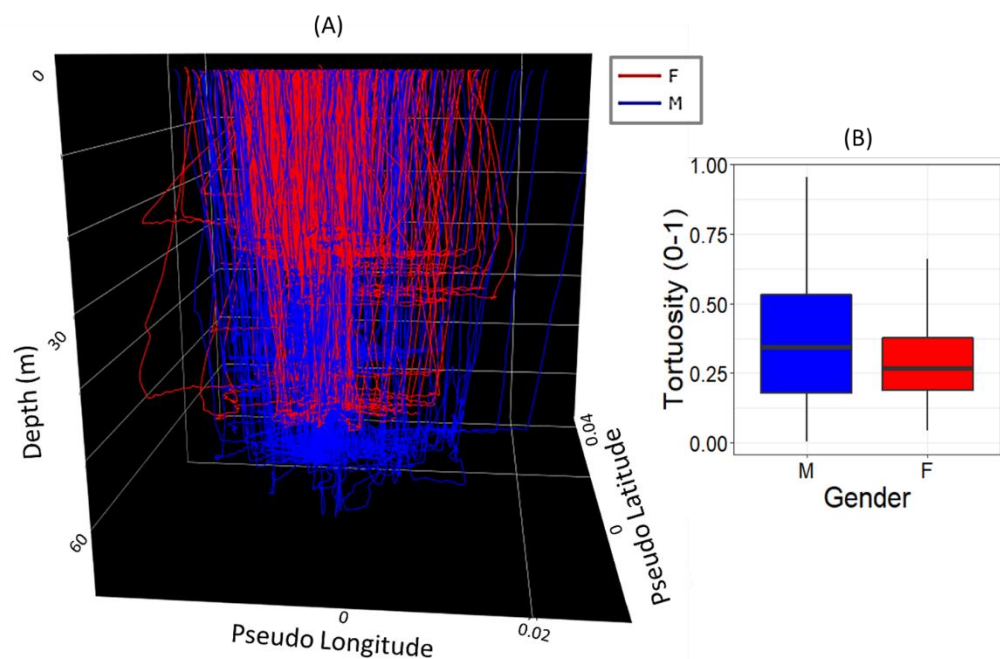


Figure 7. Dive depths and bottom phase tortuosity differ between male and female cormorants. (A) Dead-reckoned dive profiles from 15 cormorants (for 1495 dives), coloured according to gender [$M = \text{male}$ ($n = 3$); blue and $F = \text{Female}$ ($n = 3$); red]. The coordinates of each dive were zeroed off to start at 0,0 origin. (B) 3-D tortuosity was computed as the sum of the 3-D distance travelled divided by the straight-line distance over the same period. Values were subtracted from 1 so that a value of 0 reflects straight-line movement and values closer to 1 indicating more circular movement. Only the bottom phases of dives were assessed.

Determination of the details of animal movements thus seems to be critically linked to resolving animal heading over time and speed, while the energetics of movements is linked to speed and turn velocity. Taken together, these are two cornerstones of animal behavioural ecology, which feed into understanding how animal behaviours link to energy use and how both energy- and space-use over time might affect the efficiency of foraging, the probability of survival and ultimately link to lifetime reproductive success. For me, the power of simple heading data and their derivatives

lies in two facets; first, that they operate over timescales ranging from fractions of a second to lifetimes, and second, that they can be so easily combined with other metrics and indices of animal action (ranging from DBA to the specifics of behaviour) to create a matrix of understanding where the resultant is so much greater than the simple arithmetic sum of its parts. I feel privileged and excited to be part of the sensor revolution that has revealed so much about the way wild animals operate and would like to think that my contributions on heading, turning, angular velocity, dead-reckoning and the like will, in some small way, help catalyse the exhilarating hitherto unconsidered important elements of the future.

References

- Arditi, R. & Dacorogna, B. (1988) Optimal Foraging on Arbitrary Food Distributions and the Definition of Habitat Patches. *The American Naturalist*, **131**, 837-846.
- Barwick, J., Lamb, D.W., Dobos, R., Welch, M. & Trotter, M. (2018) Categorising sheep activity using a tri-axial accelerometer. *Computers and Electronics in Agriculture*, **145**, 289-297.
- Berger-Tal, O. & Saltz, D. (2019) Invisible barriers: anthropogenic impacts on inter- and intra-specific interactions as drivers of landscape-independent fragmentation. *Philosophical Transactions of the Royal Society B: Biological Sciences*, **374**, 20180049.
- Bidder, O.R., Walker, J.S., Jones, M.W., Holton, M.D., Urge, P., Scantlebury, D.M., Marks, N.J., Magowan, E.A., Maguire, I.E. & Wilson, R.P. (2015) Step by step: reconstruction of terrestrial animal movement paths by dead-reckoning. *Movement Ecology*, **3**, 23.
- Boggs, C.L. (1992) Resource Allocation: Exploring Connections between Foraging and Life History. *Functional Ecology*, **6**, 508-518.
- Brown, D.D., Kays, R., Wikelski, M., Wilson, R. & Klimley, A.P. (2013) Observing the unwatchable through acceleration logging of animal behavior. *Animal Biotelemetry*, **1**, 20.
- Chakravarty, P., Cozzi, G., Ozgul, A. & Aminian, K. (2019a) A novel biomechanical approach for animal behaviour recognition using accelerometers. *Methods in Ecology and Evolution*, **10**, 802-814.
- Chakravarty, P., Maalberg, M., Cozzi, G., Ozgul, A. & Aminian, K. (2019b) Behavioural compass: animal behaviour recognition using magnetometers. *Movement Ecology*, **7**, 28.
- Clark, R.W., Brown, W.S., Stechert, R. & Zamudio, K.R. (2010) Roads, interrupted dispersal, and genetic diversity in timber rattlesnakes. *Conservation Biology*, **24**, 1059-1069.
- Cook, T.R., Bailleul, F., Lescroël, A., Tremblay, Y. & Bost, C.-A. (2008) Crossing the frontier: vertical transit rates of deep diving cormorants reveal depth zone of neutral buoyancy. *Marine Biology*, **154**, 383-391.
- Davis, R.W. (2014) A review of the multi-level adaptations for maximizing aerobic dive duration in marine mammals: from biochemistry to behavior. *Journal of comparative physiology. B, Biochemical, systemic, and environmental physiology*, **184**, 23-53.
- Drucker, E.G. & Lauder, G.V. (2000) A hydrodynamic analysis of fish swimming speed: wake structure and locomotor force in slow and fast labriform swimmers. *Journal of Experimental Biology*, **203**, 2379-2393.
- Dupuis-Désormeaux, M., Davidson, Z., Mwololo, M., Kisio, E. & MacDonald, S.E. (2016) Usage of Specialized Fence-Gaps in a Black Rhinoceros Conservancy in Kenya. *African Journal of Wildlife Research*, **46**, 22-32, 11.
- Elliott, K.H., Woo, K.J., Gaston, A.J., Benvenuti, S., Dall'Antonia, L. & Davoren, G.K. (2009) Central-Place Foraging in an Arctic Seabird Provides Evidence for Storer-Ashmole's Halo. *The Auk*, **126**, 613-625.
- Enstipp, M.R., Ciccione, S., Gineste, B., Milbergue, M., Ballorain, K., Ropert-Coudert, Y., Kato, A., Plot, V. & Georges, J.-Y. (2011) Energy expenditure of freely swimming adult green turtles (*Chelonia mydas*) and its link with body acceleration. *The Journal of Experimental Biology*, **214**, 4010-4020.
- Foo, D., Semmens, J.M., Arnould, J.P.Y., Dorville, N., Hoskins, A.J., Abernathy, K., Marshall, G.J. & Hindell, M.A. (2016) Testing optimal foraging theory models on benthic divers. *Animal Behaviour*, **112**, 127-138.

- Forin-Wiart, M.-A., Hubert, P., Sirguy, P. & Poulle, M.-L. (2015) Performance and Accuracy of Lightweight and Low-Cost GPS Data Loggers According to Antenna Positions, Fix Intervals, Habitats and Animal Movements. *PLOS ONE*, **10**, e0129271.
- Fourati, H., Manamanni, N., Afilal, L. & Handrich, Y. (2011) Posture and body acceleration tracking by inertial and magnetic sensing: Application in behavioral analysis of free-ranging animals. *Biomedical Signal Processing and Control*, **6**, 94-104.
- Frair, J.L., Fieberg, J., Hebblewhite, M., Cagnacci, F., DeCesare, N.J. & Pedrotti, L. (2010) Resolving issues of imprecise and habitat-biased locations in ecological analyses using GPS telemetry data. *Philosophical Transactions of the Royal Society B: Biological Sciences*, **365**, 2187-2200.
- Fukasawa, M., Komatsu, T., Higashiyama, Y. & Oshibe, A. (2018) The use of accelerometer to measure sleeping posture of beef cows. *Animal Science Journal*, **89**, 488-493.
- Gleiss, A.C., Wilson, R.P. & Shepard, E.L.C. (2011) Making overall dynamic body acceleration work: on the theory of acceleration as a proxy for energy expenditure. *Methods in Ecology and Evolution*, **2**, 23-33.
- Gómez-Laich, A., Wilson, R.P., Shepard, E.L.C. & Quintana, F. (2013) Energy expenditure and food consumption of foraging Imperial cormorants in Patagonia, Argentina. *Marine Biology*, **160**, 1697-1707.
- Graf, P.M., Wilson, R.P., Qasem, L., Hackländer, K. & Rosell, F. (2015) The Use of Acceleration to Code for Animal Behaviours; A Case Study in Free-Ranging Eurasian Beavers *Castor fiber*. *PLOS ONE*, **10**, e0136751.
- Guo, Y., Corke, P., Poulton, G., Wark, T., Bishop-Hurley, G. & Swain, D. (2006) Animal Behaviour Understanding using Wireless Sensor Networks. *Proceedings. 2006 31st IEEE Conference on Local Computer Networks*, pp. 607-614.
- Halsey, L.G., Bost, C.A. & Handrich, Y. (2007) A thorough and quantified method for classifying seabird diving behaviour. *Polar Biology*, **30**, 991-1004.
- Hays, G., Hochscheid, S., Broderick, A., Godley, B. & Metcalfe, J. (2000) Diving behaviour of green turtles: dive depth, dive duration and activity levels. *Marine Ecology Progress Series*, **208**, 297-298.
- Hays, G.C., Metcalfe, J.D. & Walne, A.W. (2004) The implications of lung-regulated buoyancy control for dive depth and duration. *Ecology*, **85**, 1137-1145.
- Hayward, M.W. & Kerley, G.I.H. (2009) Fencing for conservation: Restriction of evolutionary potential or a riposte to threatening processes? *Biological Conservation*, **142**, 1-13.
- Hubel, T.Y., Myatt, J.P., Jordan, N.R., Dewhurst, O.P., McNutt, J.W. & Wilson, A.M. (2016) Energy cost and return for hunting in African wild dogs and cheetahs. *Nature Communications*, **7**, 11034.
- Hurford, A. (2009) GPS Measurement Error Gives Rise to Spurious 180° Turning Angles and Strong Directional Biases in Animal Movement Data. *PLOS ONE*, **4**, e5632.
- Ito, T.Y., Lhagvasuren, B., Tsunekawa, A., Shinoda, M., Takatsuki, S., Buuveibaatar, B. & Chimeddorj, B. (2013) Fragmentation of the Habitat of Wild Ungulates by Anthropogenic Barriers in Mongolia. *PLOS ONE*, **8**, e56995.
- Kato, A., Ropert-Coudert, Y., Grémillet, D. & Cannell, B. (2006) Locomotion and foraging strategy in foot-propelled and wing-propelled shallow-diving seabirds. *Marine Ecology Progress Series*, **308**, 293-301.
- Korpela, J., Suzuki, H., Matsumoto, S., Mizutani, Y., Samejima, M., Maekawa, T., Nakai, J. & Yoda, K. (2020) Machine learning enables improved runtime and precision for biologgers on seabirds. *Communications Biology*, **3**, 633.
- Kotzerka, J., Hatch, S.A. & Garthe, S. (2011) Evidence for Foraging-Site Fidelity and Individual Foraging Behavior of Pelagic Cormorants Rearing Chicks in the Gulf of Alaska. *The Condor*, **113**, 80-88.

- Laich, A.G., Quintana, F., Shepard, E. & Wilson, R. (2012) Intersexual differences in the diving behaviour of Imperial Cormorants. *Journal of Ornithology*, **153**, 139-147.
- Laich, A.G., Wilson, R.P., Quintana, F. & Shepard, E.L. (2008) Identification of imperial cormorant *Phalacrocorax atriceps* behaviour using accelerometers. *Endangered Species Research*, **10**, 29-37.
- Langerhans, R.B. & Reznick, D.N. (2010) Ecology and evolution of swimming performance in fishes: predicting evolution with biomechanics. *Fish locomotion: an eco-ethological perspective*, **220**, 248.
- Laplanche, C., Marques, T.A. & Thomas, L. (2015) Tracking marine mammals in 3D using electronic tag data. *Methods in Ecology and Evolution*, **6**, 987-996.
- Lempidakis, E., Wilson, R.P., Luckman, A. & Metcalfe, R.S. (2018) What can knowledge of the energy landscape tell us about animal movement trajectories and space use? A case study with humans. *Journal of Theoretical Biology*, **457**, 101-111.
- Lesbarrères, D. & Fahrig, L. (2012) Measures to reduce population fragmentation by roads: what has worked and how do we know? *Trends in Ecology & Evolution*, **27**, 374-380.
- Lewis, J.S., Rachlow, J.L., Garton, E.O. & Vierling, L.A. (2007) Effects of habitat on GPS collar performance: using data screening to reduce location error. *Journal of Applied Ecology*, **44**, 663-671.
- Li, A. & Payandeh, S. (2016) An overview of path tortuosity measures for tracking and monitoring. *2016 IEEE 7th Annual Information Technology, Electronics and Mobile Communication Conference (IEMCON)*, pp. 1-6.
- Marschall, E.A., Mather, M.E., Parrish, D.L., Allison, G.W. & McMenemy, J.R. (2011) Migration delays caused by anthropogenic barriers: modeling dams, temperature, and success of migrating salmon smolts. *Ecological Applications*, **21**, 3014-3031.
- Matyjasiak, P., Bazzi, G. & Rubolini, D. (2021) Flight Performance of Migrating Juvenile Barn Swallows *Hirundo rustica* in Relation to Fat Load and Wing Morphology. *Acta Ornithologica*, **55**, 175-186, 112.
- McCann, R., Bracken, A.M., Christensen, C., Fürtbauer, I. & King, A.J. (2021) The Relationship Between GPS Sampling Interval and Estimated Daily Travel Distances in Chacma Baboons (*Papio ursinus*). *International Journal of Primatology*.
- McClune, D.W., Marks, N.J., Wilson, R.P., Houghton, J.D.R., Montgomery, I.W., McGowan, N.E., Gormley, E. & Scantlebury, M. (2014) Tri-axial accelerometers quantify behaviour in the Eurasian badger (*Meles meles*): towards an automated interpretation of field data. *Animal Biotelemetry*, **2**, 5.
- McLean, D.J. & Skowron Volponi, M.A. (2018) trajr: An R package for characterisation of animal trajectories. *Ethology*, **124**, 440-448.
- Narazaki, T., Nakamura, I., Aoki, K., Iwata, T., Shiomi, K., Luschi, P., Suganuma, H., Meyer, C.G., Matsumoto, R., Bost, C.A., Handrich, Y., Amano, M., Okamoto, R., Mori, K., Ciccione, S., Bourjea, J. & Sato, K. (2021) Similar circling movements observed across marine megafauna taxa. *iScience*, 102221.
- Nesse, R.M. (2018) Tinbergen's four questions: Two proximate, two evolutionary. *Evolution, Medicine, and Public Health*, **2019**, 2-2.
- Noda, T., Kawabata, Y., Arai, N., Mitamura, H. & Watanabe, S. (2014) Animal-mounted gyroscope/accelerometer/magnetometer: In situ measurement of the movement performance of fast-start behaviour in fish. *Journal of Experimental Marine Biology and Ecology*, **451**, 55-68.
- Okuyama, J., Kataoka, K., Kobayashi, M., Abe, O., Yoseda, K. & Arai, N. (2012) The regularity of dive performance in sea turtles: a new perspective from precise activity data. *Animal Behaviour*, **84**, 349-359.

- Painter, M.S., Blanco, J.A., Malkemper, E.P., Anderson, C., Sweeney, D.C., Hewgley, C.W., Červený, J., Hart, V., Topinka, V., Belotti, E., Burda, H. & Phillips, J.B. (2016) Use of bio-loggers to characterize red fox behavior with implications for studies of magnetic alignment responses in free-roaming animals. *Animal Biotelemetry*, **4**, 20.
- Paiva, V.H., Geraldés, P., Ramírez, I., Garthe, S. & Ramos, J.A. (2010) How area restricted search of a pelagic seabird changes while performing a dual foraging strategy. *Oikos*, **119**, 1423-1434.
- Panzacchi, M., Van Moorter, B., Strand, O., Saerens, M., Kivimäki, I., St. Clair, C.C., Herfindal, I. & Boitani, L. (2016) Predicting the continuum between corridors and barriers to animal movements using Step Selection Functions and Randomized Shortest Paths. *Journal of Animal Ecology*, **85**, 32-42.
- Patel, A., Stocks, B., Fisher, C., Nicolls, F. & Boje, E. (2017) Tracking the Cheetah Tail Using Animal-Borne Cameras, GPS, and an IMU. *IEEE Sensors Letters*, **1**, 1-4.
- Peters, G., Wilson, R.P., Scolaro, J.A., Laurenti, S., Upton, J. & Galleli, H. (1998) The Diving Behavior of Magellanic Penguins at Punta Norte, Peninsula Valdés, Argentina. *Colonial Waterbirds*, **21**, 1-10.
- Peterson, A.N., Soto, A.P. & McHenry, M.J. (2021) Pursuit and evasion strategies in the predator-prey interactions of fishes. *Integrative and Comparative Biology*.
- Poulin, M.-P., Clermont, J. & Berteaux, D. (2021) Extensive daily movement rates measured in territorial arctic foxes. *Ecology and Evolution*, **00**, 1– 12.
- Punta, G., Saravia, J. & Yorio, P. (1993) The diet and foraging behaviour of two Patagonian cormorants. *Marine Ornithology*, **21**, 27-36.
- Pyke, G.H. (1984) Optimal Foraging Theory: A Critical Review. *Annual Review of Ecology and Systematics*, **15**, 523-575.
- Quintana, F., Wilson, R. & Yorio, P. (2007) Dive depth and plumage air in wettable birds: the extraordinary case of the imperial cormorant. *Marine Ecology Progress Series*, **334**, 299-310.
- Rahel, F.J. & McLaughlin, R.L. (2018) Selective fragmentation and the management of fish movement across anthropogenic barriers. *Ecological Applications*, **28**, 2066-2081.
- Reynolds, A.M. (2012) Fitness-maximizing foragers can use information about patch quality to decide how to search for and within patches: optimal Lévy walk searching patterns from optimal foraging theory. *Journal of The Royal Society Interface*, **9**, 1568-1575.
- Rodríguez-Baena, D.S., Gómez-Vela, F.A., García-Torres, M., Divina, F., Barranco, C.D., Daz-Díaz, N., Jiménez, M. & Montalvo, G. (2020) Identifying livestock behavior patterns based on accelerometer dataset. *Journal of Computational Science*, **41**, 101076.
- Sato, K., Mitani, Y., Cameron, M.F., Siniff, D.B. & Naito, Y. (2003) Factors affecting stroking patterns and body angle in diving Weddell seals under natural conditions. *Journal of Experimental Biology*, **206**, 1461-1470.
- Schoener, T.W. (1971) Theory of Feeding Strategies. *Annual Review of Ecology and Systematics*, **2**, 369-404.
- Schreer, J.F., Hines, R.J.O.H. & Kovacs, K.M. (1998) Classification of Dive Profiles: A Comparison of Statistical Clustering Techniques and Unsupervised Artificial Neural Networks. *Journal of Agricultural, Biological, and Environmental Statistics*, **3**, 383-404.
- Schreer, J.F., Kovacs, K.M. & O'Hara Hines, R.J. (2001) Comparative diving patterns of pinnipeds and seabirds. *Ecological Monographs*, **71**, 137-162.
- Shepard, E.L., Wilson, R.P., Halsey, L.G., Quintana, F., Laich, A.G., Gleiss, A.C., Liebsch, N., Myers, A.E. & Norman, B. (2008a) Derivation of body motion via appropriate smoothing of acceleration data. *Aquatic Biology*, **4**, 235-241.

- Shepard, E.L., Wilson, R.P., Quintana, F., Laich, A.G., Liebsch, N., Albareda, D.A., Halsey, L.G., Gleiss, A., Morgan, D.T., Myers, A.E., Newman, C. & Macdonald, D.W. (2008b) Identification of animal movement patterns using tri-axial accelerometry. *Endangered Species Research*, **10**, 47-60.
- Shiomi, K., Kokubun, N., Shimabukuro, U. & Takahashi, A. (2020) Homing Ability of Adélie Penguins Investigated with Displacement Experiments and Bio-Logging. *Ardea*, **107**, 333-339.
- Simeone, A. & Wilson, R.P. (2003) In-depth studies of Magellanic penguin (*Spheniscus magellanicus*) foraging: can we estimate prey consumption by perturbations in the dive profile? *Marine Biology*, **143**, 825-831.
- Sims, D.W., Witt, M.J., Richardson, A.J., Southall, E.J. & Metcalfe, J.D. (2006) Encounter success of free-ranging marine predator movements across a dynamic prey landscape. *Proceedings of the Royal Society B: Biological Sciences*, **273**, 1195-1201.
- Stanton-Jones, W.K., Parusnath, S. & Alexander, G.J. (2018) The impact of posture and basking orientation on thermoregulation in the Sungazer (*Smaug giganteus*). *Journal of Thermal Biology*, **75**, 45-53.
- Swain, D.L., Wark, T. & Bishop-Hurley, G.J. (2008) Using high fix rate GPS data to determine the relationships between fix rate, prediction errors and patch selection. *Ecological Modelling*, **212**, 273-279.
- Taylor, C.R., Caldwell, S.L. & Rowntree, V.J. (1972) Running Up and Down Hills: Some Consequences of Size. *Science*, **178**, 1096-1097.
- Tucker, V.A. (1975) The Energetic Cost of Moving About: Walking and running are extremely inefficient forms of locomotion. Much greater efficiency is achieved by birds, fish—and bicyclists. *American Scientist*, **63**, 413-419.
- Walker, J.S., Jones, M.W., Laramée, R.S., Holton, M.D., Shepard, E.L.C., Williams, H.J., Scantlebury, D.M., Marks, N.J., Magowan, E.A., Maguire, I.E., Bidder, O.R., Di Virgilio, A. & Wilson, R.P. (2015) Prying into the intimate secrets of animal lives; software beyond hardware for comprehensive annotation in 'Daily Diary' tags. *Movement Ecology*, **3**, 29.
- Watanuki, Y., Niizuma, Y., Geir, W.G., Sato, K. & Naito, Y. (2003) Stroke and glide of wing-propelled divers: deep diving seabirds adjust surge frequency to buoyancy change with depth. *Proceedings of the Royal Society of London. Series B: Biological Sciences*, **270**, 483-488.
- Weimerskirch, H. (2007) Are seabirds foraging for unpredictable resources? *Deep Sea Research Part II: Topical Studies in Oceanography*, **54**, 211-223.
- Weimerskirch, H., Pinaud, D., Pawlowski, F. & Bost, C.A. (2007) Does Prey Capture Induce Area-Restricted Search? A Fine-Scale Study Using GPS in a Marine Predator, the Wandering Albatross. *The American Naturalist*, **170**, 734-743.
- Williams, H., Shepard, E., Duriez, O. & Lambertucci, S.A. (2015) Can accelerometry be used to distinguish between flight types in soaring birds? *Animal Biotelemetry*, **3**, 1-11.
- Williams, T.D., Briggs, D.R., Croxall, J.P., Naito, Y. & Kato, A. (1992) Diving pattern and performance in relation to foraging ecology in the gentoo penguin, *Pygoscelis papua*. *Journal of Zoology*, **227**, 211-230.
- Wilson, J.W., Mills, M.G., Wilson, R.P., Peters, G., Mills, M.E., Speakman, J.R., Durant, S.M., Bennett, N.C., Marks, N.J. & Scantlebury, M. (2013a) Cheetahs, *Acinonyx jubatus*, balance turn capacity with pace when chasing prey. *Biology Letters*, **9**, 20130620.
- Wilson, R. (1985) The Jackass Penguin (*Spheniscus demersus*) as a pelagic predator. *Marine Ecology Progress Series*, **25**, 219-227.
- Wilson, R., Griffiths, I., Legg, P., Friswell, M., Bidder, O., Halsey, L., Lambertucci, S.A. & Shepard, E. (2013b) Turn costs change the value of animal search paths. *Ecology Letters*, **16**, 1145-1150.

- Wilson, R.P. (2002) Movements in Adélie Penguins foraging for chicks at Ardley Island, Antarctica: circles within spirals, wheels within wheels. *Polar Bioscience*, **75**, 75-87.
- Wilson, R.P., Börger, L., Holton, M.D., Scantlebury, D.M., Gómez-Laich, A., Quintana, F., Rosell, F., Graf, P.M., Williams, H., Gunner, R., Hopkins, L., Marks, N., Geraldini, N.R., Duarte, C.M., Scott, R., Strano, M.S., Robotka, H., Eizaguirre, C., Fahlman, A. & Shepard, E.L.C. (2020a) Estimates for energy expenditure in free-living animals using acceleration proxies: A reappraisal. *Journal of Animal Ecology*, **89**, 161-172.
- Wilson, R.P., Culik, B., Spairani, H.J., Coria, N.R. & Adelung, D. (1991) Depth utilization by Penguins and Gentoo Penguin dive patterns. *Journal für Ornithologie*, **132**, 47-60.
- Wilson, R.P., Culik, B.M., Peters, G. & Bannasch, R. (1996) Diving behaviour of gentoo penguins, *Pygoscelis papua*; factors keeping dive profiles in shape. *Marine Biology*, **126**, 153-162.
- Wilson, R.P., Hustler, K., Ryan, P.G., Burger, A.E. & Noldeke, E.C. (1992) Diving birds in cold water: do Archimedes and Boyle determine energetic costs? *The American Naturalist*, **140**, 179-200.
- Wilson, R.P., Liebsch, N., Davies, I.M., Quintana, F., Weimerskirch, H., Storch, S., Lucke, K., Siebert, U., Zankl, S., Müller, G., Zimmer, I., Scolaro, A., Campagna, C., Plötz, J., Bornemann, H., Teilmann, J. & McMahon, C.R. (2007) All at sea with animal tracks; methodological and analytical solutions for the resolution of movement. *Deep Sea Research Part II: Topical Studies in Oceanography*, **54**, 193-210.
- Wilson, R.P., Puetz, K., Bost, C.A., Culik, B.M., Bannasch, R., Reins, T. & Adelung, D. (1993) Diel dive depth in penguins in relation to diel vertical migration of prey: whose dinner by candlelight? *Marine Ecology Progress Series*, **94**, 101-104.
- Wilson, R.P., Ropert-Coudert, Y. & Kato, A. (2002) Rush and grab strategies in foraging marine endotherms: the case for haste in penguins. *Animal Behaviour*, **63**, 85-95.
- Wilson, R.P., Rose, K.A.R., Metcalfe, R.S., Holton, M.D., Redcliffe, J., Gunner, R.M., Börger, L., Loison, A., Miloš, J., Painter, M.S., Silovský, V., Marks, N., Garel, M., Toigo, C., Marchand, P., Bennett, N.C., McNarry, M.A., Mackintosh, K.A., Brown, M.R. & Scantlebury, D.M. (2020b) Path tortuosity changes the transport cost paradigm in terrestrial animals. *bioRxiv*, 2020.2008.2020.259390.
- Wilson, R.P., Shepard, E. & Liebsch, N. (2008) Prying into the intimate details of animal lives: use of a daily diary on animals. *Endangered Species Research*, **4**, 123-137.
- Wilson, R.P., Shepard, E.L., Laich, A.G., Frere, E. & Quintana, F. (2010) Pedalling downhill and freewheeling up; a penguin perspective on foraging. *Aquatic Biology*, **8**, 193-202.
- Wilson, R.P. & Wilson, M.-P.T. (1988) Foraging Behaviour in Four Sympatric Cormorants. *Journal of Animal Ecology*, **57**, 943-955.

Appendices

Richard M. Gunner



Photo taken by Richard M. Gunner

Chapter 2: Supplementary Information

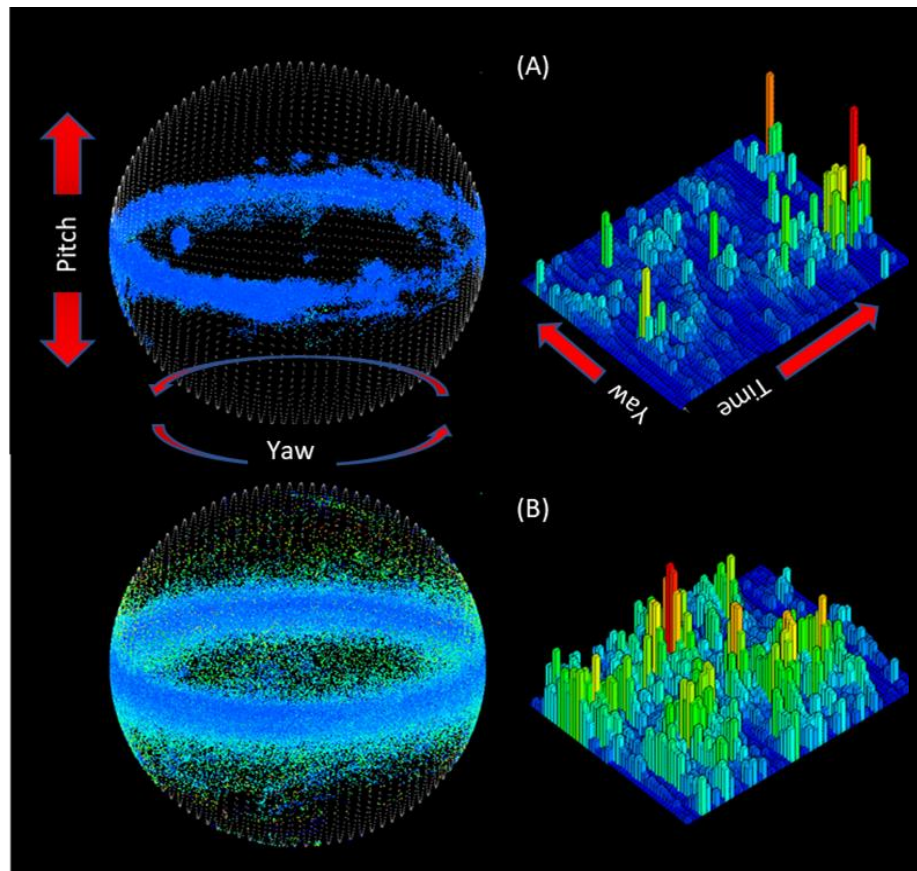


Figure S1. Visualisations of yaw during bottom phase of type 1a dives when AVEY remained less than 3 °/s (A) and greater than 3 °/s (B). Orientation-sphere visualisation [left panel] showing the simultaneous distribution of yaw angles (longitude plane) and pitch angles (latitude plane) coloured according to the magnitude of VeDBA gradient [low: blue → green → red: high]. 2-D frequency histograms [right panel] of the heading (0 - 360°) over time (bins = 50 for both x and y scales, size and colour intensity of each 'facet' represents a greater relative frequency).

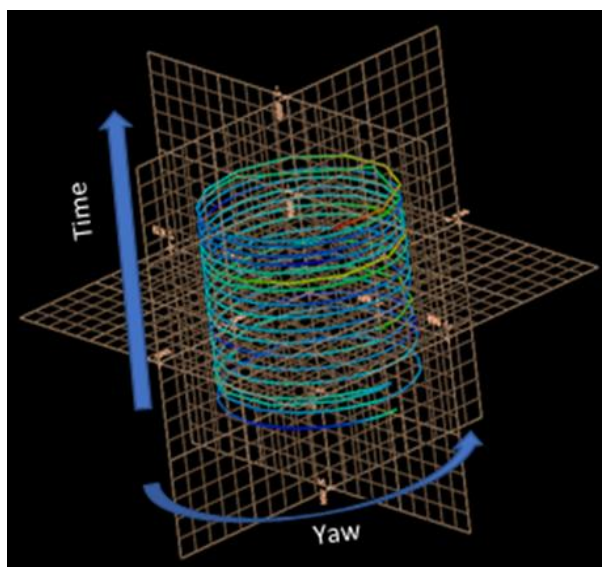


Figure S2. Yaw plotted in 3-D space. Time is represented by distance from the base colour-coded according to the magnitude of VeDBA. Data taken from a bout of circling behaviour (17 revolutions in 3 minutes 45 seconds).

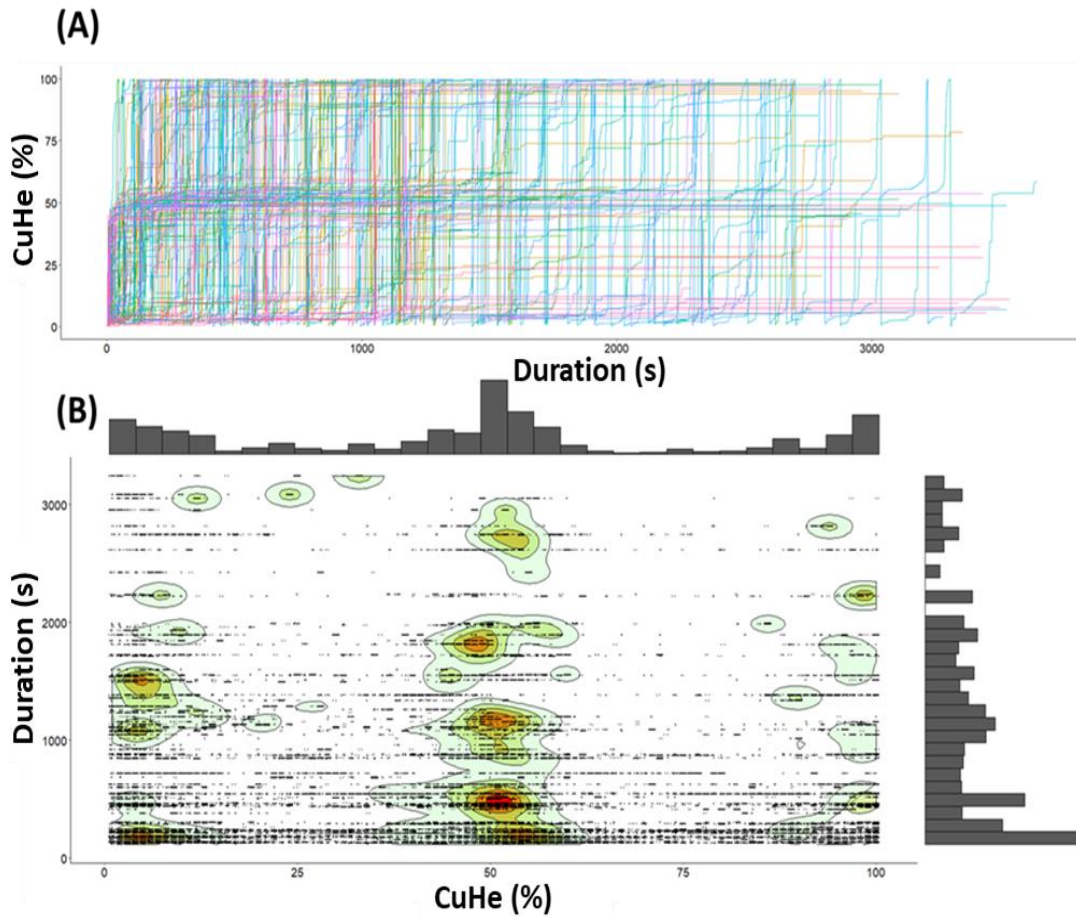


Figure S3. Patterns of CuHe across 100 random U-dives (bottom phase). This is expressed both as (A) a line graph (coloured according to dive number) and (B) a 2d contour scatterplot with marginal histograms illustrating the relationship between the most frequented CuHe percentage and the uninterrupted duration such values were frequented for (before an increment). Note, each time CuHe resets to 0, all angles of the animal's body circumference have been covered. A 1 % increase in CuHe corresponds to the body arc covering an extra 3.6 degrees (not previously covered since the last reset).

Chapter 3: Supplementary Information

Table S1. Step selection function analysis. Dive duration (s) as the response variable

Model	Coefficient ± S.E	t-value(d.f.)	p-value	CI %		R ² _r	R ² _c	AIC	ICC
				5	95				
Lmer(M1) (Null)	(intercept) 26.53 ± 1.40	18.91(4.30)	<.001***	23.06	29.95	0.00	0.03	10674	0.03
Lmer(M2) *chosen model	(intercept) 50.78 ± 2.23 log(AAV) -24.86 ± 0.58	22.75(5.76) -43.20(1269.86)	<.001*** <.001***	45.54 -23.37	54.05 -21.34	0.58	0.66	9530	0.22
Lmer(M3)	(intercept) 37.83 ± 7.20 log(AAV) -22.29 ± 0.52 log(Depth) 1.28 ± 1.43	18.03(7.44) -42.80(1269.80) 0.90(1261.74)	<.001*** <.001*** 0.37	41.83 -23.31 -1.51	53.81 -21.27 4.08	0.58	0.66	9533	0.22
Lmer(M4)	(intercept) 44.60 ± 4.49 log(AAV)*log (Depth) -2.24 ± 2.30	9.93(107.24) -0.97(1266.52)	<.001*** 0.33	35.80 -6.73	53.41 2.26	0.58	0.66	9533	0.22
Lmer(M5)	(intercept) 37.71 ± 2.10 log(AVeY) -17.49 ± 0.42	17.94(5.11) -42.01(1268.46)	<.001*** <.001***	33.59 -18.31	41.83 -16.68	0.55	0.63	9576	0.16
Gam(M4) (k=7)	(intercept)	26.19 ± 0.30	88.26						
	s(AAV)	EDF	R ² (adj)	F-value	p-value				
		5.563	0.57	288.7	<.001***				

S.E; standard error
CI; confidence interval
R²_r; marginal accounted variance
R²_c; Conditional accounted variance

*p<.05
**p<.01
***p<.001

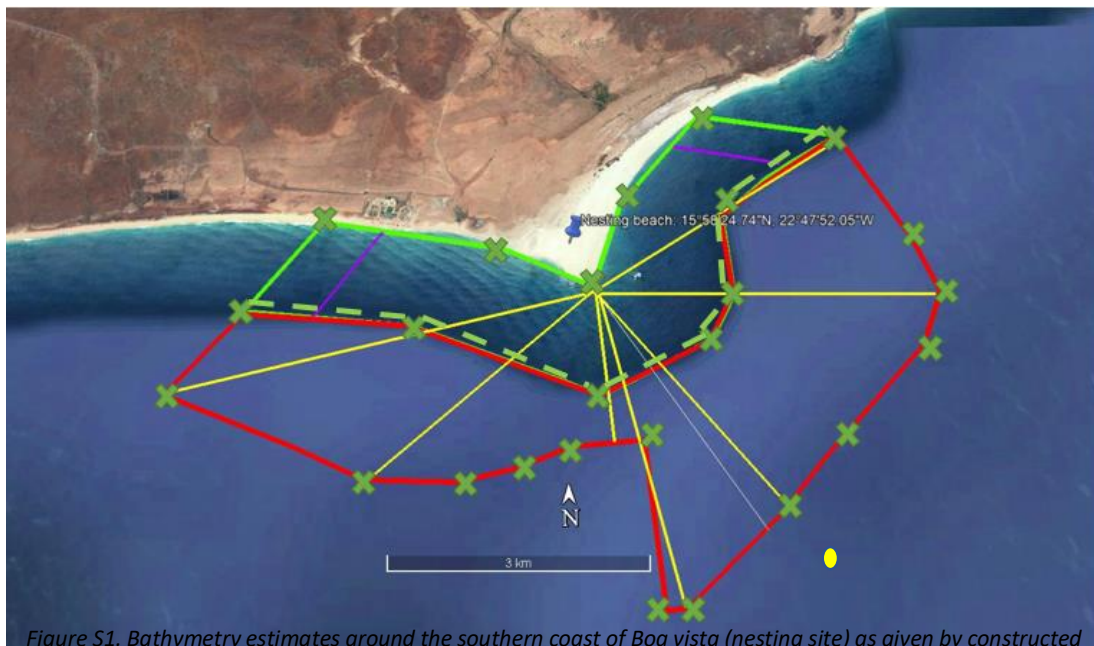


Figure S1. Bathymetry estimates around the southern coast of Boa vista (nesting site) as given by constructed polygons (green crosses denote change of angle between successive connected lines). Green polygon (perimeter = 20 km; area = 11 km²) outlines the area of sea surrounding the nesting beach. The deeper colour of blue shown in this area is a region of shallow depth (water depth < 3 m along purple transects). Red polygon (perimeter = 27 km; area = 20 km²) outlines an approximate boundary, beyond which water depth exceeds 20 m. Distance from the origin to the extremes of the yellow transects range from 2 to 5.3 km. The yellow circle shows an area of approximately 8 m depth, 3 km from the beach.

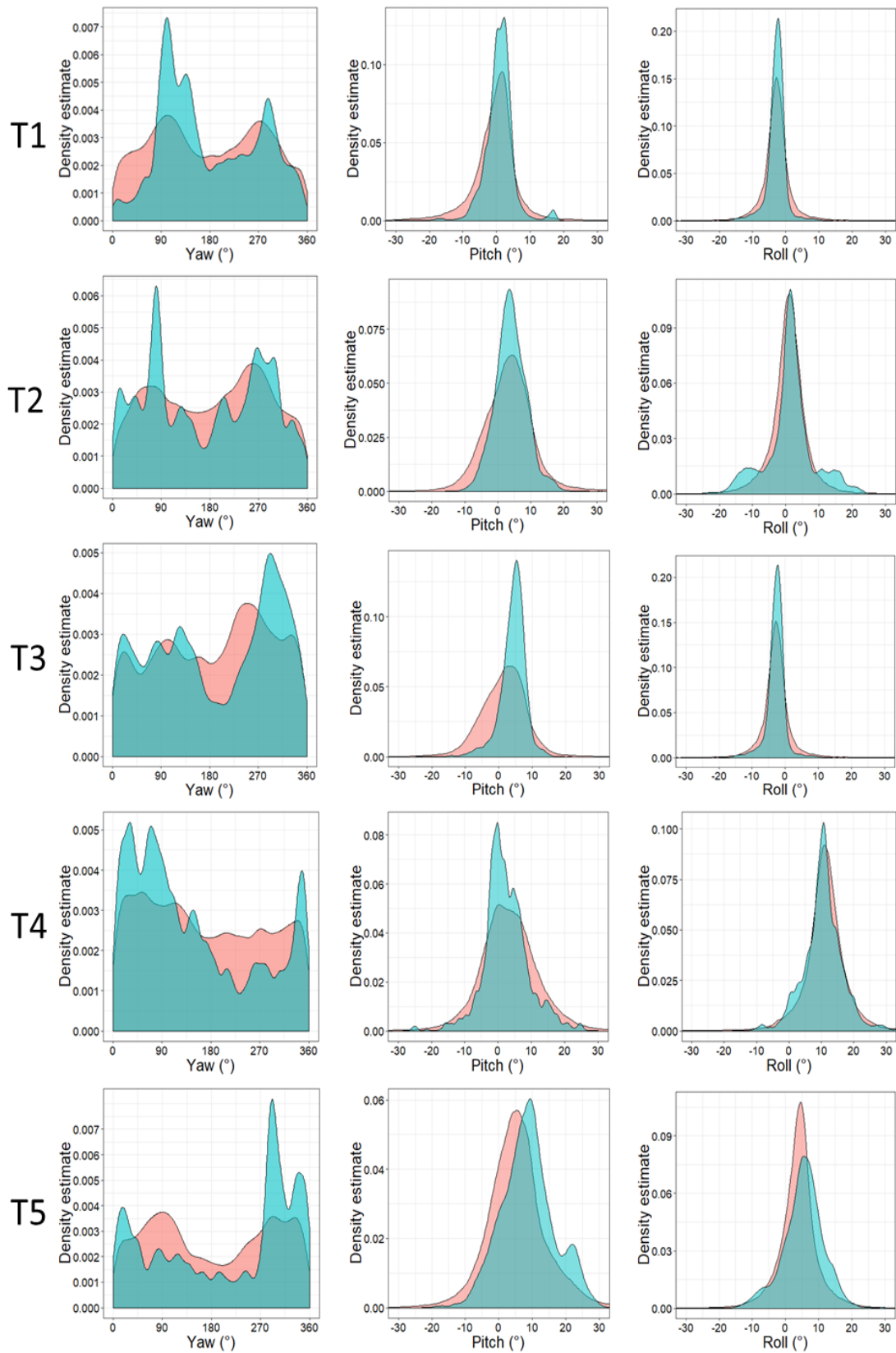


Figure S2. Density estimates for raw values of yaw (°), pitch (°) and roll (°) per turtle (T) aggregated according to resting [blue] and active [red].

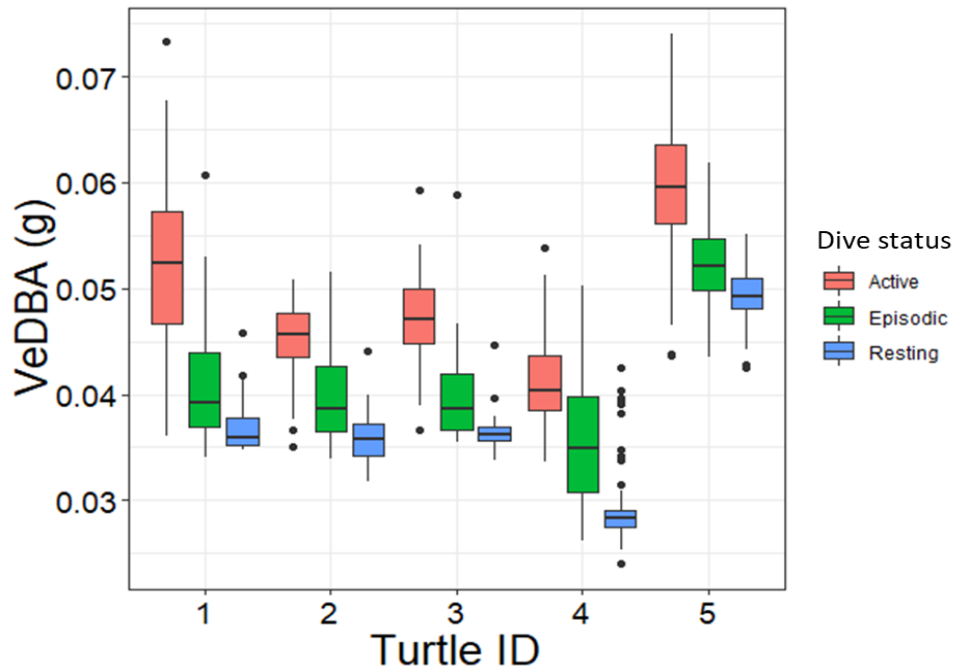


Figure S3. Mean values of VeDBA per turtle, aggregated as a function of dive status (predominately; active [red] vs episodic-rest [green] vs rest [blue]). Boxes denote the median and 25-75 % interquartile range. Whiskers extend to the minimum/maximum value no further than $1.5 * IQR$. Data points beyond this range are plotted individually. ($VeDBA (g) = \sqrt{(x^2 + y^2 + z^2)}$, where x , y & z are the derived dynamic acceleration values from each axis).

Limitation of using Euler angles

Typically, the derivation of each dimension's scale of rotation relies on a set vectoral orientation with each orthogonal channel representing a particular body plane (anterior-posterior, medio-lateral and dorsal-ventral) with respect to the earth's frame of reference (*cf.* Ozyagcilar 2012; Bidder *et al.* 2015). However, this assumption breaks down for animals that change orientations frequently at angles greater than perpendicular from their longitudinal and lateral axes of 'normal' posture and for 'severe' offsets in tag placement, in which the range for accurate angular velocity measures are restricted in one or more dimensions, whereby x , y and z values can become inversed, representing different 'surge', 'sway' and 'heave' planes. Nevertheless, this is only problematic in animals that frequently undertake body inversions greater than 90 degrees (which turtles do not).

References

- Bidder, O., Walker, J., Jones, M., Holton, M., Urge, P., Scantlebury, D., Marks, N., Magowan, E., Maguire, I. & Wilson, R. (2015) Step by step: reconstruction of terrestrial animal movement paths by dead-reckoning. *Movement ecology*, **3**, 1-16.
- Ozyagcilar, T. (2012) Implementing a tilt-compensated eCompass using accelerometer and magnetometer sensors. *Freescale semiconductor, Application Note, AN4248*, Austin, TX.

Chapter 4: Supplementary Information

Text S1 – The study design

Study area

The Kgalagadi Transfrontier Park is a large (*ca.* 38,000 km²) wildlife preserve and conservation area within the southern Kalahari Desert, encompassing both the Northern region of South Africa and South-Western region of Botswana. The terrain consists of sparse vegetation within an undulating red sand dune environment (Mills & Mills 2010). Two fossilised riverbeds (Nossob and Auob rivers) intercept this environment (Mills & Mills 2010). Artificial water holes are located along both riverbeds. As of 2005, this wildlife reserve is considered both a lion conservation unit and stronghold in Southern Africa (IUCN 2006). Dirt roads used by tourists and park rangers follow close to the fossilised riverbeds.

Collar design and set up

Fifteen LiteTrack GPS collar systems (six iridium and nine store-on-board) from Lotek Wireless Inc. were deployed. Twelve of these were fitted with Gypsy_5 Techno-smart GPS units (see later) and data from eleven analysed for this study. LiteTrack GPS units were pre-programmed to record one fix every 30 minutes. Iridium collars transmitted stored fixes every six hours. A magnet activated timed drop-off mechanism was fitted to each collar. There were two different collar sizes; five 'large' collars (two iridium, three store-on board), with an internal circumference range of 81-87 cm and ten 'small' collars (four iridium and six store-on-board), with an internal circumference range of 64-71 cm.

Daily diary (DD) logging units (*cf.* Wilson, Shepard & Liebsch 2008) recording at 40 Hz, enclosed in a water-tight aluminium housing were fitted to one side of the collar. DD units were coated with electro-lube clear protective lacquer and the inside of the housings were coated with insulating tape to prevent short-circuiting. Orthogonal acceleration measurements were logged as acceleration with respect to gravity (1 g = 9.81 m/s⁻², measuring within the range of ± 16 g) and orthogonal magnetometry measurements were recorded in Gauss (G) (magnetic intensity recorded within the

range of ± 0.88 G at 0.73 mG/LSB resolution). DD's were powered by 3 parallel circuited A-cell batteries. The combined weight of a fully equipped DD housing was 239 g. Data were stored on a 2 GB removable microSD card.

Gypsy_5 Techno-smart GPS units (attached the opposite side to DD units) were programmed to record at 1 Hz, requiring a minimum of ≥ 3 satellites before registering a fix. Gypsy_5 loggers were powered by 2 parallel circuited A-cell batteries and encased in a thick 3D-printed ABS oval plastic housing. This was to ensure signal propagation was not obstructed and to maintain robustness. Acetone was painted onto the housings to reduce porosity of plastic layers, reducing the risk of water seepage. GPS units were turned on *via* magnet activation and synced to GMT time zone from a personal computer. Once units were activated, GPS housings were coated with layers of black water-proof Tessa-tape to reduce conspicuousness (since lions are mostly nocturnal) and as an additional barrier to water ingress. The combined weight of a fully equipped Gypsy_5 Techno-smart GPS housing, was 128 g.

Male lions weighed between 165 and 215 ($\bar{x} \pm SD$ (n) = 184.3 ± 18.1 (6)) kg and female lions weighed between 99 and 136 ($\bar{x} \pm SD$ (n) = 121.5 ± 12.3 (10)) kg. Small collars weighed 1.24 kg and large collars weighed 1.33 kg (including attached DD and Gypsy_5 Techno-smart GPS units). Collars attached with all devices (*cf.* Fig. S1. 1) constituted $< 2\%$ and $< 1\%$ of the body mass of the lightest equipped female and male, respectively. Based on morphological measurements, experienced veterinary personal estimated the age of collared individuals to be between 4 and 12+ years of age.

Capture protocol

Lions were tracked and darted from vehicles during the evening and night, when weather conditions were coolest, and lions were most active. Areas of potential capture were pre-determined based on two critical parameters.

(1) Reports from trackers sent to locate prides earlier in the day prior to capture and reported sightings from tourists on game drives.

(2) Open sites close to the riverbed (where terrain is flattest) with clear 360° views.

Once in position, audio playback of a buffalo calf in distress were played from the vehicle in which darting took place. Occasionally carcasses were used for bait. Darts contained Zoletil® (tiletamine and zolazepam) and medetomidine, the latter reversed with atipamezole at the end of the procedure. Once all individuals of a pride (or those in visible vicinity) were anaesthetised, all required veterinary procedures, measurements and collar fitting were carried out according to the Standard Operating Procedures of SANParks Veterinary Services. The collars were adjusted on the lion to allow three fingers to pass through, whilst ensuring that the collar size did not exceed the lion's head circumference. Animals were monitored until ambulatory. To exclude periods of data acquisition where behaviour may have been altered due to human disturbance or drug administration, only data ≥ 6 hours after the lion's anaesthesia had been reversed were included for analysis. Full details regarding the SANParks operational procedures as detailed in SANParks' 'Standard Operating Procedures for the Capture, Transportation and Maintenance in Holding Facilities of Wildlife' are available at;

<https://www.sanparks.org/conservation/veterinary/about/animals/lion.php>.

The data were retrieved after approximately two weeks using a similar capture protocol. No females were with cubs or pregnant. At least one member of each pride wore an Iridium collar which remotely supplied the location of the individual (and thus the pride) twice daily. During the recapture, high-res GPS housings were detached, and the DD SD cards were replaced. The collars remained on the lions for

an additional 8 months (as part of a longer-term study), releasing automatically *via* the on-board timed drop-off mechanism - later found *via* the VHF beacon.

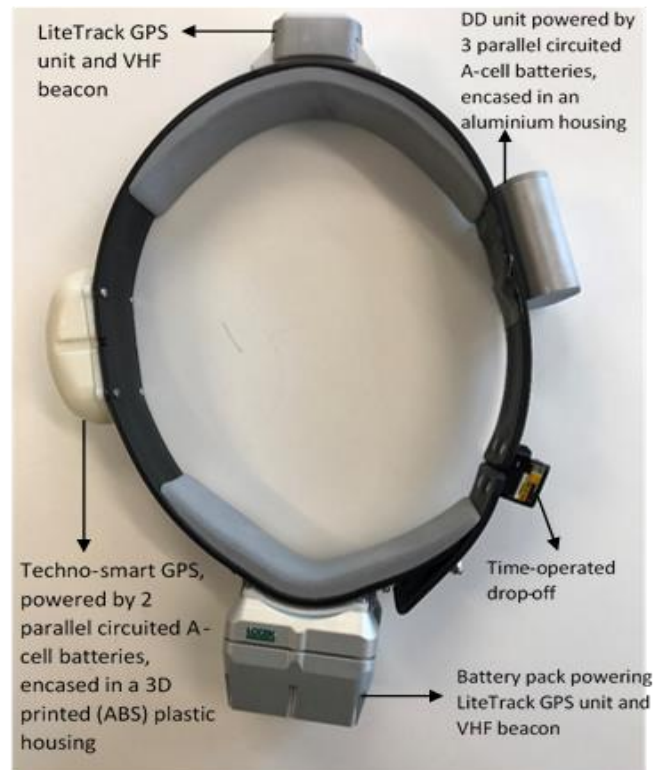


Figure S1. 1. LiteTrack (Iridium) GPS collar, fitted with a 'high-res' techno-smart GPS and Daily Diary (DD) unit.

Text S2 – The Relationship between VeDBA and GPS speed

I used the vectorial dynamic body acceleration (VeDBA) as the DBA metric;

$$\text{VeDBA} = \sqrt{(x^2 + y^2 + z^2)} \quad (1)$$

where x , y & z are the derived dynamic acceleration values from each axis (Wilson *et al.* 2020a). For this, a 2-second running mean was applied to each axis to derive the static component of acceleration, which was subsequently subtracted from the raw acceleration before the dynamic component from each axis was summed (eq 1). VeDBA values used in this analysis were post-smoothed using a rolling window of 2 seconds to ensure that both acceleration and deceleration components of a lion's stride cycle were incorporated together within any particular time period (Gleiss, Wilson & Shepard 2011).

The shortest distance (d) between two GPS fixes via;

$$d = 2 \cdot R \cdot \sin^{-1} \left(\sqrt{\sin^2 \left(\frac{\varphi_2 - \varphi_1}{2} \right) + \cos(\varphi_1) \cdot \cos(\varphi_2) \cdot \sin^2 \left(\frac{\lambda_2 - \lambda_1}{2} \right)} \right) \quad (2)$$

where R is the radius of earth (approx. 6378137 km), φ_1 , φ_2 are the latitude coordinates between point 1 and point 2 (in radians) and λ_1 , λ_2 are the longitude coordinates between point 1 and point 2 (in radians), respectively (*cf.* Chopde & Nichat 2013).

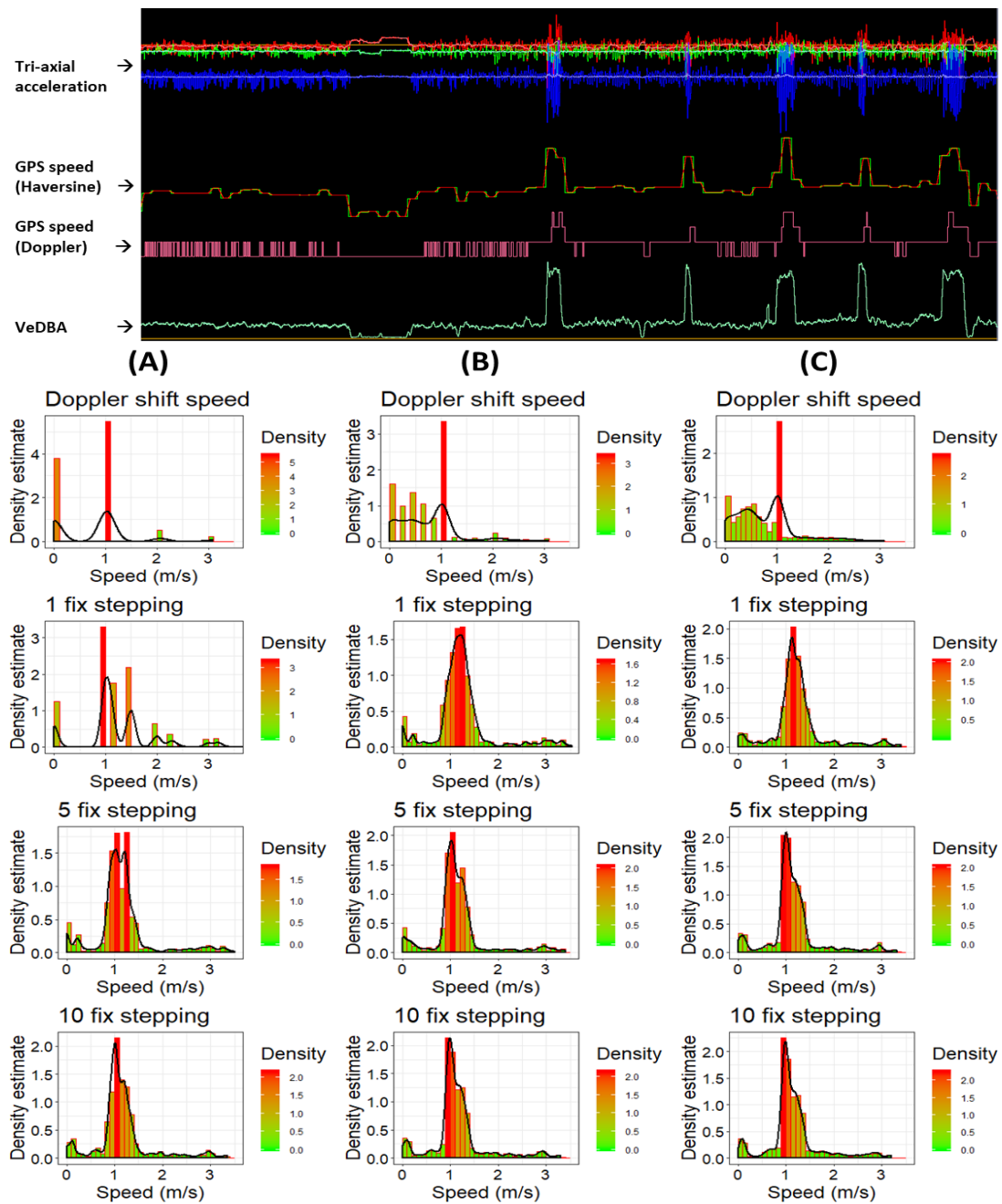


Figure S2. 1. A fifteen-minute period of predominantly traveling movement for one lion, in which the magnitude of acceleration and GPS speed are plotted against time (top plot). GPS speed (Doppler) refers to the raw speed recorded by the GPS device itself calculated using the doppler shift from orbiting satellites. GPS speed (Haversine) refers to speed calculated using the Haversine distance between fixes (using a stepping range of 5 fixes and post-smoothing window of 5 seconds). Density plots of GPS-derived speed (m/s) from this period are shown in the bottom plot. The first row shows speed calculated from the doppler shift method and the second, third and fourth rows shows speed calculated using the Haversine method at 1, 5 and 10 fix stepping ranges, respectively. The first column (A) reflects no post-smoothing filter (raw data), with column (B) and (C) reflecting 5 and 10 second post-smoothing rolling mean windows, respectively.

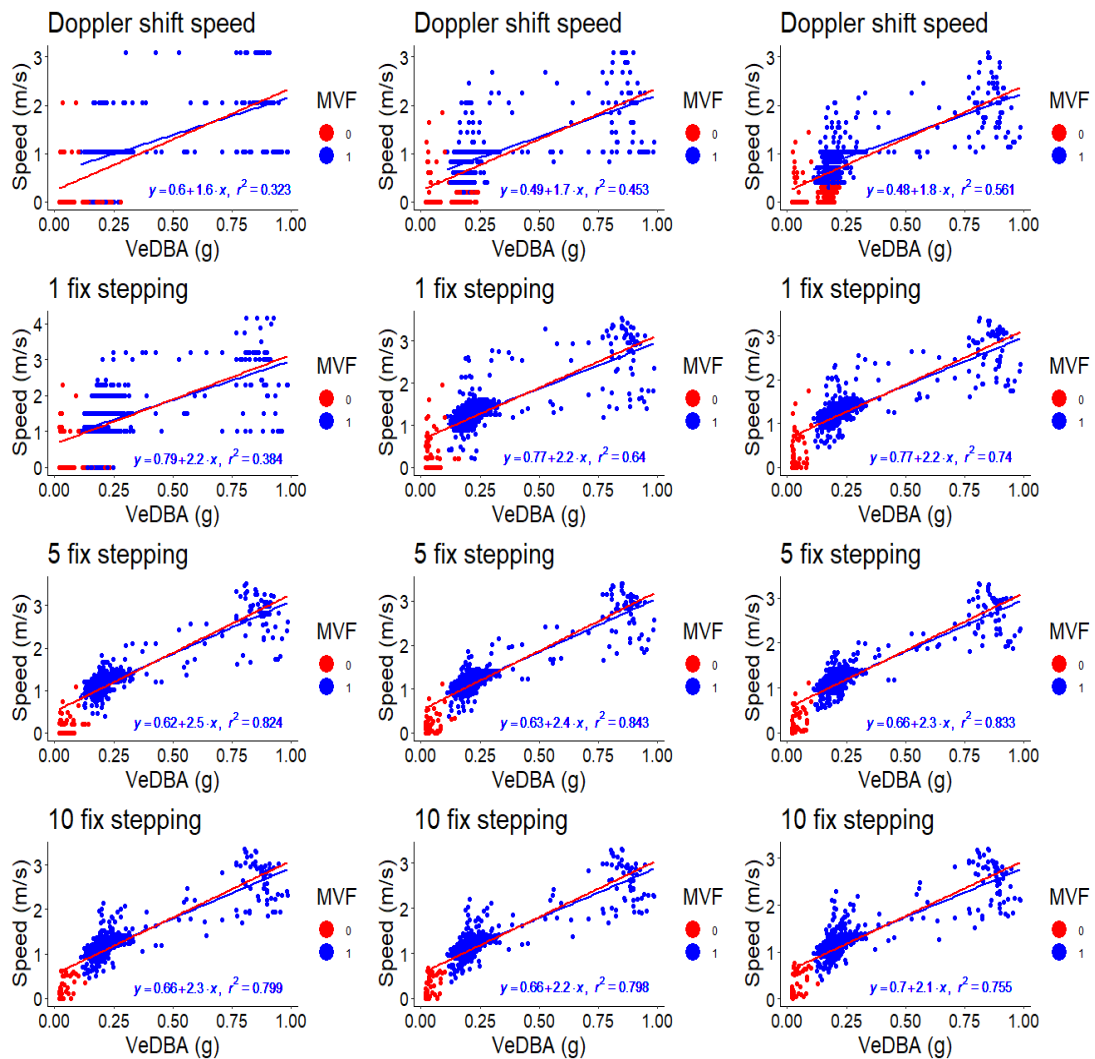


Figure S2. 2. The Relationship between VeDBA and GPS speed, with the data and order of plots following on from the same period of activity illustrated in Fig. S1. 1. Data points coloured red represent values that did not meet the MVF thresholds (0), with blue data points reflecting values that met the MVF criteria (1). Each plot consists of two linear regressions, with red lines representing a linear regression constructed from all values and the blue lines, from only values that met the MVF protocol. Regression estimates and R^2 values are given for the regression constructed from only values that met the MVF protocol.

The precision of calculated speed from both the doppler shift method and Haversine method is limited according to the number of decimal places given per GPS fix. Resampling at less frequent intervals can reduce the spurious noise associated with location error, especially when rates of moving are less than the limited spatial resolution of the GPS between fixes.

Whilst I do not know the exact means in which speed is calculated from doppler shift, it is clear that the Haversine method applied over a suitable stepping range produces

more detailed estimates of speed and a tighter relationship with VeDBA, as reflected in the more Gaussian-shaped distribution and higher R^2 values in Fig. S2. 1 & 2, respectively. The bimodal clumping of points in Fig. S2. 2 is resultant from a change in stride gait (from walking to running, as demonstrated in the disproportionate peaks in VeDBA (top plot, Fig. S1. 1)) relative to the magnitude imparted at other times. We propose that a five-fix stepping range and 5 second post-smoothing rolling mean window was suitable for this study species, providing a creditable compromise between maintaining a level of comparability to acceleration estimates whilst interpolating speed estimates at a greater than 1 m resolution, per unit time.

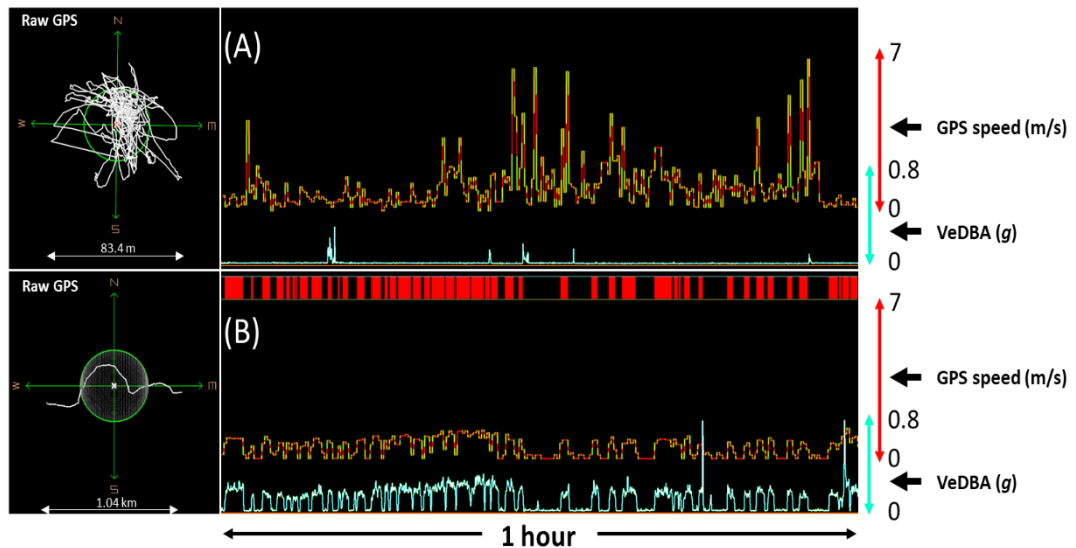


Figure S2. 3. DD- and GPS-derived data showing two different movement scenarios, each over 1 hour. In the upper panel, the animal was considered to be at rest (due to minimal DBA – All GPS fixes during this period were allocated MVF values of 0). In the lower panel, the animal was considered to be moving extensively (due to the succinctness between the patterns of magnitude between DBA and GPS speed – GPS fixes during this period that were allocated MVF values of 1 are denoted with the rug at the top of this plot coloured red). Note large locational errors prevalent during rest as manifest by inflated estimates of GPS speed and high levels of GPS jitter.

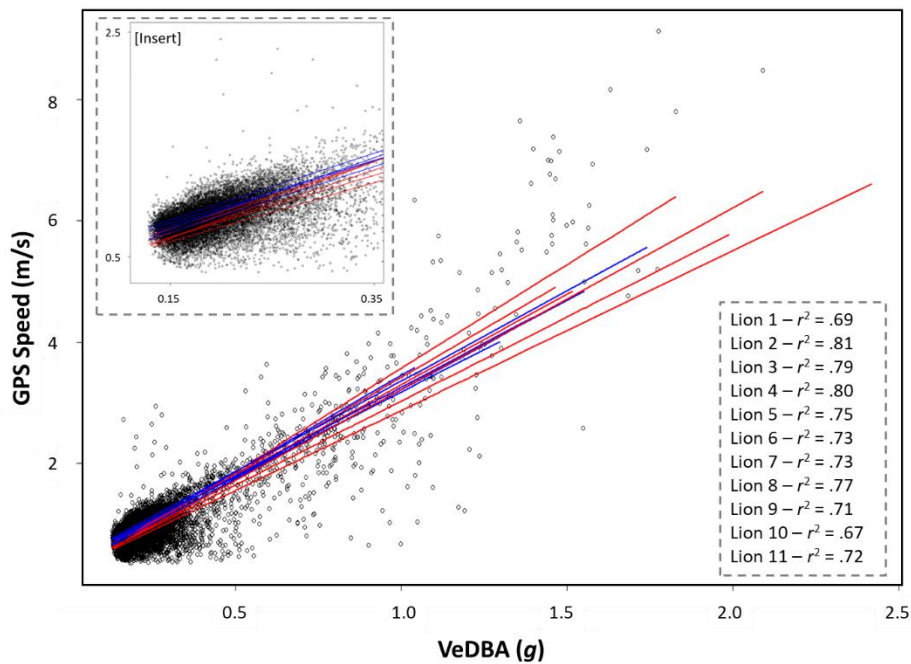


Figure S2. 4. GPS speed ~ VeDBA relationships for all lions with linear regression ($y = a + bx$). Male: blue, females: red. Data taken only from marked moving periods following the MVF method. Each data point represents the mean value per period. Insert showing a magnified section of the regression estimates is given in the top left of this plot.

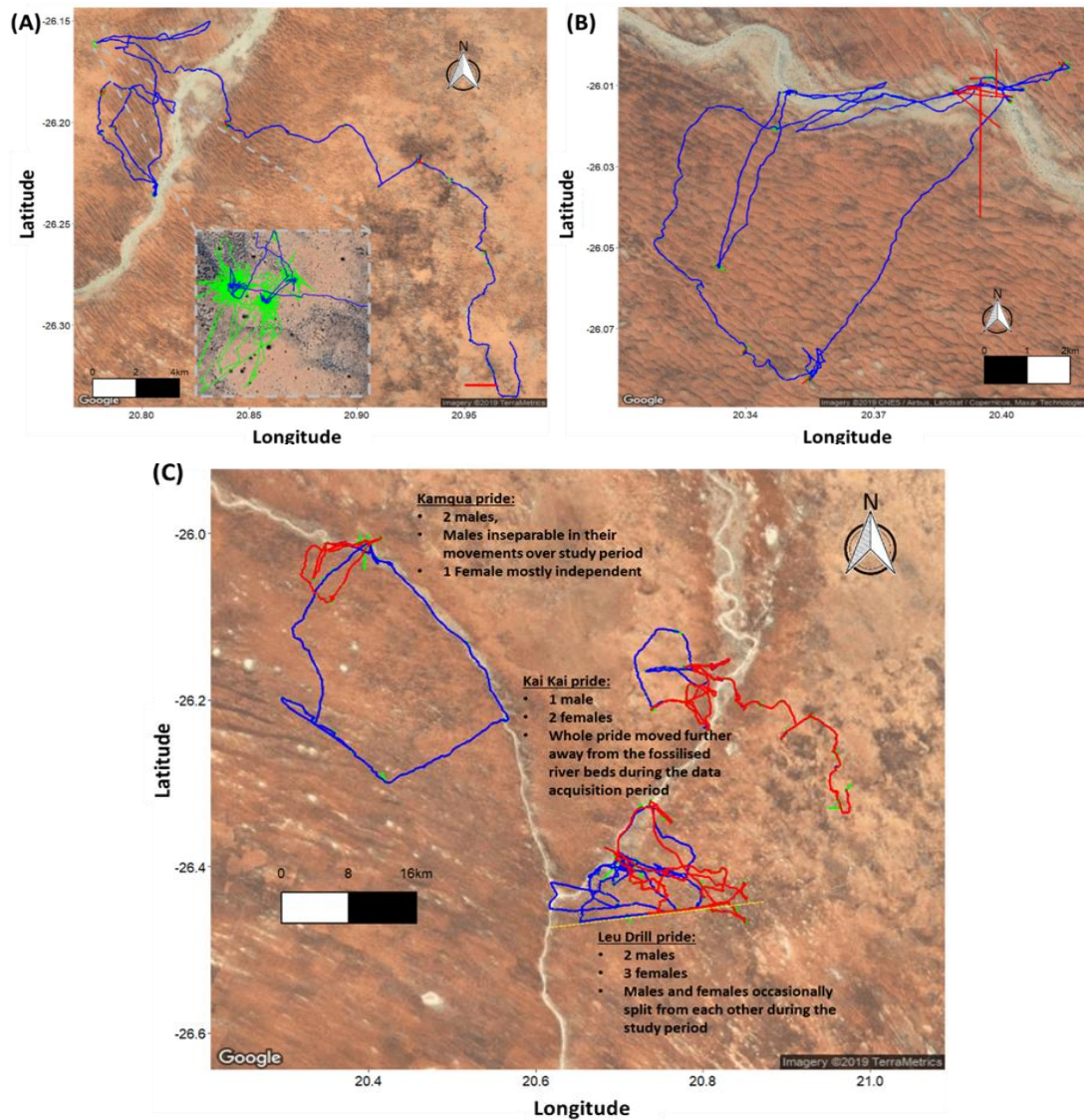


Figure S2. 5. GPS tracks for the entire data acquisition period of ~14 days, plotted according to MVF value. (A) and (B) show two individual lions from different prides; Data discerned as non-moving (MVF = 0: green) and moving (MVF = 1: blue). Missing locational data and data that failed the Z-threshold = red. Insert of (A) shows a magnified section of track with high rates of GPS jitter. (C) Each individual from the three prides plotted; Male (MVF = 1): blue, female (MVF value = 1): red. MVF values of 0 (including missing locational data and data that failed the Z-threshold): green. Brief pride dynamics of the individuals analysed given. Dotted yellow line depicts the electric fence bordering Botswana (which the Leu Drill pride females crossed).

Text S3 – Descriptive statistics comparing the MVF results

For the majority of lions, battery longevity was just enough, with the GPS units having either run out of battery on the day of retrieval (after approx. 2 weeks) or still functioning, but at low voltage capacity. Only 1 lion (lion 4) had a significantly large portion of data (approx. 12 hours) missing at the end of the data acquisition period (Fig. S3. 1). In general, though, fix success rate did not seem to vary significantly according to the length of accumulated time being switched on, whilst the duration of the GPS not registering a fix varied considerably, indicating that missing locational data was not directly attributable to battery life (and associated voltage level).

Table S3. 1. Summary parameters of fix success rate during the data acquisition period of each lion.

Lion ID	Fix success rate (%)	Duration of missing location (min)		
		Mean (± 1 SD)	Median	Maximum
1	97.08	1.89 \pm 10.27	0.05	101.28
2	95.34	3.66 \pm 11.61	0.08	67.68
3	89.06	3.23 \pm 12.86	0.08	100.9
4	92.22	6.75 \pm 53.98	0.07	720.17
5	91.73	8.62 \pm 25.76	0.1	144.65
6	96.1	3.64 \pm 12.48	0.08	68.05
7	90.02	10.06 \pm 27.47	0.13	239.18
8	89.5	5.27 \pm 15.73	0.08	102.63
9	93.31	5.73 \pm 20.47	0.08	201.3
10	94.63	2.64 \pm 13.63	0.07	134.6
11	92.25	4.54 \pm 17.44	0.1	166.81
Total	92.97 (mean)	4.44 \pm 20.86	0.08	720.17

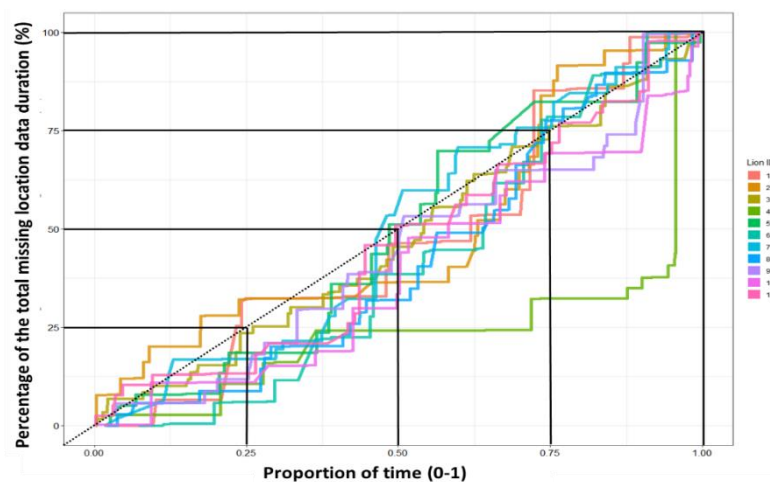


Figure S3. 1. Relative cumulative frequency of missing locational data duration (%) per lion over their respective data acquisition periods. Black solid lines reflect γ^x 25 % quantiles and the black dotted line reflects an equal distribution of missing location data over time.

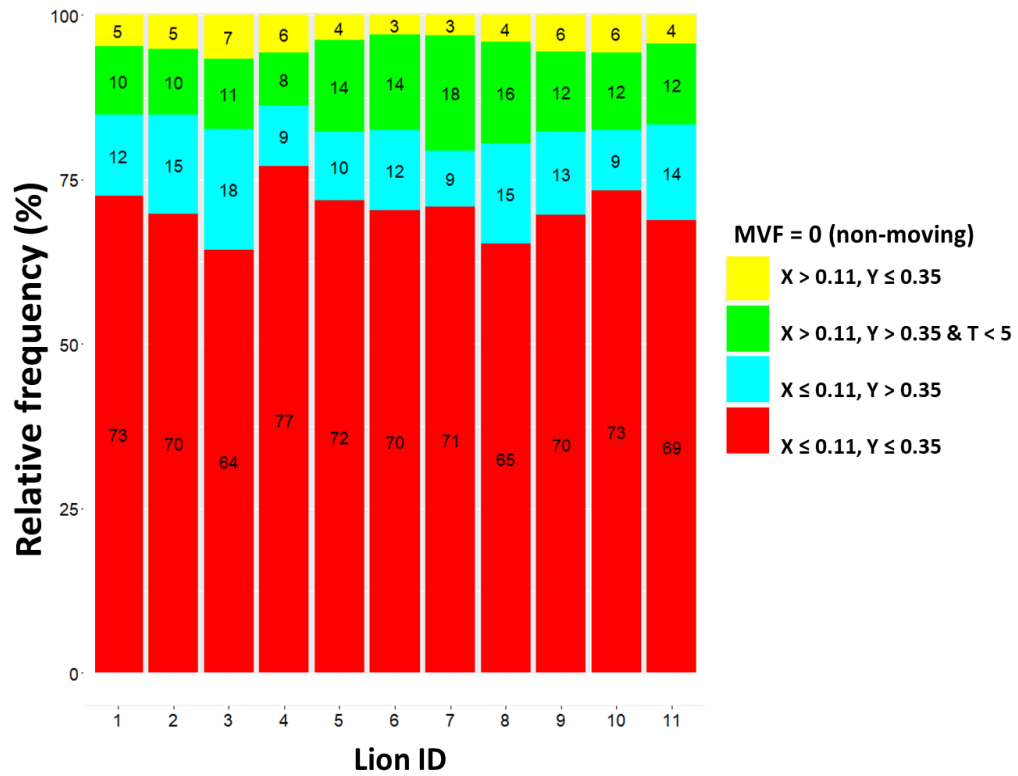


Figure S3. 2. Relative frequency of the four possible combinations of movement and time thresholds (VeDBA (X), GPS speed (Y) and time (T)) that resulted in an MVF value of zero (condition classified as non-moving). Non-traveling behaviour with little or no GPS jitter: red, non-traveling behaviour with an appreciable degree of GPS jitter: blue, either transitional movements, e.g., rolling over/feeding when GPS jitter is apparent, or temporally short travelling periods that were deemed not long enough to warrant a considerable movement bout: green, non-travelling movement: yellow. Missing locational and extreme outliers were not included in this analysis.

Table S3. 2. DD- and GPS derived summary metrics associated with data ascribed as non-moving (MVF = 0) and moving (MVF = 1) (A). Note, distance travelled estimates are used as a comparator between moving and non-moving, however these are likely highly underestimated given that times of missing location data were excluded. Such missing locational data was also excluded prior to calculating the percentage of data acquisition determined as moving. The cells filled with colour shading (ID and gender) denotes which individuals belonged to the same pride.

(A)		Assessed from DD units only										Assessed from GPS units only									
		[Mean Median 2*SD]										[Mean Median 2*SD Max]									
NM (0) M (1)	ID	Absolute pitch (°)			Absolute roll (°)			VeDBA (g)			Tortuosity (0-1) (1 = straight-line) (per period)			(1) Speed (m/s)				Duration (min) (per period)			
0	1 (F)	14.28	12.54	19.36	39.26	43.02	53.53	0.04	0.02	0.10	0.52	0.57	0.74	0.18	0.07	0.89	25.71	6.37	0.38	37.27	283.52
1	1 (F)	6.67	6.10	9.17	12.25	11.19	15.58	0.19	0.17	0.22	0.83	0.86	0.29	0.91	0.84	0.81	10.59	0.83	0.45	2.33	12.67
0	2 (F)	15.67	12.91	22.61	42.97	44.97	55.94	0.04	0.02	0.11	0.52	0.51	0.78	0.21	0.00	1.07	32.07	6.92	0.38	43.29	311.78
1	2 (F)	4.74	3.04	11.68	13.96	13.34	15.31	0.22	0.19	0.25	0.84	0.88	0.31	1.04	0.97	0.84	9.35	0.89	0.52	2.16	8.92
0	3 (M)	15.43	13.40	20.67	44.56	45.59	49.37	0.04	0.02	0.12	0.47	0.47	0.74	0.25	0.07	1.27	42.81	5.58	0.48	30.33	338.93
1	3 (M)	7.63	6.26	13.47	24.17	23.68	17.35	0.23	0.20	0.29	0.83	0.87	0.35	1.08	1.02	0.88	9.31	0.87	0.38	2.45	12.38
0	4 (F)	16.82	14.00	23.42	41.05	40.82	56.17	0.04	0.02	0.10	0.46	0.44	0.75	0.15	0.00	0.73	23.18	7.83	0.47	46.75	366.55
1	4 (F)	6.15	4.77	12.19	14.51	12.65	19.61	0.22	0.19	0.25	0.81	0.86	0.36	0.99	0.94	0.85	11.33	0.76	0.33	2.37	17.30
0	5 (M)	16.78	12.98	25.56	43.92	43.29	54.99	0.04	0.02	0.08	0.64	0.75	0.63	0.15	0.00	0.77	26.86	6.59	0.33	48.00	313.77
1	5 (M)	3.77	2.63	9.18	20.07	20.09	8.27	0.22	0.21	0.16	0.86	0.88	0.23	1.01	0.99	0.57	10.81	1.27	0.70	3.32	20.88
0	6 (M)	14.44	12.20	20.31	43.08	45.00	55.22	0.03	0.02	0.07	0.58	0.71	0.74	0.19	0.00	1.00	41.45	7.53	0.32	46.50	253.33
1	6 (M)	5.59	4.77	9.75	15.48	15.50	8.24	0.20	0.18	0.18	0.85	0.87	0.23	1.00	0.96	0.58	9.59	1.47	0.65	4.55	26.15
0	7 (M)	19.39	13.91	30.48	40.58	37.27	55.19	0.03	0.02	0.09	0.63	0.73	0.66	0.15	0.00	0.90	39.73	5.55	0.32	40.37	284.48
1	7 (M)	5.55	4.53	10.52	16.04	15.51	9.11	0.19	0.17	0.19	0.87	0.89	0.22	1.01	1.00	0.67	11.04	1.45	0.80	4.20	34.33
0	8 (M)	16.27	13.80	23.68	44.78	40.18	53.00	0.03	0.02	0.09	0.52	0.52	0.72	0.26	0.07	1.36	36.71	5.64	0.33	35.79	213.32
1	8 (M)	5.65	3.87	12.54	20.84	20.59	16.06	0.22	0.20	0.24	0.83	0.87	0.29	0.99	0.95	0.76	9.50	1.38	0.67	4.19	20.45
0	9 (F)	15.56	11.82	24.24	37.99	37.32	56.87	0.04	0.02	0.11	0.51	0.51	0.72	0.19	0.00	1.05	37.08	5.53	0.38	36.99	432.05
1	9 (F)	5.33	3.88	11.23	7.44	5.77	17.90	0.25	0.22	0.32	0.82	0.86	0.33	1.00	0.95	0.95	11.01	0.88	0.38	3.17	37.80
0	10 (F)	16.19	13.08	23.55	42.46	45.05	56.69	0.04	0.02	0.11	0.55	0.59	0.68	0.15	0.00	0.80	27.19	4.91	0.38	39.80	390.68
1	10 (F)	5.82	4.47	11.83	13.22	12.18	13.47	0.24	0.21	0.30	0.83	0.87	0.31	0.99	0.96	0.88	11.89	0.78	0.37	2.44	18.80
0	11 (F)	14.26	11.65	20.11	41.67	48.59	60.32	0.04	0.02	0.09	0.55	0.59	0.75	0.21	0.00	1.11	41.88	5.82	0.38	36.06	245.37
1	11 (F)	5.92	5.42	8.89	8.35	7.79	10.30	0.21	0.20	0.18	0.85	0.87	0.23	0.97	0.93	0.63	13.21	1.01	0.47	3.36	25.77
NM (0)		15.82	12.72	23.22	41.91	43.10	55.47	0.04	0.02	0.10	0.54	0.59	0.73	0.19	0.00	1.01	42.81	6.21	0.38	40.10	432.05
M (1)		5.66	4.47	11.08	15.08	14.11	16.79	0.21	0.19	0.24	0.84	0.87	0.30	1.00	0.96	0.77	13.21	1.02	0.48	3.19	37.80

(B)	ID										
	1 (F)	2 (F)	3 (M)	4 (F)	5 (M)	6 (M)	7 (M)	8 (M)	9 (F)	10 (F)	11 (F)
Distance travelled (km) NM (0)	297.33	334.79	364.3	224.93	198.81	256.02	187.72	203.42	266.82	231.93	269.21
Distance travelled (km) M (1)	58.39	54.84	53.48	37.40	63.57	67.21	69.24	48.80	61.95	60.97	61.48
% of data acquisition determined as moving	10.50	10.35	11.47	8.25	15.12	15.02	19.49	17.26	12.80	12.44	13.17

Text S4 - mathematical procedures for various DD- and GPS-derived metrics used to compare MVF results

Derivation of pitch, roll and heading

Prior to collars being fitted, magnetic calibrations were performed (*cf.* Williams *et al.* 2017) and, following data retrieval, compass heading was computed using methods outlined by Bidder *et al.* (2015) and Walker *et al.* (2015). Compass heading (H) with respect to magnetic North, was given *via*:

$$H = \text{mod} \left(360 + \left(\text{atan2}(-m_y, m_x) \cdot \frac{180}{\pi} \right), 360 \right) \quad (1)$$

where $m_{x,y,z}$ refer to the normalised, ellipse-fitted and co-ordinate frame-adjusted x, y and z channels of the magnetometer, respectively (Pedley 2012; Bidder *et al.* 2015; Chapter 2).

A common practice to derive animal posture (in terms of pitch and roll; required in the tilt correction procedure prior to calculating heading) is to use the static component of acceleration. This was achieved by passing a two-second rolling mean to each of the three orthogonal acceleration channels.

Pitch and roll were then computed *via*;

$$\text{Pitch } (\beta) = \left(\text{atan2}(S_x, \sqrt{S_y \cdot S_y + S_z \cdot S_z}) \right) \cdot \frac{180}{\pi} \quad (2)$$

$$\text{Roll } (Y) = \left(\text{atan2}(S_y, \sqrt{S_x \cdot S_x + S_z \cdot S_z}) \right) \cdot \frac{180}{\pi} \quad (3)$$

where $S_{x,y,z}$ refer to the static components of acceleration from the x (anterior-posterior), y (medio-lateral) and z (dorsal-ventral) channels of the accelerometer (Chapter 2).

Pitch, roll and heading values were post-smoothed using a rolling window of 1 second, which represented a trade-off between reducing some of the signal-to-noise ratio of collar roll and maintaining sensitivity to the animal's movements.

For this study site, magnetic declination (the angle on the horizontal plane between magnetic north and true north) was estimated at -16.5° so this value was added to each derived-heading value to acquire a true bearing.

The pre- and post-smoothing windows used in the derivation of the DD's static acceleration, heading, pitch and roll was carried out in DDMT at the frequency of 40 Hz, prior to sub-sampling the data.

GPS heading

Heading (bearing) (θ) from the GPS data was calculated between consecutive fixes using;

$$\psi = \text{atan2}\left(\sin(\Delta\lambda_1) \cdot \cos(\varphi_2), \cos(\varphi_1) \cdot (\sin(\varphi_2) - \sin(\varphi_1)) \cdot \cos(\varphi_2) \cdot \cos(\Delta\lambda_1)\right) \quad (4)$$

The formula (*cf.* Robusto 1957) output is in radians, so values were multiplied by $180/\pi$ to get degrees. Lastly, the range is -180° to $+180^\circ$, so to convert to the same range as DD heading (0° to 360°), I applied the logical expression;

$$H = (\psi + 360) \text{ mod } 360 \quad (5)$$

where *mod* refers to the modulo operator.

The difference between DD heading and GPS heading was calculated per second, and a logical expression applied to ensure the difference between the two never exceeded 180° (*cf.* Pewsey, Neuhäuser & Ruxton 2013). Lastly, the resultant values were made absolute since the degree of turn was of more importance than the direction for analytical purposes.

We applied a circular mean to raw values of DD-derived and GPS-derived headings per unique moving/non-moving period (*cf.* Chapter 2).

The mean resultant length (\bar{R}) was calculated *via*:

$$\bar{R} = \sqrt{(X^2 + Y^2)} / n \quad (6)$$

here X and Y are the sum of the sines and cosines of H , respectively (units in radians) and n , the length of X and Y input. Note that \bar{R} varies between 0 and 1, with values closer to 1, implying less variation in angular variance between observations.

A non-parametric circular kernel regression estimation (using von Mises kernel) was used to construct a circular covariate (DD heading) to the circular response (GPS heading) regression. This was achieved using the NPCirc package in R (Oliveira Pérez, Crujeiras Casais & Rodríguez Casal 2014). The `bw.reg.circ.circ` function was used to estimate the ideal bandwidth (to provide the least squares cross-validation smoothing parameter for the local linear estimators) and the `kern.reg.circ.circ` function (using the local linear estimator method) was used to construct a circular ~ circular regression.

Tortuosity

The tortuosity (T) was calculated by dividing the straight-line distance (SLD), that is the two-dimensional Euclidean distance between the initial fix and the end fix of the path, by the sum of the consecutive individual distance steps (SDS) between $fix_1, fix_2, \dots, fix_n$ that constituted the total path length (*cf.* Benhamou 2004) (the duration of each unique moving/non-moving period) using;

$$SLD = \sqrt{(\lambda_n - \lambda_1)^2 + (\varphi_n - \varphi_1)^2} \quad (7)$$

$$SDS = \sum_{i=1}^n \left(\sqrt{(\lambda_2 - \lambda_1)^2 + (\varphi_2 - \varphi_1)^2} \right) \quad (8)$$

$$T = \frac{SLD}{SDS} \quad (9)$$

φ and λ are the latitude and longitude coordinates (decimal format), respectively. Here, a T of 1 represents straight-line movement while values below this indicate increasing deviations.

Distance and speed estimates

Following the MVF protocol, distance and speed estimates were recalculated separately for both moving and non-moving periods. Distance was computed using a stepping range of five seconds, (same as MVF, except that the stepping range reset with each new MVF period). This meant periods of non-moving ≤ 4 s were excluded from distance estimates (moving periods were always ≥ 5 s and so this stepping range provided at least one value per period). For speed estimates, distance values were

divided by the time between the rolling stepping range (in this case, always 5 s) and values were then smoothed using a rolling mean window of three seconds, which consequently excluded speed estimates from both non-moving and moving ≤ 6 s.

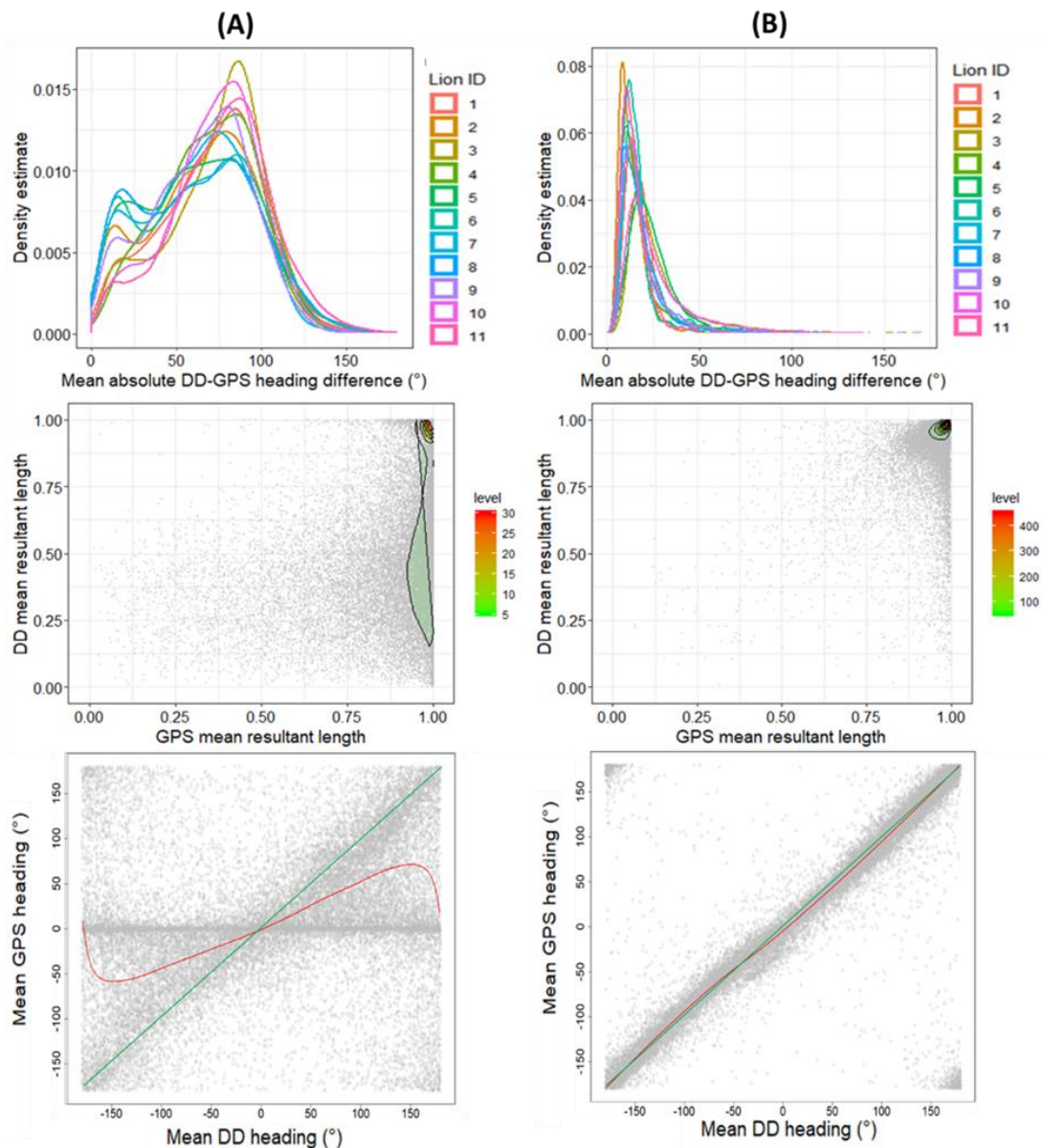


Figure S4. 1. Relationship between DD- and GPS-derived heading for both non-moving (A) and moving (B) filtered datasets (all lions). Each value reflects the circular mean calculated per unique period. A non-parametric circular kernel regression estimation (using von Mises kernel) was used to construct a circular covariate (DD heading) to circular response (GPS heading) regression (red line). A linear relationship (intercept = -180) shown for reference (green). Note the banding of GPS heading values reading 0 are a consequence of identical consecutive longitude and latitude coordinates. Also note the range of heading given between -180° to $+180^{\circ}$ (both of which represent south).

References

- Benhamou, S. (2004) How to reliably estimate the tortuosity of an animal's path:: straightness, sinuosity, or fractal dimension? *Journal of Theoretical Biology*, **229**, 209-220.
- Bidder, O., Walker, J., Jones, M., Holton, M., Urge, P., Scantlebury, D., Marks, N., Magowan, E., Maguire, I. & Wilson, R. (2015) Step by step: reconstruction of terrestrial animal movement paths by dead-reckoning. *Movement ecology*, **3**, 1-16.
- Chopde, N.R. & Nichat, M.K. (2013) Landmark based shortest path detection by using A* and Haversine formula. *International Journal of Innovative Research in Computer and Communication Engineering*, **1**, 298-302.
- Gleiss, A.C., Wilson, R.P. & Shepard, E.L. (2011) Making overall dynamic body acceleration work: on the theory of acceleration as a proxy for energy expenditure. *Methods in Ecology and Evolution*, **2**, 23-33.
- IUCN, S. (2006) Regional conservation strategy for the lion *Panthera leo* in Eastern and Southern Africa. *IUCN SSC Cat Specialist Group*.
- Mills, G. & Mills, M. (2010) *Hyena Nights & Kalahari Days*. Jacana Media.
- Oliveira Pérez, M., Crujeiras Casais, R.M. & Rodríguez Casal, A. (2014) NPCirc: An R package for nonparametric circular methods. *Journal of Statistical Software*, **61**.
- Pedley, M. (2012) eCompass-Build and Calibrate a Tilt-Compensating Electronic Compass. *Circuit Cellar-The Magazine For Computer Applications*, 1-6.
- Pewsey, A., Neuhäuser, M. & Ruxton, G.D. (2013) *Circular Statistics in R*. OUP Oxford.
- Robusto, C.C. (1957) The cosine-haversine formula. *The American Mathematical Monthly*, **64**, 38-40.
- Walker, J.S., Jones, M.W., Laramée, R.S., Holton, M.D., Shepard, E.L.C., Williams, H.J., Scantlebury, D.M., Marks, N.J., Magowan, E.A., Maguire, I.E., Bidder, O.R., Di Virgilio, A. & Wilson, R.P. (2015) Prying into the intimate secrets of animal lives; software beyond hardware for comprehensive annotation in 'Daily Diary' tags. *Movement ecology*, **3**, 29.
- Williams, H.J., Holton, M.D., Shepard, E.L., Largey, N., Norman, B., Ryan, P.G., Duriez, O., Scantlebury, M., Quintana, F., Magowan, E.A., Marks, N., Alagaili, A.N., Bennett, N.C. & Wilson, R.P. (2017) Identification of animal movement patterns using tri-axial magnetometry. *Movement ecology*, **5**, 6.
- Wilson, R.P., Börger, L., Holton, M.D., Scantlebury, D.M., Gómez-Laich, A., Quintana, F., Rosell, F., Graf, P.M., Williams, H., Gunner, R., Hopkins, L., Marks, N., Geraldi, N.R., Duarte, C.M., Scott, R., Strano, M.S., Robotka, H., Eizaguirre, C., Fahlman, A. & Shepard, E.L.C. (2020) Estimates for energy expenditure in free-living animals using acceleration proxies: A reappraisal. *Journal of Animal Ecology*, **89**, 161-172.
- Wilson, R.P., Shepard, E. & Liebsch, N. (2008) Prying into the intimate details of animal lives: use of a daily diary on animals. *Endangered Species Research*, **4**, 123-137.

Chapter 5: Supplementary Information

Text S1 – Device set up and capture protocol

I selected 3 free-living species (mixed sex) to demonstrate points being made: Twelve Magellanic penguins (*Spheniscus magellanicus*) (Argentina, San Lorenzo Magellanic penguin colony (-63.86, -42.08)), five lions (*Panthera leo*) (Kgalagadi Transfrontier Park in the Kalahari Desert (constituting parts of South Africa and Botswana) (-26.47, 20.61)) and fifteen Imperial cormorants (*Leucocarbo atriceps*) (Argentina, Punta León Imperial Shag colony (-43.06, -64.03)) were used. Daily Diary (DD) (*cf.* Wilson, Shepard & Liebsch 2008) units ('Daily Diaries' - Wildbyte Technologies, <http://www.wildbytetechologies.com>) recorded tri-axial acceleration ($1\text{ g} = 9.81\text{ ms}^{-2}$; range 0-32 g) and tri-axial magnetometry (G) at 40 Hz and GPS (Axytrek) units (<https://www.technosmart.eu>) recorded longitude and latitude positions (decimal format) at 1 Hz. Both were deployed simultaneously for each species. The DD's were also integrated with a Keller pressure sensor, with an operating pressure of 0-30 bar at 24-bit resolution for both bird species.

Penguins and cormorants were captured at the nest during the chick rearing season. Penguins were caught using the clipboard method (Wilson 1997) and cormorants *via* a crook on the end of a long pole (*cf.* Sakamoto *et al.* 2009). DD's and GPS units were fitted longitudinally to the base of the spine using Tesa® tape (Wilson *et al.* 2005; Wilson *et al.* 2010). Field work for both these species occurred in November-December, 2019. During instrumentation, birds were handled as quickly and efficiently as possible. Birds were left to execute one foraging trip at sea (typically lasting between 24 and 48h) before being re-caught at the nest and the devices recovered. Tag weight comprised < 1 % of the animal's mass.

Lion field work commenced February, 2019 - Units were collar mounted to a Litetrack collar (<https://www.lotek.com>) and caught according to the Standard Operating Procedures of SANParks Veterinary Services (see <https://www.sanparks.org/conservation/veterinary/about/animals/lion.php>) as detailed in SANPark's 'Standard Operating Procedures for the Capture,

Transportation and Maintenance in Holding Facilities of Wildlife' (Reference: 17/Pr-CSD/SOP capture, transport, holding facilities (04-17) v2) and SANParks SOP 'Fitment of tracking devices and marking of fauna in South African National Parks' (Reference: 17/Pr-CSD/pro/tracking + marking (12/16) v1).

Adult lions to be tagged were located through tourist and field ranger's observations during the day. A carcass bait secured to a tree and pre-recorded animal distress calls played using an audio system (Truck Pro, Foxpro Inc) from a darting vehicle (positioned approx. 20 m distance from the bait station) were used to attract the lion at nightfall for distance immobilisation. The drug delivery system consisted of Pneu-Dart single use powder charged darts (2cc, 1 ½" 14g wirebarbed needle) delivered with a DAN-INJECT CO2 rifle (Model JM.SP.25, DAN-INJECT) with 13 mm barrel. A combination of drugs - zolazepam/tiletamine (Zoletil®Virbac) and medetomidine hydrochloride (Medetomidine Compound, Kyron Laboratories,) at an average 1.2 mg/kg and 0.05 mg/kg, respectively were used as anaesthetic agent. Once anaesthetised, individuals were blind folded, foot shackled and translocated to a well-lit processing station. Dart sites were treated systemically by subcutaneous injection at the recommended dose with Ceftiofur (Excede®, Zoetis, 1ml per 30 kg) and meloxicam (Metacam®, Boehringer, Randburg, 0.2mg per kg) respectively. Once processed (typically 10-15 mins per individual), animals were relocated to the capture location and the medetomidine component of anaesthesia reversed intramuscularly with a mix of atipamezole (Antisedan®, Zoetis) at 2.5 times the amount of medetomidine and yohimbine (Yohimbine Compound, Kyron) at 6.25 mg per kg body weight. Animals were monitored until ambulatory. Collars attached with all devices constituted < 2 % and < 1 % of the body mass of the lightest equipped female and male animals, respectively. Data were retrieved approximately two weeks after the tag deployment using the above methods for recapture.

Text S2 – The importance of having the correct coordinate system and axis alignment

It is essential that tri-axial accelerometer and magnetometer readings are aligned to a designated tag coordinate system for accurate delineation of 3-D rotation with respect to the fixed Earth's surface. The equations and R source code detailing the tilt-compensated method (*cf.* Text S3) assumes the aerospace (x-North, y-East, z-Down) coordinate system, or 'NED' (*cf.* Fig. S2. 1). When lying flat and upright, the z-axis reads approximately 1 *g* (1 *g* = 9.81 m/s) and the x- and y-axes are near 0 *g*, inverting the device 180° negates the z-axis reading. Pointing the device 90° downward and then upward along the x- and y-axis results in readings near 1 *g* and –1 *g*, respectively. This is the reason why x-axis measurements are negated (essentially multiplied by -1) in the derivation of pitch (E₁₄ – main text), because in the NED system, a downward inversion of the x-axis results in a positive increase in measured acceleration. Assuming the magnetometer and accelerometer channels are in alignment, the x-channel magnetometer reading is at a maximum and minimum when the (whole) device (positioned flat) is pointed North and South, respectively. The y-channel is at a maximum when the device is rotated to point West and reads a minimum when the device is pointed East, with the z-channel reading remaining relatively constant. Conversely, the y-axis will read a maximum when the device is pointed East following a 180° inversion, with the z-axis reading (though still constant) being lower than the upright condition (in the Northern hemisphere), because the channel is aligned against the downward geomagnetic field vector. Using this local frame, we assume that the x, y and z axes of both the accelerometer and magnetometer sensors are aligned to the anterior-posterior (surge), medio-lateral (sway) and dorsal-ventral (heave) axes of a given animal, respectively.

Not all devices have an orthogonal set up with respect to the NED local frame, whilst discrepancies between deployment position may also change the local frame with respect to the earth's vector. Transforming between coordinate frames requires 3 x 3 rotation matrices, with the unique combination dependent on the coordinate frame of your device and the coordinate frame you are interested in (*cf.* Pedley 2013). This can become tricky however, since the direction of measured acceleration (with respect to the Earth's downward gravitational field) can differ between devices with

similar orthogonal layout. For example, the Daily Diary (DD) units (*cf.* Wilson, Shepard & Liebsch 2008) deployed on animals used in this study measure +1 *g* when lying flat and upright, similar to the NED system (Fig. S2. 1), despite an upward direction of measurement (NED being downward). Consequently, there is no 'set' rotation matrix for a given local coordinate frame transformation, whilst depending on board layout, magnetometry channels may require a variant matrix to the one used for acceleration readings. Put simply though, due to the layout of perpendicular (orthogonal) channels, any required correction just involves swapping and/or negating the measurements from your accelerometer and/or magnetometer channels until correctly aligned with the NED coordinate system (*cf.* Cheng 2011).

As a case in point using the above tilt-compensated method for DD's (*cf.* Fig. S2. 1), the y- and z- axis of the magnetometer are required to be negated, since they are measuring magnetism in the opposite direction to that governed by the NED system. As for acceleration, despite the y-axis being opposite in direction from that of NED local frame, raising the left side of the device results in a positive increase of measured acceleration, which transcends to a positive roll (*cf.* E₁₅ – main text). This is the same as the NED coordinate system, because of the point alluded to earlier whereby *g* is positive towards the downward component of earth vector for NED but negative for the DD axes configuration. If we picture a seesaw effect, as the DD y-axis tilts up, the corresponding NED y-axis tilts down, but both are measuring increasing *g* and thus depicted as rolling right. As such the y-axis does not need to be negated and in a similar manner, the z-axis also remains the same, but the x-axis does require negation, since a downward tilt (pitch) measures negative *g* for the DD configuration and positive *g* for the NED system. If a device was positioned on an animal perpendicular to 'normal' then as well as deciding channel negation, certain channels will be required to be swapped. Again, in the case of the DD, z-axis values are required to be exchanged with x-axis values (of both the accelerometer and magnetometer) following a clockwise 90° inversion about the y-axis (e.g., x-axis now points upwards and thus represents the 'heave' plane (originally reflected by z-axis values)). In this instance, the z-axis (now representing the (inverse) surge plane and swapped with x-axis values) of the magnetometer requires negating, due to a 180° inversion, though

the equivalent accelerometer channel does not (because a negative increase in measured g now corresponds to a positive pitch - same as the NED system). Lastly, the x-axis (now containing z-axis values) and y-axis values of the accelerometer and magnetometer follow the same protocol as the 'original orientation' described above.

Judicious choice of channel configuration is required for correct output of pitch, roll and yaw, though once this is obtained, the user can save the channel configuration for all future uses at this given orientation. Note, however, animals that travel with postures greater than perpendicular from one another (e.g., a penguin walking through a colony vs swimming in the ocean or a pine martin bounding across the forest floor vs climbing a tree) would require variant axis alignments according to mode of movement (when using Euler angles). Assuming a tag can be deployed at any perpendicular orientation, there are 24 possible channel local coordinate frame configurations.

To aid the above process, I recommend alongside the magnetic calibration, the user undertakes a configuration calibration, in that the device is slowly pitched up and down and rolled left and right three times at each cardinal direction, starting and ending at North, before spinning the device slowly in a circle clockwise three times, again, starting and ending at North. Note, during this procedure, the 'default' device orientation should be equivalent to that when deployed on the animal (during 'normal' traversing posture). The user can inspect results obtained during this calibration period to ensure the sequence of pitch and roll angles follow the intended direction of rotation (see Fig. S2. 1b). Further, the shape of this calibration period when dead-reckoned (using a constant progression (speed) value) should produce an approximate square shape followed by three circles, finishing at North, (see Fig. S2. 1c). Should these diagnostic plots not show what is expected, then the accelerometer and/or magnetometer alignment is wrong with respect to the coordinate system assumed within the tilt compensated compass method outlined in Text S3.

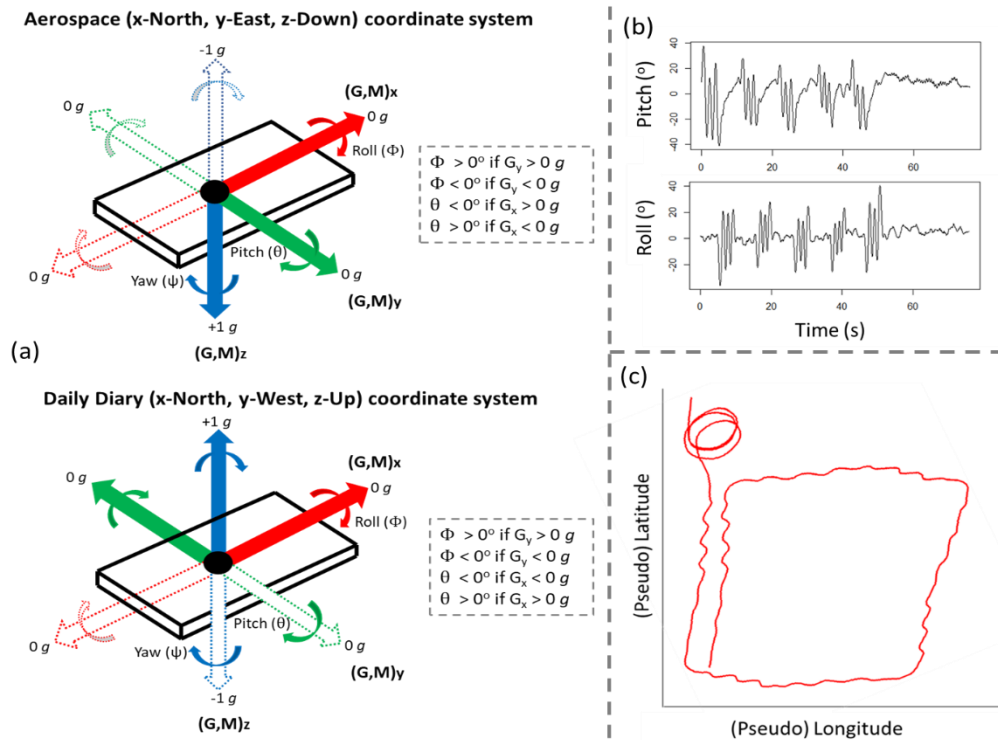


Figure S2. 1. The aerospace north-east-down (NED) coordinate system (top) and the Daily diary north-west-up (NWU) coordinate system (bottom) (a). Both systems assume the x (red), y (green) and z (blue) channels of the magnetometer (M) and accelerometer ($G = \text{gravitational component}$) are in alignment. Dotted arrows reflect a 180° inversion of each channel. Note the difference in the direction of measured acceleration ($-1 g / +1 g$) between the two coordinate systems when pointing downward in relation to the earth's gravitational vector. A clockwise rotation about the y-axis results in a positive inversion of the x-axis (pitch (θ)) and a clockwise rotation about the x-axis results in a positive inversion of the y-axis (roll (Φ)), though note, for the NED coordinate system, x-axis values are required to be negated within the computation of θ so that a positive increase in measured acceleration results in a decreasing θ . Evaluation of whether a coordinate system is correctly aligned to that required in the tilt-compensated compass method can be shown by plotting computed pitch (b), roll (b) and yaw (the latter being assessed as a dead-reckoned track (c)), from data collected during a configuration calibration (outlined in the text above).

Text S3– Magnetometer calibration, rotation correction and deriving yaw (heading)

Device calibration should be performed so that magnetic distortions to the data can be corrected post-hoc. It is recommended that the device is rotated slowly, ideally in an open space, away from potential sources of magnetic disturbance, relative to the Earth's magnetic field. Each orientation of roll, pitch and yaw should be incorporated in the device rotations (simply put, imagine a pen is attached to the end of the device being rotated and the aim is to 'colour in' all parts of a sphere). This section of data can then be used as a reference for the vectorial sum of magnetometry data across all three spatial dimensions, from which 'hard' and 'soft iron' errors which can occur in magnetometry data can be corrected. Note, only data during the calibration procedure should be used to deduce soft and hard iron offsets for each magnetometer channel, which is subsequently applied to all magnetometer readings. Hard iron deposits (e.g., ferrous materials or magnets) introduce a constant additive bias to the earth's magnetic field and thus magnetometer readings, whereas soft iron distortions (non-magnetic materials that alter the magnetic field, e.g., nickel) are caused by variations in the surrounding magnetic field. A tri-axial magnetic field intensity scatterplot of the calibration period shows such distortion (*cf.* Fig. S3. 1), with hard iron deposits causing the sphere to shift from origin and soft iron deposits, stretching the sphere into an elliptical shape. This function corrects magnetometry data for soft and hard iron distortion and performs rotation correction of the magnetic and gravity vectors (assuming they are in alignment) if the user inputs Euler angle offsets (of the tag relative to the animal's body frame), prior to computing heading.

```
Gundog.compass = function(mag.x, mag.y, mag.z, acc.x, acc.y, acc.z,
ME, pitch.offset = 0, roll.offset = 0, yaw.offset = 0, method = 3,
plot=TRUE)
```

The function inputs given below follow in the order:

- Raw tri-axial magnetometer data (mag.x,y,z)
- Tri-axial **static** acceleration data (acc.x,y,z) (for computation of pitch and roll)
- Marked events data (ME) specifying the period of the magnetic calibration period (as denoted by 'M' – any other input signifies data acquisition not part of calibration procedure).
- Pitch, roll and/or yaw device offsets relative to the animal's body frame (default values are zero)
- method
 - method = 1, is the computationally cheaper method, using scale biases with simple orthogonal rescaling (avoiding matrices altogether), outlined by Winer (2017), but may prove effective when data is less affected by noise – e.g., nearly spherical. Within this method, hard iron offsets are resolved by obtaining the average recorded magnetism bias from each channel, specifically by dividing the summed maximum and minimum values of raw magnetism by two. Soft iron scale factors are used to rescale and thus equalise the magnetometer data along the three measurement axes. Here, the average maximum chord length is calculated from the ratio of the average maximum – minimum values of each axis by the summed equivalent of all axes. This is then multiplied to all data, subsequent to hard iron distortions being removed.
 - method = 2 and method = 3 essentially compute gains and cross-axis gains (from derived eigen- values and vectors, respectively), by performing a sphere (ellipsoid) fitting. This involves centring a sphere (or ellipsoid) to (0,0,0) origin, de-rotating by multiplying by the inverse of the rotation matrix and scaling appropriately *via* multiplying by the inverse of the gains. For rotated ellipsoids use method = 3 and for near spherical data and/or influenced by heavy noise, use method = 2. For, non-rotated

ellipsoids use method = 4, when x and y channel radii the same, use method = 5, when x and z are the same, use method = 6, when y and z are the same, use method = 7 and for spherical data use method = 1, 2 or 8. Essentially, there up to eight variant methods included (default is method = 3). For a detailed review of the underlying mathematics of these methods, see Vitali (2016). Inspection of summary plots can aid in demonstrating the ‘best’ method to use.

- Plot = TRUE (default) compares 2-D magnetic field intensity scatterplots (mag.x - mag.y, mag.x - mag.z and mag.z - mag.y) of the calibration period both pre- and post-calibration from one of the user-defined methods dictated above (see Fig. S3. 1).

Note, within the function itself, $B_{x,y,z}$ refers to (uncorrected) magnetism data during the calibration period (which should be coded for by ‘M’ in ME) and $M_{x,y,z}$ refers to all (uncorrected) magnetism data (incl. calibration data). $NM_{bx,y,z}$ are the normalised channels expressed in the animal’s body frame after calibration and $NM_{bfx,y,z}$ are the calibrated, normalised data expressed in the animal’s body frame, after tilt-correction. $NG_{bx,y,z}$ are the normalised static acceleration data expressed in the animal’s body frame after calibration. Note the above notations stand when no rotation correction is performed (e.g., no Euler angle offsets supplied), since the magnetic and gravity vectors are assumed to aligned with the animal’s body-carried NED frame.

The function returns a data frame containing columns in the order:

- Normalised tri-axial **static** acceleration data expressed in the animal’s body frame ($NG_{bx,y,z}$).
- Calibrated tri-axial magnetometry data ($M_{x,y,z}$)
- Calibrated, normalised tri-axial magnetometry data expressed in the animal’s body frame ($NM_{bx,y,z}$)
- Calibrated, normalised tri-axial magnetometry data expressed in the animal’s body frame, after tilt-correction ($NM_{bfx,y,z}$)

- Marked events (ME)
- Pitch
- Roll
- Yaw

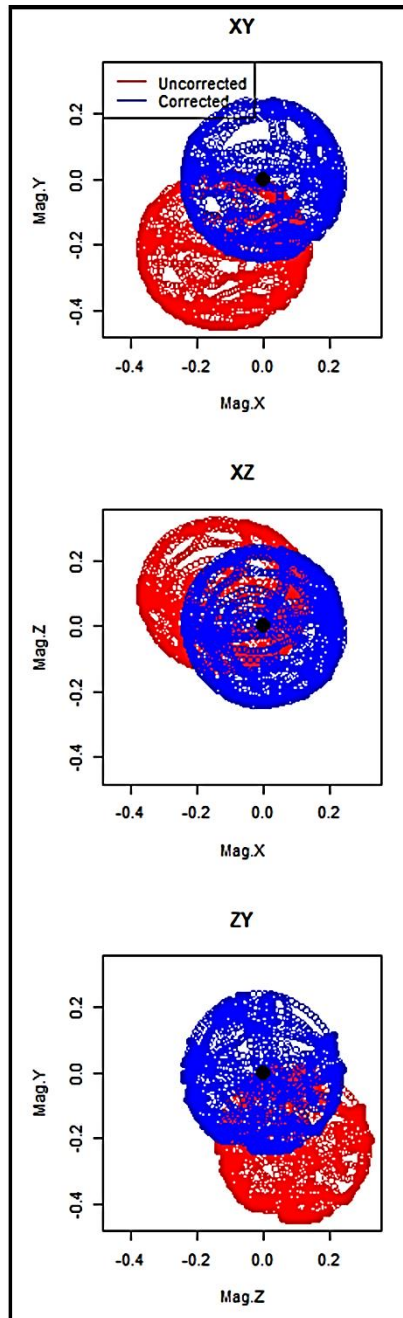


Figure S3. 1. Output summary plots from `Gundog.Compass()` (when `plot = TRUE`), showing 2-D dimensions of the `xy`, `xz` and `zy` magnetometry components during the calibration period (`ME = 'M'`), both pre- (red) and post- (blue) correction. The 0,0 origin (centroid) is denoted with a black circle.

See Text S2 for relevance pertaining to the order of variable input. This function assumes the NED coordinate frame. Changing the order of variable input/channel negation may be required. To avoid confusion, within the function, assume the `x`, `y` and `z` input fields for both magnetometry and accelerometry data represents the surge, sway heave dimensions of orientation, respectively, which the user allocates the appropriate channel and/or required negation to (dependent on the local coordinate frame of the device used).

See `Gundog.Compass.R` file for annotated function.

Text S4 – Step counts as a distance estimate

Within the main text, a step count was used as a speed proxy within *Gundog.Tracks* for twelve penguin's walking trajectories (*cf.* Fig. 7 – main text). There are multiple ways in which this could be performed. In R, if we use a Reference Vector (*RV*) and assume the duration of each stride cycle is coded for with a one (1) and anything else, a zero (0) (from some previous behavioural identifier), then the length (duration) of each uninterrupted *RV* (matching numerical) sequence can be computed (R_1). For *RV* values of 1, this is the time period per step (*TPS*). The unique incremental change of each *RV* number (each time it 'reappears' - changes from 1 to 0 or *vice versa*) can be computed ($R_{2:7}$). For *RV* values of 1, this is the step count (*SC*). Because of the nature of how *SC* is calculated, the rolling difference of *SC* provides an index of step frequency (*SF*) (with the value of 1 indexing 'another step'; R_8). One could then calculate the mean number of steps over a given window length and standardise to number of steps per second by dividing by the time difference (s) between values (*TD*; R_9 - e.g., for 40 Hz data, *TD* will be approx. 0.025 s). Multiplying this step frequency by a 'distance per step' (*d*) progression value (0.16 m used for penguins; R_{10}) gives an index of speed (m/s), which can be converted to *q* *via* dividing by the earth's radius (R_{11}).

```

TPS = sequence(rle(RV)$lengths)           (R1)
x1 = rle(RV)$values                       (R2)
x2 = rle(RV)$lengths                     (R3)
z = c()                                   (R4)
for(i in unique(x1)){                    (R5)
  z[x1==i] = 1:sum(x1 ==i)}              (R6)
SC = rep(z,x2)                            (R7)
SF = c(0, diff(SC))                       (R8)
SF = rollapply(SF, width=w, FUN=mean, fill=0, align = 'right') / TD (R9)
d = 0.16                                  (R10)
q = (SF * d) / 6378137                    (R11)

```

here, *w* should be replaced with the rolling window of choice (e.g., assuming 40 Hz data and a five second window length desired, replace with 200).

I provide a peak finder function; *Gundog.Peaks()* that locates peaks based on local signal maxima, using a given rolling window, with each candidate peak filtered

according to whether it surpassed a threshold height. The function returns a data frame containing the (original) row index position of peaks, their amplitude and periodicity between peaks. To calculate the above outlined speed proxy, the row index position of each peak (this is contained within the column termed '*Index*', from the function output) is required to be inserted within a reference vector (*RV*) the length of all other variables used within the dead-reckoning process (e.g., heading (*h*)) to match step peaks in time with motion sensor data. This is because the function output does not include inter-peak data and so output is sub-sampled from the original data input. This process can be achieved by creating a sequentially increasing numerical vector (*RN*; e.g., analogous to the row number index of a data frame, or element number index of a vector), the length of, in this case, *h* (R₁₂) and pasting the index location, '*Index*' within a vector termed '*RV*', based on the matching *Index* and *RN* values (R₁₃).

```
RN = rep(1:length(h)) (R12)
RV = as.integer(sub("\\.$", "", RN) %in% Index) (R13)
```

Note, for column operations, replace 'length' with 'nrow' (R₇₈).

Gundog.Peaks was modelled from the *find_peaks()* function within *ggpmisc* package (cf. Aphalo 2018), with inputs, function processes and outputs explained below. Note, this function requires the *zoo* package installed and required. Further, this function is only applicable to searching peak maxima, however if peak minima are of interest, I suggest that the user multiplies all values within the spectrum by minus one, subsequent to changing negative values to zero. The user can then use the function in the same way (since minima become maxima, and values originally above zero become zero). The vector sum of acceleration across all three spatial dimensions (cf. Wilson *et al.* 2020b) is the variable I recommend using.

```
Gundog.Peaks = function(TS, x, thresh = 0, LoM = 5, constant
                        = "med", ME = 1, plot=TRUE, outlier = FALSE)
```

The function inputs given below follow in the order:

- TS = timestamp data (POSIX class)
- x = the variable to locate peaks on
- thresh = the minimum height of the candidate peaks (%): size threshold relative to the tallest peak considered (though see outlier = TRUE) with constant baseline subtracted
- LoM = span (rolling window length) for local maximum, default is 5, ensure this value is odd (otherwise the function will add 1)
- constant = the constant baseline (y-axis value to be surpassed according to the height threshold) can be user defined (own constant baseline value). The default setting is "med" for median constant. For the mean, "mn" can be input; both are calculated from all values ≥ 0 that have an ME value of one (1)
- ME = marked events (default = 1) specifies which values to locate peaks on (e.g., periods of moving already demarked with a one (1), as opposed to periods to ignore, marked with a zero (0))
- plot = TRUE (default) shows the peak spectrum over time with the identified peaks, height threshold, constant baseline and marked events demarked (*cf.* Fig. S4. 1)
- outlier = FALSE (default). If changed, then the max value is not used when scaling height threshold (%) but rather, the quantile value input instead of FALSE (do not input TRUE). For example, rather than scaling a 35 % threshold height from the specified constant and the maximum value in the spectrum (with ME of 1), scale it in relation to outlier = 0.99 (0.99 quantile of data (with ME of 1)).

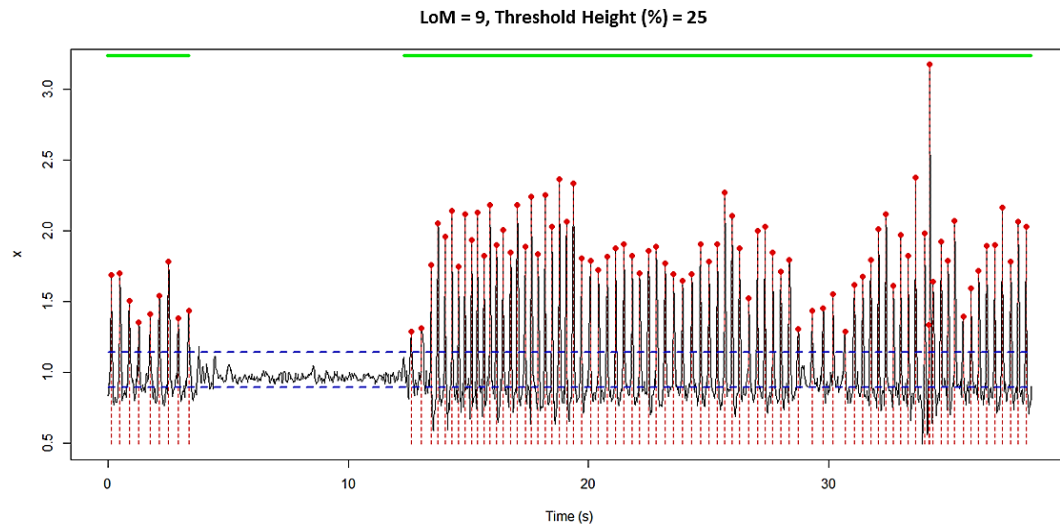


Figure S4. 1. Output plot from `Gundog.Peaks()` (when `plot = TRUE`) on a snippet of data (x ; vector sum of acceleration from a penguin walking). The green band represents ME values > 0 and each peak is signified with a red circle and dotted vertical line dissecting the peak. The user defined constant and height threshold (%) values are denoted with horizontal dashed blue lines. Here `thresh = 25`, `LoM = 9` (data = approx. 40 Hz) and `constant = "med"`.

The function returns a data frame containing columns in the order:

- Timestamp
- Index (the original row/element position of input data)
- Peak.Amplitude (value of x at peak location)
- Peak.Period (duration between peaks (s))
- Marked.events

See `Gundog.Peaks.R` file for annotated function.

Text S5 – Time Data in R (POSIXct)

In R, to determine accurate time period lengths between values, it is best to save date and time variables together as *POSIX* class (date-time format), so R recognises the character string to be manipulated. If date (*D*) and time (*T*) are within different vectors, simply paste together and convert to a *POSIXct* timestamp object (*TS*) (and specify the time zone (*R*₁)).

```
TS = as.POSIXct(strptime(paste(D, T), format = "%d/%m/%Y %H:%M:%S", (R1)
tz = "GMT"))
```

The order and type of code used in the format string composed may differ according to the original date and time format registered by the device (e.g. above, I assume date is in the format; '06/01/1995' and time; '14:15:30') (cf. Fortin *et al.* 2005).

To convert to a different format, it is best to make the *POSIXct* variable using the format dictated by device output (*R*₃; 1st format string) before converting to a character string using the format you desire (*R*₃; 2nd format string) and then converting this character string back to a *POSIXct* variable (*R*₄). In this example, I assume *D* was in the format, '1995/01/06' and *T*, '14-15-30' and I desired the original format stated in (*R*₁);

```
TS = paste(D, T) (R2)
TS = format(as.POSIXct(TS, format = "%Y/%m/%d %H-%M-%S"), (R3)
"%d/%m/%Y %H:%M:%S")
TS = as.POSIXct(TS, format= "%d/%m/%Y %H:%M:%S") (R4)
```

For data recorded at infra second frequency, it is vital to include sub-seconds within the *POSIX* object. Below I provide R code (*R*₅₋₉) using an example where date (*D*), time (*T*) and decimal seconds (*DS*) are stored in separate vectors, with date and time in the format alluded to above and decimal seconds in the format "0.555" (a zero before the decimal present).

```
DS = sub("^(-?)0.", "\\1.", sprintf("%.3f", DS)) (R5)
T = paste0(T, DS) (R6)
TS = paste(D, T) (R7)
options(digits.secs=3) (R8)
TS = as.POSIXct(strptime(TS, format = "%d/%m/%Y %H:%M:%OS", tz = "GMT")) (R9)
```


Here, I remove the zero before the decimal point of *DS*, ensuring three decimal places follow ("%0.3f"; R₅). *DS* is then appended alongside *T* (no separation; R₆) before *D* and *T* are pasted together (space-separated; R₇). I then specify the number of decimal places of the fractional seconds to express (R₈) subsequent to creating the *POSIXct* object '*TS*' (R₉) (note, '%OS' refers to decimal seconds). The resultant *TS* object has the format, '06/01/1995 14:15:30.555'.

Creating timestamp objects with *POSIX* class enables greater control and manipulation of time data, useful when preparing data to be dead-reckoned. Some useful processes include; correctly time ordering rows of a data frame (*df*; R₁₀), deleting rows with duplicated timestamp readings (R₁₁), merging two data frames together based on matching time stamps (e.g., VP data and motion sensor data; R₁₂) and importantly for the dead-reckoning calculation, computing the rolling time difference (*TD*) between data points (R₁₃).

```
df = df[order(df$TS), ] (R10)
df = df[!duplicated(df$TS), ] (R11)
new.df = merge(df1, df2, by.x = "TS" , by.y = "TS") (R12)
```

here user should replace the "TS" input after 'by.x =' and 'by.y =' with the column names of each of the two data frame's (df1 & df2) time stamp variables (assuming they have matching time format).

```
TD = c(0, difftime(TS, lag(TS), units = "secs")[-1]) (R13)
```

In conjunction with the '*lubridate*' package (Grolemund & Wickham 2011) (R₁₄), it becomes easy to add or subtract time (useful if VPs are pre-programmed to record in a different time zone; R₁₅) and to subset a data frame (*df*) between two time periods (TS₁ & TS₂; R_{16:19})

```
install.packages("lubridate") ; library(lubridate) (R14)
TS = TS + hours(3) ; TS = TS - minutes(20) ; TS = TS - seconds(55) (R15)
TS1 = as.POSIXct("2020-08-13 11:15:31.049") (R16)
TS2 = as.POSIXct("2020-08-19 17:48:11.705") (R17)
int = interval(TS1, TS2) (R18)
df = df[df$timestamp %within% int,] (R19)
```

Lastly, one can easily create a ‘pseudo’ time variable (of a given length, advanced according to a specified time interval) to act as the *TS* variable within *Gundog.Tracks()*. Below (R₂₀), a single datetime *POSIXct* variable is created (though format and time zone may differ according to user choice). This is then advanced by a user-defined time interval (default assumes seconds) – In this example, this is a 0.025 second interval between values (assuming 40 Hz). This incremental time column is advanced to a specified bounded length (here I use a data frame column ‘VeDBA’ to act as the (row-wise) dimension limit.

```
df$TS = seq.POSIXt(from = as.POSIXct("1995-01-06 05:07:28.05",      (R20)
format = "%Y-%m-%d %H:%M:%OS", tz = "GMT"), length.out = length(df$VeDBA),
by = 0.025)
```

Text S6 – VPC dead-reckoning – *Gundog.Tracks*

***Gundog.Tracks*(*TS*, *h*, *v*, *elv* = 0, *cs* = NULL, *ch* = NULL, *m* = 1, *c* = 0, *ME* = 1, *lo* = 0, *la* = 0, *VP.lon* = NULL, *VP.lat* = NULL, *VP.ME* = FALSE, *method* = NULL, *thresh* = 1, *dist.step* = 1, *bound* = TRUE, *Outgoing* = TRUE, *plot* = FALSE)**

Gundog.Tracks() input and output variables are explained within the main text (Table. 2 & 3). The function outputs written messages to the console to update the user of the progressions of each stage. Important assumptions for variable input include:

- Heading (*h*) (with magnetic calibration and any required declination angle already applied); scale 0° to 360° (both corresponding to true North - or 0° to 359°)
- Either speed (m/s) or a DBA proxy input (*v*). If inputting a DBA proxy, *m* and *c* values should be modulated
- Depending on whether *outgoing* = TRUE or *outgoing* = FALSE (reverse dead-reckoning), user supplies either starting or finishing longitude (*lo*) and latitude (*la*) coordinates, respectively. VP data input as decimal format (e.g., 26.31989, -06.11995)
- **Required packages installed: 'dplyr' & 'zoo'** (these will be checked as dependencies and installed within the function)
- If carrying out VPC, VP data should be synced up alongside motion sensor data within the same length columns/elements. Missing VP data should be replaced with NA or 0.
- Timestamp (*TS*) must be in specific format (*POSIXct* object) (cf. Text S5). Function calculates time differences between values in seconds, thus infra-second units must be included in *TS* object if data frequency is > 1 Hz. No duplicates are allowed.
- Only supply pitch (*p*) if user wants radial distance modulated according to pitch (cf. E27 - main text).
- No missing data (NA's) for; *TS*, *h*, *v*, *elv*, *p*, *TS*, *ME*, *m*, *c* variables. The variables *ch* and *cs* may have NA's but observations are carried forward and thus at

least the first row/element must contain values (though this can also be supplied as a single value input – analogous to m and c values)

- User can select a different *dist.step* value (default = 1) to change the stepping interval when computing distance between VPs (within the '*method = distance*' method of VP under-sampling and VP distance moved summary outputs)
- Data from only one animal should be dead-reckoned at a time

The 3-D distance and speed proxies are output using variants of the *disty(method = Hav.SLD)* function which is posited and fully annotated within the subsection of *Gundog.Tracks()* termed; '#2) Prepare '*disty*' (distance) and '*beary*' (bearing) functions for VPC and/or summary variables'.

See *Gundog.Tracks.R* file for annotated function. Note more information detailing input and output is given at beginning and end of the .R file. See Fig. S6. 1 for an indication of processing times (on a MSI GP72 7RD Leopard laptop with intel core i7 processor). Notably, system time seems appropriate to dead-reckon weeks-months long datasets at reasonable speeds (e.g., a few mins), though only when dead-reckoning at lower frequencies (e.g., 1 Hz).

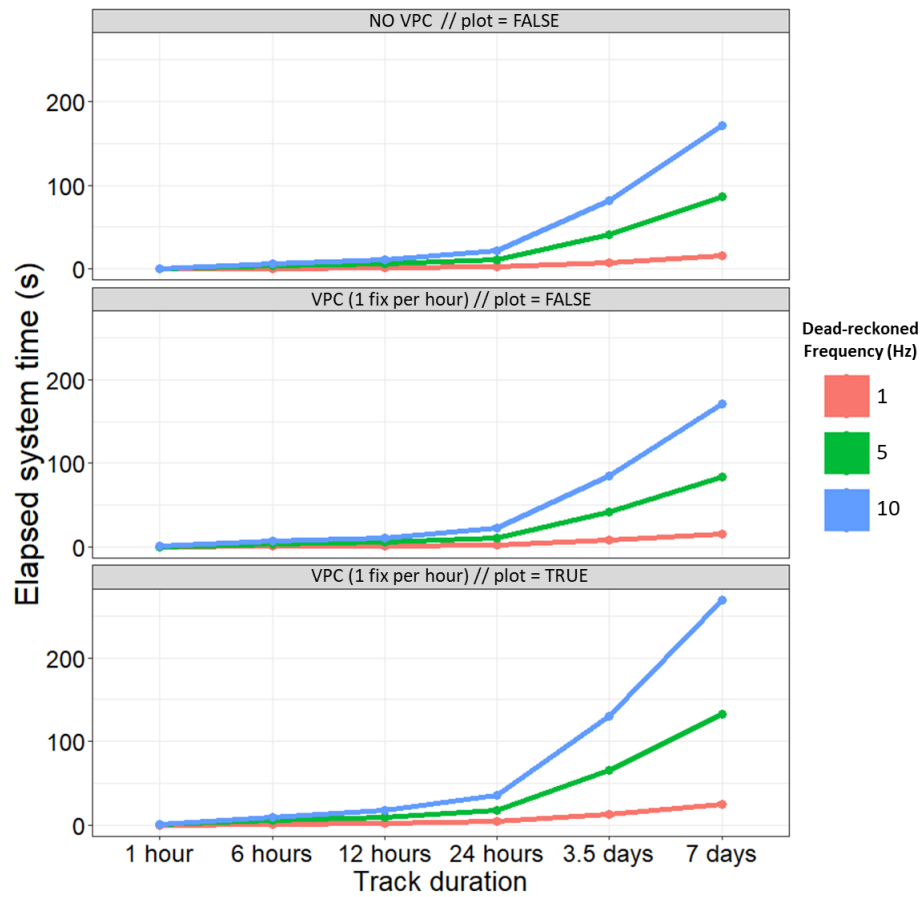


Figure S6. S1. Elapsed system time (s) to execute Gundog.Tracks according to the duration of data acquisition, frequency (Hz) of motion-sensor derived speed and heading estimates and user defined inputs (plot = TRUE vs FALSE and whether VPC occurred). Note that the biggest increase in computation time is the frequency of initial data input. The biggest source of system time is the for-loops used when dead-reckoning, plotting the tracks and computing the summary metrics (e.g., distance, speed etc.) at the end. This is why there is not much difference in computation speed when carrying out the method and degree of VPC as opposed to when not (VPC rate was chosen as 1 fix per hour here). This analysis was carried out on a MSI GP72 7RD Leopard laptop with intel core i7 processor. Whilst various changes in other user-defined inputs may modulate processing speeds somewhat, DR frequency and executing the summary plots are the main modulators.

References

- Aphalo, P.J. (2018) Ggpmisc: Miscellaneous Extensions to 'Ggplot2'. *R package version 0.3*, **3**.
- Cheng, G. (2011) How to Convert 3-Axis Directions and Swap XY Axis of Accelerometer Data within Android™ Driver. *FreeScale, Document Number AN4317*.
- Fortin, D., Beyer, H.L., Boyce, M.S., Smith, D.W., Duchesne, T. & Mao, J.S. (2005) Wolves influence elk movements: behavior shapes a trophic cascade in Yellowstone National Park. *Ecology*, **86**, 1320-1330.
- Grolemund, G. & Wickham, H. (2011) Dates and times made easy with lubridate. *Journal of Statistical Software*, **40**, 1-25.
- Pedley, M. (2013) Tilt sensing using a three-axis accelerometer. *Freescale semiconductor. Application Note 2461*, **1**, 1–22.
- Sakamoto, K.Q., Sato, K., Ishizuka, M., Watanuki, Y., Takahashi, A., Daunt, F. & Wanless, S. (2009) Can Ethograms Be Automatically Generated Using Body Acceleration Data from Free-Ranging Birds? *PLOS ONE*, **4**, e5379.
- Vitali, A. (2016) Ellipsoid or sphere fitting for sensor calibration, Dt0059. *ST Microelectronics, Design Tip*.
- Wilson, R.P. (1997) A method for restraining penguins. *Marine Ornithology*, **25**, 72-73.
- Wilson, R.P., Rose, K.A., Gunner, R., Holton, M., Marks, N., Bennett, N.C., Bell, S., Twining, J., Hesketh, J. & Duarte, C.M. (2020) Forces experienced by instrumented animals depend on lifestyle. *bioRxiv*.
- Wilson, R.P., Scolaro, J.A., Grémillet, D., Kierspel, M.A.M., Laurenti, S., Upton, J., Gallelli, H., Quintana, F., Frere, E., Müller, G., Straten, M.T. & Zimmer, I. (2005) How do Magellanic Penguins cope with variability in their access to prey? *Ecological Monographs*, **75**, 379-401.
- Wilson, R.P., Shepard, E. & Liebsch, N. (2008) Prying into the intimate details of animal lives: use of a daily diary on animals. *Endangered Species Research*, **4**, 123-137.
- Wilson, R.P., Shepard, E.L., Laich, A.G., Frere, E. & Quintana, F. (2010) Pedalling downhill and freewheeling up; a penguin perspective on foraging. *Aquatic Biology*, **8**, 193-202.
- Winer (2017) Simple and Effective Magnetometer Calibration. *GitHub repository* (ed. G. repository).

Chapter 6: Supplementary Information

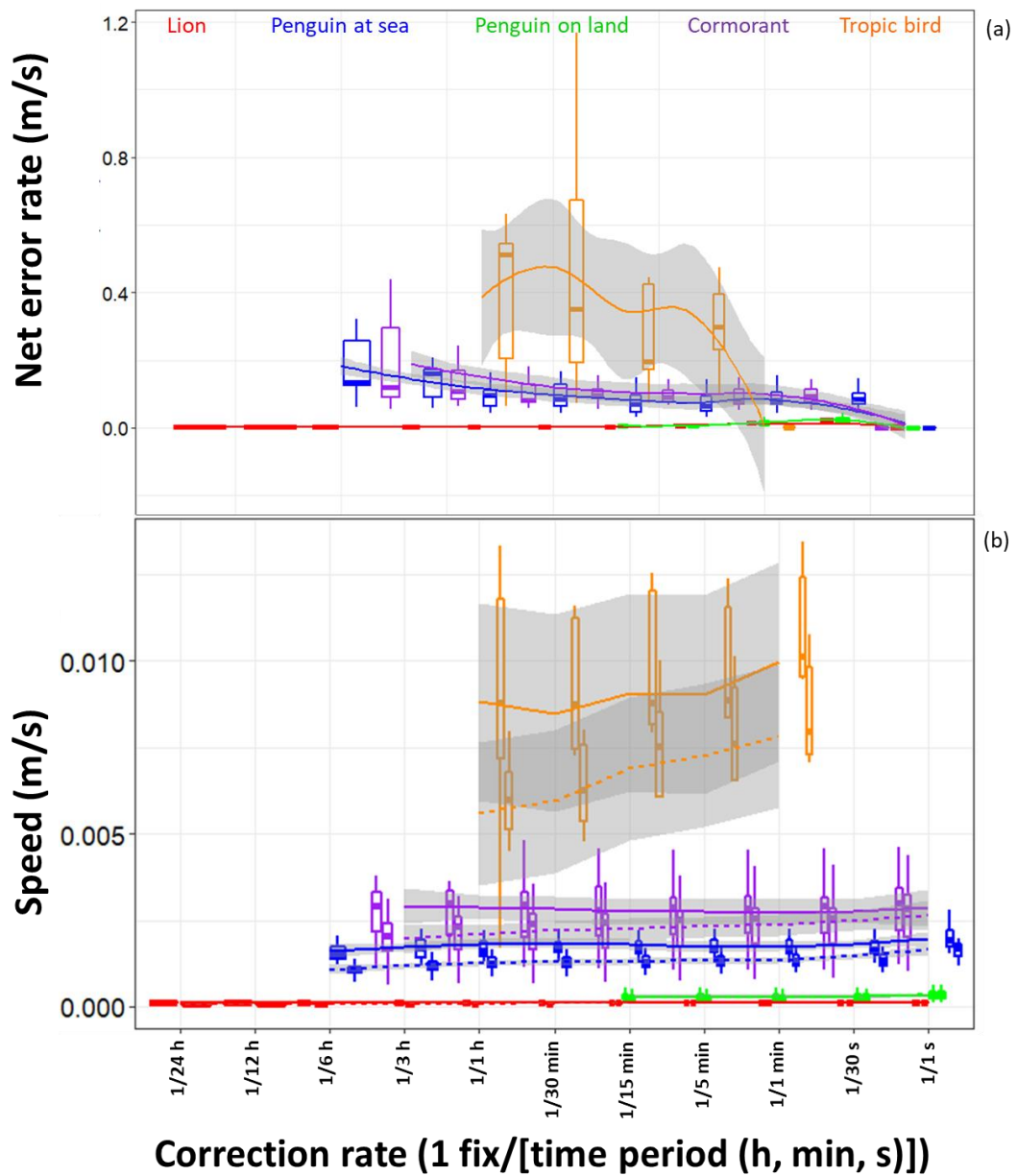


Figure S1. Boxplots demonstrating the magnitude of net error (top panel) and distance moved (bottom panel), per VP correction rate and animal. Net error (a) is standardised according to the mean time between corrections (m/s) and distance moved (b) is standardised according to trip duration, respectively, per individual and VP correction rate to provide an approximate rate in m/s. Mean values were aggregated per individual and VP correction rate. Boxes encompass the 25-75 % interquartile range and horizontal bars denote the median value with 'loess' smooth line (grey shading show the standard error and Whiskers extend to 1.5 * Interquartile range). Note net error drops to zero when the VP correction rate equates with GPS recording

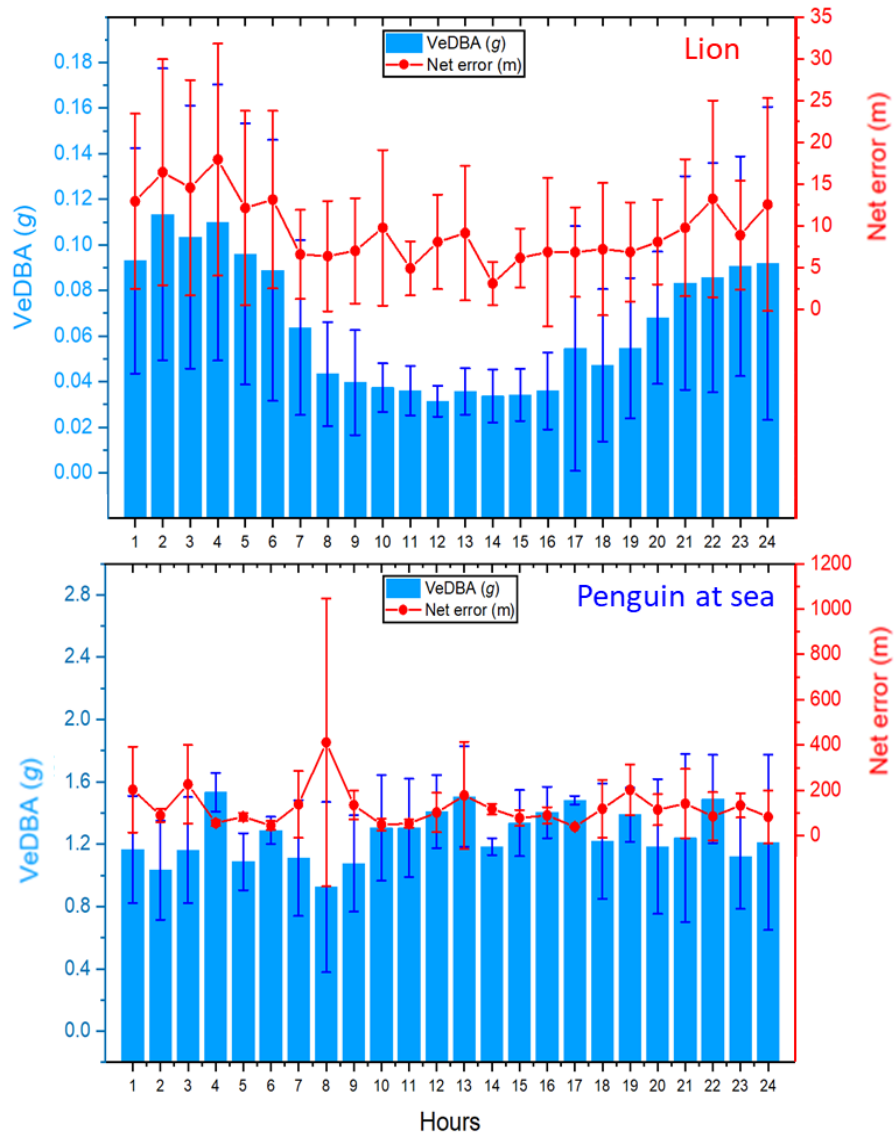


Figure S2. Mean (± 1 SD) VeDBA (column/bar) and net error (line & symbol) per hour over the duration of three individual lion (top panel) and three penguin (bottom panel) dead-reckoned tracks, VP corrected approx. every 30 minutes. Note that the net error of lions was generally slightly higher and more variable during the night when they were more active, although net error was still appreciable during the day when lions were predominantly resting, principally due to VP error. On the other hand, penguins demonstrated no clear circadian trends in activity or net error, in part due to the high variability between the dynamism of recorded movement and speed of travel (e.g., due to preening behaviour during 'surface rest' periods and the constant presence of external current flow vectors), as well as the variability in the time of day (and duration) of rests. Note that the y-scales differ between

Text S1. Dead-reckoning formulae

1) Compute the distance coefficient (q)

$$q = \frac{s \cdot TD}{R}$$

where s refers to speed (units in m/s), TD refers to the time difference between values (units in s) and R is the approximate radius of the earth ($R = 6378137$ m).

2) Derive longitude and latitude coordinates

$$\begin{aligned} Lat_i &= asin(\sin(Lat_0) \cdot \cos(q) + \cos(Lat_0) \cdot \sin(q) \cdot \cos(h)) \\ Lon_i &= Lon_0 + atan2((\sin(h) \cdot \sin(q) \cdot \cos(Lat_0)), (\cos(q) - \sin(Lat_0) \cdot \sin(Lat_i))) \end{aligned}$$

where Lat_0 , Lat_i and Lon_0 , Lon_i are the previous and present latitude and longitude coordinates, respectively, h is the heading and q is the distance coefficient. Note that the coordinates and heading must be supplied in radians.

3) VP-correct procedure

The distance (d) and bearing (b) between consecutive VPs (used to correct) and consecutive (time-matched) dead-reckoned positions are calculated based on the below formulae;

$$\begin{aligned} d &= 2 \cdot R \\ &\cdot \sin^{-1} \left(\sqrt{\sin^2 \left(\frac{Lat_i - Lat_0}{2} \right) + \cos(Lat_0) \cdot \cos(Lat_i) \cdot \sin^2 \left(\frac{Lon_i - Lon_0}{2} \right)} \right) \end{aligned}$$

where R is the Earth's radius and the output d is in metres. Note this is the Haversine formula.

$$b = atan2 \left(\frac{\sin(Lon_i - Lon_0) \cdot \cos(Lat_i), \cos(Lat_0) \cdot \sin(Lat_i - Lat_0) \cdot \cos(Lat_i) \cdot \cos(Lon_i - Lon_0)}{\pi} \right)$$

where b output is in the scale -180° to $+180^\circ$. To convert b to the conventional 0° to 360° scale, 360 should be added to values < 0 .

The distance between each VP is divided by the distance between the corresponding dead-reckoned positions to provide a distance correction factor;

$$Distance_{corr.factor} = \frac{Distance_{VP}}{Distance_{DR}}$$

The bearing (or rather, heading) between each VP is subtracted by the bearing between the corresponding dead-reckoned positions to provide a heading correction factor;

$$Heading_{corr.factor} = Bearing_{VP} - Bearing_{DR}$$

To maintain a maximum potential difference of 180° in either circular direction, 360 should be added to values < -180 and 360 subtracted from values > 180. All intermediate q values are multiplied by the distance correction factor and the heading correction factor is added to all intermediate h values (ensuring that h values are in degrees). To ensure circular range remains between 0° and 360° for the updated h values, 360 should be subtracted from values > 360 and added to values < 0. Note, these corrections for ensuring that circular range is maintained (adding/subtracting 360°) when deriving and applying the heading correction factors are not required if both b and h are in radians. It can be more intuitive though to have units in degrees when assessing biases in motion sensor derived heading offset/error, relative to VPs. After the correction factors have been applied, step 2 is repeated. Occasionally more than one iteration of the formulae (steps 2 and 3) is required for the path to adhere 'exactly' with the ground-truthed locations.

Chapter 7: Supplementary Information

Text S1 – Identifying walking and pausing periods in DDMT software using the LoCoD method.

The Boolean time-based decision-tree template LoCoD (Wilson *et al.* 2018) expressions used for depicting walking behaviour, outlined below, were modelled around the DD recording at 40 Hz and GPS recording at 1 Hz. During walking periods, the DD was positioned approximately perpendicular relative to the ground. That is, the x-axis was pointing towards the sky, the y-axis towards the penguin's left, parallel to the ground and the z-axis pointing away from the penguin's back, parallel to the ground. The ordered sequence to describe the LoCoD for discerning individual stride cycles is given in Table S1. 1 - see Wilson *et al.* (2018) for the conceptual and practical methodology for implementing this method, including definition of the terms presented in Table. S1. 1.

In essence, the patterns of sway acceleration, represented by the y-axis is a valuable descriptor of walking (used here, see Fig. S1. 1) due to penguins possessing a 'waddling' gait with each step inducing appreciable 'side-to-side' motion which is chiefly picked up by this channel (given the device orientation used). The pattern of its differential was used since derivatives are less affected by discrepancies between tag placement and angle of the substrate travelled over, producing a more consistent pattern of oscillations over time. Put simply, the template initiates a search when the rate change of sway acceleration (smoothed to some degree, *cf.* Table. S1. 1) exceeds zero, after which the differential must go above a given threshold above zero ('right step'), followed by a given threshold below zero ('left step') before returning to zero whilst remaining within a VeDBA remit and registering GPS-derived speed greater than zero. This sequence of events denotes a single stride cycle.

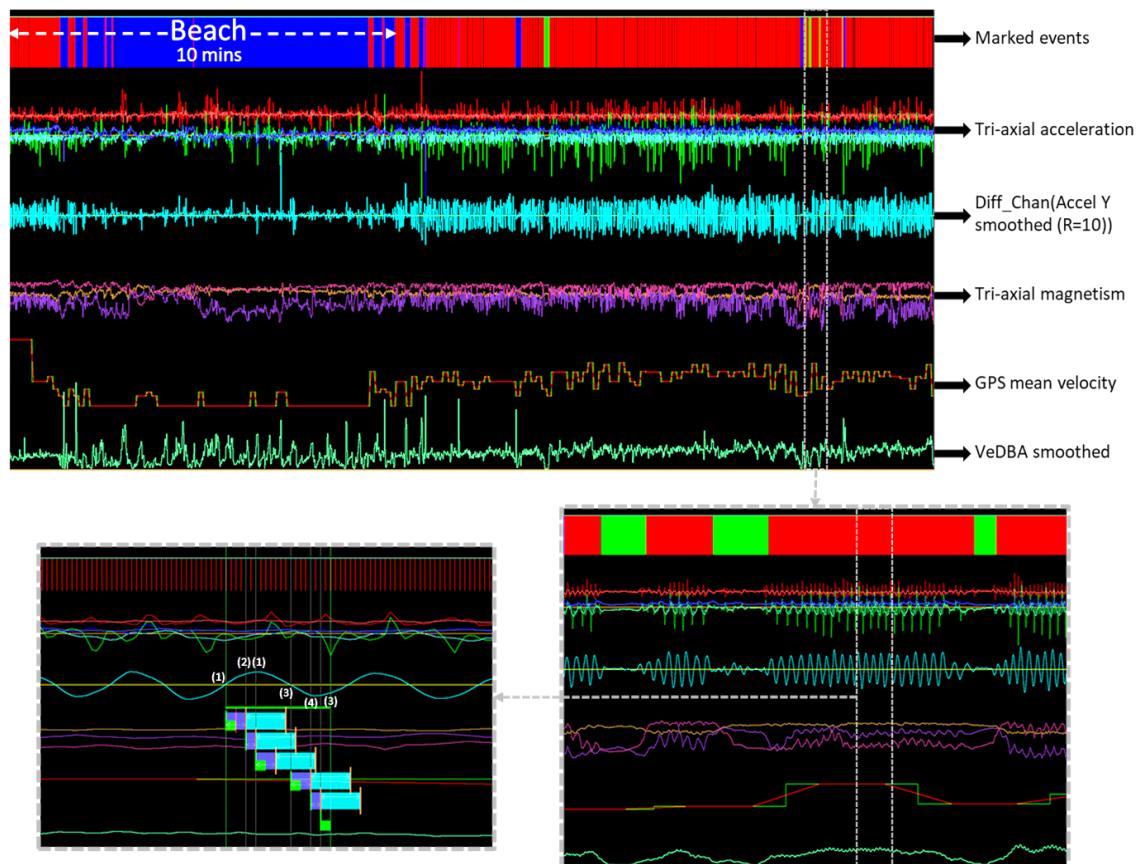


Figure S1. 1. Values from the motion sensor and GPS unit outputs (represented as 2D waveforms versus time), including marked events based on the LoCoD rules of behaviour classification [red = walking periods (discerned from the LoCoD rules), blue = pauses either > 10 s duration or associated with appreciable DBA, likely attributed to preening, green = pauses \leq 10 s duration with minimal DBA (pause type manually discerned between the bouts of marked walking)]. A 45 s section of the top panel is magnified [bottom right] to demonstrate the oscillating pattern that the differential of y-axis acceleration has during walking. This is zoomed in further [bottom left] to demonstrate the Boolean time-based search template as given by allocated LoCoD sequence, with each behavioural element having to have passed its associated rules within given time frames of one another as stated in Table. S1.

The expressions documented below yielded > 99 % precision and an overall recall of ~94 % pre-manual corrections. Most false negatives occurred at the start of incoming trips because GPS-derived speed was used in the expressions (to aid in reducing the number of false positives attributed to preening that also invoke oscillating sway movements similar to walking), and occasionally fixes (and thus GPS speed) would not occur for some time after submersion in water, preventing this template search to be valid at such times.

Table S1. 1. Acceleration- and GPS-based metrics used for identifying single stride cycles (one left step and one right step) per ('flexible') unit time. Prior to setting out the rules of each element the following pre-processing was performed:

- 1) *VeDBA smoothed* → Acceleration smoothing for $VeDBA = 80$ events. *VeDBA smoothed* over 40 events (1 s).
- 2) *GPS mean velocity* → In DDMT GPS-derived speed (termed 'velocity' in DDMT) is computed by dividing the Haversine distance (computed according to the stepping range between fixes) by the time period between values. The stepping range was set at 5 (every 5th fix) and the smoothing was set at 200 events (5 s).
- 3) *Diff_Chan (Accel Y smoothed)* → Acceleration smoothing of raw values = 10 events (0.25 s). The rolling differential of the smoothed y-axis values was then calculated using a stepping range of 10 events (0.25 s) and the resultant values were smoothed over 10 events (0.25 s).

Time-based sequence	Element	Rules	Events valid for (presence)	% time valid for	Range to begin next search	Flexibility after	Extend to?
1	1	i) <i>VeDBA smoothed</i> > 0.1 ii) <i>VeDBA smoothed</i> < 0.8 iii) <i>GPS mean velocity</i> > 0 iv) <i>Diff_Chan(Accel Y smoothed (R=10))</i> > 0	3	100	4	8	✓ (1 before)
2	2	i) <i>VeDBA smoothed</i> > 0.1 ii) <i>VeDBA smoothed</i> < 0.8 iii) <i>GPS mean velocity</i> > 0 iv) <i>Diff_Chan(Accel Y smoothed (R=10))</i> > 0.15	1	100	2	8	✓ (1 before)
3	1	i) <i>VeDBA smoothed</i> > 0.1 ii) <i>VeDBA smoothed</i> < 0.8 iii) <i>GPS mean velocity</i> > 0 iv) <i>Diff_Chan(Accel Y smoothed (R=10))</i> > 0	3	100	4	8	✓ (1 before)
4	3	i) <i>VeDBA smoothed</i> > 0.1 ii) <i>VeDBA smoothed</i> < 0.8 iii) <i>GPS mean velocity</i> > 0 iv) <i>Diff_Chan(Accel Y smoothed (R=10))</i> < 0	3	100	4	8	✓ (1 before)
5	4	i) <i>VeDBA smoothed</i> > 0.1 ii) <i>VeDBA smoothed</i> < 0.8 iii) <i>GPS mean velocity</i> > 0 iv) <i>Diff_Chan(Accel Y smoothed (R=10))</i> < -0.15	2	100	2	8	✓ (1 before)
6	3	i) <i>VeDBA smoothed</i> > 0.1 ii) <i>VeDBA smoothed</i> < 0.8 iii) <i>GPS mean velocity</i> > 0 iv) <i>Diff_Chan(Accel Y smoothed (R=10))</i> < 0	3	100	4	1	

(1) Set up behavioral elements (rules)

The exact form of the base elements within DDMT's 'behaviour builder' take the expressions:

- (1) If ((Ch (VeDBA smoothed) > 0.1) AND (Ch (VeDBA smoothed) < 0.8) AND (Ch (GPS mean velocity) > 0) AND (Diff_Chan (Accel Y smoothed (R=10)) > 0)) then mark events
- (2) If ((Ch (VeDBA smoothed) > 0.1) AND (Ch (VeDBA smoothed) < 0.8) AND (Ch (GPS mean velocity) > 0) AND (Diff_Chan (Accel Y smoothed (R=10)) > 0.15)) then mark events
- (3) If ((Ch (VeDBA smoothed) > 0.1) AND (Ch (VeDBA smoothed) < 0.8) AND (Ch (GPS mean velocity) > 0) AND (Diff_Chan (Accel Y smoothed (R=10)) < 0)) then mark events
- (4) If ((Ch (VeDBA smoothed) > 0.1) AND (Ch (VeDBA smoothed) < 0.8) AND (Ch (GPS mean velocity) > 0) AND (Diff_Chan (Accel Y smoothed (R=10)) > 0.15)) then mark events

(2) Add them in a time-based sequence

These are added into the time series tab, taking the expressions:

- (1) Element (1): present for 3 events, %time 100, with next expression starting from range 4, flexibility after of 8 and ETNE 1 before
- (2) Element (2): present for 1 events, %time 100, with next expression starting from range 2, flexibility after of 8 and ETNE 1 before
- (3) Element (1): present for 3 events, %time 100, with next expression starting from range 4, flexibility after of 8 and ETNE 1 before
- (4) Element (3): present for 3 events, %time 100, with next expression starting from range 4, flexibility after of 8 and ETNE 1 before
- (5) Element (4): present for 1 events, %time 100, with next expression starting from range 2, flexibility after of 8 and ETNE 1 before
- (6) Element (3): present for 3 events, %time 100, with next expression starting from range 4, flexibility after of 1

(3) Manual evaluation

Within DDMT, the user can easily add/remove marked events manually. Any required corrections were performed prior to merging stride cycles occurring ≤ 40 events (1 s) from one another.

Text S2 – Descriptors of movement

Heading (derived using the tilt-compensated compass method (*cf.* Pedley 2012)) and VeDBA values were smoothed using a rolling window of 40 events (1 s) (circular mean used for heading - (*cf.* Pewsey, Neuhäuser & Ruxton 2013). This was to reduce variations manifest by the ‘waddle’ of the stride cycle. For each trip, uncorrected dead-reckoned tracks were compared alongside the (1 Hz) GPS equivalent to determine the m-coefficient multiplier within the DBA~speed derivation process [$speed = (VeDBA \cdot m) + c$] (*cf.* Bidder *et al.* 2012). The m-value that produced the greatest adherence in terms of proportion scaling relative to GPS path (pre-drift correction) was selected. Dead-reckoned paths were only advanced at times of elucidated travelling movement (*cf.* Fig. S1. 1). Dead reckoned tracks were GPS corrected approximately every 50 m moved (as estimated between GPS locations using the Haversine formula (Harja & Sarno 2018); Fig. S2. 1). This was determined a reasonable compromise between correcting for inevitable error accumulation and not relying too frequently on GPS, given they themselves are not perfect with fix accuracy, precision and success rate (*cf.* Chapter 4). Following the GPS-correction procedure, the Haversine distance between (every) GPS and corresponding (time-matched) dead-reckoned positions from pooled trajectories was estimated at 1.5 ± 1.0 m [$\bar{x} \pm 1$ SD].

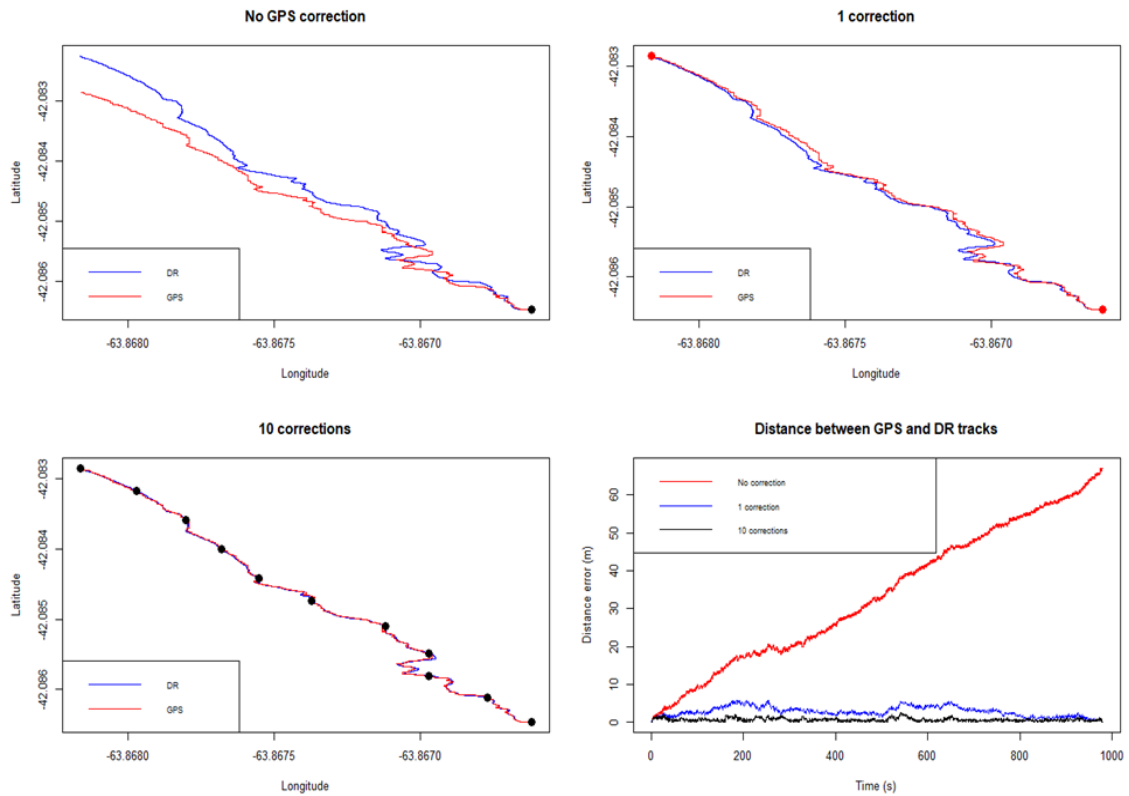


Figure S2. 1. A 30-minute, ~525 m dead-reckoned track, pre-VP correction [top left], VP corrected once [top right] and corrected 10 times (approx. every 50 m distance moved), with the resultant net error estimates relative to GPS for each track plotted as a function of time [bottom right].

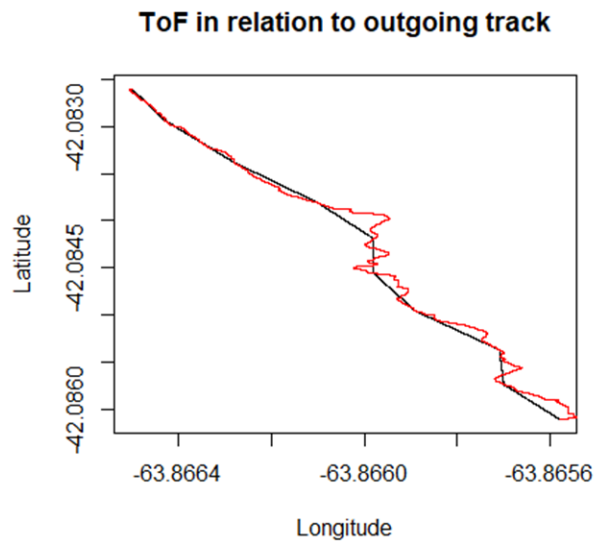


Figure S2. 2. Example of the matchstick approach of deriving the ToF (red) based on linearly interpolating between GPS fixes used in the drift correcting procedure.

Text S3 – Model parameters

Table S3. 1. Significant terms of two linear mixed effect models (LMM) with distance travelled as the response variable, and an extension of the generalised liner mixed effect model (GLM - glmmadmb), with tortuosity as the response variable.

Predictors	LMM: Distance travelled			LMM: Distance travelled (Incoming)			glmmadmb: Tortuosity (family="beta")		
	Estimate	CI	p	Estimate	CI	p	Estimate	CI	p
(Intercept)	477.96	388.80 – 567.13	<0.001	455.9	262.06 – 649.73	<0.001	-2.51	-2.95 – -2.07	<0.001
DR.Cumulative.Distance							0	0.00 – 0.00	0.015
Status: Outgoing	Reference			Reference			Reference		
Status: Incoming ToF	89.52	18.94 – 160.10	0.017	0.72	0.58 – 0.86	<0.001	0.22	-0.12 – 0.56	0.199
Random Effects									
σ ²	13970.12			4040.94			1.35		
τ ₀₀	30620.16 _{ID}			36452.98 _{Nest}			0.00 _{ID}		
ICC				0.9			0		
N	24 _{ID}			4 _{Nest}			24 _{ID}		
Observations	48			48			48		
Marginal R ² / Conditional R ²	0.128 / NA			0.200 / 0.920			0.043 / 0.043		
AIC	642.763			561.596			-120.721		

Table S3. 2. GAM output, displaying the effect size of vegetation density (c), and the additive effect of the proportion of distance travelled (Prop.of.distance) smoothed and in interaction with the factor of status (incoming vs outgoing - for pause duration (s)).

Predictors	Pause duration (family = Inverse gaussian, link="log")		
	Estimates	CI	p
(Intercept)	2.16	1.95 – 2.37	<0.001
c: None	Reference		
c: Medium	0.18	-0.05 – 0.41	0.116
c: High	0.05	-0.21 – 0.31	0.714
	EDF	F	
s(Prop.of.distance):StatusOutgoing	1.0	0.31	<0.001
s(Prop.of.distance):StatusIncoming	1.92	1.42	0.242
Status: Outgoing	Reference		0.518
Status: Incoming	-0.01	-0.16 – 0.14	0.918

Table S3.3. GAM output, displaying the effect size of vegetation density (c), and the additive effect of the proportion of distance travelled (Prop.of.distance) smoothed and in interaction with the factor of status (incoming vs outgoing) - for Tortuosity (0-1), travelling speed (m/s) and number of 'significant' turns [per 10 m].

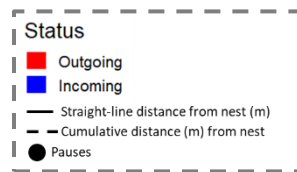
<i>Predictors</i>	Tortuosity [10 m] (family = Beta regression, link="logit")			Speed (family = Inverse gaussian, link="log")			Turns (family = zero inflated Poisson, link="identity")		
	<i>Estimate</i>	<i>CI</i>	<i>p</i>	<i>Estimate</i>	<i>CI</i>	<i>p</i>	<i>Estimate</i>	<i>CI</i>	<i>p</i>
(Intercept)	-2.34	-2.45 - 2.23	<0.001	-0.89	-0.92 – 0.86	<0.001	0.17	0.09 – 0.25	<0.001
c: None	<i>Reference</i>			<i>Reference</i>			<i>Reference</i>		
c: Medium	0.23	0.11 – 0.35	<0.001	-0.01	-0.04 – 0.02	0.560	0.23	0.15 – 0.32	<0.001
c: High	0.47	0.35 – 0.60	<0.001	-0.01	-0.04 – 0.03	0.660	0.41	0.31 – 0.50	<0.001
	EDF	Chi.sq		EDF	F		EDF	Chi.sq	
s(Prop.of.distance):StatusOutgoing	3.09	40.38	0.028	2.86	5.85	<0.001	3.48	47.70	0.001
s(Prop.of.distance):StatusIncoming	3.06	10.66	<0.001	8.69	12.09	0.027	4.12	20.49	0.014
Status: Outgoing	<i>Reference</i>			<i>Reference</i>			<i>Reference</i>		
Status: Incoming	0.20	0.13 – 0.27	0.01	0.04	0.02 – 0.06	<0.001	-0.00	-0.05 – 0.05	0.953

Table S3. 4. GAM output, displaying the effect size of vegetation density (c), and the additive effect of the proportion of distance travelled (Prop.of.distance) smoothed and in interaction with the factor of status (incoming vs outgoing) - for number of pauses [per 10 m], 'significant' turn extent (°) and extent of turn following a pause (°).

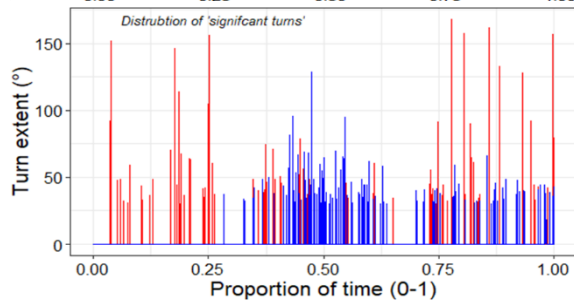
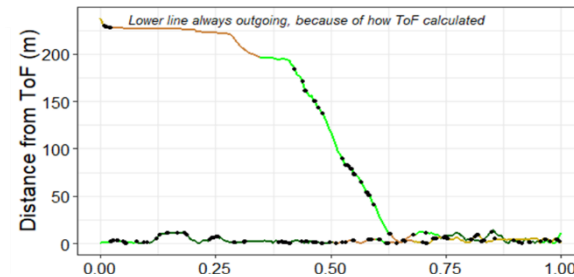
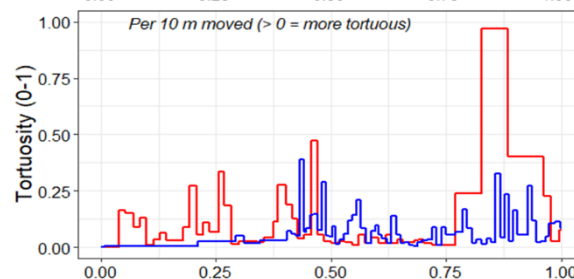
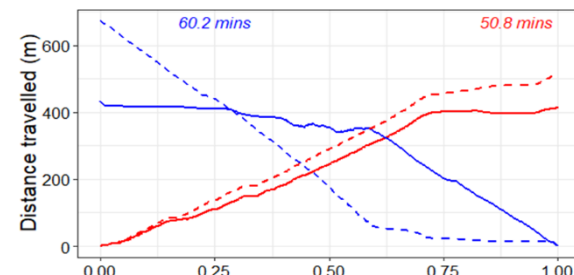
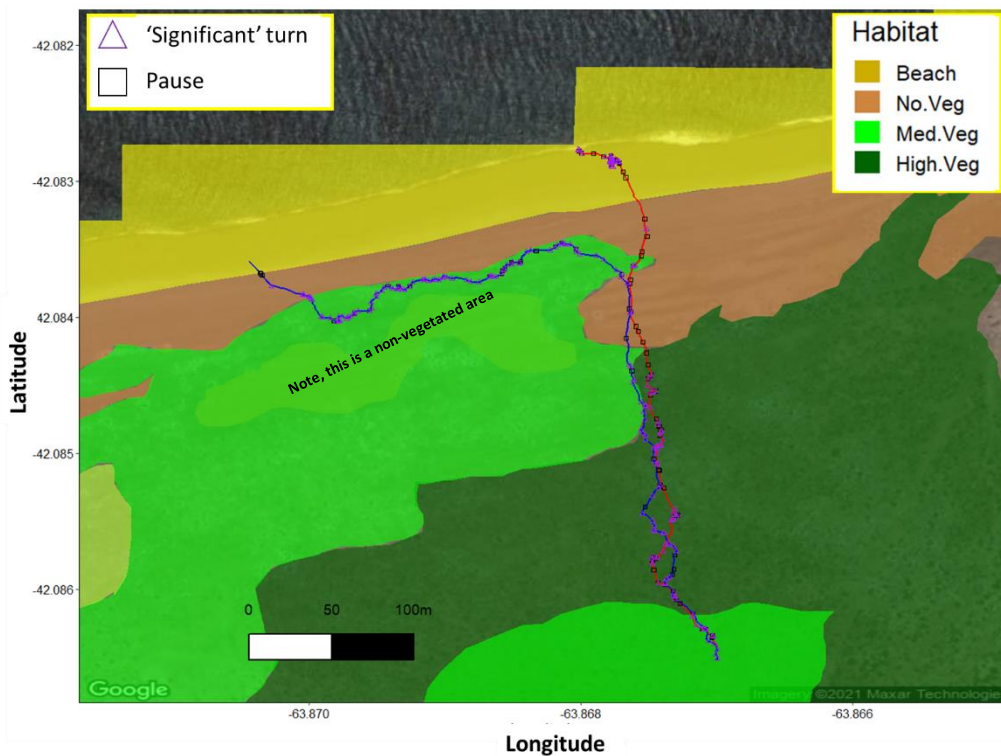
Predictors	Pauses (family = zero inflated Poisson, link="identity")			Turn extent (family = Gamma, link="log")			Turn extent following a pause (family = Gamma, link="log")		
	Log-Mean	CI	p	Estimates	CI	p	Estimates	CI	p
(Intercept)	-0.13	-0.36 – 0.09	0.245	3.73	3.67 – 3.78	<0.001	2.78	2.54 – 3.02	<0.001
c: None	Reference			Reference			Reference		
c: Medium	0.16	-0.09 – 0.41	0.197	0.07	0.01 – 0.13	0.017	0.09	-0.17 – 0.36	0.484
c: High	0.08	-0.21 – 0.36	0.597	0.12	0.05 – 0.18	<0.001	0.45	0.15 – 0.75	0.004
	EDF	Chi.sq		EDF	F		EDF	F	
s(Prop.of.distance):StatusOutgoing	3.68	37.89	<0.001	6.46	3.41	0.031	4.75	0.21	0.352
s(Prop.of.distance):StatusIncoming	4.59	47.24	<0.001	6.76	2.08	0.243	1.88	0.34	0.322
Status: Outgoing	Reference			Reference			Reference		
Status: Incoming	-0.56	-0.72 – 0.40	<0.001	-0.07	-0.11 – 0.04	<0.001	-0.01	-0.17 – 0.15	0.919

Text S4 – The case-studies

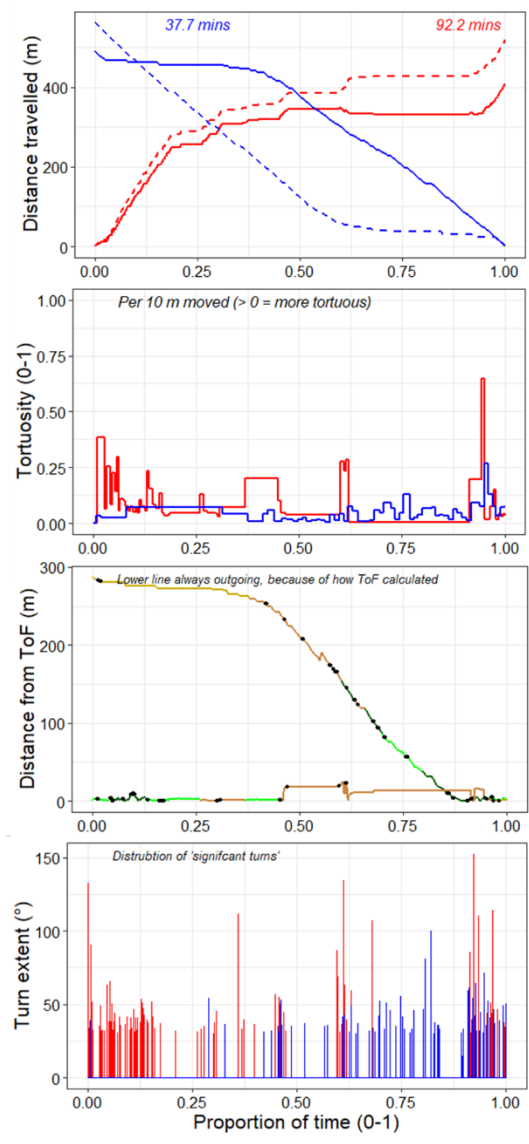
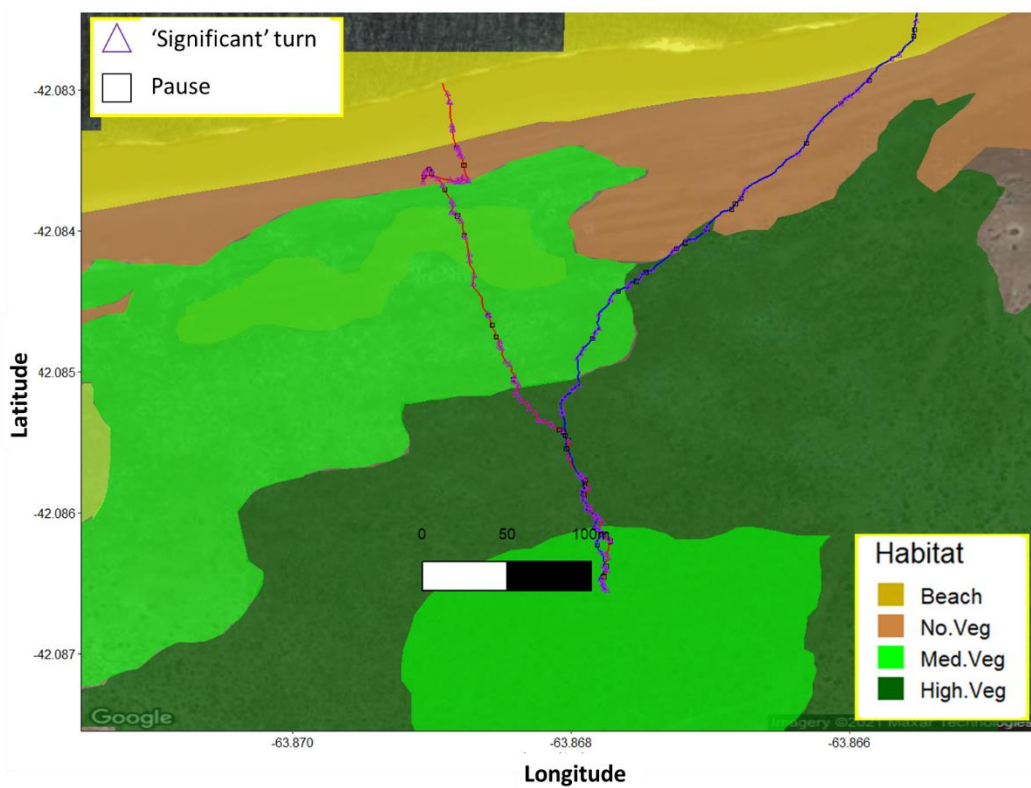
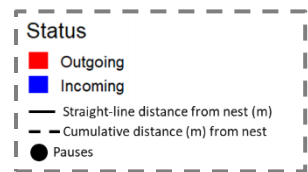
Note the metrics on the right are assessed as proportion of time (0-1) to demonstrate that many returning birds spend large periods of time at the beach prior to travelling back.



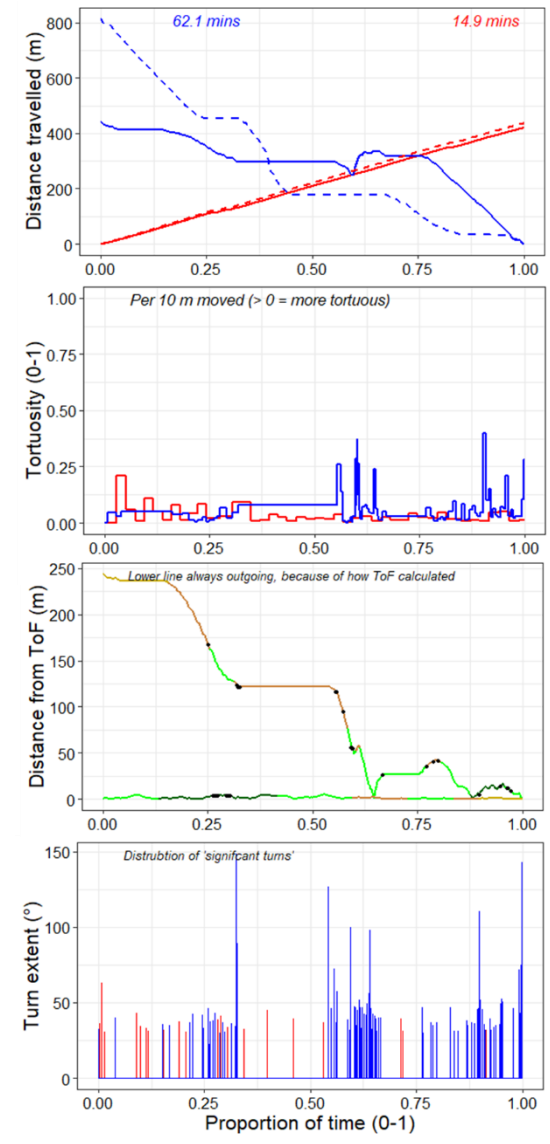
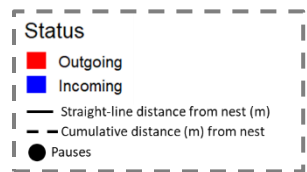
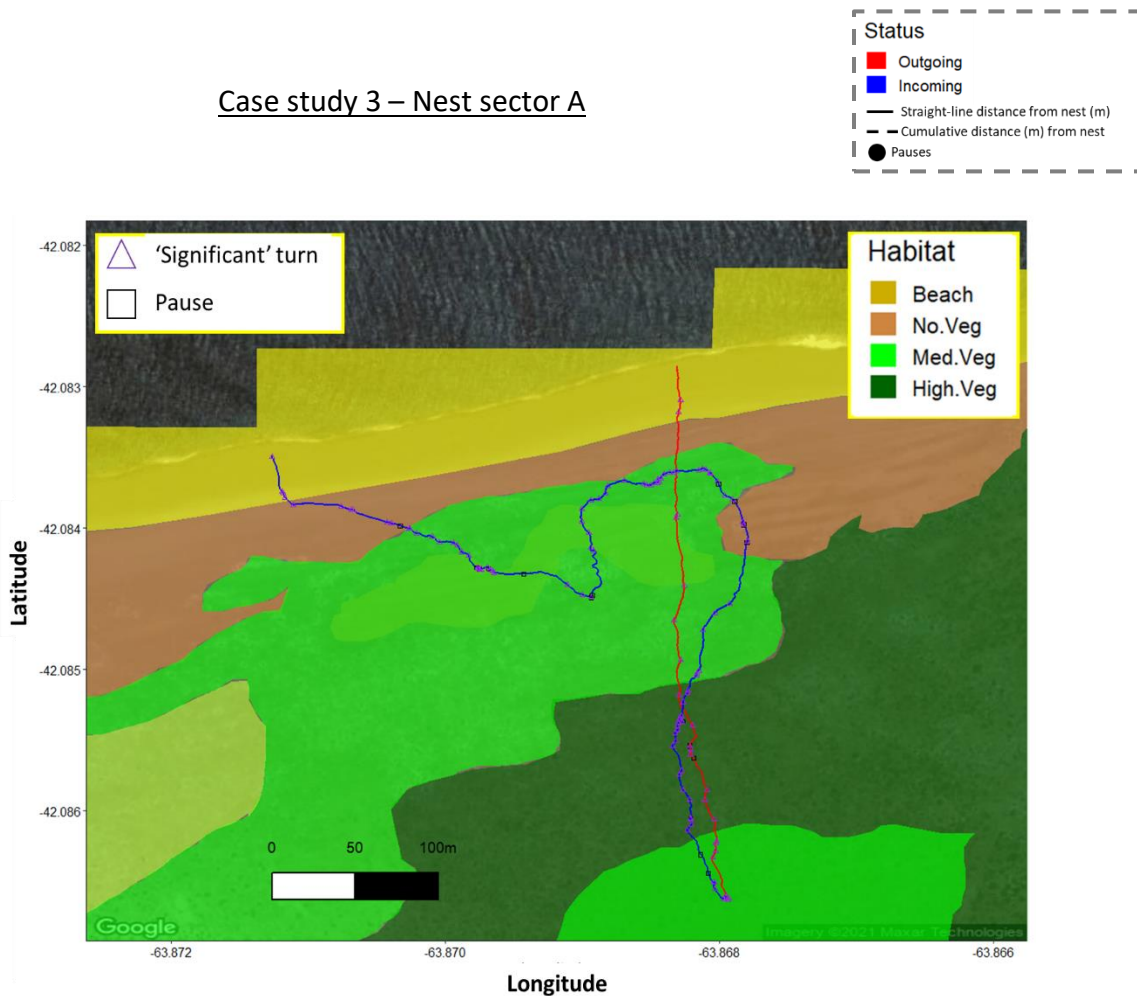
Case study 1 – Nest sector A



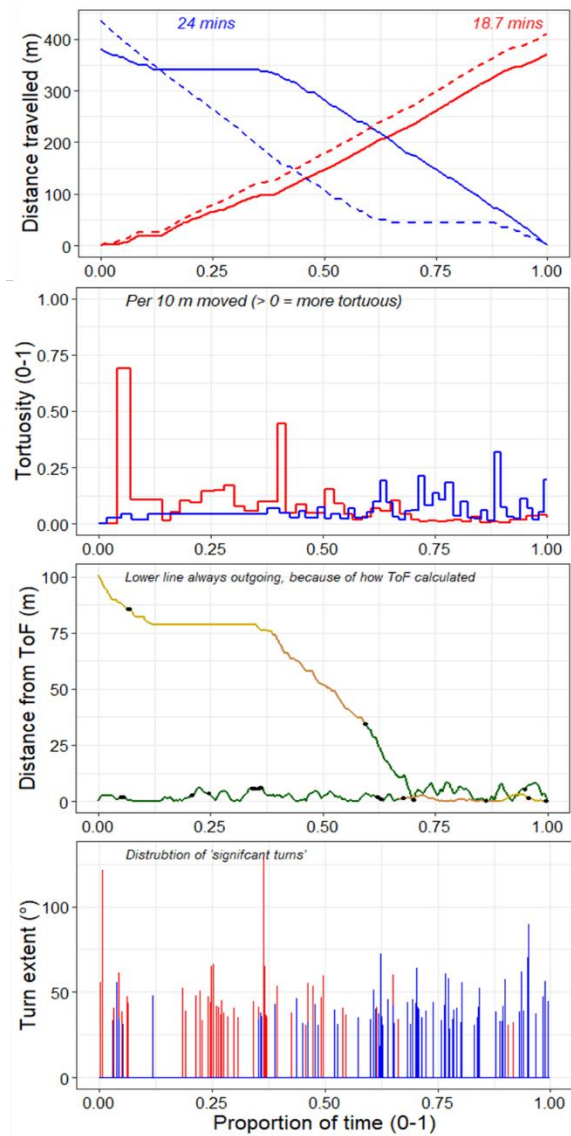
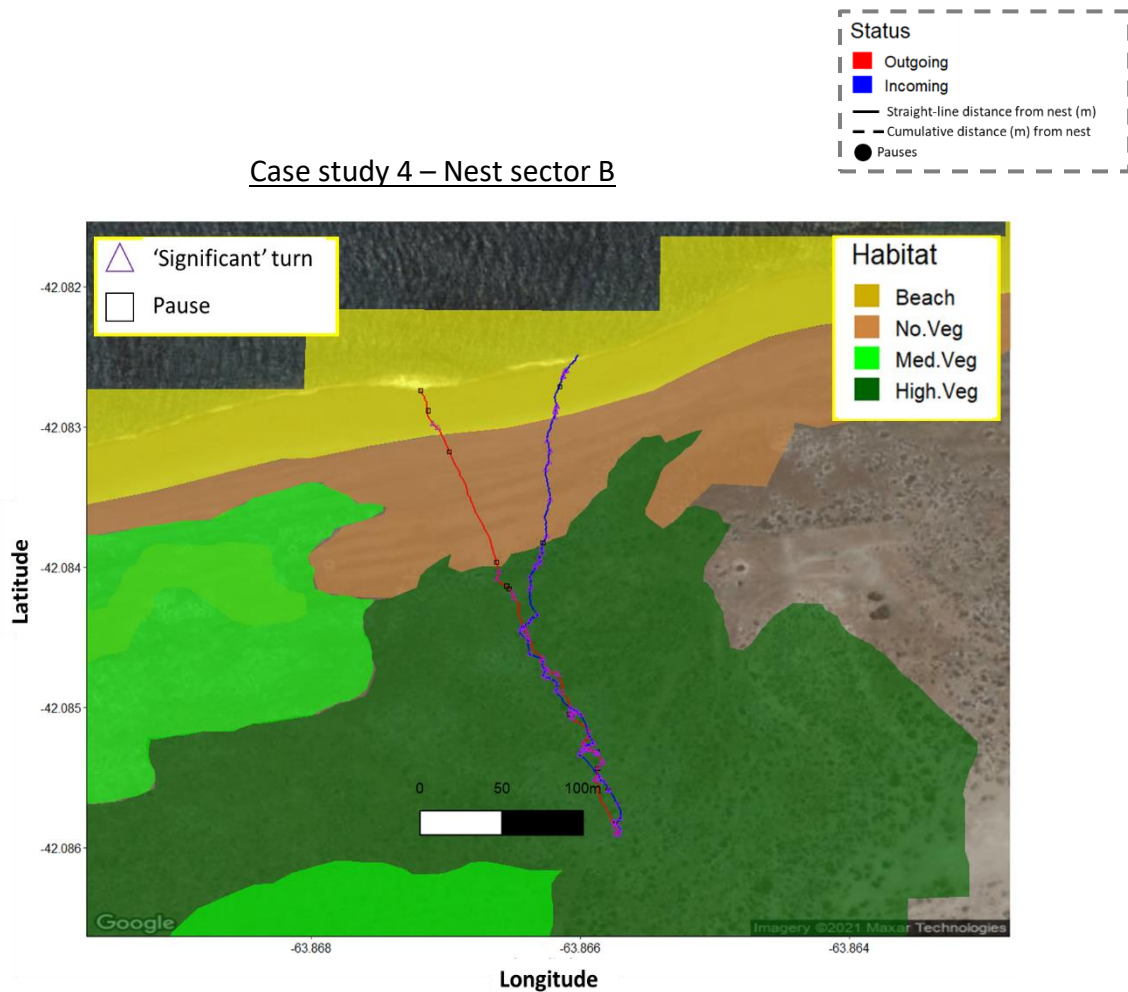
Case study 2 – Nest sector A



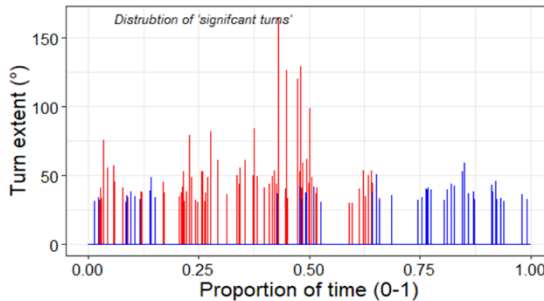
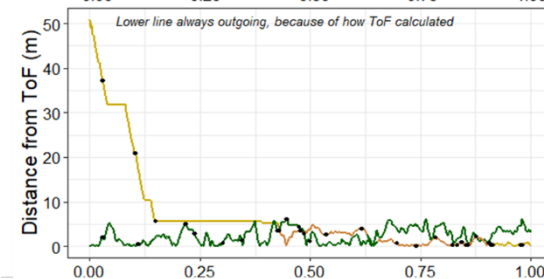
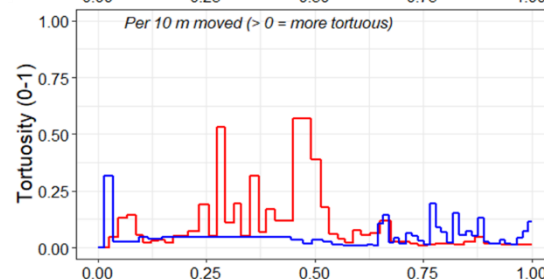
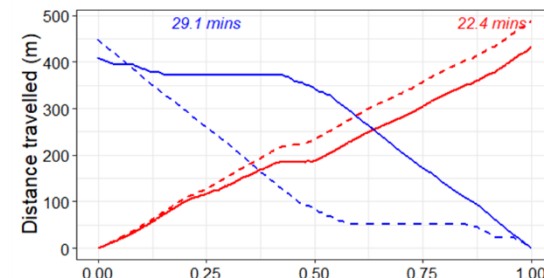
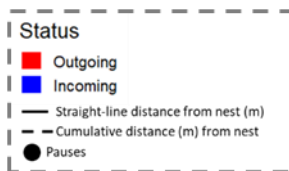
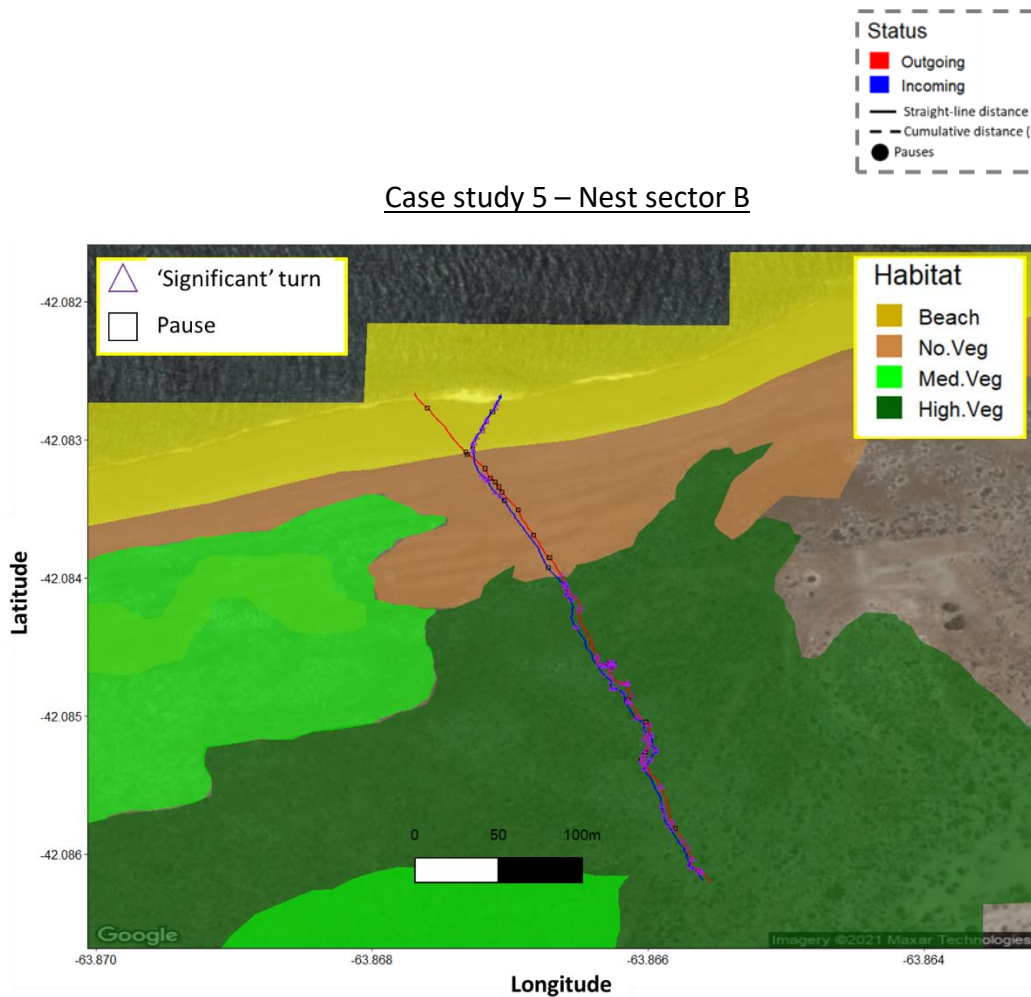
Case study 3 – Nest sector A



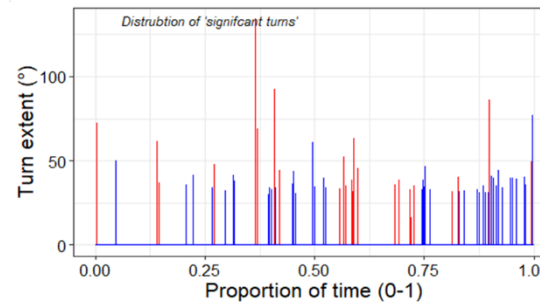
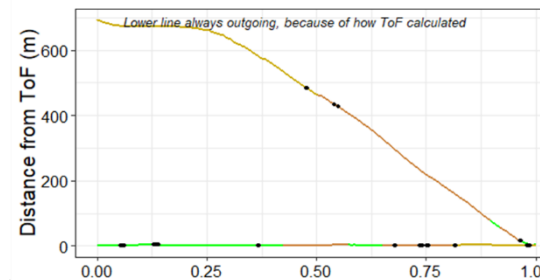
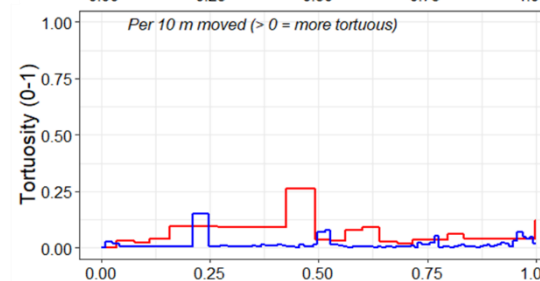
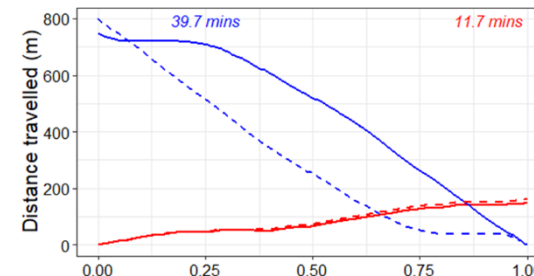
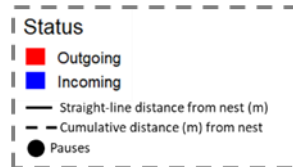
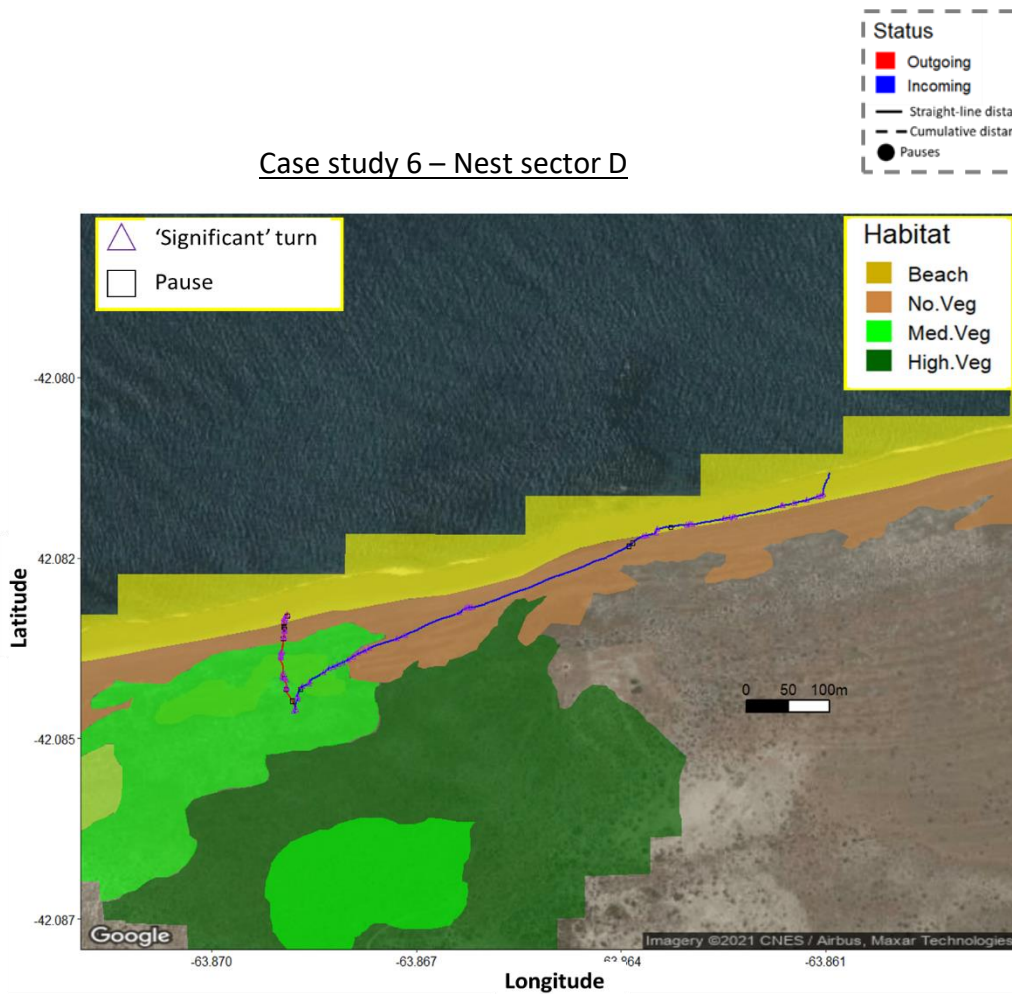
Case study 4 – Nest sector B



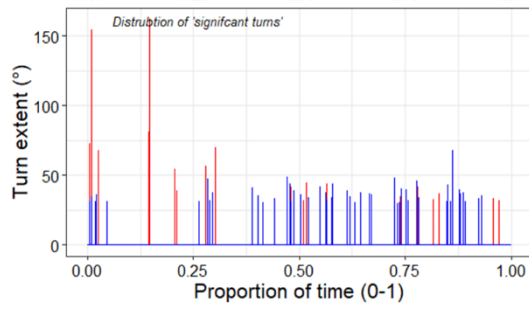
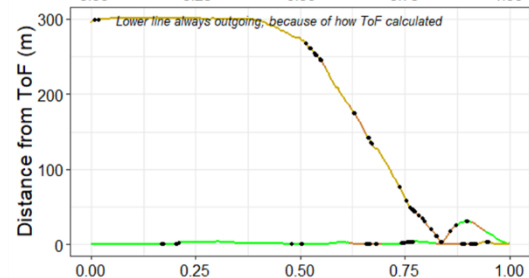
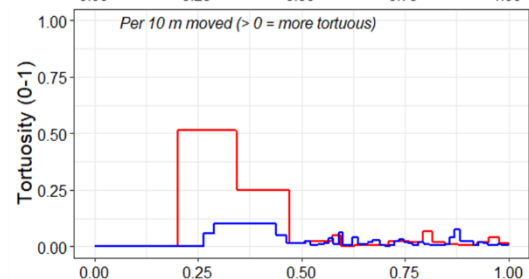
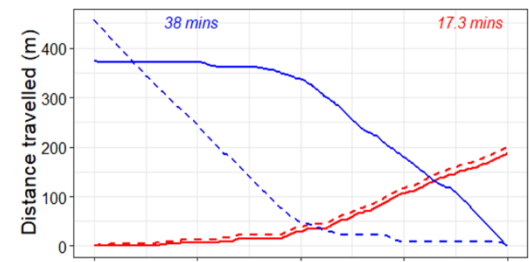
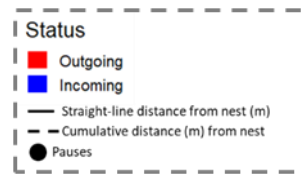
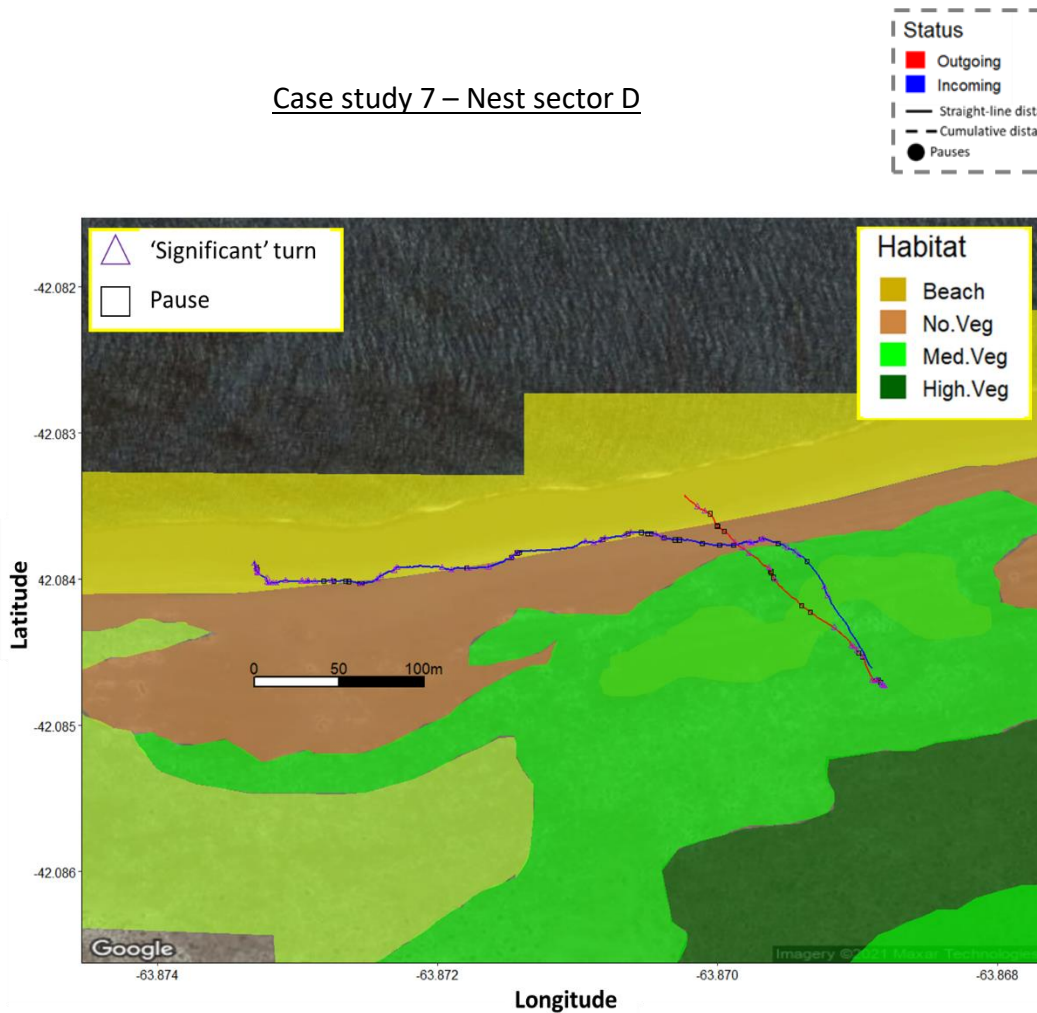
Case study 5 – Nest sector B



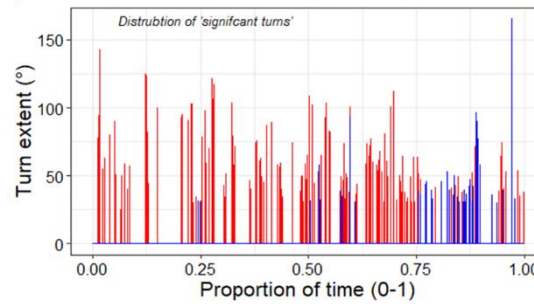
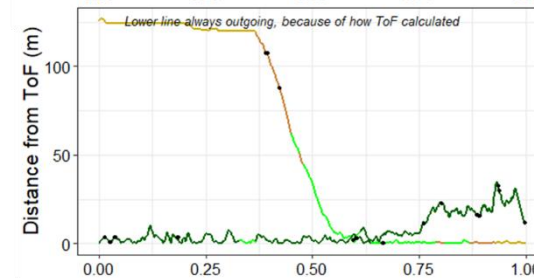
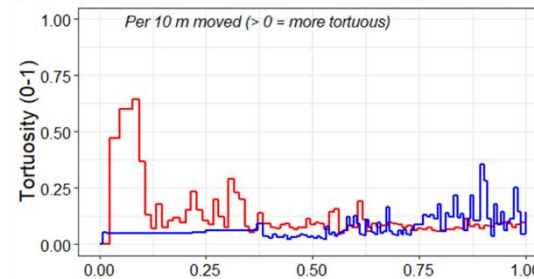
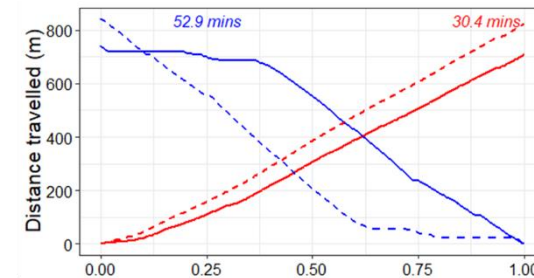
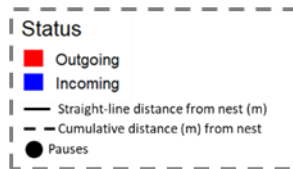
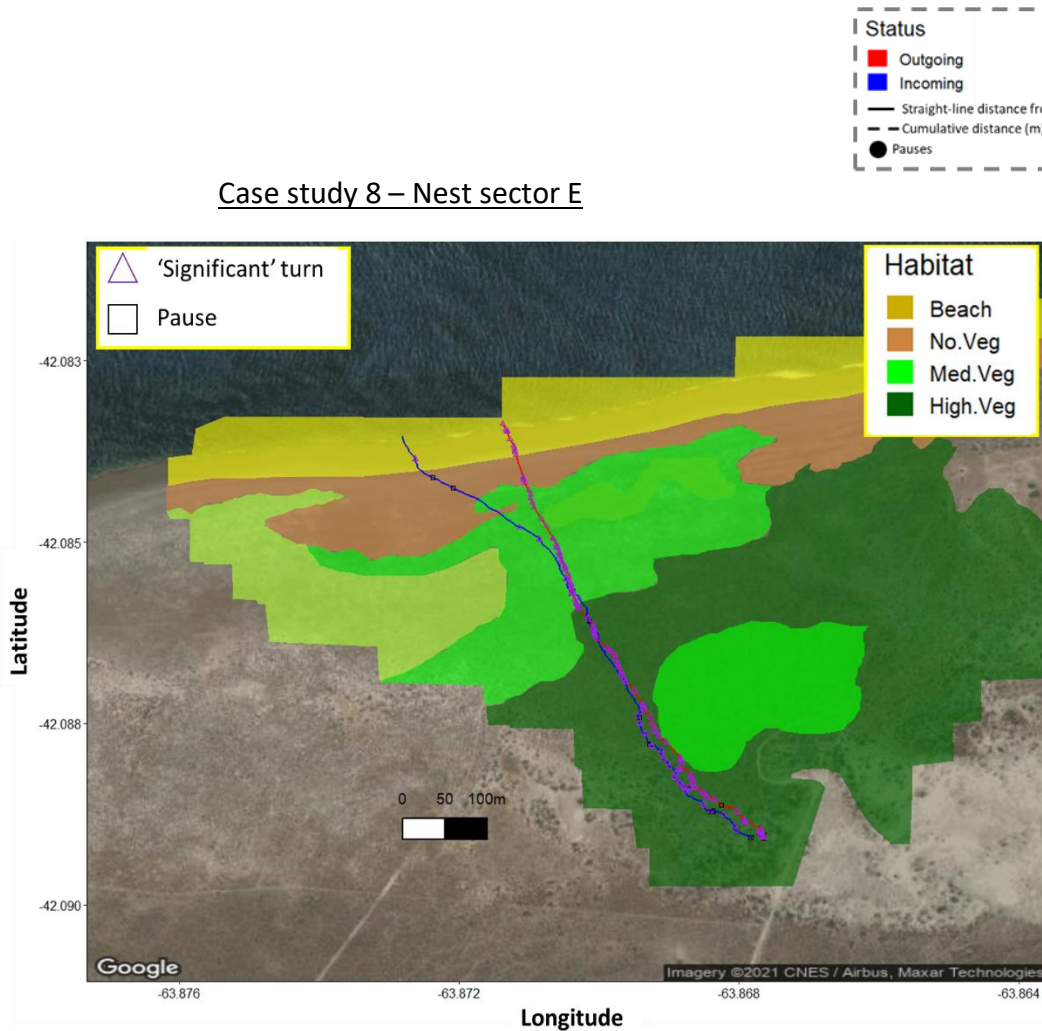
Case study 6 – Nest sector D



Case study 7 – Nest sector D



Case study 8 – Nest sector E



References

- Harja, Y.D. & Sarno, R. (2018) Determine the best option for nearest medical services using Google maps API, Haversine and TOPSIS algorithm. 2018 International Conference on Information and Communications Technology (ICOIACT), pp. 814-819.
- Pedley, M. (2012) eCompass-Build and Calibrate a Tilt-Compensating Electronic Compass. Circuit Cellar-The Magazine For Computer Applications, 1-6.
- Pewsey, A., Neuhäuser, M. & Ruxton, G.D. (2013) Circular Statistics in R. OUP Oxford.
- Wilson, R.P., Holton, M.D., di Virgilio, A., Williams, H., Shepard, E.L., Lambertucci, S., Quintana, F., Sala, J.E., Balaji, B. & Lee, E.S. (2018) Give the machine a hand: A Boolean time-based decision-tree template for rapidly finding animal behaviours in multisensor data.

Chapter 8: Supplementary Information

Text S1 – Additional results

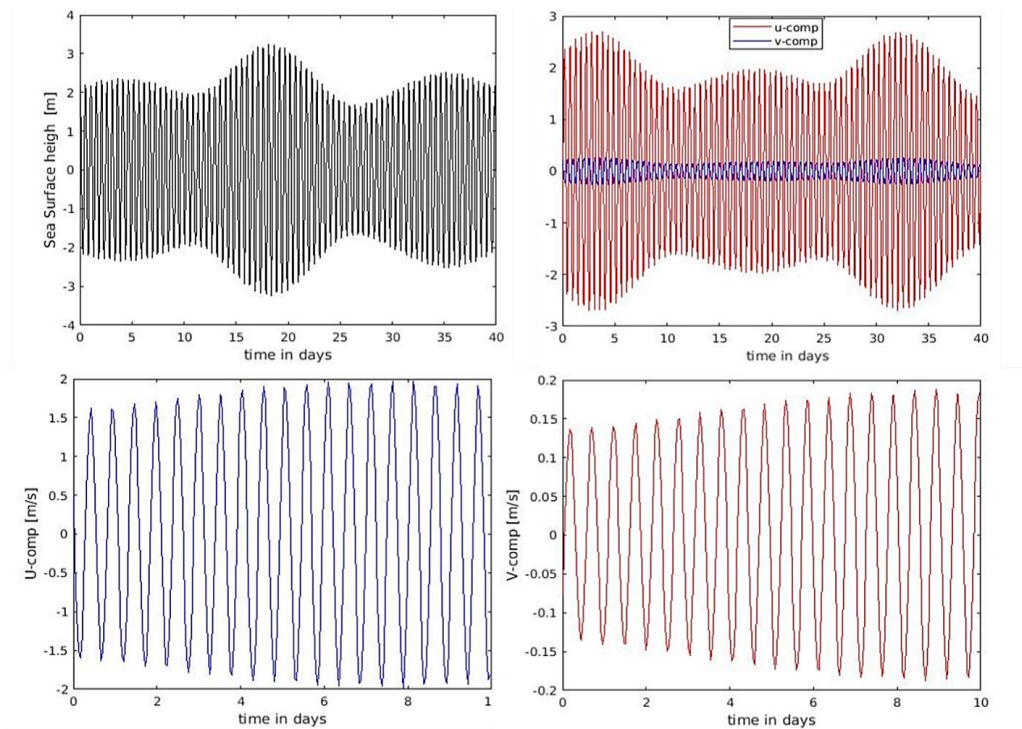


Figure S1. 1. Elevations and components (U and V) in a period of 40 days showing the variation of the region, tidal influence and dominated cross-currents (U component).

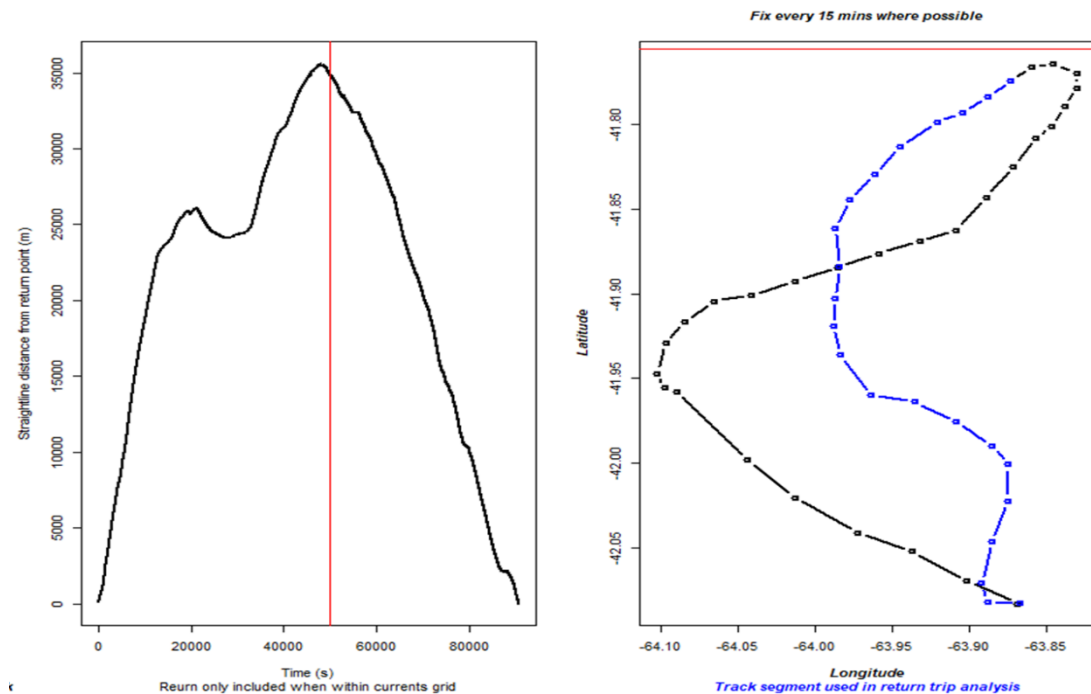


Figure S1.2. Determining the start of a penguins return journey. The red Vertical line in the left plot denotes the start of the return phase of a given penguins track, determined by selecting all data after the first GPS fix (1 fix every 15 min used; right plot) that occurred during the beginning of a continuous downward gradient of the shortest straight-line distance to the colony and was within the current model grid (horizontal red line). The blue section of track in the right plot denotes the section of track used for analysis.

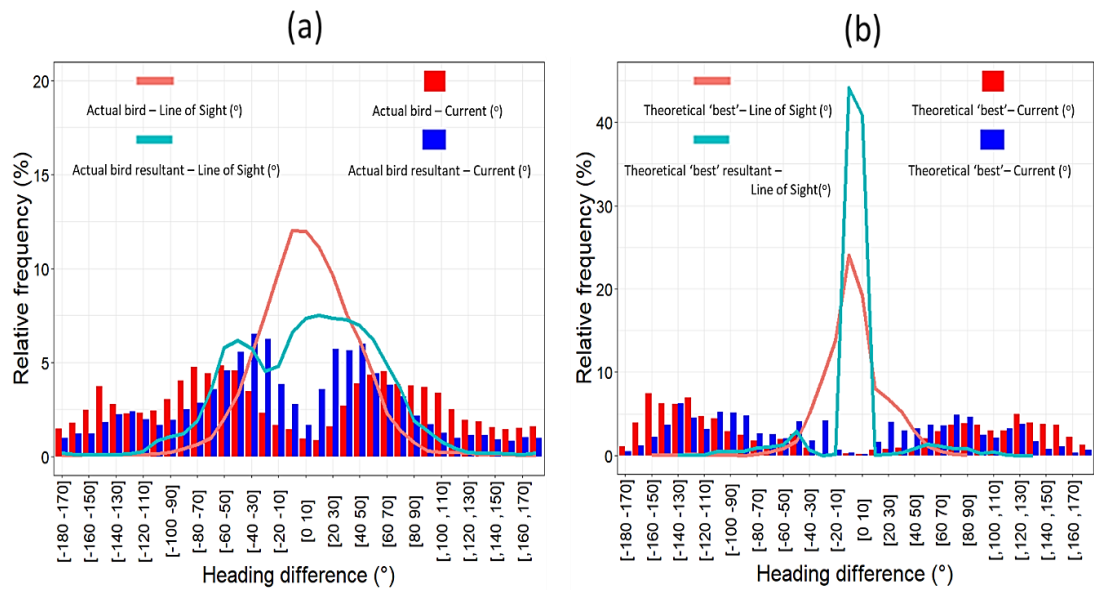


Figure S1. 3. Distributions of; (a) the actual bird heading and the Line of Sight heading difference, with respect to the actual bird heading and current heading difference and (b) the theoretical 'best' heading and Line of Sight heading difference with respect to the theoretical 'best' heading and current heading difference. The histogram bars represent the current heading difference, and the lines represent the Line of Sight heading difference within the bottom frequency plots (red = prior to current integration and blue = post current integration).

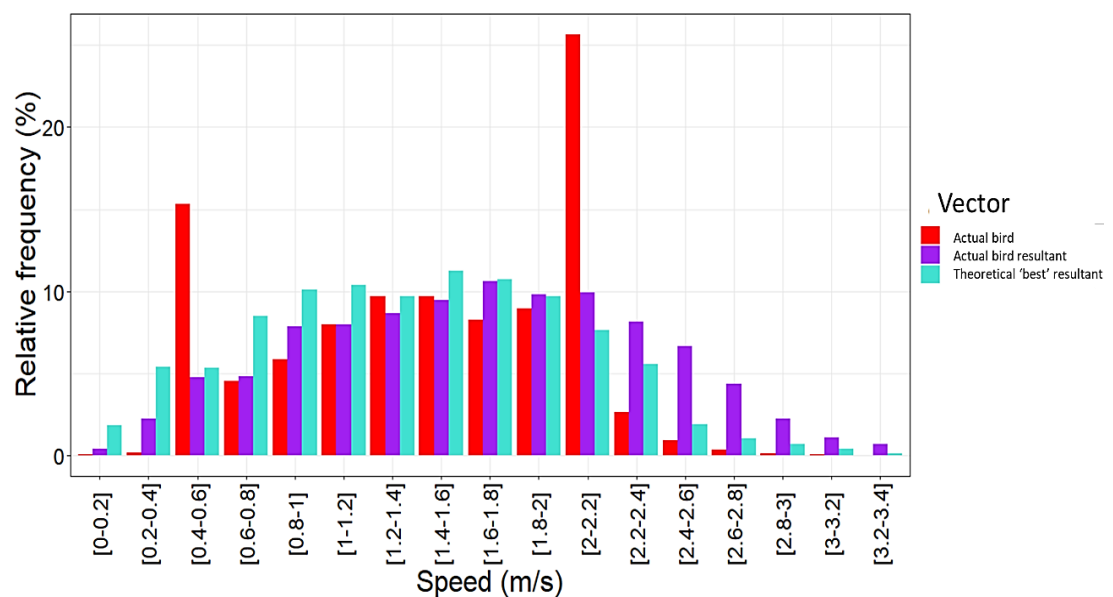


Figure S1. 4. Relative frequencies of both actual bird speed (prior (red) and post (purple) current integration) and the theoretical 'best' resultant (turquoise) during return trajectories. Notice the actual bird resultant registers tightest proportion of 'higher' speeds.

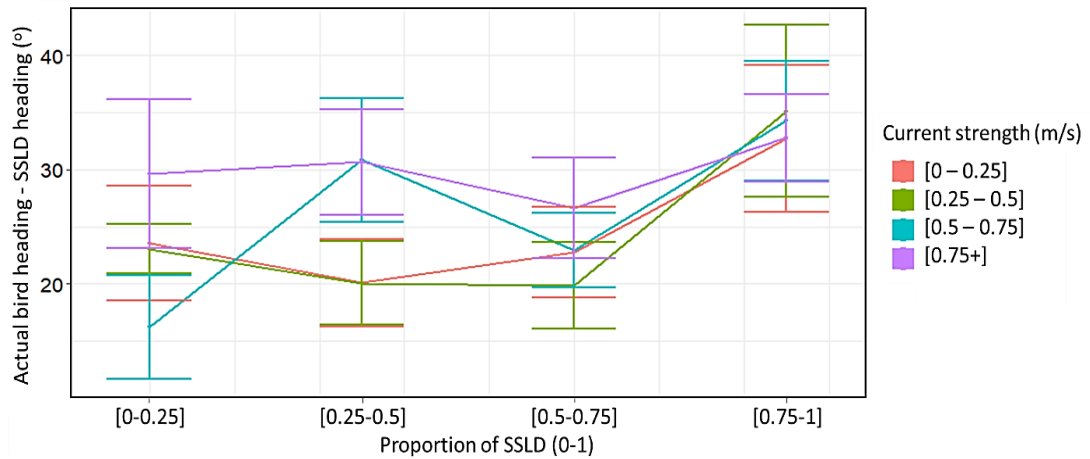


Figure S1. 5. Mean (± 1 SE) absolute difference between actual bird heading and 'line of sight' heading as a function of distance to the colony (divided into quarters with 0 = start of return trip and 1 = exit point onto the beach), grouped according to 4 current strength conditions. Error bars represent 1 SD either side of the mean. Note that, regardless of current strength, there appears no apparent trend to suggest the birds improve their homing ability the closer to the colony they get.

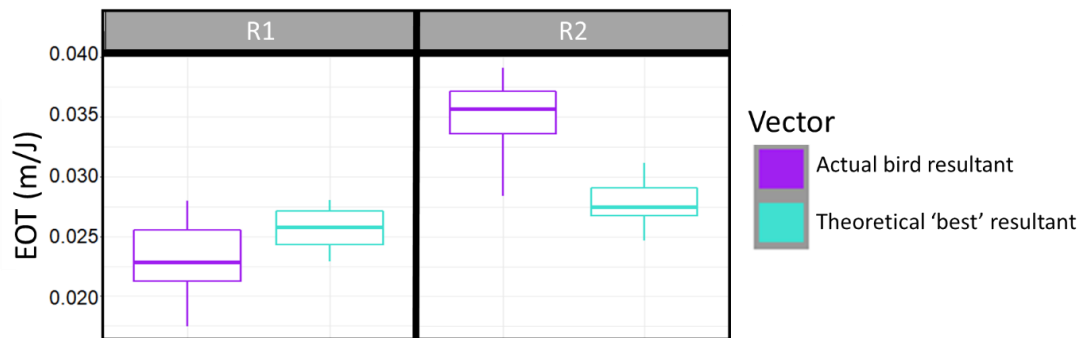


Figure S1. 6. Mean penguin ease of transport (EOT - in metres travelled per joule) for the actual bird resultant trajectory (purple) and the theoretical 'best' trajectory (turquoise). The boxplots are constructed from the grand mean of pooled values (per 0.01 epoch) per individual. Boxes denote the median and 25-75 % interquartile range. On average, the actual bird resultant R1 EOT is much higher than the theoretical 'best' resultant. In contrast, whilst similar, R2 theoretical 'best' resultant is highest.

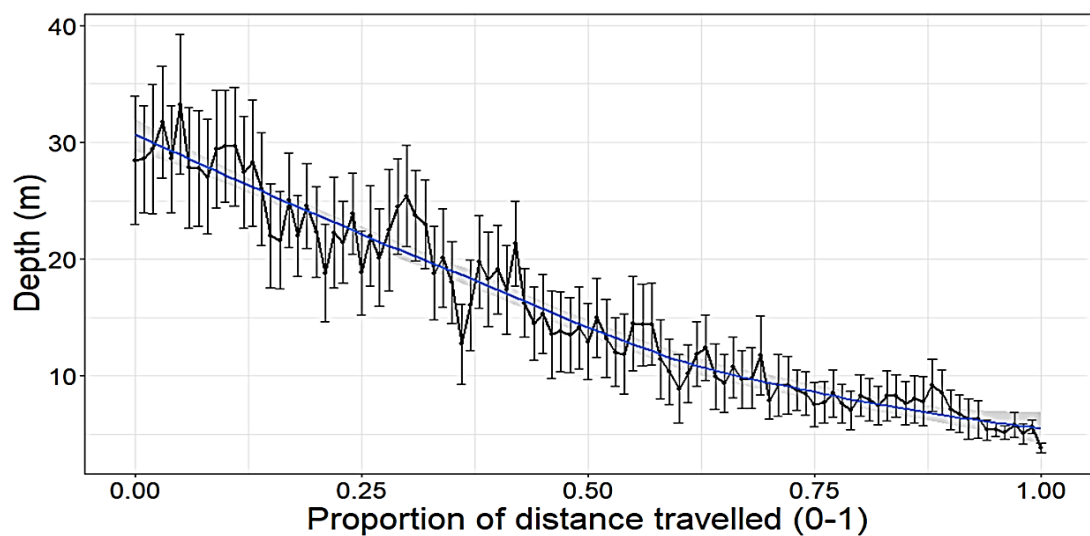


Figure S1. 7. Mean (± 1 SE) dive depth per 0.01 proportion of total distance travelled during return trajectories.

*Text S2 – Methods expanded**Accounting for Pressure drift*

In the case of depth, median pressure values were calculated when at/near the surface, governed by pressure < 10.4 m (a high upper limit of potential drift for these study animals at least (pressure recorded ≥ 10 m at surface)) and absolute values of rate change of depth ≤ 0.05 m/s (at surface differential typically did not fluctuate above this threshold - again, a high upper limit for this study species). Only median values from depicted surface periods ≥ 5 s were used. Trend Estimation with Asymmetric Least Squares (ALS; *cf.* Newey & Powell 1987) was then used on these values to depict the baseline of drift across time (*lambda*; smoothing parameter = 0.001, *p*; asymmetry parameter = 0.001, *eps*; numerical precision for convergence = $1e-8$ and *maxit*; max number of iterations = 50). This baseline was subtracted to raw depth values across time (resultant depth values < 0 m were made 0 m). Median pitch values were also pooled from the surface periods depicted above and a grand median was used as the estimated pitch offset and applied to every pitch value (logical corrections were performed to ensure pitch remained within the -90° to $+90^\circ$ range).

Correcting the dead-reckoned tracks for drift

Dead-reckoned tracks were corrected at approximately 1-minute epochs. A rolling time function was applied in which a fix was only kept when the time period between it and the previously kept fix was ≥ 60 s, after which the time counter reset and the process continued. This ensured when there was a large gap between GPS data (caused at times when penguins rarely stayed at the surface long enough for a fix to be registered), the next available fix was always included. Prior to this, it was clear that GPS fixes were sometimes displaced in time (*cf.* Bouvet & Garcia 2000), often with registered fixes occurring into the subsequent dive. As such, to ensure animal movement paths (at depth) were not corrected based on previous surface positions within the drift correcting procedure, I reallocated the last GPS fix obtained during each depicted inter-dive cycle (any data between surface periods) to the last row index of the prior surface period, disregarding all other fixes registered when the bird

was not deemed at the surface. Obvious outliers as determined visually were initially removed.

Conversions between estimates of U and V components (m/s) and heading (°) and speed (m/s)

The magnitude (or rather speed (m/s)) of a vector (\overrightarrow{VS}) was calculated via;

$$\overrightarrow{VS} = \sqrt{(U^2 + V^2)} \quad (1)$$

The direction (or rather heading (0° to 360° - 'towards the vector of travel')) of a vector (VH) was estimated via;

$$VH = \text{mod} \left(\left(90 - \text{atan2}(V, U) \cdot \frac{180}{\pi} \right), 360 \right), \quad (2)$$

where *mod* refers to the modulo operator and heading represents 'going to' rather than 'coming from' using the 0 to 360° scale.

To convert VS and VH estimates (e.g., bird speed and heading estimates) to U and V components (m/s) (+U representing currents towards the East and +V currents towards the North), 180 was first added to every VH value (because meteorological convention traditionally states the direction from which U and V vectors originate). To ensure circular range was maintained between 0° and 360°, 360 was subtracted from values > 360. Lastly, for the below formula, VH had to be converted to the -180° to +180° scale and so 360 was subsequently subtracted from values > 180°.

$$U = -VS \cdot \sin \left(VH \cdot \frac{\pi}{180} \right) \quad (8)$$

$$V = -VS \cdot \cos \left(VH \cdot \frac{\pi}{180} \right) \quad (9)$$

Calculating the Theoretical 'best' heading

This involved while() loops in R, whereby along each point along the DR track, each heading value between 0° and 360° (incrementing at 0.5° epochs) were trailed . At each epoch, U and V components were calculated and added to the U and V components of the current, before calculating the theoretical 'best' resultant heading. The theoretical 'best' U and V vectors that produced the closest heading to the 'line-of-sight' heading post current integration were used.

References

- Bouvet, D. & Garcia, G. (2000) GPS latency identification by Kalman filtering. *Robotica*, **18**, 475-485.
- Newey, W.K. & Powell, J.L. (1987) Asymmetric least squares estimation and testing. *Econometrica: Journal of the Econometric Society*, 819-847.

Papers that I have co-authored during this thesis

- Wilson, R.P., Holton, M., Wilson, V.L., **Gunner, R.**, Tysse, B., Wilson, G.I., Quintana, F., Duarte, C. and Scantlebury, D.M., 2019. Towards informed metrics for examining the role of human-induced animal responses in tag studies on wild animals. *Integrative zoology*, 14(1), pp.17-29.
- Wilson, R.P., Börger, L., Holton, M.D., Scantlebury, D.M., Gómez-Laich, A., Quintana, F., Rosell, F., Graf, P.M., Williams, H., **Gunner, R.**, Hopkins, L., Marks, N., Geraldi, N.R., Duarte, C.M., Scott, R., Strano, M.S., Robotka, H., Eizaguirre, C., Fahlman, A. and Shepard, E.L.C., 2020. Estimates for energy expenditure in free-living animals using acceleration proxies: A reappraisal. *Journal of Animal Ecology*, 89, 161-172.
- Arkwright, A.C., Archibald, E., Fahlman, A., Holton, M.D., Crespo-Picazo, J.L., Cabedo, V.M., Duarte, C.M., Scott, R., Webb, S., **Gunner, R.M.** and Wilson, R.P., 2020. Behavioral Biomarkers for Animal Health: A Case Study Using Animal-Attached Technology on Loggerhead Turtles. *Frontiers in Ecology and Evolution*, 7, p.504.
- Wilson, R.P., Williams, H.J., Holton, M.D., Di Virgilio, A., Börger, L., Potts, J.R., **Gunner, R.**, Arkwright, A., Fahlman, A., Bennett, N.C., Alagaili, A., Cole, N.C., Duarte, C.M. and Scantlebury, M.D., 2020. An “orientation sphere” visualization for examining animal head movements. *Ecology and Evolution*, 10(10), pp.4291-4302.
- Wilson, R.P., Rose, K.A., **Gunner, R.**, Holton, M., Marks, N., Bennett, N.C., Bell, S., Twining, J., Hesketh, J., Duarte, C.M., Bezodis, N. and Scantlebury, M.D., (in press). Animal lifestyle affects acceptable mass limits for attached tags. *Proceedings B*.
- Wilson, R.P., Rose, K.A., Metcalfe, R.S., Holton, M., Redcliffe, J., **Gunner, R.**, Borger, L., Loison, A., Milos, J., Painter, M.S., Silovsky, V., Marks, N.J., Garel, M., Toigo, C., Marchand, P., Bennet, N.C., McNarry, M.A., Mackintosh, K.A., Brown, M.R. and Scantlebury, M.D., 2021. Path tortuosity changes the transport cost paradigm in terrestrial animals. *Ecography*, 44(10).
- English, H.M., Harvey, L., Wilson, R.P., **Gunner, R.M.**, Holton, M.D., Woodroffe, R. and Börger, L., 2020. Multi-sensor biologgers and innovative training allow data collection with high conservation and welfare value in zoos, *Research Square*, doi: 10.21203/rs.3.rs-562677/v1. [Currently a pre-print].
- Gómez Laich, A., Patano, C., Wilson, R.P., Svagelj, W.S., Yoda, K., **Gunner, R.M.** and Quintana, F., 2021. Leg rings impact the diving performance of a foot-propelled diver, *Ibis*.
- Quintana, F., Wilson, R.P., **Gunner, R.M.**, Muzzio, F., Brogger, G.M., Dell'Omo, G., Duarte, C.M. and A. Gómez-Laich., (in review). Long walk home; strategies used by Magellanic penguins to find their nests. *Current Biology*.
- Mayer, M and **Gunner, R.M.**, (2021). Roadkill: we can predict where animals cross roads – and use it to prevent collisions. *The Conversation*.